PROCEEDINGS

EUM P 28
ISSN 1023-0416

FIFTH INTERNATIONAL WINDS WORKSHOP

LORNE, AUSTRALIA
28 February – 3 March 2000

A Workshop jointly sponsored by
BoM, EUMETSAT, JMA, NOAA and WMO

EUMETSAT

BoM

JMA
気象庁

World Meteorological Organization

NOAA

PUBLISHED AND DISTRIBUTED BY:

EUMETSAT
Am Kavalleriesand 31
D-64295 Darmstadt
Germany
Tel. ++49-6151-807-7
Fax ++49-6151-807-555

ISBN 92-9110-036-6

The papers in this book comprise the proceedings of the Fifth International Winds Workshop. They reflect the opinions of the authors. They are published as presented, without change to the contents are with only occasional changes to the layout, in the interest of timely dissemination. Their inclusion does not necessarily constitute endorsement by EUMETSAT.

The cover page shows the Twelve Apostles in front of the Great Ocean Road on the South Coast of Australia.

CONTENTS

SESSION V
NEW TECHNIQUES

SESSION VI
NEW SPACE BORNE SYSTEMS

AUTHOR INDEX

WELCOME ADDRESS

Dr. Mike Manton
Chief, Bureau of Meteorology Research Centre

Good morning Ladies and Gentlemen,

I am pleased to welcome you to the Fifth International Winds Workshop, held under the auspices of the meteorological satellite agencies and in close co-operation with the WMO Co-ordination Group for Meteorological Satellites. These workshops involve co-operation among agencies across Europe, the Americas and Asia.

We are meeting in the tourist town of Lorne, a few hours drive from Melbourne. Continuing along the coast from Lorne, one soon comes to spectacular scenery where the coast is swept by winds off the Southern Ocean. These prevailing winds meant that last century these waters were treacherous for shipping, and dozens of ships were lost along the coast.

The oceans surrounding Australia highlight the major difference between the northern and southern hemispheres. These vast oceans without conventional meteorological observations mean that satellite data are vital to us in Australia. The introduction of routine satellite imagery had a profound effect on forecasting in Australia nearly forty years ago. In particular, cloud-drift winds provide a significant source of data for our numerical weather prediction (NWP) systems. It is therefore pleasing to see the increasing availability of these data, with increasing spatial and temporal frequency.

While satellite data are critical for NWP and weather prediction in general, it is important to be aware that the record of global climate is also dependent upon satellites. This need is especially significant as we look to the future of the integrated global observing system. To some, this process has an aim of using satellites to compensate for reductions in the number of *in situ* data. In reality, what we are doing is seeking to optimise our overall observation resources to cover the full range of user needs. Key needs of the climate community are for observations that have long-term consistency and high quality. One of the aims of climate studies is the identification of trends and changes in variables, such as temperature and rainfall. Thus we are looking for a small signal against a noisy background.

For the *in situ* observations, we have established networks, subsets of the World Weather Watch, that will provide baseline observations for climate analysis. These networks, the GCOS Surface Network (GSN) and the GCOS Upper Air Network (GUAN), will also provide benchmarks or calibration standards for NWP systems. It is very encouraging to see the satellite community recognising the importance of these observations for both weather and climate applications. It is vital that we get similarly consistent and high-quality satellite observations to complement the *in situ* data.

The importance of satellite-derived winds has been recognised for a long time. Over a decade ago, the Joint Scientific Committee of the World Climate Research Programme (WCRP) was asked for its priorities for satellite observations by the space agencies. Even at that time, the highest priority for new data types was for the capability to estimate winds right across the tropics.

As we look into the future, it seems that this priority of lidar-based winds is likely to be satisfied in the next few years. This will provide a fine complement to the cloud-based winds that you are focusing on now.

If we continue to look into the future (i.e. to look at other trends), I expect that the processing of satellite imagery will evolve from the calculation of individual winds to the assimilation of radiances. Our capability to model clouds is evolving rapidly, and so our capability to utilise satellite imagery will also increase.

With these two developments (lidar-based winds and direct assimilation of imagery), it is clear that these international workshops will continue to be major forums for the consideration of major issues. In addition to the exciting science, the workshops are vital in resolving key operational issues, such as the most efficient manner to exchange the data in real time. Indeed this is a great feature of the WMO system: it brings together research and operational communities in a harmonious way.

In opening this fifth workshop, I wish you well in your deliberations over the next few days. I also trust that you will stay long enough to take that drive along the south coast I mentioned at the start. It would clearly be a business trip, allowing you to understand why the analysis of satellite winds is such a key problem for us in the southern hemisphere.

WELCOME ADDRESS

Dr. Tillmann Mohr
Director of EUMETSAT

Good morning Ladies and Gentlemen,

Following the good tradition of the previous International Winds Workshops I would like to welcome you to the 5th International Winds Workshop. This workshop is hosted by the Bureau of Meteorology and organised jointly by the Co-operative Institute for Satellite Studies (CIMSS), EUMETSAT and the Bureau of Meteorology. It is co-sponsored by the World Meteorological Organization (WMO), the Japanese Meteorological Agency (JMA) and the National Environmental Satellite Data and Information Service (NESDIS) of NOAA.

The International Winds Workshops take place under the auspices of the Co-ordination Group for Meteorological Satellites (CGMS) and as EUMETSAT acts as the CGMS secretariat I, as Director of EUMETSAT, take great pleasure in supporting the Workshops. I am pleased about the continuous creative work and success that emerges from the Winds Workshops. This success has been demonstrated through improvements to the derivation of winds from satellites over the last decade and the enhanced positive impact of satellite tracked fields on numerical weather prediction.

The Winds Workshop is a well-established forum for the exchange of ideas amongst the leading specialists in wind derivation from geostationary satellites and the user community, which is well represented through representatives from NWP centres and other institutions. The fruitful co-operation between the users, operational centres producing winds and the science community leads to the overall success. It is clear that the improvements in the wind derivation techniques would not have materialised in an improved impact of satellite winds if users, notably the NWP community, had not made significant efforts to improve the utilisation of the data. It is also noteworthy that since the third and fourth workshops, this forum has been extended to include specialists working on other methods of wind retrieval from satellites. This had been recommended by CGMS and broadens the scope of the discussion while keeping the focus on the original purpose of the workshop, which is winds from the feature tracking in geostationary satellite images.

The previous meetings have included excellent presentations providing fruitful ground for constructive discussions. The feedback of the workshops to the CGMS meetings has been very good too. The presentations at this workshop cover again the important aspects ranging from the extraction of wind fields from satellite imagery data to the utilisation in numerical forecast models. It will be interesting to hear the reports on quality indicators associated with wind vectors which help to improve the use in NWP forecast models. Various new aspects will be discussed in the working groups, amongst them the support to re-analysis efforts (e.g. ERA- 40 at ECMWF) through the reprocessing of satellite winds with state-of-the-art algorithms. The interpretation of observed feature motion is still an important science issue, in particular the use of rapid scans is still an area to be further exploited. Here I should like to give credit to Dr. Ted Fujita who passed away in 1998. Ted Fujita was a pioneer of the use and interpretation of satellite inferred atmospheric motion and many of you remember his stimulating contributions to the first and second International Winds Workshops in Washington DC and Tokyo, respectively.

I am sure this meeting will continue the success of previous meetings. Many of you will return home with new ideas and plans. I really do regret that I am not able to attend this workshop myself since I maintain a keen interest in satellite meteorology and science.

I thank the Bureau of Meteorology for hosting the 5th International Winds Workshop in this wonderful environment and I convey my gratitude to Dr. John LeMarshall and David Jaspers and their co-workers for the local arrangements. The Bureau of Meteorology has always been a strong player in the arena of satellite wind derivation and utilisation in NWP. Some of the most prominent improvements, for instance the use of high-density winds, have been pioneered by the Bureau of Meteorology. Therefore the choice of Lorne as venue for the 5th International Winds Workshop is an excellent one. Thanks are also due to Chris Velden from CIMSS, Ken Holmlund from EUMETSAT, Dr. Don Hinsman from WMO, Dr. M. Tokuno from JMA and Dr. J. LeMarshall from BoM for putting together the workshop program.

I wish you, dear colleagues, a successful and stimulating Workshop and a pleasant time.

WELCOME ADDRESS

Dr. John Le Marshall
Bureau of Meteorology

Good morning Ladies and Gentlemen,

I would like to welcome you to Lorne on behalf of the Local Organising Committee and the Bureau of Meteorology. This venue on the Surf Coast is very appropriate for the first meeting in the new millennium of the International Winds Workshop. Activities in this area have been strongly influenced by winds and their predictability. In the past, more than 140 ships have been wrecked along this section of coast and many lives have been lost as a result of adverse weather and wind conditions. A prime example of this was the Loch Ard wreck where only two people survived the catastrophic sinking.

The importance of wind, here, has not changed, with the activity of the surfing and fishing communities being dictated by wind conditions and forecasts. Of course, we understand that measurement and forecasting of wind conditions are important for many tasks. In NWP, it is well established that wind measurements are of prime importance. In the case of tropical cyclone or hurricane forecasting, we know that, in the United States, for instance, evacuation of 1 mile of coastline as a result of a hurricane warning costs of the order of $100,000. Therefore an improvement in landfall accuracy of 10 miles and its translation into evacuations saves $1 million.

The start of the new millennium is a significant time to be meeting in Lorne. We are now beginning a new era where we will have better spatial and temporal resolution data; we have new instruments on the drawing board which will observe at better and considerably more frequencies. The assimilation methods now available to use the resulting near quasi-continuous data have developed considerably in the late nineties and hold great promise in terms of improved analysis, initialisation and forecasting potential. Importantly, the burgeoning computer power, now available in operational meteorological centres, provides us with the means of collecting, processing, assimilating and forecasting with data from these new instruments and clearly points to improvement in forecast capability in the near future.

I think that to underline what will be available, soon, in the new millennium, a brief description of some of the capabilities of the GIFTS (Geostationary Imaging Fourier Transform Spectrometer) instrument is appropriate. This instrument will take 16,384 soundings, every 10 seconds, at 4 kilometre resolution and less than 1 degree RMS in the vertical. It will allow wind determination, using 3,000 channels at 4 kilometre resolution in the infrared and, even in comparative darkness, it will provide 1 kilometre resolution, quarter moonlight visible imaging for wind estimation.

This, combined with the considerable wind fields provided by QuikScat at the surface and the mooted flight of a Doppler Wind Lidar certainly paint a positive picture for the future and make it a pleasure for scientists and technologists to work in this area, optimistic of producing significant benefits for humankind.

I hope that, during your stay in Lorne, you are able to address many of the issues needing consideration. The generation and use of quality flags, optimal observing methods for wind generation and continuous data assimilation are amongst many issues requiring attention. In closing, I also hope that your stay on the Surf Coast is both personally and professionally rewarding and I trust that it will benefit future activities.

SUMMARY OF THE FIFTH INTERNATIONAL WINDS WORKSHOP

The Fifth International Winds Workshop (IWW5) was held in Lorne, Australia from 28 February – 3 March 2000. The Workshop was organised jointly by the Co-operative Institute for Satellite Studies (CIMSS), EUMETSAT and the Bureau of Meteorology (BoM). BoM was responsible of the local arrangements providing an excellent venue and facilities.

The IWW5 was attended by 40 scientists from thirteen countries (Australia, China, Denmark, France, Germany, India, Japan, The Netherlands, Spain, Switzerland, Taiwan, United Kingdom and United States of America) and four international organisations (ECMWF, WMO, ESA and EUMETSAT). It is noteworthy that all satellite operators operationally producing Atmospheric Motion Vectors (AMVs) and most global NWP centres were present and that scientists from both the research and scientific community working in this field was also well represented.

The Winds Workshop provide an established forum for data providers, users and the science community to exchange experience and knowledge on the use and interpretation of the AMVs derived from multi-spectral satellite imagery data. It also provides an important way for the these communities to improve the use of the satellite data in NWP. The previous workshop (IWW4) maintained the high standard of the previous workshop and it was felt that the specific new achievements were; expansion of the winds user community, inauguration of high density winds, characterisation of the strengths (and weaknesses) of different Automatic Quality Control (AQC) procedures, demonstration of applications in nowcasting, comparisons of impact from direct assimilation of radiances vs. AMVs, expansion of the NWP impact studies, realisation of FGGE like data sets and the initiation of a dialogue with the community representing other kind of space borne instruments providing wind information. In the view of the success and importance of the previous workshops the expectation for the IWW5 were again high.

The Workshop was opened by Dr. M. Manton, Bureau of Meteorology (BoM, Australia) who pointed out the importance of the IWWs and encouraged the participants to use the opportunity of this workshop to further advance not only the extraction methodologies but also the use of the data. In a welcoming address from Dr. T. Mohr (EUMETSAT, Germany) presented by Dr. J. Schmetz underlined the importance of these meetings to the winds community pointing out the relevance of the participation of the user community. In this address also the importance of the workshops as a forum to interact with the Co-ordination Group for Meteorological Satellites was emphasised. Finally, in his opening address Dr. J. Le Marshall (BoM, Australia), re-iterated the importance of the derivation of AMVs from satellite imagery with a special focus on local weather prediction.

The Workshop proceeded with six plenary sessions. The first session on “Current Systems to Derive AMVs” gave in five papers an overview of the current status at the operational data extraction centres, high-lighting the latest improvements in extraction techniques and also the importance to converge the existing systems toward future new systems. Session two on “Verification and Objective Quality Analysis” contained seven papers showing the significance of continuos data monitoring as well as the importance to unify the reporting methodologies and AQC procedures. Session three on “Assimilation and Impact of AMVs in NWP” provided eight papers showing new evidence on the importance and usefulness of AMVs and other wind data derived with space borne instruments for different kind of weather patters and different seasons. Session four “New Retrieval Systems” with five papers gave an overview of the future capabilities of the AMV retrieval schemes, not only depending on improved satellite data but also on improved methodologies. Session five on “New

Techniques" included four papers presenting ways to improve not only the derivation techniques for the future but the importance of rapid scans for Nowcasting as well as methodologies useful for limited areas. The sixth and final session on "New Space Borne Systems" included five papers that continued the dialog between the community representing the AMV derivation from imagery data from geostationary satellite and the community representing wind derivation with other space borne active and passive instruments. Of special interest is to note the importance of synergy between the different user communities in order to derive a homogeneous picture of the atmospheric flow.

Three working groups convened during the meeting. These were 1) Working Group on Methods (WG I), 2) Working Group on Utilisation (WG II) and 3) Working Group on Verification and Quality Indicators. The working groups continued the work started at the previous workshop (IWW4) to improve the derivation and utilisation of AMVs. They also incorporated the requests from CGMS 31 for analysis and recommendations.

The detailed reports of all six session and three working groups are provided separately on the following pages.

The Workshop concluded with a plenary session reflecting on the achievements of the workshop. It was felt that the high expectations of the workshop were met and that the workshops should be continued in their present form. The excellent local arrangements were specially noted with gratitude to D. Jasper and J. Le Marshall from BoM. The next Workshop will be again organised by the same scientific committee and it is planned for early 2002 in Madison, USA.

Kenneth Holmlund
EUMETSAT

CHAIRPERSONS' REPORTS

SESSIONS I – VI

SESSION I

CURRENT SYSTEMS TO DERIVE ATMOSPHERIC MOTION VECTORS (AMVs)

Chairperson: Donald Hinsman

Session I included presentations from the primary producers (JMA, NOAA/NESDIS, EUMETSAT, Australian BoM and CMA/SMC).

Masami Tokuno from JMA noted that Atmospheric Motion Vectors (AMVs) were being produced on a regular four times per day schedule and in the vicinity of typhoons once a day.

Jaime Daniels from NOAA/NESDIS described new operational strategies that have resulted in improved wind products and associated increased utility in numerous applications.

Mikael Rattenborg described the current EUMETSAT AMV retrieval scheme that has continuously been improved with a goal to be ready for the Meteosat Second Generation (MSG) scheduled for launch in 2000.

John Le Marshall, BoM reviewed recent advances related to the generation and assimilation of high spatial and temporal winds from GMS-5.

Jianmin Xu gave the final presentation. He showed the results from a comparison of the quality of AMVs produced with both the EUMETSAT and CMA/SMC processing systems using the same data set.

Donald Hinsman, Chairperson of Session I
WMO, Geneva

SESSION II

VERIFICATION AND OBJECTIVE QUALITY ANALYSIS

Chairperson: Masami Tokuno

Session two covered verification and objective quality analysis of Atmospheric Motion Vectors (AMVs) and new winds from QuickScat.

The first presentation by François Lalaurette presented the integrated satellite wind monitoring report of the NWP SAF to enable the improvement of both derived satellite winds and their treatment within NWP models. Most signatures were found to be consistent when the comparison is made with respect to both NWP models, i.e., stronger low level winds in stratus area and lower high level winds in the jet stream. Participation from other NWP centres was called for.

The presentation by Ken Holmlund reported a development to try to combine the Quality Indicator scheme of EUMETSAT and the auto-editor/recursive filter analysis of CIMSS in order to derive an even better approach for AQC. The impact of the combined scheme during NORPEX-98 high-density wind fields derived with both GOES and GMS imagery data was better than of either scheme alone.

The paper by Simon Elliott presented an approach for parallel quality control of EUMETSAT wind products, with and without the use of forecast wind field, separately, with each wind. Wind vectors with both sets of quality control value are disseminated via GTS BUFR code.

François Lalaurette presented their monitoring of GOES, METEOSAT-7 and GMS-5 AMVs against model first guess and co-located platforms (Aircraft and Radiosonde). He showed that the GOES error signature differs from that of the other satellites due to the auto editor processing. An underestimation of satellite wind speeds was confirmed both with reference to the model and other in situ data.

Ad Stoffelen presented the methodology of assimilating QuickScat inverted winds in numerical weather prediction. He showed that the presented methodology is better than using radar cross-section although significant advances are still required.

P. N. Khanna presented recent improvements in the quality of INSAT derived CMWs by introducing their new scheme and their use in numerical model forecast. Improved data assimilation of CMWs in their Limited Area Model being run operationally at IMD shows positive impact on the Model forecast.

Garrett Campbell presented the results of combing existing stereo-height software from CIRA/CSU with the fully automated target extraction methodology developed at EUMETSAT. He showed that the results from the 5 km resolution IR observations are just as useful as the analysis of 2.5 km visible data. He also showed discrepancies for the derived heights for some optically very thin clouds as well as for some opaque clouds. These inconsistencies can used to improve both algorithms.

Masami Tokuno, Chairperson of Session II
Japan Meteorological Agency, Tokyo

SESSION III

ASSIMILATION AND IMPACT OF ATMOSPHERIC MOTION VECTORS IN NUMERICAL WEATHER PREDICTION

Chairperson: John Le Marshall

The Third Session of the Workshop provided eight papers addressing the assimilation of atmospheric motion vectors (AMVs) and their impact in numerical weather prediction (NWP). As in previous Workshops, it gave considerable insight into the large range of activities associated with the use of AMVs and solid evidence of their utility in NWP.

Paul Menzel discussed in detail the seasonal impact of five satellite data types on the ETA Data Assimilation/Forecast System (EDAS). The data types were two precipitable water data types, temperature data for a cloudy environment and two cloud motion data types. Examining geopotential height, temperature, u-component of the wind and relative humidity showed a modest positive impact on the forecast for all data types with cloud drift wind data having maximum impact in Winter while precipitable water has the largest positive impact during the Summer and transition seasons.

Brian Soden discussed the use of GOES AMVs for numerical hurricane prediction and climate studies at NOAA/GFDL. Cloudy and clear sky multispectral water vapour observations were used in a series of parallel forecasts to determine the impact of the GOES winds on tropical cyclone track forecasts. Over 100 cases from 10 different storms in 3 seasons were examined. On average, the assimilation of satellite winds reduced track errors at all forecast periods. Relative reductions of track error were 5% and 12% at 12 and 36 hours respectively. Also discussed were the application of hourly GOES 6.7 micron water vapour observations to an examination of the processes regulating the distribution of upper tropospheric water vapour. Use was made of an objective pattern-tracking algorithm to trace upper tropospheric water vapour features from sequential images.

A case study describing the use of METEOSAT-5 winds in an analysis of a tropical cyclone in May 1999 was presented by Ramesh Bhatia and his colleagues. This study indicated the utility of the winds in the analysis and subsequent prediction of motion of a tropical cyclone affecting the Gujarat coast in May 1999.

Jenni Evans from Pennsylvania State University described the development of the Community HUrricane Modelling System (CHUMS), based on the Penn. State/NCAR non-hydrostatic mesoscale model (MM5). The detailed physics of the MM5, down to the resolution of non-hydrostatic effects and cloud scale, and the availability of a 4-dimensional data assimilation cycle based on nudging were the reasons for the choice of this numerical system for tropical cyclone studies. An initial case study of Tropical Cyclone Floyd in 1999 was presented at the meeting, demonstrating the potential of this system for further studies.

Bruce Ingleby from the UK Met. Office described recent developments in the use of satellite winds by the UK Met. Office. Changes to the operational NWP model as a result of impact tests with METEOSAT-5, GMS and GOES high-density infrared and METEOSAT high resolution visible winds were noted as was the introduction of 3D-Var. in place of the previous optimal interpolation method of assimilation. Some initial work, looking at the impact of METEOSAT winds over the Indian Ocean and Australian Region was also recorded.

Assimilation of conventional and satellite wind observations in the global data assimilation system at NCMRWF was reported by S. R. H. Rizvi and his colleagues. The paper addressed research efforts at NCMRWF in assimilating various types of wind observations, conventional and satellite, in an operational global data assimilation system (GDAS). It was reported that conventional winds from INSAT, GMS, GOES and METEOSAT at low resolution have been used and, recently, high resolution METEOSAT-5 and ERS-2 winds have been incorporated into the operational GDAS. The procedures adopted to overcome problems in assimilating these later data and their impact at NCMRWF were recorded. A technique for assimilating surface wind speeds from recently launched Indian IRSP4 OceanSat was also noted.

XiuJuan Su and her associates reported on work toward improved use of GOES satellite-derived winds at the National Environmental Modelling Center, Washington. This work is directed towards improved assimilation of the wind data, paying particular attention to the use of Quality Indicators.

The final paper of the Session reported on a preliminary impact study using QuikScat/ SeaWinds ocean surface winds in the JMA spectral model. Yoshihiko Tahara and his colleagues reported that JMA has developed an improved assimilation system. This contains a wind retrieval system of higher accuracy, a new quality control scheme to reject erroneous wind data, a retrieval scheme for ocean surface pressure based on surface wind observations and a system to assimilate the pressure data into the NWP model. Using this assimilation system, JMA successfully showed positive impact from the use of the scatterometer data in the global model. JMA began the operational use of ERS scatterometer data in 1998. In addition to the ERS scatterometer study, a preliminary impact study demonstrating the capability to assimilate QuikScat/SeaWinds in the JMA spectral model was also presented.

Overall, the session recorded recent advances in the assimilation of high-resolution winds from satellite observations and provided evidence of gains still to be made at many NWP centres.

John Le Marshall, Chairperson of Session III
Bureau of Meteorology, Melbourne

SESSION IV

NEW RETRIEVAL SYSTEMS

Chairperson: Ramesh C. Bhatia

Main focus was on the new techniques developed for derivation of Atmospheric Motion Vectors from the Geostationary Meteorological Satellite systems. There were five presentations during this session.

The first presentation by Chris Velden brought out results of several advances in winds processing and assimilation being explored at CIMSS. These include winds derived from rapid scan imaging, the use of 3.9 um for night-time wind retrievals, water vapor assimilation into NWP and derivation of vector fields from simulated data of potential future instruments.

Tim Olander presented results of work done at CIMSS to produce a platform independent version of the UW-CIMSS processing algorithm within the McIDAS environment. The new software is currently under evaluation and will soon be made available to the interested data processing centers and research institutes. It includes the latest post-processing QC module incorporating techniques of CIMSS and EUMETSAT.

Ken Holmlund presented details of the new MSG Atmospheric Motion Vector (AMV) retrieval scheme highlighting changes with respect to the current METEOSAT AMV scheme and the expected areas of improvements. Validation results showed that the new retrieval scheme will provide improved AMVs with MSG.

Presentation by José Miguel Fernández also showed good results of work done at Satellite Applications Facility (SAF), Spain for EUMETSAT in support of nowcasting, using data from future MSG systems, particularly the HRV channel at 1 km resolution.

The last presentation by Jianmin Xu of China showed the results of new work done at National Satellite Meteorological Center, China for development of Analysis tools that is used in their AMV derivation scheme. Using these tools image animations, parameters, scatter diagrams etc. can be visualized thereby providing a way to monitor the calculation process of individual vectors. Such facilities can be very useful to investigate specific problems.

All presentations were followed by a number of questions/comments from the distinguished audience. Main conclusion of the discussions during the session was to encourage the further developments of new retrieval systems in view of their importance for a number of users.

Ramesh Bhatia, Chairperson of Session IV
India Meteorological Department, New Delhi

SESSION V

NEW TECHNIQUES

Chairperson: Jianmin Xu

In Session V, 4 papers were presented.

The paper “Polar Orbiter: stereo heights and cloud motions” presented by Garrett Campbell showed that multiple satellites are needed to measure motion with some uncertainty due to undetermined cloud height. But one multiple view satellite and an additional satellite provide enough information to derive both height and motion. This was demonstrated with data from POLDER and GOES. However the 6-km resolution of POLDER limits the accuracy. Comparison was also made to the differential Oxygen height estimate method.

The paper “On the use of rapid scan” by Joe Schmetz provided a summary of previous work of rapid scan including preliminary results from Meteosat-6 rapid scans and the perspectives for Meteosat Second Generation (MSG). MSG will have a full disk repeat cycle of 15 minutes and a twelve-channel imager, which provide new opportunities to observe the fast component of the hydrological cycle (cloud formation, convection, water vapor outflow). Results from other papers were confirmed; the rapid scans from Meteosat-6 provided more continue wind fields and more numerous wind vectors. The computation of divergence fields from these wind fields is feasible.

The paper “Investigation of cross-correlation and Euclidean distance target matching techniques in the Meteorological Product Extraction Facility (MPEF) environment” presented by Ken Holmlund provided further results of a comparison of both spatial and Fourier techniques undertaken in the MPEF environment. Significant performance benefits were achieved by computing the Fourier domain cross-correlation using Mixed Radix Fast Fourier Transform (FFT) with specific optimal data sizes. The paper also compared the displacement vectors derived by spatial and Fourier techniques. It was indicated that in low contrast regions maximum discrepancy was observed between the two techniques.

The paper “Tracking low level clouds over land on Meteosat images” by André Szantai described a reliable cloud motion wind tracking task. It was concluded that a limited number of low level cloud motion winds could be computed over land with standard time interval of 30 min. The selection can be improved with the use of climatological thresholds. An important increase of the number of CMWs is observed over land in the tropics when the time interval between images is reduced to 15 min. The use of the IR/WV correlation and the IR brightness temperature of the coldest pixels lead to similar selection of low level CMWs. CMW fields computed with a solar correction are very close to those computed without it. The method based on optical flow techniques gives a realistic motion in some areas.

Jianmin Xu, Chairperson of Session V
National Satellite Meteorology Center, Beijing

SESSION VI

NEW SPACE BORNE SYSTEMS

Chairperson: Johannes Schmetz

The sixth and last session of the workshop presented five papers on new space borne systems, new developments and perspectives for future measurements, respectively. This session was a nice finale of the workshop since it stimulated intense discussion that naturally led into the summary presentations of the Working Groups that concluded the workshop.

Bill Smith gave an enlightening talk on the Geostationary Imaging Fourier Transform Spectrometer (GIFTS) which will constitute a breakthrough in measurements from geostationary orbit. With a large focal plane array the instrument can provide full disk images at 4 km resolution with a repeat rate of five minutes. The imagery will consist of thousands of channels with very high spectral resolution thus enabling soundings with high vertical resolution and, hence the tracking of water vapour features at different levels in the atmosphere.

Charlotte Hasager delivered a paper on wind energy mapping using synthetic aperture radar data. Plans are under way to deploy offshore wind energy turbines in the seas around Denmark. This is useful because the wind speed over sea is significantly higher than over land. For planning purposes Charlotte Hasager conducts a detailed study on wind potential over sea using SAR data and physical models. It was noted that this paper presented new aspects to the workshop that had not been addressed at any previous workshop.

Paul Ingmann introduced the Atmospheric Dynamics Mission (ADM) of the European Space Agency (ESA) which will measure the global wind fields in the stratosphere up to about 26 km and in the cloud-free troposphere with a Doppler Wind Lidar (DWL). In addition the DWL will yield information on cloud top heights, the vertical distribution of cloud and aerosol properties.

Ad Stoffelen investigated the expected performance of the Atmospheric Dynamics Mission. He demonstrated a sufficiently large coverage of the measurements on the basis of a statistical analysis of cloud cover. An Observation System Simulation Experiment (OSSE) has been conducted which shows the expected overall positive impact of the new DWL wind data on numerical weather forecasts.

Jim Purdom made the final presentation of the workshop on the combined capabilities of active and passive space borne systems. He highlighted outstanding previous research on the tracking of atmospheric motion and recalled the need for a good understanding of the physics of the observations that may be often forgotten in statistical presentations of problems. Clearly this calls for research on case studies. Convincing examples were presented on recent achievements ranging from SAR image data to rapid scans from geostationary satellites. A lively discussion on the utilisation of the space observations in NWP and mesoscale models emerged from J. Purdom's talk emphasising the need for early preparation for new space borne systems in order to have the relevant science ready for applications of the new data.

Johannes Schmetz, Chairperson of Session VI
EUMETSAT, Darmstadt

WORKING GROUP REPORTS

WG I: Working Group on Methods

WG II: Working Group on Utilisation

WG III: Working Group on Verification and Quality Indicators

REPORT FROM THE WORKING GROUP ON METHODS (WG I)

Chairperson: Chris Velden

The ten-member working group on satellite-derived wind tracking methods discussed a wide range of topics. The "top ten" list of issues or research areas is presented below. Some of these topics are new, while others are re-emphasized from the IWW4 recommendations. The group felt an overarching issue was that with a growing AMV producer and user community, communication of new ideas and methods to extract wind data is increasingly essential to maintain uniform vector field quality and understanding of the data properties.

1) Standardization of processing methods by the global operational wind producing community. This includes tracking and height assignment methodology as well as unified quality control indicators. Promising new techniques from proven research studies should be introduced at IWWs for consideration of implementation by the operational wind producing centers. Code exchange is highly encouraged. The group also recommended convergence of the geostationary satellite observing system in regards to common imaging channels/frequencies for global winds production.

2) International strategies for creating more rapid scan (RS) capabilities. The group endorsed the recommendation to satellite agencies to create scanning strategies that allow RS scheduling on a more routine basis. Preliminary studies have shown the increased vector yield and quality from more frequent imaging, and the applications (e.g., tropical storms, mesoscale analyses). Further studies are encouraged to solidify the relationship between optimal scan frequency vs. spectral band and resolution, and explore the value of multiple RS image tracking (more than three images in the tracking loop). The GOES-L science checkout period can be used to design scan strategies.

3) Improvement in the specifications and performance of image navigation/registration. The production of RS winds at high resolution and use of sophisticated geometric height assignment techniques demand higher accuracy in image navigation and registration. The group re-emphasizes the recommendation from the WG of IWW4 for registration and navigation accuracy to be better than 1km for accurate RS wind determinations.

4) Focussed research on the speed bias problems. The slow bias in satellite-derived cloud-tracked vectors in the upper levels still exists, and is being treated by quality control or statistically-based increments. Clear sky water vapor winds at mid levels are also showing a slow bias, especially with GOES. The WG encourages further research into these problems and/or their solutions.

5) Vector derivation over land areas. Cloud-tracked winds over land areas offer increased difficulties. The WG endorses research into the scanning strategies (RS?) and processing/QC adjustments necessary to create vector fields over land with accuracy equal to marine regions.

6) Lessen the dependence on model first-guess information. This is a follow-up from IWW4. Methods are desired to derive displacement vectors, assign heights and QC with minimal influence of model-dependent fields.

7) Expand research on the use of other spectral bands for winds processing. The GOES 3.9 micron channel has demonstrated promise for nighttime low-level vector determinations. Other planned satellite launches will contain this channel and new channels will have the same capability. Exploitation of these spectral bands for winds is encouraged.
8) Continue to explore and refine wind derivations from microwave frequencies. The success of scatterometer winds and their use has been documented. Similar advances have been made in derivation of winds from SSM/I, SAR and AMSU. The WG acknowledges this new methodology

and endorses the continued efforts to extract winds from polar-orbiter microwave information and improve the algorithms.

9) Improvements in vector height assignment methods. This is a long-standing issue with AMV. Exploration into new methods to improve the height assignment accuracy should be continued, as well as data characterization studies (i.e. the representativeness of clear sky WV winds).

10) Investigation of tracking methodology. Preliminary work suggests correlation tracking is optimal in some cases, and the Euclidean distance method in others. New, more sophisticated methods (model-free) may lead to increased tracking accuracy. The WG recommends additional research in this area.

Chris Velden, Chairperson of Working Group I
University of Wisconsin - CIMSS, Madison

REPORT FROM THE WORKING GROUP ON UTILISATION (WG II)

Chairperson: Brian Soden

The Working Group on Utilisation (WG II) considered the application of satellite wind information in Climatological Analyses, Numerical Weather Prediction, and Nowcasting, discussed importance of Data Formatting and Access in its application, and noted the role of Education and Training in promoting the effective use of satellite AMVs. A discussion of the key achievements since the last workshop and recommendations for future efforts in these five areas are outlined below.

(1) Climatological Analyses

The potential of wind information from geostationary satellites to substantially enhance our understanding of the atmospheric circulation for climate diagnostics and model evaluation was clearly established. In light of this potential, the reprocessing of the existing geostationary archive using a consistent set of wind algorithms (to the extent feasible) was recognized as a high priority. Such an undertaking should provide near-global coverage and be designed for use by both the NWP-reanalysis and the climate diagnostics community. To facilitate the use of the wind data by this broader community, the reprocessing of the satellite archive should also offer a set of gridded, model-independent wind products. The working group further recommends that the wind retrievals be performed in conjunction with the retrieval of other quantities from the geostationary archive, such as precipitation, cloud cover, and water vapor, so that the relationship between these variables and the atmospheric dynamics can be studied.

(2) Numerical Weather Prediction

The presentations during the meeting clearly demonstrated that the production and use of AMVs for NWP has greatly expanded since the previous workshop. Presentations at this workshop offered further demonstration of the utility of cloud and water vapor motion vectors, and scatterometer data for tropical cyclone forecasting in a variety of numerical models (GFDL, NOGAPS, NCMRWF, BMRC) using both intermittent and continuos assimilation techniques. Positive impacts were also demonstrated for model forecasts on both regional (UW-Eta) and global (ECMWF) scales. In particular, several studies highlighted the importance of assimilating AMV fields in combination with other satellite products (e.g., radiances or temperature/moisture retrievals) to achieve optimal impact of the satellite AMV data. It was also noted that the assimilation of satellite data improved forecasts in both the northern and southern hemispheres, with impacts comparable to that obtained from the global radiosonde network. However, achieving these improvements required considerable effort in the development and tuning of the assimilation methods specifically for the satellite data. Furthermore, as the assimilation algorithms become more sophisticated (e.g., 4DVAR), the quality of the analysis becomes more vulnerable to the quality of the ingested data. Fortunately, data providers have made considerable progress in developing consistent and meaningful Quality Indicators (QIs) for AMVs. However, the WG recommends that the data providers continue to make improvements in the quality of the data itself, in addition to the quality of the QIs. In particular, a better understanding of the nature of the speed and altitude biases in AMVs and their possible correlation with each other was noted to be a high priority.

(3) Nowcasting

Presentations at the meeting also highlighted the continued importance of AMVs for tropical cyclone nowcasting. In addition to the AMVs themselves, products derived from AMVs, such as the UW/CIMMS vertical wind shear index, have been particularly useful for real-time monitoring and prediction of cyclone intensification. Currently, the real-time wind products are distributed via the World Wide Web (WWW). However, UW/CIMSS has recently rewritten their software to allow users to run the wind retrievals locally, rather than relying upon the WWW to obtain the real-time data.

(4) Data Format and Accessibility

The WG recognized the need for a standardized BUFR format to encode satellite wind data. Specifically, the WG recommends that CGMS requires:

- Wherever possible, the use of local BUFR table entries is avoided; and
- Where no existing table entry exists, the data provider should instigate the introduction of such an entry through the standardized WMO procedure.

Furthermore, despite the widespread availability and reliability of the core BUFR encoding/ decoding software provided by ECMWF, the WG noted that some data providers and users still have difficulty encoding and decoding satellite data. To help resolve the issue, the WG recommends that CGMS:

- Ask the centers with existing BUFR software to make their software available. This software would be provided as it is, and would form an example of the necessary procedure for other data providers.

Finally, the WG noted that the current difficulties in obtaining high-resolution satellite radiance data, from both historical and real-time archives, was a substantial impediment and prevents a significant portion of the research community from using the data. Such limitations clearly hinder the effective utilisation of the data and the WG therefore recommends that efforts be taken to facilitate the free and open access to the satellite archives. This is important in the view of a better understanding of the benefits and drawbacks between assimilation of wind data vs. radiance data.

(5) Education and Training

The WG noted the recent enhancement to the WMO strategy for Education and Training in Satellite Matters through the development of a virtual laboratory to improve satellite data utilisation, education and training. The virtual laboratory has at its core a global network of specialized centers of excellence for education and training. The virtual laboratory, with the group of centers having access to the Internet, would provide a global forum for the exchange of expertise, knowledge, and education and training with specialized focus groups such as found at the International Winds Workshops. The WG requests that the IWW use the CGMS Winds listservers and the virtual laboratory to assist in education and training for interested participants.

Brian Soden, Chairperson of Working Group II
Geophysical Fluid Dynamics Laboratory, Princeton

REPORT FROM THE WORKING GROUP ON VERIFICATION AND QUALITY INDICATORS (WG III)

Chairperson: Kenneth Holmlund

The working group on Verification and Quality Indices discussed the three following major areas:

Recommendations of the Working Group III from the 4th International Winds Workshop
- Statistics against other data sources
- Combined use, research and development of QI/RFF

CGMS actions and recommendations
- Action 27.21 NWP SAF proposal: Monitoring statistics on the Internet
- Discuss convergence toward one set of quality control flags
- Expanded use of geometric approaches (e.g. stereo) for height validation purposes

Issues raised at the 5th International Winds Workshop
- Model-to-Model statistics
- Statistics from other monitoring centres
- QI/RFF as observation errors
- Table of error characteristics assigned to AMVs at different NWP centres
- CGMS statistics

After a lively and constructive discussion on the above-mentioned topics the Working Group (III) decided to divide the recommendations in to two groups namely Monitoring/Verification and Quality Indices. With respect to Monitoring and Verification the WG III agreed on the following recommendations:

1) The table of observation errors currently accessible via the CGMS home page should be maintained. Furthermore it should be completed with the errors assigned to other types of upper air observation and more NWP centres should be included.

2) The monitoring results maintained by the NWP SAF were found valuable and should be completed with statistics for all operational satellite tracked winds.

3) The NWP SAF should propose a way to present information on background errors to the WEB for the next Workshop.

4) Other NWP centres, not currently contributing to the NWPSAF monitoring, were encouraged to publish their own monitoring statistics and provide a link to the NWPSAF monitoring page.

5) It was recommended to provide a link from the WMO and CGMS monitoring pages to the NWP SAF WEB page.

6) Recognising the value of the WMO maintained CGMS statistics the WGII recommends WMO to facilitate an easy input of the statistical tables on the WEB-site.

7) EUMETSAT to provide a paper to CGMS on modified contents of the CGMS statistics including e.g. stratification of the data in speed classes.

With respect to Quality Indices the WGIII concluded the following:

8) All data providers should strive to implement quality control procedures equivalent to the combined UW-CIMSS RFF and EUMETSAT QI scheme.

9) EUMETSAT and UW-CIMSS should make their QI-schemes readily available to all operational data providers as stand alone s/w packages.

10) NWP centres should work on methods to utilise the information given by the RFF and QI schemes and therefore the move to the use of BUFR data.

11) Data providers to provide information on height assignment methods and their accuracy and to develop methods to provide statistics on height assignment accuracy, e.g.:
    - inter-comparisons on methods
    - alternative methods
    - alternative observations (e.g. R/S, Lidar)

12) Continue the development of new and improved Quality Control schemes that do not make assumptions on atmospheric balance, e.g. current schemes are tuned towards large scale synoptic flow and are therefore not optimal for mesoscale features or extreme weather conditions (e.g. hurricanes).

Kenneth Holmlund, Chairperson of Working Group III
EUMETSAT, Darmstadt

SESSION I

CURRENT SYSTEMS TO DERIVE ATMOSPHERIC MOTION VECTORS (AMVs)

Chairperson: D. Hinsman

STATUS OF GMS-5 WIND PRODUCTS AND MTSAT WIND PRODUCTS PLANS AT MSC/JMA

Masami Tokuno

Meteorological Satellite Center, Japan Meteorological Agency
3-235, Nakakiyoto, Kiyose, Tokyo
Japan

ABSTRACT

The Meteorological Satellite Center (MSC) of the Japan Meteorological Agency (JMA) has operationally produced Cloud Motion Winds and Water Vapor Motion Winds from GMS-5 images four times a day and High Resolution Low-level Cloud Motion Winds (HRLCMW) in the vicinity of the typhoon once a day in the daytime for only one typhoon. This paper presents the current status and quality of High level Cloud Motion Winds and Water Vapor Motion Winds in the last three years. In addition, we will describe some plans for the satellite wind products with MTSAT at MSC.

1. Introduction

Meteorological Satellite Center (MSC) has produced Cloud Motion Winds (CMWs) since 1982. The following improvements have been carried out up to now. The program of high-level CMWs (HCMWs) extraction has been changed, i.e., the revision of height assignment table (1990), the second revision of height assignment table (1993), the exclusion of the area containing cumulonimbus and the introduction of IR and WV intercept technique (1995)(Takata 1993; Tokuno 1996). The program of quality control has also been changed, the introduction of intensive manual quality control technique including reassignment of wind height assigned automatically (1991) and the employment of improved manual quality control software (1992) (Takata 1993). Low-level CMWs (LCMWs) extraction scheme has not been changed since the introduction of automatic wind extraction in 1982. LCMWs are derived through man-machine interactive process as same as HCMWs for quality control. In addition, MSC has produced Water Vapor Motion Winds (WVMWs) from GMS-5 image data since June 1995. IR-WV intercept technique is used to assign wind height automatically. WVMWs are derived through automatic objective quality control process (Tokuno 1996). Recently MSC has increased the number of derived WVMWs since July 31 1998.

This report firstly shows current operational wind products of MSC and the results of evaluation of HCMWs and WVMWs in the last three years. Then we compare the results of the accuracy of WVMWs before and after the introduction of increasing the number of derived WVMWs. Finally we show a future plan for satellite wind products.

2. Current Operational Wind Products

Current GMS-5 operational wind products are shown in Table-1. Both low and high level CMWs have been produced by using visible and infrared images. The techniques of target cloud selection and height assignment were modified in September 1995. In target selection, a new processing was introduced to exclude the areas containing cumulonimbus by using brightness temperature difference between IR and WV sensor. In the height assignment, an IR and WV intercept technique was newly introduced to correct brightness temperature of non-black body clouds.

WVMWs are derived a middle and high levels in the troposphere from WV images. The WVMW extraction scheme is basically the same as that of CMW. However, its quality check is applied only by the automatic procedure, in which homogeneity of the speed, direction and height are controlled. WVMWs have been operationally disseminated via GTS since 28 March 1996. Recently MSC has increased the number of derived WVMWs since July 31 1998.

High density low level visible winds were derived from time-sequential images at 15 minute intervals around 04 UTC in May 1988. Automatic quality control procedure was introduced in 1992. In this procedure, the weak wind whose speed is less than 5 m/s and the wind whose direction is anticyclonic in regard to typhoon center are excluded.

Table 1 Operational Wind Products of MSC

Type of Product	Region of Interest	Output Frequency
Cloud / Water Vapor Motion Winds	50°N – 50°S 90°E – 170°W	00UTC, 06UTC, 12UTC,18UTC 4 times / day
High Density Low Level Visible Winds Around Typhoon	20°lat. X 20°long. Centered on the typhoon Center	Once a day (04UTC) When a typhoon exists

3. Current Status of the Accuracy of GMS-5 Cloud Motion Winds

Monthly mean differences between CMWs or WVMWs and rewinsonde winds are calculated in accordance with the method specified in the international comparison of Atmospheric Motion Winds. Vector differences of CMWs and WVMWs from January 1997 through December 1999 are shown in Fig. 1 (a), and speed differences are shown in Fig. 1 (b), (c) and (d).

3.1 Low-level CMWs

The root mean square (RMS) vector differences are 3.8~5.2 m/s and the fluctuation increases in 1999 (Fig. 1(a)). RMS speed differences are 2.7~4.5 m/s and the fluctuation increases in 1999 (Fig.1 (b)). Average speed differences (BIAS) are -0.7~0.7 m/s with a short term variation (Fig.1 (c)) and absolute value of the speed difference (ABS) is 1.9~2.6 m/s with a seasonal variation (Fig.1 (d)).

3.2 High-level CMWs

RMS vector differences are 7.6~9.8 m/s, which have an increasing tendency after the latter 1998 (Fig.1 (a)). RMS speed differences are 5.8~8.1 m/s (Fig.1 (b)) and ABS is 4.0~5.8 m/s (Fig.1 (d)). Both have an increasing tendency after the latter 1998. BIAS are -3.8~-0.8 m/s, which have an increasing tendency year by year (Fig.1 (c)).

3.3 High-level WVMWs

RMS vector differences before and after July 1998 are 7.7~10.2 m/s (means : 8.9 m/s) and 7.8~9.2 m/s (means : 6.9 m/s) (Fig.1 (a)). Those of RMS speed differences are 5.9~8.1 m/s (means : 6.9 m/s) and 6.1~7.5 m/s (means : 6.8 m/s) (Fig.1 (b)). Those of BIAS are –1.2~0.0 m/s (means : -0.6 m/s) and -0.2~0.7 m/s (means : 0.2 m/s) (Fig.1 (c)). Those of ABS are 4.4~5.8 m/s (means : 4.9 m/s) and 4.5~5.2 m/s (means : 4.8 m/s) (Fig.1 (d)). Thus the value of the later in all the cases above is a little smaller than that of the former. This result suggests that the amount of highly accurate HWVMWs increases as the total number of derived WVMWs increases.

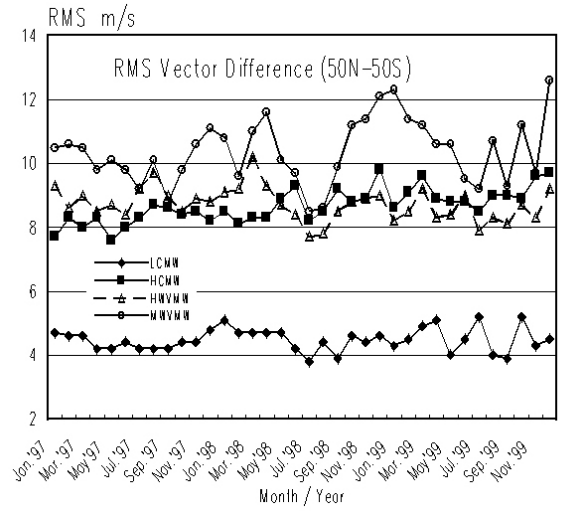

(a) RMS Vector Difference

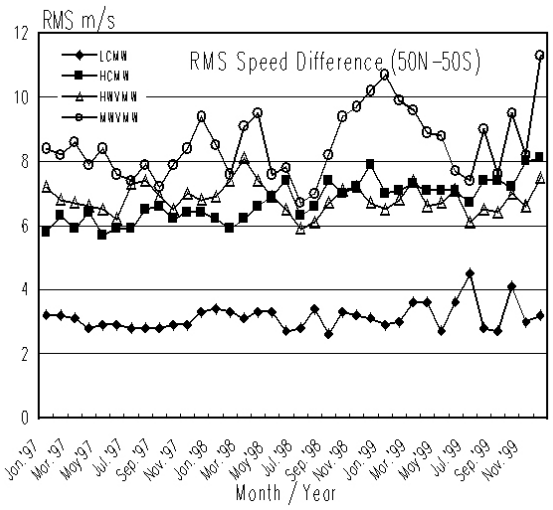

(b) RMS Speed Difference

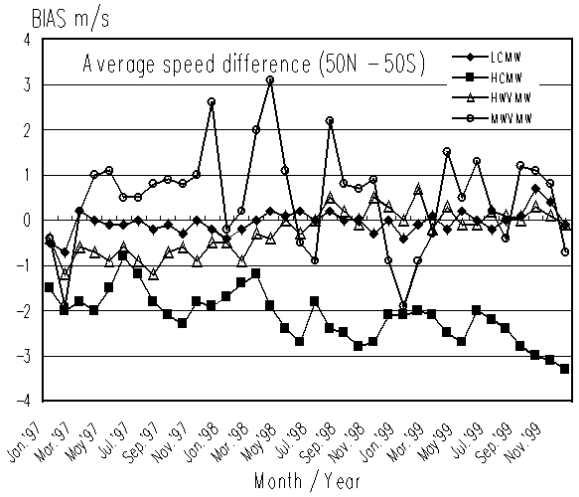

(c) Average Speed Difference

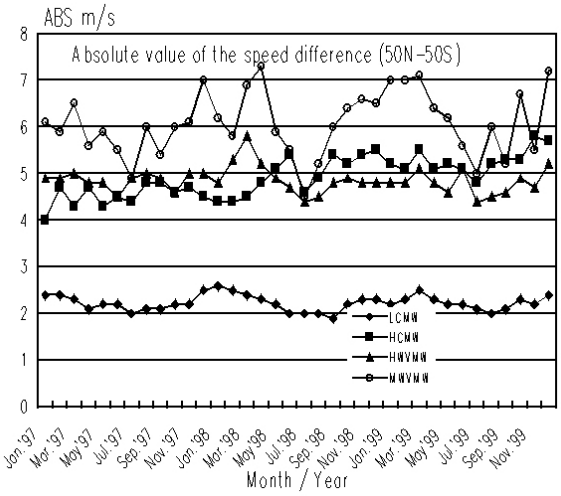

(d) Absolute Value of the Speed Difference

Figure 1. Monthly means of differences between GMS-5 CMWs or WVMWs and radiosonde wind from January 1997 through December 1999. LCMW : Low-level CMW, HCMW : High-level CMW, HWVMW : High-level WVMW, MWVMW : Middle-level WVMW

3.4 Middle-level WVMWs

RMS vector differences before and after July 1998 are 8.5~11.6 m/s (means : 10.1 m/s) and 8.6~12.6 m/s (means : 10.7 m/s) (Fig.1 (a)). Those of RMS speed differences are 6.7~9.5 m/s (means : 8.1 m/s) and 7.0~11.3 m/s (means : 9.0 m/s) (Fig.1 (b)). Those of BIAS are -1.9~3.1 m/s (means : 0.5 m/s) and -1.9~2.2 m/s (means : 0.4 m/s) (Fig.1 (c)). Those of ABS are 4.5~7.3 m/s (means : 5.9 m/s) and 5.0~7.2 m/s (means : 6.2 m/s)(Fig.1 (d)). Thus the value of the latter in above cases is a little larger than that of the former. This result suggests that the amount of inaccurate MWVMWs increases as the total number of derived WVMWs increases.

4. Comparison of High-level CMWs in 1997 with those in 1999

As shown in the session 3.2, the accuracy of HCMWs has a decreasing tendency since the latter 1998. Further investigation is carried out through the comparison of HCMWs in 1997 with those in 1999, dividing into two groups, in the summer (July and August) and the in the winter (December and next January).

Fig. 2 shows the distribution of total number of HCMWs per station used for comparison of HCMWs with rewinsode winds in the summer of 1997 and in the winter of 1997/1998. As expected, the total number of northern extra-tropical regions increases in the summer, while that of tropical regions decreases. In contrast, those of southern extra-tropical regions and tropical regions are increase in the winter. The distribution of total number of HCMWs 1999 is similar to that in 1997.

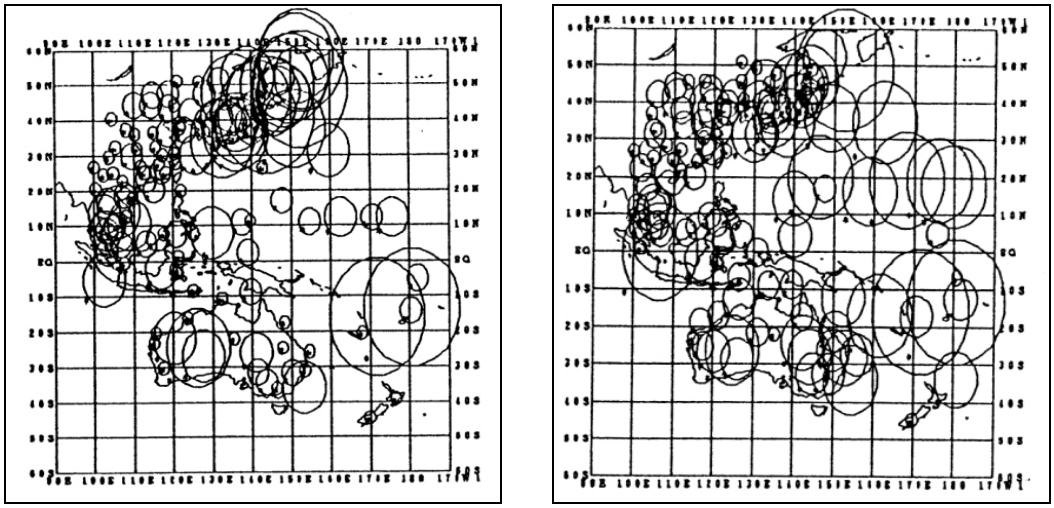

Figure 2. The distribution of total number of HCMWs per station used for the comparison.
Left HCMWs, July and August 1997. Right;HCMWs, December 1997 and January 1998

Fig. 3 shows the comparison of the vertical distribution of wind speed bias and RMS vector difference in the three latitude zones, i.e., northern extra-tropical regions (NH) (50N–20N), Tropical regions (TR) (20N–20S) and southern extra-tropical regions (SH) (20S–50S). The following features are outstanding. The negative speed bias of 1999 is apparently increased compared with that of 1997, exceptionally in both of Extra Hemisphere, that of 1999 is about 2 m/s larger than that of 1997. RMS Vector Difference in 1999 has the same tendency as that of speed bias as that of 1999 is about 2 m/s larger than that of 1997 in all regions. Thus the accuracy of HCMWs in 1999 significantly decreases compared with that of 1997, especially in the summer.

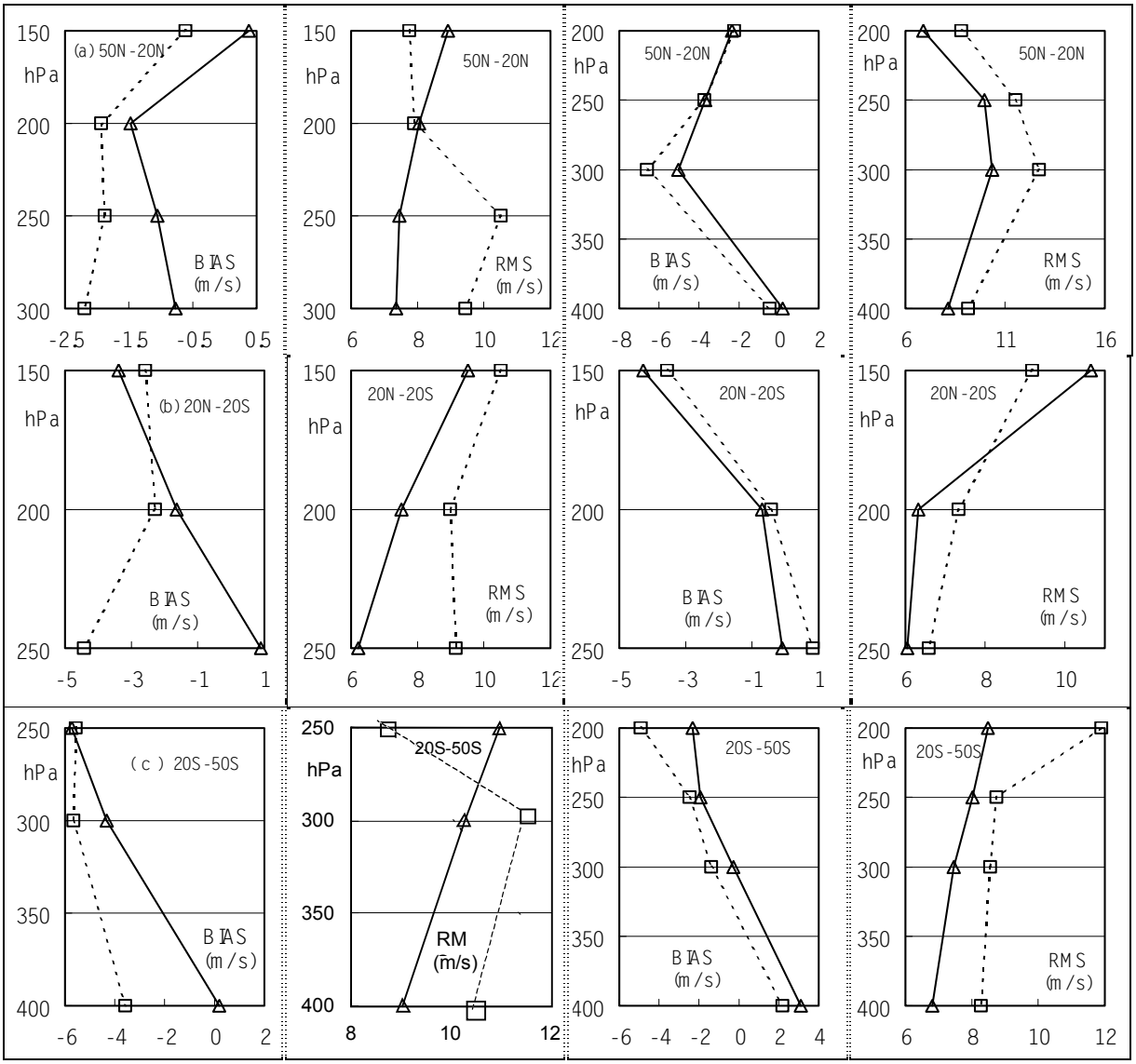

Wind Speed Bias RMS Vector Difference Wind Speed Bias RMS Vector Difference
HCMWs (Summer) Δ:1997 □:1999 HCMWs (Winter) Δ:1997/1998 □:1998/1999

Figure 3. The vertical distribution of wind speed bias and RMS vector difference in (a) NH (50N-20N), (b) TR (20N-20S), (c) SH (20S-20N) for HCMWs.

5. Comparison of WVMWs in 1997 with those in 1999

As shown in the session 3.3 and 3.4, accuracy of HWVMWs has a increasing tendency since August 1998 when the total number of WVMWs was increased. In contrast, the accuracy of MWVMWs has a decreasing tendency since August 1998. Further investigation is carried out through the comparison of WVMWs in 1997 with those in 1999 in the same way shown in the previous session.

Fig. 4 shows the distribution of total number of WVMWs per station used for comparison of WVMWs in the summer of 1999 and in the winter of 1998/1999 after the introduction of increasing the number of derived WVMWs. As expected, the total number of derived WVMWs in northern extra-tropical regions increases extremely in the summer. In contrast, that in southern extra-tropical regions and in tropical regions increases extremely in the winter.

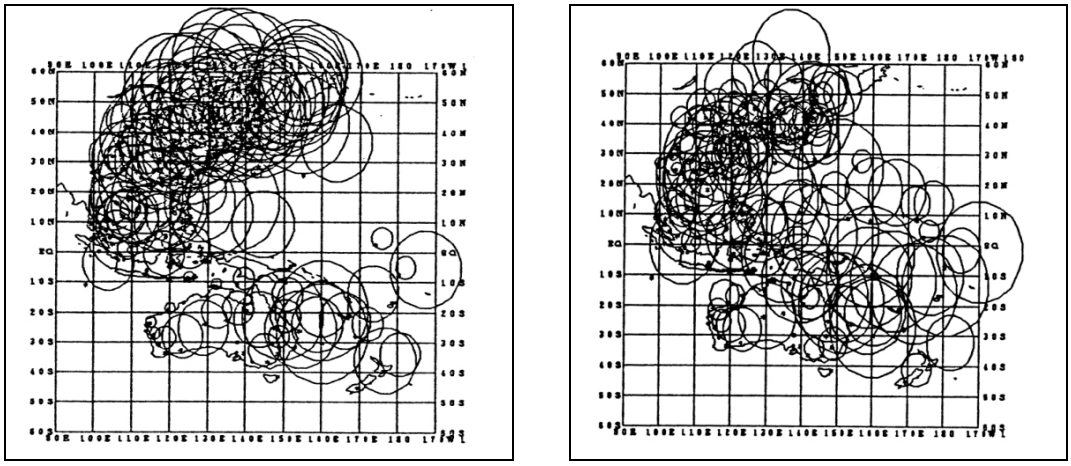

Figure 4. The distribution of total number of WVMWs per station used for the comparison.
Left; WVMWs, July and August 1999 right; WVMWs, December 1998 and January 1999.

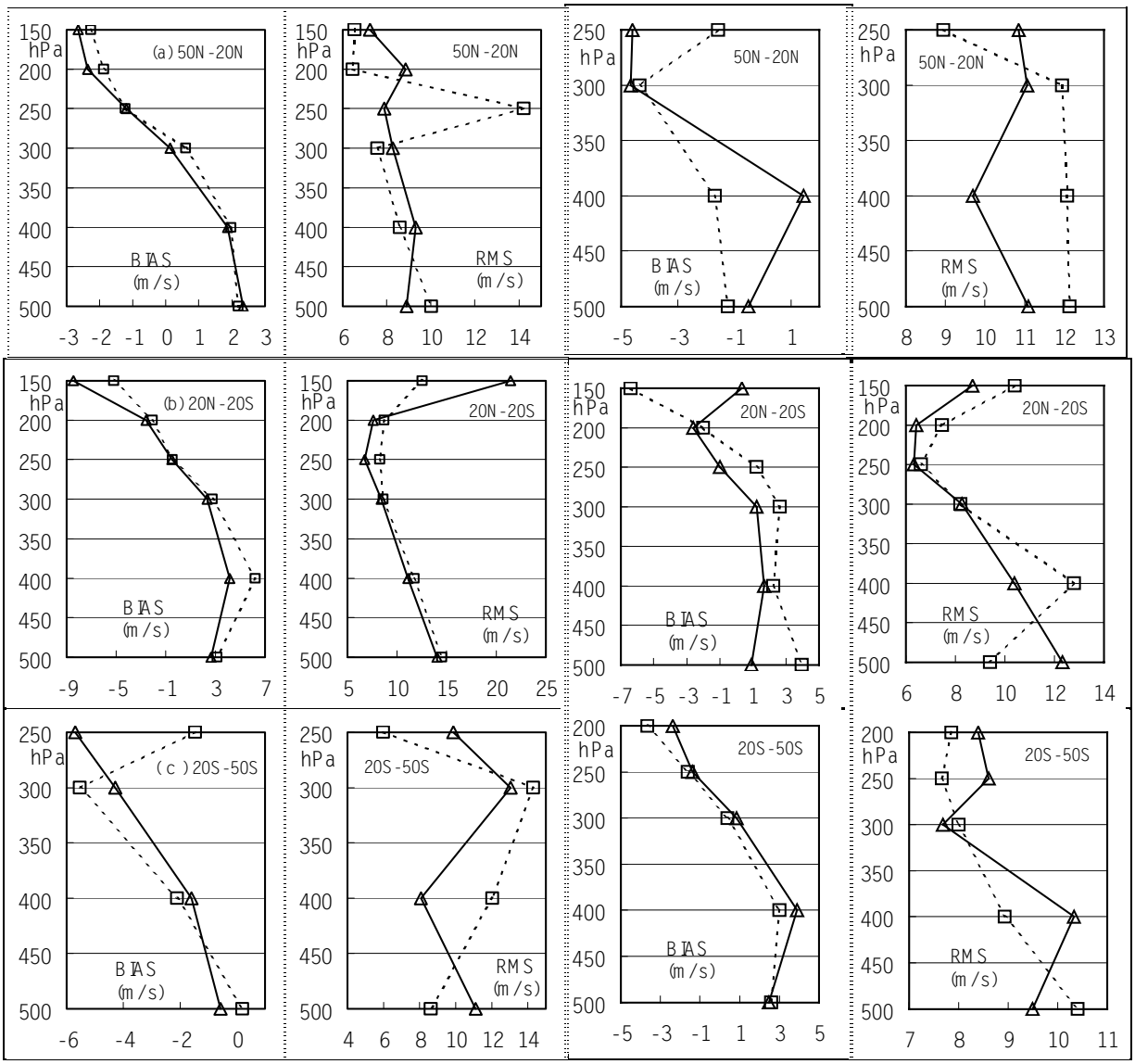

Wind Speed Bias RMS Vector Difference Wind Speed Bias RMS Vector Difference
WVMWs (Summer) Δ:1997 □:1999 WVMWs(Winter) Δ:1997/1998 □:1998/1999
Figure 5. The same as Figure 3 for WVMWs

Fig. 5 shows the comparison of the vertical distribution of wind speed bias and RMS vector difference in the three latitude zones. The following features are outstanding. In the summer, there is no significant difference between 1997 and 1999 in wind speed bias. RMS vector difference at 250 hPa of 1999 in NH region is greatly larger than that of 1997. In addition, RMS vector difference in SH region in 1999 is about 2 m/s larger than that in 1997. In the winter, negative speed bias of 1998/1999 in NH region is larger than that of 1997/1998. In contrast, negative speed bias of 1998/1999 in TR region is smaller than that of 1997/1998. RMS vector difference of 1998/1999 is larger than that of 1997/1998 between 300 hPa and 500 hPa. Thus RMS vector difference of 1998/1999 has a increasing tendency compared with that of 1997/1998 in the winter of both NH and SH region.

6. Future plan

Although MTSAT's launch did not succeed due to trouble of the launch vehicle on November 15, we are planning to launch MTSAT-1R as a replacement of MTSAT in the end of FY 2002 and a follow-on MTSAT-2 in FY 2004. The operation of MTSAT-1R will begin in FY 2003. Functions of the meteorological mission of MTSAT-1R will be almost the same as the planed MTSAT.

MSC will partly change the way of producing satellite winds when MTSAT-1R is operated in FY 2003, shortening the interval between images for wind tracking from 30-minute to 15-minute. It is expected that this change will bring an increase of the number of infrared winds by about 20 % more than the present product (Tokuno 1997). Taking an advantage of images at 15-minute intervals, MSC will also produce HRLCMWs four times a day for all observed typhoons to support typhoon analysis at the Forecast Division of JMA headquarter. In addition, the information on the HRLCMWs will be transmitted on LRIT to national Met Services that may be affected by the typhoons.

MSC currently has medium-term targets of wind products: increase in the number of derived wind vectors, provision of high-density winds, improvement of the height assignment method, full automated quality control, adding quality information to each vectors, dissemination of products in the BUFR format and adaptation to data assimilation with 4D-Variation method in the numerical prediction model.

In order to achieve these goals, it is necessary to improve the efficiency of software development and computation performance. MSC has begun shifting the facility to produce satellite wind from mainframe computers to work stations. Hereafter, we will gradually develop and replace the algorithms and finally complete then in 2004, when 4D-Var methods is to be introduced into JMA numerical model.

MSC is planning to begin the operation of deriving high-density winds around up to five typhoons at the same time using 15-minute interval visible images by early 2000. High-density winds are presently derived for only one typhoon at a time (Fig. 6).

7. Conclusion

Forgoing analysis leads to the following conclusion. The accuracy of HCMWs in 1999 significantly decreases compared with that of 1997 in the last three years. The accuracy of WVMWs after the introduction of increasing the number of derived WVMWs also decreases in the winter of both NH and SH region although the accuracy of WVMWs does not decrease in other seasons and in TR region The cause is not yet cleared. Therefore the effort is inquired to clear up the cause.

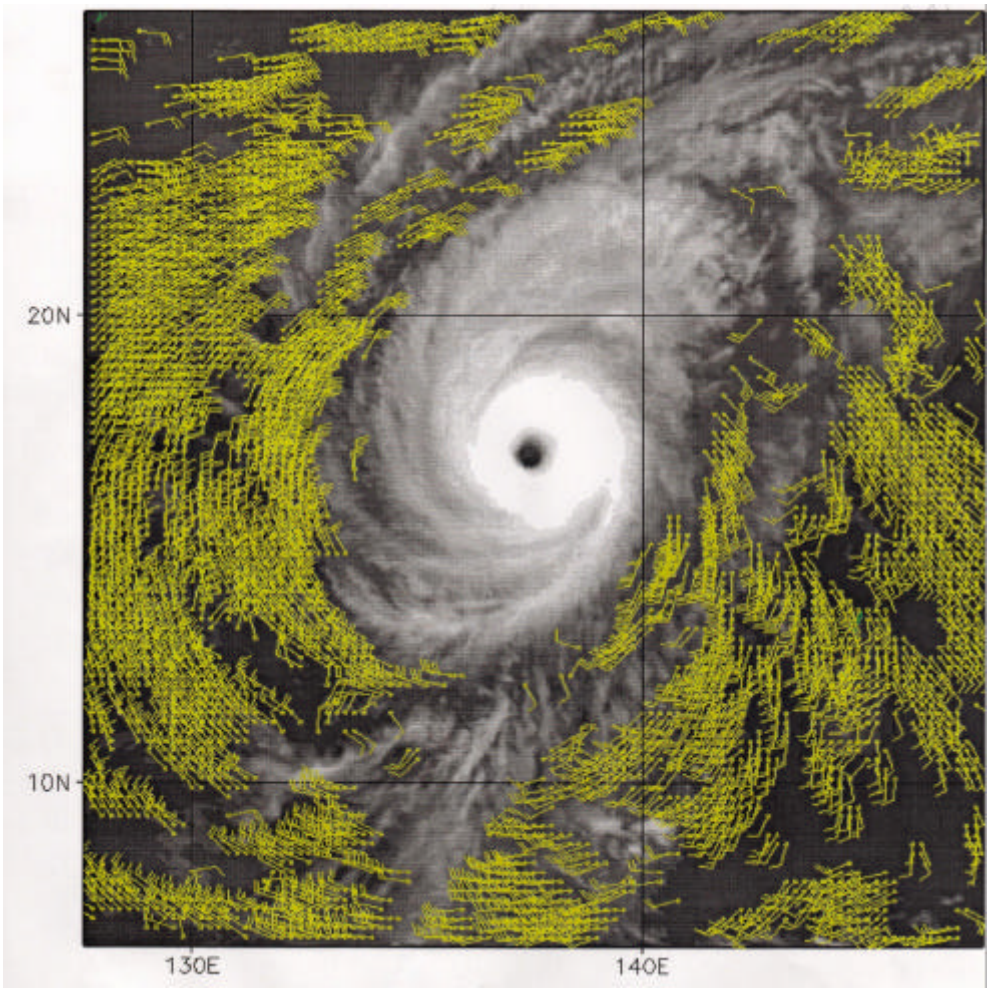

Figure 6. Illustration of the high density visible CMWs in typhoon vicinity at 04 UTC 20 Apr. 1997.

REFERENCES

Takata, S., 1993: Current status of GMS wind and operational low-level wind derivation in a typhoon vicinity from short-time interval images. *Proceedings of Second International Winds Workshop*, Tokyo, 17 – 15 Dec. 1993. EUMP14, 29-36.

Tokuno, M, 1996: Operational system for extracting cloud motion and water vapor motion winds from GMS-5 image data *Proceedings of Third International Winds Workshop*, ASCONA, SWITZERLAND, 10 –12 June 1996. EUMP18, 21-30.

Tokuno, M, 1997: Development of new products for MTSAT. *Proceedings of 1997 Meteorological satellite data users' conference*, Brussels, Belgium 29th September – 3rd October 1997.

STATUS AND DEVELOPMENT OF OPERATIONAL GOES WIND PRODUCTS

Jaime Daniels[1], Christopher Velden[2], Wayne Bresky[3] and Antonio Irving[4]

[1)] *NOAA/NESDIS*
Office of Research and Applications
Camp Springs, Maryland 20746

[2)] Cooperative Institute for Meteorological Satellite Studies (CIMSS)
University of Wisconsin, Madison, Wisconsin

[3)] Raytheon Information Technology and Scientific Services
Lanham, Maryland 20706

[4)] NOAA/NESDIS, Office of Satellite Data Processing and Distribution
Camp Springs, Maryland 20746

ABSTRACT

NOAA/NESDIS and the Cooperative Institute for Meteorological Satellite Studies (CIMSS) continue to be very active in improving the quality of Atmospheric Motion Vectors (AMVs) derived from the GOES-I/M series of satellites. The NOAA/NESDIS winds processing system continues to be incrementally upgraded with updated wind algorithms, new wind products, and new processing strategies. High quality visible cloud-drift (CD) winds are now being generated from GOES-8 and GOES-10 on an operational basis for the Northern and Southern Hemispheres. GOES sounder water vapor wind products have also been added to the operational wind production suite. The operational NESDIS wind products are now being distributed in the unified BUFR template. This development opens up opportunities for improved use of the wind products by the major numerical weather prediction centers. New operational processing strategies take advantage of the higher frequency interval imagery available to derive the wind products. These new strategies have resulted in improved wind products which, in turn, has resulted in improvements in their utility in numerous applications. These geostationary wind products serve as critical input to a wide range of applications that include assimilation into regional and global prediction systems, oceanic analyses, and tropical storm analyses.

1. Introduction

NOAA/NESDIS and the Cooperative Institute for Meteorological Satellite Studies (CIMSS) continue to be very active in improving the quality of Atmospheric Motion Vectors (AMVs) derived from the GOES-I/M series of satellites. The NOAA/NESDIS winds processing system continues to be incrementally upgraded with updated wind algorithms, new wind products, and new processing strategies. High quality visible cloud-drift (CD) winds are now being generated from GOES-8 and GOES-10 on an operational basis for the Northern and Southern Hemispheres. GOES sounder water vapor wind products have also been added to the operational wind production suite. The operational NESDIS wind products are now being distributed in the unified BUFR template. This development opens up opportunities for improved use of the wind products by the major numerical weather prediction centers. New operational processing strategies take advantage of the higher frequency interval imagery available to derive the wind products. These new strategies have resulted in improved wind products which, in turn, has resulted in improvements in their utility in numerous applications. These geostationary wind products serve as critical input to a wide range of applications that include assimilation into regional and global prediction systems, oceanic analyses, and tropical storm analyses.

2. Overview of the NOAA/NESDIS wind product system

An overview of the operational NOAA/NESDIS winds processing system is shown in Figure 1. The major components of the system include automated image registration quality control, target selection, wind target height assignment, target tracking, and automated quality control of derived winds.

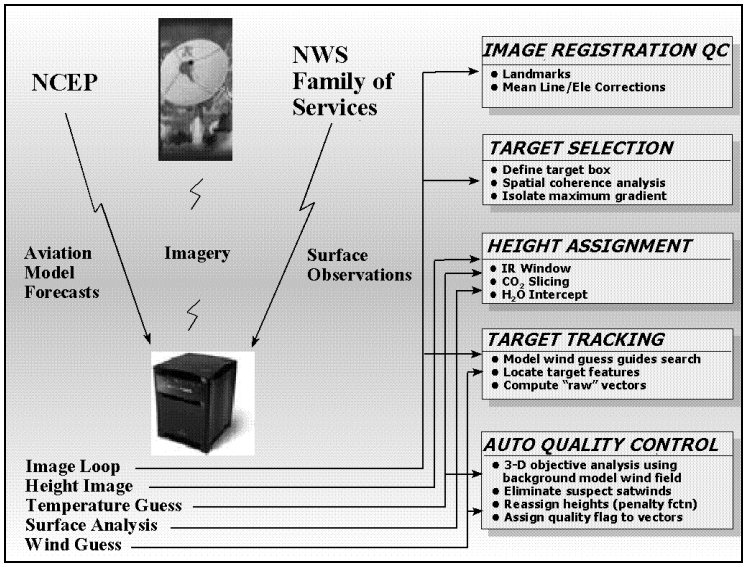

Figure 1. Overview of NOAA/NESDIS Winds Processing System

GOES imagery is acquired soon after ingest to build loops of imagery at the desired time intervals. Aviation model forecast data is made available at 3 hour forecast intervals and at 1^o x 1^o resolution by the National Centers for Environmental Prediction (NCEP)/ Environmental Modeling Center (EMC). Surface observations are made available every hour by the National Weather Service (NWS). The first image in the loop is currently used for the target selection and height assignments. Subsequent imagery is used during the tracking phase where a Euclidean distance pattern-matching technique is used. Automated quality control of the satellite winds is then performed. This step involves a three-dimensional objective analysis (Hayden and Purser, 1995) of the wind field using background information from the NCEP/EMC global aviation numerical weather prediction model.

3. Current and new operational wind products and new processing strategies

The current operational wind products being generated at NOAA/NESDIS are shown in Table 1. The frequency at which each product is produced, together with the GOES image sector used, and image interval is presented in this table.

Table 1. NOAA/NESDIS Operational Wind Products

Wind Product	Frequency (Hours)	Image Sector(s)	Image Interval (minutes)
IR Cloud-drift	3	Extended NH; SH	30
Water Vapor	3	Extended NH; SH	30
Vis Cloud-drift	3	RISOP	7.5
	3	PACU/CONUS	15
	3	Extended NH; SH	30
Sounder WV (7.4um)	3,6	CONUS/Tropical	60
Sounder WV (7.0um)	3,6	CONUS/Tropical	60

The newest operational wind products include the visible cloud drift and GOES sounder water vapor motion winds. The visible cloud-drift wind products are generated routinely for GOES-8 and GOES-10 every three hours during daylight hours over the Northern and Southern Hemisphere. The GOES sounder water vapor winds are generated every three hours over the Continental United States (CONUS) and every six hours over the adjacent oceanic regions. An example of the GOES-10 visible wind product at 23Z on February 14, 2000 is shown in Figure 2 where the low level flow around a cyclonic weather system approaching the western United States is well depicted. Figure 3 illustrates the GOES sounder water vapor winds and the sounder coverage offered over CONUS and nearby oceans from both GOES-8 and GOES-10 at 12Z on February 14, 2000. As discussed in Velden et. al., 1997, the 7.0um and 7.4um sounder water vapor channels can be used to track water vapor features radiating from lower layers of the atmosphere. While there may be some redundancy between the imager water vapor winds and sounder water vapor winds in terms of vertical coverage, additional information is gained from the sounder channels, especially in the cloud-free regions.

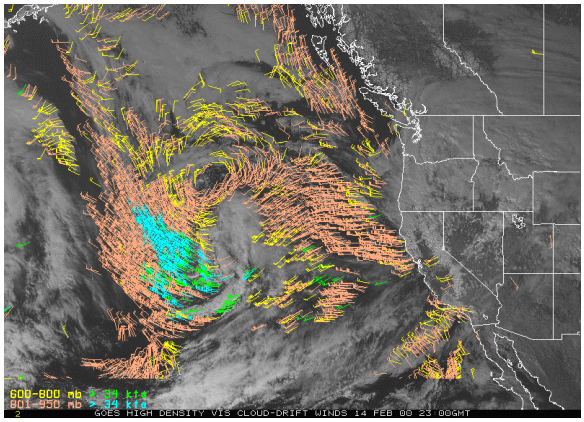

Figure 2. GOES-10 low-level visible cloud-drift winds at 23Z on February 14, 2000.

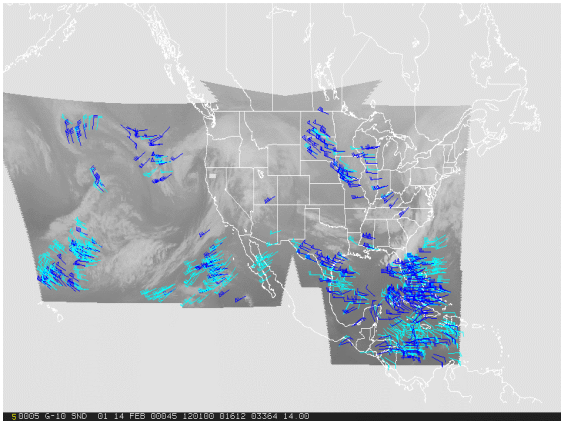

Figure 3. GOES-8 and -10 sounder 7.0 um and 7.4 um water vapor winds at 12Z on February 14 2000.

a) Use of Higher Frequency Interval Imagery

New processing strategies have been developed for operational wind processing to take advantage of the higher frequency interval imagery offered by the current GOES scanning schedules. The capability to routinely use higher frequency interval imagery in the operational derivation of visible CD satellite wind vectors has recently been added to the wind production suite at NOAA/NESDIS. The GOES 15-minute CONUS and PACUS image sectors are now used routinely for the generation of low level visible cloud-drift wind vectors for GOES-8 and GOES-10, respectively. In addition, the more frequent 7.5-minute imagery rapid scan imagery is automatically utilized when the GOES imager is placed in rapid scan mode. The Northern Hemispheric image sectors, which are scanned every 30 minutes, are used to generate wind products outside the CONUS, PACUS, and RISOP domains in order to achieve full Northern Hemispheric coverage. The Southern Hemispheric image sectors, which are scanned every 30 minutes, are used to achieve coverage in the Southern Hemisphere. These image sectors are illustrated in Figure 4.

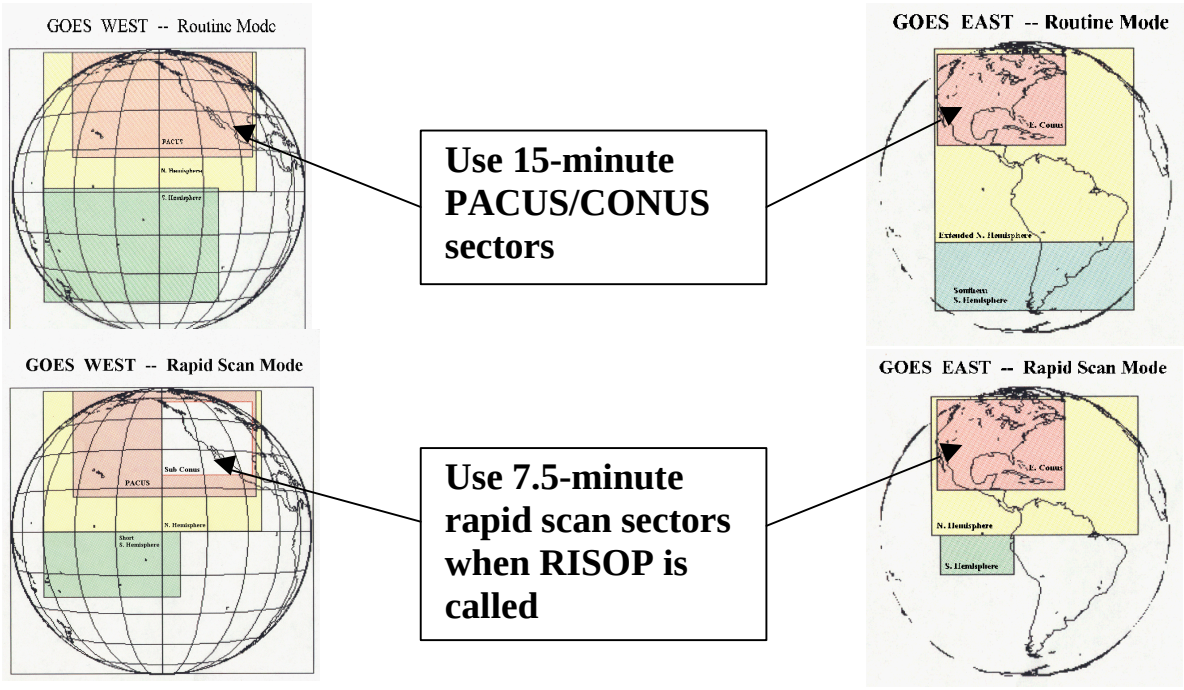

Figure 4. GOES East and GOES West Image Sectors. Use of CONUS, PACUS, and RISOP sectors offer benefits to wind processing.

The importance of image frequency in target selection for tracking is well recognized. Successful tracking of features such as cumulus over land, whose lifetimes can be considerably less than 30 minutes, demands the use of visible imagery whose time interval is in the 5-15 minute range. Velden et al, (2000) investigated the impact of using GOES rapid and super rapid scan imagery on the coverage and quality of various derived wind products. The authors presented validation statistics to help identify the optimal image frequency for various wind product types. An example showing the impact of using higher frequency interval imagery on the GOES-10 visible wind product is shown in Figure 5. This figure shows GOES-10 low level cloud-drift winds around Hurricanes Dora and Eugene, where 15-minute PACUS and 30-minute Northern Hemisphere imagery were used. Note the dramatic increase in vector coverage and the more uniform flow associated with the 15-minute wind field. As noted above, the operational NESDIS winds production cycle includes the processing of both image sectors to produce a combined visible wind product. A similar processing strategy will be implemented in the near future for the IR cloud-drift wind products.

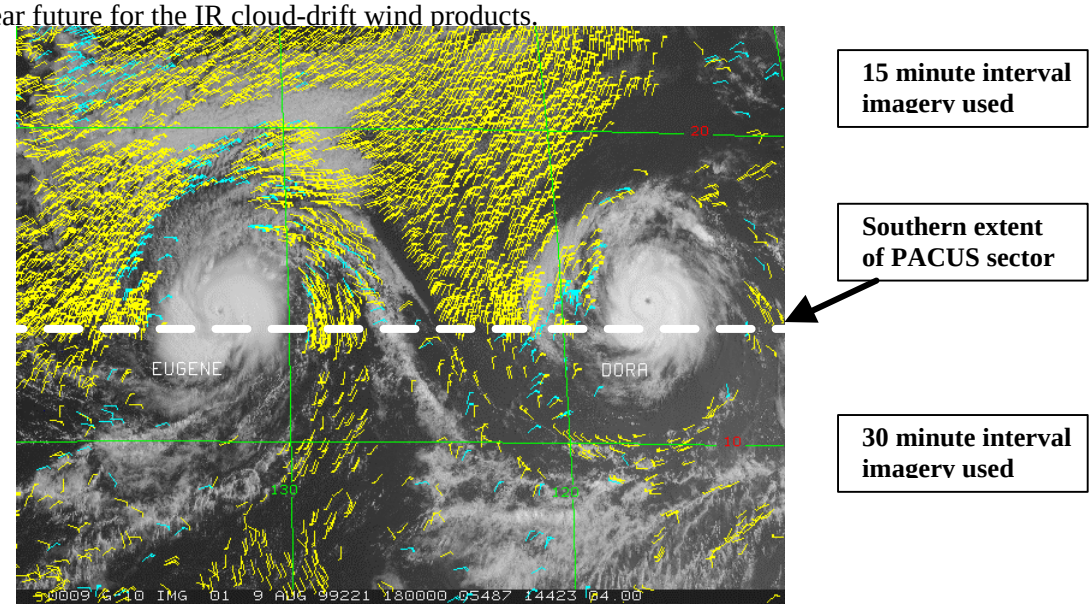

Figure5. GOES-10 low level visible cloud-drift winds around hurricanes Dora and Eugene using 15-minute and 30-minute interval visible imagery.

b) Low Level Cloud Tracer Height Assignments

Low-level cloud tracer height assignments are typically based on IR window methods which use a coincident model temperature profile to assign the tracer height at cloud top. Numerous studies, however, have indicated that low level cumuliform cloud motion is best estimated by assigning the derived wind vector at cloud base (Hasler et al, 1979). Since cloud base temperature cannot be measured directly from satellite measurements, a reasonable estimation technique is needed. Such a technique has been developed at the Australian Bureau of Meteorology. The technique involves constructing a histogram of IR pixels in the target scene, applying a Hermite polynomial expansion to the histogram, and taking the second derivative of the polynomial expansion to identify/estimate where the cloud base is. This technique has been implemented within the NESDIS tracer height assignment algorithm. Results indicate that this approach lowers the vector height assignments some 40-50mb. Verification statistics, using rawinsondes as ground truth, show a reduction in vector rms error of nearly 0.5 m/s.

c) Product Distribution

All of the operational NESDIS wind products shown in Table 1 are now encoded into the unified BUFR format and available on a NESDIS server. All of the products, with the exception of the sounder water vapor winds, continue to be encoded into the SATOB format and distributed over the GTS. The BUFR wind product datasets will be disseminated out over the GTS once NESDIS and the National Weather Service (NWS) work out the communication interfaces associated with the new NWS computer system.

4. Quality of GOES satellite wind products

The traditional means of assessing the accuracy of satellite derived winds at NOAA/NESDIS is to collocate satellite derived winds with rawinsondes. Time series of daily verification statistics for visible and IR CD and WV winds for GOES-8 is shown in Figure 6. Figures 7 shows the daily verification statistics for GOES-8 sounder band 10 (7.4um) and band 11 (7.0um) water vapor winds for the same period. It should be noted that the visible CD winds include only low level winds below 600mb. Updated time series of these wind verification statistics can be found online on the NESDIS web page: http://orbit-net.nesdis.noaa.gov/goes/winds/html/tseries.html

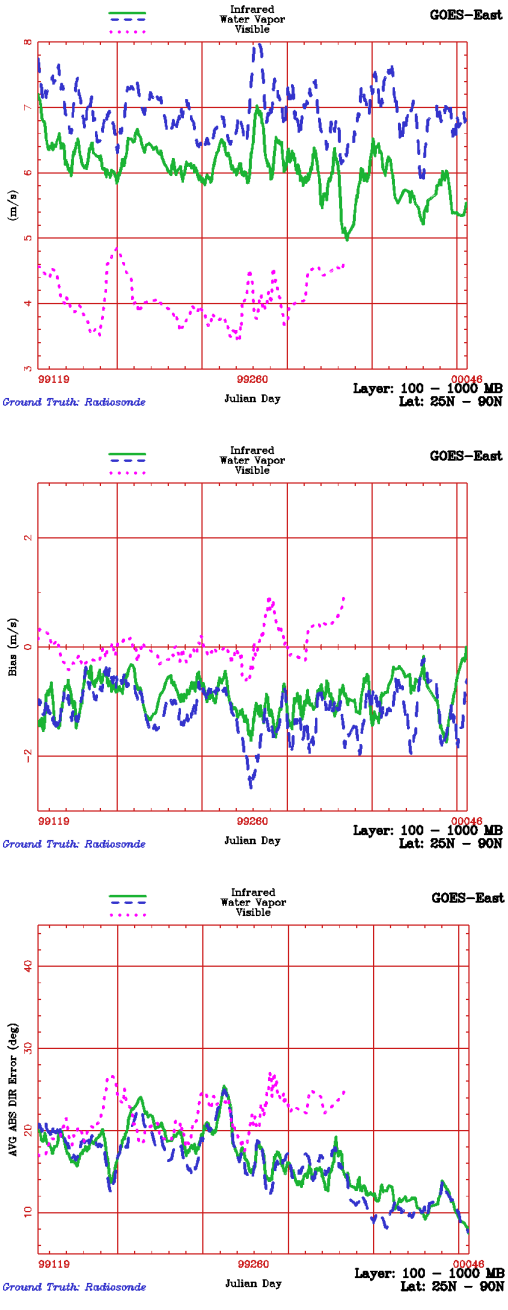

Figure 6. Mean vector difference (top), bias (middle), and directional difference (bottom) for IR,WV,VIS winds.

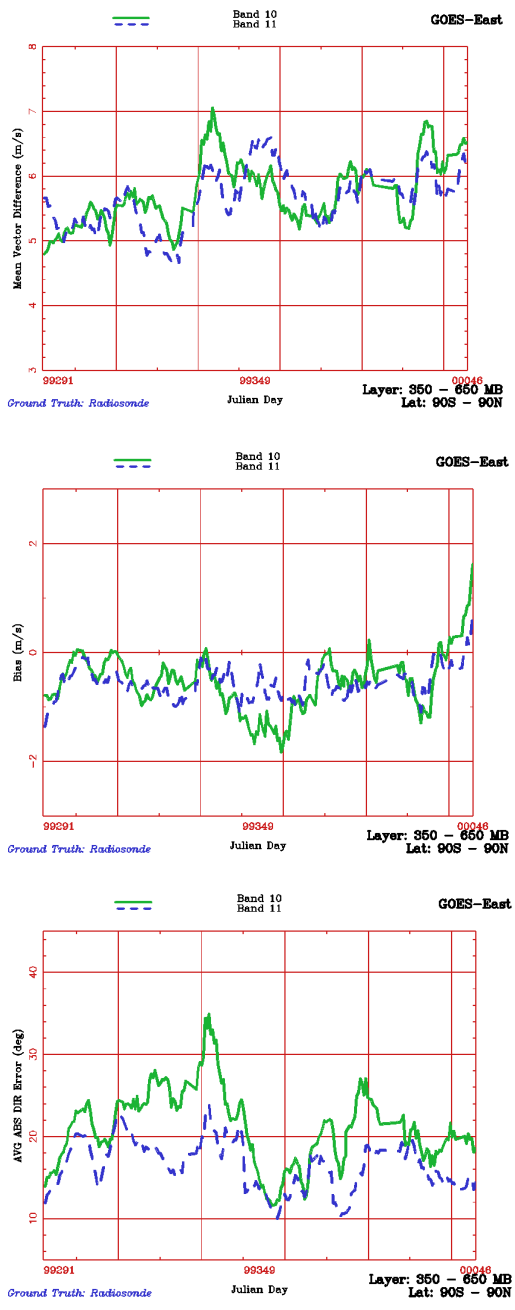

Figure 7. Mean vector difference (top), bias (middle), and directional difference (bottom) for sounder WV winds

Addressing the Slow Bias for GOES Water Vapor Winds at Middle (400-700mb) Levels

The above time series show that the water vapor winds exhibit a considerable slow bias. In this section we address possible causes for this bias and present a proposed solution.

The mid-level slow bias evident in the water vapor winds has been observed for some time by the major numerical weather prediction centers. Given their observed quality, most if not all, of the major NWP centers exclude the use of these wind products in their data assimilation schemes. Water vapor

winds at these middle levels of the atmosphere are predominantly tagged as "clear-air", indicating that moisture features having some finite depth are being tracked. The "cloud-top" WV winds fall predominantly in the high level category. These winds are treated much like the IR (10.7um) cloud-drift winds in that the cloud tracers are provided the benefit of using the multi-spectral water vapor intercept height assignment technique and are afforded the opportunity of a speed bias correction providing they meet certain criteria.

Tables 2 and 3 show our statistics at high (100-400mb) and mid-levels (400-700mb) levels derived from collocated WV winds (cloud-top and clear-air) and radiosonde winds over approximately a two year period (1998-2000). While a slow bias exists for both layers, it is much more pronounced in the mid-level layer. In addition to the usual set of statistics that get generated (mean vector difference, speed bias, etc) we computed the mean magnitude of the u-component and v-component for the satellite WV winds and the collocated radiosonde winds. We took the absolute value of each individual component when constructing the mean. We then computed the percent difference between the satellite WV winds and radiosonde for each component. At high levels, both satellite wind components are approximately 8% too slow relative to the radiosonde wind. At mid levels, however, the statistics indicate that the WV wind v-component is more than twice as slow as the u-component relative to the radiosonde wind. To investigate whether there was a dependence on direction we further stratified our statistics by radiosonde wind direction and computed these statistics for 30 degree bins (345deg-15deg; 15-45 deg, etc). These results are shown in Figure 8.

Table 2. Collocation statistics for High Level (100-400mb) GOES-8 Water Vapor Winds for the period 1998-2000. Radiosondes serve as ground truth.

Statistic	*SAT*		*GUESS*	*RAOB*
RMS Difference (m/s)	7.60		7.19	
Mean Vector Difference (m/s)	6.36		5.94	
Standard Deviation (m/s)	4.17		4.04	
Speed Bias (m/s)	**-1.03**		-1.73	
Mean | u-component | (m/s)	**17.81**	(-8.0 %)		**19.24**
Mean | v-component | (m/s)	**9.51**	(-8.6 %)		**10.33**
|Directional Difference|(deg)	13.47		13.87	
Speed (m/s)	22.31		21.62	22.91
Sample Size	282317		282317	

Table 3. Collocation statistics for mid-level (400-700mb) GOES-8 Water Vapor Winds for the period 1998-2000. Radiosondes serve as ground truth.

Statistic	*SAT*		*GUESS*	*RAOB*
RMS Difference (m/s)	8.49		7.14	
Mean Vector Difference (m/s)	7.07		5.67	
Standard Deviation (m/s)	4.70		4.33	
Speed Bias (m/s)	**-2.50**		-1.41	
Mean | u-component | (m/s)	**14.32**	(-11.4 %)		**15.96**
Mean | v-component | (m/s)	**7.19**	(-25.2 %)		**9.00**
|Directional Difference|(deg)	18.02		18.24	
Speed (m/s)	17.21		18.29	19.70
Sample Size	37755		37755	

The v-component line shows that the satellite WV wind v-component is slower than the corresponding radiosonde v-component in all bins except for two. The wind directions for these two bins are 90 deg (easterly) and 270 deg (westerly). Similarly, the u-component line shows that the satellite WV wind u-component is slower than the corresponding radiosonde u-component in all bins except for two. Not surprising, they are at 0 degrees (northerly) and 180 degrees (southerly). The behavior of the two curves at these angles is indicative of the problem of estimating small displacements with discrete

observations. Clearly, it will be extremely difficult to determine the v-component of a tracer moving in a nearly easterly or westerly direction. The horizontal resolution of the imagery used becomes increasingly important for being able to resolve such component motion where slower speeds are prevalent. What is bothersome in our statistics in Table 3 is the fact that the mid-level satellite WV wind v-component difference is nearly twice that of the u-component difference.

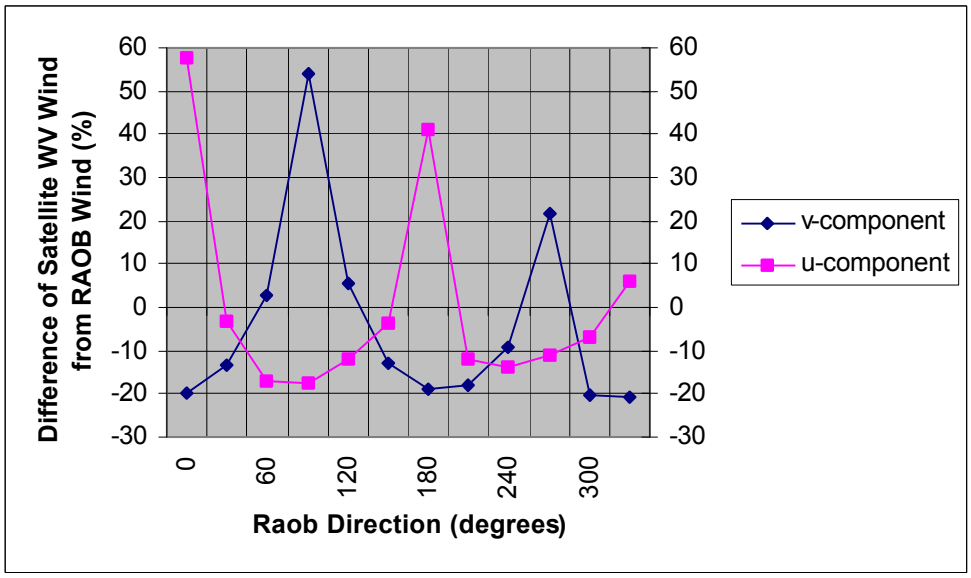

Figure 8. Percent difference between GOES-E WV wind (mid and high levels) u and v-components and corresponding u and v-components of RAOB wind as a function of RAOB wind direction.

We believe that the lower north/south resolution of the GOES water vapor imagery is likely to be a contributing factor for the mid-level slow bias. The resolution of the GOES water vapor imagery in the north-south (N/S) direction is 8km versus 2.3km in the east-west (E/W) direction where the data is over-sampled. This implies that small N/S displacements are not being resolved as well as E/W displacements in the water vapor imagery. At middle levels, where wind speeds are slower, it is logical to assume that the resolution of the data becomes even more important.

In order to bring out the impact of wind speed on the behavior we are observing in the u- and v-components, we plotted the component absolute difference (satellite – radiosonde) versus the component magnitude. This is shown in Figure 9. From this figure we conclude the following:

1) The smaller slope of the v-component line shows that the v-component is less sensitive to increases in speed. This is most likely a result of the lower N/S resolution of the WV imagery.
2) The coarser N/S resolution of the WV imagery, coupled with the slower overall magnitude of the v-component, contributes to larger relative differences.
3) Our acceleration checks tend to remove the largest “resolution” errors, while leaving the smaller (slower) errors. As such, the remaining error is biased (ie.,non-random) in the slow direction.

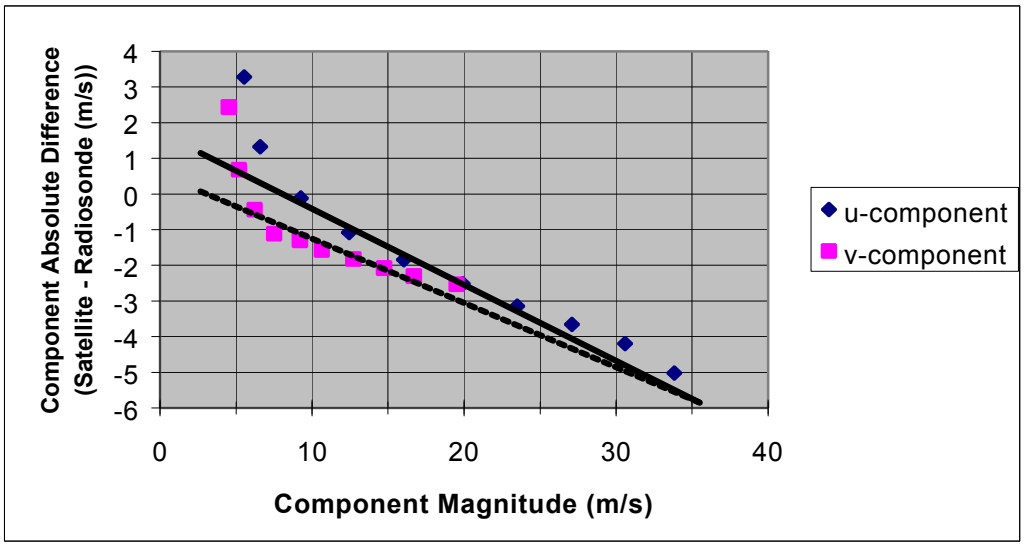

Figure 9. Component absolute differences (GOES-E WV satwinds – radiosonde) versus component magnitude.

So, what have we concluded from this exercise and where do we go from here? The coarser resolution of the water vapor imagery is a contributing factor to the differences observed in the water vapor wind u and v-component statistics. As pointed out by Merrill (1989), one must consider the temporal resolution of the imagery being used in relation to its spatial resolution. Given this, we must consider whether 30-minute temporal resolution is optimal for generating GOES water vapor winds. Using 60-minute interval imagery to derive GOES water vapor winds may be a possible answer to minimizing the resolution effects and improving the overall quality of these winds. In fact, doing this may actually make more physical sense given the nature of this data and the scale of motion which can adequately be resolved with it. We have in fact tried this and the results are quite striking. Figures 10 and 11 illustrate the raw (pre-autoeditor) water vapor winds using 30-minute and 60-minute interval data, respectively. Using the 60-minute interval imagery has resulted in a more coherent wind field. At the same time, the vector coverage at middle levels has increased by over 50% in this one case. When comparing these raw water vapor winds (30-minute and 60-minute) against radiosondes, the mean vector difference improved by 1.5-2.0 m/s. Absolute directional differences improved by over 5 degrees overall. Given these findings, we may be on the right track.

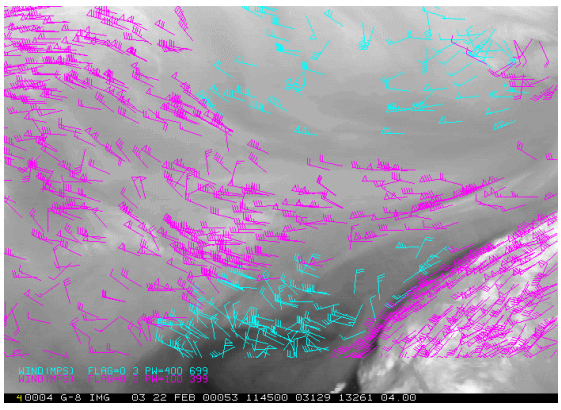

Figure 10. Raw WV winds derived from 30-min imagery

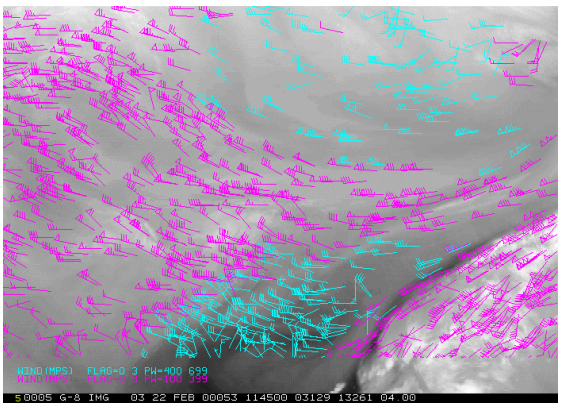

Figure 11. Raw WV winds derived from 60-minute imagery

Of course, other factors can also contribute to the observed slow bias. One is the "image aperture problem" (Jaehne, 1991) where uncertainties in tracking features along "edges" of an image are prevalent; flow can only be estimated perpendicular to an edge. This is a known problem and can be observed routinely in the water imagery where water vapor structures tend to have their strongest

gradient features perpendicular to the wind direction. The coarser resolution of the WV imagery in the N/S direction will only enhance this problem. Typical cases involve the tracking of an elongated cloud or WV feature in the vicinity of jet streams. Another contributing factor is possible source contributing to the observed slow bias in the WV winds involves mis-assigning the height to tracers. Often times, lower level features are tracked and assigned too high up in the atmosphere. Tracking features in transverse bands in high shear environments can also lead to large slow biases.

5. Summary

NOAA/NESDIS, together with its CIMSS partner, continue to improve the wind product suite at NOAA/NESDIS. New wind products now operationally supported include the high density visible cloud-drift winds from the GOES imager and water vapor motion winds derived from the GOES sounder 7.0um and 7.4um moisture channels. All of the NOAA/NESDIS wind products are now being encoded into the unified BUFR template. This opens up opportunities for improved use of these products by the major NWP centers.

Recent emphasis has been placed on better utilization of higher frequency interval imagery for the derivation of satellite winds by the satellite wind community. In response to this, NOAA/NESDIS has enhanced its processing strategies to utilize available 15-minute and 7.5-minute for the derivation of visible cloud-drift winds. These new processing strategies will be applied to the IR cloud-drift winds in the very near future. Existing GOES image scanning schedules need to re-examined to determine if more optimal scanning strategies can be employed which will benefit the wind products for use in mesoscale models and by our NWS severe storm forecasters.

Statistics regarding the quality of our wind products have been presented. The quality of the products continues to look good. The slow bias observed in the imager WV winds, particularly at middle levels (400-700mb) of the atmosphere has been addressed. The coarser North/South resolution of the GOES water vapor imagery is being considered as a significant contributor to this slow bias. One potential solution involves the use of 60-minute interval imagery; preliminary results are promising. Other factors contributing to the slow bias problem include the image aperature problem, tracer height assignment, and vertical shear. More work is planned to better characterize this problem.

REFERENCES

Hasler, A.F., W.C. Skillman, and W.E. Shenk, 1979: In situ aircraft verification of the quality of satellite cloud winds over oceanic regions. *J. App. Met*., **18**, 1481-1489.

Jaehne, B., 1991: Digital Image Processing: Concepts, algorithms, and scientific applications. Springer, 1991. 383p.

Hayden, 1993: Recent research in the automated quality control of cloud motion vectors at CIMSS/NESDIS. *Proc. Second Intl. Winds Workshop*, Tokyo, Japan, EUMETSAT, 219-226.

Hayden, C.M. and R.J. Purser, 1995: Recursive filter objective analysis of meteorological fields: Applications to NESDIS operational processing. *J. Appl. Meteor*., **34**,3-15.

Velden, C.S., C.Hayden, S.Nieman, W.P. Menzel, S. Wanzong, and J. Goerss, 1997: Upper-tropospheric winds derived from geostationary satellite water vapor observations. *Bull. Amer. Meteor. Soc*., **78**, 173-195.

Velden, C.S., D. Stettner, and J. Daniels, 1999: Wind vector fields derive from GOES rapid scan imagery. *Preprints 10th Conference on Satellite Meteorology and Oceanography*, Long Beach, CA

OPERATIONAL METEOSAT WIND PRODUCTS TOWARDS MSG

Mikael Rattenborg

EUMETSAT, Am Kavalleriesand 31, D-64295 Darmstadt, Germany

ABSTRACT

The Operational Meteosat Meteorological Products are produced by the MPEF, a facility in the Meteosat Ground Segment operated by EUMETSAT. The most important MPEF products are the wind products, derived from all three Meteosat channels.

The current operational wind products are Cloud Motion Winds, derived from 5 km resolution imagery in all three Meteosat channels, High Resolution Visible winds (HRV), derived from full (2.5km) resolution visible images and Clear-Sky Water Vapour Winds, derived from WV images in cloud-free areas. The current status and quality of these wind products is presented.

The planned development of the products from the current Meteosat satellite is driven by the meteorological community requirements for higher spatial and temporal coverage and for consistent reliability indicators. It is planned to satisfy these needs by a number of developments: more frequent wind distribution, BUFR distribution of winds with quality information, increased HRV coverage through improved tracer selection techniques, high resolution winds from the Water Vapour channel and associated WV radiance information. These developments and their relationship to the development towards the Meteosat Second Generation (MSG) products are described and discussed in detail.

1. Introduction

The EUMETSAT Meteosat Transition Programme (MTP) ground segment controls the Meteosat satellites and provides ground processing for all Meteosat services. The MTP ground segment includes a Mission Control Centre (MCC) located in the EUMETSAT headquarters building in Darmstadt, Germany.

The MTP products are produced in the Meteorological Products Extraction Facility (MPEF), which is a facility in the MTP Mission Control Centre. The core products are the wind products, extracted from all three Meteosat channels in near-real time, and distributed on the GTS.

The operational Meteosat satellites are Meteosat-7 at 0°E and (in support of the Indian Ocean Service) Meteosat-5 at 63°E. The Meteosat Second Generation Ground Segment is under development, and the MSG MPEF will be the follow-on facility for extraction of meteorological products from the MSG satellites.

2. Status and quality of Meteosat products

The current range of operational products consists of:

- Cloud Motion winds (CMW)
    - Combined wind product from Infrared, Water Vapor and low resolution Visible images
    - Distributed on GTS in SATOB at 00Z, 06Z, 12Z, 18Z
- Expanded Low Resolution winds (ELW)
    - Multi-channel cloud track wind product from Infrared, Water Vapor and low resolution Visible images
    - Distributed on GTS in standard BUFR format every 90 minutes
- Clear Sky WV winds (WVW)
    - Wind product from Water Vapor images in cloud-free areas
    - Distributed on GTS in standard BUFR format every 90 minutes
- High Resolution WV winds (HWW)
    - Wind product from Water Vapor images in cloudy areas
    - 16x16 Pixel target areas, giving higher spatial resolution
    - Distributed on GTS in standard BUFR format every 90 minutes
- High Resolution Visible Winds (HRV)
    - Produced from high resolution Visible images
    - Distributed in GTS in BUFR at 06Z, 09Z, 12Z, 15Z, 18Z (-3 hours for 63°E Service)
    - Parallel distribution in standard BUFR format and in simplified BUFR format.
- Clear Sky Radiances (CSR)
    - WV cloud-cleared radiances, scale 160 km
    - Distributed on GTS in BUFR format hourly
- Upper Tropospheric Humidity (UTH)
    - Distributed on GTS in BUFR at 06Z, 09Z, 12Z, 15Z, 18Z (-3 hours for 63°E Service)
- Sea Surface Temperatures (SST)
    - Distributed on GTS in SATOB at 00Z, 12Z
- Cloud Analysis (CLA)
    - Distributed on GTS in SATOB at 00Z, 06Z, 12Z and 18Z
- Climate Data Set (CDS)
    - Hourly, available from METEOSAT archive
- ISCCP Data Set (IDS)
    - Reduced resolution Image Data for ISCCP
    - 3-hourly, available from METEOSAT archive
- High-resolution Precipitation Index (HPI)
    - 3-hourly IR histograms for GPCP

All products are produced fully automated, with no human intervention. The Manual Quality Control for all METEOSAT products was discontinued on Sep 7 1998. The standard BUFR format contains definitions of quality control parameters and product derivation details and has been officially approved by the WMO CBS Working Group on Data Management and has entered into force as a standard WMO table in November 1998.

Major recent updates to the product extraction system have been:

- Jan 27 1999
    - Introduction of new inversion height assignment scheme
        - Old scheme:
            - Direct temp -> pressure conversion based on IR EBBT
            - Problem: Multi-valued conversion in inversion areas, causing large height assignment errors
        - New scheme:
            - Temperature: unchanged, based on EBBT
            - Pressure: If inversion present at low levels, pressure is set to bottom of inversion layer from forecast profile
        - Impact:
            - Comparison with St. Helena radisondes shows decrease in RMS
            - ECMWF rejection rates in South Atlantic strongly reduced
- July 1 1999
    - Cloud base height re-assignment scheme parameters changed
        - Adjustment of sigma parameter
        - - Limit on downward correction
    - Multi-channel spatial consistency test
        - All channels are used for the spatial consistency, if within 50 hPa
    - Pre-operational distribution of High-Resolution Water Vapour Winds
        - 16x16 pixels target, BUFR, every 90 minutes, cloud-track only
        - Positive feedback from ECMWF regarding product quality
- March 16 2000
    - High Resolution WV Winds fully operational
        - Distributed every 90 minutes in WMO standard BUFR

More information about the MTP products, including schedules, GTS headers, full statistics and full description of the standard BUFR format, can be found on the MPEF WWW pages at www.eumetsat.de/en/area3/topic3.html. These pages will shortly also contain statistics on product volumes and product quality. Information about operational radiosonde collocation statistics from all satellite wind producers can be found at www.wmo.ch/hinsman/CGMShome.html

3. User requirements

The key driving forces for the development of the Meteosat products have been the support to the global NWP operators, the support to the synoptic forecasters and the support to the WMO climate programs. By and large this will remain so in the coming years. The following key developments in the user community are foreseen in the coming years and should be supported by the MPEF.

Variational data assimilation

The migration of the optimum interpolation analysis schemes to variational methods has already started. ECMWF has for several years employed variational schemes for assimilation of TOVS radiances and is planning the operational assimilation of METEOSAT clear-sky radiances. The variational methods make possible the assimilation of data containing non-model variables by the use of so-called observation operators, which define a relation between model variables and observed data. An example of an observation operator is a forward radiative transfer model, defining a relationship between a profile of temperature and humidity and observed radiances in specific channels. The variational methods then makes it possible to assimilate satellite radiances, even if they cannot be directly converted into a real profile.

The variational technique can also be used to assimilate bulk data like deep-layer mean winds. Such a procedure could be employed for clear-sky WV winds, but no significant development work in this area has yet been done in the user community.

4-D data assimilation
The analysis schemes of at least the major NWP centres will over the next decade be migrated to the next generation 4-D variational methods and this will considerably change the data requirements. Whereas the NWP analysis schemes now depend almost solely on synoptic data, they will evolve into continuous data-assimilation systems with no special dependency on synoptic hours. As the geostationary satellites are the main continuous source of asynoptic data this will become a very important driving force for the METEOSAT products.

An ongoing debate in the NWP community addresses the issue of 4-D assimilation of satellite geophysical products, e.g. winds, vs. direct assimilation of satellite radiances. Theoretical arguments would suggest that 4-D assimilation of cloud-cleared radiances would generate a wind field consistent with the wind field derived directly from the images. This would indicate no need to assimilate clear-sky winds directly. This is however a theoretical argument, as direct assimilation of the radiances at instrument resolution in space and time is quite out of reach with current assimilation systems. Therefore a more pragmatic approach seems to prevail, namely the concurrent assimilation of radiances and winds at an appropriate resolution in space and time.

Other major NWP operators are planning operational implementation of 4-D Var.

4. Development plans

4.1 Pre-processing

Calibration
Based on data collected on the performance of the METEOSAT-7 black-body calibration a new calibration scheme is under development to be based on black-body measurements performed at least twice a day, as well as a simplified front-optics model. This scheme gives promising results, and the new calibration scheme will become operational in May 2000. For METEOSAT-5 a scheme for operational cross-calibration with METEOSAT-7, based on the overlap area, has been developed and will become operational in October 2000.

Improved spatial resolution of forecast data
On Mar 1 1999, the migration of ECMWF forecast data used in MPEF from GRID fields with very coarse horizontal and vertical resolution (3x3 deg, 10 pressure levels), to high-resolution GRIB data (1.5x1.5 deg, model hybrid-sigma levels (currently 50) was completed. The high-resolution forecast data provides very significant improvements in the description of deep low-level trade inversions and together with the new inversion height assignment scheme, this has significantly improved the quality of the low-level wind products in the subtropics.

Improved resolution of diurnal cycle
Improving the resolution of the diurnal cycle in surface temperature is important for the prediction of IR radiances for surface scenes. Because of the 6-hour resolution in time, the diurnal cycle variation has to be simulated in a separate step. The present scheme will be improved by the use of 3 hourly forecast fields, if these become available operationally, to provide a better resolution of the diurnal cycle.

Improved Semi-Transparency correction
Studies indicate that the height assignment of IR and WV winds in many cases fail because of failure to apply a correct semi-transparency correction to the cloud clusters. Several factors can contribute to an improvement in this area:

- The Semi-Transparency correction can be calculated by using a linear regression on the individual pixels. This eliminates the requirement for background scene identification.
- The quality of the humidity forecast is crucial in determining the radiance curve, and with the rapidly improving humidity fields supplied from the NWP centres an improvement will be expected.
- A posteriori adjustment of the radiance curve to fit the observed background clusters could be investigated.
- The Semi-Transparency model could be refined to more truly represent semi-transparent clouds
- Improvements of the stability of the WV vicarious calibration will have a significant effect on the semi-transparency correction.

An improved semi-transparency correction scheme, primarily based on the linear regression technique, is being developed as part of MSG MPEF, and it is planned to integrate the complete MSG MPEF scenes analysis and semi-transparency correction in MTP MPEF later in 2000.

4.2 Wind products

General
The wind products are computed by identifying and localising the same pattern ("tracer") in consecutive METEOSAT images (Buhler and Holmlund, 1993). This tracking is done in all 3 spectral channels independently. Using the knowledge of the tracer displacement, combined with the measurement of its temperature, the following values are extracted which constitute the wind product : wind location, wind speed, wind direction, temperature and pressure level.

The first operation performed is the selection of the structures that will be used as the tracers, based on the information provided by the Histogram Analysis. This tracer selection is done in a channel-specific way, including cluster merging or rejection when necessary. When a useful tracer has been identified, height assignment is performed and the corresponding wind component can be extracted. The wind-component extraction process comprises the definition of the Target and Search areas taken from the current and previous image, their enhancement, followed by their cross-correlation.

For CMW and ELW the tracers are clouds identified from 5 km imagery from all channels, for HRV clouds identified from 2.5 km visible imagery and for WVW the tracers are cloud-free tracers identified from 5km WV imagery.

The extracted wind components are thereafter subject to automatic quality control (AQC) (Holmlund, 1996). The AQC process calculates a number (currently 5) of consistency indicators for the extracted wind, and combines these as a weighted mean into an overall reliability indicator. The intermediate wind products contain all extracted winds and associated reliability indicators. No manual quality control is applied.

The intermediate wind products are encoded into GTS formats. For the CMW product the best wind per geographical location, as determined by the value of the overall reliability indicator, is selected from this intermediate product, and encoded into SATOB, if the reliability indicator exceeds a certain threshold value (currently 80%). For the ELW, HRV, HWW and WVW products, the winds are encoded in BUFR, together with the reliability indicators themselves. All winds down to a low reliability (30%) are included, but for each product, a suggested reliability indicator threshold is provided in the BUFR format.

The BUFR and SATOB products are distributed on the GTS. The original intermediate products are archived in the Meteosat archive facility (MARF) and are thus available for historical retrievals.

Further details about the wind extraction process are provided in (Rattenborg and Holmlund 1996) and (Schmetz et.al.).

The following areas can be identified, where further improvement of the current MPEF wind products are desired:

- Low level coverage around developing tropical systems. The deficient cloud motion-wind coverage in the vicinity of developing and developed tropical disturbances is an important issue for hurricane forecasting.
- Medium-level coverage. Although this area presents fundamental meteorological problems, the MPEF wind coverage at medium levels seems to be too low.
- High-level height assignment for cloud tracked winds. Significant scope for improvements to the semi-transparency correction.
- Clear-sky tracking using cross-correlation is not performing satisfactorily
- Provision of reliability indicators independent of first-guess fields
- Provision of reliability indicators for speed, direction, pressure and temperature

The needs of the user community will be addressed through improvements to the existing operational wind products (CMW, HRV, HWW and WVW) and partly through the introduction of new wind products.

HRV tracer selection improvements
The tracer selection and height assignment for HRV will be based on averaging pixel counts over the target area in the pixel-classified image instead of using the segment-based cluster information. This will provide more HRV winds in mixed cloud segments and better coverage in areas with developing systems.

Medium-level IR winds
The quality and coverage of the medium level IR winds is relatively poor. This is mainly a reflection of the complex physics and dynamics of the mid-level atmosphere, especially over the continents, and no single internal problems causing this have been identified, but the medium-level winds issue will continue to be investigated.

WV winds from cloud-free areas
The tracking of water vapour in cloud-free areas provides a wind product with extensive coverage. This product (WVW) at a resolution of 160 km is now available as an operational product, using the single-level height assignment based on the cluster EBBT, and an alternative height assignment is also included in the BUFR message, based on the WV contribution function calculated in the Radiative Transfer Model.

Low-level tracking over land
The tracking of low-level clouds over land presents significant problems because of the short lifetime of low-level clouds over land, the impact of surface features on the tracking and of flow deformation/curvature effects. The feasibility of advanced techniques to address these issues using the MSG spacecraft is being addressed in a EUMETSAT study, and if the results of this study are promising and applicable an implementation in the MTP system will be considered.

Clear Sky WV tracking
Investigations have shown that tracking in cloud-free areas with the cross-correlation tracking algorithm produces high numbers of spurious fast winds. Investigations are ongoing to assess the impact of using Minimum Euclidean Distance tracking.

Better geographical positioning
Presently the extracted winds are positioned at the segment centres, introducing an inaccuracy of up to half a segment size. A better positioning can be obtained by explicit tracer location in the image. Initial results are encouraging and this change will be introduced operationally in 2000.

Increased time-frequency of winds distribution
The MPEF distributes winds in BUFR format every 1.5 hours. A further reduction of the wind extraction cycle to 1 hour, made possible by more powerful workstations, will bring the schedule inline with the MSG baseline and is planned for 2000.

Move winds derivation to synoptic times
To leave enough time for manual quality control, the derivation of the wind products has historically been performed 1 hour before the main synoptic hours, e.g. 12Z products were derived from the three images ending at 10:30Z, 11:00Z and 11:30Z. As all procedures are now fully automated, this is no longer required, and the wind extraction times will be moved to match the synoptic hours. Planned for 2000.

Automatic Quality Control
A core issue to be addressed for the MPEF CMW product is the definition of the AQC processes and parameters. The process is essential to ensure a maximum yield of high-quality winds for all channels and all levels and to ensure the availability of stable reliability indicators for the user community. A very important aim is also to provide quality indicators which are independent of the forecast wind fields. The AQC tuning is based on the continuously growing data set of collocated radiosondes and MPEF satellite winds, as well as on comparisons with ECMWF first-guess fields. The AQC definition process is ongoing with continuous improvements over the next year. A main goal is to introduce a quality indicator, independent of the first-guess field.

With an optimal AQC the size and coverage of the SATOB encoded product can be increased and meaningful reliability indicators for the BUFR product, including individual reliability indicators for speed, direction and height, can be provided, as well as quality indicators with and without forecast information. It could also be investigated whether estimates for the error distribution functions can be produced, which could be used in the NWP data assimilation schemes.

The optimised AQC system will be used as a basis for tuning the MSG MPEF, as the MSG system will employ the same AQC system as MTP.

Verification improvements
The verification of the CMW product is currently based exclusively on radiosondes and forecast fields. Use of other data (e.g. AIREP/ASDAR/ACARS) for verification is foreseen.

4.3 Other products

80 km clear sky radiances (CSR)
These data are derived on a scale of 16x16 pixels (80 km), i.e. half the scale of the current UTH product, and provide clear-sky equivalent blackbody temperatures and radiances from both WV and IR channels, for 4D-VAR assimilation in NWP models. The product also includes upper tropospheric humidity, the standard deviation of the temperatures within the clear parts of the 80km quadrant, and

the fraction of the quadrant clear and cloudy for every quadrant in the processing area. The method employed is essentially the same as in the current 160km UTH product.

There is quality control information included (percentage confidence) which is currently simply based on a threshold amount of cloud cover for temperature and radiance data, and on a threshold amount of cloud cover and a threshold humidity limit for the upper tropospheric humidity. This scheme has scope for future enhancement by also using the standard deviation of the temperatures to give an indication of cloud contamination, and hence of reduced confidence in the data.

The CSR product has been distributed to ECMWF for testing since Jan 20 1999 and it is planned to introduce the product as fully operational when the new calibration procedures (see above) are operational.

5. Reprocessing

Recognising the increasing interest in the processing of historical image data, EUMETSAT has established a reprocessing environment, directly connected to the METEOSAT archive MARF. During the summer of 1999, 1 year (1996) of visible image data from METEOSAT-5 have been reprocessed to produce a pixel-level surface albedo product, using an algorithm developed at the Space Applications Institute (SAI) at the EU Joint Research Centre, Ispra. The surface albedo product is currently undergoing initial validation and will be presented to beta-testers later in 1999, after which it is planned to make the product generally available.

Starting spring 2000, reprocessing of METEOSAT-2 data (1981-1988) will start to reconstruct the record of cloud motion winds in support of the ECMWF 40 year re-analysis.

6. Transition from MTP to MSG

The first MSG spacecraft MSG-1 will be launched in October 2000. The development of the MSG system is very advanced, and the MSG MPEF algorithms are well defined (EUMETSAT, 1998). The MTP wind products development strategy, as detailed above, takes the following issues into account:

The User community requirements will continue to evolve before the start of MSG operations.
The capabilities of the NWP systems to assimilate wind and radiance products asynoptically at increased spatial resolution will continue to grow.

The User community transition to the MSG products baseline should be as smooth as possible.
The standard BUFR template for the wind products, developed for the MTP products, will also be employed in the MSG MPEF system, thus securing minimum user community effort required for the transition to MSG. Also later this year, the MTP system will produce wind products hourly, equivalent to the MSG system.

MSG will benefit from early operational exploitation in MTP of new developments.
There is a significant synergy effect from early implementation of MSG product developments in the MTP system. This applies to areas like the semi-transparency correction, higher resolution WV winds, usage of pixel-level classification in tracer selection and the automatic quality control.

Meteosat-7 has an estimated end-of-life of 2004.
The mission concept for the approved continuation of the MTP programme until the end of 2003 has not been finalised, but a continued derivation of wind and radiance products from Meteosat-7 for the meteorological user community could be envisaged.

Meteosat-5 continues the 63°E service.
An extension of the 63°E service till at least the end of 2001 was approved at the June EUMETSAT Council, and this means that for considerable amount of time there will be an operational MTP spacecraft operating over the Indian Ocean. This in turn means, that the MTP MPEF products and algorithms will have to be operated and maintained in parallel to MSG, and it is therefore envisaged to cross-exploit certain key areas like scenes analysis.

7. Conclusions

The MTP MPEF system will continue to develop the wind products to provide the user community with higher quality wind products, and a clear continuity of service towards the MSG MPEF system will be achieved.

REFERENCES

Buhler, Y. and Holmlund, K., 1994: The CMW Extraction Algorithm for MTP/MPEF, *Proceedings of the Second International Winds Workshop*, Tokyo, 13 -15 Dec 1993. EUM P14, Published by EUMETSAT, D-64294 Darmstadt, 205-217

Elliott, S. S., 1998: The Generation, Quality Control and Distribution of High Resolution Water Vapour Winds from Meteosat Data, *Proceedings of the Ninth Conference on Satellite Meteorology and Oceanography*, Paris, 25-29 May 1998, EUM P 22, Published by EUMETSAT, D-64294 Darmstadt, 353-355

EUMETSAT Seviri Science Plan, , www.eumetsat.de/en/area2/publications/severi_sp270398.pdf , Issue 1 March 98

Holmlund, K, 1996: Normalised Quality Indicators for EUMETSAT Cloud Motion Winds, *Proceedings of the Third International Winds Workshop*, Ascona, 10 –12 June 1996. EUM P18, Published by EUMETSAT, D-64294 Darmstadt, 155-165

Rattenborg , M. and Holmlund, K., 1996: Operational wind products from new Meteosat Ground Segment, *Proceedings of the Third International Winds Workshop*, Ascona, 10 –12 June 1996. EUM P18, Published by EUMETSAT, D-64294 Darmstadt, 53-59

Schmetz, J., Holmlund, K., Hoffman, J., Strauss, B., Mason, B., Gärtner, V., Koch, A. and L. van de Berg, 1993: Operational Cloud-Motion Winds from METEOSAT infrared images; *J. Appl. Meteor.,* **32,** 1206-122

RECENT ADVANCES IN THE GENERATION AND ASSIMILATION OF HIGH SPATIAL AND TEMPORAL RESOLUTION SATELLITE WINDS

J. Le Marshall[1], N. Pescod[1], R. Seecamp[1], A. Rea[2], C. Tingwell[1] , G. Ellis[2] and Hao Shi[3]

1 Bureau of Meteorology Research Centre, Bureau of Meteorology, Melbourne, Australia
2 Dept. of Land Information, RMIT University, Melbourne, Australia
3 Victoria University, Melbourne, Australia

ABSTRACT

This paper reviews work related to the generation and assimilation of high spatial and temporal resolution winds from GMS-5 Stretched VISSR data. It notes the physical basis used in the wind estimation and the accuracy of the resultant vectors. Winds are currently generated from tracers selected in 11μm, 12μm, 6.7μm and low and high resolution 0.5μm images. They are estimated hourly and, four times per day half-hourly. Height assignment uses the GMS-5 IR channels. The gains made in wind yield using a special experimental set of winds from 15-minute observations provided over the Southern Hemisphere by the Japanese Meteorological Agency will also be shown. For the first time, these experimental data provide an indication of the increased yields in Australian Region wind data expected from MTSAT.

The winds have been used in a series of (real time) data assimilation experiments and have been shown to have positive impact on both Regional and Global operational Numerical Weather Prediction (NWP) using intermittent data assimilation methods. The use of the winds has also been extended to include very high resolution 4D variational assimilation which has been employed to forecast tropical cyclone characteristics. Use of hourly and half-hourly high spatial resolution cloud and water vapour drift winds via high resolution 4-D variational assimilation at 15 km or higher resolutions (up to 1 km) has been found to provide tropical cyclone track forecasts which are more accurate than those produced by the current operational forecast system. In the cases examined, use of very high resolution (5 km or better) 4-D variational data assimilation in conjunction with hourly and half-hourly high spatial resolution cloud and water vapour drift wind data has also provided improved estimates of tropical cyclone intensity. Work underway related to cloud drift wind generation from FY-2 is also noted.

1. Background

In the Australian Region, observations taken from polar orbiting and geostationary satellites are vital to sub-synoptic scale analysis and forecasting (Le Marshall et al. 1997). Estimates of temperature, moisture, total ozone and wind are made from real time radiance observations, taken by the NOAA polar orbiting satellites and from the Geostationary Meteorological Satellite which is situated at 140°E, over the Australian Region. These data are pivotal for both analysis and forecasting in the Australian Region. In particular, the benefits obtained from using the almost continuous wind observations, available from the GMS-5 satellite for operational forecasts, have been quantified. In addition, benefits obtained using these winds, in combination with modern 4-D variational continuous data assimilation methods, are significant (Leslie et al. 1998, Le Marshall and Leslie, 1998, Le Marshall and Leslie, 1999). The anticipated improvement in data distribution, expected to result from the introduction of 15-minute observations by MTSAT, is also demonstrated using data from a special observation period in April 1999.

2. High spatial and temporal resolution winds

Hourly and, four times per day, half-hourly, GMS-5 Stretched VISSR (S-VISSR) infrared, water vapour and high-resolution visible images are received in Melbourne, navigated and calibrated and stored in cyclic data sets in the Australian Region McIDAS system at the Bureau of Meteorology (BoM). From these images, targets are selected automatically, using specific gradient criteria for each of the image types used in tracking (Le Marshall et al. 1994, Le Marshall et al. 1999).

After selection, the targets are tracked automatically, using a model forecast to initiate the search for selected targets on sequential images. A lag correlation technique is used to estimate the vector displacement. Pressure altitude assignment to the motion vectors is similar to that described in Le Marshall et al. 1994, with refinements to allow for the changes in the spectral response functions and calibration associated with the new GMS-5 S-VISSR data. In particular, the operational system used by the Bureau of Meteorology uses both the dynamic calibration associated with the GMS-5 imagery and data from the split window channel for pressure altitude assignment (see, for example, Le Marshall et al. 1998). For the visible winds, the altitude assignment uses infrared imagery at the central time of the image triplet used for wind estimation. Water vapour cloud wind altitude assignment is similar to that for upper level infrared vectors while for mid-level, clear air water vapour motion vectors, it uses the mean temperature of the tracers (Le Marshall et al. 1999). After velocity and altitude assignment, quality control produces winds with expected errors assigned according to several objective criteria (Le Marshall et al. 1994).

Currently, in operational mode, the system generates winds, four times per day, from sets of three infrared images, separated by half an hour. It also produces visible, high resolution visible, and water vapour-based winds from half-hourly images, four times per day. Hourly infrared, visible, high resolution visible and water vapour images are used to produce hourly wind data. These data are distributed to the National Meteorological Operations Centre (NMOC), Regional Forecast Centres (RFCs) and Tropical Cyclone Warning Centres (TCWCs). A summary of the winds produced is given in Table 1.

Table 1. Cloud and water vapour drift wind types generated in the BoM. Type (Op. = Operational, LR = Low Resolution, HR = High Resolution, IR = Infrared VIS = Visible, WV = Water vapour), Image resolution, Frequency, Time of wind extraction and the separation of image triplets (T) are included.

Wind type	Image res.	Freq.	Time (UTC)	Wind triplet ((T)
Op. IR, WV, LR VIS., (HR VIS)	5, 5, 5, (1.25) km	6 hr.	05, 11, 17, 23	30 min.
IR, WV, LR VIS., (HR VIS)	5, 5, 5, (1.25) km	1 hr.	00, 01, ... 23	1 hour

An example of the winds produced between 05 and 07 UTC on 25 March 1999 is seen in Figure 1 and a diagram of the differences between the motion vector winds and those taken from radiosondes within 150 km are seen in Figure 2.

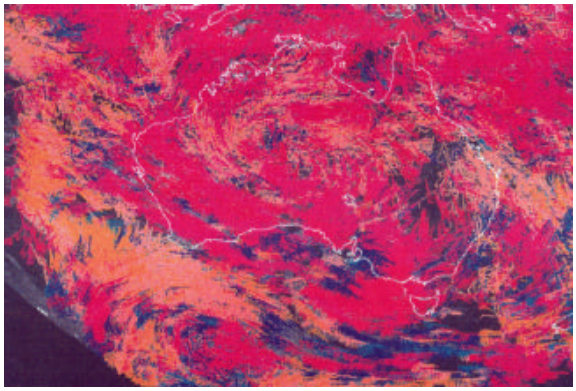

Figure 1. Local cloud and water vapour drift winds generated around 06 UTC on 25 March 1999 from visible, high resolution visible, infrared and water vapour absorption band images.

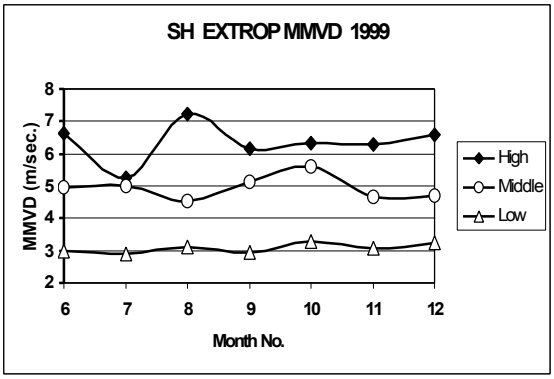

Figure 2. The mean magnitude of vector difference (MMVD) for local Southern Hemisphere extra Tropical IR cloud drift winds compared to radiosondes within 150 km June to December 1999

.

3. The 1999 special observation period

As a prelude to the launch of a replacement satellite for GMS-5, the Japanese Meteorological Agency (JMA) and the Bureau of Meteorology (BoM) undertook a collaborative project to observe the Australian Region at higher temporal resolution than had been undertaken before. In addition to the usual observation sequence, undertaken by the GMS-5 satellite, images were taken over the Southern Hemisphere on the 7, 20, 21, 22 and 23 April 1999 at 0330, 0345 and 0400 UTC, providing 15-minute observations of the southern section of the full-earth disc.

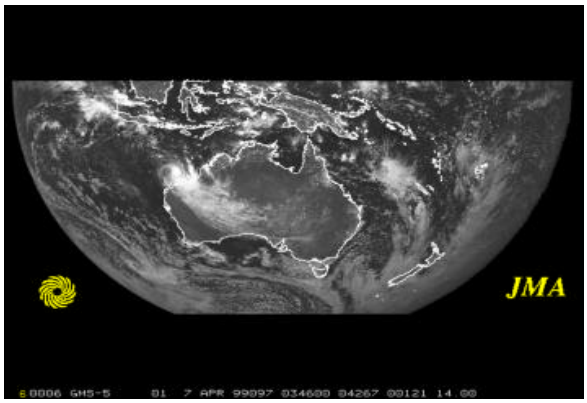

Figure 3 (a). Coverage during the Southern Hemisphere Special Observing Period - April 1999.

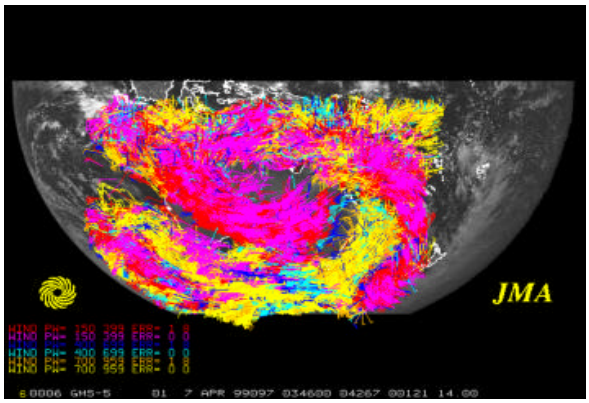

Figure 3 (b). Winds generated using 15-minute imagery on 7 April 1999.

The coverage provided during this observing period is shown in Figure 3 (a). Winds generated using these 15-minute observations on 7 April 1999 are shown in Figure 3 (b). These winds include 11µm infrared, low-resolution visible, high-resolution visible and water vapour image based motion vectors. The numbers of winds/high quality winds generated from these 15-minute observations as compared to those from hourly and half-hourly observations have been examined, as has the variation in wind numbers as visible image resolution is increased from 5 km to 1.25 km. In the case of observations taken on 7 April 1999, the area around Tropical Cyclone Gwenda has been examined in detail. Vectors generated in a 900 by 1280 pixel box, centred on the tropical cyclone, have been calculated at hourly, half-hourly and 15-minute intervals. The total number high resolution visible (HRVIS) vectors generated in the box, centred on Tropical Cyclone Gwenda, at different time periods on 7 April 1999, is displayed in Figure 4.

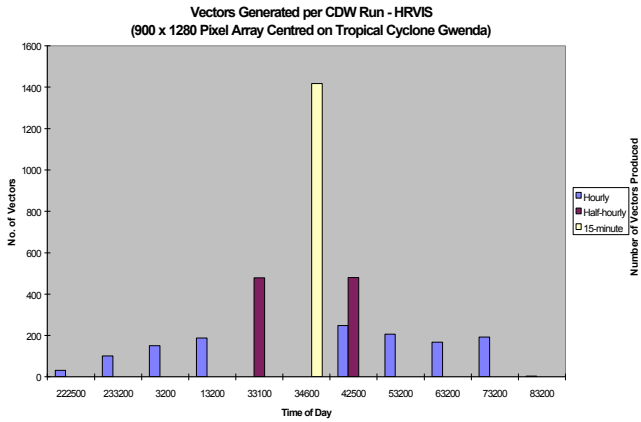

Figure 4. The variation in vector numbers for a high resolution visible image 900 x 1280 pixel box around TC Gwenda for different image frequencies (1/4, 1/2 and 1 hour).

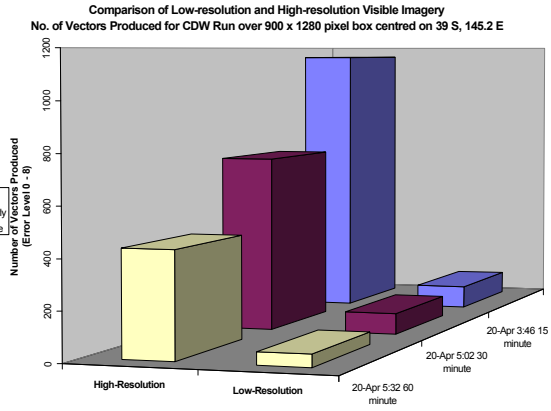

Figure 5. Comparison of low and high resolution visible imagery vectors mproduced in a 900 x 1280 pixel box centred on 39 °S, 145.2°E.

There is a significant gain in the numbers of vectors at higher temporal resolution, for this high-resolution image based data. The 15-minute observations provide significantly more data than the half-hourly and hourly observations. The influence of solar illumination is also clearly seen in these observations where the rising and setting of the Sun are clearly defined.

The effect of image resolution and target selection in the local system is seen in Figure 5 where high quality vector numbers calculated from high and low resolution visible images (1.25 km, 5 km respectively), separated by ¼, ½ and 1 hour over a 900 x 1280 pixel box centred on 39°S, 145.2°E over South Eastern Australia are shown. The total numbers of high quality vectors over the southern portion of the full-earth disc observed at different temporal resolutions are shown in Figure 6. An increase in high quality vector numbers with increased temporal resolution is seen for low resolution visible winds and, to a diminishing extent, for the infrared and water vapour winds.The winds generated from these SOP images are being used with other wind data from 7 April 1999 in a study of TC Gwenda. Preliminary results are shown later.

Overall, a clear increase in the density and coverage of high quality winds available from the system is evident with these higher temporal resolution observations. This is a clear indication of the improved observational capability associated with MTSAT, which, in principle, will allow five minute observations, defining wind fields in increased detail by tracking, for example, features in clouds associated with tropical cyclones right up to the inner core.

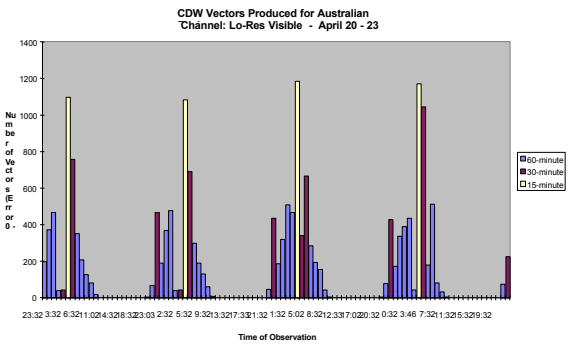

Figure 6 (a). Vector numbers for Low Resolution 5km) Visible Image based winds over the Australian Region (20 - 23 April 1999).

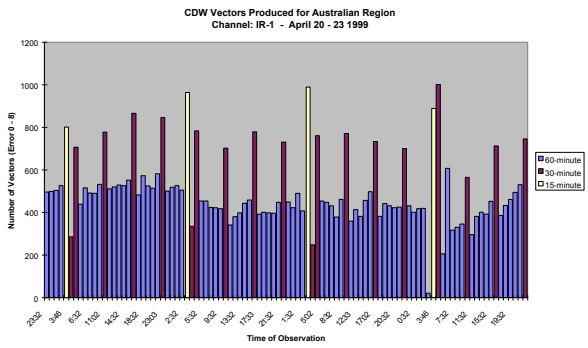

Figure 6 (b). Vector numbers for IR1 (11µm, 5km) Image based winds over the Australian Region (20 - 23 April 1999).

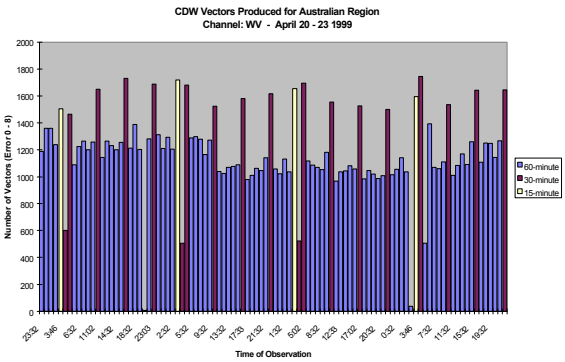

Figure 6 (c). Vector numbers for Water Vapour Band (6.7µm) Image based winds over the Australian Region (20 - 23 April 1999).

4. Intermittent assimilation of motion vector data

Real time data assimilation experiments, documenting the utility of local cloud and water vapour motion vectors for operational numerical weather prediction (NWP) over the Australian Region are complete. The operational Limited Area Prediction System (LAPS, Puri et al. 1998) has been used as the control. The experimental system employed has been a parallel, near real time LAPS system run, identical to the operational system, apart from the addition of local real time cloud and water vapour motion vectors to the data base. The analyses on which the forecasts reported here are based start with a BoM Global Analysis (Seaman et al. 1995), valid 12 hours before the forecast start time. This is used as first guess to the Regional Analysis which then provides a base analysis, an initialised 6-hour forecast, a subsequent analysis and a further initialised 6-hour forecast. This forecast is then used as a first guess to the final analysis from which 24-hour forecasts have been run. The forecasts are nested in fields of the most recent Bureau of Meteorology Global Model forecast. The LAPS analysis and forecast models have the same latitude/longitude/sigma co-ordinate system of 160 x 110 grid points at 0.75° spacing in the horizontal and 19 levels in the vertical. The upper sigma level is at 0.05.

Three experiments have been completed. The first gauged the impact on the operational regional forecast system of local IR1 cloud drift winds, based on the 11µm window channel imagery. It was reported in Le Marshall et al. 1998. The winds were estimated from triplets of half-hourly GMS-5 imagery at 05, 11, 17 and 23 UTC. The NMOC operational forecast system and the operational data base included NESDIS TOVS, local TOVS and available JMA cloud drift winds. The second experiment gauged the impact of local hourly cloud drift winds on the operational prediction system (Le Marshall et al. 1998). This experiment was performed after the local 11µm winds had been introduced into the operational system. The third experiment gauged the impact of local water vapour image based motion vectors on the operational system (Le Marshall et al. 1999). The results of these three experiments are seen in Figure 7 which shows the improvement in regional S1 skill scores estimated on the official NMOC verification grid. It is interesting to note that most impact is seen at lower levels except in the water vapour wind study where the upper and mid-level vectors have provided most benefit at upper levels.

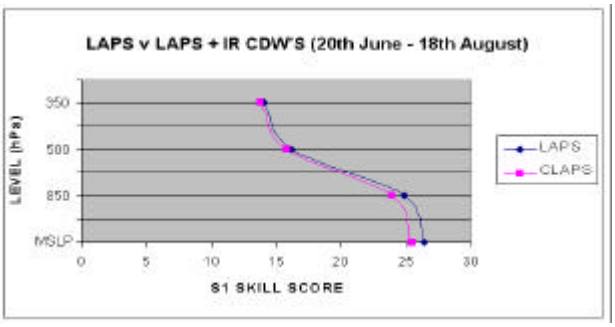

Figure 7 (a). S1 skill scores for 24-hour LAPS forecasts for Operations (Ops) and Ops plus IR1 winds.

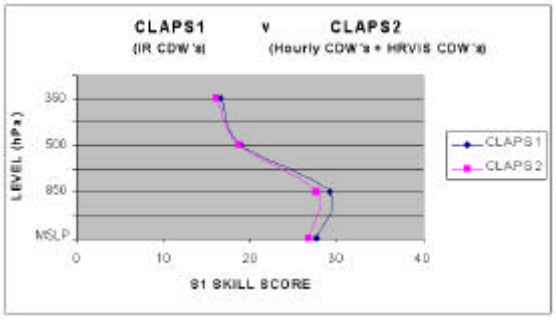

Figure 7 (b). S1 skill scores for24-hour LAPS forecasts for Operations (Ops) and Ops plus hourly winds.

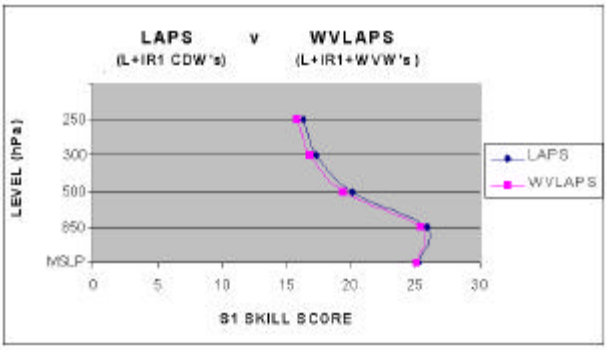

Figure 7 (c). S1 skill scores for 24- hour LAPS forecasts for Operations (Ops) and Ops plus Water Vapour winds.

5. Continuous assimilation of motion vector winds

Improvements in TC track forecasting have been made recently through the use of high resolution modelling, an enhanced data base and modern data assimilation techniques. For example, Le Marshall et al. (1996), Leslie et al. (1998) and Le Marshall and Leslie (1998) have shown that high-resolution (15 - 5 km) modelling and the use of high spatial and temporal resolution cloud and water vapour motion vector data with continuous 4-dimensional (4-D) variational assimilation (Bennett et al. 1996, 1997) has the ability to significantly improve TC track forecasting. The accuracy of eleven tropical cyclone track forecasts using high-resolution data and 4-D variational assimilation is shown in Figure 8.

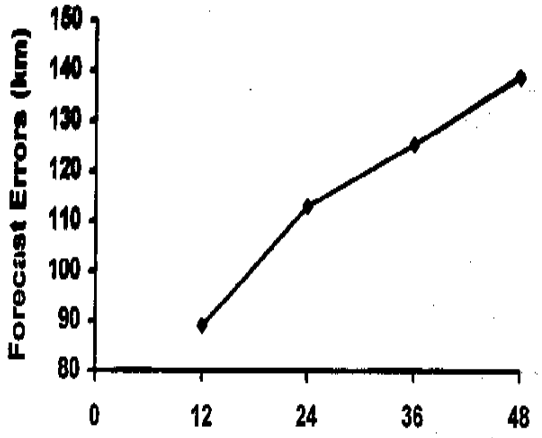

Figure 8. Forecast position error versus forecast length using 4-D variational assimilation for the eleven tropical cyclones.

Four-dimensional variational assimilation with the new high spatial and temporal resolution data source has incorporated additional data at non-synoptic times and assured an initial state which is in dynamic balance and is consistent with the observations taken during the previous 24 hours. It has produced 48-hour track forecast errors considerably below those now associated with operational forecasts (Gordon et al. 1998). Although these experiments are representative of recent increases in the accuracy of forecasting tropical cyclone tracks, the prediction of tropical cyclone intensity is still a vexing issue. We have extended the strategy employed above and have used high spatial and temporal resolution satellite data with very high resolution continuous assimilation and modelling. The wind-field associated with the tropical cyclone has again been depicted by several thousand wind observations over a 24-hour period prior to forecast start. These winds generally in the 200 - 3000 km range from the cyclone describe both the cyclone and the environment into which it moves. They also help define the upper level divergence associated with these storms, aiding the estimation and prediction of intensity (Bosart et al., 1998). We have used 4-dimensional variational assimilation to ensure that these data are incorporated correctly at non-synoptic times and we have assimilated both the data and modelled the cyclone at 5 km resolution to allow an adequate depiction of both cyclone structure and intensity. Five kilometres resolution appears to be within the range required to resolve adequately the area of maximum wind speed and provide a realistic depiction of storm dynamic and thermodynamic structure.

The model configurations used in these studies were 25 levels, 25 km resolution (180 x 180 grid points), 15 km resolution (301 x 301 grid points) and 5 km resolution (601 x 601 grid points). The early stages of two tropical cyclones are shown. The first was Tropical Cyclone Olivia which developed explosively off the NW coast of Western Australia during the forecast period. High spatial and temporal resolution cloud and water vapour winds were assimilated for 24 hours between 12 UTC on 5 and 6 April 1996 using 4-D variational assimilation. The resolution of the assimilation and forecast system was varied from 25 km, through 15 km down to 5 km. The variation of storm central pressure with time from 12 UTC on 6 April 1996 for the control and 4-D variational forecasts out to 72 hours is seen in Figure 9(a) for each resolution.

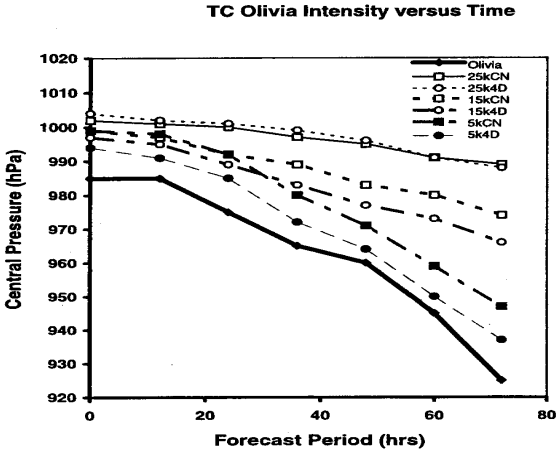

Figure 9 (a) TC Olivia intensity versus forecast period for different resolutions and data.

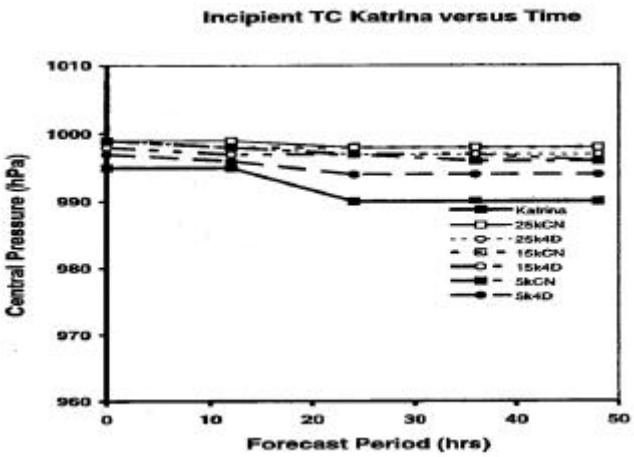

Fig. 9 (b) Forecast intensities for TC Katrina from 0000 UTC 3 January 1996 with varying grid resolutions, for the control and 4-D variational assimilation cases

Figure 9 (b). TC Katrina intensity versus forecast period for different resolutions and data..

The beneficial impact of the high resolution wind data used during initialization is evident. While there is little difference between the control and 4-D assimilation forecasts at lowest resolution, the difference progressively increase with higher model resolution. The winds associated with TC Olivia at 0000 UTC on 9 April 1996 are shown in Figure 10. This is a southwest to northeast cross section of the winds at 900 hPa. The winds are a 15 minute average. The maximum wind speed in this case is 63 m/s at 900 hPa and compares well with the NCC surface maximum winds of 46 m/s, which is close to 0.75 of the 900 hPa estimate.

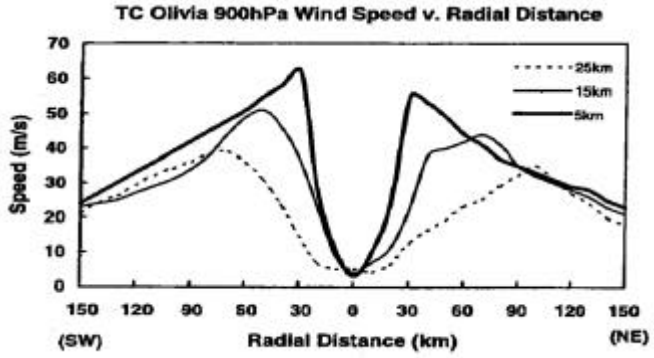

Fig. 10 A SW to NE cross-section of winds through TC Olivia at 900 hPa at 00 UTC 9 April 1996

Figure 10. A SW-NE cross-section of winds through TC Olivia at 900 hPa at 00UTC 9 April 1996.

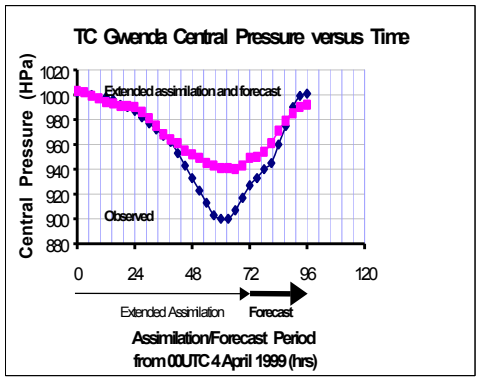

Figure 11. Modelled TC Gwenda central pressure using extended 4D variational assimilation.

The second cyclone examined in this study was TC Katrina. The time for the start of the forecasts was 00 UTC on the 3 January 1998. This cyclone formed very slowly in the Coral Sea. The intensities forecast in this case are summarised in Figure 9 (b). In recent developments, continuous data from 00 UTC on 4 April 1999, around TC Gwenda, has been used to forecast intensity. Warm running at 1 and 5 km resolution via 3 days of 24 hour 4D variational assimilation has provided a 24hr forecast (See Figure 11). Here again the benefits of very high resolution 4-D variational assimilation and modelling and high resolution data are evident.

6. Summary and Conclusions

We have briefly described the real time generation of cloud drift winds in the Australian Region from GMS-5 Stretched VISSR data. We have also used the test data available from a special observing period in April 1999 to show the improved coverage of winds expected from MTSAT. We have briefly documented the beneficial impact of the locally generated winds on regional numerical weather prediction. In relation to tropical cyclone track forecasting, while it is well established that high resolution numerical modelling and an enhanced data base are important to accurate tropical cyclone forecasts, here, we have summarised work showing high resolution modelling, high spatial and temporal resolution data and continuous data assimilation being combined and applied to the forecast problem. This approach allows the benefit of high resolution modelling to be obtained, both in the assimilation and forecast process, while continuous assimilation incorporated with the high spatial and temporal resolution data at non-synoptic times and ensured an initial state which is close to dynamic balance and consistent with observations. Although initial position errors are still a contributor to forecast errors, overall, the results show that the wind data base and the assimilation methodology adopted here have significantly reduced the forecast errors associated with tropical cyclone track prediction, , particularly in difficult forecast situations.

In relation to modelling tropical cyclone intensity, we have shown two contrasting tropical cyclones - a developing and non-developing storm. In these cases studied, horizontal resolution has been revealed to be a key element in predicting storm intensity. The winds used were mainly in the upper outflow region of the storm and had a significant impact on the overall accuracy of both the initialised fields and the subsequent forecasts. In addition to this, we have, for the first time, shown the benefits of warm running using 4-dimensional variational assimilation to enable initialisation of the model over a very intense cyclone and to successfully allow the modelling of the cyclone dissipating.

ACKNOWLEDGMENTS

Thanks are due to T. Adair for his work in the preparation of this manuscript.

REFERENCES

Bennett, A.F., B.S. Chua and L.M. Leslie, 1996. Generalised inversion of a global numerical weather prediction model. *Meteorology and Applied Physics*. **60**, 165 - 178.

Bennett, A.F., B.S. Chua and L.M. Leslie, 1997. Generalised Inversion of a Global Numerical Weather Prediction Model II Analysis and Implementation. *Meteor., Atmos. Phys*., **62**, 129 - 140.

Bosart, L.F., W.E. Bracken, J. Molinari, C.S. Velden and P.G. Black 1998. Environmental influences on the rapid intensification stage of Hurricane Opal (1995) over the Gulf of Mexico. *Symposium of tropical cyclone intensity change.* 11-16 January 1998 Phoenix Arizona . American Meteorological Society D(VT) 1/98-400.

Gordon, A., W. Gude, R. Schwerdtfeger, R. Byron-Scott, 1998. Dynamic Meteorology : A Basic Course, Arnold, London, 325 pp.

Le Marshall, J., N. Pescod, R. Seaman, G. Mills and P.Stewart, 1994. An Operational System for Generating Cloud Drift Winds in the Australian Region and Their Impact on Numerical Weather Prediction. *Wea. and Forecasting*, **9**, 361 - 370.

Le Marshall, J.F., L.M. Leslie and A.F. Bennett. 1996. Tropical Cyclone Beti - an example of the benefits of assimilating hourly satellite wind data. *Aust. Meteor. Mag*. **46**, 275 - 279.
Le Marshall, J., L.M. Leslie, N. Pescod, C. Spinoso and R. Morison. 1997. The importance of direct readout satellite data in sub-synoptic scale data assimilation and numerical weather prediction. *Adv. Space Res.* **19(3)**, 413 - 422.

Le Marshall, J. N. Pescod, R. Seecamp, C. Spinoso and A. Rea.1998, Improved weather forecasts from continuous generation and assimilation of high spatial and temporal resolution satellite data. *Proceedings of the Fourth International Winds Workshop*, Saanenmoser, Switzerland, October 20-23, 1998. (EUM P24), 101 – 108

Le Marshall,J.F. and L.M. Leslie. 1998. Tropical Cyclone Track Prediction - Using High Resolution Satellite Data with a New Methodology. *Aust. Meteor. Mag.*, **47**, 261 - 266.

Le Marshall, J., L. Leslie, R. Morison, N. Pescod, R. Seecamp, C. Spinoso, 1998c. Recent Developments in the Continuous Assimilation of Satellite Wind Data for Tropical Cyclone Track Forecasting. *Advances in Space Research*. In press..

Le Marshall, J. N. Pescod, R. Seecamp, K. Puri, C. Spinoso and R. Bowen 1999, Local Estimation of GMS-5 Water Vapour Motion Vectors and their Application to Australian Region Numerical Weather Prediction. *Aust. Meteor. Mag.*, **48**, 73 - 77.

Le Marshall, J. F. and L. M. Leslie, 1999. Modelling Tropical Cyclone Intensity. *Aust. Meteor. Mag.*, **48**, 147 - 152.

Leslie, L.M., Le Marshall, J.F., Morison, R.P., Spinoso, C., Purser, R.J., Pescod, N. and Seecamp, R. 1998. Improved hurricane track forecasting from the continuous assimilation of high-quality satellite wind data. *Weath. Rev.*, **126**, 1248-57.

Puri, K., G.S. Dietachmayer, G.A. Mills, N.E. Davidson, R.A. Bowen and L.W. Logan, 1998. The BMRC Limited Area Prediction System, LAPS *Aust. Meteor. Mag*. **47**, 203 - 224.

Seaman, R., W. Bourke, P. Steinle, T. Hart, G. Embery, M. Naughton, and L. Rikus, 1995. Evolution of the Bureau of Meteorology's Global Assimilation and Prediction System, Part 1 : Analysis and Initialisation. *Aust. Meteor. Mag.* **44**, 1 - 18.

A COMPARISON OF TWO ATMOSPHERIC MOTION VECTOR DERIVATION SCHEMES: THE EUMETSAT MSG PROTOTYPING SCHEME AND THE NSMC SCHEME

Xu Jianmin, Kenneth Holmlund, Zhang Qisong, Johannes Schmetz
(NSMC/CMA) (EUMETSAT) (NSMC/CMA) (EUMETSAT)

ABSTRACT

In order to examine the effectiveness of the NSMC scheme, a comparison was arranged under the co-operation frame between EUMETSAT and CMA (China Meteorological Administration). Two periods of data from Meteosat-5 including IR and WV channels were processed and compared by both the EUMETSAT and NSMC schemes. The comparison periods were one week long each, and in January and July respectively. The comparison results show that EUMETSAT AMVs with QI above 0.90 have the least difference compare to ECMWF model output and radiosonde reports. But EUMETSAT AMVs with QI above 0.90 holds less data. NSMC AMVs are closer to ECMWF model output and radiosonde reports than EUMETSAT AMVs with QI above 0.6 and 0.75. In case the two schemes giving different height assignment at IR channel or giving different tracking results, NSMC AMVs are closer with ECMWF model output than EUMETSAT AMVs with QI above 0.6 and 0.75. The NSMC scheme supplies high density AMVs with good quality. This is because the NSMC scheme takes procedure to distinguish high and low clouds before height assignment and takes quality control and optimisation at both tracking and horizontal consistency examining components.

1. Introduction

At the third and the fourth International Wind Workshops detailed papers on ”Calculation of Cloud Motion Wind with GMS-5 Images in China” and “Cloud Motion Winds from FY-2 and GMS-5 Meteorological Satellites” were presented by Xu and Zhong (1996, 1998). The second paper proposed a novel approach to height assignment, using the fact that there is a close correlation between IR and WV channels for high clouds. Thus, correlation between IR and WV measurements is used to distinguish high and low clouds before height adjustment. The height adjustments are only performed for tracers classified as high clouds. Other major differences of the NSMC scheme in comparison to other schemes currently in operational use are as follows:

i) The NSMC scheme does not have a target selection. It makes full use of the targets no matter how small the dynamical range of the target brightness temperature is.
ii) the target tracking is achieved through an optimised search procedure which avoids computing full correlation surfaces. With this procedure, only about 1/6 points on the matrix need to be calculated for the maximum of correlation to be picked up.
iii) The maximum and the second peak of maximum at the two successive image pairs are both considered for more continuous tracking.
iv) Quality control is performed at each component of the NSMC AMV derivation scheme, rather than only at the last step of the scheme.

In order to examine the effectiveness of the NSMC scheme, a comparison was arranged under the co-operation frame between EUMETSAT and CMA (China Meteorological Administration). This paper provides comparison results.

2. Comparison Data and Methods

Two periods of data from Meteosat-5 including IR and WV channels were processed and compared by both the EUMETSAT and NSMC schemes:

- Period 1: from 1200z Jan 1 1999 to 2300z Jan 7 1999, including 14 sets of IR and WV images.
- Period 2: from 1200z July 1 1999 to 2300z July 7 1999, including 14 sets of IR and WV images.

The following comparisons are made:
- Differences between AMVs from the two schemes;
- Differences between ECMWF grid data and AMVs from the two schemes;
- Differences between radiosonde data and AMVs from the two schemes;
- AMVs from the two schemes with large height assignment differences;
- AMVs from the two schemes with large wind speed differences.

ECMWF NWP analysis and forecast data and radiosonde data were used as reference in the comparison. In the NSMC scheme, only AMVs that pass quality control are retained; while in the EUMETSAT scheme, all AMVs derived are kept , however quality indices are assigned to each vector. The NSMC AMVs are compared with the EUMETSAT AMVs with QIs exceeding 0.6, 0.75 and 0.9 , they are written as C, E, G and F respectively.

Comparisons are made for pairs of AMVs in 1-degree latitude/longitude. High level (above 399 hPa), middle level (400-699 hPa) and low level (under 700hPa) AMVs are compared respectively. Interpolations in vertical directions were made for ECMWF and radiosonde data taken part in the comparison. Bias, absolute mean (ABM) and root mean square (RMS) of speed, direction and vector differences are compared for the two comparison periods.

The of the schemes is tested statistically using the F-test. Suppose quantities X and Y are compared. X and Y may be differences of speed, direction or vector speed. Samples of sizes N_X and N_Y are gathered respectively from the two populations X and Y. Suppose RMS_X is larger than RMS_Y . Let $FF=(RMS_X/RMS_Y)^2$. This FF has a F-distribution with (N_X-1, N_Y-1) degree of freedom. In case the value of FF computed from the sample exceeds the critical value at significant level 0.01, with an error probability 0.01 we can say X is larger than Y. By using F-tests, comparison quantities with significant differences are filtered out. The scheme producing AMVs with smaller differences compared with radiosonde or ECMWF grid data are assessed as better.

3. Product Density Associated with Quality Indexes

AMV calculations are performed at different grids in the two schemes. The NSMC scheme calculates winds at every 1-degree latitude/longitude, while the EUMETSAT scheme at every 80-pixels. The grid sizes are different. In the area near sub satellite point, EUMETSAT grid lengths are smaller (Tracers processed are denser); while in the area further from the sub satellite point, NSMC grid lengths are smaller (I.e. more tracers are processed). To make the results comparable, the ratio of the number of AMV products to the total number of tracers processed is adopted as a characteristic quantity . It is named as product ratio. In the EUMETSAT scheme only tracers that meet tracer selection criterion are taken part in the data processing. In the product ratio calculation, tracers not used in data processing are not accounted in total number of tracers processed. For the two comparison periods, product ratios are listed in table 1.

Table 1: Product Ratios for the two omparison periods for NSMC scheme and EUMETSAT scheme with QI 0.6, 0.75 and 0.9, respectively.

Channel, Period	NSMC (C)	EUMETSAT QI 0.6 (E)	EUMETSAT QI 0.75 (G)	EUMETSAT QI 0.9 (F)
IR, Jan.1-7 1999	$\frac{67652}{138334}=48.90\%$	$\frac{42020}{68226}=61.59\%$	$\frac{32878}{68226}=48.19\%$	$\frac{11098}{68226}=16.27\%$
IR, July1-7 1998	$\frac{73141}{138334}=52.87\%$	$\frac{88311}{142628}=61.92\%$	$\frac{66385}{142628}=46.54\%$	$\frac{19472}{142628}=13.65\%$
WV,Jan.1-7 1999	$\frac{74167}{138334}=53.61\%$	$\frac{76885}{141037}=54.51\%$	$\frac{56917}{141037}=40.36\%$	$\frac{22004}{141037}=15.61\%$
WV July1-7 1998	$\frac{76366}{138334}=55.20\%$	$\frac{87899}{155794}=56.42\%$	$\frac{63854}{155794}=44.99\%$	$\frac{18951}{155794}=12.16\%$

From table 1 it is noticed that for IR channel the NSMC scheme and the EUMETSAT scheme with QI 0.75 have a similar product ratio around 50%; for WV channel, NSMC scheme and EUMETSAT scheme with QI 0.6 have similar product ratio around 55%. EUMETSAT scheme with QI 0.9 have much smaller product ratio (around 15%) than NSMC scheme (around 50%). The comparisons between NSMC and EUMETSAT with QI 0.75 for IR channel and between NSMC and EUMETSAT with QI 0.6 for WV channel are considered equal in ability of producing similar density of AMVs.

4. Differences between AMVs derived by the Two Schemes

At first, differences between AMVs derived by the two schemes are compared. Comparison results are as follows:

- AMV speeds from NSMC scheme are smaller than the ones from EUMETSAT scheme. The speed biases of NSMC AMVs minus EUMETSAT AMVs are all negative. This may be due to the tracer size difference;tracer sizes for NSMC and ECMWF are 32*32 and 24*24 pixels respectively.
- All the absolute means of direction differences are less than 10 degrees. Absolute means of speed and vector differences are normally less than 3 m/s, except for WV channel in middle level where the absolute mean speed and vector differences of NSMC AMVs compare with EUMETSAT AMVs with QI above 0.6 and 0.75 reach 4 to 5 m/s.
- Comparison between AMVs derived by the two schemes shows that except for differences of NSMC AMVs compare with EUMETSAT AMVs with QI above 0.6 and 0.75 at WV channel in middle level, all differences are reasonably small. Larger differences of NSMC AMVs compare with EUMETSAT AMVs with QI above 0.6 and 0.75 at WV channel in middle level will be further analysed in section 8.

5. Differences between AMVs and ECMWF Analyses

AMVs derived by both the schemes are compared with the ECMWF grid wind vectors. In the observation area of Meteosat-5, the radiosonde stations are not well distributed. ECMWF model output is the reality examination data with good distribution.
The comparison results above 0.01 statistical significant level at F-tests were shown in table 2.

Table 2: Speed, Direction and Vector Differences of AMVs Versus ECMWF Data above 0.01 Statistical Significant Level at F-tests.

Channel Level	January Speed	January Dir.	January Vector	July Speed	July Dir.	July Vector
IR High Level	F/C C/G C/E	F/C C/G C/E	F/C C/G C/E	F/C C/G C/E	F/C C/G C/E	F/C C/G C/E
IR Middle Level	F/C G/C E/C	F/C C/G C/E	F/C	F/C C/G C/E	F/C C/G C/E	F/C C/G C/E
IR Low Level	C/G C/E	C/G C/E	C/G C/E	F/C C/G C/E	F/C C/E	F/C C/G C/E
WV High Level	F/C C/G C/E	F/C G/C E/C	F/C	F/C C/E	F/C G/C E/C	F/C C/G C/E
WV Middle Level	F/C C/G C/E	F/C G/C E/C	F/C C/G C/E	F/C C/G C/E	F/C	F/C C/G C/E

C is NSMC AMVs. E is EUMETSAT AMVs with QI above 0.6. G is EUMETSAT AMVs with QI above 0.75. F is EUMETSAT AMVs with QI above 0.9. Schemes list as numerators are assessed with significantly smaller difference compare with ECMWF model output.

In each box of table 2, comparisons with statistical significance are shown. The schemes listed as numerators are the ones with significant smaller differences compared with radiosonde data. In case the F-test is not passed, the related box remains empty. From table 2, it is shown clearly that EUMETSAT AMVs with QI above 0.9 have the least differences comparing with ECMWF model output. Considering EUMETSAT AMVs with QI above 0.9 have already simulated into the ECMWF analysis, this is expected. Since the NSMC scheme is independent from NWP output, reasonable larger differences may mean that there is information in the NSMC AMVs. It is also noticed that product ratio of EUMETSAT AMVs with QI above 0.9 is around 15%-- less than one third of the NSMC scheme.

For most comparison items, the NSMC scheme has smaller differences than EUMETSAT AMVs with QI above 0.6 and 0.75. This fact clearly shows ability of the NSMC scheme at producing good quality AMVs with high density. The product ratio of the NSMC scheme is normally above 50%. In low level EUMETSAT IR AMVs with QI above 0.6 and 0.75 have quite large differences compare with ECMWF output. The amount of low level IR AMVs produced by EUMETSAT scheme is also very limited especially in January 1-7 1999. On the other hand, NSMV AMVs are relatively more in number and closer to ECMWF model output. This may be due to the height assignment procedure adopted by the NSMC scheme.

6. Differences between AMVs and radiosonde wind vectors

Differences between AMVs and radiosonde wind vectors are compared. The comparisons with 0.01 significant level of statistics at F-tests were shown in table 3.

Table 3 Speed, Direction and Vector Differences of AMVs Versus Radiosonde Data above 0.01 Statistical Significant Level at F-tests

Channel Level	January Speed	January Dir.	January Vector	July Speed	July Dir.	July Vector
IR High Level	F/C	F/C C/G C/E	F/C C/E	C/F C/G C/E	C/G C/E	C/F C/G C/E
IR Middle Level		C/E C/G		F/C C/G C/E	C/G C/E	F/C C/G C/E
IR Low Level				C/G C/E	C/E	C/G C/E
WV High Level	C/G C/E	F/C C/G C/E	F/C C/G C/E	F/C C/G C/E		F/C
WV Middle Level	C/G C/E	F/C C/E	C/G C/E	C/G C/E	C/G C/E	C/G C/E

In each box of table 3, comparisons with statistical significance are shown. The schemes list as numerators are the ones with less difference compared with radiosonde data. In case the F-test is not passed, the related box remains empty. Table 3 shows that in general EUMETSAT AMVs with QI above 0.9 have the smallest difference compare with radiosonde data. But in July 1-7 1998 in high level, IR AMVs of NSMC have smaller differences compared with radiosonde data than the ones of EUMETSAT with QI above 0.9. In low level, the amount of EUMETSAT AMVs with QI above 0.9 is too small to get significant statistic results. This fact shows the good performance of NSMC scheme at IR channel especially in Northern Hemisphere summer. The good performance of NSMC IR winds at both high and low levels is explained because of the algorithm to distinguish high and low clouds before height assignment. This ability will be further verified in section 6. Table 3 also shows that for the comparison with radiosonde data in all the cases, NSMC AMVs have smaller differences than EUMETSAT AMVs with QI above 0.6 and 0.75. This will be further discussed in section 7.

7. Comparison of AMVs with Large Height Assignment Differences

In the same location (in 1-degree latitude/longitude), in case the height assigned by the two schemes exceed 400 hPa, pairs of data are picked out and compared with ECMWF wind vectors respectively. F-tests were performed at speed, direction and vector differences with ECMWF model output respectively. The comparison results above 0.01 significant level of statistics at F-tests were shown in table 4.

Table 4 Differences between ECMWF Data and IR AMVs Derived from NSMC and EUMETSAT for cases exceeding Height Assignment Differences of 400 hPa tested for a 0.01 Statistical Significant Level with an F-tests

Period	Speed	Direction	Vector
Jan.1-7 1999	C/F C/G C/E	C/F C/G C/E	C/G C/E
July1-7 1998	F/C C/G C/E	C/F C/G C/E	F/C C/G C/E

In each box of table 4, comparisons with statistical significance are shown. The schemes taken as numerators are the ones with less difference compared with ECMWF data. In case F-test not passed, the related box leaves empty. Table 4 shows, for the cases the two schemes give different height assignment for the IR channel, which scheme produces AMVs closer to the ECMWF model output. In both periods for all the comparison items NSMC AMVs are closer to ECMWF model output than EUMETSAT AMVs with QI above 0.6 and 0.75. In January 1-7 1999 NSMC scheme performs even better than EUMETSAT AMVs with QI above 0.9 at speed and direction comparisons. This comparison shows that NSMC scheme has a good ability for IR channel height assignment. This is because the NSMC scheme has a novel procedure to distinguish high and low clouds before height assignment.

8. Comparison of AMVs with Speed Difference

In the same location (in 1-degree latitude/longitude), in case the vectors tracked out by the two schemes exceed 6 m/s, pairs of data are picked out and compared with ECMWF wind vectors respectively. F-tests were performed at speed, direction and vector differences with ECMWF model output respectively. The comparison results above 0.01 significance level for the F-tests are shown in tables 5 and 6. Tables 5 and 6 are for IR and WV AMVs respectively.

Table 5: Differences between ECMWF Data and IR High Level AMVs Derived from NSMC and EUMETSAT with Speed Difference Exceed 6 m/s and above 0.01 Statistical Significant Level at F-tests

Period	Speed	Direction	Vector
Jan.1-7 1999	C/F C/G C/E	C/F C/G C/E	C/G C/E
July1-7 1998	C/G C/E	C/F C/G C/E	C/G C/E

The schemes listed as numerators are the ones with less difference compared with ECMWF data. In case F-test not passed, the related box leaves empty.

Table 6 Differences between ECMWF Data and WV AMVs Derived from NSMC and EUMETSAT with Speed Difference Exceed 6 m/s and above 0.01 Statistical Significant Level at F-tests

Period	Speed	Direction	Vector
Jan.1-7 1999	C/F C/G C/E	C/G C/E	C/G C/E
July1-7 1998	C/F C/G C/E	C/G C/E	C/G C/E

The schemes list as numerators are the ones with less difference compared with ECMWF data. In case F-test not passed, the related box leaves empty.

Tables 5 and 6 show, that in cases the two schemes give different tracking results, which scheme produces AMVs closer to the ECMWF model output. For all comparison items NSMC AMVs are closer with ECMWF model output than EUMETSAT with QI above 0.6 and 0.75. For some comparison items in some periods, NSMC AMVs are even closer with ECMWF model output than EUMETSAT with QI above 0.9.

9. Conclusion and Summary

Major comparison results are as follows:

- For the IR channel the NSMC scheme and EUMETSAT scheme with QI 0.75 have similar product ratio around 50%. For WV channel, NSMC scheme and EUMETSAT scheme with QI 0.6 have similar product ratio around 55%. EUMETSAT scheme with QI 0.9 have much smaller product ratio (around 15%) than NSMC scheme (around 50%).
- Comparison between AMVs of the two schemes shows no major differences. All the ABM direction differences are less than 10 degrees. ABM speed and vector differences are normally less than 3 m/s.

Comparison with ECMWF model output and radiosonde data

- Comparing with ECMWF model output and radiosonde data, EUMETSAT AMVs with QI above 0.9 have the smallest differences, however at the expense of supplying a smaller amount of data. For most comparison items, NSMC AMVs are closer to the ECMWF model output and radiosonde reports than EUMETSAT AMVs with QI above 0.6 and 0.75. This fact clearly shows ability of the NSMC scheme to produce good quality AMVs with high density.

Comparison to IR tracers at same location but being assigned by the two scheme with different heights.

- In case the two schemes give different heights using the IR channel, NSMC AMVs are closer to ECMWF model output than EUMETSAT AMVs with QI above 0.6 and 0.75. In January 1-7 1999 NSMC scheme performs even better than EUMETSAT AMVs with QI above 0.9 at speed and direction comparisons. This comparison shows that NSMC scheme has a good ability for IR channel height assignment. This is because the NSMC scheme distinguishes high and low clouds before height assignment.

Comparison to tracers at same location but being tracked as to have different motion

- In case the two schemes give different tracking results, NSMC AMVs are closer with ECMWF model output than EUMETSAT AMVs with QI above 0.6 and 0.75. For some comparison items in some periods, NSMC AMVs are even closer with ECMWF model output than EUMETSAT with QI above 0.9. This is because the NSMC scheme performs quality control and optimisation at the tracking and the step when horizontal consistency examined. At tracking step, a most consistent pair is chosen from the two largets correlation peaks. For the horizontal consistency examination height assignment results are adjusted by re-selecting results previuosly rejected. Quality control and optimisation at each component of the data processing give contribution to dense data with good quality.

Figure 1 supplies samples of AMV products from the two schemes. In general EUMETSAT AMVs with QI above 0.90 have the smallest difference in comparison to ECMWF model output and radiosonde reports. But EUMETSAT AMVs with QI above 0.90 supply less data. NSMC AMVs are closer to ECMWF model output and radiosonde reports than EUMETSAT AMVs with QI above 0.6 and 0.75.

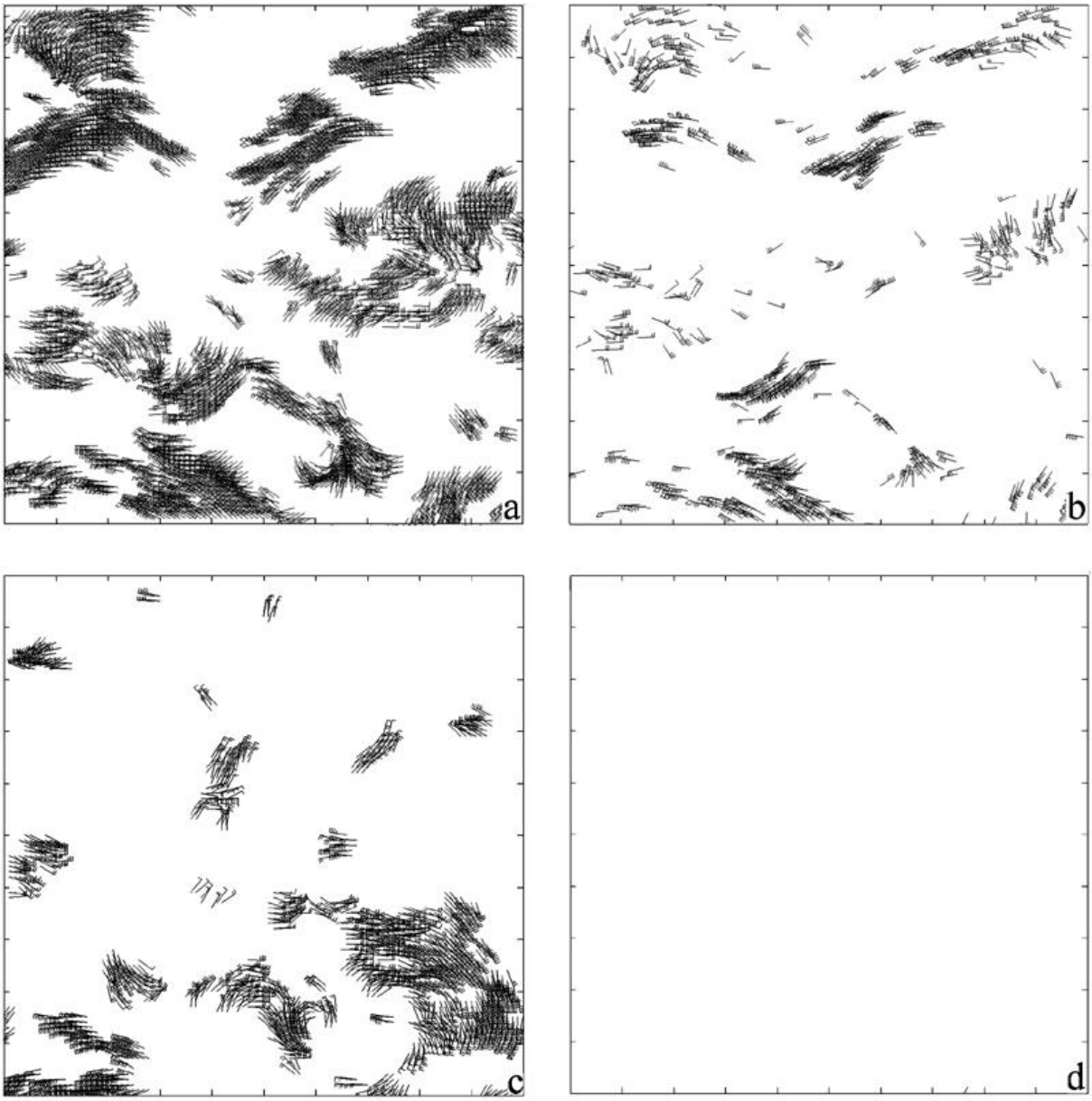

Fig.1 IR AMVs at 1200Z January 3 1999 a) High level AMVs derived by NSMC b) High level AMVs derived by EUMETSAT scheme with QI 0.9 c) Low level AMVs derived by NSMC d) Low level AMVs derived by EUMETSAT scheme with QI 0.9

REFERENCES

Baker W. E., 1991: Utilisation of Satellite Winds for Climate and Global Change Studies, Proc. NOAA Conference on Operational Satellites: Sentinels for the Monitoring of Climate and Global Change. *Global Planetary Change*, **4**, 157-163 (special issue)

Baum B. A., Arduini R. F., Wielick B. A., Minnis P. and Tsay S.L., 1994: Multilevel Cloud Retrieval Using Multispectral HIRS and AVHRR data: Night Time Oceanic Analysis, *J. G. R.*, **99**(D3) 5499-5514

Hayden C. M. and Purser R. J., 1995: Recursive Filter Objective Analysis of Meteorological Fields: Applications to NESDIS Operational Processing, *J. Appl. Meteor.* , **34**, 3-15

Inoue T., 1985: On the Temperature and Effective Emissivity Determination of Semi-Transparent Cirrus Clouds by Bi-Spectral Measurements in the 10 μm Window Region, *J. Meteor. Soc. Japan*, **63(1),** 88-89

Kallberg E., Uppala S., Gustafsson N. and Pailleux J., 1982: The Impact of Cloud Track Wind Data on Global Analysis and Medium Range Forecast, ECMWF Tech. Rep. 34, 60pp.

Kalnay E., Jusem J. C. and Pfaendtner J., 1985: The Relative Importance of Mass and Wind Data in Present Observing System, Report of the NASA Workshop on Global Wind Measurements, Baker W. E. and Curran R. J. Eds. , A. Deepak Publishing, 1-5

Leese J. A., Novak S. and Clark B., 1971: An automated technique for obtaining cloud motion from geosynchronous satellite data using cross correlation, *J. Appl. Meteor.* , **10**, 118-132

McLeese D. J. and Wilson L. S., 1976: Cloud Top Heights from Temperature Sounding Instruments, *Quart. J. Roy. Meteor. Soc.*, **102**, 781-790

Menzel W. P., Smith W. L. and Stewart T. R., 1983: Improved Cloud Motion Wind Vector and Altitude Assignment Using VAS, *J. Clim. Appl. Meteor*., **22**, 377-384

Nieman S. J., Schmetz, J. and Menzel W. P., 1993: A Comparison of Several Techniques to Assign Heights to Cloud Tracers, *J. Appl. Meteor.* , **32**, 1559-1568

Pailleux J., 1987: The Impact of Satellite Data on Global Numerical Weather Prediction, Remote Sensing Applications in Meteorology and Climatology, Vaughan R. A. Ed., 173-187

Parol F., Buriez J. C., Brogniez G. and Fouquart Y., 1991: Information Content of AVHRR Channel 4 and 5 with respect to the Effective Radius of Cirrus Cloud Particles, *J. Appl. Meteor*., **30**, 873-984

Schmetz J., Holmlund K., Hoffman J. and Strauss B., 1993: Operational Cloud Motion Winds from Meteosat Infrared Images, *J. Appl. Meteor.* , **32**, 1206-1225

Schmetz J., Hinsman D., Menzel W.P., 1999: Summary of the Fourth International Winds Workshop, B. A. M. S., 80, 893-899

Szejwach G., 1982: Determination of Semi-Transparent Cirrus Cloud Temperature from Infrared Radiance Application to Meteosat, *J. Appl. Meteor.* , **21**, 384-393

Wu Q. X., 1995: A Correlation-Relaxation-Labelling Framework for Computing Optical Flow---Template Matching from a New Perspective, *IEEE Trans. On Pattern Analysis and Machine Intelligence*, **17(9)**, 843-853

Xu Jianmin and Zhang Qisong, 1996: Calculation of Cloud Motion Wind with GMS-5 Image in *China, The Third International Wind Workshop*, 45-52

Xu Jianmin, Zhang Qisong and Fang Xiang, 1997: Height Assignment of Cloud Motion Winds with Infrared and Water Vapour Channels, *Acta Meteorologica Sinica*, **55**, 408-417

Xu Jianmin, Zhang Qisong, Fang Xiang and Liu Jian, 1998: Cloud Motion Winds from FY-2 and GMS-5 Meteorological Satellites, *The Forth International Wind Workshop*, 41 – 48

SESSION II

VERIFICATION AND OBJECTIVE QUALITY ANALYSIS

Chairperson: M. Tokuno

MONITORING SATELLITE WINDS AT ECMWF

F. Lalaurette and A. Garcia-Mendez

European Centre for Medium-range Weather Forecast
Shinfield Park, Reading GB-RG2 9AX

ABSTRACT

Although most of the satellite wind monitoring information is now part of the joint UKMO-ECMWF participation in the NWP-SAF presented by Butterworth et al., some monitoring information is not part of this initiative. Information on data availability that is presented is kept updated daily on ECMWF web site with public access. It is also shown that aircraft data that are now available in increasing numbers are confirming the longstanding issue of satellite winds underestimation first revealed by radiosonde collocations. This bias puts a major limitation on the real impact of satellite winds in the jet areas. It is therefore suggested that bias correction methods are tested that would allow numerical models to use this information were it could be of crucial importance for the timely forecast of extratropical developments.

1. Introduction

The main changes in the monitoring activities of ECMWF in recent years have been related to slowly bringing the information to the users (data providers and forecast users) in a more friendly way using our Web server (http://www.ecmwf.int). Although most of this effort has been shared with the UK Met. Office as part of the NWP SAF initiative (see the co-signed contribution Butterworth et al. in the same volume), some types of useful information do not fit in this framework. They are mainly related to data availability and coverage and to intercomparison with independent sources of observation. Recent findings derived from these diagnostics will therefore be summarised in this contribution, together with some discussion on the impact of satellite winds on the model description of the atmospheric state and on plans for future developments.

2. Data monitoring information made available on ECMWF WEB server

This information is publicly available at the following address:

http://www.ecmwf.int/services/dcover/index.html

It includes data coverage maps over the last 24h (four assimilation cycles) and time series showing the amount of data received over the last 30 days. In contrast with comments made at the last Winds Workshop (Lalaurette et al., 1998), only minor problems could be found in recent months. The flow of data was mostly uninterrupted, and one of the only disruptions is visible in Figure 1 when data were missed for a few days when Meteosat7 went through its decontamination program.

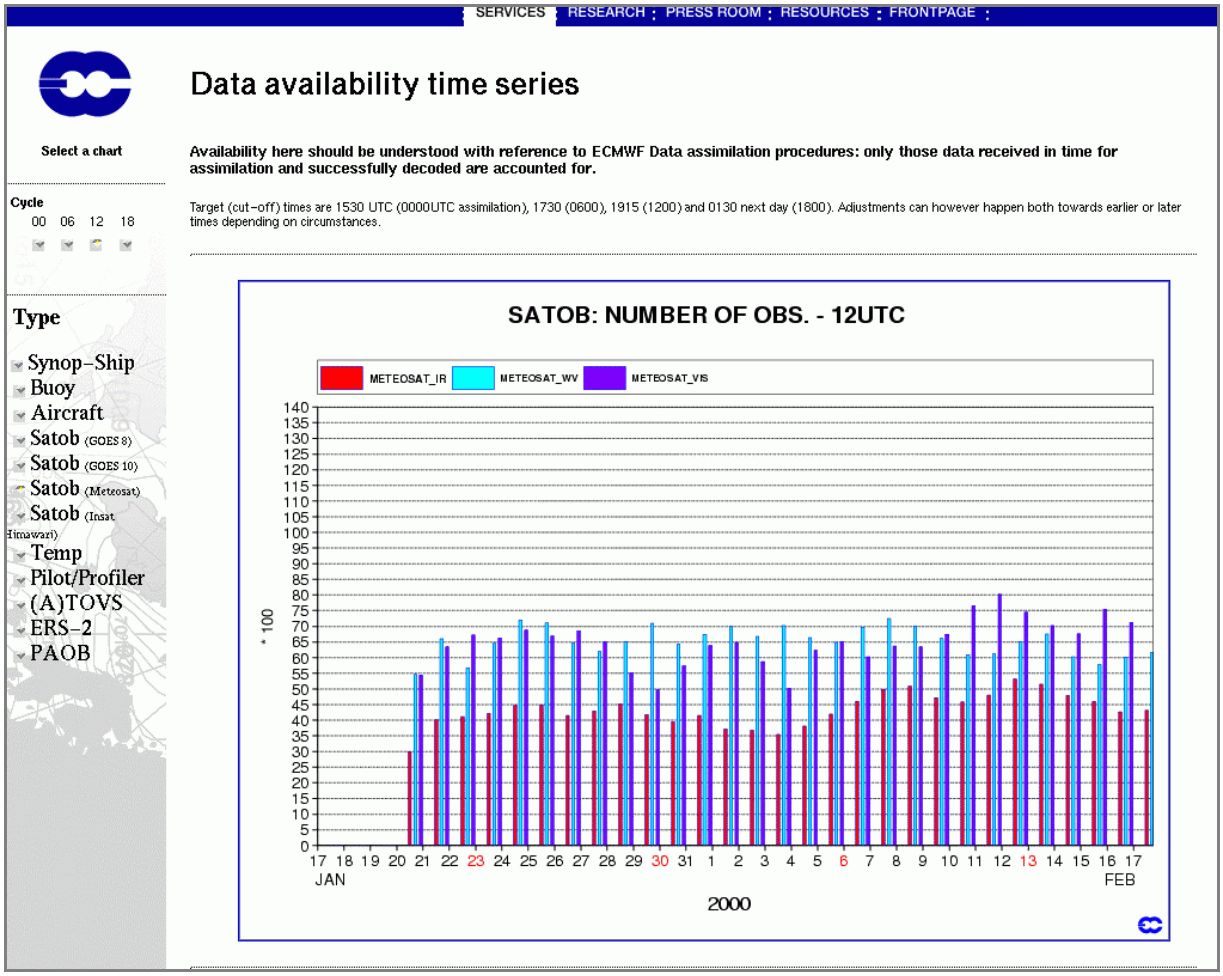

Figure 1. Time series of Meteosat-7 winds available at ECMWF from 18 January to 17 February 2000 (9-15UTC). No data selection or thinning is applied at this stage. The information is shown as available from ECMWF Web site.

Since the quality control decisions are now delayed to the data assimilation stage in the case of METEOSAT winds processed in BUFR format together with their Quality Indicator, the coverage can be seen to have increased again (Figure 2). This service is currently under development. More information on the data monitoring (satellite radiance should be the first step) and daily information on the data active and/or rejected should also be added. These although are likely to be given limited access by ECMWF Member States except when data providers have given permission to issue such information – as is the case with NESDIS and EUMETSAT for raw radiance.

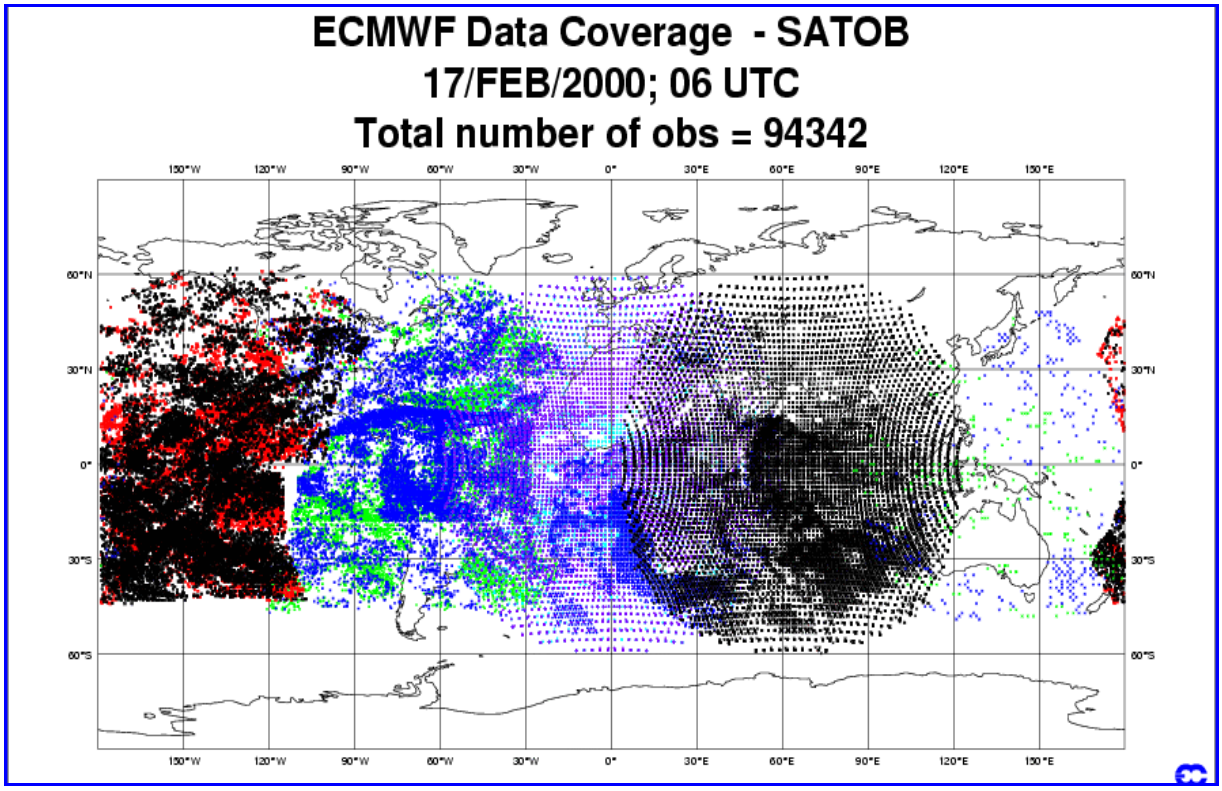

Figure 2. Data coverage given by all satellite winds dated 17 February 2000 between 03 and 09UTC and processed at ECMWF. No data selection or thinning is applied at this stage. The information is shown as available from ECMWF Web site.

3. Collocation statistics (aircraft and radiosondes)

Although model performance is steadily improving with time, the fit of satellite winds to the model cannot be taken as an absolute reference, the last reason not being that the quality of these observed data is also due to improve following refinements in both instrumentation and wind retrieval techniques. This is why in complement to statistics based on model comparisons (Butterworth et al.) statistics are gathered when satellite winds are collocated with other sources of observations. Although most of the emphasis is usually put on the comparison to radiosondes, there is an increasing benefit to be taken from a comparison to aircraft measurements. The reasons for this are:

1) the large improvement in quality that has followed the automation of most reports and
2) the increased coverage of data that followed the efforts paid by several Meteorological Agencies to collect these data from their national airlines for the common benefit of the meteorological community (Figure 3)

As a result, it can probably be safely argued that the total number of in-situ data has increased very significantly in recent years, at least for those atmospheric layers where most commercial air traffic occurs (400-200 hPa). Aircraft data have the further advantage of covering some oceanic areas where radiosondes are usually not available.

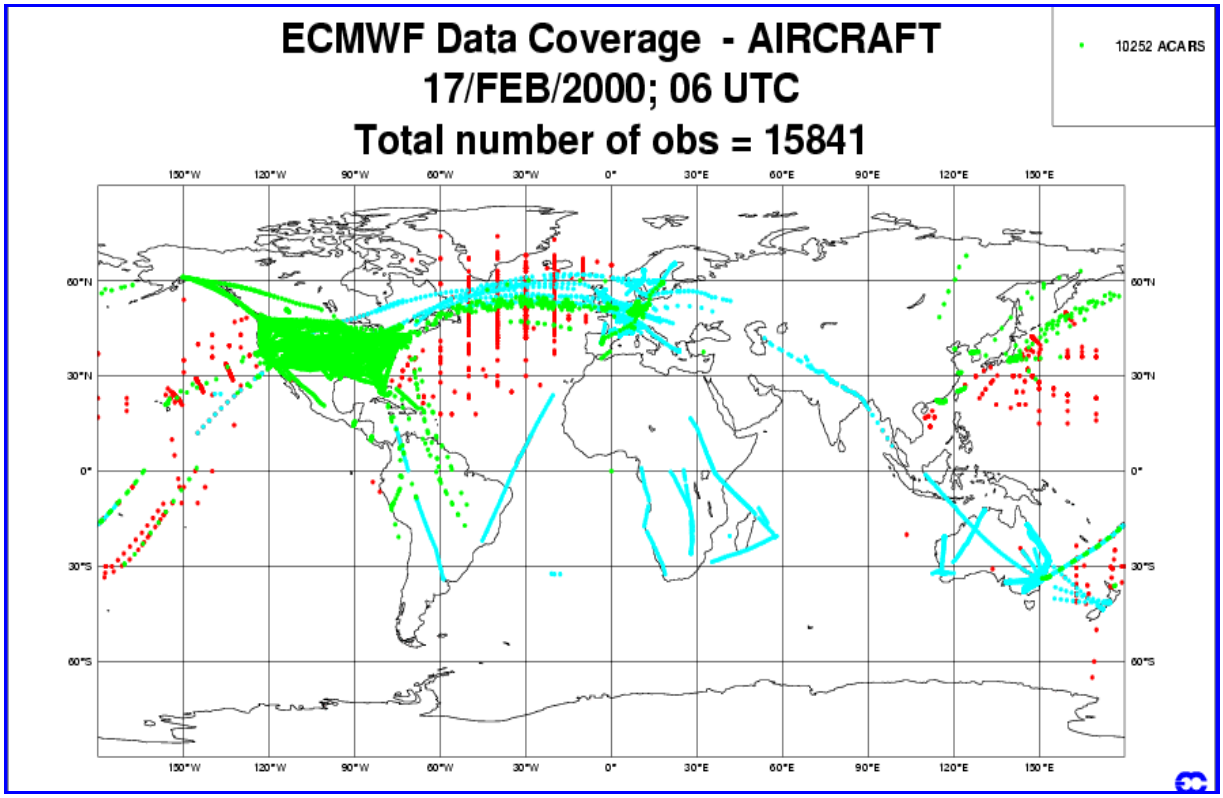

Figure 3. Data coverage given by all aircraft reports dated 17 February 2000 between 03 and 09UTC and processed at ECMWF. No data selection or thinning is applied at this stage. The information is shown as available from ECMWF Web site.

Collocation statistics usually point to the same conclusions whether satellite winds are compared to aircraft or radiosonde data, except by the end of the distribution when data are not available in large enough numbers to retrieve stable statistics (Figure 4). METEOSAT and HIMAWARI show similar signatures: an increasing underestimation for increasing values of the satellite wind, by about 10% in the case of METEOSAT, almost 20% for HIMAWARI. The bias for high-level GOES winds is almost independent of the wind speed, and point to an underestimation by about 2-3 $m.s^{-1}$ in the range 10 to 60 $m.s^{-1}$. That there is no dependence on the observed range of wind speed shows that the linear correction applied by the data providers is correct, a procedure that is not applied to METEOSAT and HIMAWARI data. It cannot however from these figures be deducted whether the bias is related to an underestimation of the wind by the target displacements, or to height assignment errors. A remarkable feature of GOES winds on the other hand is that the fit to the model is better than to in-situ observations (at least for ranges below 45 $m.s^{-1}$). This could be the result of the recursive filters applied to the GOES winds before dissemination that transform the data into winds that are more representative of the scales observed by the model (50-100km) than in-situ measurements by aircraft and radiosondes.

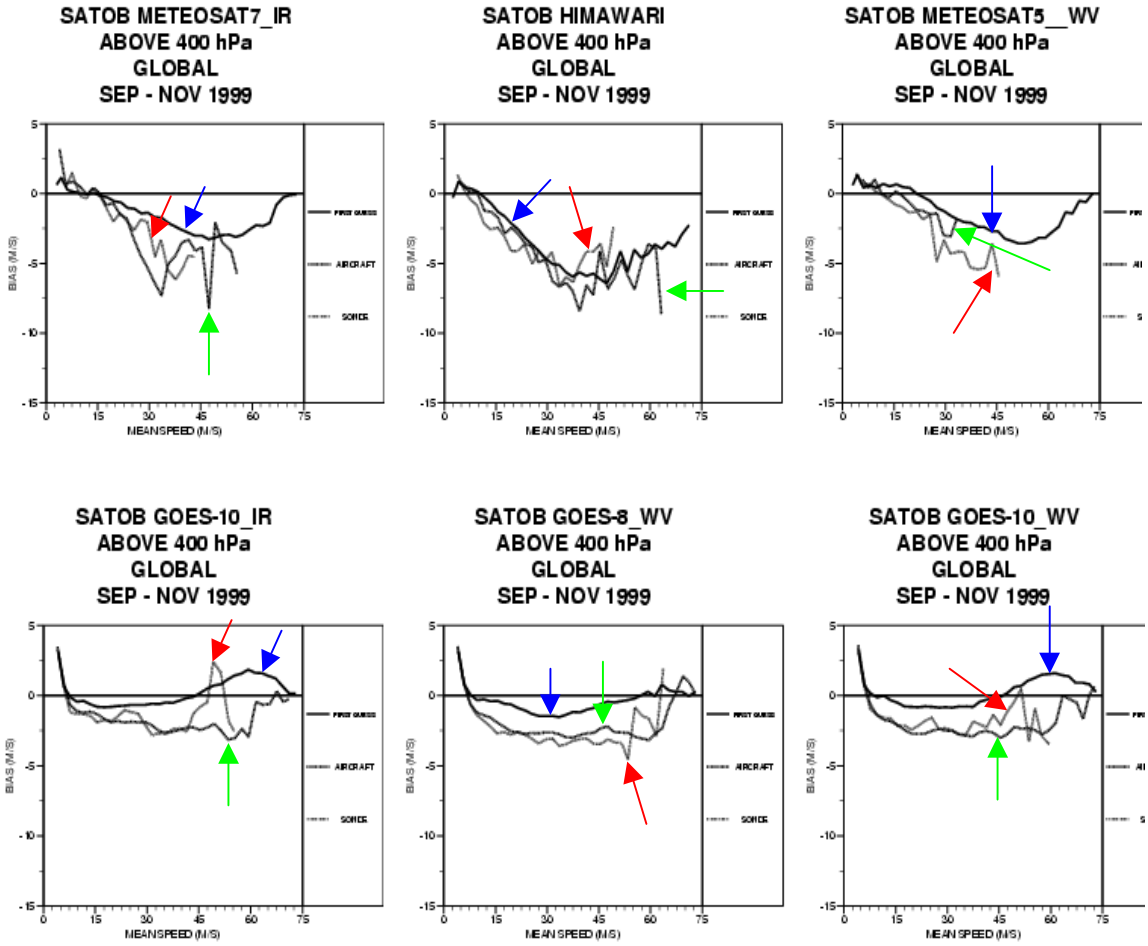

Figure 4. Comparison of high level (P<400hPa) satellite winds with collocated model winds (blue) and winds measured from radiosondes (red) and aircraft (green). Horizontal axis is labelled according to the satellite wind speed, vertical axis is the mean bias (collocated – satellite).

Data from aircraft are now coming in numbers large enough to allow scatter diagrams to be drawn that will avoid some of the problem that may affect the bias curves such as shown in Figure 4 when dealing with one-sided distributions. Such scatter diagrams are shown in Figure 5. They very clearly confirm the overall underestimation of the winds provided by both METEOSAT and HIMAWARI. They also show that there is little information to be taken from the mean bias values, as the bias exhibits roughly a linear dependency with observed winds. The mean bias is likely to largely underestimate the underestimation problem as strong winds are outnumbered by slow winds in the global statistics.

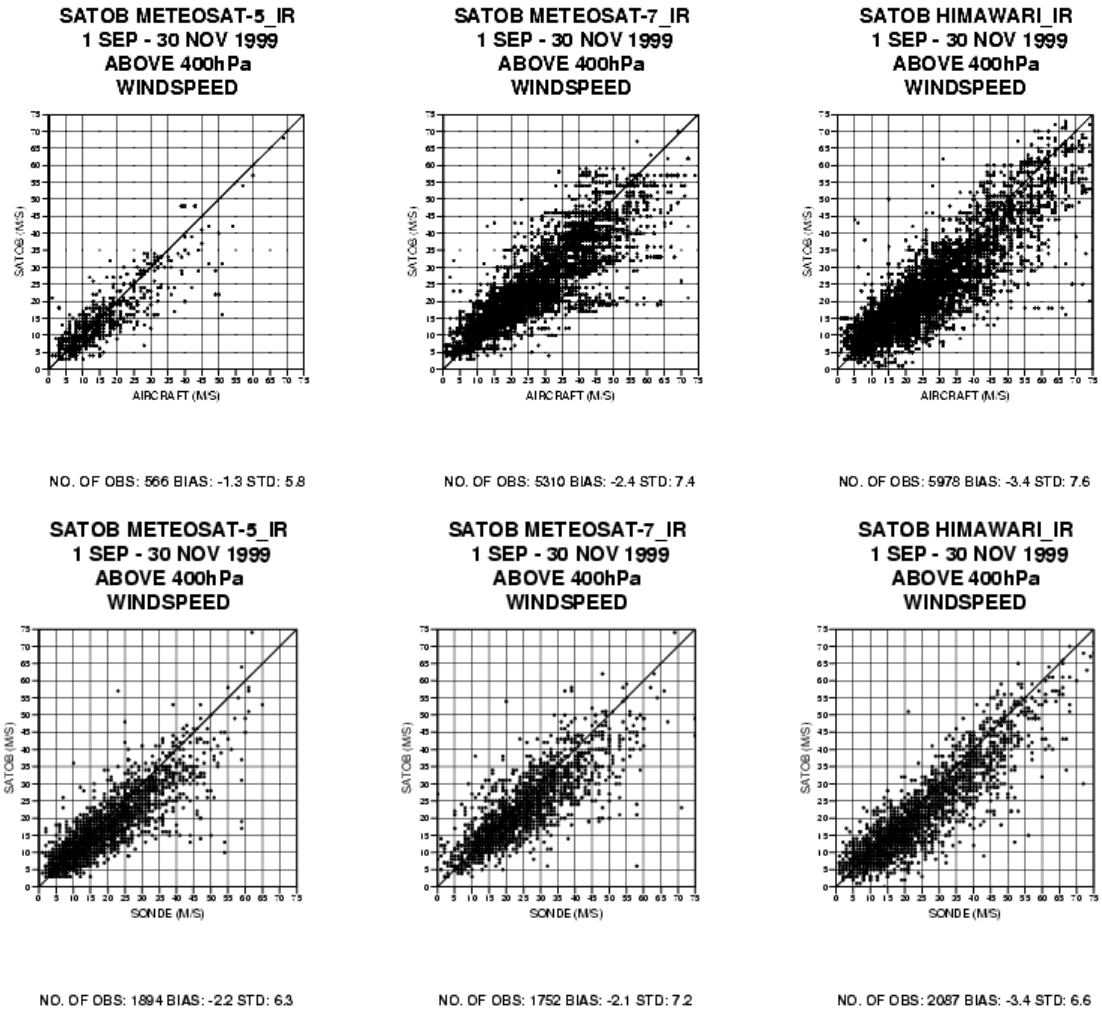

Figure 5: Scatter diagrams showing satellites winds (vertical axis) compared to collocated measures from aircraft (upper row) and radiosondes (lower row).

4. Summary: Can we make a better use if satellite winds?

Current data assimilation methods can handle random observation or representativity errors, but not systematic (biased) ones. This is why bias correction methods have to be applied before the data are provided to the model assimilation software, which is a common calibration process applied to data as different as scatterometer data, radiosonde temperatures or satellite brightness temperatures. Such calibrations are currently not applied to satellite winds, on the basis that the tracking techniques do identify motion vectors directly – and not through a quantity that is only indirectly related. An example of the latter type of winds are scatterometer winds that are related to the electromagnetic signal backscattered to space through the sea surface properties, which in turn are well related to the surface wind. However whatever the physical interpretation, results like seen on Figure 4 and Figure 5 confirm that satellite winds cannot be used as any other winds by the data assimilation system, as they will systematically slow down the most active jet streams.

The present solution used to overcome this problem is to introduce an asymmetric check on satellite winds. This check gives more confidence to slow winds than to fast ones, with the effect that any satellite wind slower than the model forecast by more than 4ms^{-1} for ranges beyond 60ms^{-1} will be rejected. This results in satellite winds being not used in those areas where they should be of crucial importance to early detect jet streams perturbations or jet streaks. A typical such rejection map is shown in Figure 6.

In order to let satellite winds bring their full information in situation that really matters, it is therefore suggested that the bias problem identified in section 3 is addressed with a high priority. This calibration should never be applied blindly and overwrite the basic displacement information provided by the automated tracking software. Whether the problem is solved by refining the height assignment procedures or by applying the bias correction to the wind value is a matter for careful studies.

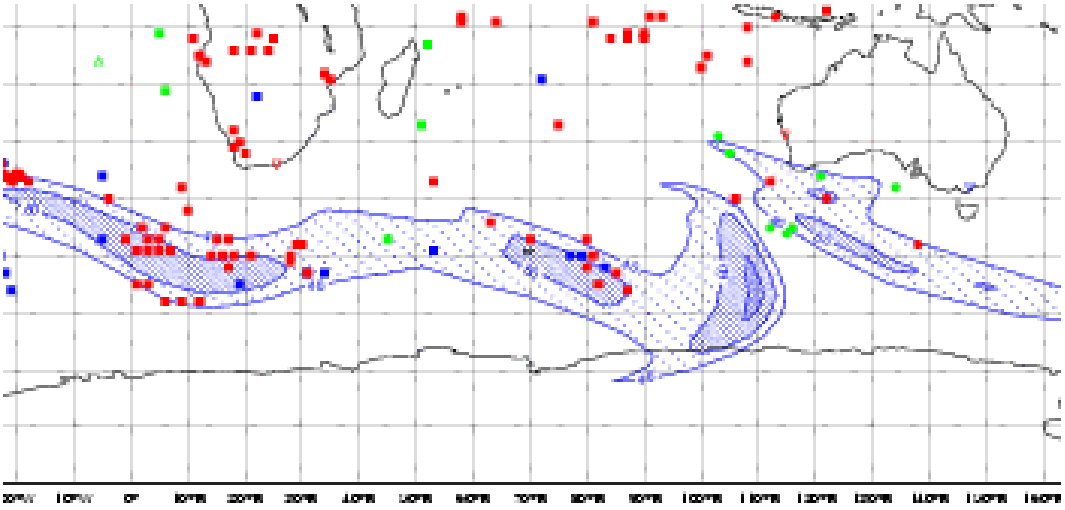

Figure 6. Rejection map (17 Feb. 2000 12UTC) showing the collocation of rejected data with the jet stream (shaded blue).

REFERENCES

Butterworth P., F. Lalaurette, B. J. Conway and A. Garcia-Mendez (2000). The NWP SAF integrated satellite wind monitoring report. Proc. 5th Int. Winds Workshop, Lorne, Australia, March 2000.

Lalaurette F., A. Garcia-Mendez and M. Rohn (1998) Monitoring AMV at ECMWF. Proc. 4th Int. Winds Workshop, Saanenmoser, Switzerland, October 1998.

Tomassini, M., G. Kelly and R. Saunders (1997) Use and impact of satellite atmospheric motion winds on ECMWF analyses and forecasts. EUMETSAT/ECMWF Fellowship Research Programme Report, November 1997.

IMPROVED QUALITY ESTIMATES OF ATMOSPHERIC MOTION VECTORS UTILISING THE EUMETSAT QUALITY INDICATORS AND THE UW/CIMSS AUTO-EDITOR

Kenneth Holmlund[1], Christopher S. Velden[2]
and
Michael Rohn[3]

1) EUMETSAT, Darmstadt, Germany
Am Kavalleriesand 31
64293 Darmstadt
Germany

2) Co-operative Institute for Meteorological Satellite Studies, Madison, Wisconsin
3) European Centre for Medium range Weather Forecasting, Reading, UK

ABSTRACT

The development of reliable Automatic Quality Control (AQC) schemes has played a key role in the development of the new high density and high frequency Atmospheric Motion Vector (AMV) products at UW/CIMSS and EUMETSAT. Despite the fact that the AQC schemes in the two organisations differ significantly it has previously been shown that both schemes are capable of assigning reliability factors to every extracted vector. The two approaches both seem to have areas where they perform well, but simultaneously they also have some shortcomings. Therefore it has been a natural development to try to combine the two schemes in order to derive an even better approach for AQC.

The preliminary comparisons of the two schemes were already presented at the 4th International Winds WorkShop. Based on these results a combined AQC-scheme was developed and verified. This new approach was applied to high-density wind fields derived with both GOES and GMS imagery data during the North Pacific Experiment (NORPEX-98). In the combined approach the QI was used as a precursive filter to the AE and within the ECMWF assimilation scheme for data screening. The impact of the combined scheme was better than either scheme alone. This paper will present the new combined approach and the validation results from NORPEX-98.

1. Introduction

Since the launch of the first geostationary satellites the data has been used to improve the knowledge and description of atmospheric flow especially over the large ocean regions that are void of traditional land based observations. Today the Atmospheric Motion Vectors (AMVs) derived from sequences of image data from the geostationary meteorological satellites have established themselves as an imperative part of the global observation system essential to medium range weather forecasting (e.g. Kelly, 1993) and also for the prediction of severe weather (e.g. Velden 1998). The main problem of the AMV extraction schemes is that several of the extracted targets are not suitable to be used as passive tracers for atmospheric flow and that the matching techniques do not always find the correct target location in the subsequent images. Furthermore the height assignment invariable gives gross errors in the pressure estimates. Therefore it is imperative to employ quality control to remove poor vectors that do not represent the instantaneous atmospheric flow. The large amount of vectors that are currently derived is too demanding for manual editing. Therefore, emphasis has been placed on the research and development of robust Automated Quality Control (AQC) procedures that are capable of removing suspect vectors related to tracking, height assignment and tracer representation errors. Furthermore, these schemes are being designed to provide a quality estimate for each individual displacement vector,

as well as provide information on how representative these vectors are to instantaneous motion at a single tropospheric level. These quality estimates can be employed by the user community to select the part of the vector field that best suites their application, as well as in data assimilation schemes for optimising the data selection procedures.

The AQC schemes developed at EUMETSAT and UW-CIMSS that are currently employed at their respective national AMV extraction centres have already been presented at the 4th International Winds Work Shop (Holmlund and Velden, 1996). The results from their inter-comparison study showed the strengths and weaknesses of the two respective approaches. Based on the previous work a new combined quality control approach that takes advantage of the strengths of each method was developed. This scheme is presented together with validation results based ECMWF (European Centre for Medium range Weather Forecasts) model forecast impact studies based on a common data set derived during the NORPEX (NORth Pacific Experiment) field campaign.

2. Comparison of the EUMETSAT and the UW-CIMSS AQC Schemes

The results from the initial comparison of the EUMETSAT AQC and the CIMSS RFF scheme were presented at the previous winds workshop (Holmlund and Velden, 1996). The main conclusions from the inter-comparison were the following:

Both schemes classify in general the AMVs in a similar fashion
The UW-CIMSS scheme is capable of deriving more coherent wind fields
The UW-CIMSS scheme can recover some height assignment failures by re-adjusting the derived heights
The EUMETSAT scheme is capable of retaining more winds in fast flow regimes
The EUMETSAT scheme lends itself more easily for implementation and interpretation
The best vectors are those accepted by both schemes whereas the winds rejected by both schemes simultaneously seem to have the lowest reliability as single point measurements. These findings are summarised in Table 1, showing the nrms (rms normalised with wind speed for four quality categories.

Table 1. nrms for AMVs vs. NCEP 12-hr forecast at different levels (High=H (above 400 hPa), Medium=M (400 – 700 hPa) and Low=L (below 700 hPa), for three channels (IR, WV and VIS) and for different combinations of RFF and QI. The number of collocations is in brackets for each case. Winds with a RFF > 50 are accepted by the CIMSS scheme, whereas winds with a QI > 0.60 are considered to be good by the EUMETSAT scheme.

	RFF > 50 QI > 0.60	RFF < 50 QI > 0.60	RFF > 50 QI < 0.60	RFF < 50 QI < 0.60
IR, H	0.39	0.47	0.70	0.78
WV, H	0.39	0.41	0.69	0.66
IR, M	0.26	0.56	0.57	1.12
WV, M	0.24	0.43	0.47	0.82
IR, L	0.35	1.48	0.51	1.45
VIS	0.32	0.37	0.72	0.93

3. Validation in the ECMWF Assimilation Scheme

Based on the previous experience with the two systems, several different combinations of the QI and the RFF schemes were explored. Three main experiments were undertaken using different QI values to select which vectors would be subjected to the RFF scheme. The selected minimum QI values were 0.3, 0.6 and 0.9. These thresholds were selected as 0.3 represents the operational cut-off, 0.6 provides a good coverage and reasonable quality and 0.9 as it only retains very good winds. Additionally to utilising the QI as a pre-filter it was also used to select the best vector for each assimilation box in the

model as explained in section 4 a. The impact studies showed that the most promising approach was to use the QI with threshold 0.6 to pre-filter the raw wind field before submitting to the RFF scheme. The reason for the QI threshold of 0.3 not doing too well was that only a small number of very poor vectors were removed and these the RFF handles well. The QI threshold of 0.9 again did not keep enough vectors for the RFF to perform a coherent analysis of the data. Therefore the results for the QI threshold of 0.6 (RFFQI60) are discussed in more detail.

For our evaluation of this approach, all winds derived between 1 to 7 February 1998 during NORPEX were quality controlled by the RFF based approach only (RFF), and then also with the combined scheme using the QI information as a pre-filter to the RFF scheme. All data sets were disseminated to ECMWF. The AMVs are compared to the wind fields of the ECMWF 6-hour operational forecast with 31 model levels and T319 spectral resolution (Courtier et. al., 1998, Rabier et. al., 1998). For the statistical evaluation the background field was interpolated on a latitude longitude grid with 1.5° resolution. The model winds were then interpolated to the location and pressure of the satellite wind observations. For the evaluation, the wind vectors were sorted into quality classes based on their quality estimates. Each quality class was 0.02 wide (0.0 – 0.02, 0.02 – 0.04, 0.04 – 0.66, etc) and the mean wind speed (dashed line), rms departure (solid line) and bias (dotted line) as against the model winds was computed separately for each quality class.

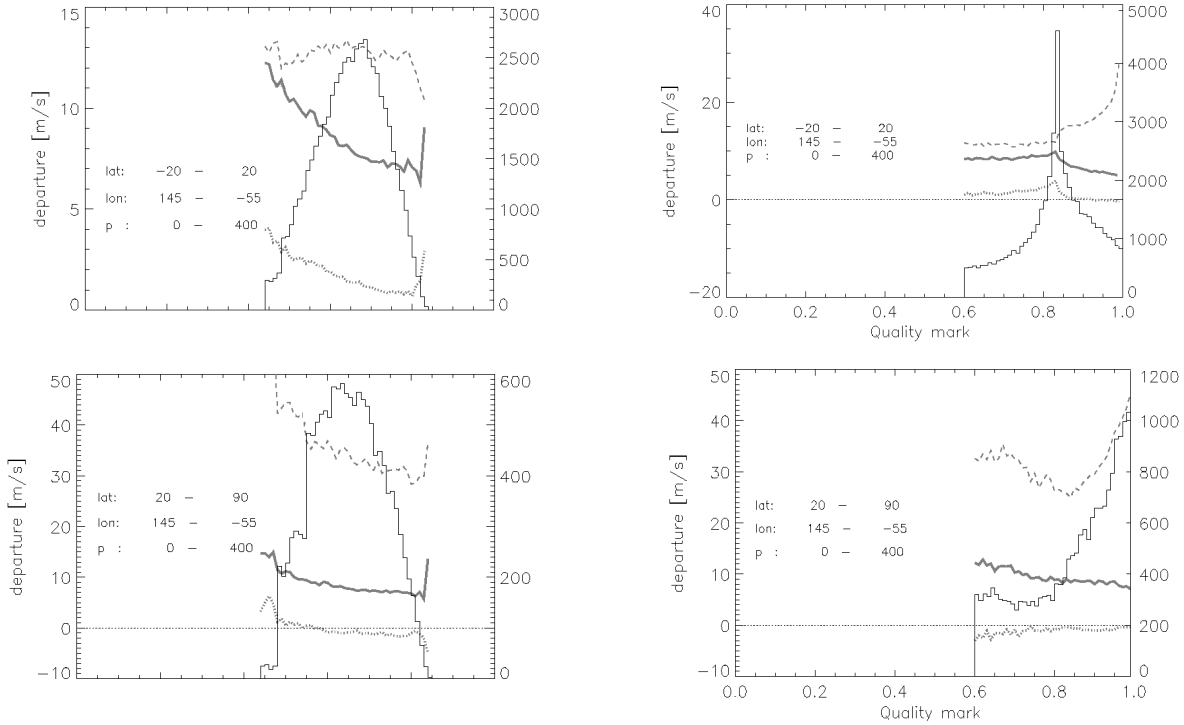

Figure 1. Comparison of background departures (The line for rms is solid, for speed bias dotted and for mean background speed dashed) of high level (p < 400 hPa) extratropical (bottom two figures) and tropical (top two figures) IR winds from the original NORPEX dataset (RFF only) to assigned RFF quality estimates. (The line for rms is solid, for speed bias dotted and for mean background speed dashed) of high level (p < 400 hPa) extratropical IR winds from the revised NORPEX dataset (RFFQI60) to assigned QI quality estimates.

Figure 1 presents these results for the IR high (above 400 hPa) and low (below 700 hPa) winds for the northern hemispheric extratropics (20° < latitude < 90°) and the tropics (0° < latitude <= 20°). The number of observations in each quality class is indicated by the histogram. Both quality indicators (RFF and QI) show decreasing rms departures and bias with increasing quality mark. The mean wind speed is almost constant for the RFF approach whereas it increases in the combined approach against the QI. The RFFQI60 winds reveal a pronounced step around QI=0.85 that is probably related to one of the EUMETSAT consistency tests indicating the need of further tuning for the tropical region. Below this threshold the rms departures are large and the mean wind speed low whereas above this threshold the bias and the rms departures decrease rapidly with an increase in the mean wind speed. This finding indicates the 0.6 threshold is not optimal for all channels, and the impact of this will be addressed in the next section.

4. Forecast Impact Studies with the ECMWF Model

4.1 Assimilation Strategy

For our study, the operational version of the ECMWF 4DVAR with an analysis resolution identical to the configuration under 5c is employed for data impact and sensitivity (Klinker et. al., 1999). The findings presented above are used to identify QI thresholds for selection of the winds to be considered for assimilation into the ECMWF analysis. The experiments using the original NORPEX high-density winds followed the operational usage of GOES-9 cloud-tracked winds, i.e. only winds with a quality estimate of RFF > 50 were considered. This follows the current practice of the ECMWF operational assimilation of GOES cloud drift winds from the IR and WV channels. Additionally, cloud drift winds from the VIS channel were introduced at low levels. Additionally to cloud drift winds, winds from cloud free regions are produced from the WV imagery data operationally. Also during NORPEX these so-called clear sky winds were produced and the medium and high level vectors were activated for the assimilation experiments.

The assimilation strategy for the revised data set using the QI as a pre-filter for the RFF scheme was based on the results described in section 4c). In the Northern Hemisphere extra-tropics all winds with a QI > 0.60 were considered. In the tropical belt a more restrictive use was introduced based on the findings in Figure 10, with a minimum QI value of 0.85 for high levels in the tropical belt. This is similar to the approach for the current operational usage of Meteosat winds, which is currently under investigation (Rohn et. al., 1998).

The NORPEX high-density winds were assimilated during the two-week period from 25 January to 7 February 1998. Early experiments with the high density data showed some problems in assimilating large volumes and is likely to be related to horizontally correlated errors in the observation data and by out weighting other observations. Therefore the high-density wind data needed to be thinned prior to assimilation by selecting one vector per analysis grid point location. For each case the vector with the highest quality within a selection box was chosen for assimilation. This results in a minimum horizontal distance between assimilated observations of roughly 1.25°. In the vertical, only one satellite wind is allowed per nearest model pressure level (50, 70, 100, 150, 200, 250, 300, 400, 500, 700, 850, 925, 1000 hPa). In the situation of very dense coverage of observations, the QI flag is further employed in the RFFQI60 experiment as a criterion in order to assimilate only the one observation with the highest QI value.

4.2 Forecast Impact

Since the main objective of the NORPEX campaign was to test adaptive observing strategies in order to improve the forecast skill over the US (Langland et al. 1999), we follow the evaluation used in the investigation of the combined impact of both high-density winds and dropsondes on the NOGAPS (Navy Operational Global Atmospheric Prediction System) forecasts (Szunyogh et al. 1999 and Langland et al., 1999) at the Naval Research Laboratory. The rms errors of the 48-hour forecast for both the 1000 hPa and 500 hPa geopotential surfaces are summarised in Table 2. The verification is restricted to a western North American region (30° < latitude < 60°; -130° < longitude < -100°) in agreement with the studies by Szunyogh et al. (1999) and Langland et al. (1999).

Table 2. Influence of the experimental assimilation of high-density winds on ECMWF model 48-hr forecast errors of the 1000 hPa and 500 hPa geopotential surfaces. The relative forecast impact is given as rms error differences between forecasts starting from the analysis using the experimental satellite winds derived by UW-CIMSS for NORPEX, and the control analyses using only the operationally available GOES-9 and GMS winds over the Pacific. Results are shown for the RFF-only, QI-only and the combined RFF/QI60 experiments. The evaluation period is 25 January to 7 February 1998. Both the absolute forecast rms errors and the difference values are averaged over the region of interest (30°<latitude<60°; -130°<longitude<-100°). Negative difference values indicate forecast improvement over the control. The forecasts are verified against their own analyses.

Description	Pressure level	48h forecast mean difference (m)	48h forecast rms error (m)
RFF-only	1000 hPa	-0.56	17.91
	500 hPa	-1.82	23.23
QI-only	1000 hPa	1.24	19.71
	500 hPa	0.64	25.70
Combined (RFF/QI60)	1000 hPa	-1.29	17.19
	500 hPa	-2.65	22.40

Both data sets that used the RFF scheme (RFF only, RFF/QI60) lead to reduced forecast errors, whereas the QI-only scheme increased the errors. Note that the control system uses the operational GOES winds that have been subjected to the RFF scheme as well. Therefore it is encouraging to see that by utilising the combined approach further improvements are made. From the theoretical aspect of data assimilation any dependency of the observation data to a short-term numerical forecast is not desirable as it feeds the model. This is especially important in the context of the re-adjustment of speed and height as outlined in section 3. The current results demonstrate on the other hand the gain from the RFF scheme in the current assimilation of AMVs. The rms error of the 48-hour geopotential forecasts is further decreased by the combined scheme (RFF/QI60). This can be explained by that the QI-scheme is able to provide a more consistent data set for the RFF scheme, which is then able to perform a more consistent analysis of the data.

The restriction to a particularly limited verifying region and a single forecast time requires caution especially regarding the relatively short experimentation period of two weeks. We therefore include the geographical distribution of short term forecast error in Figure 2. Both panels show the differences in the averaged rms error (14 cases) of the geopotential forecast at 250 hPa between the system initialized with the RFF/QI60 data and the Control. The forecast field is verified against its own analyses. Negative values indicate reduced forecast errors and are marked in yellow shading. Positive values are marked green. The 48h forecast error differences (left panel) reveal an extended area of reduced errors over the north Pacific which is less pronounced in the forecast based on the RFF-only analysis (not shown). In the bottom panel the forecast impact has moved east showing propagation into the NORPEX target area (northern America).

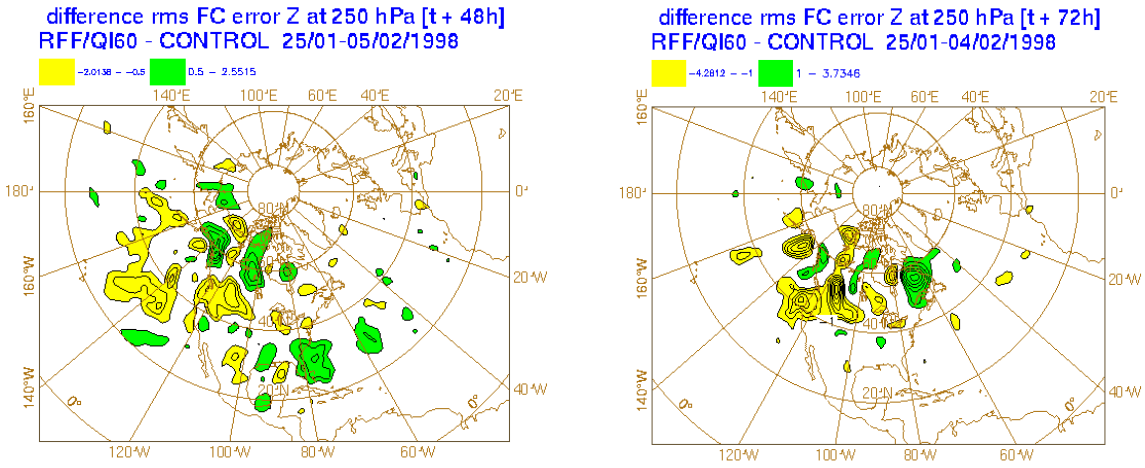

Figure 2. Differences of rms forecast error for the geopotential at 250 hPa between the RFF/QI60 experiment and the Control. Left: 48 hour forecast, Right: 72 hour forecast. Negative values indicate reduced forecast errors and are marked in yellow shading whereas positive values are marked green. All other areas do not show a significant change and are clear.

This development is supported by the verification of the forecast of vector wind at 850 hPa and 200 hPa within the Northern Hemisphere (Figure 3). All forecasts are verified against the Control analysis that explains the differences up to day one. The assimilation of the QI-only data results in increased rms errors in the medium range in agreement with the tendency indicated in Table 2. The combined quality control (RFF/QI60) shows a mainly neutral impact through day 2 and a small reduction of the medium range forecast errors beyond. These results support the positive impact of the presented combined quality control approach together with data screening decisions based on the quality estimates (RFFQI60).

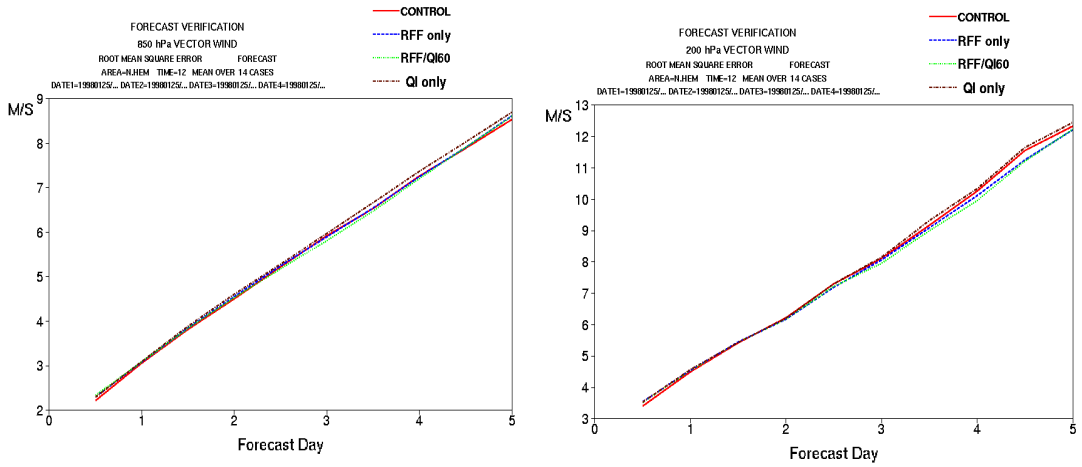

Figure 3. Verification of the rms forecast errors for vector wind at 850 hPa (left) and 200 hPa (right) in the Northern Hemisphere. All forecast are verified against the Control analysis.

5. Conclusions

The current operational automatic quality control schemes for satellite-derived atmospheric wind vector fields at high densities as applied at NOAA/NESDIS (UW-CIMSS scheme) and EUMETSAT have been briefly summarised. Even though the two schemes differ in their respective approaches, they generally classify the quality of vectors in a similar fashion. Both schemes have been shown to have advantages and disadvantages. The UW-CIMSS scheme is capable of providing more coherent wind fields and adjusts for some height assignment problems. The EUMETSAT scheme is capable of retaining more winds in the fast flow regimes and lends itself more easily for analysis and interpretation due to its straightforward formulation. It has been shown that the best vectors are generally those accepted by both schemes, whereas winds rejected by the two schemes simultaneously have a low reliability as single-level point measurements. In the case of disagreement between the two schemes, the EUMETSAT QI-scheme is capable of identifying and retaining more high-level water vapour and low-level visible winds, whereas the UW-CIMSS RFF based scheme retains a better low-level IR vector field.

Numerical model forecast impact experiments were performed on a two-week dataset during the NORPEX field program. The first two experiments used the original QC methods (RFF-only and QI-only), and the third assimilated a revised data set based on the application of the QI filter prior to the RFF based scheme and using the quality indicators to select the final winds for input. In general, results from the forecast impact studies show the assimilation of the high-density cloud and water vapour drift winds provided over the North Pacific region during NORPEX leads to a positive impact on the ECMWF model two-day forecast of the 1000 hPa geopotential height over a western North America region which was used as the primary verifying area for the NORPEX campaign. This result is consistent with the positive experience of using the NORPEX satellite-derived data set in other assimilation and forecast systems (Szunyogh et al., 1999; Langland et al. 1999).

The assessment of the geographical distribution of mean rms forecast errors differences appear to introduce an improvement by the revised QC strategy at day 2 which propagates into the NORPEX target area over the North West of the United States at day3. This tendency is supported by the verification of the rms forecast errors for vector wind at 850 hPa and 200 hPa in the Northern Hemisphere beyond day2. Note that in contrast to the comprehensive study by Langland et al. (1999) these results are based on the comparison to a Control system which uses the at that time operationally available GMS and GOES-9 satellite winds over the North Pacific.

Detailed analysis of the NORPEX cloud and water vapour drift wind sets by comparison with the ECMWF 6 hours forecasts revealed insight into the information content of the two different automatic quality control estimates, namely the recursive filter flag (RFF) and the quality indicator (QI). The QI+RFF value indicates the potential to mark the quality of single observations with respect to rms background departure and speed bias for data assimilation purposes. This study yields good evidence for the use of the combined QI and RFF values within the screening decisions of the ECMWF (and other) data assimilation system. The most promising approach was to use the QI with threshold 0.6 to pre-filter the raw wind field before submitting to the RFF scheme, and to subsequently use the QI, especially in high density areas, to select the best of the retained winds for data assimilation into a forecast model. A more complete analysis is given in Holmlund et. al. (2000).

Future work will concentrate on optimising the combined AQC approach described initially in this study. The effort on the data assimilation side should attempt to correct the representativeness error by modelling the vertical uncertainty of clouds and water vapour structures. Furthermore the discrepancy between the resolution of the extracted vector fields and the numerical analysis (Kelly et. al. 1996) should be reduced. In the area of AMV-extraction the efforts will be directed towards better target selection and height assignment methodologies including uncertainty estimates.

ACKNOWLEDGEMENTS

The work of M. Rohn was conducted under the EUMETSAT fellowship program at ECMWF.

REFERENCES

Courtier, P., E. Andersson, W. Heckley, J. Pailleux, D. Vasiljevic, M. Hamrud, A. Hollingsworth, F. Rabier and M. Fisher, 1998: The ECMWF implementation of three-dimensional variational assimilation (3D-Var). Part 1: formulation. *Quart. J. Roy. Meteor. Soc*., **124**, 1783-1807.

Holmlund, K. and C. Velden 1996: Objective determination of the Reliability of Satellite-Derived Motion Vectors. *Proc. Fourth Int. Winds Workshop*, Saanenmoser, Switzerland. EUMETSAT, 215-224.

Holmlund K., C. Velden and M. Rohn, 2000: Enhanced Quality Control Applied to High-Density GOES Winds during the North Pacific Experiment (NORPEX-98). Conditionally accepted in *Mon. Wea. Rev.*

Kelly, G. A., M. Tomassini and M. Matricardi, 1996: METEOSAT cloud-cleared radiances for the use in three/four dimensional variational data assimilation. *Proc. Third Int. Winds Workshop*, Ascona, Switzerland. EUMETSAT, 105-116.

Klinker, E., F. Rabier, G. Kelly and J.-F. Mahfouf, 1999:The ECMWF operational implementation of four-dimensional variational assimilation. Part III: Experimental results and diagnostics with operational configuration. ECMWF Research Dept. Tech. Memo 273, 27 pp. [Available from ECMWF Librarian, Reading, Berkshire RG2 9AX, United Kingdom.] (Submitted to *Quart. J. Roy. Meteor. Soc*.)

Langland, R. H., Z. Toth, R. Gelaro, I. Szunyogh, M. A. Shapiro, S. J. Majumdar, R. E. Morss, G. D. Rohaly, C. Velden, N. Bond, C. H. Bishop, 1999: The north Pacific experiments (NORPEX-98): Targeted observations for improved north American weather forecasts. *Bull. Amer. Meteor. Soc.,*

Rabier, F., McNally, A., Andersson, E., Courtier, P., Undén, P., Eyre, J., Hollingsworth, A., and Bouttier, F., 1998: The ECMWF implementation of three dimensional variational assimilation (3D-Var). Part II: Structure functions., *Quart. J. Roy. Meteor. Soc.*, **124**, 1809-1830.

Rohn, M., G. Kelly, and R.W. Saunders, 1998: Use and impact of atmospheric motion vectors at ECMWF. *Proc. 9th Conference on Satellite Meteorology and Oceanography*, Paris, France, 360-363.

Szunyogh, I., Z. Toth, S. Majumdar, R. Morss, C. Bishop, and S. Lord, 1999: Ensemble-based targeted observations during NORPEX. Preprints, *Third Symp. on Integrated Observing Systems*, Dallas, TX, Amer. Meteor. Soc., 74-77.

Velden, C.S., T.L. Olander and S. Wanzong, 1998: The impact of multispectral GOES-8 wind information on Atlantic tropical cyclone track forecasts in 1995. Part 1: Dataset methodology, description and case analysis. *Mon. Wea. Rev*., **126**, 1202-1218.

PARALLEL QUALITY CONTROL OF EUMETSAT WIND PRODUCTS, WITH AND WITHOUT THE USE OF FORECAST WIND FIELDS.

Simon S. Elliott

EUMETSAT
Am Kavalleriesand 31
D-64295 Darmstadt
Germany

ABSTRACT

It is widely felt among the numerical weather prediction community that the use of forecast wind fields in the quality control of atmospheric motion vectors should, in principle, be avoided. This is because of the concern that a feedback could be introduced into the system, whereby only those winds which are in any case similar to the forecast, would be disseminated for assimilation into the forecast models. Where the satellite winds could have the most useful impact on a forecast is in the very areas where the forecast is incorrect, and the satellite winds could help to get it back. However, in these cases a consistency check against forecast data would give the satellite wind a bad score and it would probably not be distributed.

Statistical analysis of co-location data shows that among the various tests used by EUMETSAT, the forecast test gives, on average, the most reliable measure of quality, measured in terms of the vector difference from radiosonde data. Removing it from the suite of tests, which form the automatic quality control scheme can, therefore, only worsen the overall performance this scheme. We will show, however, that by carefully performing the optimisation of the weights of the remaining checks, this effect can be mitigated. e use the flexibility offered to us by BUFR encoding to include quality control information calculated with and without the use of forecast data, separately, with each wind. The use of BUFR Table B entries defining the quality control process allow the two sets of information to be distinguished, and used independently if required.

1. Introduction

The mechanism by which we select the relative weights given to the various automatic quality control tests is as discussed in Elliott, 1998. The fundamental idea is to assume that the tests themselves are (a) fixed in terms of the values they give for a particular wind vector, and (b) mutually independent.

The first of these assumptions is certainly a simplification, but does not invalidate the basic process. In fact, the precise performance of the individual tests is continually analysed and the exact parameterisation of their functional forms is subject to constant review. As we will discuss below, the calculation of the weights does not appear to be unduly sensitive to the fine detail of the input data, and so unless an individual test has been significantly modified, the weights would not need to be re-calculated. If the tests were truly an independent set of measurements of the quality of the wind vectors, the processing of optimising the various weights assigned to them would be relatively straightforward. There is, however, a clear overlap between some of the tests. This is most obvious when we consider the impinging triptych of the speed, direction and vector consistency tests. The speed consistency test gives a score relating the difference in speed between the two components of a combined vector, a small difference giving a higher score. The direction consistency test works in a similar way but for the difference in direction. The vector difference between the constituent component vectors is used directly to calculate the third test score. Since the wind vectors themselves are only two dimensional, there cannot be three independent pieces of information to use for three separate tests. Any two of the three tests are sufficient to contain all the information, which is present.

A further dependency between the results of the tests derives from the vector extraction method itself. The tracking of a target across consecutive images is, in the vast majority of cases, either successful, or very bad. There are very few cases where the tracking is "not bad" or "quite good". Since the three tests mentioned above are all measuring the quality of the target tracking, the nearly always give similar results.

Since the analysis presented in Elliott, 1998 was performed, an additional quality control test has been activated in the wind extraction process. The correlation consistency test gives a value relating to the mean of the height of the selected correlation peak, for each of the forward and reverse correlation surfaces. The strength of this test is that it actually is independent of the others used. Its usefulness is, however, limited by the fact that in the large majority of cases it has a very high value. In fact its behaviour can be summarised by stating that any wind (good or bad) can get a high score, but a low score is a strong indication of a bad wind. We use this test naïvely in a linear combination with the other tests for the following analysis. Investigation into the potential use of the correlation consistency test as a multiplicative filter on the combined score of the other tests are currently in progress (*priv. comm.*, J. Gustafsson, 2000).

2. Core tuning results

Fig. 1 shows the distribution of results from a standard set of experiments using various combinations of automatic quality control tests. All the co-location data were used. The x-axis is the standard deviation of the best-fit straight line drawn through the scatter plot of normalised vector difference (NVD)[§] as a function of final quality control score. The y-axis is the correlation between the NVD and the final quality control score. The correlation coefficient is always negative, because a wind vector with a large difference from the radiosonde should get a small quality control score, and vice versa. In an ideal case, there would be an exactly linear relationship between the two sets of data, and this being the case (i) the standard deviation would be zero, (ii) the correlation coefficient would be –1.0, and (iii) we would be able to write an equation of the form

$$NVD = (a \times QC) + \beta, \qquad [1]$$

where QC is the final quality score of a wind vector, and a and β are arbitrary constants. The better a particular set of weighted tests perform in achieving a relationship of the form in Eq. 1, the further into the lower left corner of the plot our result will be.

The nine configurations of the quality control tests used are shown in Table 1. Test case (TC) 1 was a first guess at what a potential choice of tests could be for the quality control process without forecast data being used. TC 2 represents the best possible choice because all the tests are used and their weights are then optimised. The third and forth test cases represent the current operational configuration, and a similar configuration without forecast data respectively. In both cases, the weights used for the tests are prescribed based on experience, and are not calculated automatically. TCs 5 and 6 are almost the identical; neither includes the correlation test and both have the weights of the tests optimised, but TC 5 additionally excludes forecast data. We consider two possible configurations using only three tests in TCs 7 and 8. Both use the spatial and correlation tests, but TC 7 uses the direction test, where as TC 8 uses the vector test. Finally, TC 9 can be considered together with TCs 2, 5 and 6. Together these 4 can be juxtaposed to show the four binary combinations of with/without the forecast test, and with/without the correlation test.

The four results clustered together in the top left-hand corner are from TCs 1, 7, 8 and 9. These all use correlation test data, but exclude the forecast test. The two results in the top right corner are from TCs 4 and 5, both of which exclude the forecast test and the correlation test. These two groups differ primarily in their standard deviation, which can infer is reduced by the inclusion of the correlation test.

[§] The normalised vector difference, or NVD, is the vector difference between an extracted wind vector and the co-located radiosonde wind, normalised by the speed of the radiosonde wind.

The bottom left and right results are from TCs 2 and 6 respectively. Both these cases use the forecast test, but TC 6 excludes the correlation test (and so has a higher standard deviation, as we might expect). Comparing these two results with the first two clusters shows that the main impact of including the results of the forecast test is to improve the correlation coefficient, and therefore to do a better job of achieving a relationship like that given in Eq. 1.

Table 1. Details of the various combinations of quality control tests used. Where 'Opt.' appears, the weight assigned to the test was derived using the optimisation method. The highlighted cells containing 'None' indicate that that quality control test was not used for that case. The bold numbers are prescribed weights determined by experience of real data.

Test case	Description	Direction test weight	Speed test weight	Correlation test weight	Forecast test weight	Spatial test weight	Vector test weight
1	Intuitive without forecast	Opt.	Opt.	Opt.	None	Opt.	None
2	Optimal with forecast	Opt.	Opt.	Opt.	Opt.	Opt.	Opt.
3	Current operational	**0.167**	**0.167**	None	**0.167**	**0.333**	**0.167**
4	Operational without forecast	**0.200**	**0.200**	None	None	**0.400**	**0.200**
5	Optimal without forecast or correlation.	Opt.	Opt.	None	None	Opt.	Opt.
6	Optimal without correlation.	Opt.	Opt.	None	Opt.	Opt.	Opt.
7	Simple-I without forecast	Opt.	None	Opt.	None	Opt.	None
8	Simple-II without forecast	None	None	Opt.	None	Opt.	Opt.
9	Optimal without forecast	Opt.	Opt.	Opt.	None	Opt.	Opt.

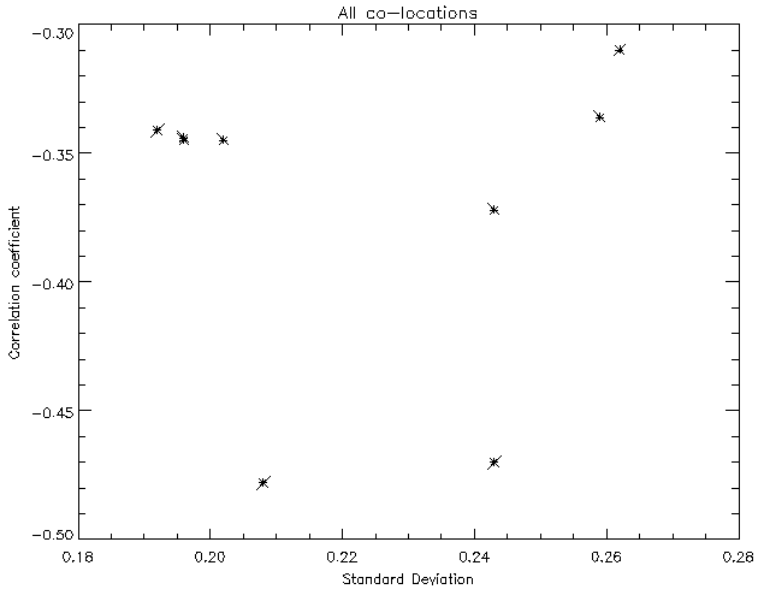

Figure 1. An inter-comparison of the performance of the various combinations of quality control tests used to derive an overall quality score. Those combinations that perform well fall towards the lower left part of the figure. These cases always include the forecast test.

TC 3 falls a little over half way up the plot on the left-hand side. This represents the operational configuration, which does use the forecast test. The plot suggests that simply by changing the weights given to the tests used operationally today, we could move toward TC 6 and by adding in the correlation test, we could move toward TC 2. It is also clear that in terms of standard deviation, the current operational setting is only marginally better than TCs 1, 7, 8 and 9, none of which use forecast data. This reinforces the idea that careful use of independent non forecast based tests can give a final quality control score which does almost as well as the current operational configuration.

3. Sensitivity to filtering by co-location vector difference

When one examines the co-location data set used for the analyses presented in this paper, it is clear that there is a small number of co-locations with a very large NVD. This can be the result of a failure in the semi-transparency correction mechanism, meaning that a fast moving thin cirrus tracer is mistakenly assigned to a low level. This vector is then co-located with a radiosonde wind at low level, which would have a much lower speed, and the resulting NVD can approach 100.0.

In order to ensure that the optimisation of the weights assigned to the quality control tests is not perturbed by these few rogue co-locations, it is possible to filter out co-locations where the NVD exceeds some threshold value from the tuning process. This step helps to ensure that the optimisation method is statistically robust. It is important, however, to consider the effect of these weights not only on only the selected set of co-location data used for the tuning process itself, but also on the entire co-location data set. Fig. 2 shows a similar set of results to that presented in Fig.1, but for a filtered set of co-locations with NVD < 5.0. The left hand plot shows the results when only the filtered-in set of co-locations used to determine the weights which are assigned to the tests are used for the evaluation. The right hand plot shows the result of applying the weights derived from the filtered set of co-locations to all the original co-locations.

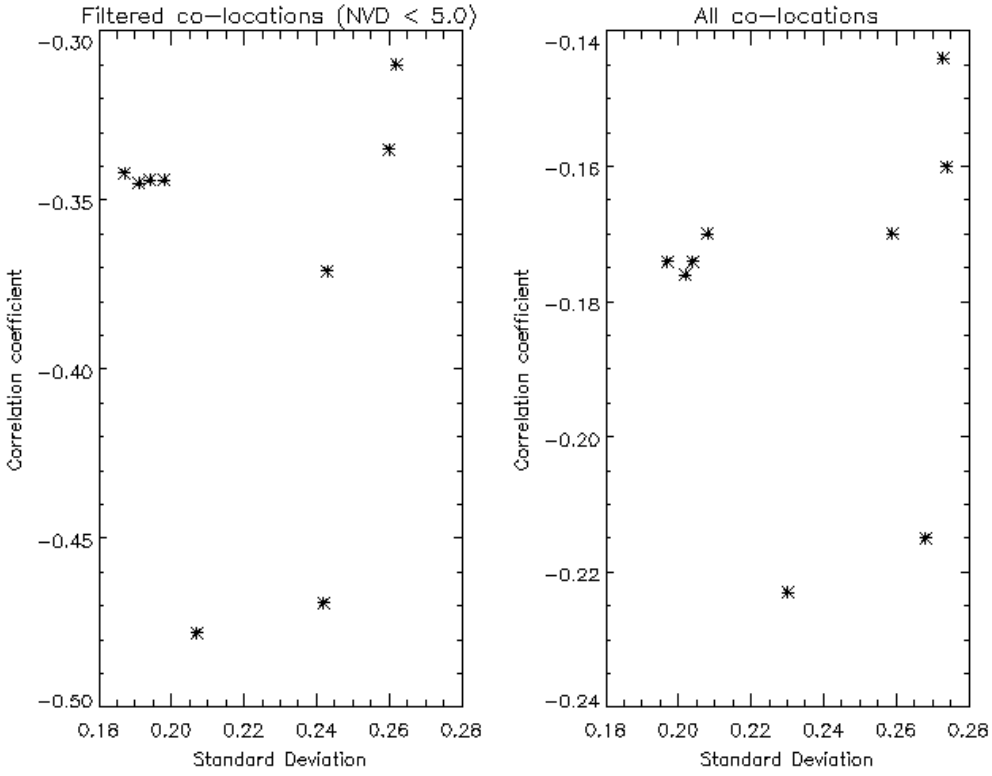

Figure 2. An inter-comparison of the performance of the various combinations of quality control tests, where the weights are selected using a set of co-locations filtered such that those with an NVD > 5.0 are excluded.

The results shown in Fig. 2 lead to two observations:

(i) In relative terms (comparing the left and right plots), there is very little difference between the results of applying the weights derived from the filtered set of co-locations to only those co-locations, or to the whole set. This means that the weights derived from the filtered set of co-locations can be used for all the co-locations with equanimity.

(ii) Comparison with Fig. 1 suggests that the exclusion of the outlying co-locations from the optimisation process actually made only a small difference. The general distribution of the various test cases remains essentially the same, and the values of the weights themselves were changed by typically less than 10 %.

The choice of a threshold value of 5.0 for the NVD was somewhat arbitrary. In an attempt to make a more calculated choice for the threshold value, the distribution of NVD within the co-location data set was examined. Fig. 3 shows this distribution.

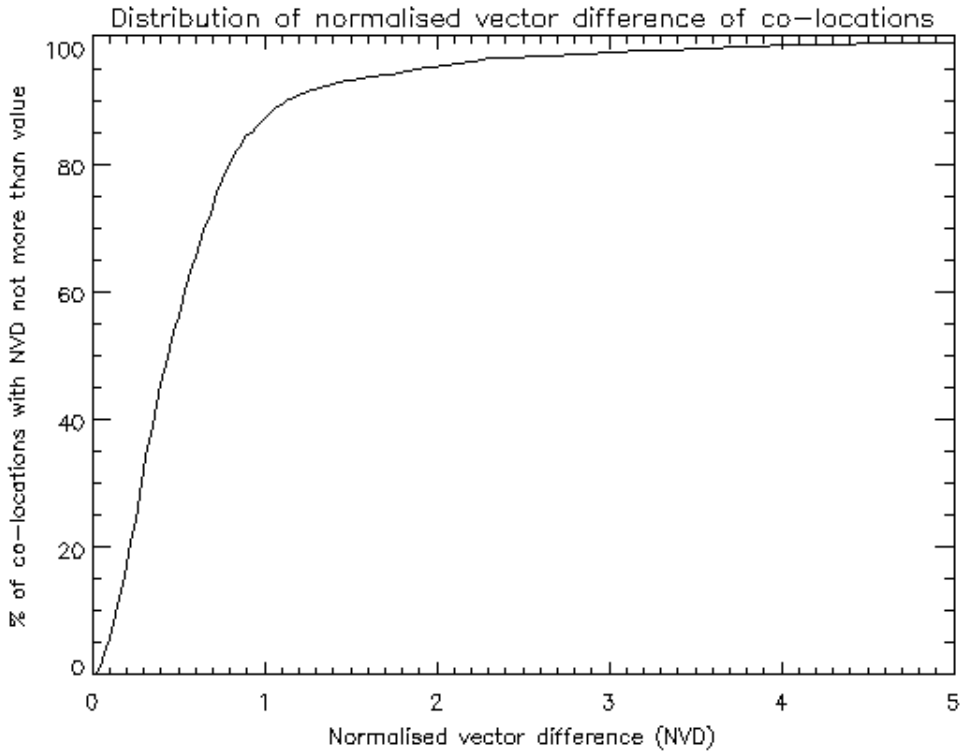

Figure 3. The distribution of NVD across the complete set of co-locations. There is a clear bend in the curve when the NVD is near 1.0, hence the choice of this as a preferred threshold value.

The graph in Fig. 3 shows that ~85% of co-locations have a NVD less than 1.0. The form of the curve is similar to that of a cumulative Poisson distribution function. For threshold values lower than 1.0, the number of co-locations remaining reduces rapidly. For this reason, the NVD threshold value of 1.0 was used, and the same set of test cases, as defined in Table 1, were re-run. The results are shown in Fig. 4.

By comparing Figs. 2 and 4, we can see that the only significant effect of reducing the NVD threshold value is to scale up uniformly the correlation coefficient values assigned to the test cases for the filtered set of co-locations. In fact, the only significant effect of filtering the co-locations used in the tuning process by NVD, is in the performance of the TC 1, 7, 8 and 9 cluster of results. When the weights are calculated using these filtered co-locations and applied to the whole data set, the aforementioned TCs have an improved correlation coefficient, relative to the other TCs in Fig. 1. This result alone does,

however, indicate that there is value in applying an NVD threshold filter to the co-location data before the optimisation of the weights is performed.

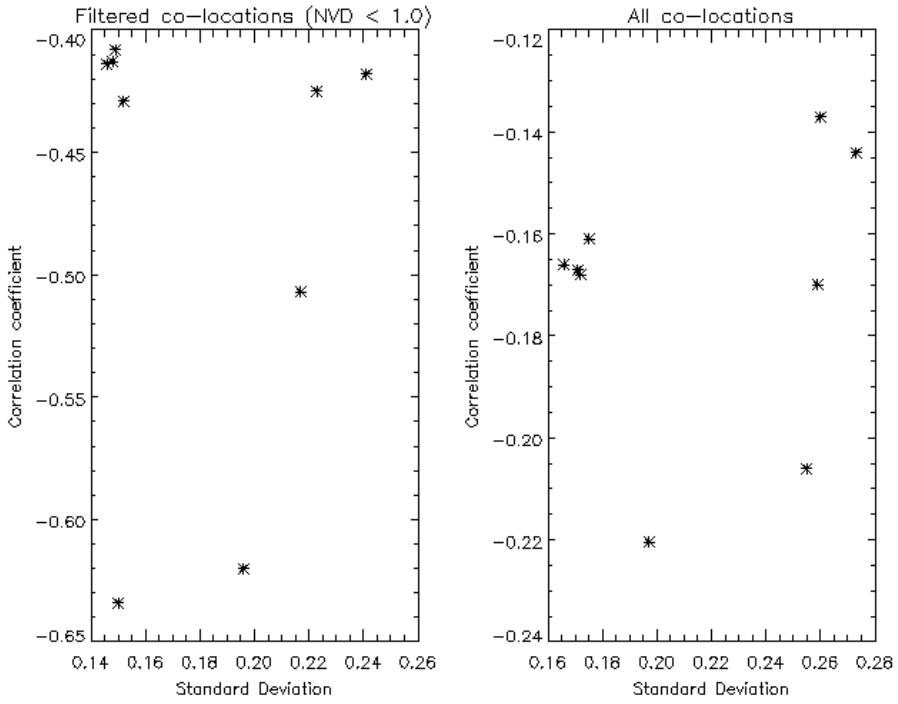

Figure 4. An inter-comparison of the performance of the various combinations of quality control tests, where the weights are selected using a set of co-locations filtered such that those with an NVD > 1.0 are excluded.

4. Limitations of optimisation method

As we have mentioned in Sect. 1, the entire optimisation process is critically dependent on the independence of the quality control tests, which we know is not the case. The performance of the optimisation when the tests are dependent is, at best, unpredictable, and can be in fact be improved upon by an intelligent choice of weights based on experience of the performance of the various tests.

The limitations of the optimisation method have been illustrated by several examples (*priv. comm.*, J. Gustafsson, 2000). For instance, when considering one set of low level wind co-locations, the following results were obtained,

- Manually weighted with forecast test: NRMS = 0.35
- Optimised with forecast test: NRMS = 0.36
- Forecast test only: NRMS = 0.37
- Operational setting: NRMS = 0.41
- Manually weighted without forecast test: NRMS = 0.58
- Optimised without forecast test: NRMS = 0.62,

where NRMS is the root mean square of the vector difference between the extracted wind vector and the co-located radiosonde wind, normalised by the mean radiosonde wind speed across the sample. In both the cases where test weights were derived using the optimisation method, the equivalent cases using manually assigned weights performed slightly better.

The reason for this limitation can be described by an analogy between optimising the results of n of test results and finding the co-ordinates of a point in an n-dimensional space. In the ideal case, each of out tests would be like an orthogonal basis vector in the space. The co-ordinates of the point are not very

sensitive to small changes in the direction of a basis vector. If, however, the basis vectors spanning the space are all nearly parallel (so the tests all give similar results), the co-ordinates of the point change significantly if the direction of one of the vectors changes a little bit. This means that the weights assigned to tests that perform similarly to each other are very sensitive to the exact performance of the test on a particular set of co-location data.
For this reason, the results from the optimisation process are best considered as an indication of the approximate weight to be assigned to each test. We have also shown that changes in the weights of the order of 10% make only marginal difference to the relative performance of each test case (as described in Table 1).

5. Use of BUFR for representing parallel quality control data

The flexibility offered by the BUFR encoding of disseminated wind products can be exploited, to allow the inclusion of quality control information calculated with and without the use of forecast data, separately, with each wind. The use of BUFR Table B entries defining the quality control process allows the two sets of information to be distinguished, and used independently if required.
A hypothetical example applied to a wind consisting of only four parameters (speed, direction, temperature and pressure) is shown in Table 2. A real wind has 103 parameters, but the same principle applies.

Table 2. An illustration of the way in which BUFR can be used to include parallel quality control information within a message. The table should be read from left to right and then downwards. Fields highlighted in grey can be read down the columns to see what information is given for each parameter (Speed, Direction, *et c.*). Fields without a highlight do not correspond to any particular parameter.

Speed	Direction	Temperature	Pressure
QC follows	Define bitmap		
QC Included	QC Included	QC Included	QC Included
		EUMETSAT QC	QC1, with forecast
% confidence	% confidence	% confidence	% confidence
QC follows	Re-use bitmap	EUMETSAT QC	QC1, with forecast
Confidence threshold	Confidence threshold	Confidence threshold	Confidence threshold
QC follows	Re-use bitmap	EUMETSAT QC	QC2, without forecast
% confidence	% confidence	% confidence	% confidence
QC follows	Re-use bitmap	EUMETSAT QC	QC2, without forecast
Confidence threshold	Confidence threshold	Confidence threshold	Confidence threshold

Table 2 should be read left to right and from top to bottom. By reading down the columns and looking at the highlighted cells it is possible to see which quality control values are given for which parameter value.

Immediately after the measured parameters, a descriptor (222000) is used to indicate that quality control information follows. Next follows a descriptor (236000) to indicate the presence of a 'data present' bit map, followed by the bit map itself (four 031031 descriptors). Each entry in the bit map is set to indicate whether or not there will be quality control information following for the associated parameter. Then follows a descriptor (001031) indicating the originating/generating centre (EUMETSAT, 254), and one for the generating application (001032). It is by setting the value of this element that we can indicate which type of quality control has been performed, 1 being with forecast data being used, and 2 being without. Next a set of values relating to the parameters as per the bit map is given (033007 for % confidence, for example). Then follows the same pattern of descriptors for each successive set of quality control values, namely (i) quality control information follow (222000), (ii) re-use previously defined bit map (237000), (iii) originating/generating centre (001031), (iv) generating application (001032), and (v) the quality control values relating to the original parameters.

During the summer of 2000, EUMETSAT will use this method of BUFR encoding to send test bulletins on the GTS. The wind data in these bulletins will be the same as the operational wind data, but the quality control section will contain the two parallel sets of indicators, calculated both with and without the use of the forecast test.

6. Summary and conclusions

The principle conclusion to be drawn from this study is that a set of quality control values for the wind products can be calculated without using a forecast consistency test. The values calculated in this way will have a less well defined relationship to the actual quality of the winds (compared to co-located radiosonde data), but there will be less error correlation. The EUMETSAT wind products will be disseminated with both sets of quality control information attached.

The method used to optimise the weights assigned to each test is dependent on the tests being independent, which they are not. For this reason, the results from the optimisation process are best considered as an indication of the approximate weight to be assigned to each test. We have also shown that changes in the weights of the order of 10% make only marginal difference to the relative performance of each test case (as described in Table 1).

In an effort to make the optimisation more statistically robust, we have assessed the impact of filtering the set of co-location data used for the tuning process, by limiting the maximum NVD to be considered. The distribution of NVD within the sample of co-location data led to the choice of an NVD threshold value of 1.0, excluding ~15% of the data. This filter led to a slight improvement in the performance of the optimisation, particularly for the test cases using the correlation test, and not the forecast test.

During the summer of 2000, EUMETSAT will distribute test bulletins on the GTS, which will contain the two parallel sets of quality information, calculated both with and without the use of the forecast test. The users will then be able to decide which set of information they should use.

REFERENCES

Elliott, S. (1998). The application and implications of the use of a unified BUFR template for the exchange of satellite derived wind data. In *Proceedings of the fourth international winds workshop*. EUMETSAT, EUM P24.

THE NWP SAF INTEGRATED SATELLITE WIND MONITORING REPORT

P. Butterworth,* F. Lalaurette,# B. J. Conway* and A. Garcia-Mendez#

*NWP Division, The Met. Office, London Rd, Bracknell RG12 2SZ, U.K.
and #ECMWF, Shinfield Park, Reading RG2 9AX, U.K.

ABSTRACT

The NWP SAF (Satellite Application Facility for Numerical Weather Prediction) is a 5-year EUMETSAT-sponsored project to develop processing methods and software to enable satellite data to be exploited for NWP purposes by the EUMETSAT Member States. One of the first deliverables from the NWP SAF is the Integrated Satellite Wind Monitoring Report, which displays observation-background differences for different NWP models (currently those of ECMWF and The Met. Office). These statistics are being gathered in order to try to separate the contributions from the two sources, observation and background, and thus to improve the derivation of satellite wind observations, their use within NWP models, and the NWP models themselves. After four months of operation, some results are highlighted here, illuminating certain characteristics of the winds and the models. It is hoped that in forthcoming months, both the set of quality statistics displayed and the number of NWP centres contributing to the report will increase. The 5th International Winds Workshop will make a clear recommendation to CGMS for maintenance and enhancement of the satellite wind monitoring report, allowing the satellite producers to give formal permission for the publication of their data. The satellite wind monitoring report is available for viewing at http://www.met-office.gov.uk/sec5/NWP/NWPSAF/satwind_report/

1. Introduction

The NWP SAF (Satellite Application Facility for Numerical Weather Prediction) is one of currently seven EUMETSAT-sponsored SAFs. The purpose of the SAFs is to develop processing methods and software to enable satellite data to be exploited in various meteorological application areas. Each SAF is a 5-year research and development (R+D) collaboration of a few EUMETSAT Member States, with the likelihood of a subsequent operational phase to apply and extend the products of the R+D phase. More information about SAFs is available at the EUMETSAT web-site, http://www.eumetsat.de. The report is available for viewing at http://www.met-office.gov.uk/sec5/NWP/NWPSAF/satwind_report/

The NWP SAF was approved by EUMETSAT Council in November 1998. The Kick-off Meeting was held in February 1999 and the SAF's planned 5-year term will end in February 2004. The SAF is led by The Met. Office, with partners ECMWF, KNMI and Météo-France.

The objectives of the NWP SAF are as follows:

- to improve the benefits derived by European NMSs from NWP, by developing techniques for more effective use of satellite data, and
- to prepare for effective exploitation within NWP of data and/or products from satellites in the EPS and MSG Programmes and related programmes of other agencies.

The main development activities of the SAF are concerned with the processes required to generate the intermediate products of the full data assimilation process, not with the products themselves, and the

work of the SAF is structured according to input data (i.e. by instrument: ATOVS, IASI, ASCAT, SEVIRI, etc.) rather than according to geophysical parameter.

The main deliverables from the SAF's activities will be software packages for implementation at NWP centres within their data assimilation schemes, or at EUMETSAT central processing facilities or at other SAFs. The SAF will focus on development activities, but will also provide support to implementation activities.

The emphasis of the SAF's activities is on development, rather than research. However, it is also proposed that there should be some scope for support of associated research activities, through the EUMETSAT SAF Associate/Visiting Scientist programme.

2. The integrated satellite wind monitoring report

One of the first deliverables from the MVIRI/SEVIRI section of the NWP SAF is the Integrated Satellite Wind Monitoring Report, which displays differences between satellite wind observations and NWP models. The comparison is between the transmitted observation of wind and a 6-h forecast of wind from the NWP model, valid at the observation time, that provides the background data for the new model forecast. Both the satellite wind observation and the model forecast contribute to these differences; neither can be assumed to be true, and therefore the differences are model dependent. The report presents, in similar formats, differences found in different NWP models in order to try to separate the contributions from the two sources (observation and model). This should enable the improvement of both derived satellite winds and their treatment within NWP models, as well as highlighting differences in the characteristics of the models. NWP centres contributing to the report are ECMWF and The Met. Office at present.

Currently (February 2000) there are two separate types of statistical quality plot. The first is a wind speed contour map, which plots observation vs background wind speed and gives the density of observations on a logarithmic scale. From these plots can be seen the average wind speed bias, and areas of significant departure from the 1:1 line. The second type is a global map of wind speed bias and standard deviation, plotted for different wind types (infrared, water vapour, visible) and at different pressure levels. From these can be seen the geographical areas where there is significant mismatch between observation and models. The similarities between these maps can highlight where the observations are not matching the real wind, and the dissimilarities can highlight where the NWP centres are modelling features differently.

A set of data has been collected for four months so far (October 1999 - January 2000), and these plots will form the basis of a continual set, at least for the lifetime of the NWP SAF. However, there is still potential for the introduction of new types of quality plot, and the website for the Integrated Satellite Wind Monitoring Report will continue to be developed.

In general, the agreement between the background fields and the observations is good; indeed the satellite winds would not be assimilated routinely into NWP models if it were not. Some examples are given below where significant differences were seen between the background and observed values.

2.1. Comparison of wind speed contour plots

Figures 1a and 1b compare the wind speed contour plots for ECMWF and The Met. Office, respectively, for Meteosat-5 infrared low-level (700 - 1000 hPa) winds in the tropics (20ºN - 20ºS), averaged for January 2000. The difference in the number of winds shown from the two centres is due to the fact that ECMWF monitors (and uses) those winds from EUMETSAT received in BUFR code, whereas The Met. Office monitors (and uses) those winds received in satob code. Notwithstanding the numerical difference, the statistics and features of the plots are very similar. Most notable is the plume

of winds reporting an observation speed in excess of background speed. This is due to erroneous height assignment of these winds (high faster winds being assigned to a low height where the wind speeds are actually slower) and is a known problem at EUMETSAT. The problem is often that the wind-tracking algorithm is following semi-transparent cirrus clouds and assigning the motion to a lower height. However there is another cause of incorrect height assignment. An NWP model vertical profile is used to match brightness temperature with height. It was found at EUMETSAT (Gustaffson and Lindberg, 2000) that due to the coarse resolution of the model profile, in regions where maritime temperature inversions exist, an incorrect height can be assigned. Gustafsson and Lindberg (2000) corrected the wind-production method to take account of this and subsequent time-series of quality statistics has confirmed that there has been an improvement in observation-background agreement since this change was made. Thus it can be deduced that the remaining winds that have the wrong height assigned are probably due to the tracking of cirrus clouds. Interestingly, equivalent plots for visible winds show that this problem does not feature in The Met. Office's use of visible winds (at low resolution), yet does show up in ECMWF's use of high-resolution visible winds in BUFR code. (Not featured, see Monitoring Report website.)

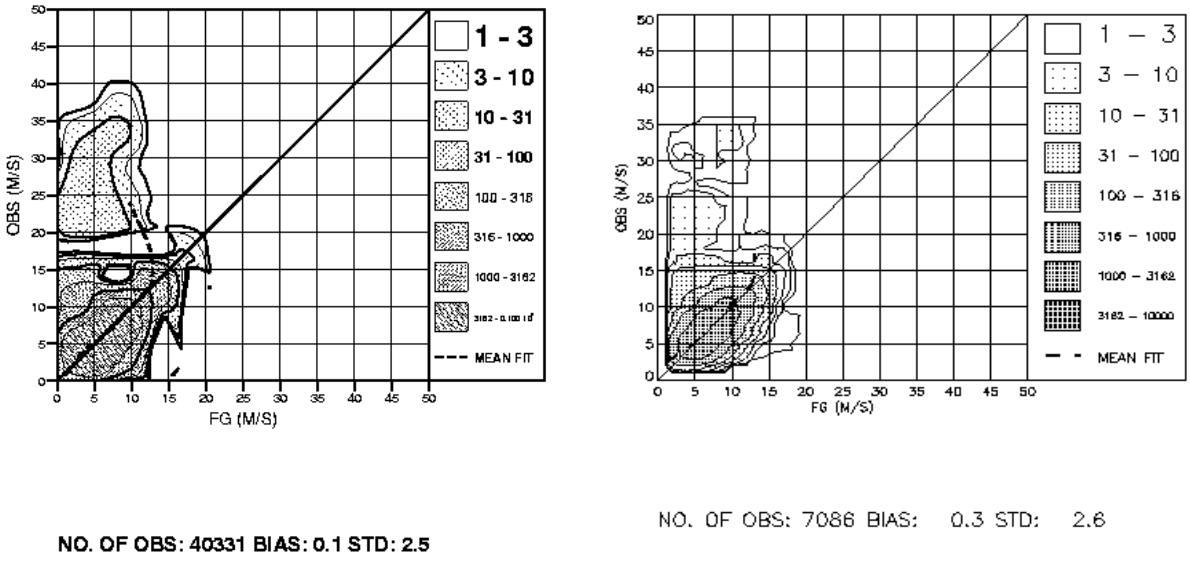

Figure 1. Wind speed contour plot for Meteosat-5 infrared winds in the tropics (20ºN - 20ºS) at low level (700-1000 hPa), averaged for January 2000, compared with the a) ECMWF (left panel) and b) The Met. Office (right panel) background field.

2.2. Comparison of wind speed bias global maps

The second type of graphical plot is a global map of observation-background wind speed bias and standard deviation. Figure 2 shows some examples of this type of plot. The top panel shows observation-background wind speed bias for high-level infrared winds vs the ECMWF model and the bottom panel shows the same vs The Met. Office model. The data are averaged for January 2000. It can be seen that there is some consistency in the signals that are seen from the two centres. For example, both ECMWF and The Met. Office show consistent small-scale features of persistent negative speed bias in the northeastern and southeastern Pacific ocean. Similarly, both centres show large positive wind speed biases around the coastlines of northern and western South America. Taken in isolation it is tempting to conclude that in these areas the wind production method for the GOES winds is in error. However, since the production of GOES winds relies heavily on the use of the NESDIS auto-editor (Nieman et al., 1997), there is the possibility that the NCEP model is the source of the problems. Another suggestion is that both the global models at ECMWF and The Met. Office have erroneous wind speeds in these areas. Further investigation is therefore necessary: communications

with the satellite wind producers, investigation into radiosonde-reported wind speeds from the regions affected, if any, and a knowledge of the persistent biases inherent in each model. It must again be emphasised that the point of the NWP SAF Integrated Satellite Wind Monitoring Report is to help to improve both the production and the use of satellite winds, and that deficiencies may be revealed in the satellite winds, the NWP models, or both.

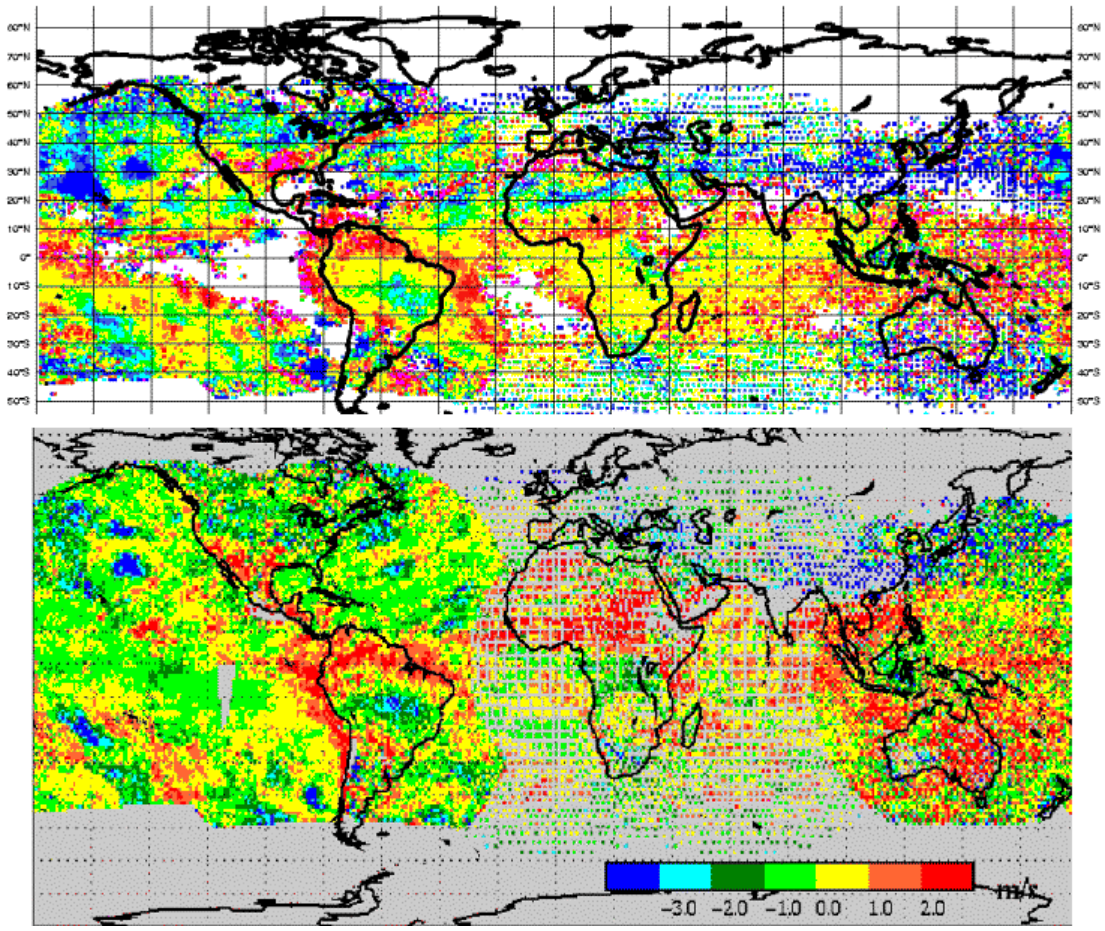

Figure 2. Observation-background wind speed bias. Top: high-level infrared satellite winds vs ECMWF background field, bottom: high-level infrared satellite winds vs The Met. Office background field.

In contrast, some differences between the plots can be seen with respect to high-level infrared winds from GMS. ECMWF biases are strongly negative in the extratropics, whereas those shown by The Met. Office have some strong positive areas. Referring to the contour wind speed plots of high-level GMS infrared winds (Figs 3a and 3b), it is seen that, although overall the wind speed bias is calculated as negative for both centres, it is more strongly negative for ECMWF, implying that average wind speed in this region is greater in the ECMWF model than in The Met. Office model.

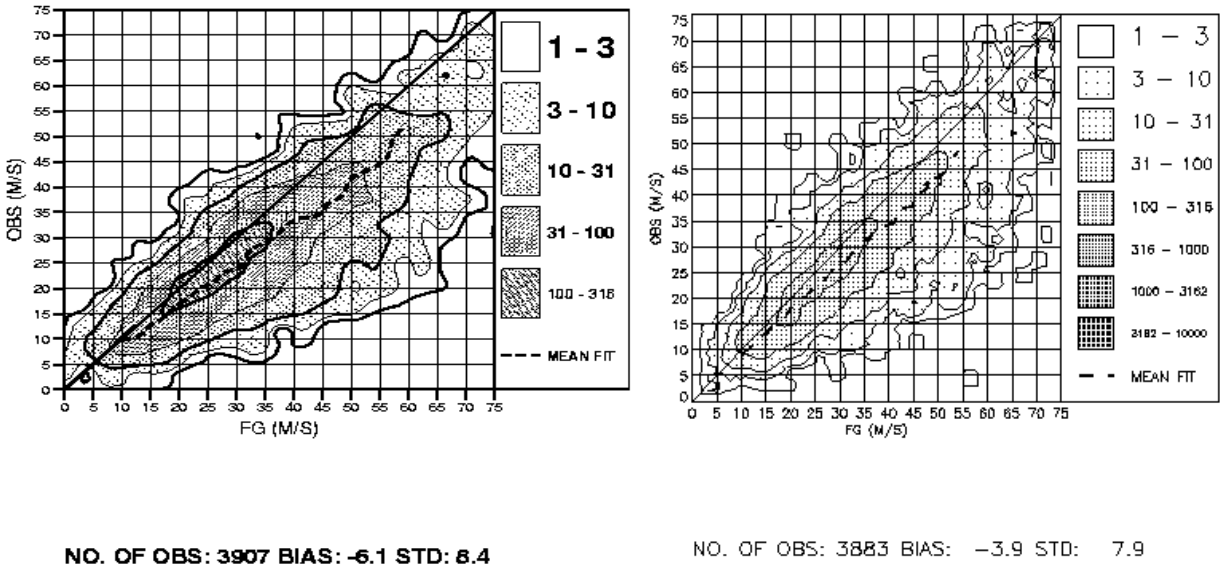

Figure 3. Wind speed contour plot for GMS infrared winds in the northern extratropics at high level, averaged for January 2000, compared with a) the ECMWF(left panel) and b) The Met. Office (right panel) background field

The top panel in Fig. 2 shows that use of new BUFR-coded satellite winds from EUMETSAT is providing much more resolution in the wind field than the use of satob-coded winds (ECMWF uses and monitors high-resolution winds provided by EUMETSAT in BUFR code). Relatively small-scale features can be seen over northern Africa in the data, which are not as obvious when the lower resolution satob-coded product is used (Fig. 3, bottom panel). However, some features are consistent, for example, the small plume of positive wind speed bias emanating from southwestern Africa.

3. Future developments

This paper has featured just a small selection of the plots that are available from the NWP SAF Satellite Wind Integrated Monitoring website. The information is freely available on the internet and it is hoped that it will be of interest to the satellite wind community worldwide; it is not intended solely for the NWP SAF. It is thus intended to stimulate thought and discussion and eventually to lead to improved production and use of satellite winds, as well as improvements in NWP models and assimilation procedures. Other NWP centres are invited to contribute to this report, not just those involved in the NWP SAF, and this invitation is extended to centres outside Europe. Data will continue to be added on a monthly basis, and future plans are for cross-links to access the CGMS satellite wind monitoring site, to encompass comparison of satellite winds vs radiosondes and aircraft. Feedback is invited from viewers of the website (a contact link is provided), and the format is expected to evolve accordingly. A summary of preliminary results will be compiled in spring 2000. It is envisaged that this website will eventually replace the ECMWF quarterly satob monitoring report.

REFERENCES

Gustaffson J. and M. Lindberg (2000) CMW low-level height assignment. *Proc. EUMETSAT Satellite Data Users' Conf.*, Copenhagen, September 1999. EUMETSAT, Darmstadt (in press).

Nieman S., J. Daniels, D. Gray, S. Wanzong, C.S. Velden and W.P. Menzel (1997) Recent performance and upgrades to the GOES-8/9 operational cloud motion vectors. *Proc. 3rd Int. Winds Workshop*, Ascona, Switzerland, June 1996. EUMETSAT, Darmstadt, EUM P 18.

TOWARDS THE ASSIMILATION OF QUIKSCAT WINDS

Ad Stoffelen[1], Marcos Portabella, and Aart Voorrips

Ad.Stoffelen@knmi.nl
Royal Netherlands Meteorological Institute, KNMI

ABSTRACT

At the fourth winds workshop a paper was presented on the importance of ERS scatterometer observations for the forecasting of tropical cyclones with the ECMWF model. Recently, SeaWinds scatterometer measurements from QuikScat have become. SeaWinds on QuikSCAT provides great coverage over the oceans. However, rain contamination, wind direction noise characteristics, and wind direction ambiguity patterns need further study. We describe our work on QuikScat product validation and inversion of the backscatter data to winds. A new procedure to quality control (QC) SeaWinds scatterometer observations, in particular to screen out rain-contaminated points, and a new procedure to assimilate QuikScat observations are presented. Our QC method is based on a methodology that was used to screen anomalous ERS and NSCAT backscatter triplets or quadruplets respectively. The methodology checks whether the consistency of the backscatter measurements at a particular Wind Vector Cell (WVC) is compatible with the consistency as predicted by the Geophysical Model Function (GMF). Rain contaminated points are screened out effectively thus opening the way to effective wind information assimilation. The ERS scatterometer data assimilation procedure is generalised to deal with ambiguous solution sets with more than two solutions of varying probability and quality. ERS provides two ambiguities with about the same quality and probability. Extension of the assimilation procedure is essential to deal with the average 80% probability of the first rank SeaWinds solution and the occurrence of high-probability third and fourth rank solutions.

1. Introduction

ERS scatterometer winds have proven to be very useful for the forecasting of dynamic weather (Isaksen and Stoffelen, 2000; Atlas and Hoffman, 2000). Increased coverage, such as from tandem ERS-1 and ERS-2 measurements, clearly improve the situation (e.g., Stoffelen and Beukering, 1998; Le Meur et al, 1997). Improved coverage from the Ku-band scatterometers NSCAT and SeaWinds have thus great potential. Preliminary attempts to assimilate SeaWinds data have been carried out with mixed success, and improved data characterisation is needed.

The SeaWinds on QuikSCAT mission from NASA is a “quick recovery” mission to fill the gap created by the loss of data from the NASA Scatterometer (NSCAT) after the ADEOS-1 satellite lost power in June 1997. QuikSCAT was launched from Vandenberg Air Force Base (USA) in June 19, 1999. A similar version of the SeaWinds instrument will fly on the Japanese ADEOS-II satellite currently scheduled for launch in late 2001.

The SeaWinds instrument is an active microwave radar designed to measure the electromagnetic backscatter from the wind roughened ocean surface. The instrument is a conically scanning pencil-beam scatterometer, which in comparison with the NSCAT fan-beam scatterometer has the following advantages: higher signal-to-noise ratio, smaller in size, and superior coverage. On the other hand, QuikSCAT has an antenna geometry that is dependent on node number or cross-track location, due to its circular scans on the ocean. The skill of the wind retrieval algorithm depends very much on the number of measurements and their polarization (horizontal HH or vertical VV) and azimuth diversity, where "azimuth diversity" is defined as the spread of the azimuth looks among the measurements in the WVC. The nadir region has fore and aft looks of both beams (HH and VV) nearly 180º apart. At the edges of the swath the outer VV beam fore and aft looks are nearly in the same direction and no inner HH beam information is available. In both areas, the skill of the wind retrieval algorithm is decreased with respect to the rest of the swath (called the sweet zone) where there are four measurements (fore-HH, fore-VV, aft-HH and aft-VV) with enough azimuth diversity.

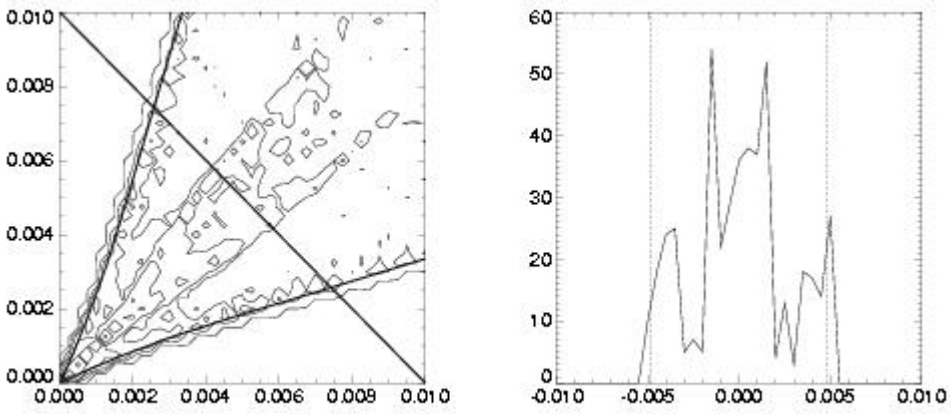

Figure 1. Left: Density-contoured scatter plot of backscatter values for the outer beam for simulated SeaWinds data at WVC 50 with nominally 142 degrees separation between fore and aft look. The scatter plot is build up from Lissajous-type curves that follow an inner revolution and an outer revolution as wind direction changes. The boundary of the outer revolution is shown by the thick lines from the origin outward produced using the NSCAT-2 GMF. Right: Number density along the cross-diagonal thick line of the left plot. The boundaries of the outer and inner Lissajous revolutions are now clearly discernible (Voorrips, 1999). Cross sections of this type are being used to validate aspects of the GMF definition.

The inversion software based on the ERS scatterometer processing (Stoffelen, 1998) modified by Julia Figa (2000) for NSCAT has been adapted for QuikSCAT. In was verified to closely mimic JPL's inversion (Portabella and Stoffelen, 2000). SeaWinds simulations confirm a higher standard deviation of speeds and directions in the outer and nadir parts compared to the sweet zone of the swath. No significant bias is seen in any part of the swath.

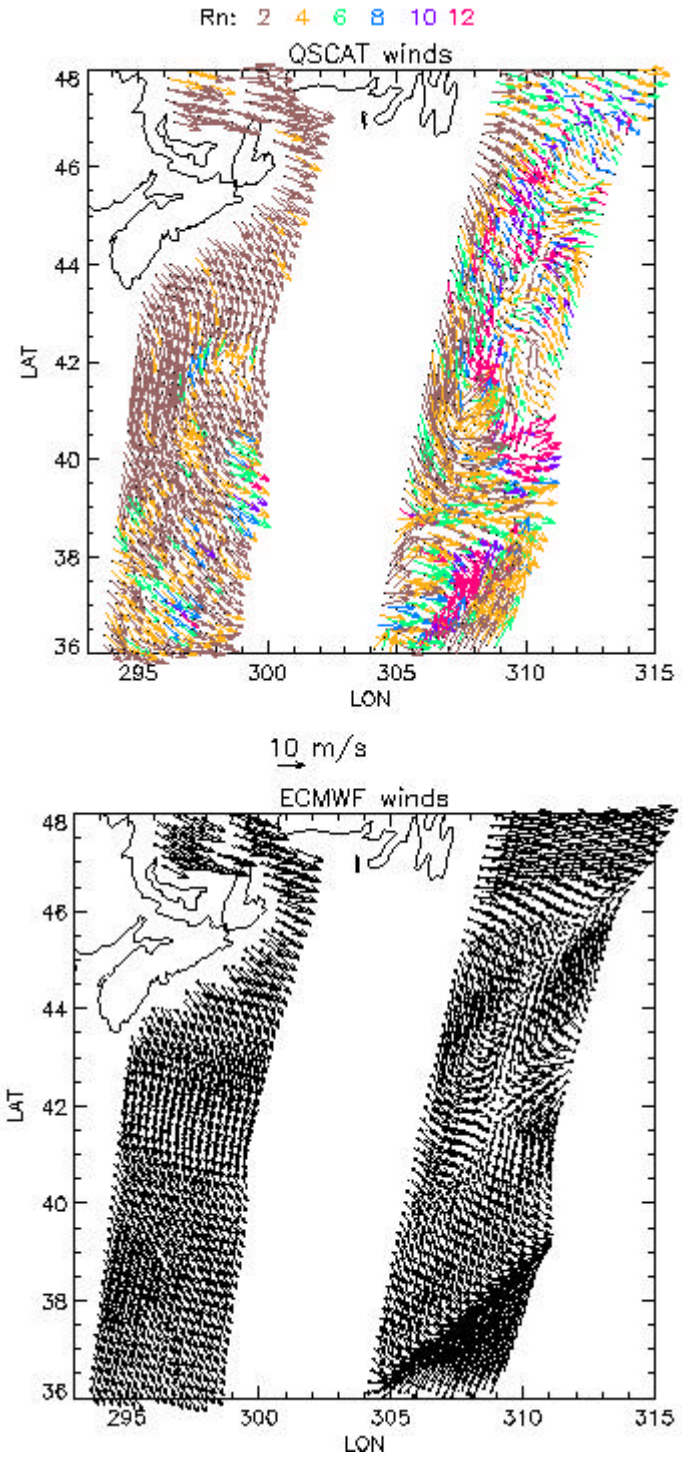

Figure 2. a) Top panel: QuikScat winds in the Atlantic in the development zone of the devastating storms that hit Western Europe during Christmas 1999. Date and time of observation are December 24 22 GMT. The inversion residual is normalised as a function of speed and WVC, such that a number Rn results with an expectation value of one. Rn values for good quality winds between 2 and 4 are thus unlikely, and winds at values above 4 are verified to be generally of bad quality (Portabella and Stoffelen, 2000). The colour code for the Rn values is shown above the plot. Anomalous winds have generally Rn > 4. For Rn < 4 large areas remain that depict relevant and important mesoscale features of the wind field.b) Bottom panel: As for top panel, but ECMWF winds. Dynamical features particularly appearing in the right SeaWinds swath are not well represented in the ECMWF first guess, for example the through orientation and position, and the low at 308E and 41N.

2. Quality control and rain elimination

In contrast with C-band scatterometers such as on ERS and ASCAT, Ku-band scatterometers are sensitive to rain and procedures need to be developed to screen out rain-contaminated measurements.
A quality control procedure is being developed for SeaWinds based on the QC methodology for the ERS scatterometer (Stoffelen and Anderson, 1997; Stoffelen, 1998). In addition to a screening similar to ERS, the procedure acts to remove rain contaminated points (Figa and Stoffelen, 2000). The methodology checks whether the consistency of the backscatter measurements at a particular Wind Vector Cell (WVC) is compatible with the consistency as predicted by the Geophysical Model Function (GMF). A measure of this consistency is provided by the inversion residual. A limitation of this approach is obviously that anomalous geophysical conditions that are still compatible with the GMF are not screened out, such as a few rain points that appear as 15 m/s winds. Such points should ideally be rejected by the QC procedures of NWP data assimilation systems

Alternatively, one could- use the backscatter polarisation ratio, but this has the same limitation and is more restricted (Wentz, 1999); or use the SeaWinds passive noise measurement to detect rain, though this has low accuracy (of 13 K) and a relatively large footprint (> 75 km; Jones, 1999) Particularly in those parts of the SeaWinds swath where azimuth view diversity or polarisation coverage is lacking, notably around nadir and in the far swath, the wind vector may be underdetermined and QC by a consistency check, such as in the above-described methodology, impossible. The part of the swath where this occurs is limited fortunately. SeaWinds on ADEOS may profit from AMSR for rain screening, when all parts of the swath may be controlled.

3. Observation smoothing

SeaWinds data are nominally provided with a sampling of 25 km, whereas most NWP models use scatterometer data at a 100-km density. To reduce wind retrieval noise it is better to average backscatter measurements, σ^0, to lower resolution before wind retrieval. For ERS and ASCAT observations the same applies, where it has been shown that averaged winds compare better to the HIRLAM (2000) first guess than thinned data (Stoffelen and Beukering, 1998). A procedure is being tested and incorporated in the inversion module to average backscatter measurements in a resolution cell of varying size.

4. SeaWinds assimilation

Stoffelen (1998; chapter VI) describes the problem of the assimilation of variables that are related in a non-linear way to the NWP model variables, such as scatterometer backscatter measurements. As a practical solution, he suggests to assimilate retrieved scatterometer winds. This approach is further pursued here for SeaWinds scatterometer observations. Scatterometer winds can be retrieved accurately, since backscatter noise is generally small for all scatterometer systems. Backscatter-only noise results in a wind vector uncertainty of only about 0.5 m/s. However, the interpretation of a radar backscatter measurement, that is more directly related to the anisotropic roughness of the ocean topography, as a wind at 10m height introduces a much larger uncertainty, that can be well modelled as a normal wind component error distribution. Wind vector measurements from a scatterometer have an estimated accuracy of about 2 m/s. The larger uncertainty in the wind domain makes the assimilation of retrieved winds more attractive than the direct assimilation of backscatter measurements. In the direct assimilation of backscatter observations, one transforms the first guess errors and the uncertainty in the Geophysical Model Function (GMF) in a non-linear way to the backscatter space, resulting in a usually skew error distribution in this space. The precise form of the error distribution would depend on wind speed, wind direction, and view configuration. The maximum probability in a skew distribution does generally not overlap with the mean of the distribution, nor has the maximum symmetric properties. The optimal observation cost function is not a priori clear in such a case and requires considerable thought (Stoffelen, 1998). By the assimilation of retrieved winds this problem disappears.

5. Ambiguity removal

NSCAT and SeaWinds use horizontal and vertical polarisation measurements, whereas ERS or ASCAT are solely based on vertical polarisation. This in combination with a varying measurement geometry results in a different wind direction ambiguity structure than for ERS or ASCAT. The near-nadir and far swath areas of SeaWinds are particularly difficult to QC and invert, due to poor sampling in azimuth.

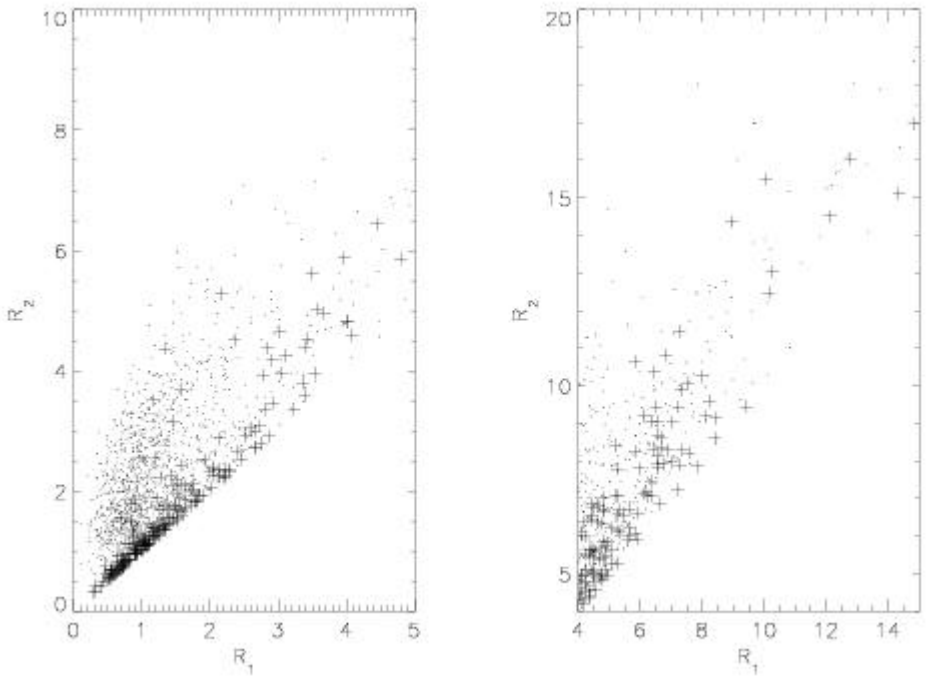

Figure 3. Scatter plot of first rank normalised inversion residual R_1 against second rank solution residual R_2 only for cases with two solutions. Dots indicate pairs where the first rank is the one closest to the NWP wind velocity; plusses are pairs where the second rank is selected. The left panel highlights the lower range residuals of 1,500 pairs, whereas the right panel only shows higher range pairs of a total of 15,000 pairs. For Rn values smaller than three the first rank is almost always selected, unless $R_1 \approx R_2$. For higher Rn either rank may be selected, indicating less predictive value in Rn. Note however that many of these are screened by our QC. As such, SeaWinds ranking information in Rn appears to be an excellent predictor.

The ERS scatterometer cost function may be generalised to be able to cope with all scatterometer data. All scatterometer data can be characterised by multiple wind vector ambiguities that each have different probability and accuracy. A procedure is being developed that estimates this probability and accuracy and as such provides the input for a general scatterometer cost function. The working of the cost function for ambiguity removal is being tested and documented (Voorrips, Stoffelen, and Portabella, 2000).

Generally data assimilation systems constrain to a background or first guess field and to observations (e.g., Courtier, 1998 and 1999). The observation term consists of a contribution from each observation and is related to the probability of a meteorological state, given the measurements. For scatterometer data we may write

$$p(\mathbf{s}^0 \mid \mathbf{v}) = \sum_{i=1}^{M} p_i^p \, p_i(Rn_i) N(\mathbf{v}_i, \mathbf{e}_i) \qquad (1)$$

where p_i^p is the prior probability of a solution i, $i \in [1, M]$, i.e., without knowledge of Rn. It is solely dependent on the wind direction sector that a solution represents and only relevant in case of more than two solutions ($M > 2$). $p_i(Rn_i)$ is the probability of a solution based on the normalised residual of the solution i. It is assumed to be independent of p_i^p. $N(\mathrm{v}_i, \varepsilon_i)$ is a normal distribution with maximum at the

wind solution v_i and error width ε_i. For ERS scatterometer data (Stoffelen, 1998) the values $M = 2$, $p_i^p = 0.5$, $p_i(Rn_i) = 1$, and $\varepsilon_i = 1.5$ m/s are used. For NSCAT or SeaWinds, the prior probability p_i^p just depends on the azimuths of the solutions (Figa and Stoffelen, 2000). Since the wind error in the sweet zone is mainly dependent on the geophysical interpretation and less on the retrieval process, ε_i does not vary much from one solution to the next, As such, the main modelling effort is in $p_i(Rn_i)$. Figures 4 and 5 illustrate this. Figure 5 shows that *Rn* can very well be interpreted as a probability, thus facilitating the implementation of equation 1.

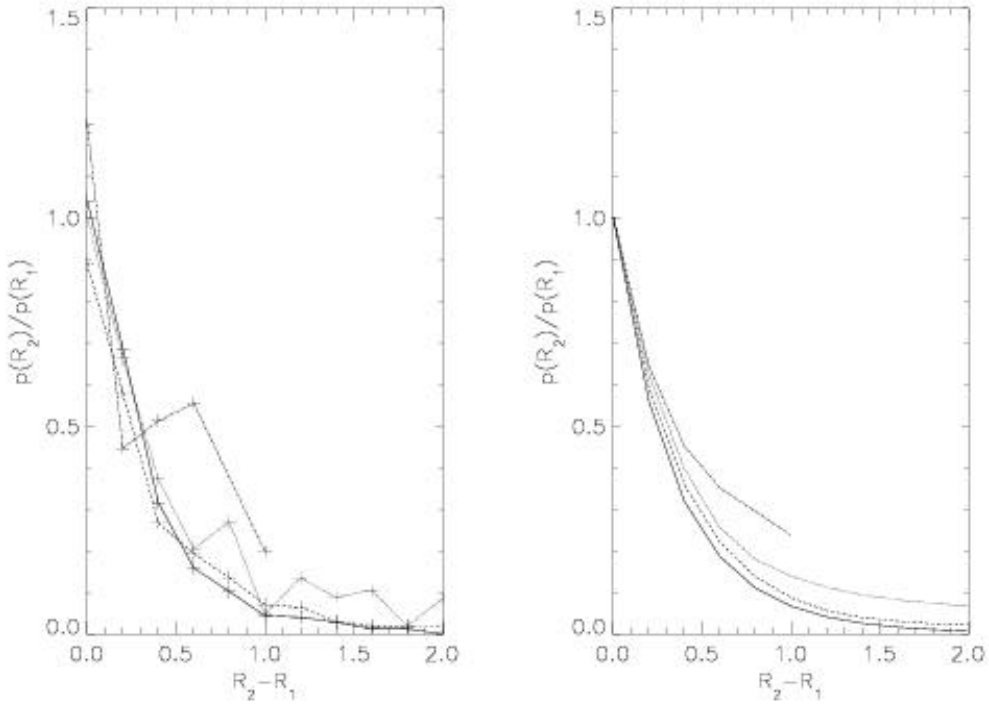

Figure 4. Ratio of the number of realisations of R2 and the number of realisations of R1 as a function of R2 – R1, and for values of R1 = 0.5 (solid), R1 = 1.1 (dashed), R1 = 1.7 (dotted), and R1 = 2.1 (dash-dot). The left plot is based on real data and the right plot is constructed using an exponential relationship p(Rn). The normalised residual can be well explained in terms of a wind solution probability.

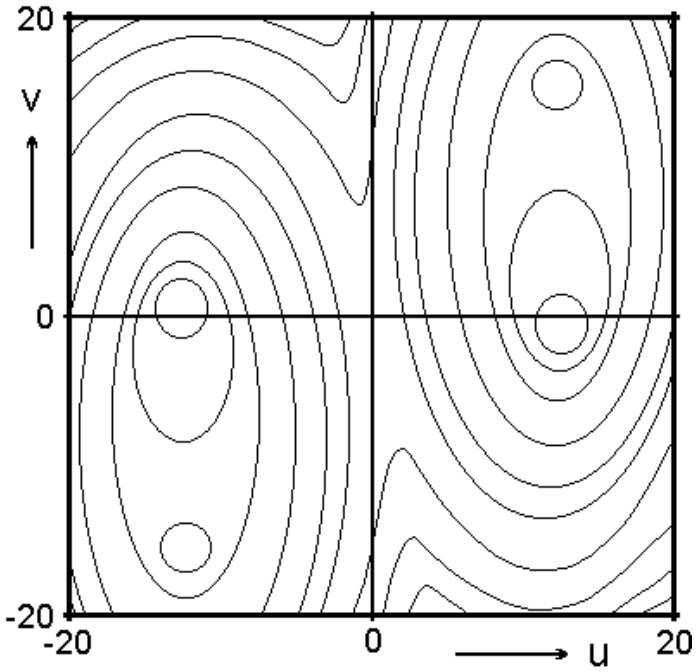

Figure 5. Illustration of wind probability contours as a function of the wind components u and v for a SeaWinds wind vector cell with measurements at four different azimuths including two polarisations. Multiple minima exist, resulting in a slightly more complex variational assimilation.

The generalised methodology may also be applied for those parts of the swath where the wind vector cannot be fully determined, because of limited azimuth or polarisation coverage, and where the ambiguity pattern can be of greater complexity. However, in these parts of the swath the solution minima may be less well defined than in the sweet zone. In that case, the width of the minimum can be decomposed into two independent wind components, e.g., along the wind vector solution and across or any other orthogonal set, that model the possible anisotropy of the retrieval solution minimum width. ε_i is then determined by these widths and the isotropic geophysical interpretation error of about 1.5 m/s in a component. Another limitation is that for some parts of the swath QC may be difficult and assimilation therefore more risky (see section 2 above). AMSR on ADEOS-II is likely to ease this problem.

6. Conclusions

Within the EUMETSAT-funded NWP Satellite Application Facility, SAF, a SeaWinds processing package is being developed that checks, spatially averages, and inverts backscatter data. After these steps a 2D-VAR ambiguity routine will be run to investigate the ambiguity removal properties of the cost function and observation operator as proposed here. After these tests, application in 3D- or 4D-Var (e.g., Courtier, 1998 and 1999) data assimilation systems is a straightforward development.
Following our procedure, we expect that carefully screened, smoothed, and assimilated SeaWinds scatterometer data from QuikSCAT and ADEOS-II have great potential in NWP.

ACKNOWLEDGEMENTS

We acknowledge NASA and NOAA for providing the QuikSCAT data and help using it, and the project and science teams for their inspiring meetings. The collaboration with ECMWF, and more in particular Mark Leidner, on visit from AER, and Lars Isaksen has proven very fruitful. EUMETSAT supports our activities within the context of the NWP SAF and by providing an EUMETSAT fellowship.

REFERENCES

Atlas, R., and R.N. Hoffman, 2000: The Use of Satellite Surface Wind Data to Improve Weather Analysis and Forecasting? , To appear in *Satellites, Oceanography, and Society*.

Courtier, P., et al, 1998, The ECMWF implementation of three dimensional variational assimilation (3D-Var). Part I: Formulation, *Quart. J. Royal Meteol. Soc.* 124, 1783-1808.

Courtier, P., et al, 4D-Var, ECMWF documents, 1999.

Figa, J., and A. Stoffelen, 2000, "On the Assimilation of Ku-Band Scatterometer Winds for Weather Analysis and Forecasting", IEEE-IGARS special issue on scatterometer applications, accepted.

HIRLAM, 2000:
http://www.knmi.nl/hirlam.

Isaksen, L., and A. Stoffelen, "ERS-Scatterometer Wind Data Impact on ECMWF's Tropical Cyclone Forecasts", IEEE-IGARS special issue on scatterometer applications, accepted.

Jones, Linwood, and David G. Long, 1999, QuikSCAT Radiometric Calibration and Special Brightness Temperature Product, *Proceedings from the QuikSCAT cal/val - early science meeting,* 2-5 November 1999, JPL, Pasadena, California.

KNMI satellite section web site.
http://www.knmi.nl/onderzk/applied/en/sd_index.html

Le Meur, Didier, Lars Isaksen, and Ad Stoffelen, ? Impact of ERS-1/ERS-2 scatterometer tandem on the ECMWF 3D-var assimilation system? , *Proc. Of the third ERS symposium – space at the service of our environment*, Florence, 17-21 March 1997, ESA special report, ESTEC, Noordwijk, the Netherlands, 1997.

Portabella, Marcos, and Ad Stoffelen, EUMETSAT QuikSCAT Fellowship Progress Report, KNMI, de Bilt, the Netherlands, 2000.

Stoffelen, Ad, 1998a, "Scatterometry", PhD thesis, ISBN 90-393-1708-9.
http://pablo.ubu.ruu.nl/~proefsch/01840669/inhoud.htm.

Stoffelen, A. C. M. and D. L. T. Anderson, 1997c, Ambiguity removal and assimilation of scatterometer data, *Q. J. Roy. Meteorol. Soc*., 123, 491-518.

Stoffelen, Ad and Paul van Beukering, "The impact of improved scatterometer winds on HIRLAM analyses and forecasts", BCRS study contract 1.1OP-04, report published by BCRS, Delft, The Netherlands, and HIRLAM technical report #31, published by IMET, Dublin, Ireland, 1997.

Voorrips, Aart, 2000, Preliminary work in the QuikSCAT observation operator definition, KNMI.
(PDF http://www.knmi.nl/onderzk/applied//pdf/QuikSCAT_OO.pdf)
(Postscript http://www.knmi.nl/onderzk/applied/ps/QuikSCAT_OO.ps)

Vries, de, John, and Ad Stoffelen, 2000, 2D variational ambiguity removal, Project report for the BCRS, KNMI, de Bilt, the Netherlands.

Wentz, Frank, Deborah Smith, and Carl Mears, 1999, Rain and the QuikSCAT winds, *Proceedings from the QuikSCAT cal/val - early science meeting,* 2-5 November 1999, JPL, Pasadena, California.

RECENT IMPROVEMENTS IN THE QUALITY OF INSAT DERIVED CMVS AND THEIR USE IN NUMERICAL MODEL FORECAST

P. N. Khanna , R. C. Bhatia and Devendra Singh.
India Meteorological Department New Delhi 110003, India.

ABSTRACT

INSAT derived Cloud Motion Vector (CMVs) have been improved recently by introducing the new scheme proposed during 4th International Wind workshop (Khanna et al. 1998). India Meteorological Department (IMD) is generating Limited Area Model (LAM) forecast operationally for last five years. Earlier Quality Assurance (QA) tests of INSAT derived CMVs were done using low resolution 12 hour forecast from NCEP Washington or ECMWF. These forecasts earlier did not use satellite derived CMVs from INSAT or other satellites from data sparse Indian Ocean. Other centers did not find INSAT CMVs of reliable quality. Before July 98, no other satellite except INSAT covered the data sparse Indian Ocean. In July 98, METEOSAT-5 was shifted over Indian ocean at 63 deg. E. Recently improved algorithm uses LAM forecast in QA tests. Pressures and heights are assigned on the basis of mean temperature of certain percentage of cloud population at the cold end of the spectrum. Detailed comparison of CMVs from INSAT and METEOSAT-5 has been done. The improved CMVs from INSAT and METEOSAT-5 show quite good agreement qualitatively. The bias and RMS also show improvements. Zonal winds reported earlier have shown improvement. The lesser number of INSAT CMVs is due to lower spatial resolution of INSAT radiometer compared to METEOSAT–5. The two sets of CMVs generated from triplet of images are being combined, taking care of excluding the collocated CMVs in the two sets. The improved INSAT derived CMVs have shown positive impact on the Model forecast. This is mainly due to proxy data (CMVs) assimilation in the model.

1. Introduction

The Cloud Motion Vector derivation is a challenging job. The challenges involve, 1) Tracer, Target image registration and navigation, 2) Passive tracer selection, 3) Pattern matching of the reference window of tracer image at different lag positions in search window of target image, 4) Vector computation, 5) Height assignment to derived vector, 6) QA tests on derived vectors 7) Manual editing any spurious vectors. Height assignment is the most challenging. LAM (Krishnamurti T. N. et. al, 1990) is being used operationally in IMD since 1995. The model has horizontal grid of 1^0x 1^0, in latitude/longitude and uses 12 sigma levels. The model uses all conventional and satellite derived information in its assimilation scheme covering, vast data sparse Oceanic areas around India. It was, therefore felt that presently generated IMD LAM forecast is more reliable for QA tests. Recently METEOSAT-5, an additional data source over Indian Ocean has become available. However, it will take some time before this data can be assimilated into the model. The only limitation of LAM model forecast is the limited area (40 deg. E to 129 deg. E, -29 deg S to 45 deg N). There is scope for improvements in quality of INSAT derived CMVs. The approach needed improvement in image to image registration, and image navigation. Any error in registration translates into additional vector thereby resulting in poor quality of CMVs (Daniels J. M et. al. 1990). The quality of the numerical weather forecast has also direct impact on the quality of CMVs since the forecast is used in QA tests for CMVs. It is, therefore desirable that the numerical forecast uses conventional as well as satellite derived information from Indian ocean area in its data assimilation scheme. The model forecasts from NCEP and ECMWF did not assimilate INSAT CMVs into the model. This resulted in rejection of CMVs in QA tests. The zonal flow, high speed bias and RMS compelled other centers not to use INSAT CMVs. Forecast over Indian Ocean indicated improvement, when model for the region assimilated INSAT or METEOSAT-5 CMVs for oceanic area. Any other approach only marginally improved CMVs. In view of the above problems the improvements in CMVs were attempted in phased manner. After every change, the quality of CMVs were monitored by analyzing the statistics. These

statistics were computed using the formulae used in ECMRWF SATOB Monitoring reported in the proceedings of third International Wind workshop.

2. CMV generation prior to the improvements

Before the improvement, the selection of cloud tracers was done on four-bin histogram basis. The four-bin histogram classified cloud tracers to low, medium, high or of mixed type. In the case of mixed clouds, the computation was not attempted. The same approach was applied for various lag positions of search window and CMVs were computed using Sequential Similarity Detection Algorithm (SDDA) for pattern matching at different lag positions (Kelkar R.R and Khanna P.N 1986). Later pattern matching has been done, using cross-correlation technique. The navigated images provided wind vectors. The two sets after going through spatial, temporal consistency and QA test were submitted for the manual editing. CMVs were flagged at each stage when they failed. Finally the second set was transmitted on GTS. This provided CMVs with zonal flow and fewer in number. The coarser resolution of model forecast used in QA tests and coarser resolution of imagery resulted in zonal flow.

3. Improvements made in the derivation of CMVs

The improvements in INSAT CMVs were attempted in phased manner. After each attempt the CMVs were monitored to ensure steady and gradual improvements. The attempts were made in three phases.

3.1 Phase 1 (Introduced operationally from 1st Nov, 1999)

The existing registration / navigation approach was not changed and the tracer selection was done on the basis of four bin histogram. The histogram with maximum frequency was the basis of cloud tracer selection. Low medium and high clouds were assigned pressure 925 to 601 hPa., 600 to 301 hPa., and 300 to 200 hPa. The tracer image chip in tracer image and target image chip for different lag positions were pattern matched using cross-correlation. This has been the approach by most of the centers generating CMVs. The tracers in southern hemisphere south of 20 deg. S bring out cloud motion clearly and the coverage of CMVs is very good. These tracers are generally passive and provide CMVs with good coverage and high confidence. The derived CMVs were assigned height and pressure level using LAM forecast to the level at which temperature of cloud cluster matched best with LAM forecast. The CMVs were then quality controlled using collocated forecast, because It uses INSAT derived CMVs in its assimilation scheme and is of high spatial resolution. The quality of INSAT CMVs as reported by UKMO showed smaller speed bias (Fig. 1a, 1b, 1c and 1d) and slight improvement in RMS error for all levels (Fig. 2a, 2b, 2c and 2d). The gap in the data plots for June, 99 is due to missing data. Other centers were still not using INSAT CMVs in their assimilation scheme. After these changes INSAT derived CMVs showed better agreement with METEOSAT-5 derived winds in qualitative terms.

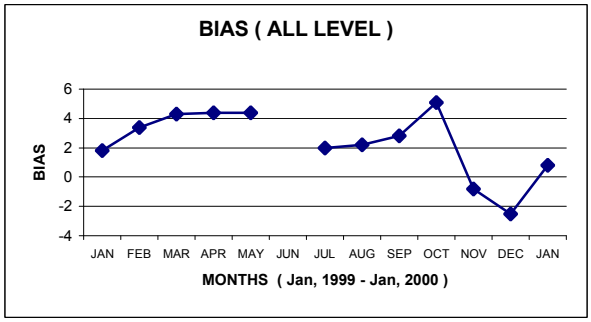

Fig - 1a

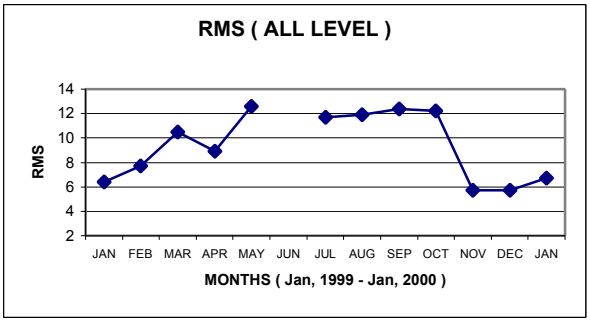

Fig – 1b

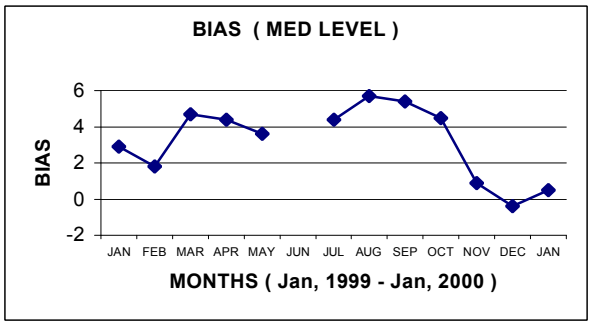

Fig – 1c

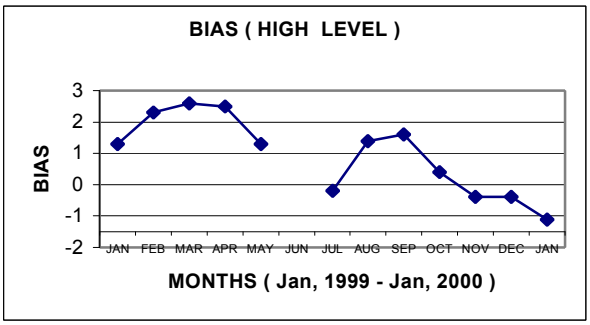

Fig – 1d

Fig 1. Statistics of INSAT CMVs with UKMO Forecast at different levels Note: Data for June, 1999 is not available.

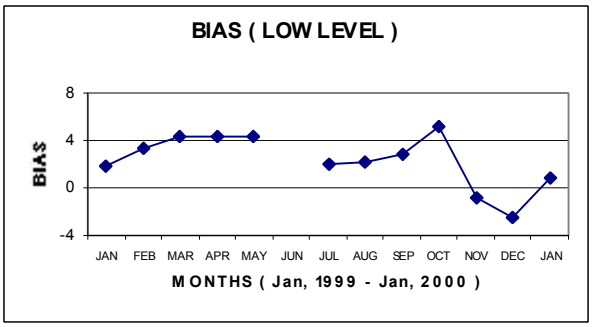

Fig – 2a

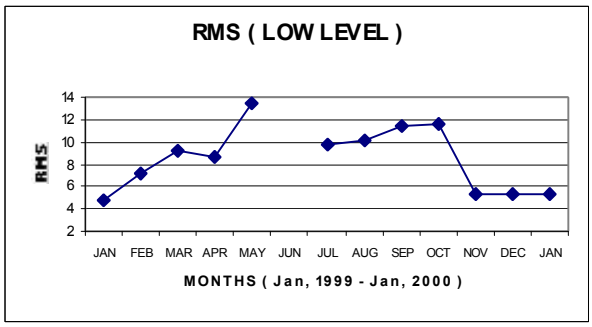

Fig – 2b

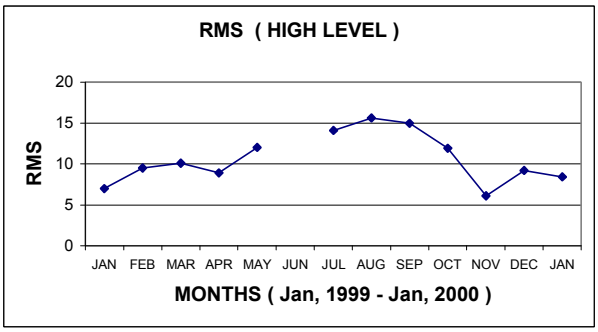

Fig – 2c

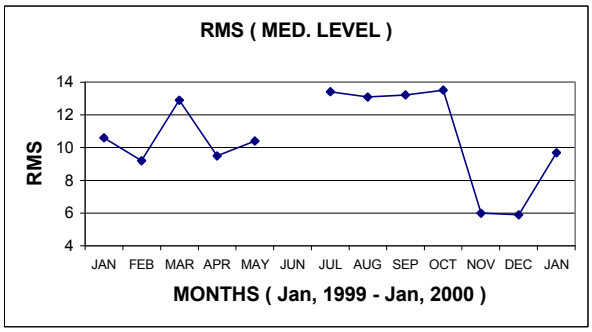

Fig – 2d

Fig 2. Statistics of INSAT CMVs with LAM Forecast/Analysis, Note: Data for June, 1999 is not available.

3.2 Phase 2 (Introduced operationally from 2nd Dec., 1999)

At present INSAT-1D is the only operational Indian satellite, providing meteorological services much beyond the normal expected life. It is now operating in an inclined orbit with its inclination close to 1.8 deg. The successive half–hourly images show poor registration when the images are seen in line/pixel coordinate system. Since all the images are navigated individually, the images in geocentric coordinates system are reasonably registered. The land features showed appreciable movement in the line/pixel coordinate system but in lat/long coordinate system these features show very little movement. The tracer selection for passive tracers was retained to use four-bin histogram. These tracers were tracked using cross-correlation for pattern matching. The height assignment and QA tests were done in the same way. Since LAM has been assimilating INSAT CMVs, it showed gradual improvement as a result of continued use. RMS error (Fig 3) and Speed bias (Fig. 4) for INSAT CMVs show improvement.

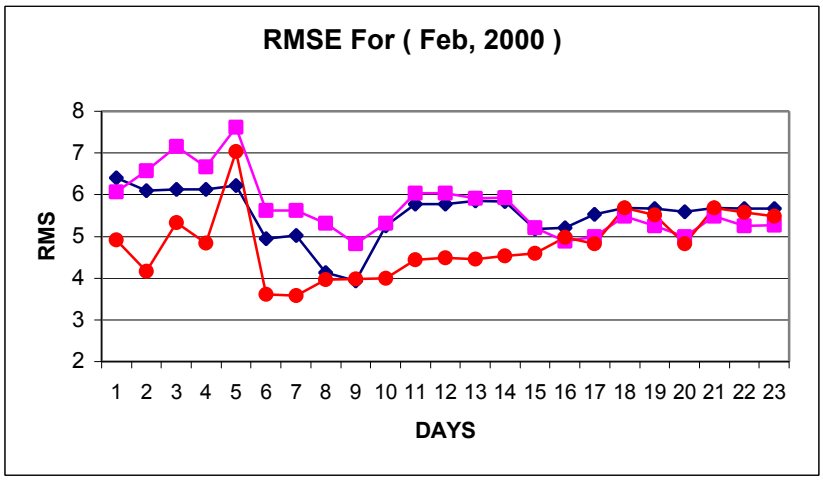

Fig – 3 25 – 601 hpa (Blue) , 600 – 301 hpa (Pink) , 300 – 200 hpa (Red)

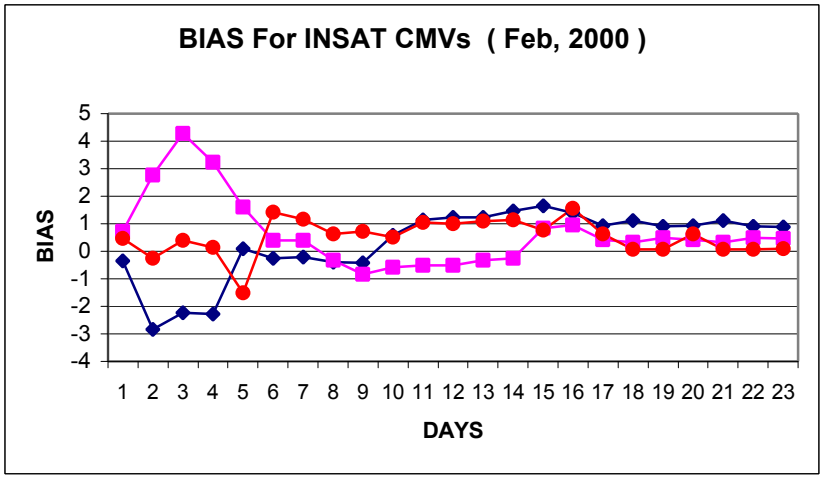

Fig – 4 925 – 601 hpa (Blue) , 600 – 301 hpa (Pink) , 300 – 200 hpa (Red)

3.3 Phase 3 (Introduced operationally from 2nd Feb., 2000)

Registration of images was further improved and height was assigned on the basis of the cloud top temperature using mean temperature of 25% of the coldest pixels (Nieman S. J et al. 1997). The cloud types and cloud heights were reassigned on this basis. These changes brought out very well even strong winds with speeds 80 to 100 kts, generally experienced during winter at 10 to 12 km height. These features were not being brought out earlier. These improved CMVs are in close agreement with METEOSAT-5 derived CMVs. Some meteorological features which were not brought out earlier by INSAT CMVs are being brought out very clearly. INSAT CMVs agreed very closely with METEOSAT–5 CMVs. QA tests with LAM forecast have improved INSAT CMVs. Inter-comparison of RMSE for GOES, GMS, MEOSAT-5 and INSAT from NCMWF shows close agreement (Fig. 5).

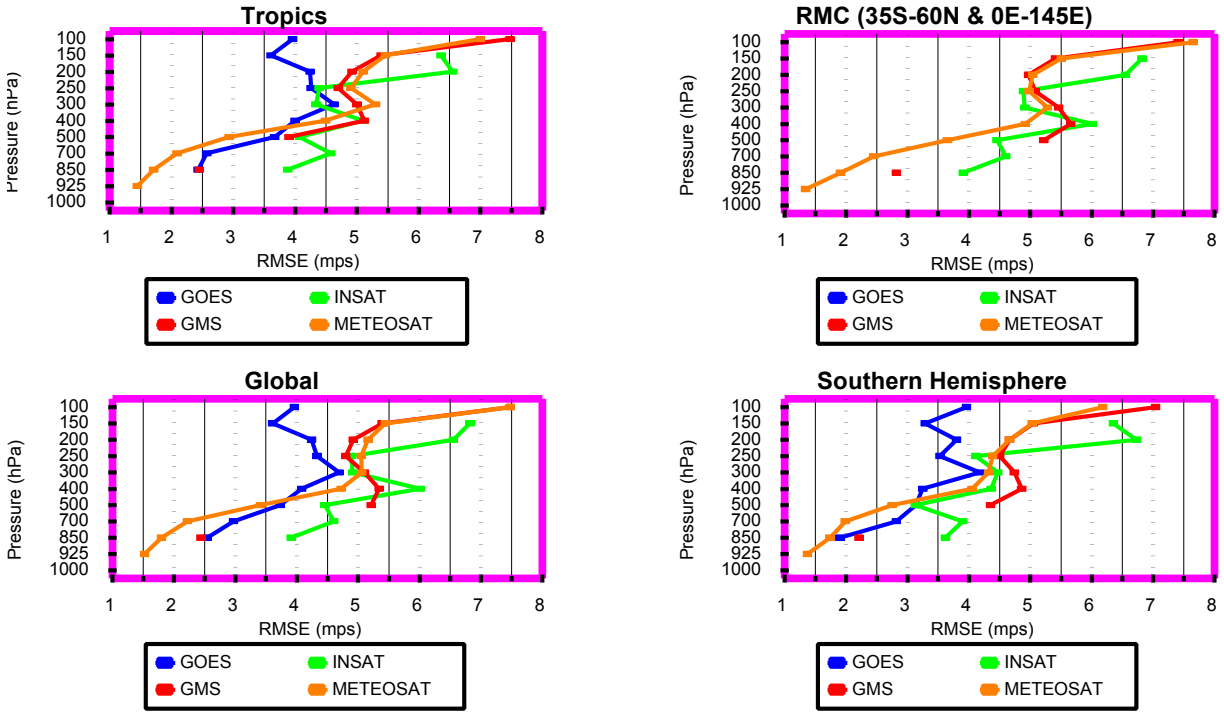

Fig - 5 Vector Wind RMSE of different Satellite with NCMWF Forecast (Jan & Feb, 2000)

4. Development plan for future

Further improvements have been planned based on the cluster classification using objective analysis (Cockley, Bretherton 1982; Schmetz et. al. 1993). This is expected to improve the quality of CMVs, bringing their overall quality closer to those generated by other centers. INSAT-3A VHRR with Infrared, visible and water vapor channels of higher spatial resolution, than that of INSAT 1D, will be available in the year 2001. It will also have a CCD payload with 1km resolution in Visible, Near IR and Short-wave IR bands. The ground processing system is being upgraded for additional processing load. It will provide CMVs more frequent and of better quality. In addition Water Vapor Winds (WVWs) will also be derived operationally providing extensive coverage more frequently. CCD will provide capability of more rapid scanning which will be useful to provide high resolution CCD CMVs more frequently using thermal IR and WV bands from VHRR for correct height assignment using IR - WV intercept approach (Nieman et. al. 1997). This is expected to provide more frequent, extensive coverage of satellite derived winds from CCD, IR and WV bands of VHRR (Velden C. S et al 1997).

5. Conclusions

Use of high spatial resolution LAM forecast produced in IMD has shown the improvements in the derived CMVs. This is because the model assimilates INSAT derived CMVs and has higher spatial resolution. The spatial resolution also partially removed the zonal flow reported earlier. INSAT does not have CO_2 ratioing or IR – WV intercept option, this caused poor height assignment resulting in CMV rejection in case of sub-pixel sized clouds or thin Cirrus with lower emissivity. Taking recourse to mean temperature of certain percentage (25 %) of coldest cloudy pixels helped reducing the emissivity problem.

ACKNOWLEDGEMENT

Authors wish to acknowledge the help rendered by Mr. Mukherjee S. K., of Satellite Division for providing lot of useful technical assistance for completion of work.

REFERENCES

Coakley J. A. and Bretherton F. P., 1982: Cloud cover from high resolution Scanner data: Detecting and Allowing for partially filled field of view, *J. Geophys. Res.*, **87**, 4917- 4933.

Daniels J. M. et. al., 1998: Recent advances to the operational GOES wind processing system at NESDIS, *Proc. of 4th International Wind workshop,* Oct. 20-23, Saanenmoser, Switzerland, 29-39.

Kelkar R. R, Khanna P. N, 1986: Automatic extraction of cloud motion vector from INSAT 2B imagery, *Mausam*, **37**, 495-500.

Khanna P. N, Sant Prasad 1998 " New Approach for Height Assignment and Stringent Quality Control Tests for INSAT derived Cloud Motion Vector, *Proc. of 4th International Wind Workshop,* Oct. 20-23, Saanenmoser, Switzerland, 255-262.

Krishnamurti T. N., Arun Kumar; et. al., 1990: Performance of a high resolution mesoscale tropical predction model, *Adv. Geophys*., **32**, 133-286.

Nieman S. J. et. al., 1997: Fully automated cloud drift winds in NESDIS operation, *Bull. Amer. Meteor. Soc*., **78**, 1121-1133.

Robert T. M. et al, 1990: A report of recent NOAA's upgraded capability to derive satellite winds, CIMSS, Madison, Wisconsin.

Schmetz J. et al 1993: Operational cloud motion winds from Meteosat Infrared images, *J. Appl. Meteor*. **7**, 1206-1225.

Velden C. S, et al 1997," Upper tropospheric winds derived from Geostationary satellite water vapor observation" BAMS Vol.78, 2,173-195pp.

GEOMETRIC CLOUD HEIGHTS FROM METEOSAT AND AVHRR

G. Garrett Campbell[1] and Kenneth Holmlund[2]

[1] Cooperative Institute for Research in the Atmosphere
Colorado State University

[2] EUMETSAT

ABSTRACT

Geometric cloud height estimation provides an alternative to cloud top temperature methods if two satellites view the same cloud. First we demonstrate the stereo cloud height derivation with a combination of Meteosat 7 and Meteosat 5 5 km resolution Infrared data. Comparison with the temperature technique shows consistency in the majority of the clouds, but some differences. This demonstrates the stereo method as a verification tool for satellite cloud top temperature height retrievals. A case study of Meteosat plus AVHRR shows that the geometric technique can be extended beyond the range of overlapping geosynchronous observations. This uses an asynchronous stereo technique because the observations are not simultaneous.

1. Introduction

Estimating winds from cloud motion measured by satellite imagery has been studied for more than twenty years (Menzel, 2000). It is now being performed operationally for weather forecast model initialization. One source of uncertainty in the resulting wind fields is the height of the wind vector (). Combining the cloud top temperature, cloud emissivity and a temperature profile is the standard method for estimating cloud heights. Observations from different view points of the same cloud provides a method to measure cloud heights just from the geometry of the observations. This can be done with simultaneous stereo or asynchronous stereo where the cloud motion is derived at the same time as the geometric height().

2. Simultaneous Stereo: Meteosat 7 plus Meteosat 5

At EUMETSAT an automatic procedure has been developed to track clouds across sequences of images to estimate cloud motion (Schmetz et al. 1993). This has been adapted to the stereo problem. First a Meteosat 5 image from the INDOEX project (63^{o}E subpoint) was remapped to the Meteosat 7 projection (0^{o}E subpoint). This remapping assumes the input and output grids are on the geoid. Then the images were feed into the automatic tracking program to select and match cloud locations. The pair of latitude, longitudes were then analyzed for geometric height. These locations differ because of different parallaxes from the different view points. In essence the stereo software draws a line from the observation point and the apparent location of the cloud. A least squares fit is used to find the closest approach of the two lines from the different view points. With perfect measurements, the lines would intersect, but the fit is required because small measurement errors and navigation errors preclude the intersection of the two lines.

Figure 1 shows a Meteosat picture with superimposed cloud heights represented as colored spots. The first test of the algorithm is spatial consistency: are the heights random or organized like the underlying clouds. Qualitatively, the heights seem reasonable.

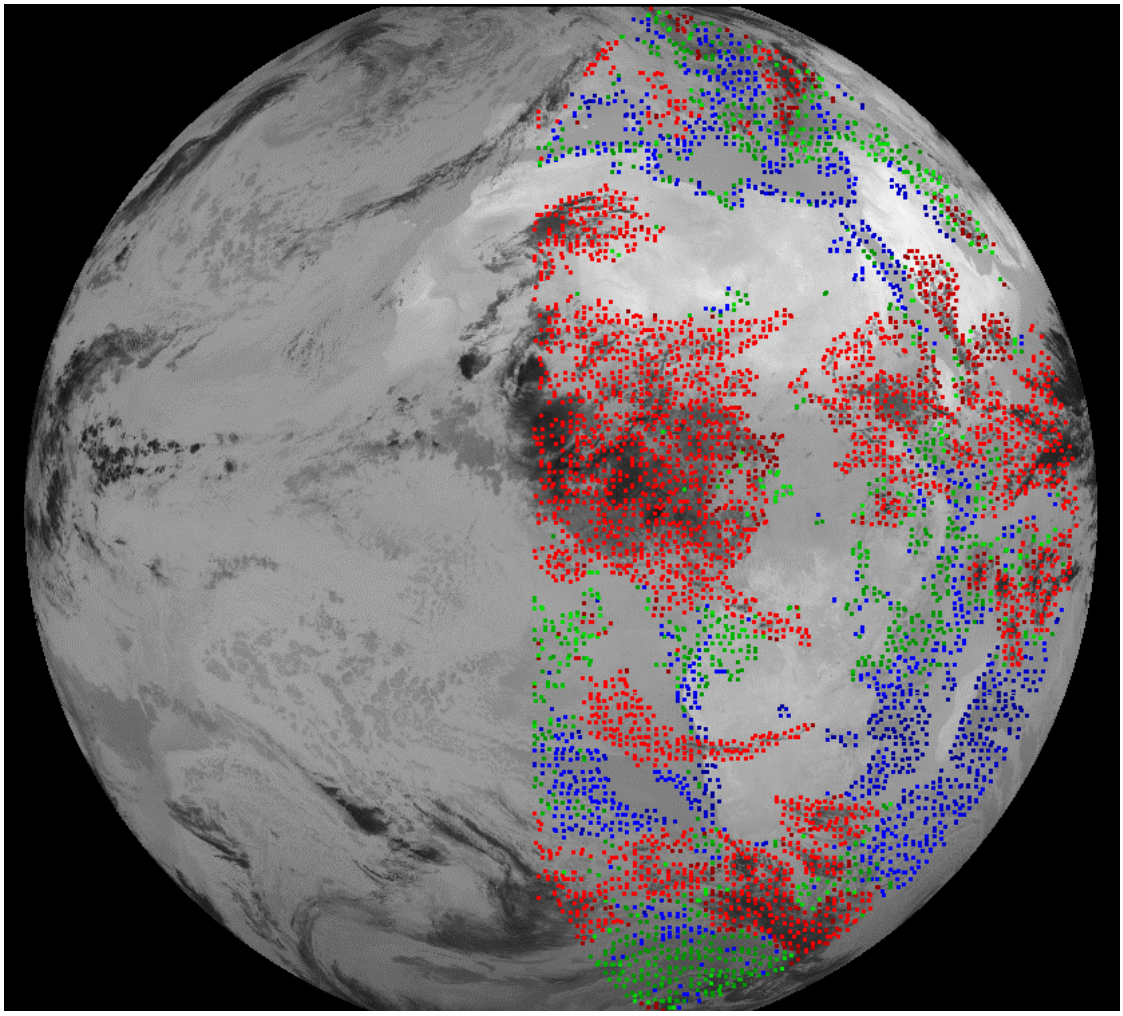

Figure 1. IR stereo cloud height analysis June 21, 1998: Consistency shows that the technique produces reasonable results. Red >7 km; Green 4 km < Z < 7 km; Blue < 4 km

This was applied to 5 km resolution infrared data. At first sight, this would seem too coarse a resolution to detect the subtle parallax shifts of cloud at different levels. But in fact the location of groups of pixels can be located to better than $\pm$ one pixel. This is incorporated in the standard EUMETSAT tracking software.

In the EUMETSAT cloud track procedure, the cloud top temperature is converted to cloud top pressure using the ECMWF temperature profile prediction for the time of the image (Schmetz et al 1993). Using the same profile, the geometric cloud heights were converted to pressure for comparison. Figure 2 shows a scatter plot of the two cloud top pressure estimates. In the majority of the cases, there is a match in heights within 107mb. This consistency is similar to other cloud top height comparisons (Nieman et. al., 1993).

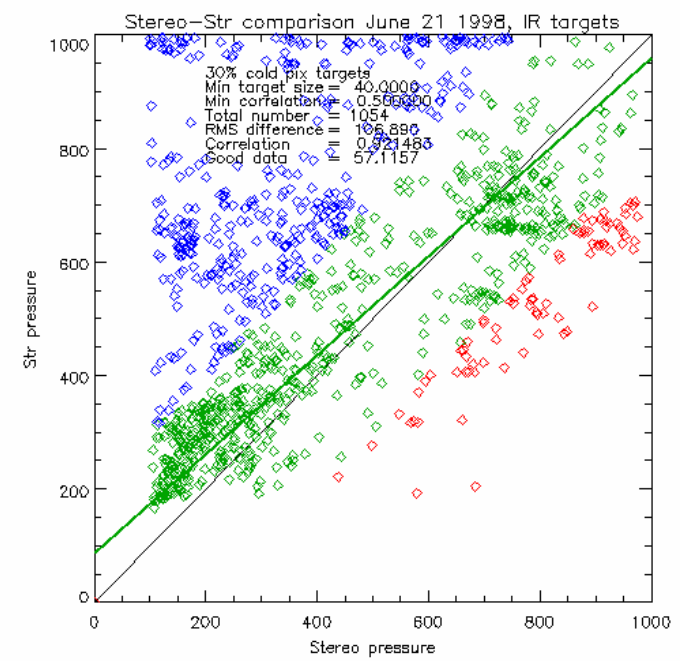

Figure 2. Cloud pressure derived from a simple cloud top temperature scheme (30% coldest pixels of a target) compared to the stereo pressures. The clusters in green show good correspondence. The red and blue clouds show areas of disagreement and potential algorithm improvement.

A further segregation of the cloud types is preformed in the automatic analysis. From the radiance in the window channel and the water vapor channel it is possible to distinguish semitransparent clouds. Figure 3 and 4 shows a comparison of the semitransparent clouds with stereo results. The cloud from the blue locations are clearly areas where the semi-transparent analysis should have been applied. The has been verified by a thorough image analysis showing that all these points originate from one extremely thin cloud for which the semi-transparency correction scheme did not sufficiently correct the pressure. The red areas indicate areas where the semi-transparent analysis was applied and in some cases over corrected the heights. The geometric scheme measures the height of the cloud edge but the temperature scheme searches of the coldest cloud top. Further study on the mismatched locations is warranted.

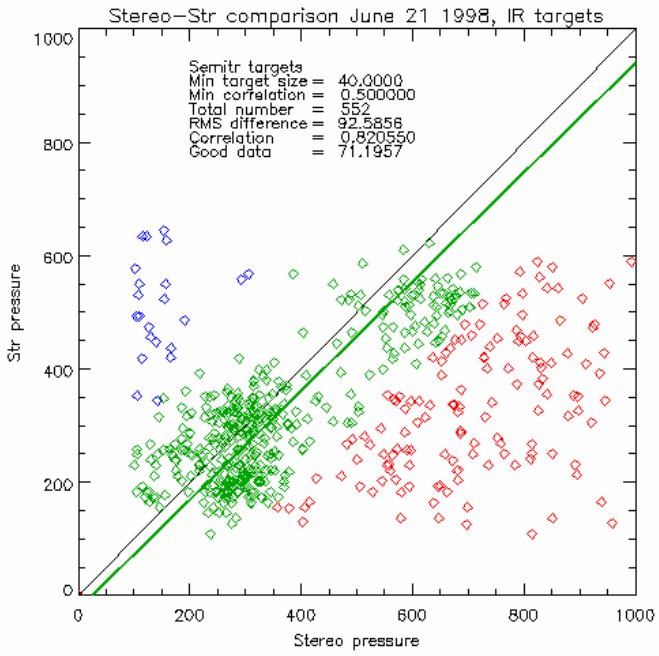

Figure 3. Cloud pressure from the semi-transparent cloud height analysis and stereo pressure.

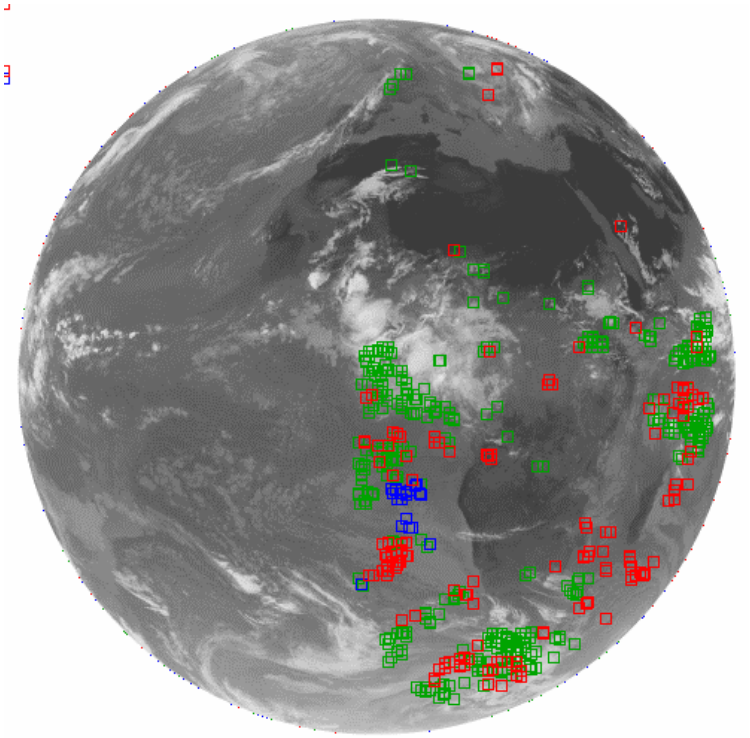

Figure 4. Cloud height matching between stereo heights and height derived with the semi-transparency scheme. The red targets clustered over the South Atlantic are related to very thin cirrus that were not detected by the temperature scheme. The blue targets east of Africa were falsely interpreted by the temperature scheme as transparent clouds.

3. Asynchronous Stereo: AVHRR + Meteosat 7 or Meteosat 5

To further test the geometric technique, a merger of AVHRR and Meteosat was performed. Here an asynchronous stereo analysis is required, because the observations are not simultaneous and the clouds often move between observations. The idea of fitting is performed here as well but allowing the cloud to move between observations. (Campbell 1998)

Figure 5 shows an image of AVHRR remapped to the Meteosat 7 projection, 1999 day 150 near 17:00. A movie loop of the M7 image at 17:00, AVHRR and M7 at 17:30 shows displacements of the clouds due to motion in time and parallax from the different view points. Again the automatic cloud selection and tracking software was run on these images to find successive cloud locations from the three images. The asynchronous technique uses the times, view points and locations of each cloud track to derive both motion and geometric height. Superimposed on the figure 7 are the cloud height estimates. As in the simultaneous stereo case, regional consistency shows the technique is working qualitatively.

As a reference, stereo heights were derived from the pair of Meteosat 5 and 7 images at 17:00. Figure 6 shows a scatter plot of heights of matching clouds. Very similar heights were obtained from the two. A hand adjustment was needed to the remapped AVHRR image, because the operational navigation of AVHRR is often not accurate to $\pm$ 10 km. This is not an inherent problem of the satellite, but a choice of NOAA operational procedures.

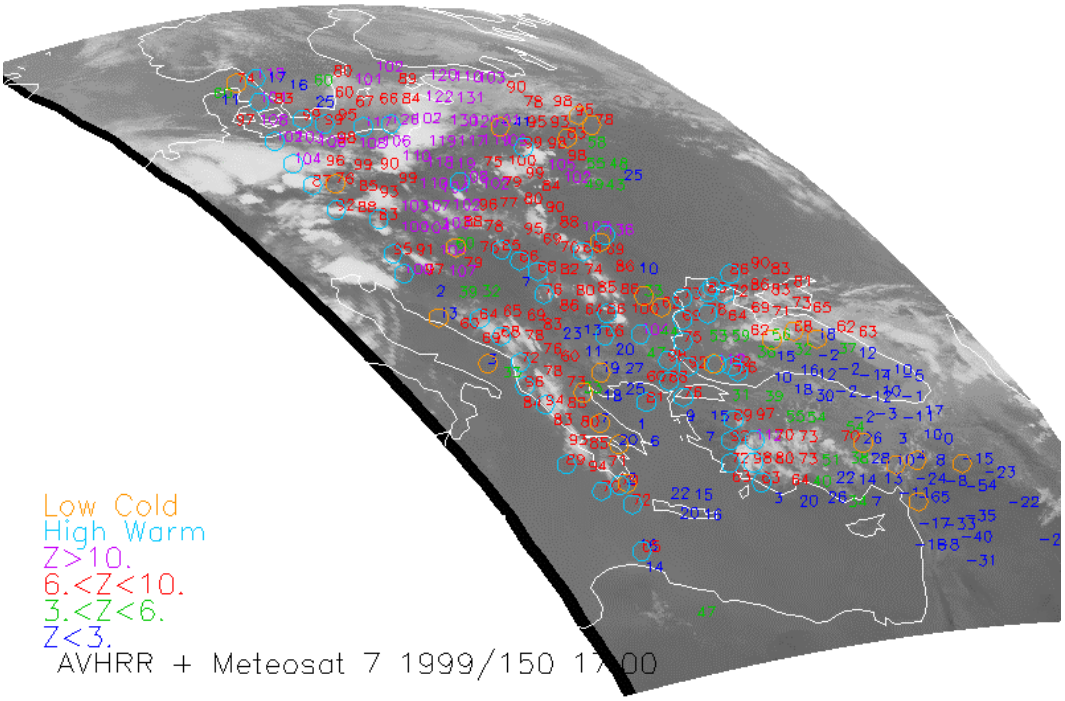

Figure 5. Asynchronous Stereo heights in hectometers (10=1km) from Meteosat 7 at 17:00 and 17:30 and AVHRR between those times for day 150 of 1999. As discussed below, geometric heights with large disagreements between temperature and heights are noted as colored circles: warm high objects (blue) and cold low objects (orange).

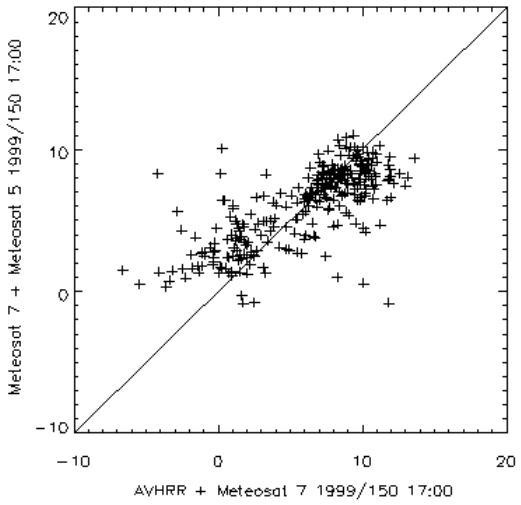

Figure 6. Asynchronous stereo AVHRR + M7 vs Stereo M7 + M5.

Similarly a comparison is possible between the geometric cloud height and the cloud top temperature. Figure 7 shows qualitative consistency: high clouds are colder that low clouds. Cloud which are warm and high (geometric) and cold and low (geometric) are noted in figure 5 with colored circles. As in the first case discussed above, there is some organization to the anomalous clouds, they appear at the edges of the cloud systems and thus have less well defined temperatures.

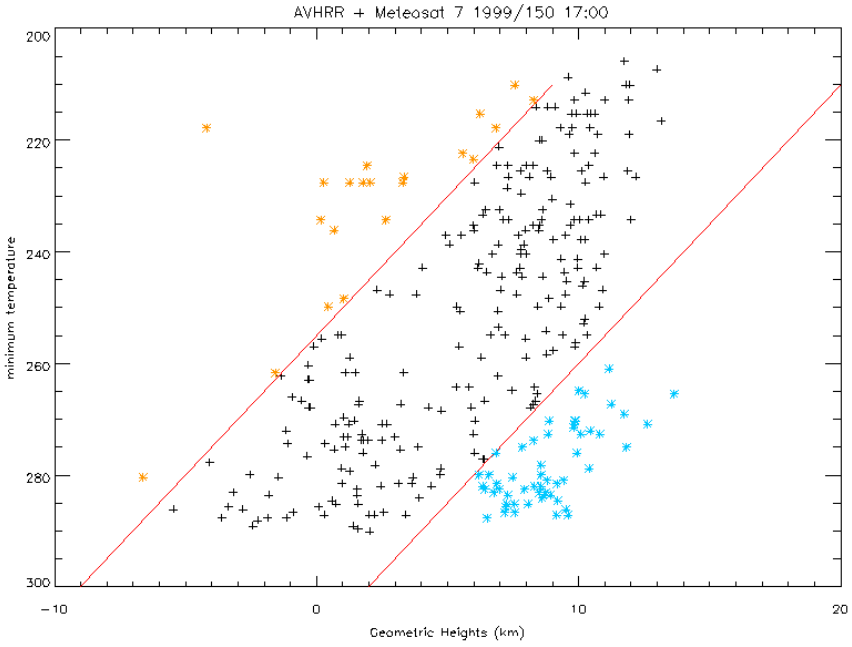

Figure 7. Scatter diagram of geometric heights vs cloud top temperature (the coldest pixel in the 50 km region of the cloud.

4. Discussion

The stereo cloud height estimates from Meteosat 5 km resolution data are not more accurate that the temperature methods, basically because 5 km pixels do not provide accurate enough cloud locations for stereo heights better than $\pm$ 2 km. But we did demonstrate that geometric methods can locate problem clouds for testing temperature methods. This will lead to improved temperature methods with algorithm refinements.

On the other hand, the comparison shows that stereo cloud height estimates of cloud with variable cloud top temperatures do not measure the cloud top height. The stereo method is actually measuring the height of the cloud edge. If one wants just cloud top heights, the inhomogeneous clouds should be dropped from the stereo reports because there are clouds with complicated cloud top shapes and in fact do not have a single cloud top heights. Less successful tests were also performed with Meteosat visible channel observations. There was more scatter in cloud heights in regions across the overlap area between the two satellites.

With higher resolution MSG observations, the stereo method will improve. Combination with GOES IR observations or the older Meteosat will require the asynchronous method because simultaneity will not occur very often with different scanning schedules.

The stereo analysis will be used in the verification of the cloud tracking software once MSG is launched later this year. Modest improvements will be made in the temperature height retrieval with more accurate temperature measurements, but that technique is limited by knowledge of the temperature profile. The geometric techniques are not limited by the fact that the atmosphere is isothermal near the tropopause so more precise results are possible with improving resolution and better cloud matching.

5. Conclusion

We have demonstrated geometric cloud height estimation using a simultaneous stereo to analyze automatically selected clouds and cloud locations. In comparison to the standard cloud top height estimate from temperature, the stereo method is able to identify problem areas in the temperature results leading to algorithm improvements. Similarly, rejecting the clouds with variable cloud top temperature will improve the stereo results.

The merger of polar orbiter and Meteosat observations shows that the geometric cloud height analysis can be extended beyond the regions of overlap between geosynchronous satellites.

Some of the images in the report can be viewed in animation at: http:///acamar.cira.colostate.edu.

ACKNOWLEDGEMENTS

This research was supported by NOAA (Grant NA67RJ0152) and EUMETSAT. Campbell would especially like to thank EUMETSAT for hosting a visit in the summer of 1999 during which much of this work was done.

REFERENCES

Campbell, G.G., 1998, Asynchronous Stereo Height and Motion Analysis: Applications, *Proc. Fourth International Winds Workshop*, EUMETSAT, EUM P24.

Menzel, P., 2000, Cloud tracking with satellite imagery: From the pioneering work of Ted Fujita to the present, *Bull. Amer. Meteor. Soc.*, accepted for publication.

Nieman, S. J., J. Schmetz and W. P. Menzel, 1993: A comparison of several techniques to assign heights to cloud tracers. *J. Appl. Meteor*., **32**, 1559-1568.

Schmetz, J., K. Holmlund, J. Hoffman, B. Strauss, B. Mason, V. Gartner, A. Koch and L. van de Berg, 1993, Operational Cloud-Motion winds from Meteosat Infrared Images. *J. Appl. Meteor*., **32**, 1206-1225.

SESSION III

ASSIMILATION AND IMPACT OF AMVs IN NWP

Chairperson: J. Le Marshall

IMPACT OF SATELLITE TEMPERATURE, MOISTURE, AND WIND OBSERVATIONS IN THE ETA DATA ASSIMILATION SYSTEM OVER THREE SEASONS

Tom H. Zapotocny [1], James P. Nelson III [1], James A. Jung [1], and W. Paul Menzel [2]

1 - Cooperative Institute for Meteorological Satellite Studies
2 - NOAA/NESDIS
1225 West Dayton Street, Madison, Wisconsin 53706, USA

ABSTRACT

The seasonal impact of five satellite data types in the Eta Data Assimilation/Forecast System (EDAS) is studied. The five data types include two precipitable water data types, temperature data in a cloudy environment, and two cloud motion wind data types. The case studies chosen include 11-day periods during December 1998, April 1999 and July 1999. During these periods six EDAS runs were executed twice daily; they include a control run of the EDAS, which utilizes all 34 operational data types, and five experimental runs in which one of the five satellite data types is denied. The 00-hr sensitivity and 24-hr forecast impact of these data types in the EDAS are investigated. Evaluation of conventional meteorological parameters at mandatory pressure levels reveals modest positive forecast impact from all five of these data types in all three seasons. The cloud motion wind information has the largest positive forecast impact during the winter season, while the precipitable water information has the largest positive forecast impact during the summer and transition seasons.

1. Introduction

The seasonal impact of five satellite data types in the Eta Data Assimilation/Forecast System (EDAS) is studied. The five data types include three layer (GOESM, Menzel et al. 1998) and vertically integrated precipitable water (SSMI, Alishouse et al. 1990), temperature data down to cloud top (TOVCD, Reale et al. 1994), infrared cloud drift winds (GOESC, Nieman et al. 1997) and water vapor winds at cloud top (GOESW, Velden et al. 1997). Only reports over water were used.

The case studies chosen include 11-day periods during December 1998, April 1999 and July 1999. During these periods six EDAS runs were executed twice-daily. The six runs include a control run, which utilizes all operational data types used in the EDAS, and five experimental runs in which one of the five satellite data types is denied. Differences between the experimental and control runs are then accumulated during the 11-day periods and analyzed to demonstrate the 00-hr analysis sensitivity and 24-hr forecast impact of these data types in the EDAS. Conventional meteorological terms evaluated include geopotential heights, temperature, u-component of the wind, and relative humidity on five mandatory pressure levels.
If a data type does not affect the analysis, there are four possible explanations. First is that the data were too few in number. Second is that the data received too little weight. Third is that the environment sampled by the observation was already successfully depicted by the EDAS. Fourth is that the data may not have passed an assimilation quality control check. It is beyond the scope of this study to separate these possibilities.

2. Experimental Design and Implementation

Three-dimensional variational analysis (3DVAR) (Parrish et al. 1996) became the data assimilation technique of the operational EDAS in February 1998. Procedures for utilizing EDAS forecasts as the first guess, thereby “fully-cycling” the system on its own first guess, were also developed and

implemented in operations during the summer of 1998. Details of the operational 3DVAR portion of the EDAS configuration can be found in the work of Rogers et al. (1997). The EDAS has since been updated (NWS 1999); experimental results presented here are generated with a May 1999 version of both 3DVAR and the Eta forecast model.

A total of 396 separate EDAS runs were required to isolate the extended length contributions from each of these five observational data types. An additional 220 EDAS simulations were performed to study conventional data denials during December 1998 and July 1999. Data used in the experiments reported here were obtained from an 80 kilometer, 38 level EDAS which was being executed at NCEP twice-daily "parallel" to the 32 kilometer operational EDAS. All 616 EDAS simulations performed herein are also run at 80 kilometers and 38 levels.

Sensitivity of the EDAS assimilation to the five data types is only evaluated at 00-hr, meaning after a complete 12-hr 3DVAR assimilation. The Root Mean Square (RMS) sensitivity **S** is defined as

$$S = \sqrt{\frac{\sum_{i=1}^{N} (D_i - C_i)^2}{N}} \quad , \qquad (1)$$

where **C** is the control assimilation containing all the data types, **D** is the assimilation containing all but the one denied satellite data type and **N** is the total number of grid points on the isobaric level being evaluated. Since (1) only contains two analyses and does not contain an independent verification, the sensitivity diagnosed by (1) does not indicate whether the 00-hr analysis is better or worse with the denied satellite data type. Seasonal sensitivity statistics are only presented at 00-hr.

The RMS forecast impact **FI** of an individual data type is evaluated as

$$FI = \sqrt{\frac{\sum_{i=1}^{N} (D_i - A_i)^2}{N}} - \sqrt{\frac{\sum_{i=1}^{N} (C_i - A_i)^2}{N}} \qquad (2)$$

In (2) **N** has the same meaning as above. The variables **C** and **D** are the 24-hr control and denied forecasts, respectively, and **A** is the 00-hr EDAS control analysis valid 24-hrs after the forecast began. Unlike (1), (2) directly evaluates whether the 24-hr forecast is closer to or farther away from the EDAS analysis valid at the same time as the 24-hr forecast. In (2) the first term can be considered the error in the denied forecast. The second term in (2) can be considered the error in the control forecast.

Both the 00-hr sensitivity and 24-hr forecast impact diagnostics are delayed one day after the start of each 11-day seasonal period. This delay in evaluating the statistics allows more time for the impact of the denied data to be removed from the initial first guess, and reduces the 11-day time periods to 10 days diagnostically.

Each of the 616 EDAS simulations consisted of the complete 12-hr assimilation cycle and a 48-hr forecast cycle. Data were assimilated via 3DVAR at T-12, T-9, T-6, T-3, and T-0, using 3-hour Eta model forecasts between each assimilation step. At each assimilation time, all data within ± 1.5 hours are included. In this study, SSMI typically contributed about 3000 reports, GOESM about 20000, TOVCD about 20000, GOESC about 5000, and GOESW about 4000. Errors assigned to the observations in the EDAS (Table 1) influence the weighting each report gets. The result of the 12-hr assimilation cycle is the complete analysis before the Eta model's forecast cycle begins.

TABLE 1. Errors assigned to observations in the EDAS at six pressure levels. The data type, description and units are shown at left. Rawinsonde (RAOB), aircraft (ACAR) and GMS errors are included for later discussion.

ID	Description	1000	850	700	500	300	200
RAOB1	Temperature (K)	1.2	0.8	0.8	0.8	0.9	1.2
ACAR1	Temperature (K)	1.5	1.1	1.0	1.0	1.0	1.0
TOVCD	Cloudy temperature (K)	7.6	7.1	6.6	6.6	7.0	6.7
RAOB1	Specific humidity (%)	5.0	7.0	10.0	20.0	20.0	20.0
SSM/I	Marine precip. water (mm)	8.0	8.0	8.0	8.0	8.0	8.0
GOESM	Marine precip. water (mm)	8.0	8.0	8.0	8.0	8.0	8.0
RAOB2	Winds (m s^{-1})	1.4	1.5	1.6	2.1	3.0	2.7
ACAR2	Winds (m s^{-1})	2.5	2.5	2.5	2.5	2.5	2.5
GOESC	IR Cld drft winds (m s^{-1})	1.8	1.8	1.9	2.1	3.0	3.0
GOESW	Cld top water wapor (m s^{-1})	1.8	1.8	1.9	2.1	3.0	3.0
GMSLO	IR/VIS Cld drft winds (m s^{-1})	1.8	1.8	1.9	2.1	4.6	5.0

3. Results

Sensitivity diagnostics include time-summed RMS differences over the entire model domain for four quantities (Z, T, u and R.H.) on five mandatory pressure levels (1000, 850, 700, 500, and 300 hPa). Differences between the various experimental 12-hr assimilation runs and the control 12-hr assimilation run provide a measure of the sensitivity of the EDAS to each individual data type for these three extended length time periods. Similarly, time-summed differences between the 24-hr experimental forecasts and the 24-hr control forecast provide a measure of the positive or negative forecast impact of each data type in the Eta model.

The 00-hr bar chart sensitivity results (Figs.1-3) presented below have the same vertical scale by data type and time period. The 24-hr forecast impact results (Figs. 4-6) have the same vertical scale with respect to each other, but a different vertical scale than the 00-hr sensitivity results.

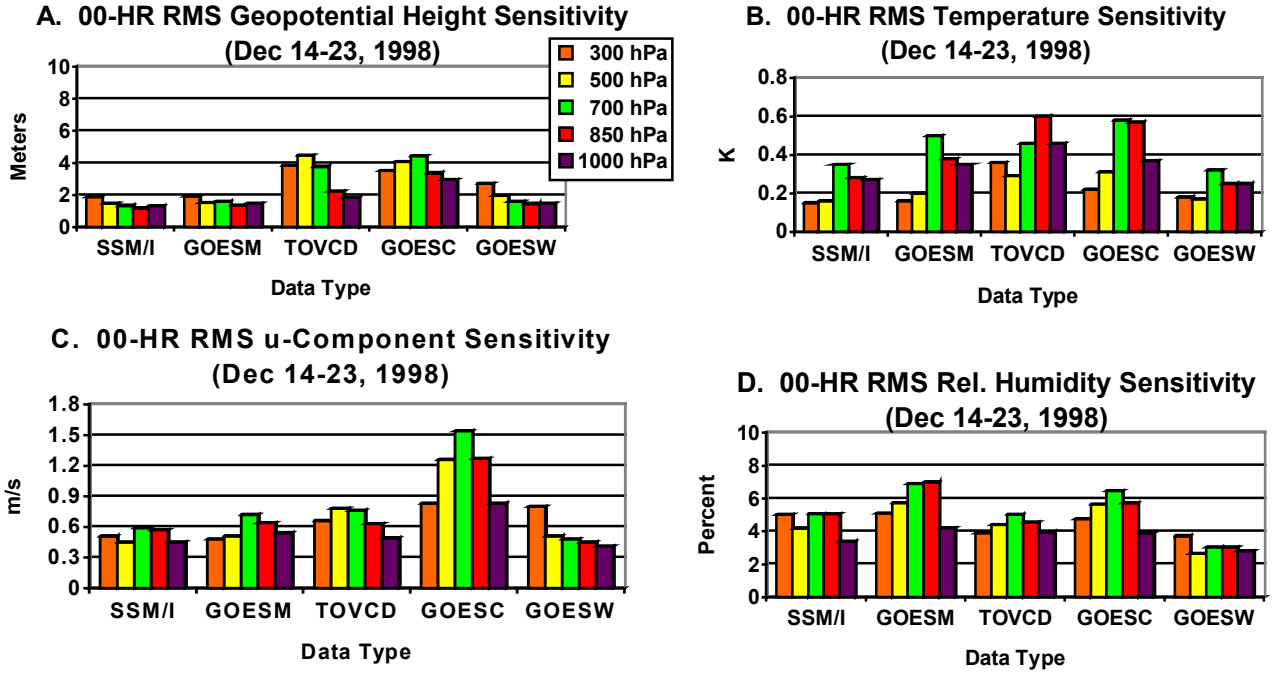

Fig. 1. Sensitivity of the five satellite data types after a complete 12-hr 3DVARassimilation. These results are formed by summing over time the results of (1) for each period from 0000 UTC 14 December 1998 through 1200 UTC 23 December 1998. The units of each field are listed on the y-axis.

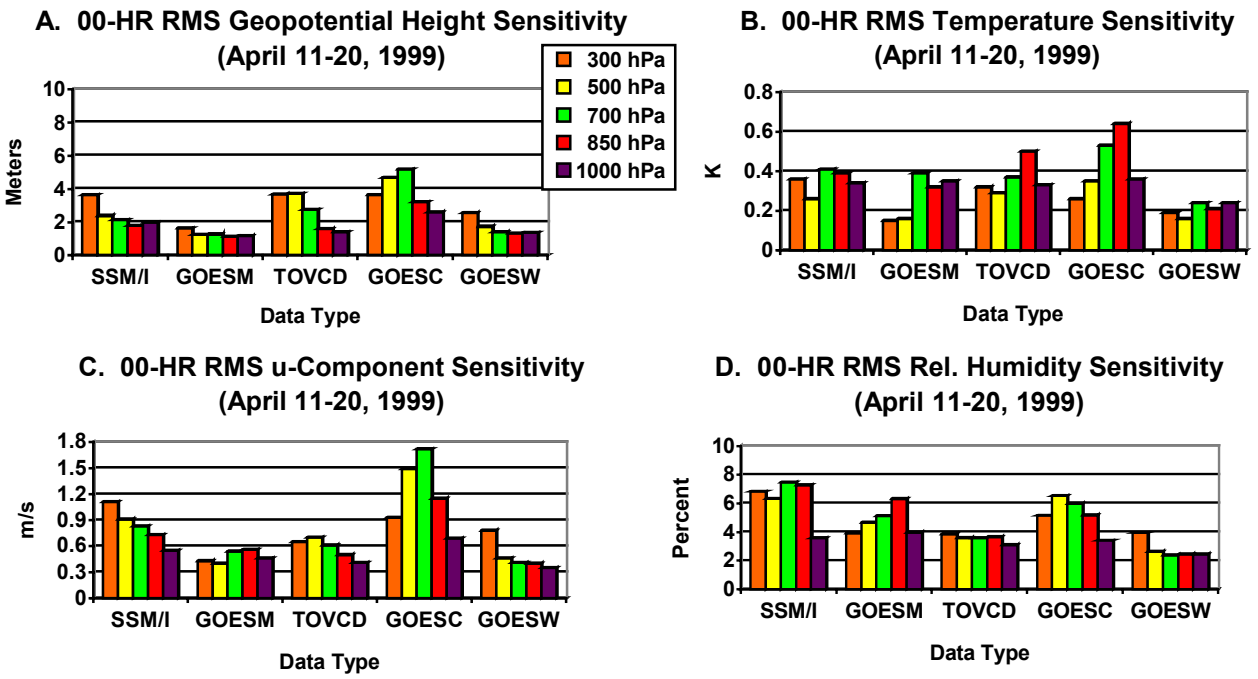

Fig. 2. Same as Fig. 1 except for the period 0000 UTC 11 April 1999 through 1200 UTC 20 April 1999.

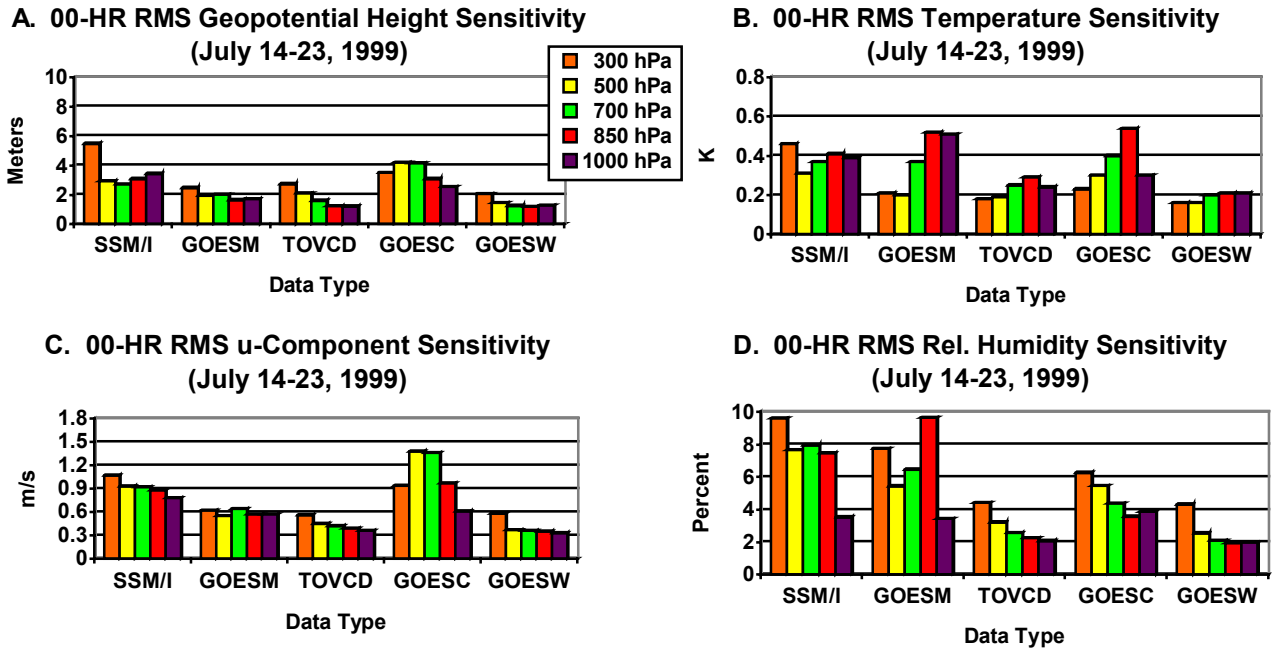

Fig. 3. Same as Fig. 1 except for the period 0000 UTC 14 July 1999 through 1200 UTC 23 July 1999.

3A. 00-hr sensitivity results

The time-summed 00-hr sensitivity results of geopotential heights, temperature, u-component of the wind and relative humidity for the 13-23 December 1998 time period are presented for five mandatory pressure levels in Figs. 1A-D, respectively. Largest overall wintertime geopotential height sensitivity (Fig. 1A), which represents a vertically integrated effect, is to TOVCD and GOESC. Both these data types provide up to a 4.5 meter change in the middle troposphere. The other three data types (SSM/I, GOESM, and GOESW) are in general near a 2 meter impact on all five isobaric levels.

Larger relative variation by isobaric level and data type is noticed in the 00-hr wintertime temperature sensitivities (Fig. 1B). The TOVCD and GOESC data types again provide the largest overall impact, up to 0.6 K in the lower to middle troposphere. However, other data types such as GOESM at 700 hPa also prove to be nearly as significant (0.5 K). In general the temperature sensitivities are larger in the lower to middle troposphere than aloft. For the most part this is an expected result, since the gradients of temperature in the wintertime hemisphere are largest at lower altitudes.

During this extended time period in December 1998, the 00-hr u-component analysis is clearly most sensitive to GOESC data at nearly all levels (Fig. 1C). For this period GOESC provides an impact of 1.5 m s^{-1} at 700 hPa. The 300 hPa GOESW, 500 and 700 hPa TOVCD and 700 hPa GOESM sensitivities have the next largest contributions, but these are all less than 0.9 m s^{-1}. Other data types, such as SSM/I and the remaining levels of GOESW show sensitivities less than or equal to a 0.6 m s^{-1} impact in the time-summed December 1998 results.

The 00-hr wintertime relative humidity sensitivities (Fig. 1D) demonstrate the most uniformity of the four standard meteorological fields presented here, at least when comparing data type to data type and level to level. Except for GOESW the 00-hr sensitivity provided by these data types average between 4 and 6%, with GOESM approaching 7% at 700 and 850 hPa. The GOESW sensitivities are 4% or less and the smallest for all levels by data type. A 7% relative humidity sensitivity seems like a much larger impact than a 0.6 K temperature or 1.5 m/s u-component sensitivity.

The 10-20 April 1999 and 13-23 July 1999 sensitivities are presented in Figs. 2 and 3, respectively. The April and July sensitivities are examined by comparing the time summed impact of these data types with their December counterpart. Concentration will focus on the precipitable water data types, which should logically have the largest impact in July and the smallest impact in December.

Comparing the relative humidity sensitivities during December 1998 and July 1999 (Figs. 1D and 3D respectively) clearly indicates that the impact of SSM/I data at all levels and GOESM data at 850 and 300 hPa is more significant in July (Fig. 3D) than December (Fig. 1D).

While relative humidity shows a larger 00-hr impact in July than December, the same cannot be said about the sensitivity of GOESC and GOESW cloud motion data types. Considering each of these two data types, their average impact might be slightly larger in winter than summer, but in general their impact remains fairly constant from season to season regardless of the field examined. (Compare GOESC and GOESW for all four fields within Figs. 1 and 3.) The only data type to show a significant drop in sensitivity from December to July is TOVCD. For this data type the July values are in some cases less than one-half the magnitude of their corresponding December values.

During the transition month of April (Fig. 2D) SSM/I has more impact on the analysis than GOESM, in contrast to what was seen in December (compare Figs. 1D and 2D). On the whole, April relative humidity sensitivities from SSM/I and GOESM are somewhat closer to their December values than their July values.

3B. 24-hr forecast impact results

Figures 4A-D show the 24-hr forecast impact for the same four fields presented above during the December 1998 time period. An examination of the four fields indicates that each of the five satellite data types cumulatively have a positive impact. GOESC clearly has the most positive forecast impact for the geopotential heights and u-component, and shows the largest positive impact when all four data types are combined. On the other hand, GOESW is the smallest contributor to nearly all fields, with cumulative results for the four fields producing only a slightly positive impact. The other three data types (SSM/I, GOESM and TOVCD), while not as positive overall as GOESC, each produce a cumulative positive forecast impact for the four fields added together.

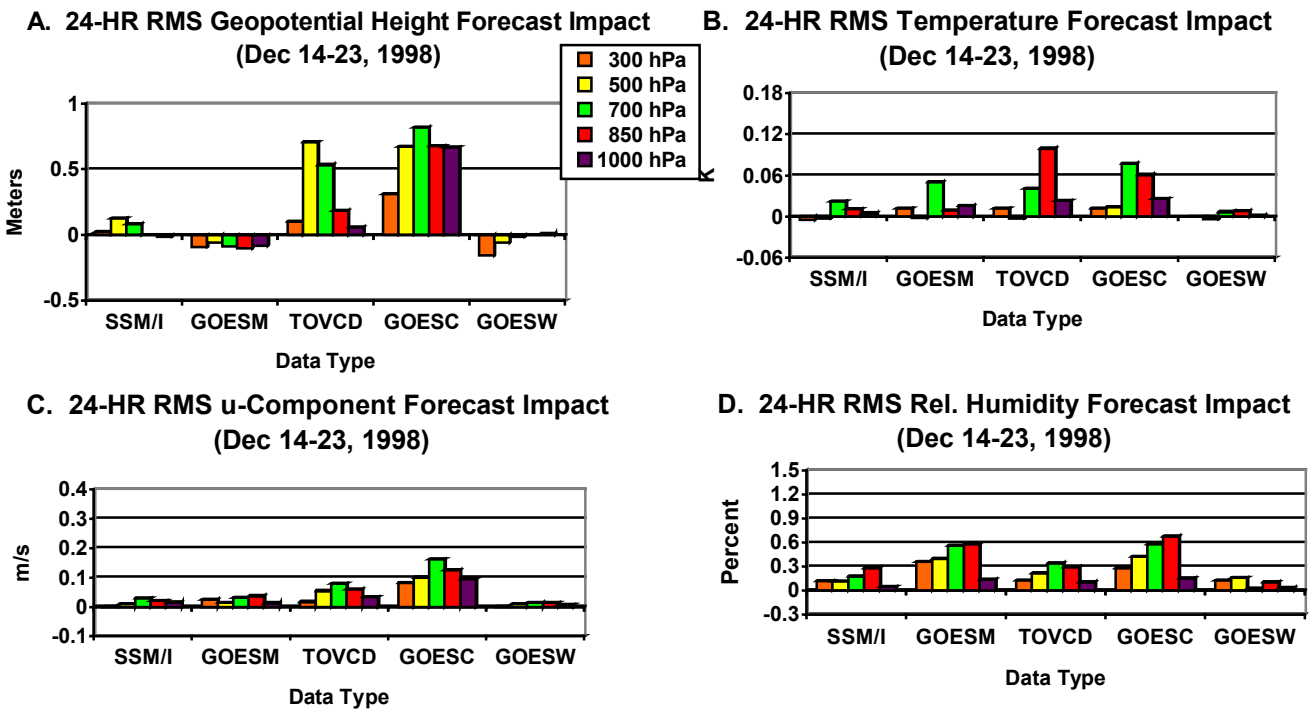

Fig. 4. Forecast impact of the five satellite data types after 24-hrs of Eta model integration. These results are formed by summing over time the results of (2) for each period from 0000 UTC 14 December 1998 through 1200 UTC 23 December 1998. The units of each field are listed on the y-axis.

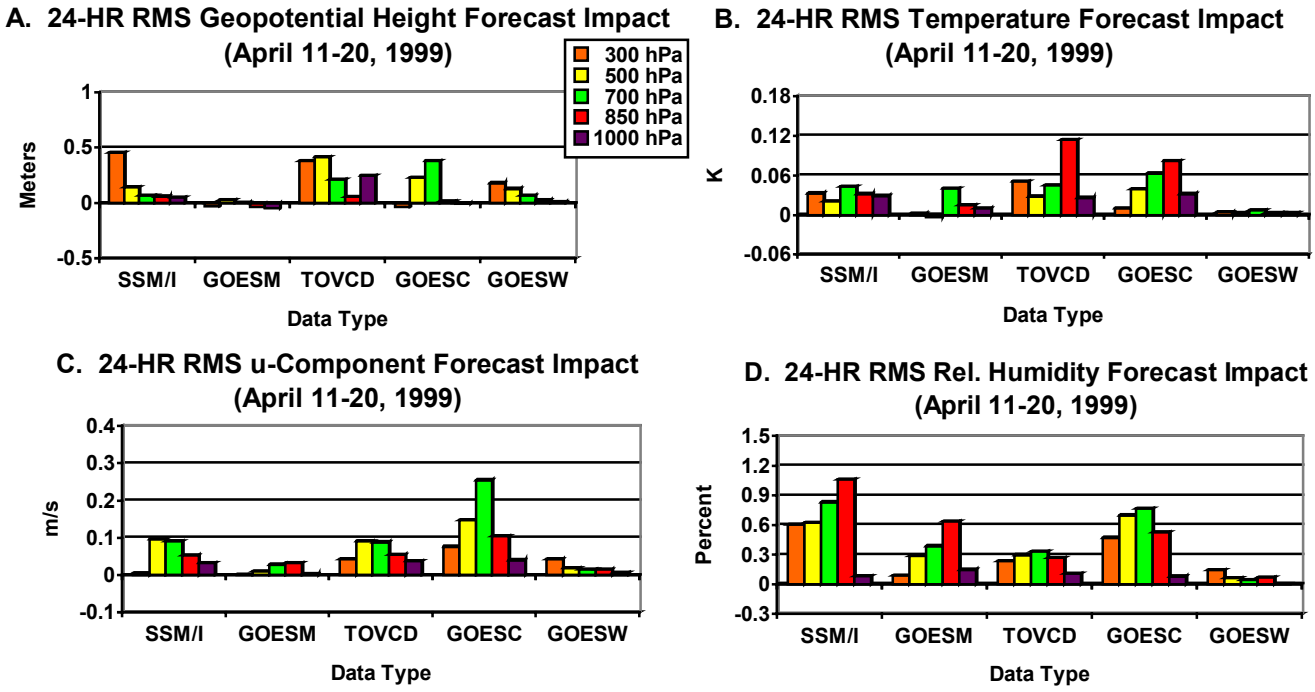

Fig. 5. Same as Fig. 4 except for the period 0000 UTC 11 April 1999 through 1200 UTC 20 April 1999.

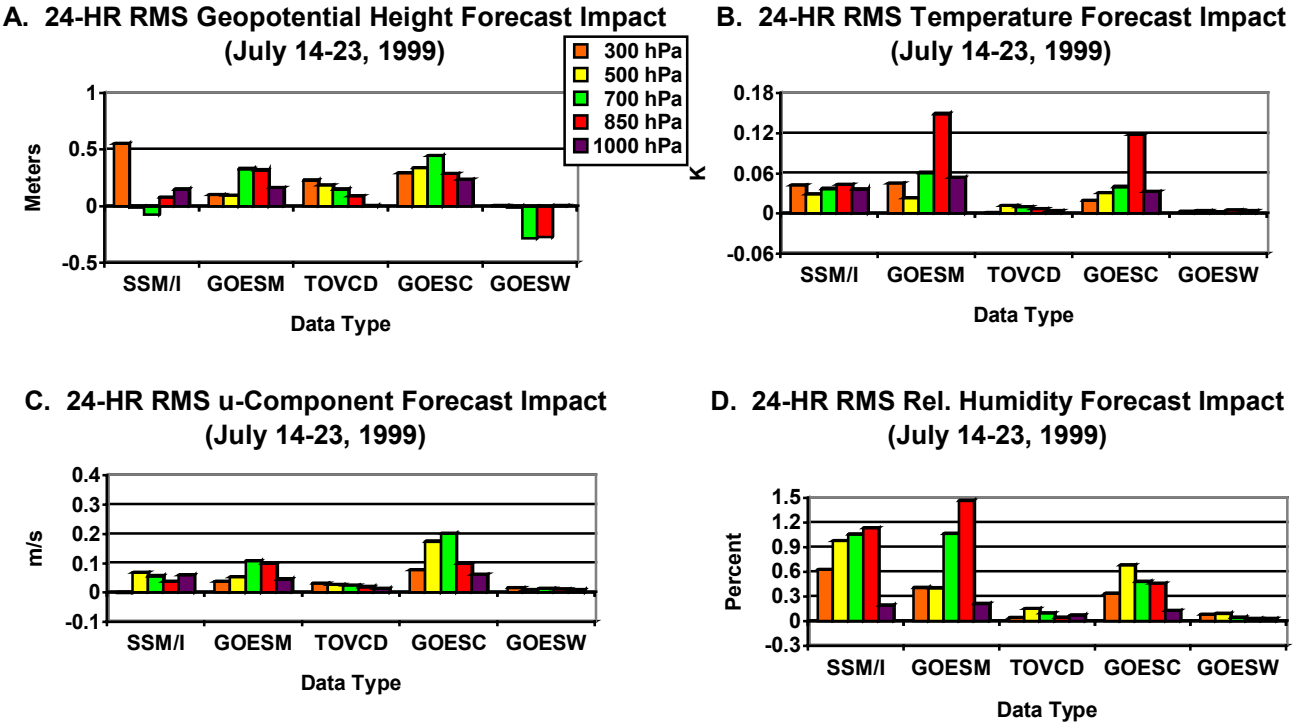

Fig. 6. Same as Fig. 4 except for the period 0000 UTC 14 July 1999 through 1200 UTC 23 July 1999.

The 24-hr April and July 1999 forecast impact results are displayed in Figs. 5 and 6, respectively. Comparing the SSM/I and GOESM precipitable water data types from December 1998 (Fig. 4) and July 1999 (Fig. 6) indicates that, a larger atmospheric moisture content in July nearly always translates to a larger positive forecast impact in July than December for all four fields presented. In fact, by July the precipitable water data sets provide some of the largest positive forecast impacts, even for fields not intrinsically related to moisture (see GOESM at 850 hPa in Fig. 6B and SSM/I at 300 hPa in Fig. 6A). The negative impact of GOESM in geopotential heights in December 1998 (Fig. 4A) has also reversed and is neutral by April (Fig. 5A) and modestly positive by July 1999 (Fig. 6A).

With respect to the non-moisture data types, a December 1998 and July 1999 comparison indicates that the impact of GOESC and TOVCD is positive for virtually every level and field in December, and for all levels and fields in July (compare Figs. 4 and 6). However, similar to the 00-hr sensitivities, the overall magnitude of the positive forecast impact for these two data types decreases somewhat from winter to summer, especially TOVCD impacts. Furthermore, while GOESW is modestly negative in the lower and middle troposphere in terms of geopotential heights in July (Fig. 6A), its overall impact remains slightly positive during all three 11-day periods when cumulatively examining all four fields.

3C. The importance of several conventional data types

The impact of several conventional data types were also be examined. The five data types are rawinsonde temperature and moisture observations (RAOB1), Aircraft Communications Addressing and Reporting System (ACARS) temperature data (ACAR1), rawinsonde wind observations (RAOB2), ACARS wind observations (ACAR2), and Geostationary Meteorological Satellite low-level infrared/visible cloud drift wind observations (GMSLO).

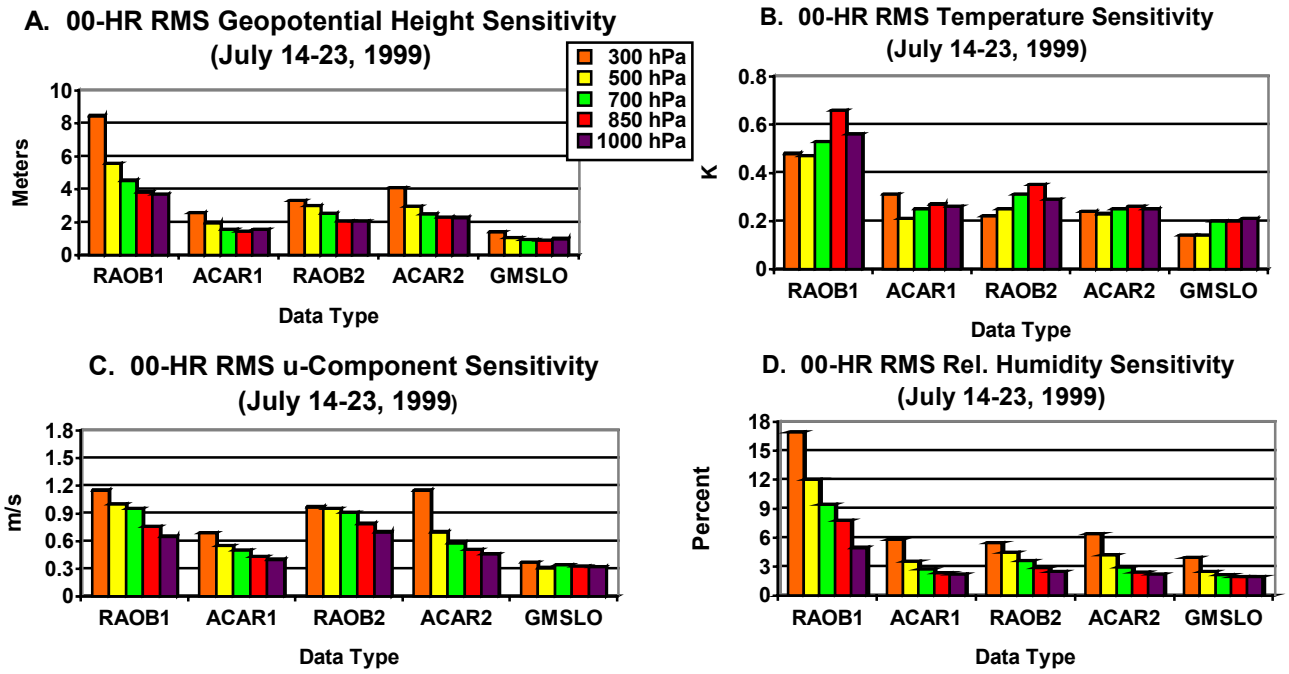

Fig. 7. Sensitivity of four more conventional data types as well as cloud drift wind information from GMS after a complete 12-hr 3DVAR assimilation. These results are formed by summing over time the results of (1) for each period from 0000 UTC 14 July 1999 through 1200 UTC 23 July 1999. The units of each field are listed on the y-axis.

Figure 7 displays the 00-hr sensitivities of these five new data types during the July 1999 time period. Note that the vertical scale is the same as the previous sensitivity figures, except for relative humidity where the vertical axis has been expanded from 10% in section 3A to 18% here. Inspection of these four fields reveals that the EDAS has the largest sensitivity to RAOB1 data for all four fields, especially geopotential height, temperature and relative humidity. The remaining three conventional data types (ACAR1, RAOB2 and ACAR2) all demonstrate a nearly equal sensitivity with each other, and as little as one-half the overall RAOB1 sensitivity. The GMSLO sensitivity is clearly the smallest for all four fields. Another interesting aspect of these results is that the sensitivities are in general larger in the upper troposphere than in the lower troposphere. This is especially true for the geopotential height, u-component and relative humidity sensitivities (Figs. 7A, C and D) and different than the satellite data types of Fig. 3, which appear somewhat more random with height.

Comparing satellite and non-satellite data sensitivities reveals several interesting features. With respect to geopotential height, the RAOB1 sensitivities are clearly the largest at all five isobaric levels (compare Figs. 3A and 7A). RAOB1 is also the largest at every level for temperature sensitivity, although the 850 and 1000 hPa GOESM, 850 hPa GOESC and 300 hPa SSM/I sensitivities come in a close second (compare Figs. 3B and 7B). GOESC provides the largest overall u-component sensitivity, especially at both 500 and 700 hPa where values approach 1.4 m s^{-1}. RAOB1, RAOB2 and SSM/I provide the second largest sensitivities and are of nearly equal importance (compare Figs. 3C and 7C). RAOB1 is also the most important for overall relative humidity sensitivity, and is particularly important at 500 and 300 hPa (compare Figs. 3D and 7D, noting the different y-axis scales).

Figure 8 displays the 24-hr forecast impact of these five new data types during the July 1999 time period. Similar to the five July satellite data types presented in Fig. 6, these more conventional data types also provide a positive impact for nearly all fields and levels. GMSLO impact is small due to the lack and location of these observations within the EDAS model domain.

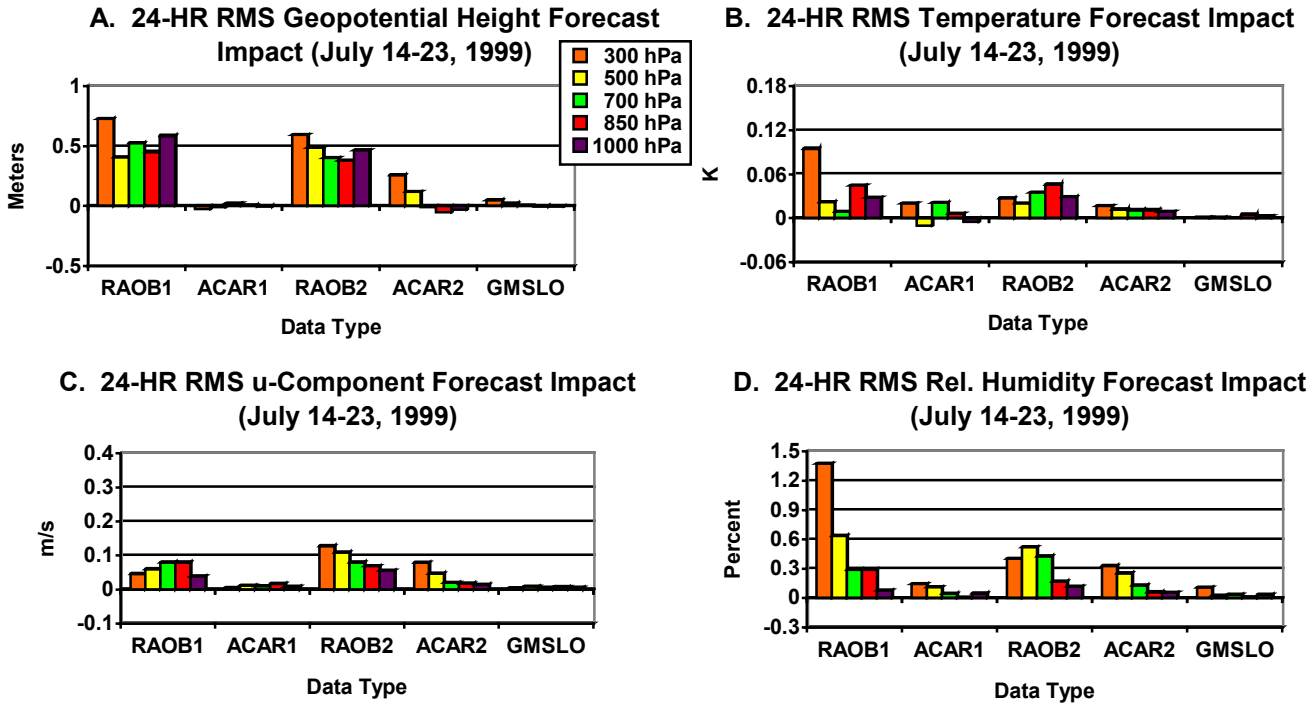

Fig. 8. Forecast impact of four more conventional data types as well as cloud drift wind information from GMS after 24-hrs of Eta model integration. These results are formed by summing over time the results of (2) for each model run from 0000 UTC 14 July 1999 through 1200 UTC 23 July 1999. The units of each field are listed on the y-axis.

The results from both RAOB and ACAR data types are not as easy to understand. These two data types are assigned relatively small errors to the observation (large importance), at least with respect to the satellite data types. However, when comparing Figs. 6 and 8, it is clear that the RAOB and ACAR data (Fig. 8) have generally speaking similar or smaller positive forecast impact than most of the five satellite data types (Fig. 6). Interestingly, ACAR1 forecast impact is very small for the four fields presented, even though its 00-hr sensitivity was as large as RAOB2. ACAR2 impact is still small but more significant than ACAR1 for both the u-component (Fig. 8C) and relative humidity (Fig. 8D) fields during the July 1999 time period. Of the five data types presented in this subsection, the RAOB1 and RAOB2 impacts are clearly the largest overall. However, in spite of what one might expect, their contributions are similar to or slightly smaller than many of the five satellite data types.

Several specific details about these summertime forecast impacts are now highlighted. First, with respect to geopotential height, RAOB1 and RAOB2 clearly provide the most positive forecast impact of the 10 data types presented for July (compare Figs. 6A and 8A). Second, with respect to temperature forecast impact, GOESM and GOESC have the largest overall positive contribution of the 10 July data types, due in large part to the significant positive impact at 850 hPa (compare Figs. 6B and 8B). Third, GOESC is the largest contributor to u-component forecast impact, RAOB2 is second most important (compare Figs. 6C and 8C). Fourth, the SSM/I and GOESM precipitable water data types are dominant with respect to overall positive forecast impact for relative humidity; however, RAOB1 has the largest positive forecast impact in the upper troposphere (compare Figs. 6D and 8D). Finally, the largest contribution of the five satellite data types is generally at 700 and 850 hPa, at least for the data types which have a significant impact (Fig. 6). On the other hand, the more conventional data types presented in this subsection tend to have their largest positive impacts at 300 and 500 hPa, especially RAOB1's relative humidity forecast impact (Fig. 8D).

4. Summary

This paper summarizes the 00-hr sensitivities and 24-hr forecast impacts of the EDAS to five satellite data types during 11-day periods in a winter, summer and transition season. The five satellite data types are SSM/I, GOESM, TOVCD, GOESC, and GOESW. The three 11-day periods are 13-23 December 1998, 10-20 April 1999, and 13-23 July 1999. Sensitivity and forecast impact statistics were presented for four standard meteorological fields, at each of five isobaric levels. The fields consisted of geopotential heights, temperature, u-component of the wind and relative humidity. While only the u-component statistics were presented, the v-component statistics for both sensitivity and forecast impact were found to be very similar to the u-component.

The 00-hr sensitivity results indicate that GOESC has nearly equal impact during all three time periods, while the precipitable water data types of SSM/I and GOESM have nearly twice as much impact in summer as winter. During the assimilation and forecast, most data types impact the fields they do not observe as much as the ones they do. For example, precipitable water data sets impact the u-component of the wind as much as GOESC cloud drift winds impact the relative humidity. Of the non-satellite data types, rawinsonde observations of temperature and moisture (RAOB1) were the most important of any data type in the 00-hr EDAS analysis.

The 24-hr forecast impact results indicate that all five of the satellite data types provide some positive impact. GOESC had the most positive overall forecast impact during the course of these simulations, at least when considering all fields examined during all three 11-day periods. The precipitable water data sets of SSM/I and GOESM had the most positive forecast impact during summer in terms of relative humidity, but their importance was reduced significantly during winter. GOESW had the smallest impact of all five satellite data types, with its overall contribution being just slightly positive. While the positive forecast impact is termed modest, it is important to note that very few negative forecast impacts were observed, either for the three 11-day periods as a whole (only 28 of 295 were negative), individual 11-day periods (16 of 100 were negative during July), or individual time periods. A separate investigation into the importance of more conventional data (both RAOB and ACAR) during winter and summertime established that their positive forecast impact was about the same or slightly smaller than the five satellite data types investigated, even though they were more important in the 00-hr sensitivities.

REFERENCES

Alishouse, J. C., S. Snyder, J. Vongsathorn, and R. R. Ferraro, 1990: Determination of oceanic total precipitable water from the SSM/I. *IEEE Trans. Geosci. Rem. Sens*., **28**, 811-816.

Menzel, W. P., F. C. Holt, T. J. Schmit, R. M. Aune, A. J. Schreiner, G. S. Wade, and D.G. Gray, 1998: Application of GOES-8/9 soundings to weather forecasting and nowcasting. *Bull. Amer. Meteor. Soc*., **79**, 2059-2077.

Nieman, S. J., W. P. Menzel, C. M. Hayden, D. Gray, S. T. Wanzong, C. S. Velden, and J. Daniels, 1997: Fully automated cloud-drift winds in NESDIS operations. *Bull. Amer. Meteor. Soc*., **78**, 1121-1133.

NWS, 1999: EDAS. NWS Technical Procedures Bulletin found at [http://www.nws.noaa.gov/om/tpb/3d-eta.htm.]

Parrish, D., J. Purser, E. Rogers, and Y. Lin, 1996: The regional 3D variational analysis for the Eta model. Preprints, *11th AMS Conference on Numerical Weather Prediction*, Amer. Meteor. Soc., Norfolk, VA, 454-455.

Reale, A. L., M. W. Chalfant, R. V. Wagoner, and T. J. Gardner, 1994: TOVS operational sounder upgrades: 1990-1992. NOAA Tech. Report NESDIS 76, 67 pp. [Available from www.ntis.gov.]

Rogers, E., M. Baldwin, T. Black, K. Brill, F. Chen, G. DiMego, J. Gerrity, G. Manikin, F. Mesinger, K. Mitchell, D. Parrish, and Q. Zhao, 1997: Changes to the NCEP Operational "Early" Eta Analysis / Forecast System. NOAA/NWS Tech. Procedure Bull. 447. [Available from Office of Meteorology, National Weather Service, 1325 East-West Highway, Silver Spring, MD 20910.]

Velden, C. S., S. J. Nieman, W. P. Menzel, and S. T. Wanzong, 1997: Upper-tropospheric winds derived from geostationary satellite water vapor observations. *Bull. Amer. Meteor. Soc.*, **78**, 173-195.

THE IMPACT OF SATELLITE-DERIVED WINDS ON GFDL HURRICANE MODEL FORECASTS

Brian J. Soden[1] and Christopher S. Velden[2]

1) Geophysical Fluid Dynamics Laboratory
National Oceanic and Atmospheric Administration
Princeton, New Jersey, USA

2) Cooperative Institute for Meteorological Satellite Studies
University of Wisconsin-Madison
Madison, Wisconsin, USA

ABSTRACT

A series of experimental forecasts are performed to evaluate the impact of satellite-derived winds on numerical hurricane track predictions using the GFDL model. Over 100 cases are examined from 10 different storms covering 3 seasons (1996-1998), enabling us to account for the large case-to-case variability in the forecast results when assessing the wind impact. On average, assimilation of the GOES winds reduces track error at all forecast periods. The relative reductions in track error range from ~5% at 12 hours to in excess of 12% at 36 hours. Statistically significant reductions in track error are noted for the 24, 36, and 72 hour forecast periods. A composite analysis of the initial flow fields suggests that the reduction in track error may be associated with the ability of the GOES winds to more accurately depict the strength of vorticity gyres in the environmental flow.

1. Introduction

Numerical prediction of hurricane forecasts require accurate representation of the current meteorological conditions. Unfortunately, conventional measurements used to initialize forecast models are unavailable for vast areas of the tropical oceans. The sparsity of observations, both near the storm center and in the surrounding environment, is a key factor in limiting the accuracy of hurricane forecasts. Satellite winds from geostationary satellites offer a valuable supplement to conventional observations by providing measurements in these data sparse regions. This study seeks to determine the extent to which GFDL model forecasts can benefit from the direct assimilation of GOES winds. For this purpose, a series of over 100 parallel forecasts were performed spanning 10 storms and 3 Atlantic hurricane seasons (1996-1998).

2. Forecast Model: The GFDL Hurricane Prediction System

The dynamical model used in the hurricane prediction system is an outgrowth of a research model developed at GFDL and adopted by the National Weather Service as an operational hurricane forecast model in 1995. The prediction system uses a limited area, baroclinic model which solves the primitive equations using a finite-difference method in spherical coordinates with 18 sigma levels. To resolve the interior structure of a hurricane, a multiply-nested grid system is used consisting of two inner movable meshes ($1/6^o$ and $1/3^o$ resolution) nested within a coarser 75^ox75^o outer mesh (1^o resolution). The initial and lateral boundary conditions are defined by the NCEP global analysis. A 3-dimensional optimum interpolation (3DOI) scheme was developed to assimilate the GOES winds directly into the GFDL model.

3. Impact of GOES Winds on GFDL Track Forecasts

This section compares model forecasts integrated from two sets of experiments - a control run (CTRL) and an experimental run which includes the GOES winds (WIND). A set of 103 cases are examined for different 10 Atlantic storms spanning 3 seasons. For each case, 72 hour forecasts are performed. On average the assimilation of satellite winds improved forecasts for all verification times, with the reduction in track error ranging form 4% at 12 hr to 12% at 36 hr, with statistically significant reductions (95% confidence level) at 24, 36 and 72 hr (Figure 1). With the exception of the 12 hr forecasts, the inclusion of the satellite winds typically improved 60% of the cases.

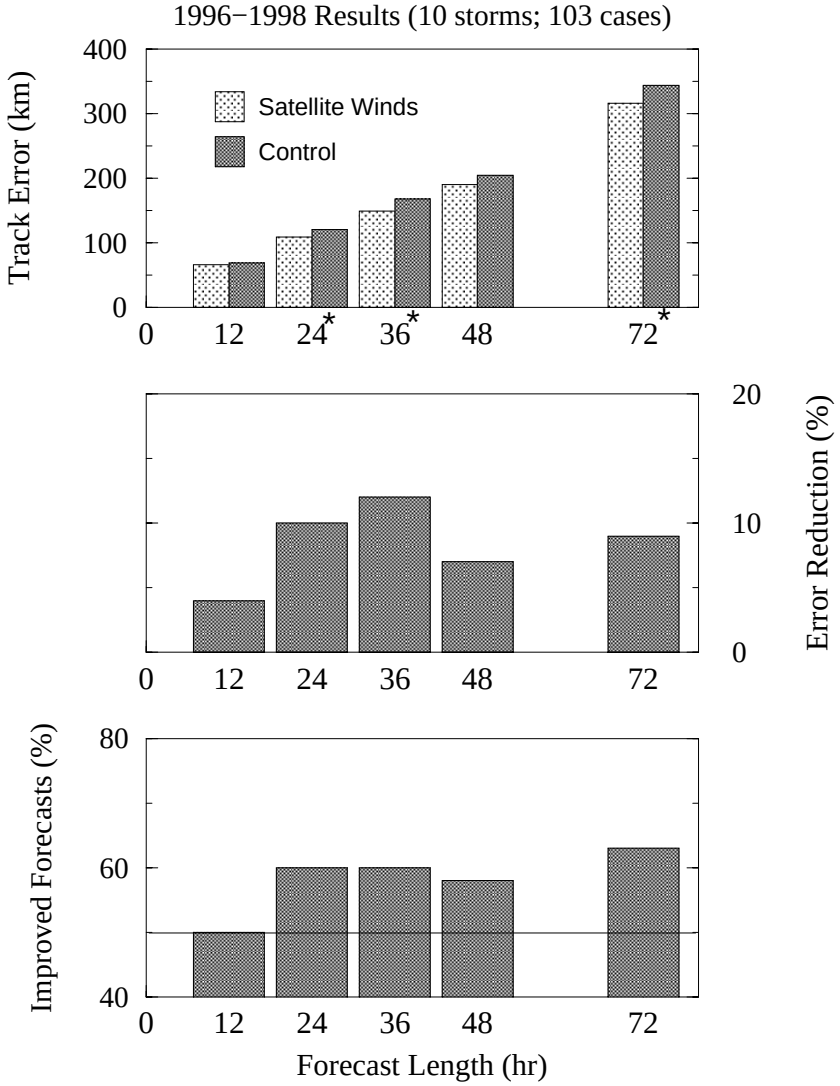

Figure 1. Summary of track errors. The mean track error (top), the percentage reduction in track error (middle), and the percentage of improved forecasts (bottom) due the assimilation of GOES winds. The reduction in track error are statistically significant at the 95% confidence level for the 24, 36 and 72 hour forecasts. The average error reduction for all forecast lengths (12-72 hr) is also statistically significant at the 95% confidence level.

To determine the impact of the satellite winds on the model flow fields, the initial wind conditions from the CTRL and WIND experiments are compared. Rather than examine the winds at individual model levels, we compute deep-layer-mean (DLM) flow, defined as the vertical pressure-weighted average of the initial condition wind field, for both the CTRL and WIND runs. To highlight the large-scale environmental or "basic" flow patterns, the DLM fields are then low-pass filtered with a wavenumber cutoff of ~1000 km. Since there are over 100 cases, each with widely differing synoptic conditions, it is difficult to analyze each case individually and reach a general conclusion. Instead, we

have constructed composites of the mean track forecasts (Figure 2) and the mean DLM flow fields (Figure 3) by using the storm center as the frame of reference.

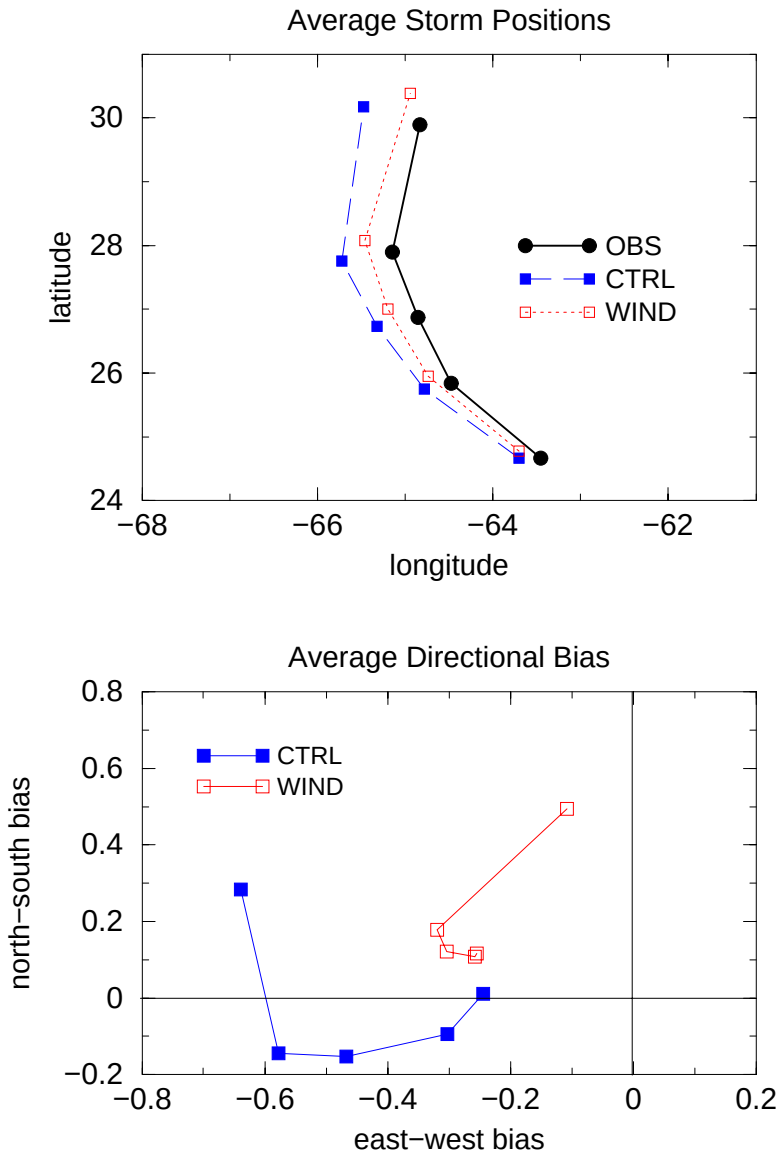

Figure 2. A composite of the mean storm tracks (top) from the observations (filled circle) and the CTRL (filled square) and WIND (open square) experiments. The bias in the CTRL and WIND predicted tracks are presented in the bottom.

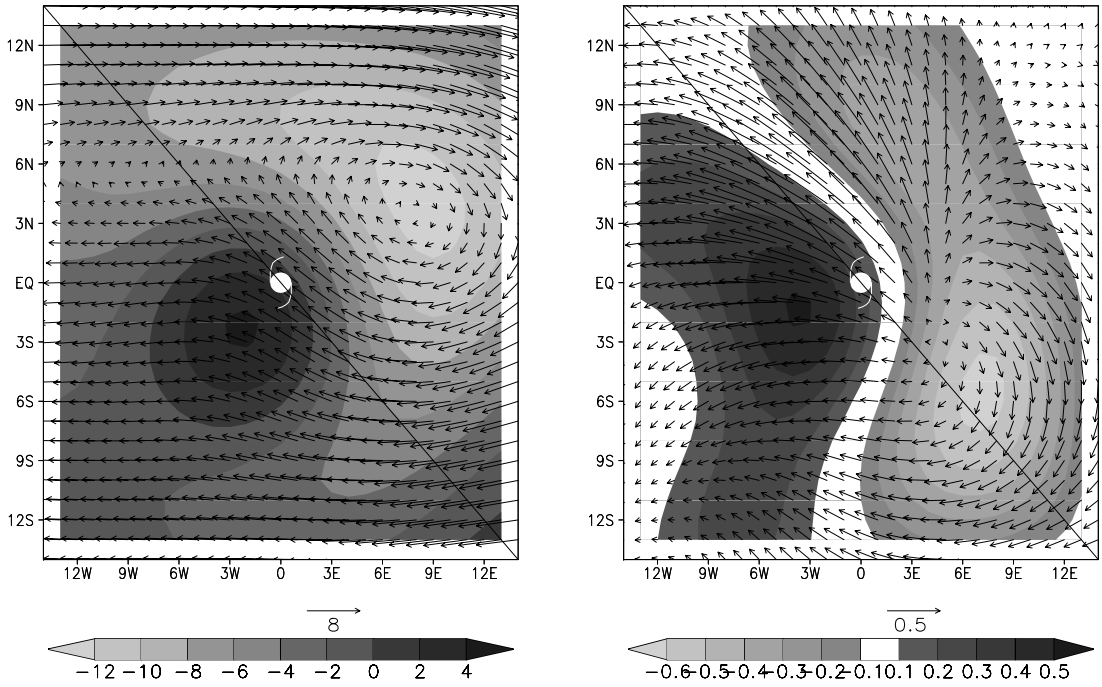

Figure 3. A storm-relative composite of the large-scale steering flow from the CTRL simulations (left) and the difference (WIND - CTRL) due to the assimilation of GOES winds (right) averaged over all 103 cases. Vectors depict the deep layer mean winds (in m/s) and shading depicts the corresponding vorticity field (in 10^6 s^{-1}). The hurricane symbol identifies the center of the storm used as the frame of reference to form the multi-storm composite.

Comparison of the mean forecast tracks for the CTRL and WIND experiments, from all 103 cases (Figure 2, top), provides a convenient summary of the improved performance of the track forecasts following the assimilation of GOES winds. The WIND forecasts clearly exhibit a tighter recurvature which, in turn, results in a marked reduction in the westward bias of the track forecasts (Figure 2, bottom), although at the expense of a modest increase in the northward bias. Since the WIND forecasts tend to move farther north than the CTRL, this would tend to hasten their recurvature (by moving the storms closer to the mid-latitude westerlies) and is consistent with the reduction in westward bias. Also note that the increased meridional bias relative to the CTRL only occurs for the 72 hr forecast, whereas the reduction in zonal bias is evident at all forecast times.

To examine the impact of the GOES data on the initial wind fields, Figure 3 illustrates the time-mean composite of the mean DLM flow from the CRTL runs (left) and the difference in DLM flow field (WIND-CTRL) due to the assimilation of GOES winds (right). In both these figures, the DLM flow is presented as vectors while the vorticity of the DLM vectors is depicted by shading. A key feature in the CTRL DLM field is the presence of a distinct β-gyre as evidenced by the anticyclonic circulation to the northeast and cyclonic circulation to the southwest of the storm center. Moreover, the difference in the vorticity of the DLM flow due to the assimilation of GOES winds also exhibits a distinct dipole structure (Figure 3, right). The DLM flow for the WIND experiments tends to have greater anticyclonic circulation to the northwest of the storm and greater cyclonic circulation to the southeast of the storm, consistent with an enhanced β-gyre. This suggests that, while the initial wind field from NCEP does contain a β-gyre like structure the strength of these gyres are, on average, underpredicted relative to that inferred from the GOES retrievals. This is consistent with the tendency for coarser resolution models (such as that used to provide the CTRL initial conditions) to form a weaker storm circulation and thus undepredict the advection of planetary vorticity. The stronger northward flow associated with

the enhanced β-gyre in the WIND experiments agrees qualitatively with the northward displacement of the storm tracks relative to the CTRL (Figure 2), although it does not offer an immediate explanation for the reduction in westward bias.

4. Summary

Recent enhancements in the wind retrieval algorithm and improved satellite instrumentation has provided unprecedented capabilities to observe the atmospheric circulation over the traditionally data-sparse tropical oceans with high spatial and temporal resolution. As shown here, the assimilation of these winds, even in a relatively simplified manner, were able to make a significant contribution to the reduction in track error. Specifically, assimilation of the GOES winds reduced the average track error at all forecast periods with reductions in track error of up to ~40 km and relative reductions in track error ranging from roughly 4-12%. The number of improved forecasts also outweighed the number of degraded forecasts following the assimilation of the satellite winds, especially for the 24, 36, and 72 hour forecast periods where over 60% of the forecasts were improved.

While these results are encouraging, substantial work remains in this area and further improvements appear possible. In particular, the use of improved assimilation techniques, such as 4-D variational analysis, which can utilize the high-time resolution of the satellite data are particularly promising. In addition, more work is needed to better define the nature of the model error covariances which is critical to both 3D and 4D assimilation methods. In the future, we hope to pursue such directions in collaboration with existing efforts both within NOAA and abroad.

USE OF METEOSAT-5 DERIVED WINDS FOR ANALYSIS OF TWO TROPICAL CYCLONES AFFECTING GUJARAT COAST ON 20 MAY, 1999 AND ORISSA COAST ON 29 OCTOBER, 1999

R. C. Bhatia, P. N. Khanna, K. Prasad and D. Singh
(India Meteorological Department Lodi Road, New Delhi, India)
and
M. Das Gupta
National Centre for Medium Range Weather Forecasting, New Delhi. India

ABSTRACT

Since last 2 years the coverage and quality of satellite derived winds over the Indian Ocean region has improved considerably with the operation of METEOSAT – 5 from 63 deg E longitude starting July 98. Due to availability of water vapour channel on this satellite, good quality water vapour winds at middle to upper tropospheric levels are now available in large numbers. METEOSAT - 5 derived winds have been used to diagnose the motion of the two tropical cyclones that formed over the oceanic areas during the year 1999, including the one which struck Orissa coast on 29 October, 1999 causing a very widespread devastation. The data has also been found to be useful for understanding factors responsible for intensification of cyclone and to provide better insight into the possible causes of movement of tropical cyclones in particular directions. Impact studies on the track prediction by assimilating METEOSAT – 5 winds in the Limited Area Model forecast run operationally at IMD and in the Global Spectral Model run at NCMRWF show positive results. Use of METEOSAT – 5 winds in the model improves the track predictions.

1. Introduction

Persistent efforts of last several years by a few centres have culminated into production of high quality satellite derived winds operationally by many satellite operators. These winds have proved to be of immense use for a number of applications, particularly by the Numerical Weather Prediction Centres world over. A number of studies have been reported earlier showing the impact of satellite derived winds, particularly Water Vapour Winds (WVWs), on objective analysis and numerical forecasts. Velden et al. (1992) have shown that by including high- density satellite derived winds into the tropical cyclone analysis, the error of objective track forecasts can be reduced. Subsequently, while studying the sensitivity of GOES derived WVWs on spectral barotropic numerical hurricane track forecast model, Velden (1996) found that inclusion of WVWs gives rise to improvement in numerical track forecast. More recently, Velden et al. (1997) have reported results of assimilating the data into the State-of-the art primitive-equation analysis and prediction systems such as those developed at GFDL and NRL. Study of four storms during the year 1995 has shown improvements in hurricane track forecasting. It has been shown that assimilation of wind information results in a reduction of mean forecast error by 6 - 13% over the 24 – 72 hrs forecast period. The 6.7 μm channel derived WVWs contribute significantly to the improvements of medium and longer - range forecasts.

During 1999 two cyclonic storms affected Indian coasts. One had struck North Gujarat coast and adjoining areas of Pakistan coast on 20 May, 1999. The second one had crossed Orissa Coast on 29 Oct., 1999 and caused widespread damage to the Orissa state as it had attained the stage of a super cyclone. Meteosat-5 derived winds were obtained from EUMETSAT for these two events covering the entire period right from their inception to maturity stage. These data were used to better understand the movements of the storms in the particular directions in a qualitative manner. Impact studies were also done by ingesting these winds into the Limited Area Model (LAM) being run operationally at IMD in order to assess the sensitivity of this new data to the objective analysis and numerical prognoses . In particular, their impact on objective track forecast errors was studied and results obtained have been compared with similar studies conducted in the past by other authors. WVWs derived operationally by

CIMSS, University of Wisconsin using METEOSAT-5 data and disseminated through INTERNET , were also used in this study to examine particularly the factors responsible for strengthening of Orissa cyclone.

2. Current studies

In the present work a preliminary study of the impact of METEOSAT-5 derived winds on the cyclone track predictions by Limited Area Model has been carried out. These data have also been used to understand the motion of the two tropical storms mentioned above, focusing particularly on the question whether the observed track of the storms could be explained by the steering flow as inferred from the METEOSAT-5 winds. The problems of the data sparseness in oceanic regions and the consequent limitations of the track predictions by NWP model are well known. The present study is motivated by the need to fill the data gaps in the areas surrounding Indian Sub-continent with satellite derived information. With this end in view an attempt has been made to examine the utility of METEOSAT-5 derived CMVs and Water Vapour Winds for improving NWP model forecasts.

3. Super Cyclonic Storm Over the Bay of Bengal (25-31 October,1999)

It was the most intense cyclone in last 114 years for the state of Orissa. It was bettered for more than 2 days by its fierce winds and intense rains. It also produced huge storm surge and catastrophic floods causing severe damage in 12 districts of Orissa affecting a population of about 120 lakhs. It started as an initial disturbance on 24 October near Gulf of Thailand and emerged in North Andaman sea as a well marked low pressure area on the morning of 25 October. It concentrated into a depression in the evening of the same day and moved further in a west northwesterly direction. Meteosat-5 derived winds at 200 hPa level on 25 October (1200 UTC) clearly bring out the steering flow responsible for this movement. Subsequently , the system intensified further and developed in to a cyclonic storm on 26 October at 03 hrs UTC. The system had been moving northwestwards under the influence of a steering flow caused by a subtropical ridge to its northeast at 200 hPa level. The conventional meteorological observations are inadequate to define this flow clearly. However, METEOSAT-5 derived winds bring out this flow very clearly (Fig. 1) and were found to be useful in track prediction. By 03 hrs UTC of 27 October , the system intensified to the stage of a severe cyclonic storm and came under the influence of 200 hPa ridge axis providing upper level outflow favourable for its further developments. Once again METEOSAT-5 winds brought out very clearly this flow which is known to be conducive for further intensification. After 0900 hrs UTC of 27 October , 200 hPa anticyclone got positioned over the system as a result of which its movement was slowed down. These features are very well noticed in METEOSAT-5 winds. It was further upgraded to the stage of VSCS at 1500 hrs UTC on 27 October and moved in a west northwesterly direction.

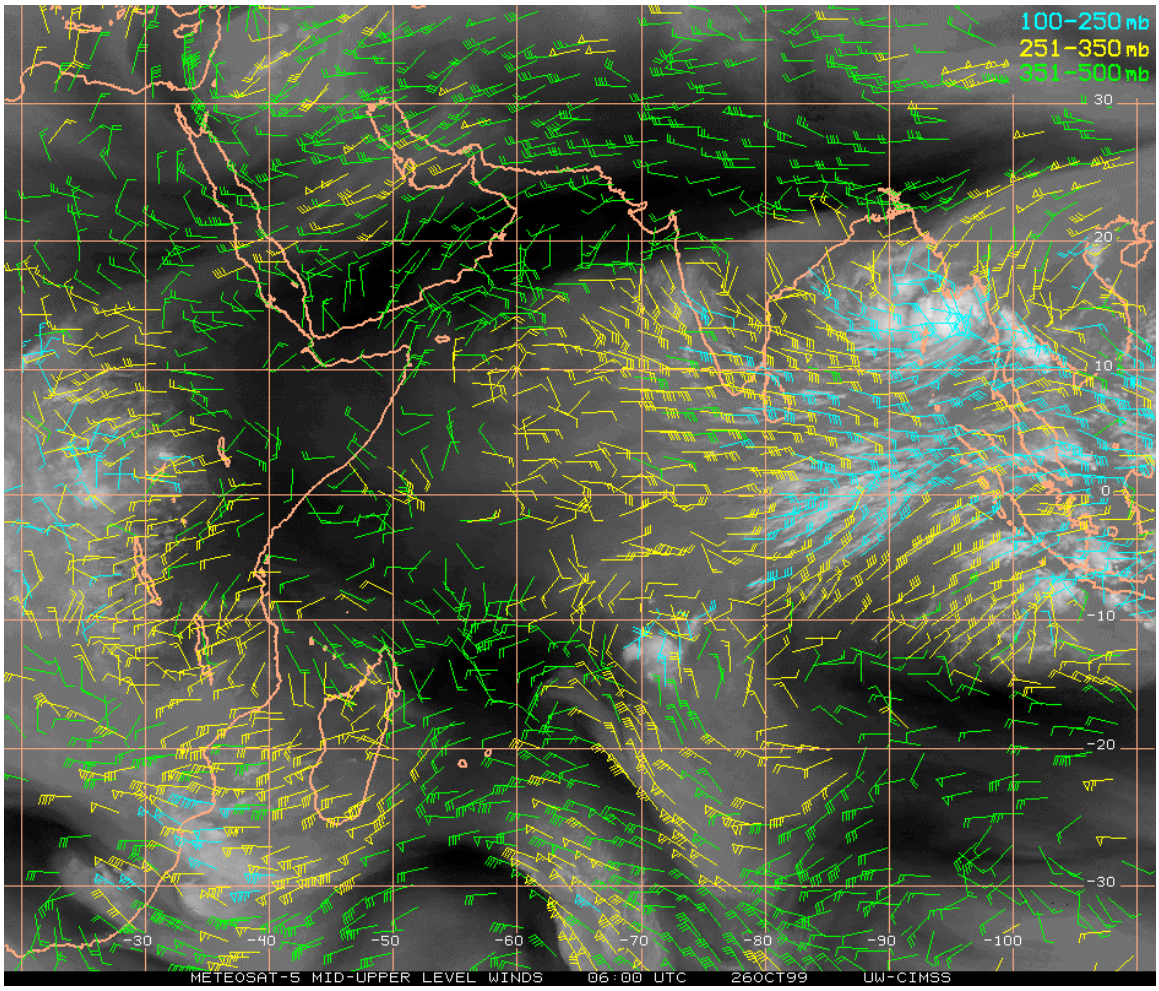

Figure 1. Meteosat-5 mid and upper level winds 26 October 1999 0600 GMT.

At this stage upper level flow as seen in METEOSAT-5 winds continued to be favourable for further development. A slight northward jog in the track was noticed which is well correlated with METEOSAT-5 winds. Forward motion was again slowed down and by 1800 hrs UTC of 28 October it become a super cyclone between 00 and 03 hrs UTC. It attained peak intensity at 03 hrs UTC just before landfall. It crossed Orissa coast close to and south of Paradip between 0430 and 0630 hrs UTC of 29 October. Next day morning (30 October) it was located in the col region (Fig 2) at 200 hPa with an anticyclone to its west over the western and adjoining areas of central India and another to the east covering parts of north Bay of Bengal and up to China sea. The Col region is brought out better in the METEOSAT – 5 derived winds. This situation continued up to 30th evening. The middle and upper tropheric WVWs by CIMSS with METEOSAT-5 also provided useful information on absence of shear in the upstream environment of the storm. Hence there was no disruptive influence on the storm as a result of which it continued its development process.

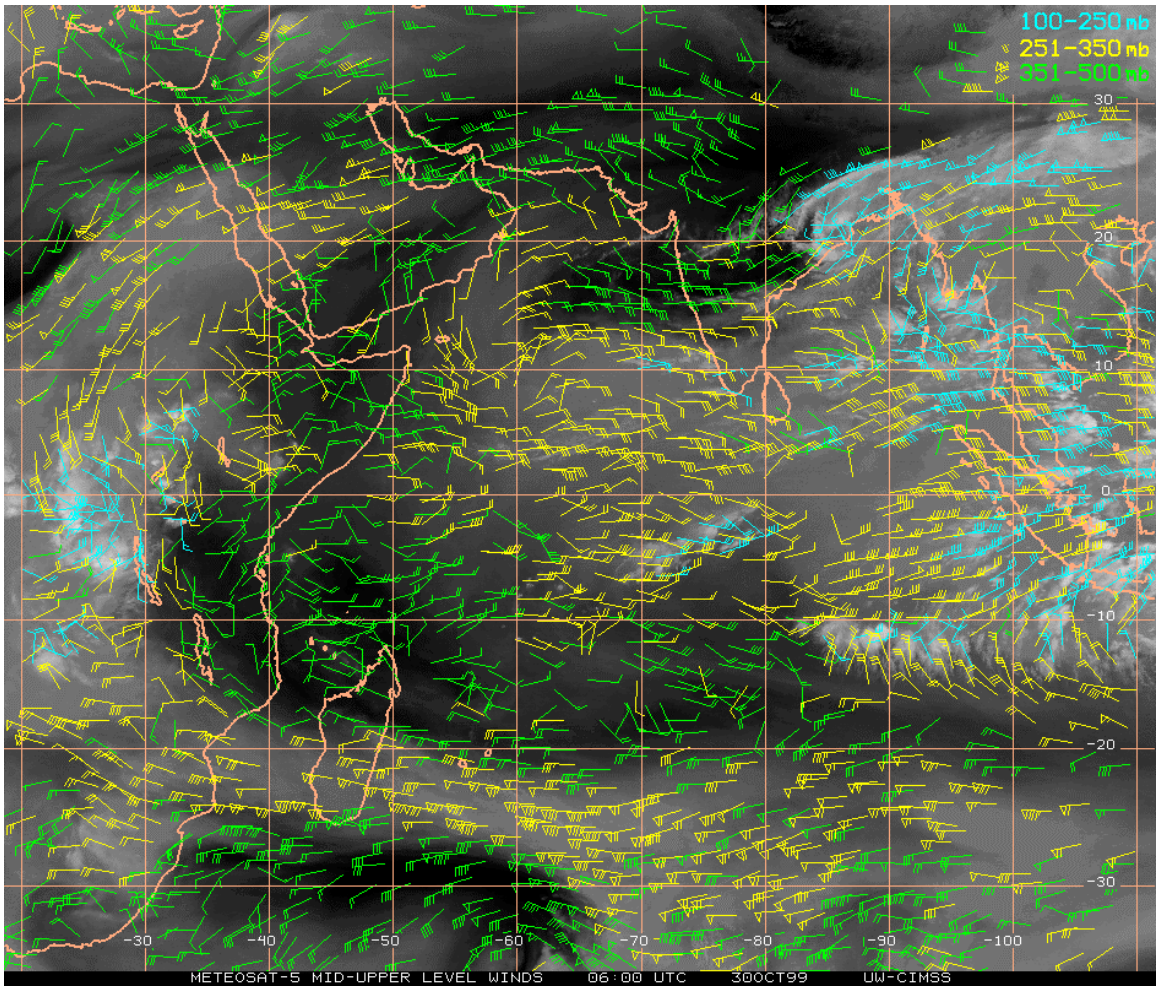

Figure 2. Meteosat-5 mid and upper level winds 30 October 1999 0600 GMT.

4. Very Severe Cyclonic Storm (VSCS) over Arabian Sea (16 - 22 May, 1999)

It was the case of one of the rare and intense storms that crossed into Pakistan coast of Sind which has not been visited by any tropical cyclone since 1948. It started as a low pressure system over southeast Arabian sea on 15 May ,1999 which intensified into a deep depression by 1800 hrs of 16 May and rapidly further intensified to the stage of VSCS by 1200 UTC of 17 May. Initially it was moving in a northwesterly direction , but after 0300 UTC of 18 May , 1999 it moved in a dead northerly direction. It skirted the Indian coast of Gujarat before crossing Pakistan coast close to the international border on 20 May , 1999. Subsequently it moved in a north eastward direction and lay over Jaisalmer in West Rajasthan as a deep depression at 1800 hrs UTC of 22 May. Its unique feature was northerly movement along 68 deg E longitude for a considerable period of time. The reason for this movement can be very well understood from the direction of middle level steering flow as seen from METEOSAT - 5 derived winds (Fig 3) for the period 18 – 19 May, 99. Storm was embedded in a persistent nearly Southerly steering flow for a considerable period. The ridge line at 200 hPa lay to the north of the system over Arabian Sea along 23 deg N latitude. Conventional charts could not bring out this feature adequately due to lack of data. Another feature noticed was that its movement was slow (8 - 10 knots) between 17 to 19 May, 1999. METEOSAT – 5 derived winds have provided better insight into the movement of this cyclone. There were generally weak winds at middle to upper tropospheric levels during this period.

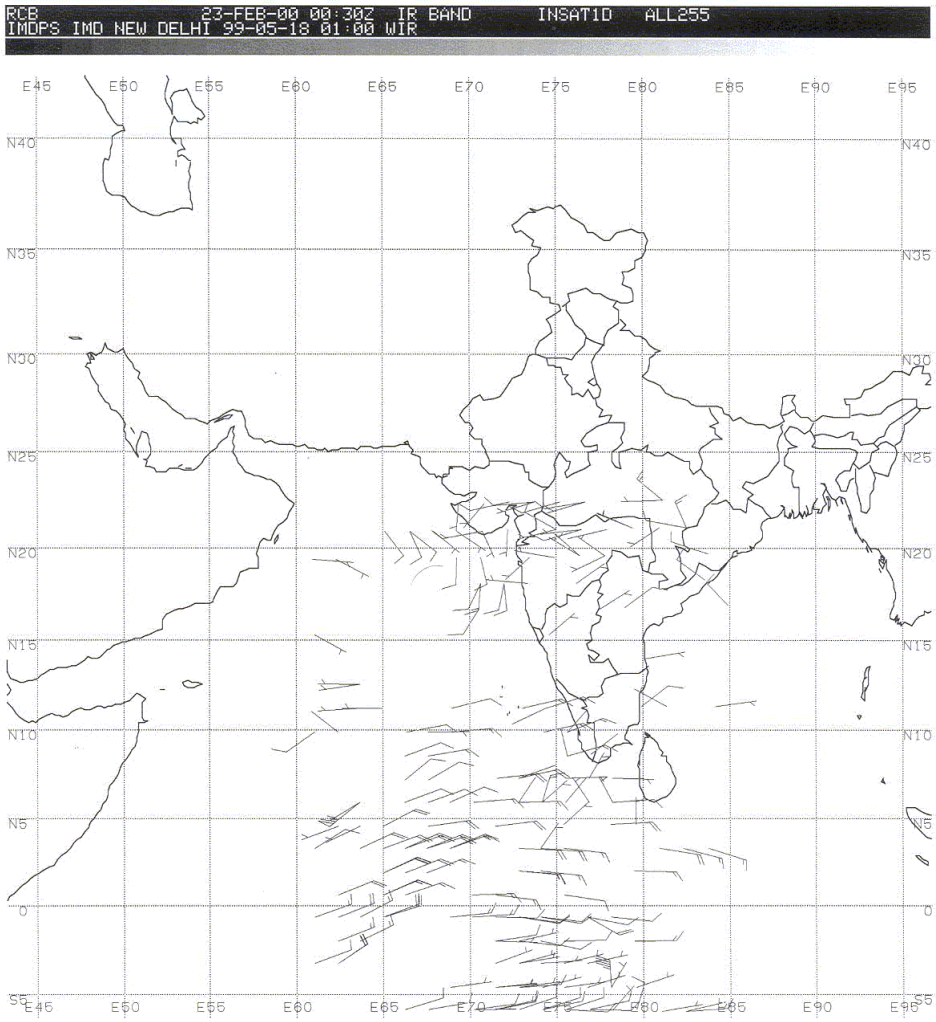

Figure 3. METEOSAT - 5 derived winds disseminated as SATOBs for the period 18 – 19 May, 99.

5. Impact studies on model forecast of a Limited Area Model

A Limited Area Model (LAM) adopted from Florida State University (Krishnamurti et al., 1990) is being run operationally at IMD since 1995. To start with, the model was run on NCMRWF's CRAY XMP – 14 Computer in experimental mode. It was made operational in August, 1995 on IMD's Cyber – 2000 computer. The model has at present a horizontal resolution of 1 deg x 1 deg lat./long. and 12 sigma levels in the vertical covering a geographical domain of 30 deg - 125 deg E and 25 deg S to 45 deg N. It is run operationally twice a day based on 00 and 12 UTC maps using real time GTS data. The data inputs include INSAT derived CMVs, but not the METEOSAT - 5 derived CMVs disseminated normally on GTS. Apart from generating the forecast of normal meteorological parameters with LAM for operational use, the track prediction model is also specially run at the time of formations of cyclonic storms and track forecasts are generated for use.

Experience of track predictions with the performance of LAM shows that the initial wind analysis over the oceanic areas is often inadequate as a result of which vortex is generally not brought out in the analysis. At times bogussing of data is resorted to and a synthetic vortex is implanted over the region of

cyclonic storm. This obviously results in poor performance of the model in capturing significant synoptic disturbances developing over the sea areas. METEOSAT - 5 derived winds which provide good coverage over the cyclone field could alleviate this problem to a some extent due to improved general analysis of the environment flow. In order to examine the impact of these data on track forecasts, above two cases of cyclones one over Bay of Bengal and one over Arabian Sea, were examined.

5.1 May, 1999 Cyclone

A control run (without METEOSAT–5 winds) and an experimental run (Including METEOSAT–5 winds) was executed on the initial conditions of 17 May, 1999. The Control run failed to take the track to the actually observed position and deviation was about 150 kms. However, the experimental run showed better results and the observed deviation from the actual track was found to reduce to 120 kms. The track predictions were also extended up to 48 hrs and it is noticed that even in the 48 hrs forecast, results of experimental run are slightly close to the actually observed track. The track is better predicted in the experimental run using METEOSAT– 5 derived winds.

5.2 29 October, 1999 Cyclone

Similar tests were also run on the initial conditions of 25 October, 1999 to find out impact on the 24 hrs and 48 hrs track forecasts for the devastating cyclone which struck Orissa on 29 October, 1999 using Global Spectral Model run at NCMRWF. Fig. 4 and Fig. 5 depict the results. It is noticed that use of METEOSAT-5 winds improves the track forecasts and also reduce the error. Mean error in analysis of four positions reduced from 5.5^0 to 3.7^0 and the mean error in forecast of two positions was reduced from 6.8^0 to 3.5^0 by using METEOSAT–5 winds. However, the problem of large error in the initial position still persists (though there was slight improvement) and further studies are needed to resolve it.

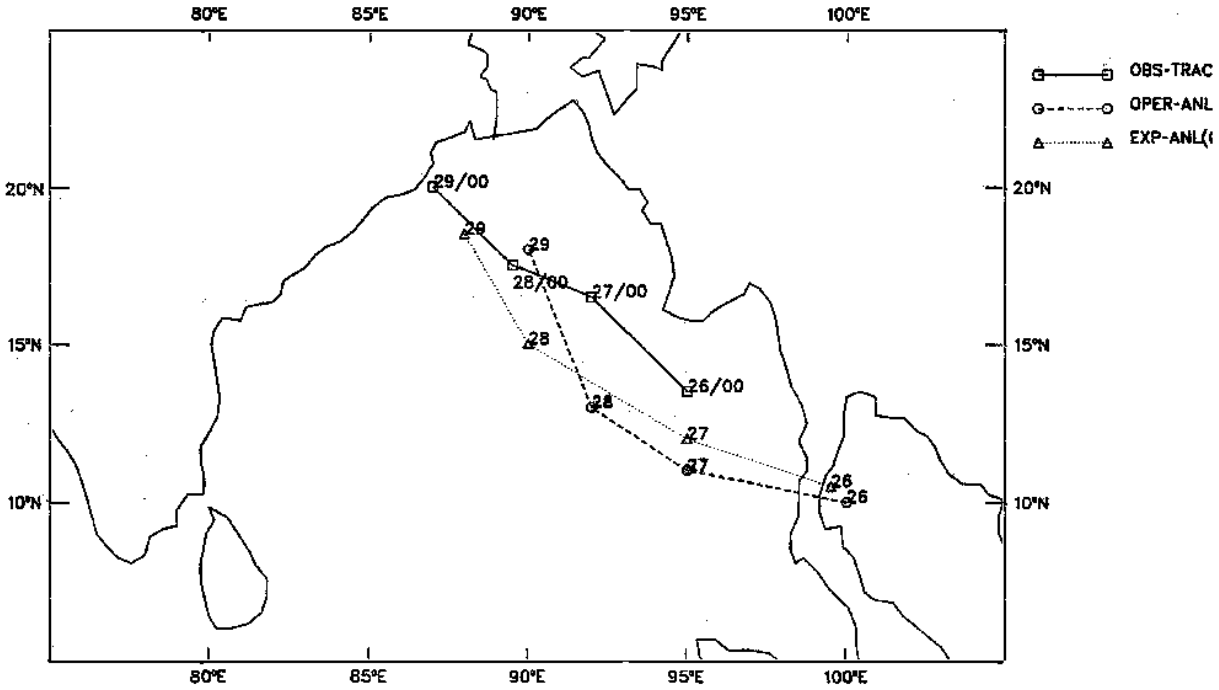

Figure 4. Analysis of the location of the storm Orissa.

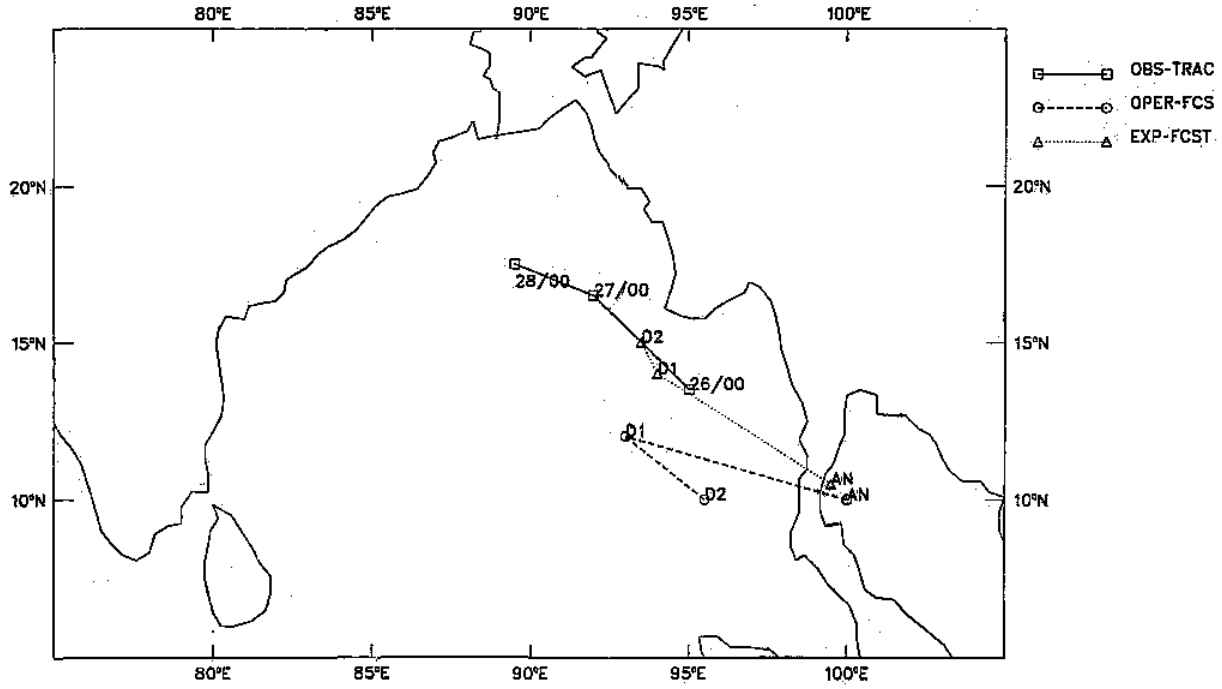

Figure 5. Forecast of the location of the storm Orissa.

The above two studies thus clearly bring out the slight positive impact of using METEOSAT-5 derived winds on the cyclone track forecasts based on Limited area and Global Models. These results are also consistent with findings of Velden et al. (1997).

6. Conclusions

METEOSAT-5 derived winds provide very good supplement to other conventional data sources over India and neighbouring oceanic regions and are useful for operational work of cyclone warning by providing better insight into the processes responsible for intensification of Tropical Cyclones and their movement. The middle level water vapour winds derived from METEOSAT – 5 are particularly useful to provide information on the effects of wind shear which are sometimes not observed in conventional satellite imagery. This information is very useful for forecasting intensity of Tropical cyclone which is vital for cyclone warning services. High level winds are found to be useful for depicting certain features above the center of the storm which are conducive to its further intensification.

Even for forecasting the movement of tropical cyclones METEOSAT-5 derived winds provide very useful guidance as they help to better define the direction of steering flow of the environment in which the storm is embedded. Use of this data in the track prediction done with the help of Limited Area and Global Models shows a slight positive impact on the track forecast. Impact is noticed in the form of better match between the actual and predicted track of the cyclone. Hence there appears to be a good potential in the use of METEOSAT-5 derived winds in improving the qualitative intensity forecasts of tropical cyclones and the track predictions by numerical models. They are also useful for track forecasts in a qualitative manner.

ACKNOWLEDGEMENT

Authors are grateful to EUMETSAT for promptly supplying the original METEOSAT – 5 derived winds data sets for the purpose of this study. Thanks are also due to Mr. S. K. Mukherjee of Sat. Met. Directorate for providing lot of useful technical assistance for completion of work.

REFERENCES

Krishnamurty T. N; Arun Kumar; et. al., 1990: Performance of a high resolution mesoscale tropical predction model, *Adv. Geophys*., 32, 133-286.

Velden, C. S, C. M. Hayden, W. P. Menzel, J. L. Franklin and J. Lynch, 1992: The impact of Satellite – derived Winds on numerical hurricane track forecasting. *Wea. Forecasting*, 7, 107 – 118.

Velden, C. S, 1996: Winds derived from geostationary Satellite moisture channel observations : Applications and impact on numerical weather prediction, *Meteor, Atoms. Physics*, 60, 37 – 46.

Velden, C. S, C. M. Hayden, S. J. Nieman, W. P. Menzel, S. Wanzong and J. S. Goerss, 1997: Upper – tropospheric Winds Derived from Geostationary Satellite water vapour observations, *Bull. Amer. Met. Soc.*, 78, 173 – 195.

ASSIMILATION OF SATELLITE–DERIVED WINDS INTO THE COMMUNITY HURRICANE MODELING SYSTEM (CHUMS) AT PENN STATE

Jenni L. Evans[1]

Department of Meteorology, The Pennsylvania State University
503 Walker Building, University Park PA 16802
USA
[1]Presently on sabbatical: Bureau of Meteorology Research Center,
Bureau of Meteorology, 150 Lonsdale Street, Melbourne
AUSTRALIA.

ABSTRACT

Challenges relating to forecasting in the tropics often differ from the midlatitudes due to: (i) weak dynamical constraints, (ii) rapidly evolving, mesoscale weather systems, (iii) the important role of convection and (iv) sparseness of the conventional data network in the tropics. Faithful representations of divergent flow and mesoscale features are necessary to resolve and simulate tropical weather phenomena accurately. The argument is that improving the initial conditions (IC) of a proven numerical model will optimize the reliability of the forecast.

Hurricane Floyd (1999) was the deadliest hurricane to affect the United States since Agnes in 1972 (NHC 1999). Hurricane Floyd (1999) tracked along the entire eastern seaboard of North America on its way out into the Atlantic towards Britain. The standard observing network lay to the left of the storm center as it tracked up the coast. This asymmetric coverage of the standard observations on a rapidly changing storm provides an ideal test of the potential impacts of using satellite–derived wind data to define the mesoscale detail of a rapidly evolving, intense weather system. Static analyses (with and without these wind data) of hurricane Floyd are compared for two key times in the storm's evolution. The radius of influence (horizontal and vertical) and observations/ analysis weightings mix are varied. The second component of this study is to perform a four dimensional data assimilation (FDDA) of these winds into the Penn State Community Hurricane Modeling System (CHUMS). In the present study, only satellite–derived winds are used. Asymmetries in the distribution of the satellite winds aloft seem to contribute to a degradation of the FDDA product. The results obtained here indicate that thermal fields, which can be derived from the AMSU–A sounder may hold promise for FDDA improvements. The impacts of moisture soundings from AMSU–B should also be investigated.

1. Experiment Design

Two approaches to assimilation of the winds data are presented here: a static, Cressman–type analysis and the MM5 four dimensional data assimilation (FDDA) cycle. Each approach has merits in assessing the value of the satellite winds to the analysis of the storm system structure. VIS, IR and WV winds (satwinds) from both GOES–8 and METEOSAT–7 are incorporated into both analysis systems. Data incorporated into the analyses presented here are not the operational GTS winds, but are an advanced version of high-density multispectral vectors derived in real time at CIMSS. These satwinds are derived using the advanced UW-CIMSS/NOAA-NESDIS algorithm (Velden *et al.* 1997; 1998). The data is processed to 60ºN however, the satwinds density at the highest latitudes is greatly diminished due to scan angle considerations. Two time periods in the lifecycle of hurricane Floyd were compared using this technique (see below).

Once read into MM5, the satwinds are sorted and their heights are estimated against a (case–specific) thermodynamic reference state. They are then incorporated into the model initial conditions through either the Cressman or FDDA procedure. US Navy Operational Global Atmospheric Prediction System (NOGAPS) and NCEP AVN model analysis fields (interpolated to the mesoscale model grid) are used as the first guess fields and also control analyses against which the impacts of the winds on the analyses are evaluated. While some satellite–derived winds are assimilated into these global models in real time, the data density is dramatically improved here. All available satwinds (CIMSS quality control only) within the vertical layers specified are incorporated into the Cressman analyses presented. Typically, over 2500 winds (additional quality control) are successfully assimilated in the CHUMS analyses at all times through the FDDA cycle. A 60 h continuous nudging FDDA cycle is compared with an equivalent 60 h forecast for the time leading up to the landfall of hurricane Floyd (1999) in North Carolina. Before reviewing these results, a brief review of the key elements in the lifecycle of hurricane Floyd (1999) is presented.

2. Case Study of Hurricane Floyd (1999)

Hurricane Floyd (1999) was responsible for 56 deaths in the United States, making it the deadliest US hurricane since Agnes (1972). In spite of quite reasonable track forecasts, this storm was the third in a series of hurricanes to make landfall in the Carolinas in the 1999 season and caused devastating flooding in large areas of the mid–Atlantic states. The storm was almost a category 5 system (921 hPa) as it approached the Bahamas on September 13, 1999. After exiting the islands, Floyd turned northward ahead of an approaching midlatitude trough and made landfall in North Carolina around 0630 UTC on 16 September 1999 as a weak Category 3 storm (965 hPa). It then tracked along the US east coast and Canadian Maritimes for over 2 days from until late on 18 September 1999. In all of this time, the structure of Floyd was continually evolving from a tropical, warm–cored system toward a midlatitude, cold–cored system as the storm underwent an extratropical transition. Floyd began to transition when it was offshore of New York state late on September 16th and completed transition about 72 h later, as it sped across the Northern Atlantic Ocean near 48ºN, caught up in the westerlies. While the U.S. National Hurricane Center (NHC) ceased tracking the system on 1800UTC at 19 September 1999, post–processing of global model analyses (both AVN and NOGAPS) reveals that the system was reintensifying to at least 985hPa at 10ºW as it approached Britain. This and a number of other recent studies compel us to recall the work of earlier researchers, who highlighted tropical systems as a potential source of damaging midlatitude storms.

3. Wind Assimilation Effects

While Floyd tracked along the North American coast, the standard network data was concentrated to its west. This asymmetric data distribution is problematic, especially as this storm is undergoing extratropical transition: a process of evolution from a relatively symmetric, tropical system to a highly asymmetric, extratropical system. The supplementary satellite–derived winds incorporated in the analyses presented here was almost entirely ocean–based. Rather than eliminating a data distribution bias, this asymmetry in data type produced its own complications.

3.1 Cressman Analyses

The Cressman–type analyses are static interpolations of the wind fields and have no temporal integration of the observations. This straightforward approach has the advantage of being very fast, allowing rapid assessment of a large variety of weighting structures for the asynoptic observations. These analyses are used to experiment with horizontal and vertical weighting functions for the satwinds. The control simulation uses a horizontal radius of influence (ROI) of 250 km and a vertical range of ±25 hPa from the model level. Two variations on this weighting structure have been tested: ROI=250km at all levels, ±50 hPa and varying ROI with height such that ROI=500km at 200 hPa,

ROI=250km at 500hPa, and ROI=100km at 850hPa (vertical range of ±25 hPa at all levels). This last experiment is designed to reflect the decreasing inertial stability of the tropical cyclone with height. For weak inertial stability (at 200 hPa) external forcing will have more impact over a wider area than the highly inertially stable lower levels. In all cases the winds are weighted either at the same level as the analysis (50/50) or as the dominant observation (85/15) wherever they exist. The 85/15 weighting is an attempt to approximate the effects of the winds if little or no other data were available for an analysis cycle (if satellites were the only data source, for example!).

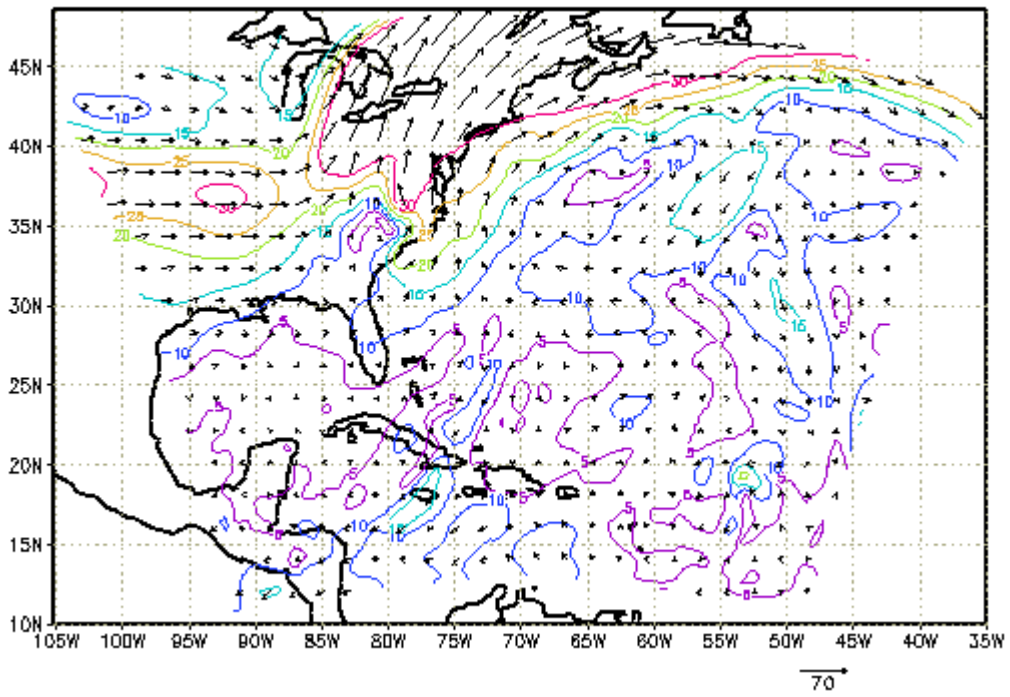

Figure 1. 200 hPa winds at 1200 UTC on 16 September 1999. Hurricane Floyd is located just off the North Carolina coast at (35.7ºN, 76.8ºW) and has minimum central pressure of 965 hPa.

Snapshots of two distinct stages in the lifecycle of Hurricane Floyd were studied in detail: (i) a weakening Category 3 hurricane (965 hPa) just exiting the North Carolina coast [16 September 1999 1200UTC] and (ii) a rapidly accelerating extratropical system in the midlatitude westerlies [18 September 1999 0000UTC]. Only analyses from the 16 September 1999 1200UTC are presented.

The 200 hPa winds for 1200UTC, 16 September 1999 are plotted in Figure 1. The tropical cyclone is at (35.7ºN, 76.8ºW) recurving just ahead of a midlatitude upper trough; the trough is associated with a surface front. These are the only significant flow features evident in the region. The poleward outflow jet of Floyd appears to merge with the strong upper jet ahead of the approaching trough.

Figure 2 is designed as a summary plot, highlighting the key features of the ROI and weighting variation. In all cases, the winds in the vicinity of the tropical cyclone modify the outflow near the storm center and in the vicinity of the trough/jet feature. In all cases, the poleward steering flow over the storm is weakened and a more cyclonic shear is evident over the storm. Not surprisingly, these effects are amplified for stronger weighting of the satwinds. Increasing the ROI also amplifies these changes (compare panels (a) and (c)), as well as weakening Floyd's poleward outflow jet and increasing the divergent flow in the right jet entrance region. This last wind change could affect low level cyclogenesis in the region (Lackmann et al. 1997). Modifications evident in the tropics are unlikely to have any effect on the evolution of Floyd which is accelerating into the midlatitudes at this time.

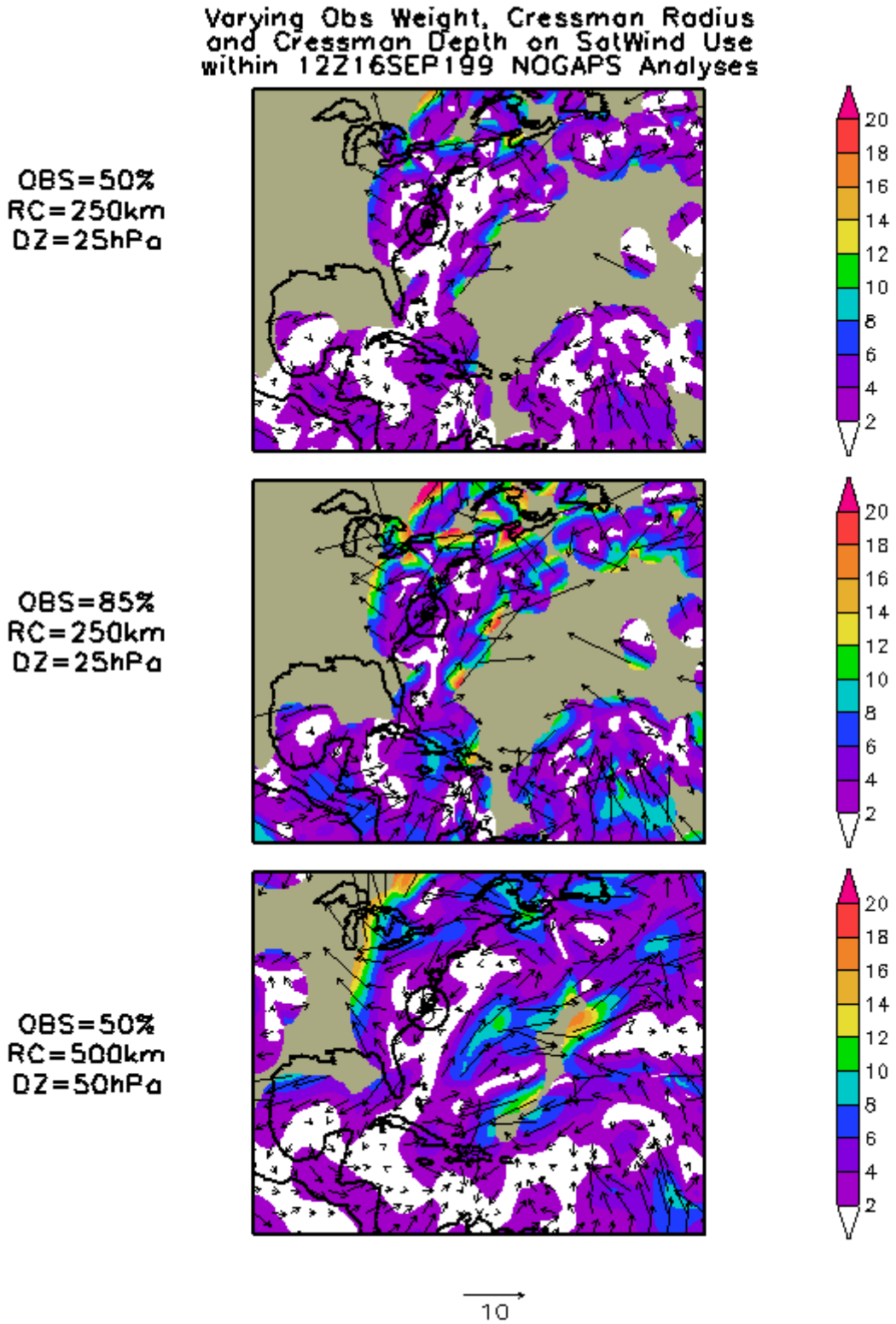

Figure 2. Impacts of different satwinds treatments on the 200 hPa wind analysis. 200 hPa difference fields (*satwinds*–control) for NOGAPS first guess fields are plotted: (a) ROI=250km, δp=±25, ω=0.5; (b) ROI=250km, δp=±25, ω=0.85; and (c) ROI=500km, δp=±50, ω=0.5. Both the tropical cyclone location and a circle with radius equal to the ROI are plotted on each panel. Grey shading indicates regions which are unaffected by the satellite–derived winds (outside the ROI of the closest wind).

3.2 Four Dimensional Data Assimilation

The MM5 FDDA procedure is based on a *Newtonian relaxation* (*nudging*) procedure (Stauffer and Seaman 1994) and readily allows assimilation of asynoptic data such as satwinds. Error characteristics for different data types are assigned either objectively or subjectively and are incorporated into weightings for each observation type that have both horizontal and vertical structure. Hence, for example, near–surface winds may only be assimilated in one layer, but may have broad horizontal influence on the final analysis field.

Two 60 h model simulations are compared here: an *"FDDA run"* in which the CHUMS forecast includes FDDA (3 hourly nudging to the satwinds) for the entire forecast cycle and a *"non–FDDA"* run in which no satwinds are used. In both cases, NOGAPS *analyses* are used to provide initial and boundary conditions. Since the purpose of this experiment is to investigate the impact of FDDA on the CHUMS forecast, continuous FDDA on the entire forecast was used for maximum impact; in a real–time forecast setting, a 12 h FDDA step, followed by a 48 h forecast would be a more typical cycle. The period studied extends from 14 September 0000 UTC to 16 September 1200 UTC 1999.

The impact of the FDDA on the forecast was unexpected and raises a number of issues. The track of hurricane Floyd was well simulated by the control (no satwinds) forecast of the model is shown in Figure 3. Inclusion of the satwinds in this case has resulted in a degradation of the track forecast. The intensity forecast (not shown) is improved by 5-10% in the FDDA simulation, although the model resolution is too coarse to expect it to agree closely with observations.

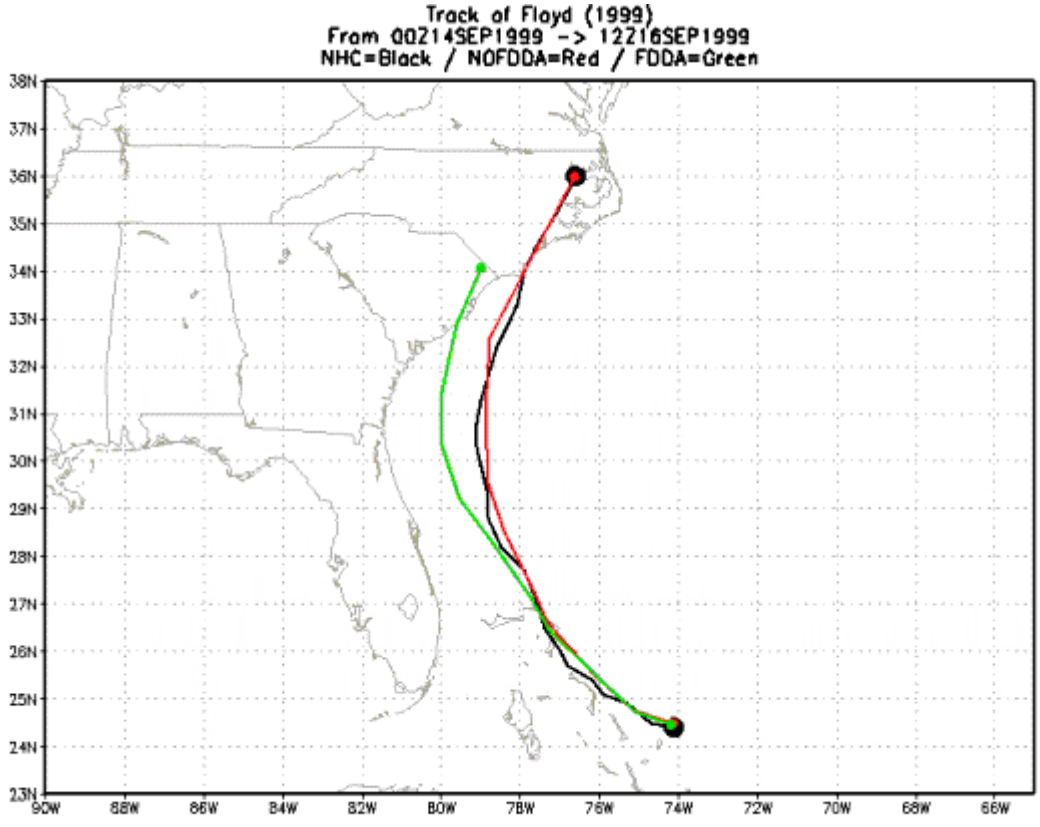

Figure 3: Comparison of the tracks of Floyd: NHC best-track (black), 60 h control forecast (red) and 60 h FDDA satwinds forecast (green). Forecasts initialized on 0000 UTC 14 September 1999.

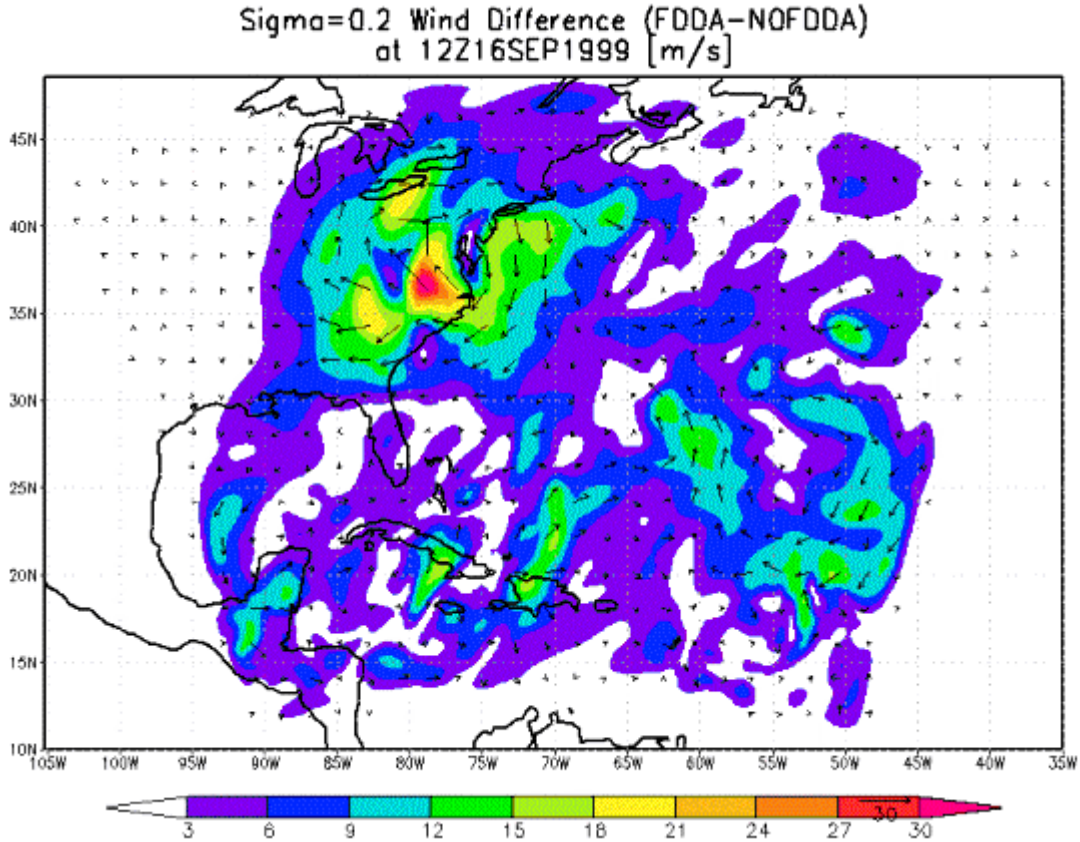

Figure 4: 200 hPa wind difference (FDDA-control) for 16 September 1999 at 1200UTC.

A number of avenues are being explored to progress from this result. The immediate work involves incorporating a more uniform coverage of satwinds and repeating the experiment. For 20/22 datasets used here, we had satwinds over the ocean only. Thus, inclusion of these winds vastly increased the description of the upper troposphere over the ocean, without directly impacting the flow over land. Even at 60h, the differences in upper tropospheric flow are predominantly over the ocean or in the immediate vicinity of the storm (Figure 4). Optimal satwinds weights and ROI are also being sought.

4. Summary

Cressman analyses of combined satwinds and global model analyses demonstrated the potential for variation of the radius of influence (ROI) of observations with height (Figure 2) and allowed for efficient exploration of optimal ROI values for this case. The time presented here (16 September 1999 at 1200 UTC) was one of two windows in which the satwinds data available were distributed across the entire (land and ocean) domain show here.

While initial results for the FDDA are somewhat disappointing, the bias in the satwinds spatial distribution is an obvious cause for concern. Simulations with full resolution satwinds will be repeated immediately and these results will be presented at the AMS Tropical Meteorology and Tropical Cyclones Conference in May 2000.

ACKNOWLEDGEMENTS

Support for this research by the Large-Scale Dynamics Program of the National Science Foundation (grant ATM-9911212) is gratefully acknowledged. Many thanks to Mr Robert Hart of Penn State for his excellent programming and graphics work. The satwinds data used here were provided by Mr Christopher Velden and colleagues at CIMSS, University of Wisconsin.

REFERENCES

Lackmann, Gary M., Daniel Keyser, Lance F. Bosart, 1997: A characteristic life cycle of upper–tropospheric cyclogenetic Precursors during the Experiment on Rapidly Intensifying Cyclones over the Atlantic (ERICA). *Mon. Wea. Rev.*, **125**, 2729–2758.

NHC staff (1999) Preliminary Report on Hurricane Floyd 7–17 September 1999: http://www.nhc.noaa.gov/1999floyd_text.html.

Stauffer, D. R. and N.L. Seaman, 1994: Multiscale four–dimensional data assimilation. *J. Appl. Meteor.*, **33**, 416–434.

Velden, C. S., C.M. Hayden, S.J. Nieman, W. P. Menzel, S. Wanzong and J. Goerss, 1997: Upper-tropospheric winds derived from geostationary satellite water vapor observations. *Bull. Amer. Meteor. Soc.*, **78**, 173–195.

Velden, C. S., T. Olander and S. Wanzong, 1998: The impact of multispectral GOES–8 wind information on Atlantic tropical cyclone track forecasts in 1995. Part I: Dataset methodology, description and case analysis. *Mon. Wea. Rev.*, **126**, 1202–1218.

RECENT DEVELOPMENTS IN THE USE OF SATELLITE WINDS AT THE UK MET. OFFICE

P. Butterworth and N. B. Ingleby

NWP Division, The Met. Office,
London Rd, Bracknell RG12 2SZ, U.K.

ABSTRACT

Impact trials carried out for July 1998 to test Meteosat-5 and GMS water vapour satellite winds showed small positive impacts, and operational changes to The Met. Office's global operational numerical weather prediction (NWP) system were subsequently made in spring 1999. Since then, a set of impact trials attempting to make use of satellite winds at a higher resolution than previously has been carried out. It was found that assimilating winds at a resolution of 2º results in a neutral impact, whereas assimilating at resolutions closer to model resolution (92- and 125-km) produces small negative impacts. The average forecast RMS error increased by 0.4 and 0.3%, respectively, even though use was made of EUMETSAT's quality indicator in the thinning of these winds. To provide a context within which to set these results, a trial was run using no satellite winds, which resulted in a degradation of forecast RMS error of 1.8% when verified against independent observations. This last result confirms that the current operational use of satellite winds is providing a significant enhancement to the forecast.

1. Introduction

Since the 4th Winds Workshop in October 1998, The Met. Office has carried out a series of impact trials in order to try and improve the use of satellite winds in its operational global NWP model, the Unified Model (UM). Improvements and modifications to the current set of satellite winds transmitted worldwide have been outlined and highlighted in the proceedings from the most recent Winds Workshops (EUMETSAT, 1997, 1999). These include the repositioning of Meteosat-5 in support of INDOEX, the generation of water vapour winds by the Japanese GMS satellite, the generation of high-resolution winds from both Meteosat and GOES, and also the transmission of winds with a quality indicator (QI) attached from Meteosat. Tests were carried out on Meteosat-5 and GMS WV winds in 1998, and, within the past year, attempts have been made to make use of high-resolution winds, including those containing a QI.

Currently (February 2000) use is made of infrared, water vapour and low-resolution visible winds from Meteosats-5, -7 and GMS-5, and infrared winds from GOES-8 and -10 (thinned to 2º). No satellite winds are used at heights below 700 hPa (low level) over land in the northern extratropics, and GMS-5 water vapour winds are not used between 400 and 700 hPa (medium level).

Other types of "satellite wind" are in use at The Met. Office: winds derived from scatterometer measurements and those from the microwave imager, SSM/I. The term satellite wind or satwind is used here to signify those data derived from geostationary imagery; winds from scatterometer or SSM/I will be named as such. Recent changes in the use of these latter winds included the switching off of scatterometer winds in December 1999 as a Y2K precaution. The Met. Office had been carrying out its own retrieval and dealiasing of ERS data since August 1993, to the benefit of the forecast system. However, this benefit had recently been negated by an error in the sea-ice check, which was introduced in January 1998 and rectified in September 1999. An impact trial on ESA-produced winds with extra quality control on the wind directions yielded neutral impact (Candy *et al*., 1999). Scatterometer

winds will be reintroduced within the operational 3DVAR assimilation system in late 2000. SSM/I wind speeds have been used operationally since October 1999. They showed a similar positive impact to scatterometer winds (largest in the southern extratropics) but there exists some redundancy between the two observation types.

2. Data assimilation developments

In March 1999 The Met. Office changed from the previous analysis correction (AC) scheme to a three-dimensional variational assimilation (3DVAR) system (Lorenc *et al*., 2000). ATOVS data from NOAA-15 were assimilated simultaneously. In October 1999, direct assimilation of radiances from satellite sounders was introduced, as were SSM/I wind speeds. There were also changes to the background error covariances and to the use of surface pressure observations. Together these changes were the most significant to the data assimilation system for many years and they resulted in forecast improvements throughout the globe, but particularly in the southern extratropics (see Fig. 1).

Salient features of the 3DVAR system are that it is performed at half the horizontal resolution of the operational forecast model (in spectral terms it is a T107 analysis) and no special account is taken of asynoptic data (plans are currently in hand to amend this). The 3DVAR system allows use of nonlinearly related observations (such as satellite radiances) and an improved covariance model controls the spreading of observational increments. For example, in the tropics there is less vertical spreading of wind and temperature increments (Ingleby, 2000). In general the system extracts more useful information from observations but it appears also to be more vulnerable to poor quality data. Thus, if one aspect of the quality control system is wrong, then it can negate the benefit of using a particular observation type (e.g. scatterometer winds). Observation errors should be regularly monitored to ensure that up-to-date estimates are used within the assimilation system. For the trials outlined below, the observation errors used at different levels for satellite winds are:

Level (hPa):	1000	850	700	500	400	300	250	200	150	100	70
Error (m/s):	1.3	1.7	2.0	2.5	3.3	3.3	3.3	3.3	3.6	5.5	5.4

A full discussion on background errors is given in Ingleby (2000).

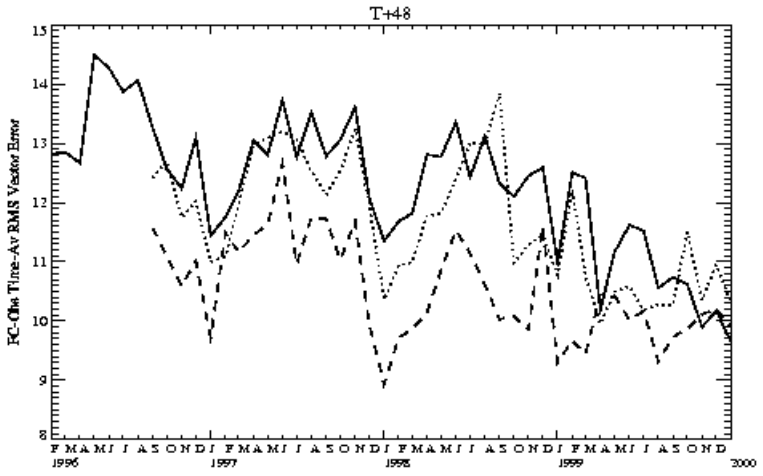

Figure 1. RMS verification of T+48 forecasts against radiosonde 250-hPa wind (m/s) for region 30-90º south: The Met. Office (solid line), ECMWF (dashed line) and NCEP (dotted line). (Courtesy of D. Matthews, The Met. Office.)

3. Impact trials

In response to the repositioning of Meteosat-5 for INDOEX over the Indian Ocean, an impact trial valid for July 1998 was run. Verifying the forecasts against observational data showed an improvement in an averaged skill score of 0.4%. This improvement was good enough for the use of Meteosat-5 winds to be made operational in the UM in February 1999. Following this, an impact trial on the use of GMS water vapour (WV) winds at high level (heights above 400 hPa), valid for July 1998 was carried out, and showed an improvement in skill score of 0.2%. Again, this resulted in an operational change, and high-level GMS WV winds were switched on in March 1999. The skill score is described briefly in section 4 of Lorenc *et al.* (2000). It places most weight on short-range (24-hour) forecasts and mean sea-level pressure.

Two subsequent trials on the use of high-resolution visible winds from Meteosat gave results that were not so encouraging. The first, using these winds thinned to one per 2 x 2º box, run during October 1998, gave a neutral result. The second, which attempted to make more use of these winds by using one per 92-km box, as well as increasing the use of GOES IR winds to this density (they are used operationally at one per 2 x 2º box) gave different results depending upon the season. Two separate trials were run. The first, valid for March 1999, showed an insignificant increase in skill score against observations (0.03%) and the second, valid for June 1999, showed a decrease in skill score of 0.3%. Due to the negative nature of the combined trials, the operational use of GOES winds remained as before, and high-resolution Meteosat visible winds were not introduced operationally. A more in-depth account of all the above trials is given in Butterworth (2000).

The transmission of Meteosat satellite winds in BUFR code, along with the QI, means that more flexibility is now possible in the use of Meteosat winds. The QI is computed at EUMETSAT during routine quality control of satellite wind observations (Holmlund, 1998), and is based on a set of five tests for consistency against neighbours and a forecast field. The QI can range from 0 to 1, and for normal satob transmissions of low-resolution winds, only those winds that have a QI above 0.8 are transmitted. In BUFR code, however, all winds with QI>0.3 are transmitted, thus allowing the NWP centre to determine its own requirement with respect to quality. The BUFR winds are also produced every 90 min (with the exception of visible winds, which are produced every 3 hours).

3.1. The Quality Indicator

Before quality control decisions based on the QI can be made within the data assimilation system, it must be verified that the QI itself is an independent measure of quality which can be used by the assimilation system. The QI contains information from another NWP model (the ECMWF model is used for the forecast check), and it is possible that a high QI measured by the EUMETSAT quality control system will not equate to a high quality when compared against our system. To this end, a week's worth of data were collected (25 October - 1 November 1999), and for each separate wind type, in different latitude regions and at different levels, the QI was compared against the observation-background differences found during observation preprocessing. Figure 2 shows some typical results. The winds were divided into QI bins of 0.01, and then plotted with the average wind speed bias and vector RMS computed for the set of winds within that bin. Number of winds in each bin and the averaged background wind speed is also shown. It is reassuring that, generally, as the QI increases, the measures of quality for bias and vector RMS improve (i.e. the bias tends closer to zero, and the vector RMS decreases). For lower values of QI (0.3 - 0.5) the signal tends to be more noisy, and for the cases of medium-level cloudy WV winds and clear-sky WV winds, the signal is not clear enough that we would currently consider testing these winds with the current assimilation system.

3.2. Details of impact trials

Two impact trials at different resolutions were run to test the use of the QI and increased resolution satellite winds. The tests ran from 26 November to 26 December 1999, using a low-resolution version of the current operational UM. Changes made in the use of satellite winds were as follows:

- Satob-coded winds from Meteosat were switched off.
- BUFR-coded winds from Meteosat were switched on, constituting high-resolution visible winds, high-resolution water vapour winds (cloudy only at high levels) and standard-resolution infrared winds.
- BUFR winds were only used for validity time closest to the operational runtime, i.e. every 6 hours, and not every 90 min.
- All satellite winds, and not just the high-resolution data, were subject to thinning.
- One trial at a thinning resolution of one wind per 92-km box was run. A second trial at a thinning resolution of one wind per 125-km box was run.
- The choice of wind within a thinning box was that closest to the centre of the box for GOES and GMS winds.
- The choice of wind within a thinning box was that with the highest QI for Meteosat, subject to a certain minimum threshold.

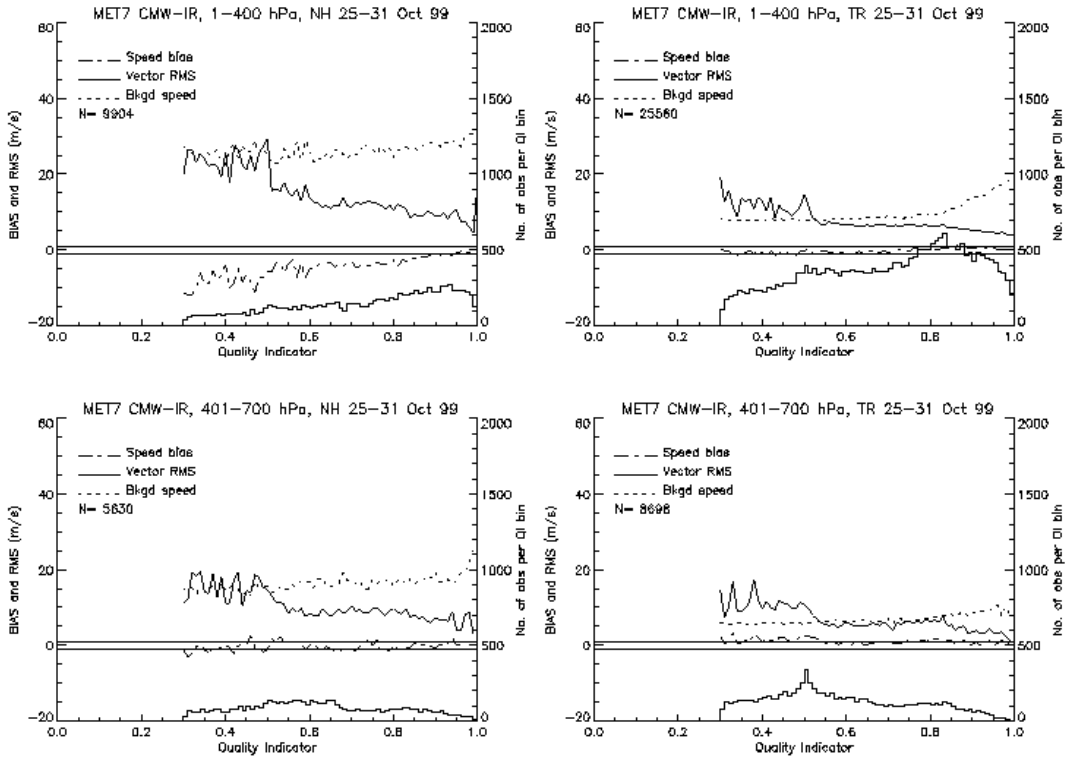

Figure 2. Quality indicator vs observation-background statistics for Meteosat-7, infrared cloud-motion winds. Top panels: high-level winds; bottom panels: medium-level winds; left panels: northern extratropics; right panels: tropics. Solid line: vector RMS; dot-dashed line: wind speed bias; dotted line: background wind speed, all relating to the left-hand scale. The number of winds in each 0.01 QI bin is also plotted, relating to the right-hand scale.

Since winds with QI above 0.3 are transmitted, it is necessary to impose a threshold limit on the winds that are allowed into assimilation. Based on the figures showing QI in relation to observation-background quality statistics, the following thresholds were chosen:

Tropics, all winds	all levels	0.90
Visible winds	low level	0.60
Water vapour winds	high level	0.80
Infrared winds	high level	0.85
Infrared winds	medium level	0.60
Infrared winds	low level	0.70

The high threshold chosen for tropical winds is not based on the QI plots (since these showed tropical winds to be quite reliable at QIs much less than 0.9), but on the experience of impact trials at ECMWF (Rohn *et al*., 1999). Those trials found that a stringent threshold should be placed on tropical winds, due to the scarcity of other observations and to avoid over-dependence on satellite winds. With regard to volume, it was found that moving from the current operational use of satellite winds to 92-km resolution resulted in double the number of satellite winds being assimilated (from *ca* 7000 to 15000 per model run).

4. Results

The forecasts were verified from 1 to 25 December 1999, allowing a generous 4-day spin-up before comparison. In each case, a set of forecast parameters were verified for the test run and the control run, both against the analysis produced by each run, and against independent observations valid for the forecast time. Forecast parameters include geopotential heights, wind, temperature and relative humidity at a range of levels (850-100 hPa), and mean sea-level pressure, all at a range of forecast times, from T+24 to T+144 h. The RMS forecast error was measured for each case, and the value of percentage change in RMS forecast error computed, whereby a positive change is a degradation from control to test, and a negative change an improvement. The percentage changes in RMS forecast error averaged in latitude bands are given in Table 1, as is the number of observations available for verification for each model run.

Table 1. Percentage change in RMS forecast error for the two trials at different resolutions, and number of observations available for verification in each latitude band. A positive change is a degradation in the forecast from control to test.

	Verification vs analysis	Verification vs observations	Obs available for verification
92-km resolution			*Surface*
NH	+0.8	+0.1	3160-3280
Tropics	+1.2	+0.4	650-850
SH	+1.4	+0.6	620-670
Average:	+1.1	+0.4	
125-km resolution			*250-hPa wind*
NH	+0.9	+0.3	310-340
Tropics	+0.8	+0.3	70-95
SH	+1.1	+0.4	70-95
Average:	+0.9	+0.3	

It can be seen from Table 1 that both trials show a negative impact from the changes introduced in the test runs. Overall, the result is worse for the 92-km resolution trial than the 125-km, yet within latitude bands the northern extratropics verifies better for the 92-km trial. Verification against observations is considered to be a better measure of forecast error, since they are independent of the forecast being verified. Analyses retain some influence due to previous forecasts and do not provide an independent reference, especially in data-sparse regions. However, a closer inspection is still needed to pinpoint the locations of the changes that are being made to the forecast by introducing the new winds and the new thinning procedures.

Figure 3 shows where the differences in analysis between test and control are taking place for mean sea-level pressure. The data are averaged for 1 - 25 December 1999, for the runs at 12 UTC, and the RMS difference between test and control is shown. It is apparent that the biggest changes are taking place in the south Atlantic and southern Indian ocean, under the Meteosat sphere of influence. With regard to upper-level parameters, Fig. 4 shows an equivalent field for the u-component of the 250-hPa wind. This time, the changes are more widespread over the Meteosat regions. Figures 3 and 4 indicate that no major changes were made to the analyses by the introduction of more GOES data due to the increased resolution, and this finding is apparent in fields of other forecast parameters. The auto-editor system at NESDIS reassigns the observation heights to give a better fit to the NCEP forecast (Nieman *et al*., 1997). This appears to improve their accuracy and their fit to our short-range forecasts, but at the cost of introducing information from another NWP system.

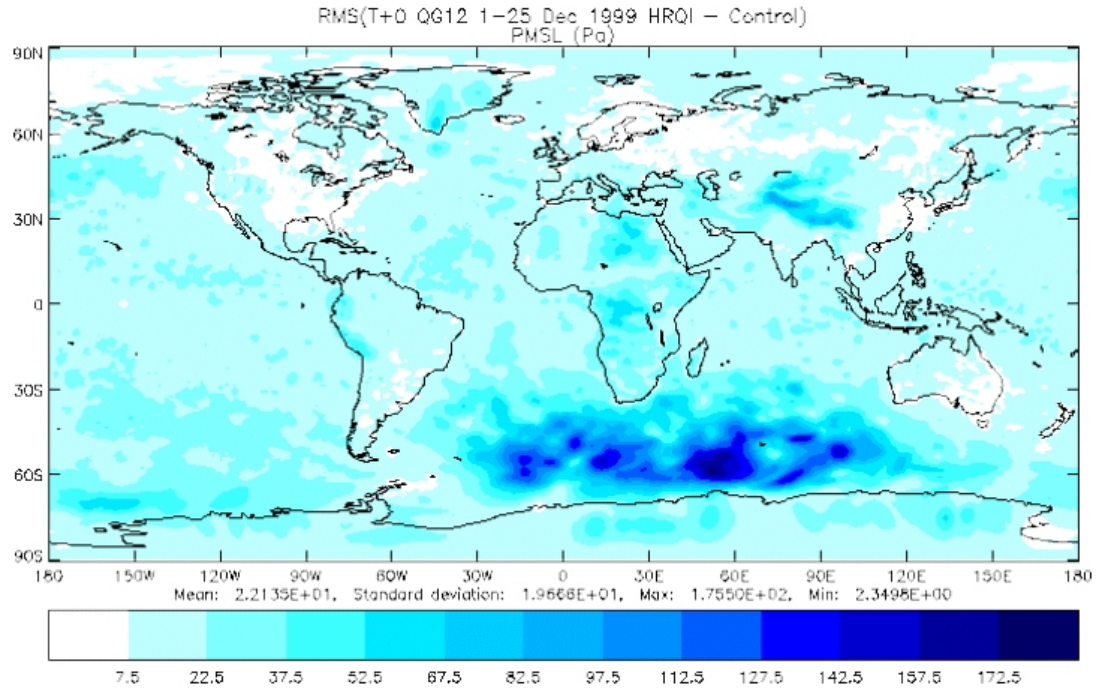

Figure 3. RMS difference (test - control) of mean sea-level pressure (Pa), averaged for 1 - 25 December 1999, model runs at 12 UTC only, for the 92-km resolution trial.

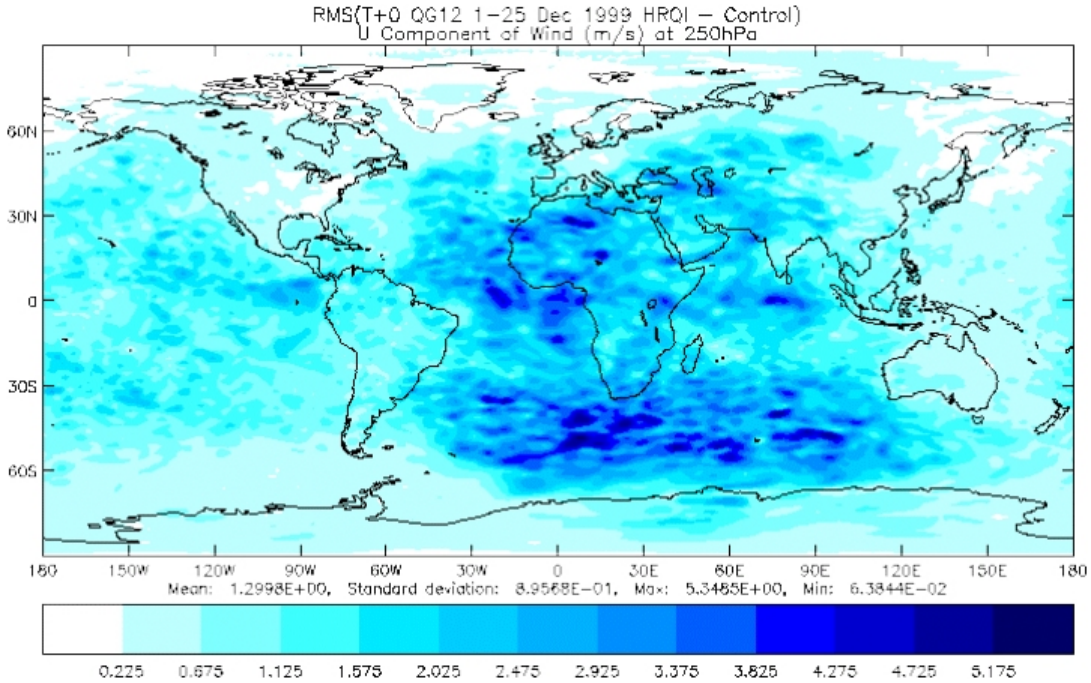

Figure 4. As Figure 3 but showing the u-component of the 250-hPa wind field (m/s).

Although the results for both trials were negative overall, the average change in percentage forecast RMS error was not very large. Of the forecast parameters that were compared against observations, mean sea-level pressure in the southern extratropics for the 92-km resolution trial showed the most sustained difference, with significant increases in forecast RMS error of 2.6, 2.7 and 3.4% at forecast times of T+72, 96 and 144 h, respectively. The biggest single changes in forecast RMS error were in the southern extratropics for 850-hPa geopotential height at T+96 and 250-hPa wind field at T+144 (both 3.9%). The 125-km resolution trial displayed a similar pattern of differences.

In order to try and place these results in context, a further trial was carried out in which all satellite wind observations were removed from the test run. In this case the control is the current operational system, which assimilates Meteosat, GOES and GMS winds at low resolution. Table 2 shows the results averaged for 1 - 25 December 1999. Against analysis, the global forecast has improved by 0.4% upon the removal of satellite winds from the system, while verifying against observations shows that the forecast is degraded by 1.8%. The improvement in forecast against analysis in the tropics is dominated by T+24 forecasts. Since persistence gives a good forecast in the tropics, adding observations here nudges the forcast away from persistence and so the verification against analysis is worse at short range. The use of satellite winds in the tropics becomes more positive at longer ranges. Due to the reasons described above, verification against observations is considered to be a better measure of impact.

Table 2. Percentage change in forecast RMS error for the "no satwind" test. A positive result implies a benefit from using the satwinds.

	Verification vs analysis	Verification vs observations
NH	+0.4	+0.9
Tropics	-2.2	+1.8
SH	+0.5	+2.7
Average:	-0.4	+1.8

Against observations, it can be seen that overall the forecast in the southern extratropics has degraded the most, by 2.7%. The biggest single changes in forecast RMS error were in the southern extratropics for mean sea-level pressure (T+144, 11.9%) and for 100-hPa wind fields in the tropics (T+24, 12.1%).

Although many forecast parameters exhibited sustained degradation throughout the forecast range when no satellite winds were used (e.g. tropics, 100- and 250-hPa wind fields, 100-hPa temperature fields; southern extratropics, 50- and 250-hPa wind fields, 250- and 850-hPa geopotential height), mean sea-level pressure in the southern extratropics displayed the largest changes, as seen in Fig. 5. These results confirm that satellite winds are a valuable part of the observing system used in data assimilation. An interesting result to come from this trial found that in the northern extratropics the satellite winds were actually degrading the short-term (24-hour) forecast when verified against radiosondes, particularly over Europe and Asia, however this was more than compensated by the benefit seen at longer forecast ranges. The implication of the degradation at short-range is that we may be overfitting the satellite winds, and perhaps need to increase the assigned observation errors.

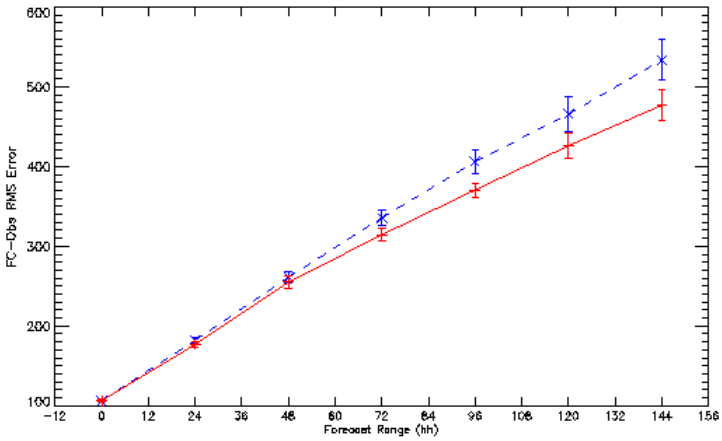

Figure 5. Forecast - observation RMS error for mean sea-level pressure (Pa), verified against surface observations for the southern extratropics (20-90 S), vs forecast range for control (solid line) and no satwind test (dashed line).

A greater selection of RMS forecast error changes for the 125-km resolution trial and the no satellite winds trial is given in Table 3.

Table 3. Percentage change in RMS forecast error for a selection of forecast parameters. Results for the 125-km resolution trial and the no satellite winds trials are shown. A positive change indicates a degradation from the control run to the test run. Changes vs both analysis and observations are given.

			125-km resolution		No satellite winds	
Area	Field	Range	vs anal	vs obs	vs anal	vs obs
NH	PMSL	T+24	0.75	1.85	1.09	0.01
NH	PMSL	T+48	0.16	1.16	1.10	1.98
NH	PMSL	T+72	0.82	0.46	0.47	1.24
NH	PMSL	T+96	1.30	1.69	0.81	0.39
NH	PMSL	T+120	1.14	1.35	1.55	5.69
NH	H500	T+24	1.73	2.14	0.04	-1.13
NH	H500	T+48	0.39	-0.45	1.59	2.88
NH	H500	T+72	0.88	-0.34	0.89	2.15
NH	W250	T+24	1.39	0.32	-0.12	-0.29
Trop	W850	T+24	0.63	0.32	-16.13	0.54
Trop	W850	T+48	0.47	0.15	-10.52	1.31
Trop	W850	T+72	0.73	0.17	-7.05	1.74
Trop	W250	T+24	-1.81	0.73	-15.76	8.61
SH	PMSL	T+24	0.09	-0.12	-1.81	2.96
SH	PMSL	T+48	0.58	0.97	0.54	2.42
SH	PMSL	T+72	0.72	2.24	3.11	6.75
SH	PMSL	T+96	0.92	2.16	3.80	9.56
SH	PMSL	T+120	1.50	0.69	5.13	9.32
SH	H500	T+24	0.41	-1.56	-3.47	-1.22
SH	H500	T+48	0.24	-0.75	2.30	4.13
SH	H500	T+72	0.65	0.10	5.32	6.59
SH	W250	T+24	1.07	-0.91	-7.26	2.78

5. Conclusion

The use of satellite winds at resolutions approaching model resolution does not improve the forecast, at least in the current configuration. Making use of extra quality information supplied by EUMETSAT is not sufficient to overcome the negative impact of assimilating so many winds. As a follow-up to the tests on high-resolution winds, an impact test using no satellite winds was also carried out. In comparison, the use of winds at 92-km resolution resulted in an average forecast RMS error degradation of 0.4% against observations (equivalent to 0.4% degradation in skill score). The use of no satellite winds resulted in an average forecast RMS error degradation of 1.8% (equivalent to 1.9% degradation in skill score), illustrating that the use of satellite winds is enhancing the forecasts, particularly in the tropics and southern extratropics. The smaller enhancement in the northern extratropics due to the use of satellite winds is to be expected in the light of the density of conventional observations in this region. Since there is some evidence that we are overfitting the satellite winds, a trial using increased observation errors is being trialled. Height assignment may also be part of the problem, and this will be investigated.

REFERENCES

Butterworth P. (2000) Impact of the assimilation of new data types on UKMO global model analyses and forecasts. *Proc.* 1999 *EUMETSAT Satellite Data Users' Conf.*, Copenhagen, September 1999. EUMETSAT, Darmstadt (in press).

Candy B., D. Li and A. Berney, 1999: The impact on forecast skill of using wind observations from different scatterometer processing methods. FR Technical Report 277, The Met. Office, Bracknell, U.K.

EUMETSAT, 1997: *Proc.* 3*rd Int. Winds Workshop*, Ascona, Switzerland, June 1996. EUMETSAT, Darmstadt, EUM P 18.

EUMETSAT, 1999: *Proc.* 4*th Int. Winds Workshop*, Saanenmoser, Switzerland, October 1998. EUMETSAT, Darmstadt, EUM P 24.

Holmlund K., 1998: The utilization of statistical properties of satellite-derived atmospheric motion vectors to derive quality indicators. *Wea. Forecasting* **13**, 1093-1104.

Ingleby N.B., 2000: The statistical structure of forecast errors and its representation in The Met. Office global 3-dimensional variational data assimilation scheme. *Quart. J. Roy. Meteor. Soc*. (submitted).

Lorenc A.C., S.P. Ballard, R.S. Bell. N.B. Ingleby, P.L.F. Andrews, D.M. Barker, J.R. Bray, A.M. Clayton, T. Dalby, T.J. Payne and F. Saunders, 2000: The Met. Office global 3-dimensional variational data assimilation scheme. *Quart. J. Roy. Meteor. Soc*. (submitted).

Nieman S.. J. Daniels, D. Gray, S. Wanzong, C.S. Velden and W.P. Menzel, 1997: Recent performance and upgrades to the GOES-8/9 operational cloud motion vectors. *Proc. 3rd Int. Winds Workshop*, Ascona, Switzerland, June 1996. EUMETSAT, Darmstadt, EUM P 18.

Rohn M. and G. Kelly, 1999: Transition to cloud motion winds from Meteosat with 90 minute time sampling and a revised screening. ECMWF Res. Dept Memorandum R43.8/MR/63, ECMWF, Shinfield Park, Reading, U.K.

ASSIMILATION OF CONVENTIONAL AND SATELLITE WIND OBSERVATIONS IN THE GLOBAL DATA ASSIMILATION SYSTEM AT NCMRWF

S.R.H. Rizvi, M. Das Gupta, A.K. Mitra, V.S. Prasad
National Center for Medium Range Weather Forecasting (NCMRWF)
Mausam Bhawan, Lodi Road, New Delhi - 110003
India
E-mail: rizvi@ncmrwf.gov.in, riffat_rizvi@hotmail.com
and
H.V. Gupta
India Meteorological Department
Mausam Bhawan, Lodi Road, New Delhi - 110003
India

ABSTRACT

For determining the three-dimensional structure of the global circulation of atmospheric fluid it is very important to assimilate wind information from all available sources through out the globe. This paper is aimed at describing efforts made at NCMRWF in assimilating various types of global wind observations, both conventional and satellite, in its operational Global Data Assimilation System (GDAS).

The conventional in-situ observations are very few and mostly confined over land, leaving behind vast amount of data sparse oceanic region. Thus it is very essential to make use of various other global wind observations like, buoy, aircraft and remote sensing data, such as cloud drift winds, scatterometer winds and microwave winds etc. There are some well known uncertainties in the remote sensing data, such as height assignment of cloud motion winds and directional ambiguity of scatterometer winds etc, which are to be addressed before assimilating these wind observations. Apart from conventional winds, satellite winds from INSAT, GMS, GOES and METEOSAT at low resolution, recently we have started utilizing high resolution METEOSAT-5 and ERS-2 winds data in the operational GDAS at NCMRWF. One of the main objectives of this work is to describe the impact of various types of wind data used in the NCMRWF operational analysis/forecasting system. Results on the intercomparison of CMVs from various geostationary satellites is also discussed. Impact of high resolution CMVs from METEOSAT is discussed as a special case study.

1. Introduction

Atmospheric data assimilation is the process of determining a consistent four-dimensional atmospheric state using various information like, meteorological observations taken from all over the globe, first guess field from a Numerical Weather Prediction (NWP) model and other physical constraints like mass-wind relationship, various type of statistical information about the observations and the background field used as first guess etc., while analyzing the data. The operational global data assimilation system at NCMRWF makes use of almost all types of both conventional and non-conventional data received on GTS.

2. NCMRWF Global Data Assimilation System

The Global data Assimilation System (GDAS) is an important component of the Analysis/Forecast system which basically provides the initial condition to the Numerical Weather Prediction (NWP) model. It consists of mainly three components. (i) Data reception and quality Control (ii) Data Analysis and (iii) the NWP model. The NWP model basically provides the first guess to the analysis scheme. The details of various components are discussed in Rizvi et al. (1997). The analysis scheme used in GDAS is based on the concept of Spectral Statistical Interpolation (SSI) technique developed originally at NCEP, USA (Parrish and Derber, 1992). It is based on the Lorenc (1986) concept of minimizing a cost function J consisting of mainly two parts as follows.

$$J = J_{ges} + J_{obs}$$

The two terms, on the right hand side of J, deal with the fit of analysis with the first guess field and the observations respectively. In order that the analysis should fit best with both the first guess and the observations, J is minimized, using conjugate gradient algorithm (Chandra, 1978) with respect to the analysis variables. Further details about the operational analysis scheme at NCMRWF can be seen in Bansal and Rizvi (1993), Rizvi and Parrish (1995) and Rizvi et al.(1998).

3. Global Data Utilization

The meteorological data from various observing platforms from all over the globe is received at Region Telecommunication Hub (RTH), New Delhi through Global Telecommunication System (GTS) and the same is made available to NCMRWF. Keeping in view that these global observations pertain to different types of instruments, both from conventional and non-conventional type, some observations deal with single level and some of them have multi-level information etc., proper processing is required to separate out these highly inhomogeneous set of observations in proper categories. This is very essential because different type of observations have different error characteristics which are to be given due weightage in their analysis. At present, various type of data used in the operational GDAS at NCMRWF are as follows.

3.1 Conventional Data

(a) TEMP and TEMP-SHIP: Wind and temperature at all the significant and mandatory pressure levels except humidity field which is up to 300 hPa. Surface temperature, wind, pressure, moisture and elevation from the surface reports are also utilized.

(b) PILOT and PILOT-SHIP: Winds at all the mandatory and significant pressure levels and all the wind reports by height.

(c) SYNOP, SYNOP-SHIP and BUOY: Surface Temperature, wind, pressure, moisture and elevation.

(d) Aircraft reports: Winds and temperature information.

3.2 Non-Conventional Data

(a) Cloud motion vectors (CMVs) Both low (> 500 hPa) and high (< 500 hPa) levels wind from INSAT, GMS, GOES and METEOSAT satellites. High resolution CMVs from METEOSAT for a limited region (00 - 150 South and 400 East to 1200 East).
(b) NOAA satellite temperature profiles and total precipitable water content.
(c) Surface wind information from ERS2 satellite.
(d) Synthetic data based on satellite T-number is also used whenever a cyclone is observed in the Arabian sea and Bay of Bengal.

As a special case , high resolution METEOSAT cloud motion vectors are used (25 Oct.-29 Oct., 1999) to study the impact on the Super Cyclone which formed in the Bay of Bengal during this period.

4. Results Discussion and Conclusions

In the present study output of operational GDAS for July, 1999 have been compared with the corresponding run for the same period without METEOSAT high resolution CMVs. It is observed that use of high resolution METEOSAT winds make positive impact on the NCMRWF analysis/forecast system. As shown in Fig.1, at 500 hPa., the forecast wind vector RMSE in Tropics (300 S to 300 N) and Indian region (100 S to 400 N, 00 E to 1450 E) are less in the operational run which uses the additional high resolution METEOSAT CMVs. For a special case study, METEOSAT high resolution CMVs data were obtained from EUMETSAT on request to study the impact on the Orissa Super Cyclone, which formed in the Bay of Bengal during October 1999.

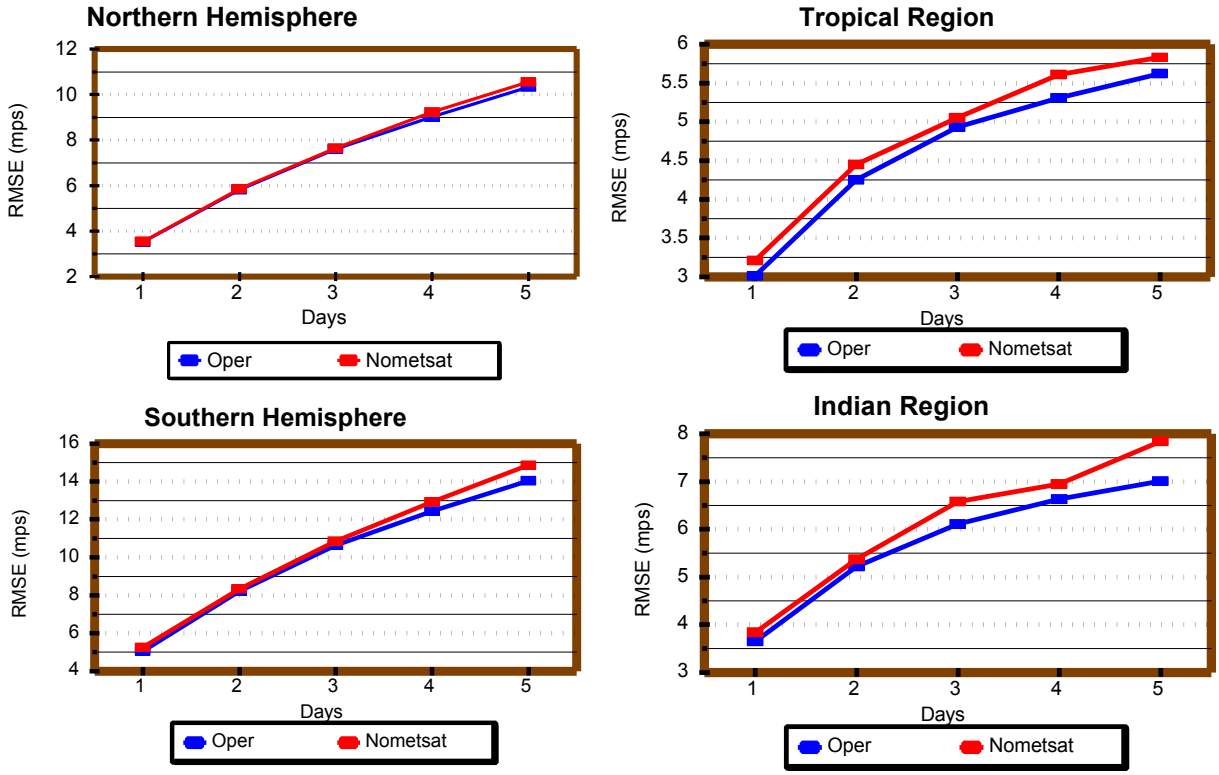

Figure 1. 500hPa forecast Vector Wind RMSE for July, 1999

The use of these winds have shown positive impact on the NCMRWF analysis during the cyclone period. As shown in Fig.2, the analysed position of the cyclone track is in better agreement with the operational cyclone track of India Meteorological Department. The use of these winds have improved 24 and 48 hour forecast. It can be seen in Fig.3, that the 24 and 48 forecast (based on initial condition

of 00 UTC of 26th October, 1999) of 850 hPa. wind flow is better defined in the experiment run specially in the NE-sector of the cyclone.

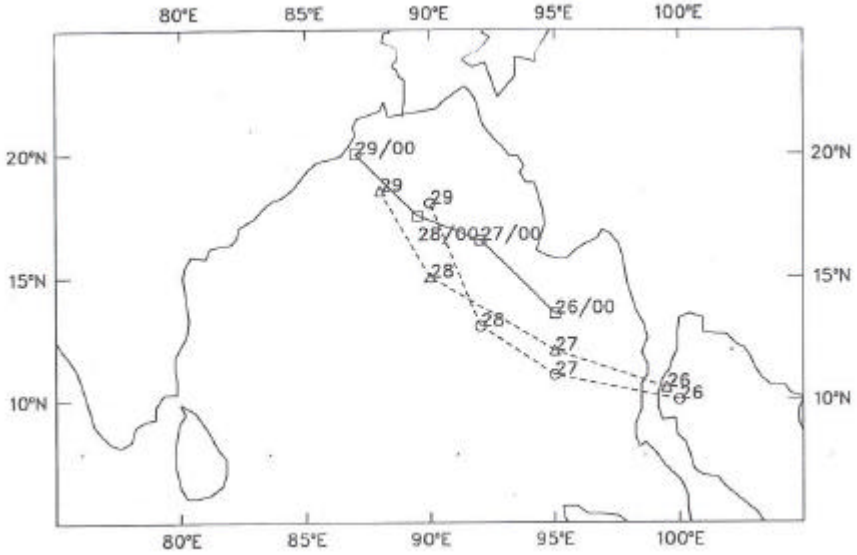

Figure 2. Analysed position of the cyclone track (OPER = circles, EXP = triangles) and observed along with the operational cyclone track of IMD, New Delhi, (OBS = squares).

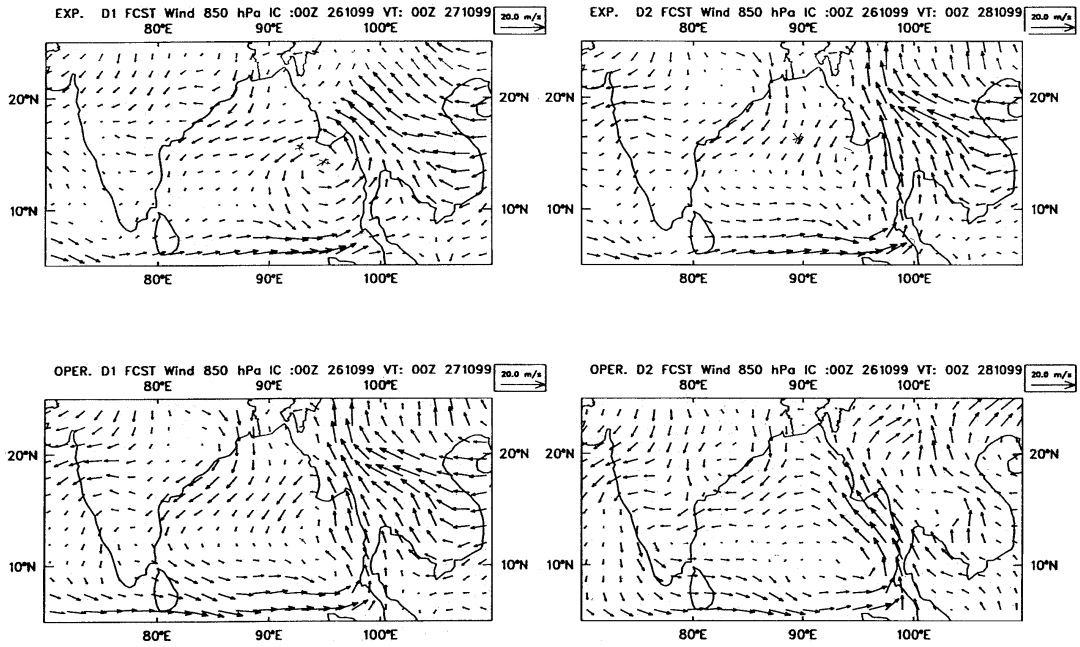

Figure 3. 850 hPa (wind flow), 24 and 48 hour forecast (OPER & EXP) IC : 00 UTC 26 October 1999.

Recently a new CMVs derivation scheme was implemented at IMD, New Delhi for computation of INSAT CMVs. To see its impact on the NCMRWF operational GDAS, 15th Jan. to 15th Feb., 2000 data was used for inter-comparison of the CMVs data from GOES, GMS, INSAT and METEOSAT satellites. GOES rmse was found to be less as compared to other satellites, specially at higher (< 500 hPa.) levels and the same is shown in Fig.4. It has been observed that INSAT CMVs are fitting well with the NCMRWF analysis / forecast system after the implementation of new INSAT CMVs derivation scheme.

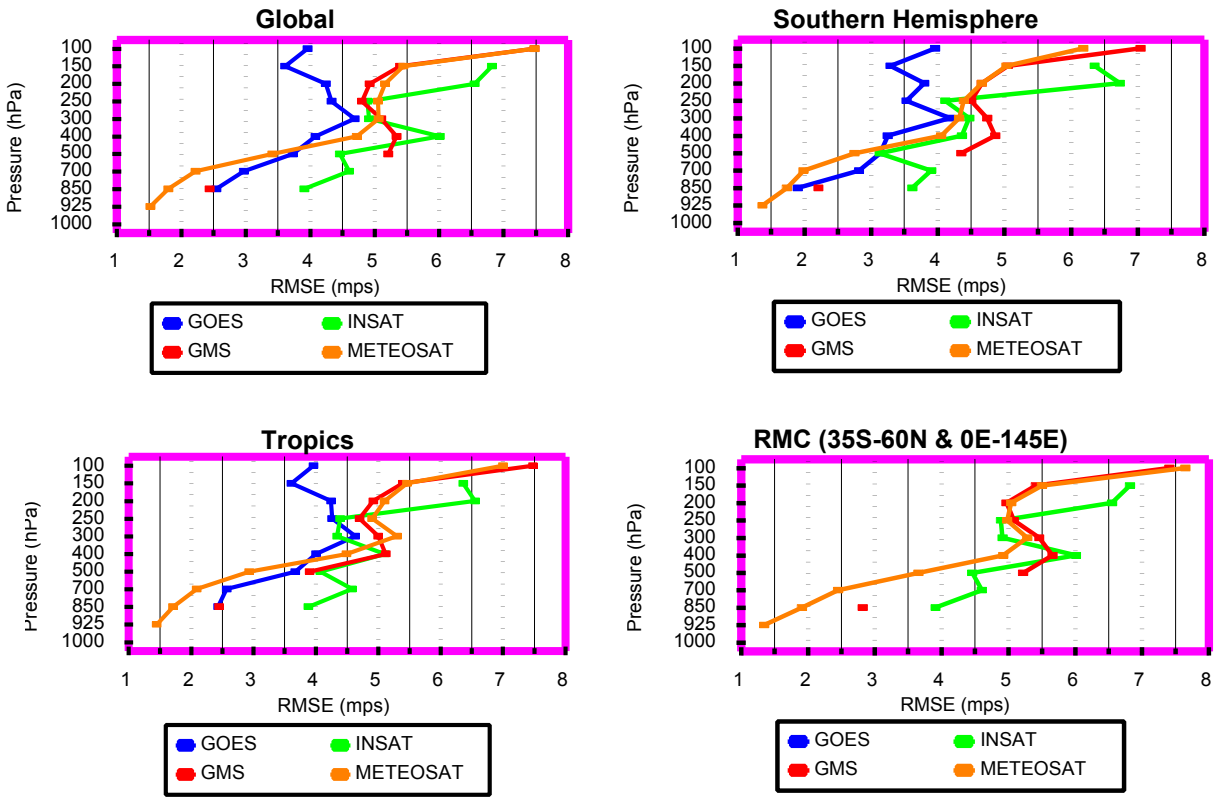

Figure 4. Vector Wind RMSE (Jan - Feb, 2000)

ACKNOWLEDGEMENTS

The authors are thankful to the Head, NCMRWF for encouragement and support. The authors are grateful to the Organizers of this workshop for giving the opportunity to present this work. Thanks are also due to DGM, IMD for providing the data and other facilities for this study. The first author sincerely acknowledge EUMETSAT for financial support for attending this workshop. Special thanks are due to Dr. K. Holmlund of EUMETSAT for providing METEOSAT data used in this study and for his keen interest and encouragement.

REFERENCES

Bansal, R.K. and S.R.H.Rizvi, 1993: A new approach to analysis problem. *Proc. Seminar Meteorology and National Development*, TROPMET-93.

Lorenc, A.C., 1986: Analysis methods for Numerical Weather prediction. *Quart. J. Roy. Meteor. Soc.*, **112**, 1177-1194.

Mitra A. K., A.K. Bohra and D Rajan, 1997: Daily rainfall analysis for Indian summer Monsoon. *Int. J. Climatol.*, **17**, 1083-1092.

Munmun Das Gupta, S. R. H. Rizvi and A. K. Mitra: Assimilation of ERS-2 Scatterometer winds data in the global data assimilation system operational at NCMRWF. (Communicated to Mausam).

Parrish, D.F. and J.C. Derber, 1992: The National Meteorological Center's Spectral Statistical interpolation analysis system. *Mon. Wea. Rev.*, **120**, 1747-1763.

Rizvi, S.R.H., A.K.Mitra, and R. Singh, 1992: Performance of NCMRWF global Data Assimilation System (GDAS) during Monsoon-90. Advances in Tropical Meteorology, TROPMET-92, pp. 470-490.

Rizvi, S.R.H. and D.F. Parrish, 1995: Documentation of the Spectral Statistical Interpolation (SSI) Scheme. NCMRWF, Technical Report. 1/1995.

Rizvi, S.R.H., R. K. Bansal and M. Das Gupta 1998: Recent developments in the analysis scheme operational at NCMRWF. *Proc. INROMET-98*.

TOWARD IMPROVED USE OF GOES SATELLITE-DERIVED WINDS AT THE NCEP ENVIRONMENTAL MODELLING CENTER

Xiujuan Su[1], John Derber[2], Steve Lord[2], Christopher S. Velden[3]

1. General Science Corporation
2. Environmental Modelling Center**,** NCEP
3. Cooperative Institute for Meteorological Satellite Studies
1,2:EMC/NOAA, 5200 Auth Rd., Camp Springs, MD 20742 USA
3:UMCIMSS, 1225 West Dayton St., Madison, WI 53706 USA

ABSTRACT

There are two types of GOES satellite derived winds which are now used operationally at NCEP. They are cloud-drift and cloud-top water vapor winds. These winds provide valuable information for numerical model initialization over regions where conventional observations are not available. However, inaccurate wind data have the potential to degrade the quality of model forecasts. Previous experiments have shown that forecast impacts from satellite derived winds are minor. Therefore, more work needs to be done in order maximize the impacts of utilizing these winds. In order to do this, a three step approach is planned. The first step is to examine the satellite derived winds, including the quality indicators such as the recursive filter flag (RFF) developed by Cooperative Institute for Meteorological Satellite Studies (CIMSS) and the quality indicator (QI) developed by European Organization for the Exploitation of Meteorological Satellites (EUMETSAT). Some relationships which need to be studied are how QI, RFF vary in relation to differences between satellite derived winds and model winds; between satellite winds and conventional wind measurements, such as radiosondes and aircraft; and between model guess and satellite derived winds. The guess fields used in the derived satellite winds algorithm are compared with our model guess field. Winds at different heights determined by different height assignment methods, will be investigated. After this step, we hope to develop other indicators besides quality mark RFF and QI for filtering derived satellite winds into analysis system. The second step focuses on the studying the impacts of satellite derived winds on our model forecasts. The impact study experiments include the different wind inputs by different RFF, QI values and the indicators developed by our study. Some case studies on storms and jet streams are chosen for the derived satellite wind impacts. As a third step, any revealed weaknesses in our data assimilation system for derived satellite will be improved.

THE PRELIMINARY STUDY OF THE IMPACT OF QUIKSCAT/SEAWINDS OCEAN SURFACE WIND DATA TO THE JMA GLOBAL MODEL

Yoshihiko Tahara

Numerical Prediction Division, Japan Meteorological Agency
1-3-4 Otemachi, Chiyodaku, Tokyo
Japan

ABSTRACT

A new scatterometer SeaWinds was launched onboard QuikSCAT satellite in June 1999. It observes surface wind vectors over the ocean with the swath of 1800km, which is more than three times wider than that of ERS-2 scatterometer. Hence its large contribution to numerical weather prediction (NWP) is expected. Using preliminary observation data of QuikSCAT, an impact study was performed with the JMA global NWP system. The results showed large positive impact over the southern hemisphere and small positive impact over the tropics and the ocean of the northern hemisphere.

1. Introduction

A space-borne scatterometer observes wind vectors over the ocean surface, and it provides precious information to numerical weather prediction (NWP) over the ocean, where conventional observations are sparse. In addition to ERS-2 scatterometer launched by European Space Agency (ESA) in April 1995, a new scatterometer SeaWinds was launched onboard QuikSCAT satellite by National Aeronautics and Space Administration (NASA) / Jet Propulsion Laboratory (JPL) in June 1999. It is designed to observe wind vectors with an accuracy of 20 degrees in direction and 2 m/s or 10% in speed, and a horizontal resolution of 25km. These are almost the same as ERS-2 scatterometer. Meanwhile the observational swath of SeaWinds along the satellite track is 1800km, which is more than three times wider than that of ERS-2, 500km. Therefore it is expected to bring larger impacts to analysis and forecast than ERS-2.

2. Assimilation system for scatterometer

In order to assimilate scatterometer data effectively, an assimilation system for ERS-2 scatterometer shown in Figure 1 was built up. The system consists of three parts.

1) Wind retrieval ERS-2 scatterometer data are received at JMA from ESA in near real-time through the Global Telecommunication System (GTS). However the quality of the wind direction data is not acceptable for use in NWP. Therefore the scheme of wind retrieval from ERS-2 backscatter measurements, which are also included in the real-time data, was built up. The retrieval method is based on the techniques described in Stoffelen and Anderson (1995). A maximum likelihood estimator is used to transform backscatter measurements into winds. Median filter and NWP nudging techniques are used in order to remove ambiguities of wind direction data. Owing to the scheme, the accuracy of wind direction data is improved significantly.

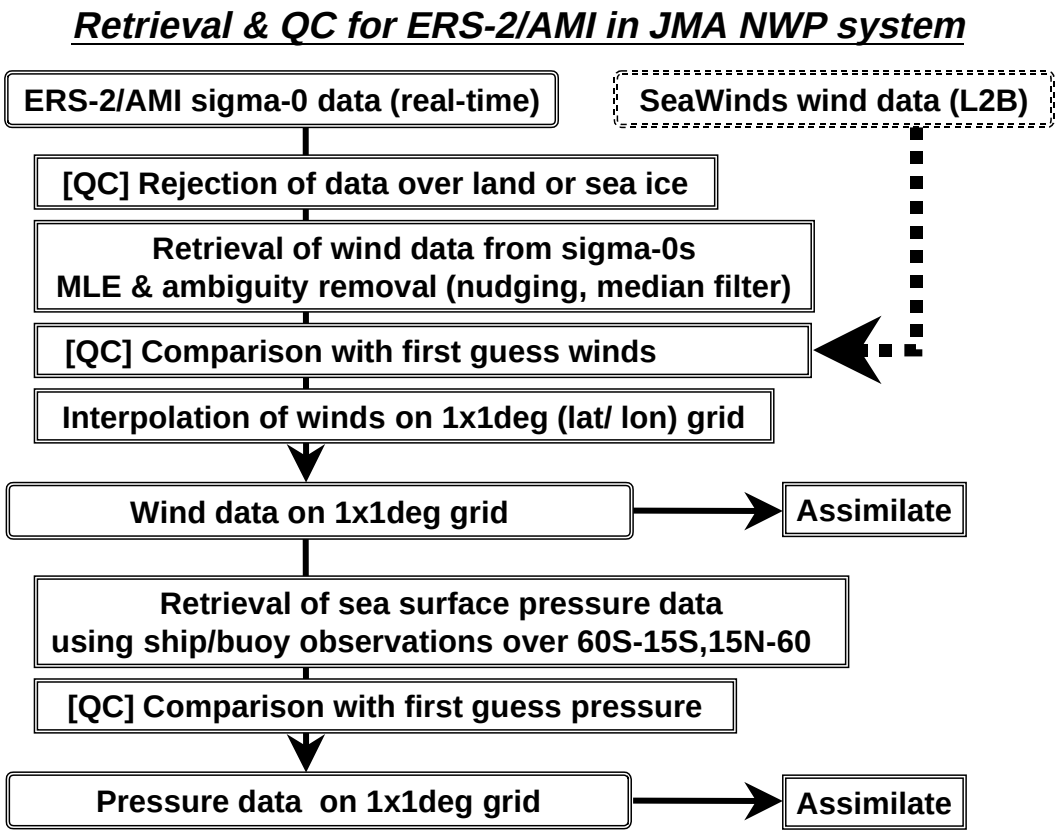

Figure 1: Wind retrieval and quality control system for ERS-2 scatterometer used in the JMA NWP system. In QuikSCAT experiment this system were used except the wind retrieval part.

2) Quality control A new quality control (QC) scheme called "group QC" is introduced in addition to conventional QC, in which observaton data are checked comparing with a first guess field individually. The conventional QC occasionally rejects correct wind data in and around severe weather system such as cyclone and front, since wind direction and speed varies sharply there and the difference between a first guess and a observation tends to be large. The observational information of these phenomena is very important for analysis. The group QC is a technique to save such important data. It consists of two steps. The first is grouping step, in which scatterometer data are divided into some groups consisting of adjacent data which have the similar wind directions and speeds. According to the grouping, the data are divided into the groups of burst error data, sporadic error data and correct data. The next is testing step, in which the data are checked group by group. Correct data, which would be rejected by conventional QC, are saved by comparing with surrounding correct data. The group QC saves a lot of correct scatterometer data in and around severe weather system successfully.

3) Surface pressure retrieval Scatterometer data represent fine structures of wind field with a high spatial density over the ocean; surface pressure patterns can be easily imagined from them. However it is not easy to represent the atmosphere states on analyzed fields through data assimilation. Because the sea surface winds reflect the phenomena at the bottom of atmosphere and complicated boundary layer physics prevents to transmit effects of the surface wind data to upper layers inside a model. In order to transfer the information of scatterometer data to analysis field effectively, we try to estimate surface pressures from surface winds

and assimilate them.

The data used for pressure retrieval are scatterometer wind data interpolated into 1x1 degree latitude and longitude mesh. The retrieval method is based on Brown (1995). The scheme consists of two steps. At first a gradient field of surface pressure over a satellite swath are calculated from dense surface wind data. To calculate a gradient field of surface pressure, the geostrophic relation is used with some modifications for an effect of surface frictions. The gradient field can be easily converted to a surface pressure field by calibration using conventional marine observations such as buoys and ships. Since the geostrophic relation is assumed, the area to calculate pressures is limited to middle latitude (60S - 15S, 15N - 60N).

Figure 2 shows the example of QuikSCAT wind and pressure data. Cyclones and anti-cyclones seen in the wind data are represented in the pressure data. Figure 3 shows the impacts of the QuikSCAT data on a sea surface wind and pressure analysis. The left of Fig 3 shows the impact of only the wind data and the right shows the impact of both the wind and pressure data. The difference of the two is apparent; pressure data can transfer the information of scatterometer data to an analysis field strongly. The similar difference can be recognized in upper atmosphere too.

By adopting the system, a positive impact was obtained by assimilating ERS-2 scatterometer data in the global model, and the operational use was started from summer 1998 at JMA.

3. Impact study for QuikSCAT data

3.1 Configuration of the experiment

An observation system experiment for QuikSCAT data was performed in order to investigate the impact of the data on analysis and forecast performance. We used 6 hourly intermittent global data assimilation system, which is the same as the operational one. The forecast model was a reduced version (T63L30) of the operational global spectral model (T213L30). The analysis scheme was three dimensional multivariate optimum interpolation. Data assimilation was started from 00UTC August 1 1999 and continued to 12UTC August 31. 8days forecasts started from 12UTC analyses have been carried out for all experimental assimilations from August 6 to August 31. Two experiments were conducted, Control run and Test run. The observation data used in Control run were conventional data, NOAA14 data, winds obtained tracking cloud and water vapor images observed by geostationary satellites and moisture bogus data statistically retrieved from black body temperature and cloud amount data observed by GMS-5. In addition to these data, QuikSCAT data were used in Test run. The assimilation system for QuikSCAT data is almost the same as that for ERS-2 scatterometer, which is used in the operational system excepted that the wind retrieval scheme was not used (Fig 1).

3.2 QuikSCAT preliminary data

QuikSCAT data used in the experiment were the preliminary data produced by JPL for the purpose of calibration and validation. The official distribution of the data is planned from the end of January 2000. Because of the design of SeaWinds wind observing method, the quality of wind data near the far swath and nadir (along the ground track of the satellite) was considered to be worse compared with the data between the middle of far swath and nadir, where QuikSCAT could observe winds skillfully and the area is called sweet spot. The decline of the quality in far swath and nadir was recognized for the preliminary observation data in

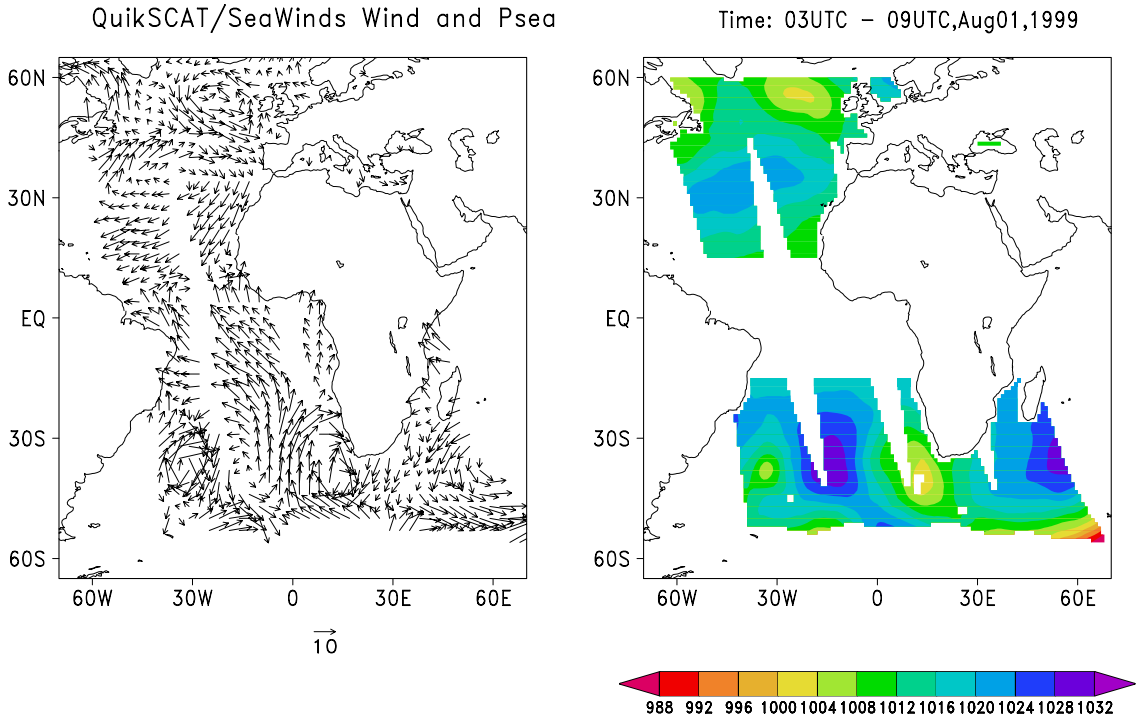

Figure 2: The left figure shows the wind data observed by QuikSCAT/SeaWinds. The right figure shows the surface pressure retrieved from the wind data in the left figure. The unit of wind vector length is m/s and that of pressure is hPa.

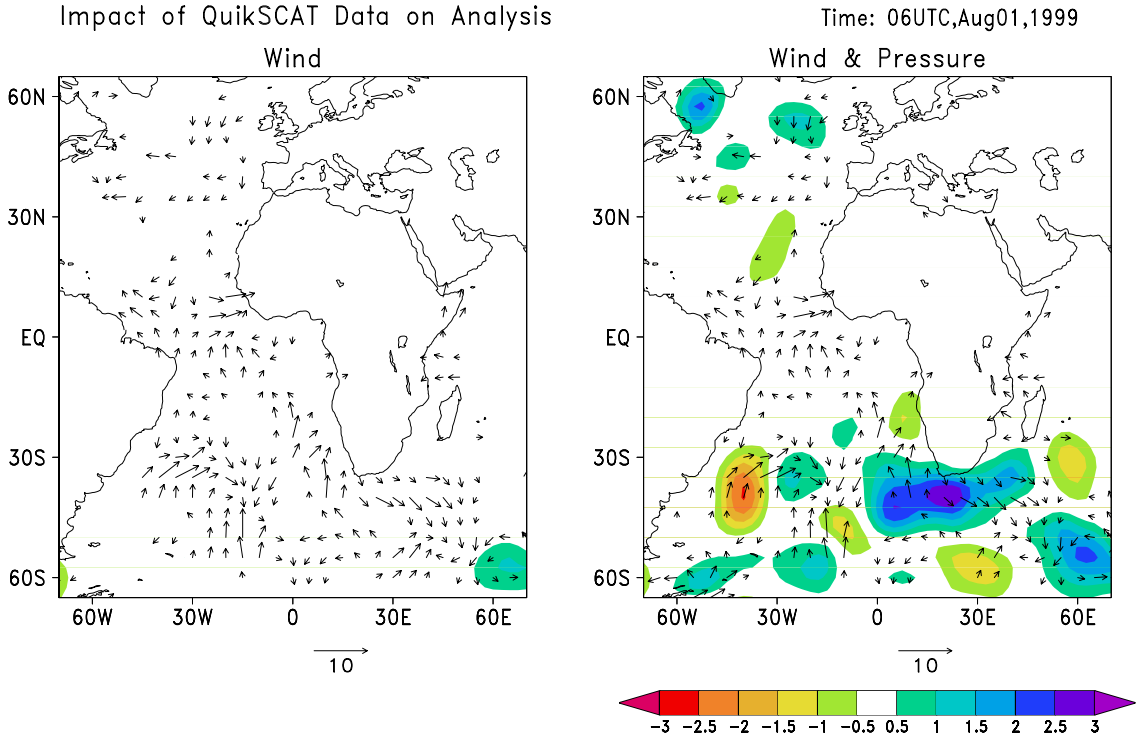

Figure 3: The figures show the impacts on analyses carried by the QuikSCAT data drawn in Figure 2, an analysis using QuikSCAT data minus an analysis without the data. The left figure shows the impact by only the wind data, and the right shows the impact by using both the wind and pressure data. The unit of wind vector length is m/s and that of pressure is hPa.

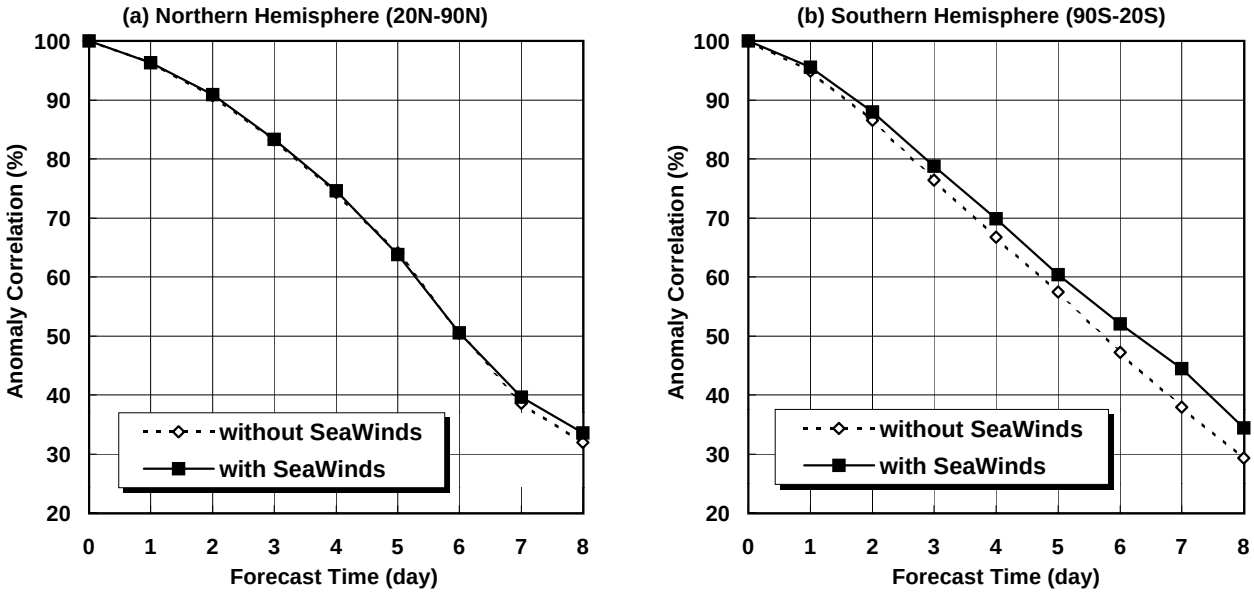

Figure 4: Mean anomaly correlation of forecasted sea surface pressure against initialized analysis over (a) the northern hemisphere (20N-90N) and (b) the southern hemisphere (20S-90S). The forecasts are carried out at every 12UTC from August 6th to 31st 1999. Dash line indicates Control run and solid line indicates Test run.

SeaWinds/QuikSCAT calibration workshop held in November 1999. Moreover other problems were found such as biases contained in backscatter measurements, rain contamination and poor observation outside 3 to 30 m/s range. However it was also recognized that the data in sweet spot had the good accuracy as expected before the launch. In the experiment these problems were ignored and whole data were treated as having the same quality.

A comparison between QuikSCAT wind data interpolated into 1x1 degree mesh and first guess wind fields resulted in 21.5 degree RMS error in wind direction and 1.92 m/s RMS error and +0.18 m/s mean error in wind speed. It means that the QuikSCAT data have good enough accuracy to be used in NWP, even if they are preliminary data.

A comparison between surface pressure data retrieved from QuikSCAT winds and first guess pressure fields resulted in 2.7 hPa RMS error and +0.28 hPa mean error. The quality check schemes used in the data assimilation system detected erroneous data of 12% in the pressure data. However 88% of the data were recognized to have a good quality, and a comparison between the data having passed the quality checks and first guess fields showed that RMS error was decreased to 1.5 hPa and mean error to 0.0 hPa.

3.3 Impacts to forecasts

Obvious positive impact to model's performance is obtained over the southern hemisphere by using QuikSCAT data. Figure 4 (b) shows mean anomaly correlations of forecasted sea surface pressure field over the southern hemisphere extra tropics (20S - 90S). The anomaly correlation is a score that evaluates agreement of patterns between analyzed field and forecasted field. The higher value indicates better forecast performance, the value of 100% means the forecast is perfect and that over 60% means useful. The figure shows that the score drops to 60% at 5.1 forecast day for Test run, but 4.7 forecast day for Control run. It means that

period of useful forecasts is extended by 0.4 day by using the QuikSCAT data. Figure 4 (a) shows the same as Fig 4 (b) but over the northern hemisphere extra tropics (20N - 60N). The similar results for forecasted 500hPa geopotential height field can be seen over both the southern and northern hemisphere too. It means that QuikSCAT surface wind data improve the NWP performance of not only surface field but also upper atmosphere. A small positive impact is also seen on 850 hPa temperature field over the tropics (20S - 20N, the figure is not shown).

Figure 5 (a) shows the difference map of the mean RMS errors of forecasted sea surface pressure fields between Test run and Control run. Forecast time is 6 day. The area in red or orange indicates an area where the forecast error of Test run is smaller than that of Control run. And the area in blue or green indicates the forecasts of Control run are better than the Test run. The red or orange area can be seen wider than the blue or green area over the middle latitude of the southern hemisphere, where QuikSCAT data improve the analysis and forecast skill significantly. Fig 5 (b) shows the same map as Fig 5 (a) but for surface wind vector fields. A similar impact by QuikSCAT data can be recognized over the southern hemisphere. Moreover a small but evident positive impact can be seen over the northern Pacific and Atlantic ocean.

4. Conclusion

The impact study for QuikSCAT data using the JMA global NWP system was performed. The assimilation method for QuikSCAT data was almost the same as operational one used for ERS-2 scatterometer except that wind retrieval scheme was not applied. Throughout the experiment, QuikSCAT data were recognized to have a good enough quality to be used for NWP, even if they were preliminary data. Pressure data retrieval from QuikSCAT winds was successfully performed, and 88% of the data were assimilated. The evident positive impacts on forecasts were recognized over the southern hemisphere and small positive impacts over the northern hemisphere and the tropics.

The official distribution of QuikSCAT data is planned from early 2000. The data will be calibrated according to the results of discussion in the QuikSCAT/SeaWinds workshop held in November 1999. We plan to receive the QuikSCAT real-time data, and we will continuously investigate the quality of QuikSCAT/SeaWinds data and their impact on NWP.

REFERENCES

Anderson, D., A. Hollingsworth, S. Uppala and P. Woiceshyn, 1991: A Study of the use of scatterometer data in the European Centre for Medium-Range Weather Forecasts operational analysis-forecast model. 2:Data Impact, *J. Geophys. Res.*, **96**, 2635-2648.

Atlas, R., P.M. Woiceshyn, S. Peteherych and M.G. Wurtele, 1982: Analysis of satellite scatterometer data and its impact on weather forecasting, *Oceans*, **82**, 415-420.

Atlas, R. and S.C. Bloom, 1989: Global surface wind vectors resulting from the assimilation of satellite wind speed data in atmospheric general circulation models, *Oceans '89 Proceedings*, 160-265.

Atlas, R., 1992: Impact of Satellite Wind Data on Ocean Surface Analysis and Numerical Weather Prediction, *ADEOS/NSCAT Science Team Meeting*, Nov. 12-14.

Brown, R. A., 1995: Revelations of surface Pressure fields from ERS-1, *Proceedings of 1995 ADEOS/ NSCAT Science Working Team Meeting*, NASDA, 214-220.

(a)

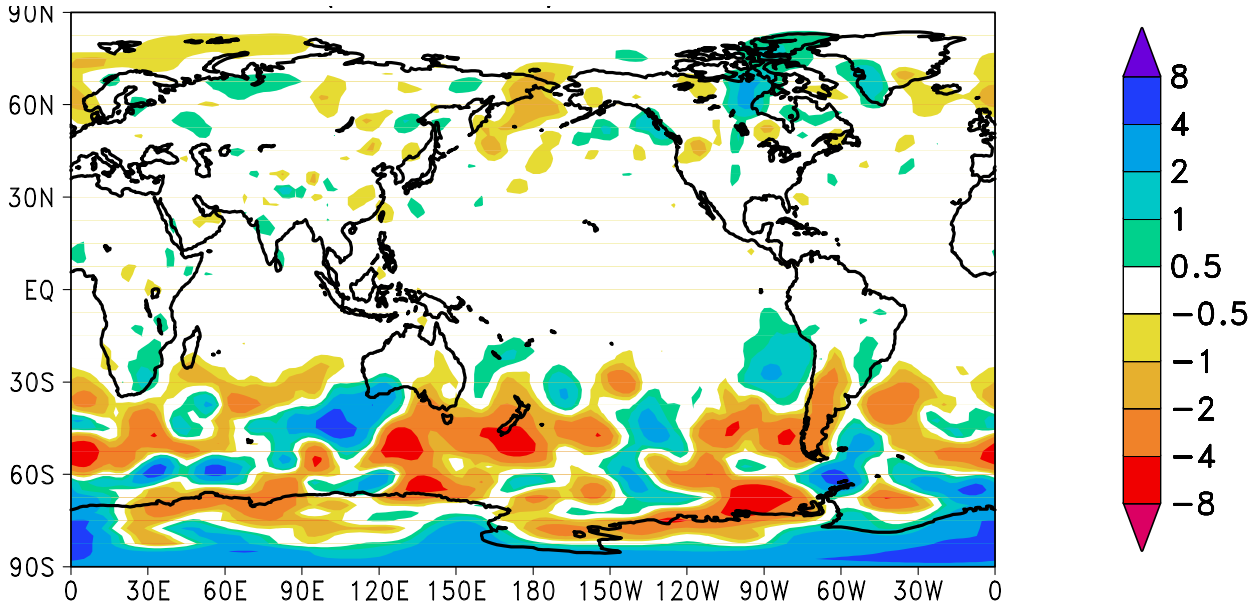

(b)

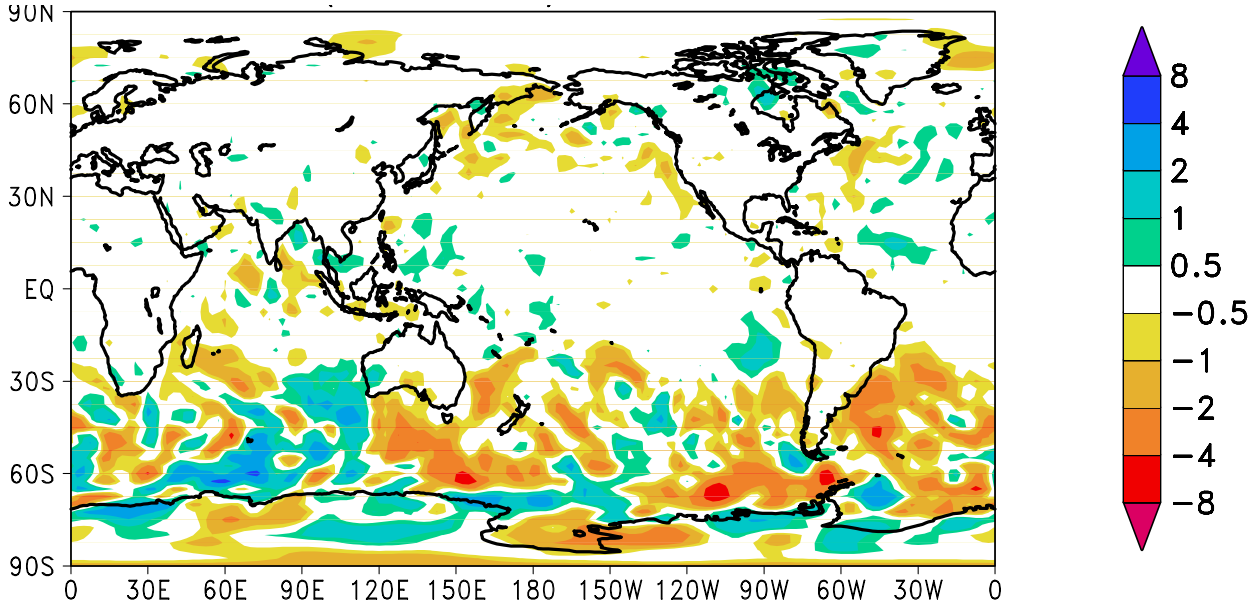

Figure 5: These figures show the differences of the mean RMS errors of 6 day forecasts between Test run and Control run. An area shaded in orange or red represents that the forecast error of Test run is smaller than that of Control run, and an area shaded in green or blue represents the forecast error of Test run is larger. Figure (a) shows a comparison over sea surface pressure field and figure (b) shows over surface wind field. The unit of pressure is hPa and that of wind speed is m/s.

Chi, C.Y. and F.K. Li, 1988: A Comparative Study of Several Wind Estimation Algorithms for Space Borne Scatterometers, *IEEE Trans. Geosci. Remote Sensing*, **26**, 115-121.

Hoffman, R.N., 1993: A preliminary study of the impact of the ERS-1 C-band scatterometer wind data on the ECMWF global data assimilation system, *J. Geophys Res.*, **98**, 10233-10244.

Hsu, C.S., M.G. Wurtele, G.F. cunningham and P.M. Woiceshyn, 1997: Construction of Marine Surface Pressure Fields from Scatterometer Winds Alone, *J. Appl. Meteor.*, **36**, 1249-1261.

Long, D.G., and some members, 1996: Current Progress in Ku-Band Model Functions, *NSCAT Science Working Team Geophysical Model Function Subcommittee.*

Nomura, A., 1992: Impact of SSM/I wind data on a Numerical Weather Prediction model, *ADEOS/ NSCAT Science Team Meeting*, Nov. 12-14.

Shaffer, S.J., R.S. Dunbar, S.V. Hsiao and D.G. Long, 1991: A Median-Filter-Based Ambiguity Removal Algorithm For NSCAT, *IEEE Trans. Geosci. Remote Sensing*, **29**, Jan, 167-174.

Stoffelen, A. and D. Anderson, 1995: The ECMWF Contribution to the Characterization, Interpretation, Calibration and Validation of ERS-1 Scatterometer Backscatter Measurements and Winds, and their use in Numerical Weather Prediction Models, *ESA Contract Report*, ESA.

Stoffelen, A. and D. Anderson, 1997: Ambiguity removal and assimilation of scatterometer data, *Q.J.R. Meteor. Soc.*, **123**, 491-518.

Undén, 1997: Recent observing system experiments at ECMWF, *Proceedings of CGC/WMO Workshop*, 7-9 Apr., 13-26.

THE USE OF THE MPEF QUALITY INDICATOR

Graeme Kelly, Michael Rohn,
European Centre for Medium Range Weather Forecasts
Shinfield Park, Reading, RG2 9AX, UK

ABSTRACT

Enhanced Meteosat wind data sets are provided every 90 minutes together with the Quality Indicator (QI) derived during the quality control of the Meteorological Product Extraction Facility (MPEF) at EUMETSAT. All three channel Cloud Motion Winds (CMW) and clear sky Water Vapour Motion Winds (WVMW) have been passively monitored by comparison to the ECMWF background field. The evaluation of the relationship between the MPEF QI and the background departures indicate possible benefits to be gained from the use of the QI within the observation screening of the assimilation system. The atmospheric motion winds (AMW) with 90 minute time sampling have been implemented into the ECMWF assimilation system. The MPEF quality indicator is used as a selection criterion within the screening. The applied thresholds are restricted in the Tropics compared to the extratropical regions where the threshold for high level winds has been relaxed below the Automatic Quality Control (AQC) at MPEF. The overall effect is an increase of active Meteosat winds by a factor of two.

1. Introduction

One step in the extraction of AMW observations is the quality control prior to the transmission of the data. Traditionally this includes a manual quality check based on a subjective comparison of the wind vector with the actual image triplet used in the retrieval. Following the increase in temporal and spatial resolution the task of a manual control became impossible. Therefore, the producers are working on the development of quality estimates for individual wind observations simultaneously to the attempts to increase the spatial and temporal coverage (Holmlund, 1998, Holmlund and Velden, 1998). The binary encoded experimental data stream from EUMETSAT contains all observations that pass a very weak quality threshold of QI>0.3 together with the final Quality Indicator (QI) assigned during the MPEF quality control.

2. Monitoring of the MPEF quality indicator

The MPEF QI value is traditionally used as a criterion by the Automatic Quality Control (AQC) to decide about the transmission of a particular datum. The current AQC set-up includes only observations which exceed a threshold of QI=0.8 in the 6 hourly CMW data set except for CMW observations from the visible imagery at high resolution (HRES VIS) where a threshold of QI=0.65 is applied. A concise description of the MPEF quality control scheme and the derivation of the QI value can be found in (Holmlund, 1998). The basic tests together with the currently used parameters are summarised in the appendix. The quality of the BUFR encoded MPEF winds have been routinely compared against the ECMWF background wind field. The background field is a 6 hour forecast of wind and pressure with 1.5° horizontal resolution at 50 vertical model levels. In particular the relation between the background departures and the assigned Quality Indicator (QI) have been monitored in order to assess the information content of the QI values towards a possible use within an assimilation system. Following the monitoring practice at MPEF the rms background departures versus assigned quality estimate are studied separately for different channels (IR, VIS low and high resolution, WV cloud and clear sky), in different geographical regions, and tropospheric layers. Due to the known problem of negative speed bias in high wind speed situations the mean wind speed and bias are

included in this monitoring. The relation between QI value and background departures for high level (p < 400 hPa) IR winds is shown in Figure 1.

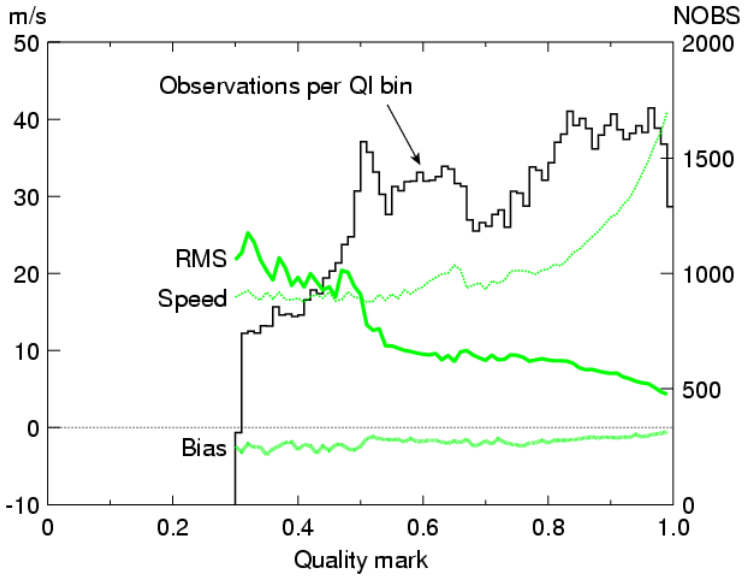

Figure 1. Monitoring of high level(p<400hPa) IR winds from Meteosat-7

Table 1. MPEF automatic quality control (AQC) thresholds.

channel	QI threshold
IR	QI>0.80
LRES VIS	
WVcloud	
HRES VIS	QI>0.65

The statistics have been computed for a period of one week from 1-7 February 1999. The departures are collected in QI bins of 0.01. The rms departures are shown by the solid line, the speed bias in dotted style, and the background wind speed as dashed line. The histogram shows the number of observations in each QI bin. All cloud tracked winds as well as the motion vectors from clear sky features within WV images have been assessed separately for the northern (lat > 20°) and southern (lat < -20°) extra tropical regions, and the Tropics (-20 °< lat < 20°). Additionally three tropospheric layers are distinguished (p > 700 hPa, 700 hPa > p > 400 hPa, 400 hPa > p). Generally, the background statistic shows decreasing rms departures and bias with an increasing quality estimate (QI). Furthermore, the mean wind speed in each quality interval is also increasing with the quality indicator. This is important in respect to the underestimation of high wind speeds by cloud tracked winds. Within the ECMWF assimilation system the so-called asymmetric check is applied as part of the first guess check of atmospheric motion vectors in order to prevent a slowing down of jet streams (Järvinen and Undén, 1997). The observed relation between quality indicator and background departures indicates the potential of the QI value as an additional parameter within the observation screening of an NWP assimilation system.

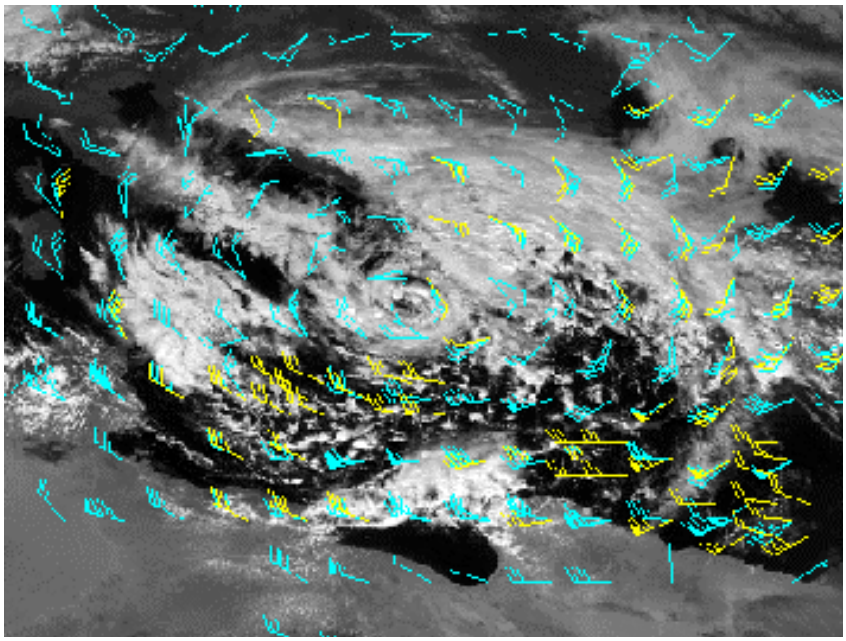

Figure 2. Atmospheric motion vector from Meteosat-7 on 19 March 1999

At 12 UTC.Observations at all levels are included.The observations which passed the automatic quality are marked in yellow. Remaining observations with QI values below the confidence threshold are plotted in blue.

3. Potential of enhanced Satellite Winds

The new data set generally provides more information due to increased spatial and temporal resolution as well as including the winds of poorer quality below the automatic quality control threshold. By the aid of a case study we illustrate the potential of the extended observation set. Figure 2 shows the visible image from Meteosat-7 on March 19, 1999 at 11:30 UTC. The vectors shown are observations between 9:00 and 15:00 UTC which passed the Automatic Quality Control (AQC) (yellow) together with the remaining observations with QI values below the AQC thresholds in Table 1. In case several observations from one imaging channel are derived within the six hour time window only one vector is plotted per channel. Multiple observations at some locations represent data from tracking of cloud features within different imaging channels. This is in contrast to the traditional wind product. It includes only one per wind per processing segment that is identified by the highest QI value. Therefore more than one observation can be provided within the same segment by tracking of clouds at different levels. Motion vectors derived in clear sky areas of WV imagery are not included in Figure 2 that illustrates only the potential of cloud tracked winds. The fleet of observations over North Africa where at first glance no clouds can be identified are results from the WV channel and indicate tracking of thin cirrus at upper level. There is a good indication that the quality control rejects many observations that appear to supplement information on the vector field in a consistent way. This is especially clear in the vicinity of the low-pressure system over the Mediterranean. A few obvious outliers are also apparent which is to be expected due to the missing quality control.

4. Use of QI for screening of atmospheric motion vectors

4.1 Blacklisting

Based on the monitoring described a set of QI thresholds is derived for blacklist decisions for the three channel cloud tracked winds. Unlike the MPEF quality control scheme, the cut-off parameters are chosen separately for channel, tropospheric layer, and geographical region. The selection that was used in the assimilation experiments described later are summarised in table 2. Generally, it led to a restriction in the use of low-level IR cloud tracked winds. At mid level IR winds were activated above QI > 0.90. These winds were not used within the operational system based on the observed background departures observed in the past (Rattenborg, 1998). The threshold for high level winds has been relaxed down to QI > 0.60 in the extra tropical region while the usage for tropical winds is restricted compared to the MPEF AQC. For VIS winds the AQC decision has been used. The VIS winds at high resolution are provided three hourly together with the low resolution VIS winds every 90 minutes. The time slots of low resolution VIS data which coincide with the high resolution VIS winds are blacklisted to avoid redundancy. These decisions are applied in conjunction with the transition to 90 minute time sampling.

Table 2. Data selection according to quality estimate QI

Area	Channel	Low 700<p<=1000	Medium 400<p<=700	High p<=400
NH	IR	QI>0.85	QI>0.90	QI>0.60
lat>20°	VIS	QI>0.65		
	WVcloud		not used	QI>0.60
TR	IR	QI>0.85	QI>0.90	QI>0.85
-20°<lat<20°	VIS	QI>0.65		
	WVcloud		not used	QI>0.85
SH	IR	QI>0.85	QI>0.90	QI>0.60
lat<-20°	VIS	QI>0.65		
	WVcloud		not used	QI>0.60

The overall effect can be expected to be a large increase in the number of satellite winds being presented to the analysis. The main reasons in order of decreasing importance are:
- 90 minute time sampling
- relaxed QI threshold at high level in the extra-tropical region
- multiple observations per processing segment from different channels at identical time slots
- introduction of IR winds at medium levels.

4.2 Selection in thinning

Besides the static QI thresholds the thinning step for atmospheric motion vectors has been extended using the MPEF QI value. The selection follows the thinning scheme applied to various observation types with high spatial coverage (Järvinen and Undén, 1997). Atmospheric motion vectors are collected in boxes of dimension as generally used for all CMW observations (Table 3). The quality estimate is included as selection criterion within each thinning box. In the presence of several observations within one thinning box the observation with highest quality estimate is retained as active in the assimilation.

Table 3. Specifications of SATOB thinning.

Parameter	value	comment
horizontal box dimension	1.25 °	
vertical extent	50, 70, 100, 150, 200, 250, 300, 400, 500, 700, 850, 925, 1000 [hPa]	varying according to nearest stand ard pressure level (50-175 hPa)
selection within a box	observation closest to analysis time preferred	

4.3 Assimilation and Forecast Experiments

The experiment hereafter referred to as ECQC-90 introduces the full 90 minute sampling using the QI thresholds based on the monitoring described in Section 2 (Table 2). Two experiments were performed using the ECMWF four-dimensional assimilation system (21 October - 10 November 1998 and 6-31 May 1999). Clear sky WV winds were not used in either the operational suite or the experiments.

Table 4. Experimental set-up for tuning of QI thresholds and transition to 90 minute winds.

experiment	Control	ECQC-90	
periods		21.10 - 10.11.1998	6.5 - 31.5.1999
time sampling	6 hour	1.5 hour	
IR/WVcloud	AQC	variable (see Table 3.), AQC passed	
low/high res. VIS	AQC		
WV clear	NO		
thinning	YES	YES including QI	

Both experiments are compared to the system which was operational during the relevant time period the main difference being the extension of the vertical resolution into the stratosphere (50 level compared to 31 level). This can be expected to be of minor importance in this context due to the similar vertical resolution between the surface and 50 hPa. The operational system (Control) uses only cloud tracked winds at the synoptic times (00, 06, 12, and 18 UTC) which passed the automatic quality control at MPEF (Table 1). The main differences in the data usage are therefore the increased time sampling, the revised blacklist decisions, and the introduction of the QI value as selection criterion as outlined above.

5. Analysis Impact

The background and analysis departures of the CMW observations used are discussed first for the experiment ECQC-90 during the autumn period. The statistics includes ten assimilation cycles at 12 UTC during the period 1 to 10 November 1998. The results are confined to the area covered by both Meteosat platforms (-55°<lat<55°, -55°<lon<118°). The number of active CMW winds in the analysis has been increased by a factor of two compared to the operational analysis(table 5).

Table 5. Number of active CMW observations during 1-10 November 1998, 12:00 UTC (55° South to 55° North, 55° West to 118° East

experiment	number of active CMW data
Control	57.263
ECQC-90	116.393

Differences in the number of active observations during the second experiment in spring are summarised in table 6 for all assimilation cycles during the 26 day period.

Table 6. Number of active CMW observations during 6-31 May 1999 00, 06, 12, and 18 UTC (55° South to 55° North, 55° West to 118° East)

experiment	number of active CMW data
Control	491.453
ECQC-90	1.089.368

The rms background and analyses departures of active CMW observations have been considerably decreased at all levels. A pronounced change of the zonal component bias occurs at mid tropospheric levels where no CMW winds from Meteosat were used in the operational analysis. The mid level observations used in the operational analysis are IR winds from GOES-8 which partly cover the Meteosat area between 55° and 15° West over the Atlantic. Since CMW observations are generally blacklisted over land below 500 hPa pressure height the differences must represent a different regime over the Indian Ocean. The fit of other observations to background and analysis within the area of influence of CMW data from Meteosat has hardly changed. Small differences in the fit of PILOT observations show decreased rms departures and bias especially at upper levels The fit of active radiosonde (TEMP) observations (remains mainly unchanged. A few additional radiosonde data are activated at low and upper tropospheric levels. Some rejections occur at medium levels and in the lower stratosphere. These changes of quality control decisions are very small (~ 0.01%) and due to changes in the background field. Minute differences in the background departures indicate an improved rms fit. The different signal in the fit of SATOB winds and other wind observations indicates that the observations are influencing different areas. This agrees with the geographical distribution of the mean rms increments discussed below.

Changes in the increments of the geopotential are further used in order to assess the quality of the modifications introduced into the analysis. The increment is defined as the difference between the analysis and the 6 hour forecast for the same time. The differences of rms increments are used in order to assess the impact over the entire experimentation period. In the following we discuss the difference field of rms increments between the experiment assimilating Meteosat winds with the ECQC-90 setup and the Control using the operational Meteosat winds with 6 hour time sampling provided by the MPEF quality control. The resulting fields for the geopotential at 250 hPa are presented in Figure 3.

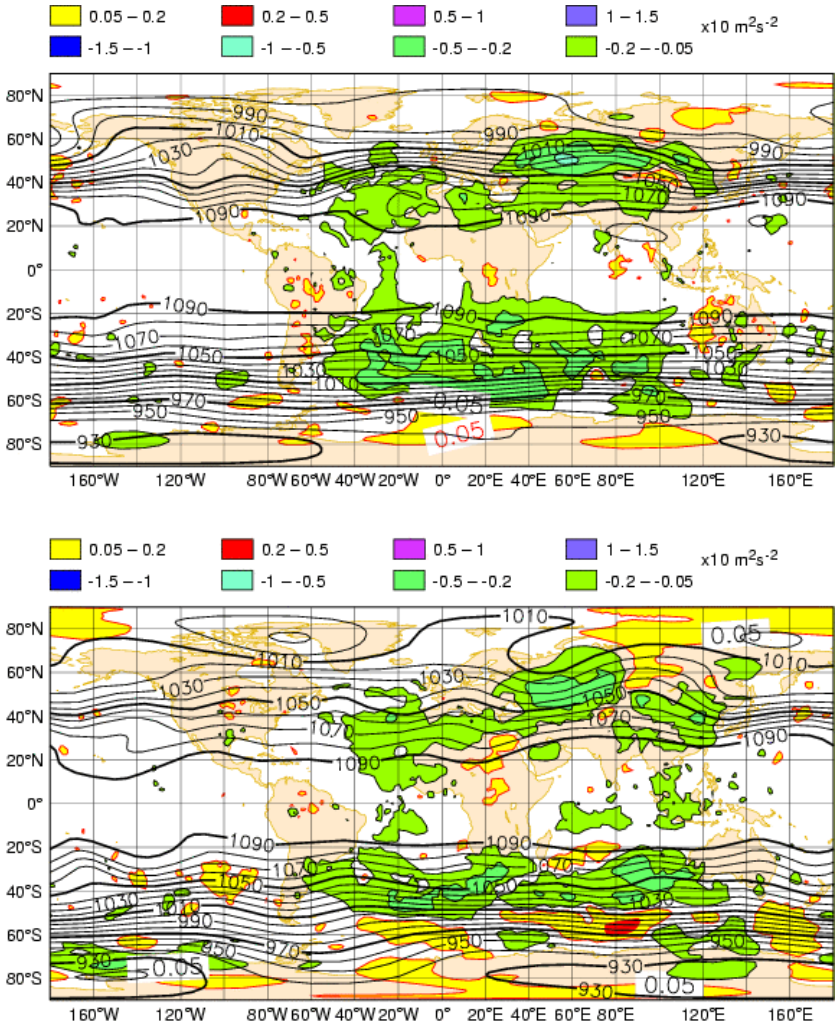

Figure 3. Differences in rms increments [x10 gpm] of geopotential at 250 hPa between experiment assimilating 90 minute winds and QI Negative values (marked in green) indicate reduced rms increment and yellow increased rms. The black contours are the mean analysed geopotential field. Top Spring experiment and bottom Winter experiment.

First of all the area of impact for Meteosat winds from both platforms is clearly visible. The observations are generally used only within a great circle of 55°. The rms increments are reduced within extended areas over the oceans especially in the Southern Hemisphere. The spring experiment (bottom panel) reveals increased rms increments right on and beyond the data boundary of 55° South. In the Northern hemisphere satellite winds are traditionally not used over land with the exception of North Africa (Tomassini *et al.*, 1997). This restriction has been relaxed with the introduction of observations from Meteosat-5 over the Indian Ocean beyond 30° East where AMW observations are active within the upper troposphere ($p < 500$ hPa). Consequently, the increment difference reveals no changes over Europe. In the area directly influenced by Meteosat winds the rms increments are reduced with a strong impact being centered over Kazakhstan. It is not intuitive that an increase in active observations by a factor two leads to reduced increments. This indicates that the changes in the observational system are consistent within itself, with the model background, and other observations within the same area (Erik Andersson, 1999, personal communication). Increased increments can indicate disagreement between satellite winds themselves, the background, or again other observations. TOVS radiances from tropospheric channels are not used over land in neither of both experiments. Remaining alternative information sources over Asia are therefore aircraft and sonde data. The strongest reduction of mean increments coincides with a data poor area over Kazakhstan. The differences in the rms increments at 850 hPa (not shown) reveal reductions only in the Southern Hemisphere coinciding with the impact on the 250 hPa field. The absence of significant impact in the Northern

Hemisphere is consistent with the fact that AMW data is generally not used over land below a pressure height of 500 hPa. The large areas of reduced increments indicate that the analysis has been improved towards a system that agrees with itself in respect to background and observational information. It should be noted that the relaxed QI threshold (QI > 0.6) for upper level observations (p < 400hPa) within the extratropical areas in the first place presents many observations with increased background departures to the analysis. The four dimensional assimilation appears to make good use of the 90 minute AMW data. An interaction between the first guess check, the variational quality control and the screening decisions dependent on the QI value also contributes to this positive result.

6. Forecast Impact

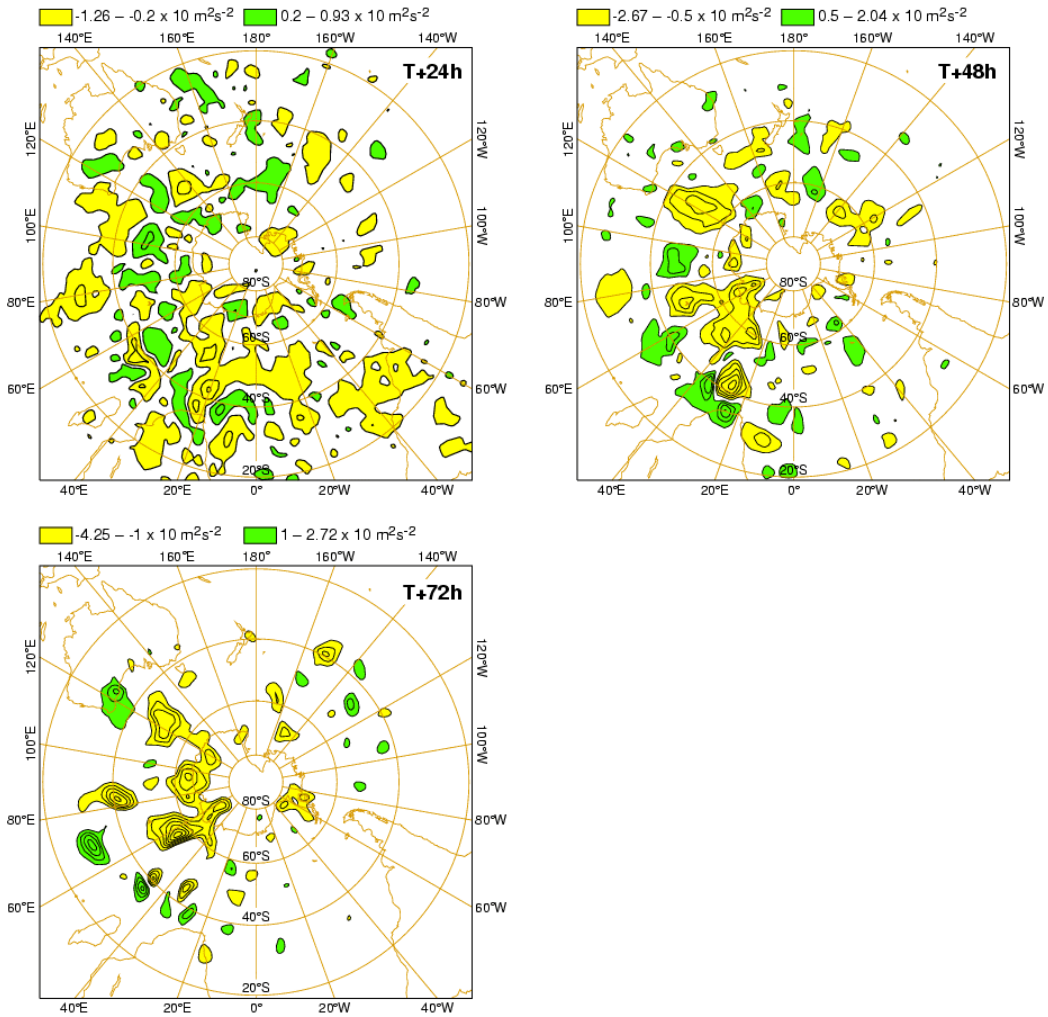

Figure 4 Differences in rms 250 hPa forecast error 21.10-7.11.1998,top left t+24h, top right t+48h and bottom t+73h. Yellow indicates decreased forecast error and green increased forecast error.

The assessment of the development of short term forecast errors between 24 and 72 hours shows the main signal in the Southern Hemisphere. Figure 4 contains the rms errors difference between the experiment (ECQC-90) during Autumn (21.10-10.11.1998) and the operational forecast of the 250 hPa geopotential. Yellow shading marks negative values and improved forecast. Green shading indicates increased rms forecast errors. The 24 hour forecast (top panel) reveals extended areas of reduced forecast errors. During the next two step (middle: 48 hour, bottom: 72 hour) the main contribution appears to concentrate in the South Indian Ocean. The Spring experiment shows similar patterns.

7. Summary

The BUFR encoded winds from both Meteosat platforms have been monitored including the MPEF QI quality estimates for use within a NWP system. The QI value appears to be capable of marking the quality regarding rms wind vector error, speed bias, and the observed wind speed. This provides good evidence to include the QI value as an additional criterion in the observation screening. A set of refined QI thresholds has been derived from the monitoring. The QI value of active observations is further used as a selection criterion within the thinning step for AMW data. This scheme is applied to Meteosat winds with 90 minute time sampling. The overall effect in the analysis is an increase in the number of active CMW data by a factor two. The two main reasons are the increased time sampling and a relaxed QI threshold at high level in the extra-tropical regions. Small contributions arise from multiple observations per processing segment from different channels at identical time slots and the less restrictive use of IR winds at medium levels. The fit of CMW data to background and analysis has been improved. The fit of other observations remains mainly unchanged. The rms increment for geopotential at 850 hPa and 250 hPa are generally reduced in extended areas over the oceans, North Africa and Asia. This indicates an improved analysis in terms of the consistency between the active Meteosat wind data, the background, and other available observations. The four dimensional variational assimilation system together with screening decisions depending on the MPEF Quality Indicator makes good use of the increased time sampling of AMW data.

ACKNOWLEDGEMENTS

This work was only possible through support from others in numerous technical and scientific issues. Thanks to all staff and consultants in both Operations and Research Departments at ECMWF. We would like to thank also Simon Elliott, Ken Holmlund, and Mikael Rattenborg at EUMETSAT for their strong support on the wind extraction side.

REFERENCES

Holmlund, K., 1998: The Utilization of Statistical Properties of Satellite-Derived Atmopheric Motion Vectors to Derive Quality Indicators, *Wea. Forecasting*, Vol. 13, No.4, 1093-1104.

Holmlund, K. and C. Velden, 1998: Objective Determination of the Reliability of Satellite- Derived Atmospheric Motion Vectors. *Proc. Fourth International Winds Workshop*, 20-23 October 1998, Saanenmoeser, Switzerland, publ. EUMETSAT, EUM P 24, 215-224.

Holmlund, K., C. Velden, and M. Rohn, 1999; Enhanced Automated Quality Control Applied to High-Density GOES Winds Derived During the North Pacific Experiment (NORPEX-98), *submitted to Monthly Weather Review*, October 1999.

Järvinen, H and P. Undén, 1997: Observation screening and back ground quality control in the ECMWF 3D-Var data assimilation system, ECMWF Technical Memorandum No. 236, 33 pp.

Rattenborg, M., 1998: Status and development of operational Meteosat wind products. *Proc. Fourth International Winds Workshop*, 20-23 October 1998, Saanenmoeser, Switzerland, publ. EUMETSAT, EUM P 24, 49-59.

Tomassini, M., G. Kelly, and R.W. Saunders, 1997: Use and impact of satellite atmospheric motion winds on ECMWF analyses and forecasts. EMWF, *EUMETSAT/ECMWF Fellowship Programme*, Research Report No. 6.

SESSION IV

NEW RETRIEVAL SYSTEMS

Chairperson: R.C. Bhatia

EXPLORATORY SATELLITE-DERIVED WINDS RESEARCH AT CIMSS

Christopher S. Velden

University Of Wisconsin – Cooperative Institute for Meteorological Satellite Studies
1225 West Dayton St., Madison, Wisconsin 53706 USA

ABSTRACT

Several advances in geostationary satellite-derived winds processing and assimilation are being explored at the Cooperative Institute for Meteorological Satellite Studies (CIMSS). This paper will focus on: 1) The study of winds derived from rapid scan imaging, 2) The use of the GOES short-wave IR channel near 3.9 microns for night-time low level cloud tracking improvements, and 3) Characterization of clear-sky water vapor winds for improved assimilation into objective analyses and NWP. Each of these exploratory studies will be briefly examined. Several other collaborative efforts are included throughout the abstract volume.

1. Winds from rapid scan imagery

Rapid scan imagery from GOES has been employed in operational forecasting for quite some time. The value of more frequent imaging is evidenced by the inclusion of a 15-minute update cycle over the CONUS sector in the current GOES schedule, and by the multitude of special NWS operational requests for more frequent sampling at 7.5 minute intervals (RISOP). Forecasters recognize the additional detail that can be captured from RISOP in events associated with rapidly changing cloud structures. On occasion, the research community has called special super rapid scan operations (SRSO). These SRSO events allow limited area coverage of one-minute interval sampling over meteorological events of interest.

1.1 GOES-10 Science checkout

Immediately after the launch of GOES-10, the satellite was put into a science test mode for almost a one-month period (March 16 – April 12, 1998). During this time, continuous 5 minute sampling over the CONUS domain was achieved in all available spectral bands.
These rapid scan data sets are used to test the impact of more frequent sampling on the UW-CIMSS/NESDIS wind-tracking algorithm (Velden et al. 1998).

Winds were derived over the central US from GOES-10 full-resolution water vapor (WV), infrared window (IR) and visible (VIS) images. Three images were employed in the displacement derivations. For our evaluation, the image spacing was varied at 5, 10, 15, and 30-minute intervals, with the shorter intervals nested inside the longer loops for the best inter-comparison. Currently, 30-minute intervals are used operationally.

Table 1 shows the vector quantities (unedited and objectively edited) derived using the different imaging intervals. There is a notable increase in the number of vectors in the VIS and IR channels (factor of two) when more frequent imaging is employed. The percentage of vectors objectively edited is also dramatically reduced, which indicates the increased quantities are generally coherent (in Table 1, EDITED = after editing). Little impact is seen with the WV channel. It should be noted that these statistics consider clear-

sky WV vectors only (WV-tracked cirrus tracers are not included). This indicates the current operational 30-min. processing interval for the WV winds may be satisfactory.

Table 1. Vector quantity versus imaging interval for three spectral bands from GOES-10 for a limited area over the central US during March/April 1998.

Band	Interval	Number of Winds RAW	EDITED
VIS	30 minutes	8915	4187
	15 minutes	10867	5392
	10 minutes	14325	7437
	5 minutes	20378	12726
IR	30 minutes	6973	3412
	15 minutes	11238	5880
	10 minutes	12642	6428
	5 minutes	12990	6009
WV (clear)	30 minutes	7281	2640
	15 minutes	6958	2631
	10 minutes	6312	2348
	5 minutes	6251	1957

Table 2. Statistical evaluation of GOES-10 VIS winds (below 600mb only) versus collocated rawinsondes and AVN model first guess, as a function of image processing interval. BIAS and RMSE are in m/sec.

	GOES-10 *VIS* SAT	GUESS
30 minutes		
BIAS	-1.21	-0.96
RMSE	5.92	4.01
Match Sample	662	
15 minutes		
BIAS	-0.67	-0.62
RMSE	5.82	3.97
Match Sample	782	
10 minutes		
BIAS	-0.71	-0.69
RMSE	6.02	4.59
Match Sample	1293	
5 minutes		
BIAS	-0.13	-0.85
RMSE	6.16	5.36
Match Sample	1963	

Statistical analyses of the wind sets (after objective editing) using rawinsonde verification are shown in Tables 2-4. This verification illustrates that the optimum processing intervals (based on data RMSE and bias relative to co-located AVN model background first guess fields used in the processing) are 5 minutes for VIS, 10 minutes for IR and 30 minutes for clear-sky WV. While the *absolute* RMSE may not be minimized at these times, our assessment takes into account the increase in vector density, and both the bias and RMSE *relative to the first guess*, since the end goal is to improve on the model guess field. These results show that more frequent image sampling improves the vector field density and quality. The optimal tracking time interval is dependent on the spectral band.

Table 3. Statistical evaluation of GOES-10 IR winds (after objective QC) versus collocated rawinsondes and AVN model guess, as a function of image processing interval. BIAS and RMSE are in m/sec.

	GOES-10 *IR*	
	SAT	GUESS
30 minutes		
BIAS	-1.04	-0.60
RMSE	7.93	7.10
Match Sample	692	
15 minutes		
BIAS	-1.39	-0.74
RMSE	7.99	7.48
Match Sample	1232	
10 minutes		
BIAS	-1.52	-0.97
RMSE	7.64	7.41
Match Sample	1323	
5 minutes		
BIAS	-1.66	-1.08
RMSE	8.13	7.63
Match Sample	1273	

Table 4. Statistical evaluation of GOES-10 WV winds (after objective QC) versus collocated rawinsondes and AVN model guess, as a function of image processing interval. BIAS and RMSE are in m/sec.

	GOES-10 *WV*	
	SAT	GUESS
30 minutes		
BIAS	-0.12	-0.80
RMSE	8.10	7.19
Match Sample	517	
15 minutes		
BIAS	0.56	-0.91
RMSE	8.58	7.42
Match Sample	512	
10 minutes		
BIAS	0.34	-0.87
RMSE	8.99	7.47
Match Sample	481	
5 minutes		
BIAS	0.34	-0.73
RMSE	9.58	7.46
Match Sample	411	

This study provides a preliminary look at the value added by geostationary satellite rapid scan imaging on wind vector determinations. It is demonstrated that the vector quantity and quality is notably improved in the VIS and IR channels using 5 and 10 minute imaging intervals, respectively, over the currently-employed 30 minute frequency. WV derived winds in cloud-less sky are less impacted, although cirrus cloud features tracked in the WV channel should also benefit as with the IR.

Further studies are being conducted. It is hoped that rapid scan imaging can become a routine part of the geostationary satellite observing system strategies worldwide. Quantities such as atmospheric motion vectors will benefit.

1.2 Hurricane applications

Special SRSO periods have been collected during several Atlantic hurricane events. The SRSO provides nearly continuous one-minute interval sampling, and these periods usually last 2 to 6 hours. Since hurricane cloud structures are characteristically fast evolving, the effects of rapid scan imaging on resultant vector wind fields should be promising. This is being evaluated with the UW-CIMSS algorithm.

Preliminary findings on a few cases are indicating the ability to retrieve mesoscale motions is notably enhanced using 3 to 5 minute imaging (Figure 1). However, use of the full 1-minute frequency is not optimal due to horizontal resolution limitations of the image pixels, and the navigation/registration inaccuracies. Applications of these data sets extend to hurricane genesis studies, and intensity change research. The impact of these data on numerical hurricane model forecasts is being examined

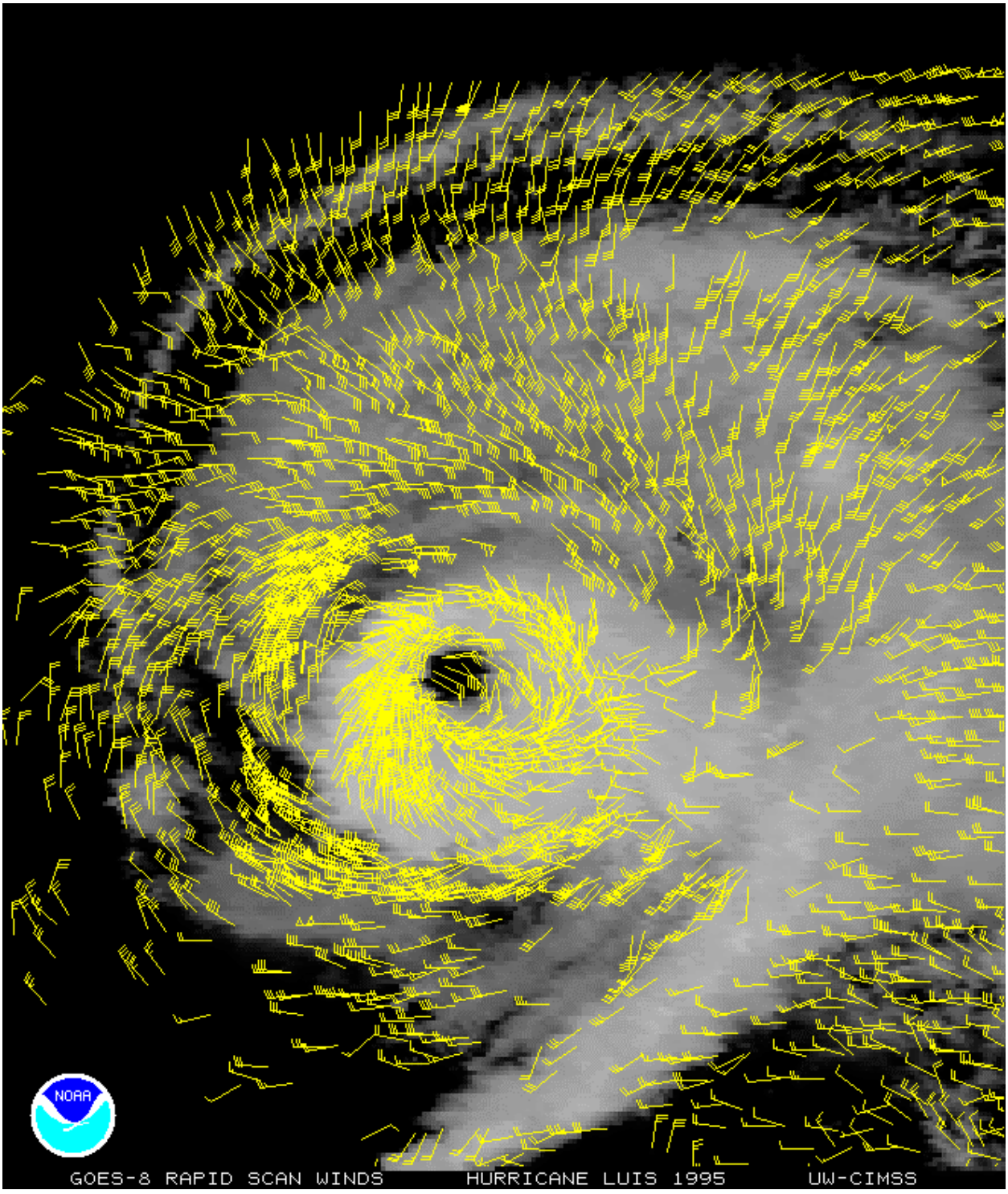

Figure 1. Satellite-derived winds from a 5-minute rapid scan sequence during Hurricane Luis of 1995. The vector field was derived from IR and VIS imagery

.

1.3 Field experiments

During the NORPEX (NORth Pacific EXperiment) and CALJET (California JETs experiment) fields programs in 1998, several SRSO periods were collected during intensive observing periods (IOPs). These experiments were conducted over the Pacific Ocean, with special observations taken from multiple aircraft. These IOPs offer the opportunity to assess the value of satellite-derived data derived over marine environments. For selected case study periods, UW-CIMSS derived wind sets from the SRSO imagery at 5-minute intervals. These data are being assessed against in-situ marine data and in numerical model impact studies. Preliminary results are suggesting the increased ability of the SRSO winds to help identify tropospheric structures and impact mesoscale model forecasts.

2. Winds from the GOES 3.9 micron channel

Traditionally, the 10.7-micron long-wave IR channel has been used to track low-level (warm) clouds at night. The relatively low resolution and resolving power of this wavelength for warm clouds have been a limiting factor on vector yield. The new generation of GOES imagers contain a channel in the short-wave IR at 3.9 microns. The response of the GOES 3.9-micron channel to warmer temperatures is greater than that at 10.7 microns. Based on the principle that the emissivity of low level water cloud at 3.9 microns is less than at 10.7 microns, differencing techniques have been developed to delineate low cloud and fog. Presumably, this will also lead to improved edge detection of low-level clouds at 3.9 microns. Therefore, this principle is being applied to nighttime tracking of low level clouds with the hopes of improving the low-level wind vector yield.

Figure 2 shows an example of low-level vector tracers achieved using both the 3.9 and 10.7-micron channels at night. All of the processing algorithm settings used to derive the winds were identical, except for the replacement of the 3.9-micron imagery in the targeting and tracing modules. Vector height assignments used the 10.7-micron channel in both cases. It is quite evident from Fig. 2 that the 3.9-micron imagery increases the low-level vector yield. Several areas, which were void of vectors using the traditional 10.7-micron imagery, now contain coherent wind information.

Since the 3.9-micron channel is susceptible to reflection of visible light, its optimal use will be limited to non-sunlit domains at a distance from the day-night terminator. This distance needs to be defined through more research and extensive processing experiments. For daily operational processing, the point in time the 3.9 micron channel becomes desirable to use over the 10.7 micron channel needs to be determined. Studies are underway at CIMSS to further evaluate this product and answer these questions.

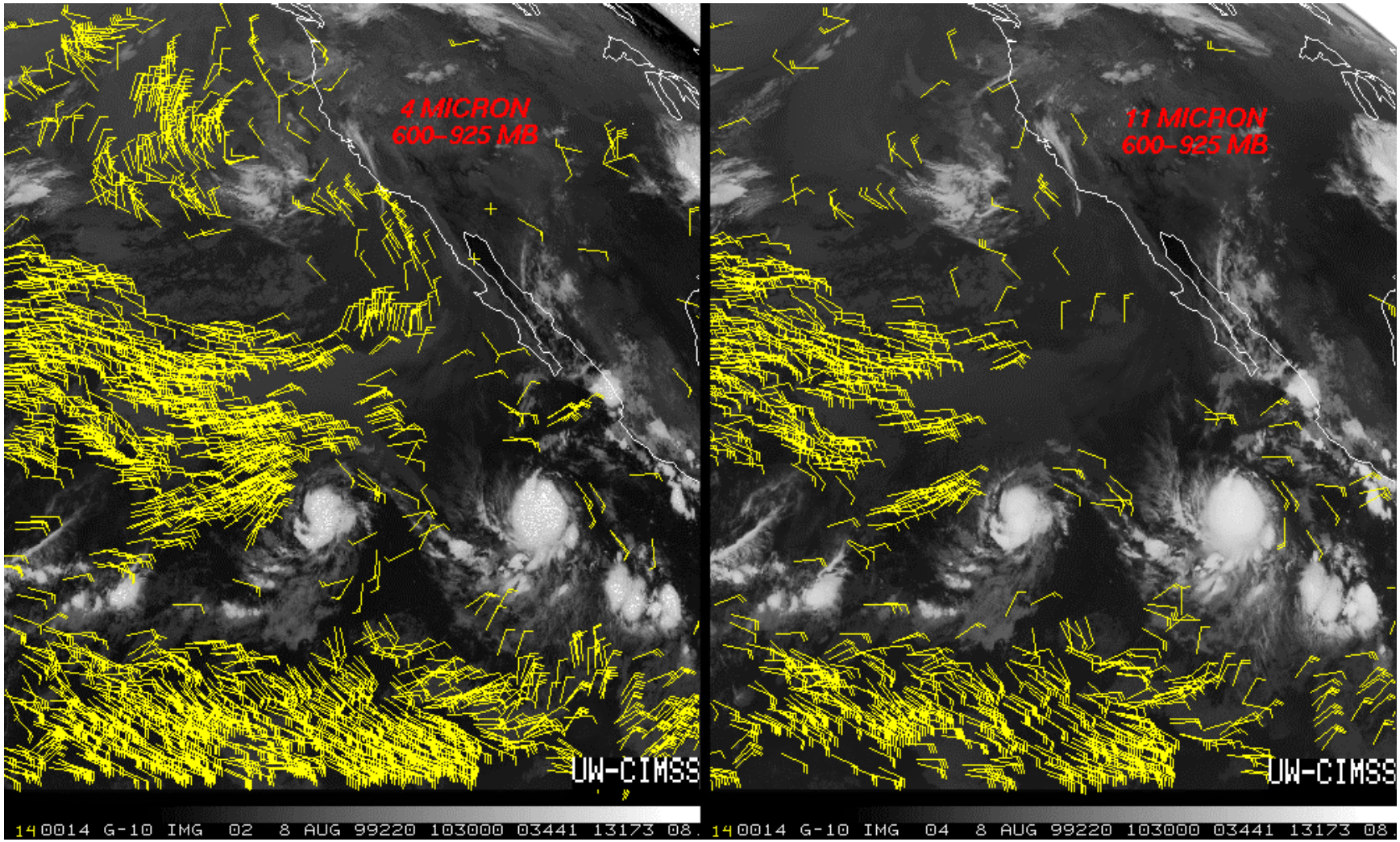

Figure 2. Example of low-level GOES-10 wind vector fields derived from 3.9 micron (left) and 10.7 micron (right) imagery. Plotted winds are those below 600mb only.

3. Characterization of clear sky water vapor winds

Since the 1980s, winds have been retrieved from geostationary satellite water vapor channels. These winds have met with mixed results in data assimilation studies. Part of the problem lies in the representativeness of the height assigned to the vector as a single level value. In reality, the features traced in the clear-sky WV channel represent layer quantities that must be treated differently than single-level reports.

In order to do this, the representativeness of the WV vectors as layer quantities must be defined. Specifically, what layer thickness do clear-sky WV vectors typically correlate with? As one approach, we subjected a large sample of clear-sky WV vectors to comparisons with collocated rawinsonde wind profiles. The level of best fit was calculated for each vector. This is defined as the minimum in the RMSE and/or normalized RMSE (NRMSE) when the vector is compared to the entire collocated rawinsonde wind profile. Figure 3 shows several levels as examples of the RMSE and NRMSE profiles that result from comparing WV winds assigned to these levels with collocated rawinsonde wind profiles over a period of about a month. Both clear and cloud WV examples are illustrated. The horizontal lines denote the selected WV height assignment levels while the arrows indicate the corresponding level of minimum values (or best vector fit). Fig. 3 suggests overall that the vector heights assigned by our current methodology match the best fit levels reasonably well, indicating the height assignments are good approximations for the tracer heights in general.

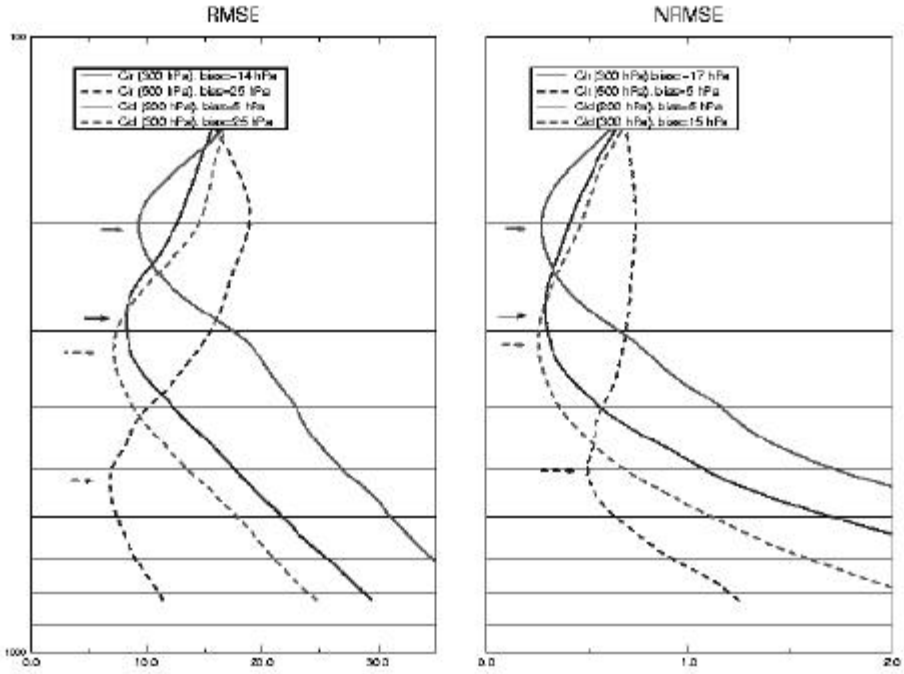

Figure 3. RMSE (left, m/s) and RMSE normalized by wind speed (NRMSE, right) for clear and cloudy WV winds against collocated total rawinsonde wind profiles. The legend indicates the selected height assignment (HA) levels while the arrows indicate the level of minimum RMSE values (LMV) for the respective profiles. Bias equals LMV minus HA.

However, the broadness of the RMSE profiles suggests the WV winds correlate with a layer rather than a single level, which agrees with theory. Therefore, a second analysis was performed in an attempt to isolate the representativeness of the WV winds as single-level approximations. An example is shown in Figure 4. In this plot the 400mb WV wind RMSE profiles are plotted against profiles from corresponding 400mb rawinsonde wind values. In other words, the 400mb rawinsonde report is compared to its own vertical profile in each case to isolate the natural correlation that exists between a measured single level report and its vertical profile of wind. This can then be compared to the WV profile. The differences will represent the layer over which the WV winds are representing motion relative to a single-level observation. Figure 4 indicates that this layer is on the order of 100mb for sharp profiles and 150mb for broad profiles. Broad (sharp) is defined as those RMSE profiles from the overall set of 400mb WV winds comparisons that were broader (sharper) than the overall mean profile. The RMSE profile gradients were also calculated and shown in the bottom panels (25 mb running average smoother applied).

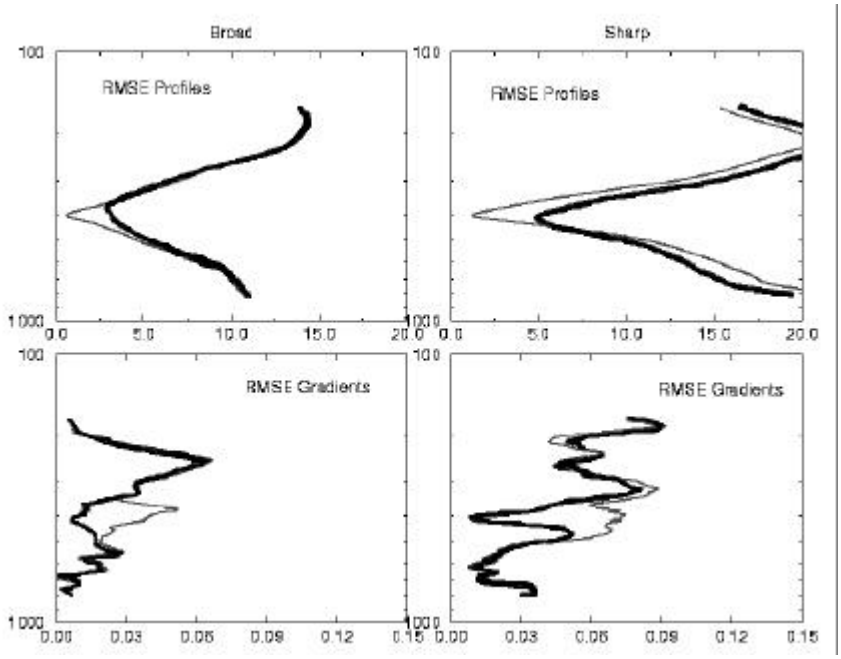

Figure 4. RMSE profiles (m/s) and gradients (m/s/2mb) for 400mb clear-sky WV winds (thick) and 400mb rawinsonde winds (thin) vs. entire collocated rawinsonde wind profiles for two categories of profile, broad and sharp. Broad (sharp) is defined as those RMSE profiles where the slopes calculated 150mb above and below 400mb were both lower (higher) than the overall mean sample profile.

The findings here suggest information on the representativeness of the WV winds as single level vector approximations. It is hoped that this type of information could aid the treatment of clear-sky WV winds in data assimilation.

REFERENCE

Velden, C.S., T.L. Olander and S. Wanzong, 1998: The impact of multispectral GOES-8 wind information on Atlantic tropical cyclone track forecasts in 1995. Part 1: Dataset methodology, description and case analysis. *Mon. Wea. Rev.*, **126**, 1202-1218.

CREATION OF A PLATFORM-INDEPENDENT VERSION OF THE UW-CIMSS GEOSTATIONARY, HIGH-DENSITY WIND DERIVATION ALGORITHM

Timothy Olander, Christopher Velden, and Connie Spinoso

University of Wisconsin - Cooperative Institute for Meteorological Satellite Studies
1225 West Dayton Street, Madison, WI 53706
USA

ABSTRACT

In response to the widespread use of geostationary satellite-derived winds in the meteorological community, a portable, platform-independent version of the UW-CIMSS winds processing algorithm has been developed. The incentive for this development derives from the desire to allow flexibility to satellite wind processing and research centers around the world to be able to locally create site-specific data sets tailored to suit their forecast, NWP or research needs using the latest advances and techniques. The prototype version of the CIMSS winds algorithm must be executed within a McIDAS environment, utilizing specific McIDAS formatted satellite data and model forecast "guess" fields. The revised algorithm will run within either McIDAS or UNIX shell environments, allowing utilization and processing of other geostationary satellite data and model guess field formats in addition to McIDAS.

This revised edition is currently being implemented and evaluated at the U.S. Naval Fleet Numerical Meteorology and Oceanography Center, and the Air Force Global Weather Center. Transfer of the new software to NOAA/NESDIS for operational testing and evaluation is also planned. The new CIMSS winds processing algorithm will soon be released and available to other interested data processing centers or research institutes. The updated algorithm includes the latest post-processing quality-control module that combines the objective-editor/recursive filter (RF) analysis developed at CIMSS with the quality indicator (QI) scheme developed by EUMETSAT. Future versions of the algorithm will continue to be advanced and supported by UW-CIMSS. Further expansion of I/O interfacing will allow easier portability to various operating systems utilizing a wide variety of input data sets. A generic X-Windows and/or IDL graphical display capability will be added to allow easier data entry, and visualization tools now supplied with the McIDAS version of the code.

1. Introduction

Wind algorithms using geostationary satellite imagery have been developed and distributed by the University of Wisconsin-Madison Cooperative Institute for Meteorological Satellite Studies (UW-CIMSS) in collaboration with NOAA/NESDIS for many years. The algorithm architecture is housed within McIDAS, a software package developed at the University of Wisconsin-Madison, and relies on McIDAS for accessing, manipulating, and displaying the required input satellite and meteorological data. While highly successful, the potential users of the algorithm are limited to sites that utilize McIDAS.

Traditionally, the latest in advanced winds processing from GOES and other geostationary satellites is demonstrated at UW-CIMSS before being transitioned to NOAA/NESDIS (Velden et al. 1998). Many other sites around the world rely on UW-CIMSS and NOAA/NESDIS to derive and distribute various

real-time satellite wind sets. This arrangement has been proven to be successful a great majority of the time, but remote users are still limited by many factors outside their control in their ability to receive data, such as internet connectivity problems. These problems could be alleviated by local production of the data sets at each site. Direct operation of the winds algorithm would also allow each site to individually tailor the algorithm to meet their respective requirements and needs. The derivation of winds by sites around the world from multiple satellite platforms using a common algorithm is also a desirable goal.

During the past few years, UW-CIMSS has received queries about obtaining the winds algorithm for use at local sites around the world. Potential applications range from research to operational support. These requests provided the impetus for developing a platform-independent version of the UW-CIMSS wind processing algorithm. This goal has been achieved during the past year and has resulted in modifications and upgrades to the prototype version.

2. Motivation

The prototype wind processing algorithm was written in the FORTRAN programming language over a period of approximately 20 years. A multitude of programmers have worked on this code both at UW-CIMSS and NOAA/NESDIS in Washington, DC. Many sections have become outdated as computer resources improved, satellite instruments/sensors evolved, and as changes were made to code logic and structure over many years (including McIDAS library functions). In order to provide a manageable algorithm for potential remote users, many sections of the code needed to be rewritten or eliminated entirely. Also, several new processing routines needed to be added to the increasingly large amount of code comprising the winds derivation package.

In addition to cleaning up the algorithm, a desire to increase compatibility with remote site-specific needs was taken into consideration during this process. Discussions with potential users indicated that a visualization package may be required with the algorithm. McIDAS users possess an interactive display platform, however many sites must either rely on visualization packages already in place or do not have such capability at the current time. Visualization tools such as X-Windows, IDL, JAVA, and TeraScan are easily compatible with or already written in the C programming language (McIDAS is also being converted to C for compatibility reasons). The C language also possesses many inherent advantages over FORTRAN, such as internal data storage (structures and global variables) and the availability of a universal C compiler, gcc, which is independent of UNIX operating systems. Therefore, the new version has been written in the C language.

By converting the algorithm into a portable, platform-independent algorithm, the user base can be increased. Remote sites around the world can have access to the latest advances in satellite wind processing. With on-site processing, users can customize wind data sets for individual needs, such as tailoring the wind set space/time resolution for targeting specific meteorological phenomena.

3. Current status

Clean-up and conversion of the primary satellite wind derivation routines have been completed. These routines comprise targeting (including height assignment procedures), vector displacement, objective Recursive Filter (RF) analysis wind editing, automatic image registration/navigation, and the newly-implemented EUMETSAT Quality Indicator (QI) routine. In addition, many ancillary routines have been converted.

Input file formats required for operation of the winds algorithm have been modified during the conversion process. Numerical model guess parameters can be ingested either directly from GRIB-

format files or from McIDAS MD-format files. Satellite imagery is still required to be in McIDAS AREA-format, due to the use of McIDAS-based internal navigation and calibration routines within the winds algorithm. Future versions will convert various formats internally, eliminating the need for the user to pre-process the image data.

Various output data file formats are available. The default output wind file format is McIDAS MD-format. Routines are provided with the new winds package to convert these files to ASCII and/or BUFR format. Also, the grid analyses from the RF editor can be output in McIDAS GRID-format, with a conversion program from GRID-format to GRIB-format being developed.

It is emphasized that all of these routines can still be utilized within the McIDAS environment for users who wish to process and display wind vectors with this system. A number of supplemental McIDAS visualization and editing routines will be converted and supplied with future wind package upgrades.

Preliminary comparisons of data sets derived by the new C version with the prototype FORTRAN version have yielded near-exact agreement. The comparisons were conducted on several UNIX platforms to check for any platform specific dependencies. Any such dependencies were eliminated, including those found within the compilation makefiles used to create the executable files. A more extensive comparison is being conducted for GOES-8 and GMS-5 wind data sets. Both versions are automated with UNIX shell scripts utilizing an identical sequence of processing commands. A sample shell script will be provided to future users as a guide for automated wind processing.

A comprehensive User's Guide is also being written. This guide will thoroughly document all procedures within the winds processing package. Flowcharts of all routines will be diagrammed in order to outline the logic comprising each procedure. All command line control keywords utilized with the procedures will be catalogued and explained, with all valid options and default values listed for each keyword. Numerous examples and current operational settings will be presented for clarity.

4. Integration of EUMETSAT Quality Indicator (QI)

In an effort to further improve the objective wind vector editing procedure, the EUMETSAT Quality Indicator procedure (Holmlund et al. 2000) has been added prior to the RF analysis routine (Velden et al. 1998). In effect, the QI acts as a pre-filter of erroneous vectors. Model forecast impact studies have documented the positive influence of the combined QI/RF procedures (Holmlund et al. 2000). Initial testing of the combined approach at UW-CIMSS is also yielding positive results. The most important issue regarding use of the QI algorithm as a pre-filter is in setting the threshold. It has been found that the QI behaves differently for each geostationary satellite. A precise definition of these properties is necessary for optimal utilization of the QI/RF for numerical modeling and research applications. Therefore, a thorough statistical analysis using rawinsonde verification is underway.

Preliminary results of this study are shown in Figure 1. Normalized root mean square (NRMS) errors for different QI value ranges are displayed for wind vectors derived using GMS-5 and GOES-10 data, as verified against collocated rawinsonde observations. Fig. 1 displays the NRMS errors for the QI-only stage, and for the QI/RF combination. A significant NRMS error reduction is achieved for each satellite after the QI/RF analysis has been performed. Most notably, the QI/RF combination leads to a large reduction in the NRMS error for wind vectors carrying lower QI values, with less editing on the higher-quality vectors. This is clearly shown in the reduction of sample size between the two comparison data sets, with a greater percentage of higher quality (high QI) winds being retained by the RF analysis.

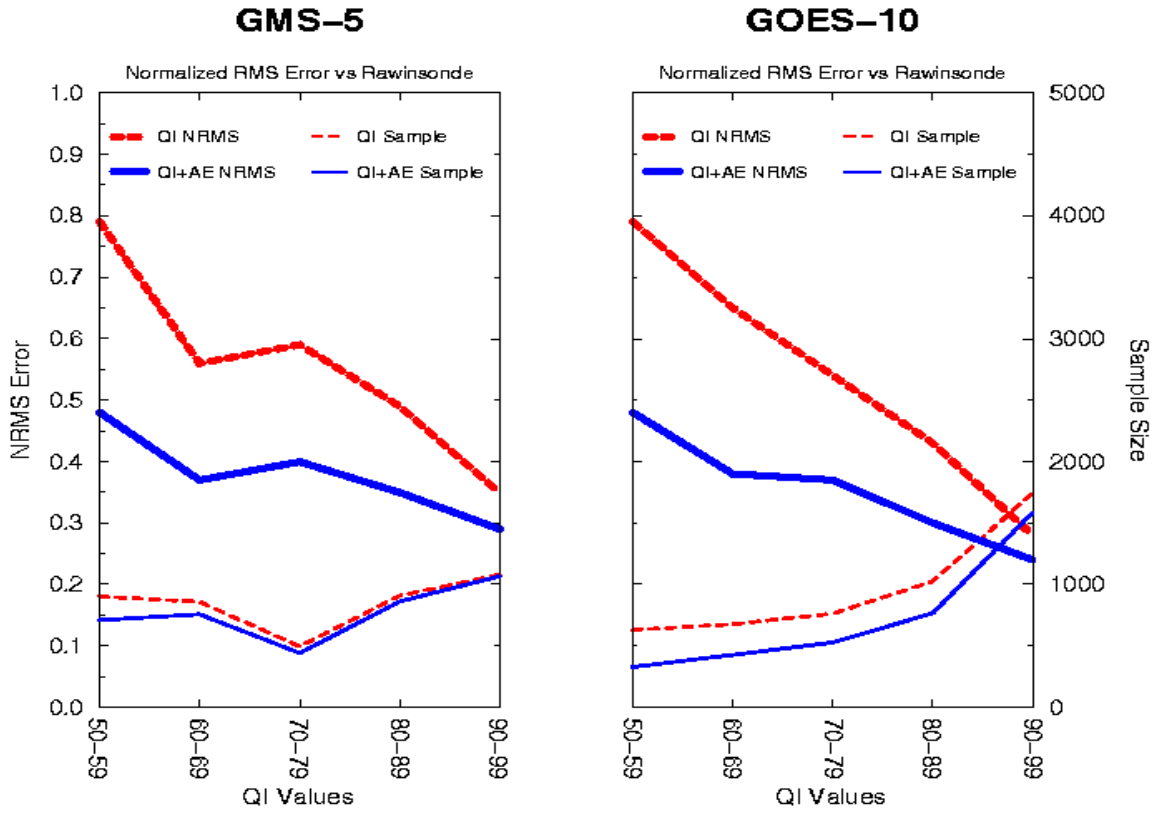

Figure 1. Normalized RMS Error versus rawinsonde observations for GMS-5 and GOES-10 satellite wind vectors prior to (red) and after RF analysis (blue) for various QI value bins (higher values of QI are considered higher quality).

One interesting feature we have noted is that the behavior of the QI routine appears to be satellite dependent. We have found the QI threshold value needs to be set about one category higher for GOES relative to GMS in order to achieve equal editing percentages. For GOES-10, there are a greater percentage of wind vectors retained by the QI=50 threshold vs. GMS-5. This is currently unexplained, and will be further examined. Other satellites will also be investigated.

5. Future plans

As mentioned previously, a generalized visualization interface will be developed for potential users not possessing McIDAS visualization tools. A generic X-Windows graphical user interface (GUI) will be provided for these users since X-Windows software is available to all UNIX-based platforms. For remote users who wish to utilize site-specific GUI software packages for visualization purposes (e.g. IDL, TeraScan), detailed explanations of pertinent input and output file formats will be provided for data file access. For McIDAS users, visualization tools/commands currently used in the FORTRAN version of the winds derivation code will be converted to C and released in future versions.

A significant goal for future UW-CIMSS wind algorithm packages is to reduce the influence of numerical model forecast guess fields. Entirely eliminating the need for model forecast fields is not likely given the reliance of the height assignment methodologies on model temperature profiles. However, studies on several new “model-independent” targeting, tracking and objective editing schemes will be performed to assess their strengths and weaknesses

6. Summary

A platform-independent version of the UW-CIMSS satellite-derived wind processing algorithm is in development. A preliminary version has been completed, with the main procedures rewritten from FORTRAN to C language to allow for greater compatibility with remote site platforms. This version retains many features distinct to the McIDAS environment, such as input and output file formats and internal navigation/calibration of the satellite imagery data, but can now be run either inside or outside of the McIDAS environment. This capability will expand the user-base of satellite-derived winds by allowing local processing, and reduce the reliance upon UW-CIMSS for distributed real-time or post-processed wind sets.

The UW-CIMSS algorithm is currently in the process of being ported to platforms for use by the U.S. Navy, and should be available for general distribution during the coming year. The algorithm will be fully supported by UW-CIMSS, with all new upgrades and additions to the software package available as warranted. A comprehensive User's Guide is being composed and will be made available to all users. This guide will fully document all methodologies utilized in the new wind algorithm. A web site is also under development.

A new addition to the objective quality control module (the EUMETSAT Quality Indicator) has been integrated into the winds processing code and is being evaluated. Preliminary indications on the impact of using a combined QI and RF wind editing approach are positive, with a significant reduction in NRMSE vs. collocated rawinsondes supporting earlier numerical model impact studies (Holmlund et al. 2000).

REFERENCES

Holmlund, K., C. S. Velden and M. Rohn, 2000: Enhanced automated quality control applied to high-density GOES winds derived during NORPEX. Conditionally accepted in *Mon. Wea. Rev.*

Velden, C. S., T. Olander and S. Wanzong, 1998: The impact of multispectral GOES-8 data wind information on Atlantic tropical cyclone track forecasts in 1995. Part 1: Data set methodology, description and case analysis. *Mon. Wea. Rev.*, **126**, 1202-1218.

THE ATMOSPHERIC MOTION VECTOR RETRIEVAL SCHEME FOR METEOSAT SECOND GENERATION

Kenneth Holmlund

EUMETSAT
Am Kavalleriesand 31
64293 Darmstadt
Germany

ABSTRACT

The advent of the Meteosat Second Generation (MSG) provides many new opportunities for improved derivation of Atmospheric Motion Vectors (AMVs) from geostationary satellite data. MSG will provide full field of view imagery data every 15 min. with a sampling distance of 3 km, already improving the capabilities to derive AMVs. Another main improvement is the large range of available channels that amongst others incorporate two water vapour absorption channels at 6.3 and 7.2 um and a CO2 absorption channel. These channels will enable the application of the IR/WV and IR/CO2 ratioing methodologies, providing a more accurate estimate of the cloud heights. Further new channels like the 3.9 um channel and High Resolution Visible channel at 1 km resolution are expected to improve especially the tracking of low level cloud structure during night and day.

This paper will present the MSG AMV retrieval scheme especially highlighting the changes with respect to the current Meteosat AMV scheme and the expected areas of improvements. Validation results of the new approach using current existing satellite data will also be provided.

1. Introduction

The current operational Meteosat satellites operated by EUMETSAT (EUropean organisation for the utilisation of METeorological SATellites) form an mandatory and integral part of the global meteorological satellite system. One of the most important products derived not only from Meteosat imagery data but from all geostationary satellites in general consists of, the Atmospheric Motion Vectors (AMVs). These vectors are extracted from sequences of well navigated and calibrated images. Typically the extraction frequency is between 1.5 to 6 hours and the horizontal density is of synoptic scale (100 km or worse). The AMVs are today an important part of the observation data fed to Numerical Weather Prediction (NWP) and are imperative over the vast data void ocean areas as shown already by Kelly (1993). Currently the scale and extraction frequency is sufficient for the NWP purposes, but in the future, global NWP as well as nowcasting will require data with a higher extraction frequency and higher density. Furthermore the height assignment that is currently one of the weakest parts of the AMVs should be improved. In order to meet these new and increased requirements new series of geostationary satellites are developed. At EUMETSAT the Meteosat-satellites will be complemented by Meteosat Second Generation in year 2001. This new satellite generation will provide enhanced capabilities to derive AMVs with a higher accuracy, extraction frequency and coverage. This paper will give a short overview of the new MSG satellite, introduce the current baseline MSG AMV extraction scheme and present validation and preparation activities.

2. The Meteosat Second Generation (MSG)

Meteosat Second Generation (MSG) is a spin-stabilised satellite in geosynchronous orbit. The spin rate is 100 rpm and with the new SEVIRI instrument the satellite will provide global imagery every 15 min. The sampling distance of SEVIRI is 3 km (1 km for High-resolution visible (HRVIS) data) and the radiometric resolution is 0.25 K. Figure 1 presents the EBBT as observed at the top of the atmosphere for Mid-latitude summer together with the infrared spectral band coverage of the MSG SEVIRI instrument. As a comparison the spectral coverage of the GMS-5 (Geostationary Meteorological Satellite, maintained by the Japan Meteorological Agency), GOES-8 (Geostationary Operational Environmental Satellite, maintained by National Oceanographic and Atmospheric Administration/National Environmental Satellite, Data and Information Service) sounder and GOES-8 imager are included.

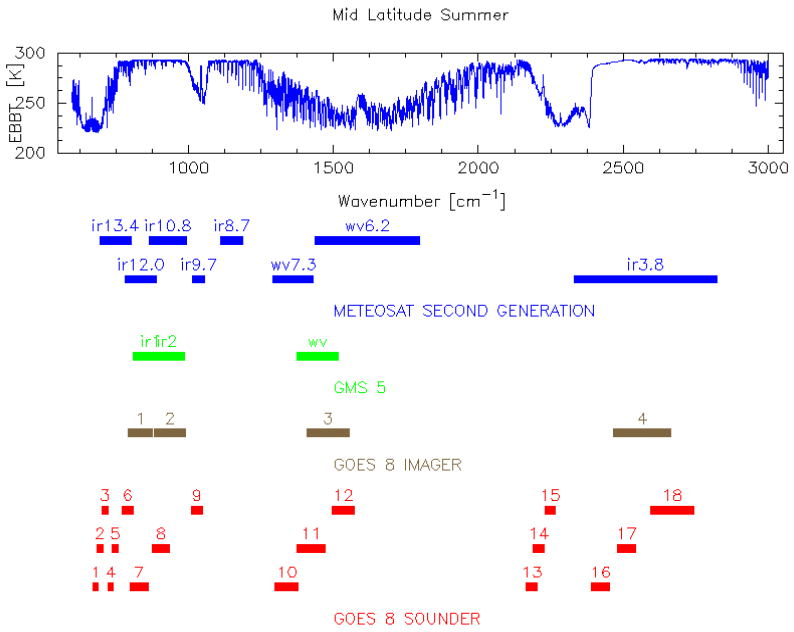

Figure 1. The EBBT as observed at the top of the atmosphere for Mid-latitude summer together with the infrared spectral band coverage of the MSG SEVIRI as well as the GMS-5, GOES-8 sounder and GOES-8 imager.

Table 1 presents the current baseline channels for AMV extraction. The table also incorporates an extended set of channels that are highly likely to provide significant and improved data, but for which there are currently no experience. It is foreseen that the AMV-products derived from these channels are not declared operational at Day-1 (First day of operational dissemination), but at a later stage when a complete validation and assessment of quality has been performed.

Table 1. The AMV channels.

Baseline channels:		
Band	Central wavelength	Prime targets
IR	10.8 µm	Clouds
IR	6.2 µm	High level clouds/Moisture
IR	7.3 µm	High/Medium level clouds/Moisture
VIS	0.6 µm	Low level clouds over sea
VIS	0.8 µm	Low level cloud over land
Extended channels:		
IR	9.7 µm	Clouds and ozone features
IR	3.9 (8.7) µm	Low level clouds at night
HRVIS	0.8 µm	Low level clouds over sea

3. The Atmospheric Motion Vector (AMV) Extraction Scheme

The Atmospheric Motion Vector (AMV) extraction scheme will in general retrieve the AMVs in a similar fashion to the current operational extraction scheme at EUMETSAT (e.g. Schmetz et. al., 1993, Bühler and Holmlund, 1993). The main components are the following:

- Target extraction
- Image enhancement
- Tracking
- Height Assignment
- Quality control

In the following sections several examples are presented. These are based on a prototype AMV extraction scheme, currently employed at EUMETSAT for development and verification purposes. This system is able to digest various kinds of image data and for these examples simulated MSG data has been used. The simulated data is based on Meteosat-6 IR, WV and VIS data that has been re-sampled and calibrated to the MSG SEVIRI resolution.

3.1 Target extraction

The main major change to the current operational AMV extraction scheme at EUMETSAT is the target extraction. Currently the AMVs are extracted on an equidistant grid (baseline 32*32 pixels) with a target size equivalent to the grid size. In the new scheme the target size and extraction grid are controlled separately. Furthermore the exact location of the target is not fixed and centred at the grid location but optimised in a search area around the grid-location. The main two reasons for this approach are; 1) Better and more stable targets for tracking, e.g. the target area contains at least a certain minimum amount of the clouds at the highest local level and 2) Avoidance of extraction of targets in multi-layered cloud situations that have proven to be difficult to handle. These conclusions were already indicated by Holmlund (1995) and by the necessity to introduce complex image enhancement procedures (Hoffman, 1990). A variable target extraction scheme is already used operationally at NOAA/NESDIS and has proven to be reliable. The EUMETSAT target extraction scheme investigates the following features of each location:

- Minimum contrast
- Minimum acceptable local standard deviation
- Minimum number of pixels with high local standard deviation
- Entropy
- Cloud configuration
- Land/Sea (water) distribution
- Overlap control

Suitable targets are typically targets that have the highest contrast and largest amount of standard deviation (highest entropy) within the optimisation area. Furthermore multilayered cloud situations should be avoided and a minimum amount of cloudy/clear sky pixels are required for respective target type. Coastal regions are avoided in the IR and VIS channel, as the coastal feature might have an impact on the tracking. Finally the overlap between targets is restricted in order to avoid vectors to be derived that contain a large amount of pixels from the same cloud (clear sky feature). This will minimise the impact of correlated errors by reducing the horizontal dependency neighbouring targets. Currently the baseline overlap is limited to 30 %

Figure 2 shows the impact of the variable target extraction. In order to enhance the performance of the location optimisation a low density grid was used. It can be seen in figure 1 that the target locations are preferably extracted along strong gradients in the coldest parts of the satellite imagery data.

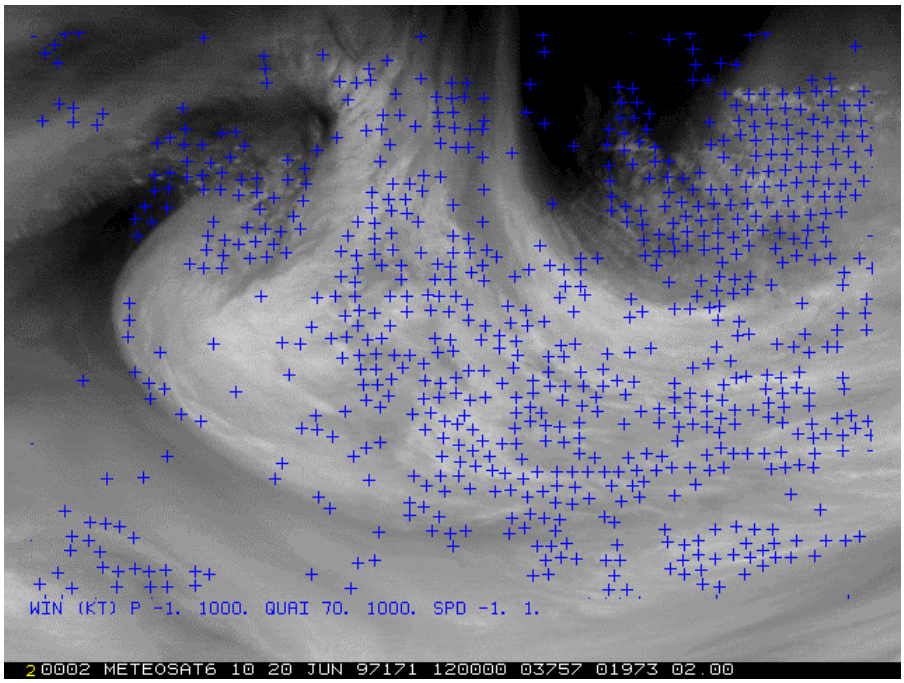

Figure 2. Low density targets extracted from MSG water vapour data simulated by WV data from Meteosat-6.

3.2 Image enhancement

The image enhancement is equivalent to the current methodologies applied at the Meteorological Product Extraction facility (MPEF) for the current Meteosat-satellites (Schmetz et. al., 1993). The only important difference is the derivation of cluster mean radiances, necessary for the image enhancement, that currently are directly retrieved from the targets analysis scheme. As the target location is only defined at the stage of AMV target-extraction a dynamical clustering has to be used. Currently it foreseen to use an approach similar to the one presented by Ebert et. al. (1993).

3.3 Tracking

The tracking of the targets is generally the task that uses the largest amount of computer resources in any AMV extraction scheme. Therefore several various alternatives have been explored in order to minimise the computational load. Generally the following methodologies have been employed; 1) Use of additional data for first guess estimates of the displacements; 2) In cases where several consecutive vector fields are derived the search area is after the initial matching reduced for any subsequent derivation; 3) Sequential derivation of matching surfaces with full surface calculated only at locations indicated by a low resolution matching surface. The first approach is often relying on NWP data and is therefore not recommended as flow with a large discrepancy to the NWP field might not be derived correctly. The second approach is better, introduces however some limitations on the timely variation on the vectors and is implicitly invoking a quality control (by limiting the search –are) that preferably is performed at a later stage. The third alternative is generally the most promising and for current satellite data and resolution it has been shown that the results are agreeing up to 97% of a full matching surface. As the available processing capacity has in the past years increased tremendously the requirement for a limited calculation of matching surfaces has decreased and therefore the calculation of the full matching surface was regarded to be feasible. Three basic matching methods have been implemented 1) Cross-correlation in the time domain, 2) Cross-correlation in the Fourier domain and 3) Sum of Squared Distances. The detailed description of the implementation of these methods are given in Dew and Holmlund (2000). Figure 3 shows an example of water vapour vector fields derived with the current software version using simulated MSG image data.

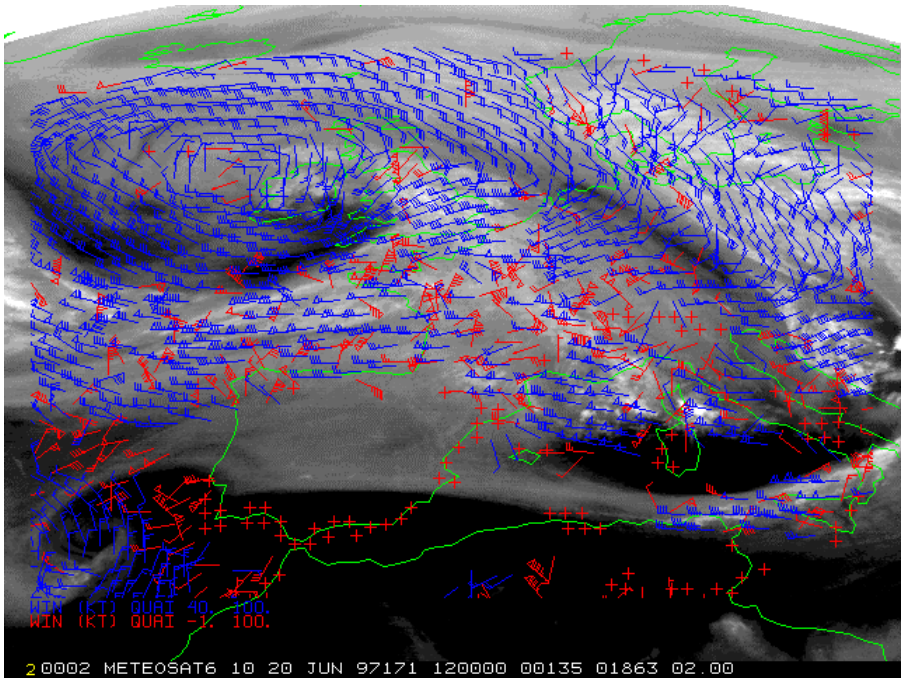

Figure 3. Water vapour vector field with water vapour imagery data from 20 June 1997.

3.4 Height assignment

The height assignment of AMVs is currently the most challenging task in the AMV extraction schemes. Broken clouds, multi-layered cloud targets, low level targets (requiring cloud base height assignment) and height assignment of clear sky targets do all require their special attention. The biggest problems however are generally encountered with semi-transparent clouds.

With the advent of MSG it will for the first time be possible to operationally derive the correct height for semi-transparent clouds using two operationally established methodologies; the semi-transparency correction utilising the WV and IR channel (e.g. Schmetz 1993) and the CO_2-ratioing method (Eyre and Menzel, 1989, Nieman et. al. 1997). Nieman et. al. (1993) showed that for high level clouds the bias of the estimated cloud height is of the order of 20 hPa and with a RMS pressure difference of ca 80 hPa between the two methods. With MSG it will be possible to simultaneously apply both methods. The implementation of these methods contains the following new features:

- channel dependant noise is included in the calculations
- refined selection of pixel or groups of pixels depending on the characteristics of the pixels and the neighbouring pixels
- various possibilities to extract background/surface information (real observations, history of previous observations, forecast, climatology)

Figure 4 presents an example of extracted IR vectors with their respective height over the South-Atlantic. The delineation between high (above 400 hPa) vectors (in red), medium (between 440 and 700 hPa) vectors (in blue) and low (below 700 hPa) level (in green) looks realistic and has been verified against operational heights derived from Meteosat-6 data. It should be noted that as these results are based on simulated MSG data based on the Meteosat-6 IR, WV and VIS data, no CO_2-channel is present and therefore only the semi-transparency correction method has been applied to the thin high level clouds.

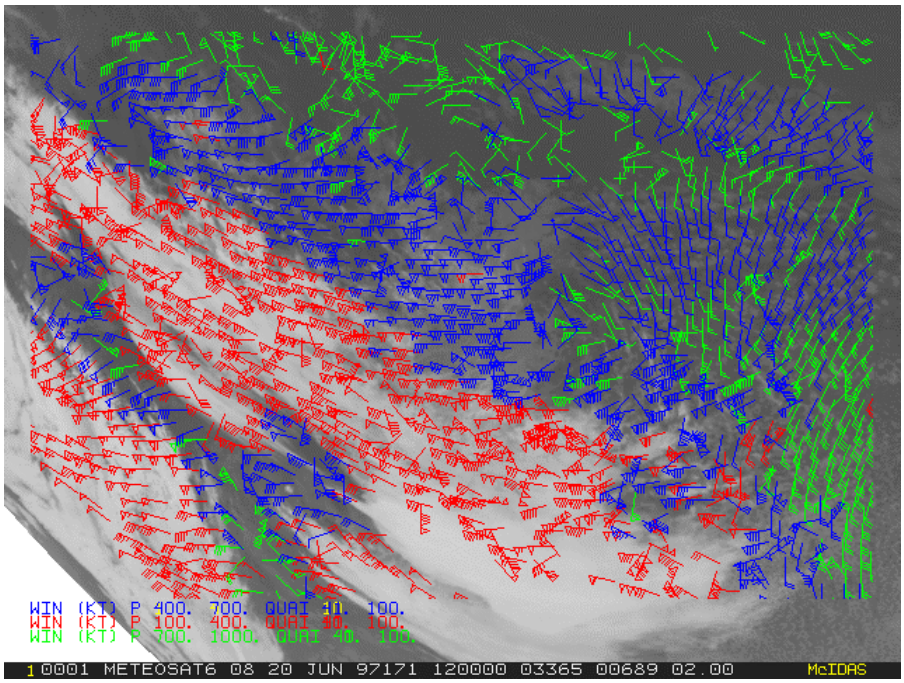

Figure 4. AMVs derived from simulated MSG images over the South-Atlantic. The image data has been simulated from Meteosat-6 data from 20 June 1997 1200 GMT. High (above 400 hPa) level vectors are coded in red, medium (between 400 and 700 hPa) level vectors are coded in blue and low level (below 700 hPa) vectors are coded in green.

3.5 Automatic quality control

The automatic quality control is based on the same principals used in MTP MPEF (Holmlund, 1998). The scheme has been further improved with latest experiences with current operational AMVs and the new capabilities provided by MSG. The baseline Automatic Quality Control (AQC) tests are based on:

- local consistency (horizontal)
- speed consistency (in time)
- direction consistency (in time)
- vector consistency (in time)
- background consistency (currently against NWP)

The extraction cycle of the baseline AMV product consists for MSG of three vector fields. All vector fields contribute to the consistency calculations enabling a better estimation of the vector reliability.

3.6 Final product

The AMV fields can be derived continuously, however the current baseline is that a final product should be extracted once every hour. The baseline product derivation is therefore set up to extract three intermediate AMV fields from four consecutive images during one hour. The targets are extracted from the first image in the sequence and are then followed in time throughout the other three images. The final vector components (speed, direction, height, temperature, quality) is based on a weighted mean of the intermediate vectors. The current baseline is however that all fields have the same weight.

4. Development approach

4.1 Pre-launch activities

The development of the MSG MPEF AMV scheme is based on previous experience with the Meteosat-satellites. It further incorporates the knowledge gained at the previous International Winds Workshops as well as information exchange during co-operation amongst the various AMV extraction centres. Finally results from various studies have been incorporated as well as in-house development activities. The development of the operational software has been given to industry and is based a formal Algorithm Specification Document and on in-house prototyping of all essential parts. The performance of the prototype code has been verified with comparisons against not only the operational extraction schemes but also with detailed case studies

4.2 Post-launch activities

The main goal for all activities is to ensure that the derived software is capable to produce from the first day of operations products that are at least as good as the current operational products. As MSG incorporates a completely new instrument with new channels and performance the tuning of the configuration parameters will be an essential activity. Therefore it is foreseen that during commissioning of the satellite an early access to image data is granted to the MSG MPEF in order to tune all algorithms (not only the AMV-scheme). The use of real MSG data is also likely to identify possible problems in the software implementation and might also identify some shortcomings in the current baseline methodologies. The MSG MPEF is designed to be modular such that it will be possible to incorporate new software modules or to replace existing modules with improved modules if necessary.

5. Conclusions

The Atmospheric Motion Vector (AMV) extraction scheme for Meteosat Second Generation (MSG) has been introduced. The new scheme is based on well-established operational algorithms enhanced with new concepts utilising the foreseen new capabilities of the satellite. It is expected that the AMVs are extracted in up to 7 image channels, with a target size of 80 km and an extraction grid of 50 km. The vectors will be disseminated hourly over the GTS. With the new capabilities of MSG it is expected that the quality of the AMV-products will improve, especially with respect to height assignment due to the new channels (especially the CO_2-channel). The launch of MSG is currently expected in mid 2001.

REFERENCES

Bühler Y. and K. Holmlund, 1993: The CMW Extraction Algorithm for MTP/MPEF. *Proc. 2nd International Winds Workshop*, Tokyo, Japan, EUMETSAT EUM P 14, pp. 205-217.

Dew, G. and K. Holmlund, 2000: Investigations of Cross-Correlation and Euclidian Distance Target Matching Techniques in the MPEF Environment. . *Proc. 5th International Winds Workshop*, Lorne, Australia, EUMETSAT, these proceedings.

Ebert, E. E., 1989: Analysis of Polar Clouds from Satellite Imagery Using Pattern Recognition and a Statistical Cloud Analysis Scheme. *J. Appl. Meteor.,* 28, pp. 382 – 399.

Eyre J. and P. Menzel, 1989: Retrieval of Cloud Parameters from Satellite Sounder Data: A Simulation Study. *J. Appl. Meteor*., **28**, 267-275.

Hoffman, J., 1990: The Use of Spatial Coherence Method for Cloud Motion Wind retrieval. *Proc. 8th Meteosat Scientific users Meeting*, Norrköping, Sweden,, EUMETSAT EUM P 05, pp. 97-100.

Holmlund K., 1995: Half Hourly Wind Data From Satellite Derived Water Vapour Measurements. Adv. Space res., Vol. 16, No 10, pp (10)59-(10)68.

Holmlund, K, 1998: The Utilization of Statistical Properties of Satellite-Derived Atmospheric Motion Vectors to Derive Quality Indicators. *Wea. Forecasting*, **13**, 1093-1104.

Nieman S. J., Schmetz J. and W. P. Menzel, 1993: A Comparison of Several Techniques to Assign Heights to Cloud Tracers. *J. Appl. Meteor*., **32**, 1559-1568.

Nieman, S.J., W.P.Menzel,C.M.Hayden,D.Gray,S.T.Wanzong,C.S.Velden, J.Daniels, 1997: Fully Automated Cloud-Drift Winds in NESDIS Operations, *Bull. Amer. Meteor. Soc.,* **78**, 1121-1133.

Schmetz J., K. Holmlund, J. Hoffman, B. Strauss, B. Mason, V. Gärtner, A. Koch and L. van de Berg, 1993: Operational Cloud-Motion Winds from Meteosat Infrared Images. *J. Appl. Meteor*., **32**, 1206-1225.

Kelly, G., 1993: Numerical experiments using Cloud Motion Winds at ECMWF, *Proc. On Developments in the use of Satellite Data in Numerical Weather Prediction*, Reading, UK, ECMWF, 331-348.

DEVELOPMENTS FOR A HIGH-RESOLUTION WIND PRODUCT FROM THE HRV VISIBLE CHANNEL OF THE METEOSAT SECOND GENERATION

José Miguel Fernández

Servicio de Teledetección, Instituto Nacional de Meteorología -I.N.M.
C/ de las Moreras, s/n, 28071 Madrid,
Spain

ABSTRACT

The Satellite Application Facility -SAF- for Eumetsat in support to nowcasting (and very short-range forecasting) develops algorithms and software to provide cloud, precipitation, air mass and synoptic analysis products, from data of the future MSG satellite system. A wind product -HRW- was also included to add some dynamical information. It is centred in the exploitation of the HRV channel at 1km horizontal resolution (s.s.p.) as closer in possibilities to the meso-scale than other channels at only 3km, more indicated for synoptic scale winds to be produced at Eumetsat Central Facilities -MPEF.

Existing techniques allow appreciable results in tracer scales around 25 to 35 pixels (km), but the HRW product should offer improved resolution (around 10 pixels) for at least some zones or tracers, whilst preserving a good level of accuracy and efficiency. It is in consequence aimed in the development to work at 2 or more different scales but with reasonable link among these, and to work on tracer features for selection and tracking.

The current approach considers mainly 3 development parts, enhancement on existing, alternative objects method, additional quality control and other aspects. The first one already boarded, on gradual enhancement of starting existing methods (the INM-VDI satellite wind procedures developed from a McIDAS core, and the use of some adapted specific elements from current or proposed Eumetsat methods): to the basic tracer selection based on the laplacian operator, have been added some optimising criteria considering tracer features (a well determined brightness frontier used as threshold to determine if enough variability in the tracer); the next step is the use of these same criteria in the tracking step (it seems in fact convenient, to avoid some errors when tracking with the usual correlation on some tracers so selected), and to determine lower scale tracers. Results from the work already done are the subject of the presentation.

1. Improvement of the tracer selection - TRAZ method.

An overview of the intended HRW product for the SAF for Nowcasting can be found at (Fernández, 1998). It is assumed that the VIS channel present distinct cloudy targets but the clouds could present less sharp edges than IR window channels (due to characteristics of the top of the cloud and illumination), so an approach including histogram classification and tracer determination of features at an intermediate resolution could be adequate, lying in-between merging between target determination based on gradients (introduced for IR channels, e.g. Hayden, 1989) or prior segment classification, and direct image matching or correlation (rather used for WV channels, e.g. Jedlovec, 1998).
The operational INM-VDI for Meteosat winds (Fernández, 1996) uses the McIDAS WINDCO gradient method -TARGET. The image is explored by segments LSIZExESIZE. Wherever a MIN threshold and a DVAL contrast area reached (cosZ-corrected brightness values in the scale 0-255), the laplacian ($\Delta R/\Delta x+\Delta R/\Delta y$)is evaluated, and the location of its maximum (unless at boundary of the segment) provides the tracer centre. Rather standard values (LSIZE, ESIZE=20, 24 pixels, MIN=75, DVAL=25 and $\Delta x=\Delta y=5$, are retained for the as starting point for the 'coarse' approach.

TARGET is generally providing good results at this resolution, but often tracers do not suggest well marked structure for eased recognition, are too linear, or too simple, and more tracer are wanted. An additional search algorithm has thus been implemented. It basically searches for a defined frontier in the brightness histogram of the pixels of the segment, serving to classify it in a 4x4 array of 'big pixels' then explored for enough 'variability', with conditions to be met. Optimisation search around initial centre is performed. The chosen TRAZ method onsiders 1 step or 2 steps around any candidate centre in the basic grid, in the first TARGET tracers are determined and then fine-adjusted in location (or rejected) with the new algorithm parts, if no result a second step only with these re-starts from the basic initial centre trying to fill holes in coverage.

The algorithm mainly includes the 2 routines dealing with histogram -HISTFRON- and 'big-pixels' creation and evaluation -SUBSEC-. HISTFRON performs again basic checks (MIN and contrast now on percent values 90%, and 97%-3% which contrast must be CONTR=30 or reduced value for 'generally bright' segments for cloud-over-cloud cases). The histogram (smoothed with a x3 passing filter), is explored -bottom to top- to get frontiers (brightness minima), evaluation of 3 terms -6 contiguous classes summed by pairs-, (1^{st} -2^{nd}) + (3^{rd} - 2^{nd}), any frontier has to be deeper than UMB_PROF=14.

The SUBSEC routine assigns 0, 1, 2 class-value to each big-pixel (in an 4x4 array) depending on the position of the frontier relative to the percentiles 30% and 70% in the big-pixel, values 0 and 2 should appear at least once. The 4x4 array is checked for each frontier (brightest to dimmest) until a good 'variability' is found in 4 directions (row, column, 2 diagonals); are checked the absolute sum of contiguous differences in class value along each linear array (of at least 3 elements) of each direction, at least equal to UMB_DIR=6 (also 4 used in the tests) , see fig.1. A second test and condition CRI_ARR, at least one 'complete' transition 2-0-2 or 0-2-0 in any linear array of at least 2 out of the 4 directions, is also used in addition (also tested alone but poorer results).

0 0 0 0 2 2 2 2	0 0 0 0 2 2 2 2	0 0 1 0	0 1 1 0
0 0 0 0 2 2 2 2	0 1 0 0 2 1 2 2	0 1 2 1	0 2 1 0
0 2 0 0 2 0 2 2	0 2 1 0 2 0 1 2	0 1 2 2	1 2 1 0
0 0 0 0 2 2 2 2	0 0 0 0 2 2 2 2	0 2 1 1	1 2 0 0
UMB_DIR=4	UMB_DIR=6		

Figure 1. 4 examples of 'extreme acceptable configurations' for target as a 4x4 array of 'big pixels', also meeting CRI_ARR condition. Target 5 meets UMB_DIR conditions (4 or 6) but not the CRI_ARR ('complete transition' only in SW-NE direction) . Last target meets CRI_ARR, but none UMB_DIR (low 'variability' N-S) . 0 if 70% of values below frontier, 2 if 70% above, 1 for the other less defined cases.

Comparative results (TARGET; and TRAZ tracers, with UMB_DIR=4 -plus CRI_ARR- and =6 -alone and plus CRI_ARR- for Meteosat -2.5km- and GOES -1km, only TARGET and last TRAZ case-) are shown in fig.2 and fig.3; TRAZ is expected to provide more determined tracers to be tracked. The TRAZ method is by now quite slow (even 2.5min for the intented regions of 1500x1500, to be compared to a few seconds for the TARGET method), but it will be ran as a pre-processing for next time-slot, at the end of the wind computation, and will provide data useful for the wind computation and quality control (tracer characteristics from the HISFRON and SUBSEC), intended to speed-up this next step which could be the critical one.

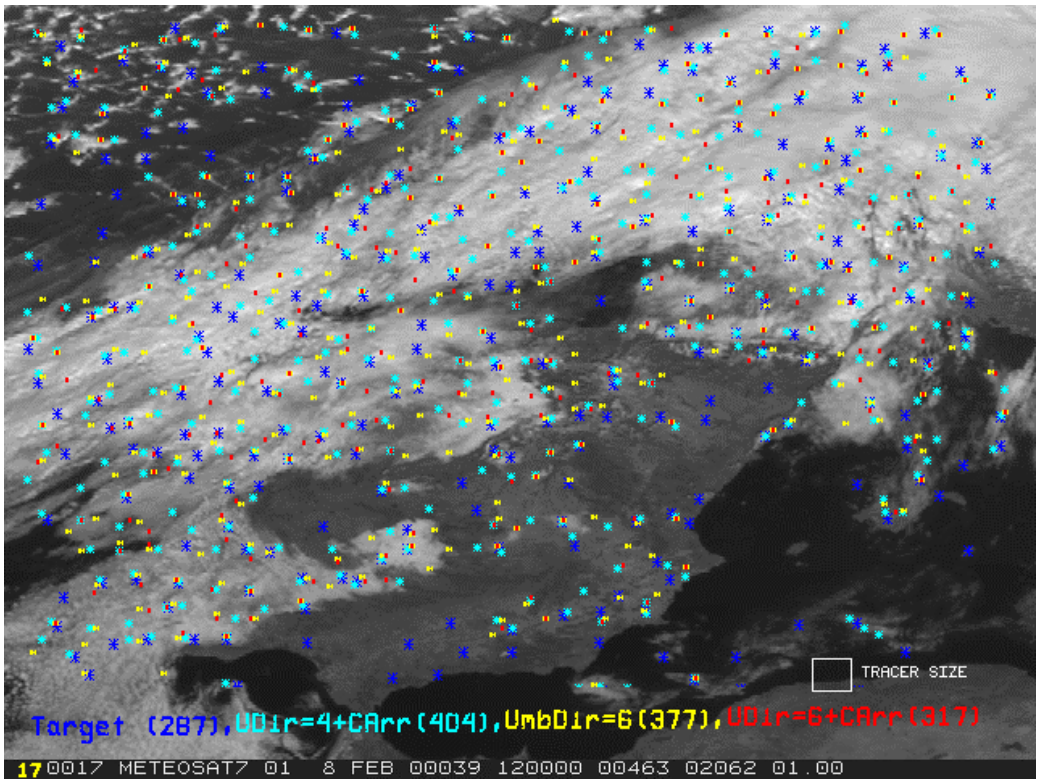

Figure 2. Meteosat example of targets, and tracers determined using 3 criteria.

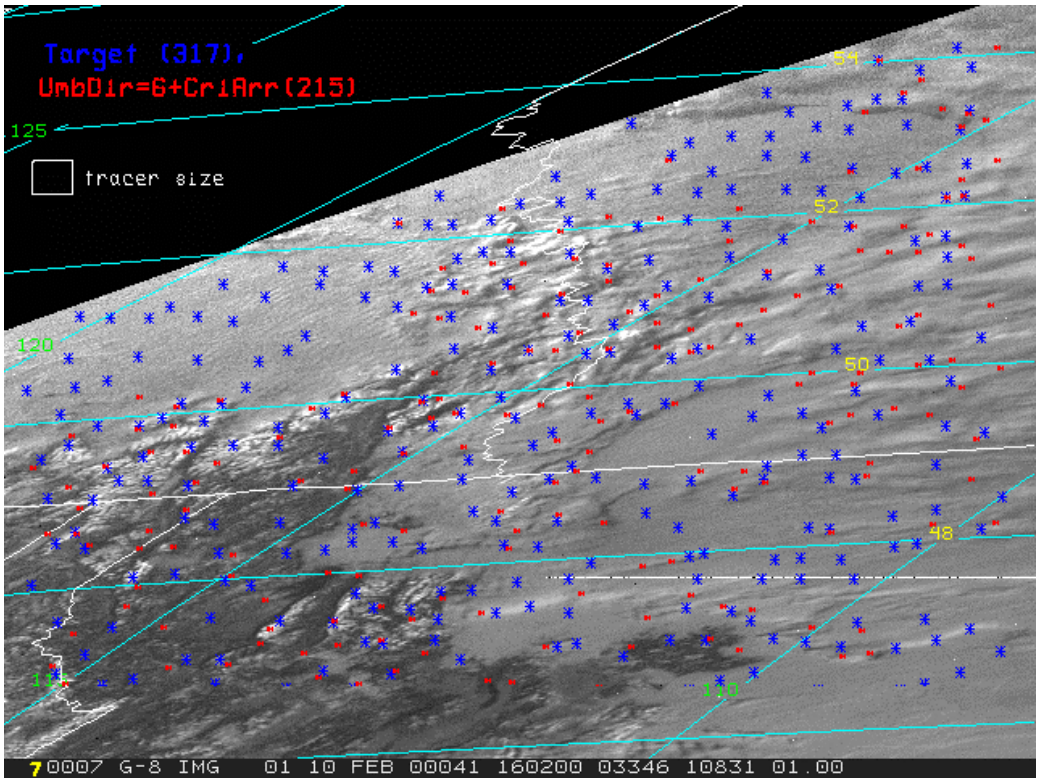

Figure 3. GOES example of targets and tracers.

2. Use of 'medium resolution' features of the tracers for approximate tracking then refined with limited cross correlation analysis -MATCH method.

The TRAZ method provides a basic set of tracers, also expected to be improved when coupling the 'coarse' tracers at around 20x24 with 'detailed' providing up to 4 tracers at around 10x12 (same initial centre) where some conditions are met for its computation. All these would be input to a tracking based in cross-correlation with a guess to reasonably shorten computations meeting some '5min' figure for the mentioned 1500x1500 region; guess winds from NWP and MPEF are considered for the HRW product.

It is also being considered to get rather independent of external guess, introducing internal considerations to reduce search zone for cross-correlation -final step, a sort of internal guess or rough step. Apart from the fact that combination of quality control with the continuous HRW could perhaps limit search area (e.g. limit search to 50% level of confidence for a previous wind), current developments explore the possibility of performing a rough step which is a pattern matching, based on TRAZ characteristics with some quality control, in the large search zone: classification in 'big boxes' (similar to that in TRAZ for the given tracer) in the final image throughout a grid of centre locations (size LLAGxELAG, =50 -Meteosat- and 60 -GOES- are chosen) centred in the tracer position in the initial image, 'candidate tracers' are compared to the initial tracer.

MATCH includes in fact 3 principal functions. The comparison of tracer -initial image- to any 'candidate' -final image- is done by absolute sum of classes differences at the same relative locations. The evaluation of the best candidate (and its centre) considers the 2 minimal difference-values (this introduces some smoothing, search of candidates is in fact computed each 3 or 2 lines and elements, only so the computation is fast enough, a factor x5 or x3, with respect to full correlation; as no great difference was found x3 was used). If more than one 'best candidate', an average centre is determined, and the final-step search zone increased accordingly, for the final cross-correlation, limited to a 9x9 or 6x6 search grid of centres. The quality acceptance includes -by now: the 'best candidate centres' should 'not be too distant', and a correlation maximum to be found which is close, with correlation value at least .55 for these coarse tracers.

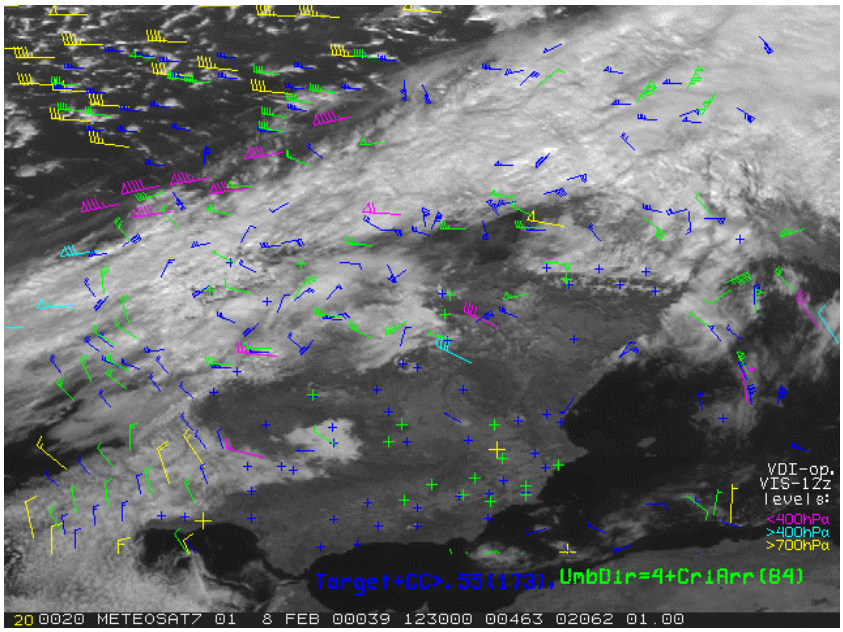

Figure 4. Meteosat VDI-INM VIS winds (computed using TARGET tracers, NWP guess wind, quality selected using sequence of 2 winds and spatial coherence including IR and WV winds). Full cross-correlation winds (CC>0.55), from TARGET tracers. TRAZ+MATCH winds (frontier as invariant), at a x3 step search, for the option providing the best apparent results (UMB_DIR=4 + CRI_ARR).

Basically, TRAZ selected frontier is the 'invariant' for MATCH. Also was checked to rather its percent (and re-compute frontiers at the final image at any candidate centre for a given tracer), based in the expectation that the percent distribution (if cloud time-changes are small) of an image should be few dependent on the illumination changes (hypothesis used for normalisation of VIS images, e.g. Binder, 1989). But this could also selects spurious candidates and slows down (not critically but sensibly) the procedure; this will be rather serve in any case to determine in the development expected changes in frontier value for changing sun elevation (a combination of both methods could be tested including application to non-normalised brightness as the normalisation method introduces noise).

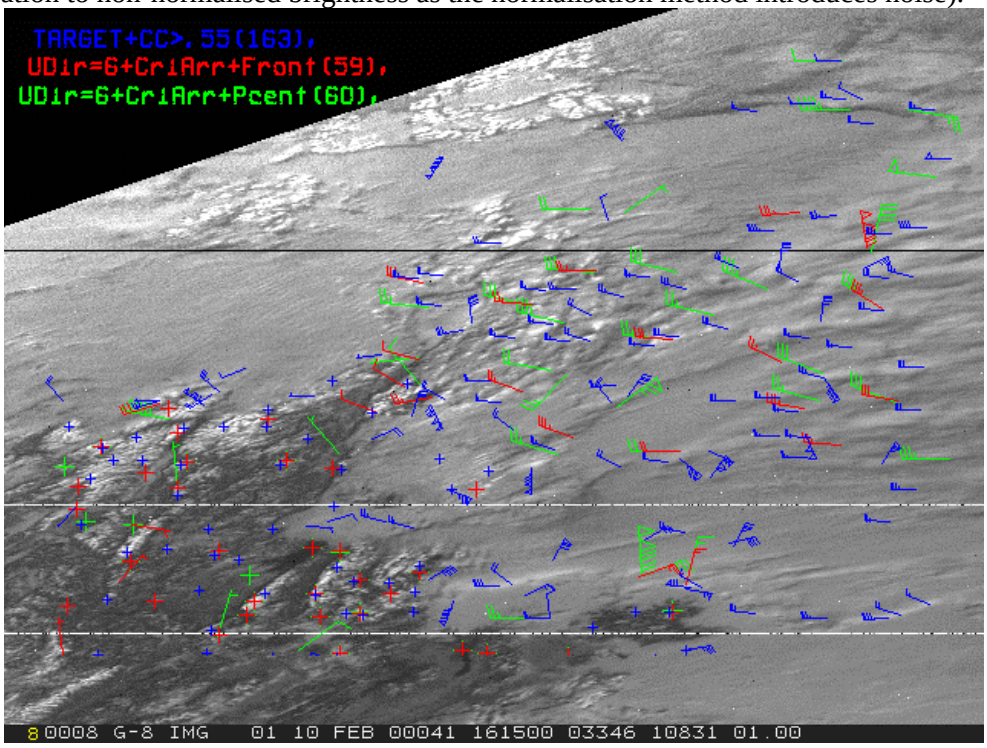

Figure 5. GOES winds: full cross- correlation (CC>0.55) from TARGET tracers. TRAZ(UMB_DIR=6 + CRI_ARR) +MATCH (frontier and frontier percent, as invariants), at a x3 step search.

Comparative examples of MATCH results are shown for Meteosat (fig.4 and fig.5, image presenting wide diversity in cloud patterns) , and GOES (fig.6, image with low view and illumination angles).

MATCH (or TRAZ+MATCH) as now needs certainly improvement. The tools implemented to check at any location tracers features and matching matrices allow to identify particular causes of errors or deletion. Among these, cloud level confusion (inside the tracer or in its tracking), a too simple determination of candidates (when different 'best candidates' could appear selection should consider additional criteria). Orography effects, and the selected frontier being too high or too low (depending on case) given a tracer few defined for tracking, are, in close connection with the former, cause of difficult tracking and errors.

Finally the whole method was tested at detailed resolution (LSIZE=10, ESIZE=12), with options quite the same of the coarse ('best' results nevertheless with UMB_DIR=4 only) and independently, with rather poor results (but some promising results in zones considered a priori of interest, as in zones of continuous Sc with few details).

3. Conclusions, further developments.

The described methods provide a basis for selection of a wide set of targets, and winds. The basic methods are desired to change little, but actions on options and thresholds should improve them. Despite this tuning can seem complex, the availability of checking tools and determination of priorities in the method improvement and tuning should partly ease this task.

TRAZ will include level assignment (and derived tracer acceptance), and the linked selection of detailed tracers. MATCH will have to improve selection of tracer matching candidates, and include quality tests.

The quality acceptance and flagging in the method is a very important issue for development. Given that in this case the fast availability (and a dense wind pattern) is a major requirement, among the tests on time and space consistency, it is assumed that some of the first (which include wind -Holmlund, 1998, and tracer and level continuity which could perhaps use related techniques) could rather serve to reduce computations, and that the second should be in this case very important for the final flagging.
In particular of importance is the final quality control with relation to orography. The combined use of external winds, orography patterns in relation to HRW winds, and other SAF products (e.g. on stability) is considered for this task.

Finally, it was considered for the HRW development on alternative methods, the tracking of objects at combined different scales; in a first study it was determined that statistical entropy (for object selection), and a pyramidal method (to go through scales) could be candidate methods. The studies could not be continued until now. Continuation on this issue is subject to evolution in described in this presentation as it could in fact provide a good part of requested from these alternative methods, and these could otherwise represent a major development or research.

REFERENCES

Binder, P., 1989.: A normalisation procedure for Meteosat visible channel data. *Journal of the Amer. Meteor. Soc*., **6**, 67-75.

Fernández, J.M., F. Martín, 1996: Satellite winds calculated at INM and its potential usefulness for the operational forecasters. *Proc. 3rd international wind workshop*, EUM P18, 117-123.

Fernández, J.M., 1998: A future product on HRVis winds -HRW- from the MSG for the nowcasting and other applications. *Proc. 4th international wind workshops*, EUMP24, 281-288.

Hayden C.M., R.T: Merrill, R.T., 1989: Recent NESDIS research in wind estimation from geostationary satellite images. *ECMWF Seminar proceedings on data assimilation and the use of satellite data*, Vol II, 273-293.

Holmlund, K., 1998: The utilisation of statistical properties of satellite-derived atmospheric motion-vectors to derive quality indicators. *Wea. Forecasting*, **13**, 1093-1104.

Jedlovec G.J., Atkinson R.J., 1998: The Marshall automated wind algorithm: Error analysis, quality control and climate applications. *Proc. 4th international wind workshop*, EUM P24, 247-254.

ATMOSPHERIC MOTION VECTOR (AMV) ANALYSIS TOOLS IN THE NSMC AMV DERIVATION SCHEME

Zhang Qisong and Xu Jianmin
(National Satellite Meteorological Center, China)

ABSTRACT

Atmospheric Motion Vector (AMV) derivation tools used in NSMC AMV derivation scheme are introduced. The AMV product is sensitive to the data processing scheme. A small change in algorithm may cause a big difference at the results. Statistics of product performance is often utilized to estimate impact from changes at data processing algorithm. Although statistics has ability to diagnose inappropriate points at data processing, it needs a long validation period and a larger amount of samples to perform well.

In the NSMC AMV derivation scheme, man machine interactive tools have been designed. With these tools, image animations, parameters, scatter diagrams, even measurements of individual pixels at the screen in form of images, graphics or texts can be visualized. The calculation process of individual wind vectors can therefore be monitored providing a way to watch the data and learn from the data.

The major tools are as follows:
- Watch image of any individual tracer at different channels
- Watch animation of any individual tracer on the image
- Watch correlation of any individual tracer on the image
- Watch scatter diagram of any individual tracer on the image
- Watch intermediate parameters of individual AMVs, such as position of tracers expressed as i j accounts latitudes and longitudes, maximum and minimum measurements, maximum and minimum brightness temperatures, correlation coefficient between IR and WV measurements, slope at IR WV scatter diagram, brightness temperature before and after adjustment, pressure level, wind velocity etc.
- Watch NWP and radiosonde reports
- Display AMVs at different projections
- Simultaneously display AMVs, radiosonde wind vectors, radiosonde temperature and humidity profile, and parameters useful at height assignment
- Error statistics and display
- Comparison at different ways of error statistics is discussed.

1. Introduction

AMV derivation programs are large and complex. In the programs, judgements and paths need to be decided. Thresholds are chosen at making decisions. AMV product quality is sensitive to thresholds or paths chosen. A small difference at thresholds or paths chosen may cause a big difference at AMV calculation results.

Statistics of AMV product performance are often adopted to estimate impact of AMV programs or algorithms at the product quality. Although statistics does have ability at diagnosing algorithm or program performance, it needs a long validation period and a large amount of samples.

In the NSMC AMV derivation scheme, man-machine interactive tools are used to assist thresholds choosing and performance estimation. In this paper, tools of analysis and diagnose used in the NSMC AMV derivation scheme are introduced.

2. Display Functions

The display program shows not only AMV products, but also detail information of individual AMVs and comparison data.

On the screen, AMVs are overlapped with image. Overlay display of AMVs with image supplies sophisticated tool in image analysis. It also helps at diagnosing the AMV distribution pattern.

The detail information of each wind vectors can be accessed with mouse clicking. This information helps AMV derivation personal to understand the calculation process. Four times a day AMVs are processed. The latest products always cover the previous ones. Thus, only the detail parameters of the latest processed are maintained in the system and accessible. The content of accessible parameters is shown in Table 1.

Table 1. The content of accessible parameters

Position of tracer (i, j)
Position of tracer (Lat., Lon.)
Movement of tracer
Correlation coefficient matrix at tracing component
Maximum and minimum measurements in the tracer region
Maximum and minimum bright temperature (BT) in the tracer region
Correlation coefficient between IR and WV measurements
Slope at IR—WV scatter diagram
5% minimum BT before and after adjustment
Wind velocity
Wind direction
Pressure level of AMV

In order to estimate quality of AMVs, NWP grid data, radiosonde data and AMV data from other centers are assessable together with NSMC AMV data. Radiosonde data are also shown in graphic form.

Variety display function can easily be reached by mouse clicking at menus: view latest IR images, view latest WV vectors, view archived vectors, Lat./Lon projection display (NWP grid data display included), Animation display, screen zooming display and comparison display. At present, the detail information of each wind vectors can be accessed only at viewing latest IR or WV images. In viewing archived images, this is not yet reached, because the information is not maintained in the historical data. The Projection, animation, and zooming functions are available for users.

3. Utilization Examples

3.1 Tracing Component

In order to diagnose tracing results, the following parameters can be monitored by mouse clicking:

- Position of tracer (i, j)
- Position of tracer (Lat., Lon.)
- Movement of tracer
- Correlation coefficient matrix at tracing component

Display to (i, j)/(Lat., Lon.) position and movement of individual tracer helps the AMVs derivation personal to judge the correction of tracing result.

Maximum correlation is the bases of tracer tracing. Sometimes multi maxims appear on the correlation matrix. In the NSMC scheme, the most continuous first and second maximum peaks between two continuous tracing pairs are chosen to calculate wind vector. To diagnose, mouse clicking can monitor the first and second maximum peaks.

3.2 Height Assignment Component

The NSMC scheme does not make efforts to select targets. After monitoring a great number of cases, it is considered not necessary to select targets. Mouse clicking displays the following height assignment information:

- Maximum and minimum measurements in the tracer region
- Maximum and minimum bright temperature (BT) in the tracer region
- Correlation coefficient between IR and WV measurements
- Slope at IR—WV scatter diagram
- 5% minimum BT before and after adjustment
- IR—WV scatter diagram

IR—WV scatter diagrams are helpful at height assessment. By comparison of individual cases, appropriate thresholds are chosen to distinguish high and low clouds. In the NSMC scheme, target height assessment is performed before target height adjustment.

3.3 Quality Control Component

Although quality controls are made at the end of each component, total quality assessment is still performed. Wind velocity, wind direction, pressure level of AMVs is accessible by mouse clicking. Radiosonde data and AMV data from other centers are displayed together with NSMC AMV data. Radiosonde data are also shown in graphic form. At present, this function is not performed in real time. When radiosonde data and AMVs of other centers arrive, the AMV operation has already terminated, and the AMV products sent out. The simultaneous display function helps at diagnosing.

4. Summary

Variety of display function of the NSMC AMV derivation scheme that monitors the whole process of AMV derivation and help at improving product quality has been presented.

REFERENCES

Xu Jianmin and Zhang Qisong, 1996: Calculation of Cloud Motion Wind with GMS-5 Image in China, *The Third International Wind Workshop*, EUMETSAT, EUM P18, 45-52

Xu Jianmin, Zhang Qisong and Fang Xiang, 1997: Height Assignment of Cloud Motion Winds with Infrared and Water Vapour Channels, *Acta Meteorologica Sinica*, 55, 408-417

Xu Jianmin, Zhang Qisong, Fang Xiang and Liu Jian, 1998: Cloud Motion Winds from FY-2 and GMS-5 Meteorological Satellites, *The Fourth International Wind Workshop*, EUMETSAT, EUM P24, 41-48

SESSION V

NEW TECHNIQUES

Chairperson: J. Xu

POLAR ORBITER: STEREO HEIGHTS AND CLOUD MOTIONS

G. Garrett Campbell
CIRA/CSU
Ft. Collins CO, USA

Francois-Marie Breon
CEA/DSM/LSCE, Gif sur Yvette, France

ABSTRACT

As a demonstration, a combination of POLDER and AVHRR images were used to calculate geometric cloud heights and motions. Reproducibility of the height is 1km with the 6 km resolution pixels of Polder. This is supported by simulation studies and example real world clouds near Point Barrow in Alaska. A similar demonstration mixing POLDER and GOES is discussed. Also a comparison is made to the Oxygen A band cloud height estimates.

1. Introduction

The analysis of cloud motions in polar regions is difficult due to the lack of geosynchronous satellite observations used for this purpose in tropical and mid latitude regions. Using pairs of polar orbiters satellites will allow some estimate of motion, but additional parallax adjustments are required, so one needs to know the cloud height from a separate source. Here we discuss the use of POLDER data with the addition of one other view point to estimate cloud motion and geometric height.

The POLDER instrument concept allows the observation of the surface below up to 14 times at different view angles within 4 minutes (Deschamps et al 1994). It was originally designed for bi-directional reflectance measurements, but we are testing its use for stereo height estimates. The sequence of POLDER views were mapped into a common projection assuming the reflecting object came from the surface of the earth. Any displacement from one view to an other is due to the fact that the cloud is above the surface (parallax) or has moved (wind) between the measurement times. There is actually an ambiguity between along track motion and height above the ground so at least one additional image from a different view point is required to resolve the motion. For these tests, we use either GOES or AVHRR observations more than 10 minutes away from the mean POLDER observations.

2. Alaska case study

Figure 1 shows an image from POLDER of clouds over Alaska near Point Barrow (71^{o}N, -156^{o}W). The imaged area is roughly 1000x1000 km^2; the continent being in the lower-right corner as indicated by the coastline. The analysis proceeds by selecting a circular patch of pixels at the center time of the sequence, then correlating with the other images in the sequence. This matching was also performed with the remapped AVHRR image. The POLDER data has 6 km resolution visible pixels which would seem too large to provide stereo information, but in fact the correlation matching is able to measure the displacements to better than $\pm$ one pixel. Aligning with the edge of an extended object provides enough information to estimate positions to about $\pm$ 2 km (Campbell 1998). These apparent locations, viewpoints, and times were analyzed with the Asynchronous Stereo scheme (Campbell, 1998). This performs a least squares fit to estimate the height and motion of the object.
Shown in figure 1 are the cloud motion vectors and an estimate of the height. For instance the cloud over the land south of Point Barrow in the image is moving north at about 4km altitude. In the circle

are the corresponding winds at different heights from the Point Barrow radiosonde. That is not coincident in time, so a precise match should not be expected.

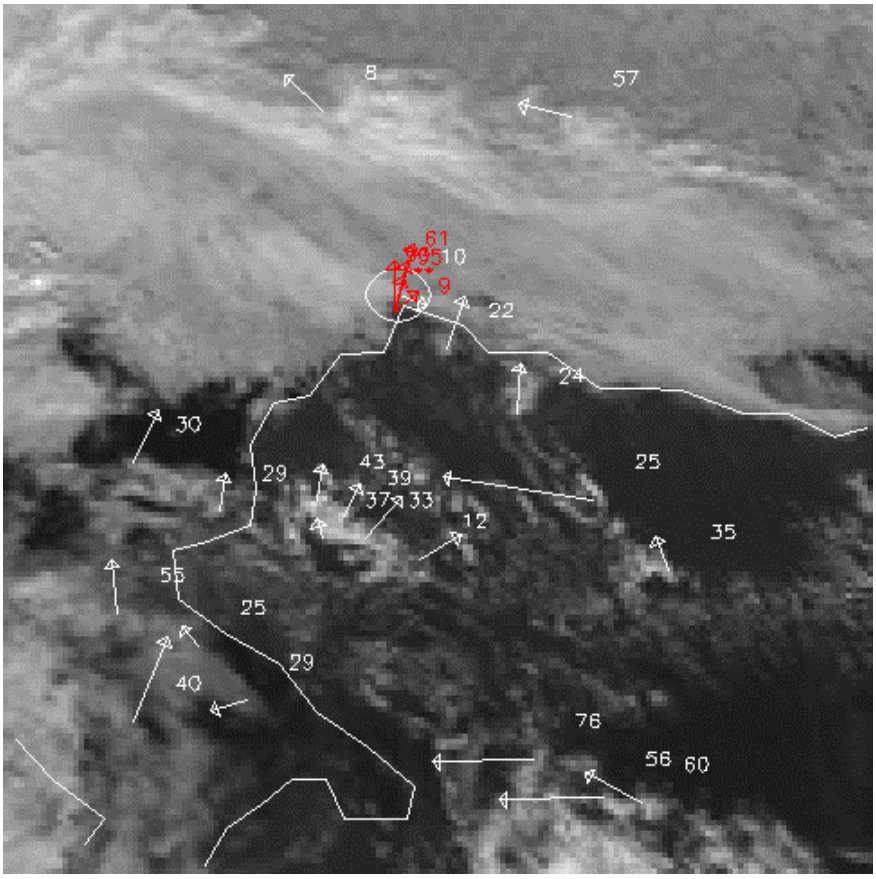

Figure 1. Image of Polder visible radiances over Alaska on June 19, 1997 at 22:30Z. Super imposed are estimate of the cloud motions and heights (hectometers). The red or black wind rose in the circle shows the Point Barrow radiosonde at 0Z, June 20.

To get some estimate of the accuracy of the measurements, some test clouds were tracked repeatedly, starting at locations offset ± one pixel east-west and north-south. Table 1 shows a list of the heights, motions and standard deviations from this boot strap reproducibility study. This is really a test of the tracking procedure and small errors in matching the clouds from the different scenes.

Table 1. Sample reproducibility test. Av = average of 5 heights, sd = standard deviation of the 5.

Averages (5 trials)			Standard Deviations (5 trials)		
Height	U (m/sec)	V (m/sec)	Height	U (m/sec)	V (m/sec)
0.73	-2.72	1.60	0.26	0.69	0.30
-0.39	0.85	3.80	0.13	0.38	0.33
3.39	0.51	7.02	0.04	0.28	0.14
4.66	3.82	5.77	0.45	0.70	1.17
2.67	-4.66	0.09	0.19	0.76	0.20
2.30	3.97	7.63	0.34	1.36	1.07
1.17	0.69	-0.87	0.24	1.87	1.13
0.45	0.70	1.17	0.49	1.30	1.26

3. Baja California case study

A second example was analyzed merging GOES and Polder viewing clouds over Baja, Mexico, figure 2. Here we were able to make a comparison with the asynchronous stereo analysis of GOES 8 plus GOES 9. This comparison of two geometric techniques is a better measure of the accuracy of the analysis. Figure 3 shows the GOES analysis, which actually appears more consistent in the cloud motions and heights than the Polder result (fig 2). The GOES data was actually mapped into the Polder projection at 6 km resolution before the analysis.

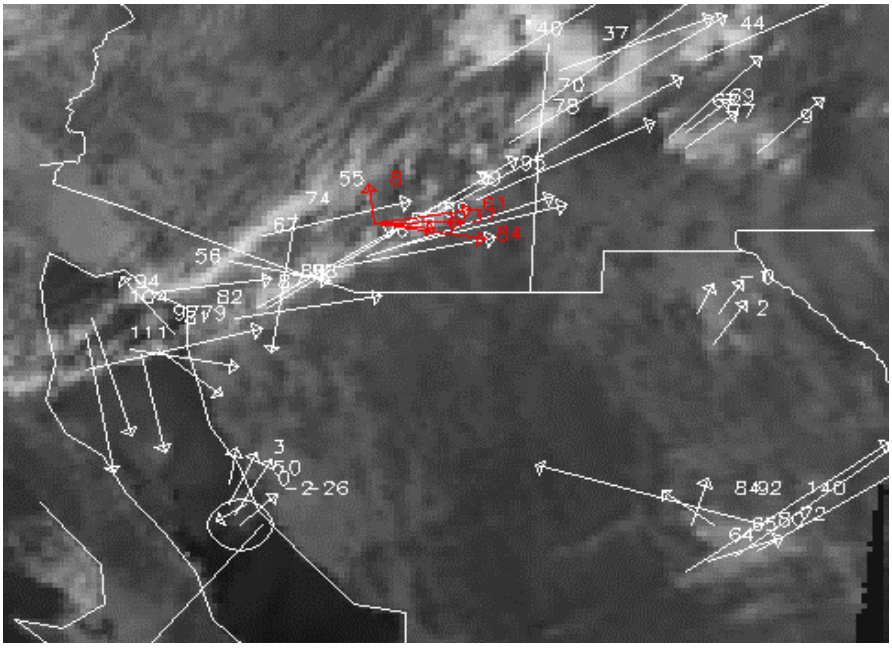

Figure 2. Polder visible radiances over Baja on April 29, 1997, 18:47Z. The heights are shown in hectometers. Notice that there is some residual motion of the islands in the Gulf of California. The Tucson sounding winds are shown in red.

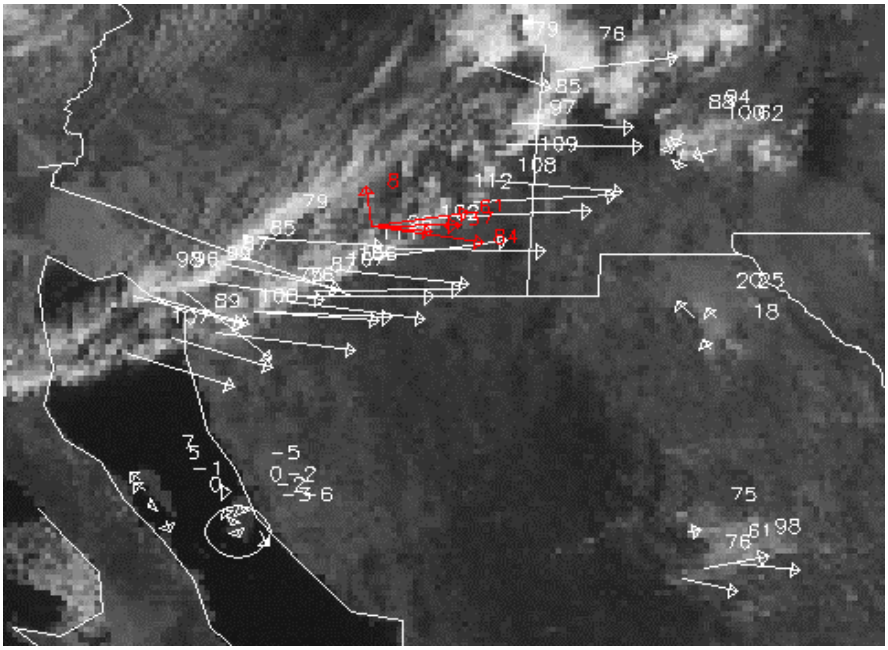

Figure 3. Image of GOES 9 visible radiances over Baja on April 29, 1997, remapped to the Polder projection. Notice that the islands in the Gulf of California do not move.

Figure 4 is the scatter diagram of the heights of the two geometric analyses over Baja. From the scatter of the heights and the variation in cloud motion vectors in figure 2, the results based on POLDER observations are not very accurate. An improvement is possible to these results by forcing the motion of the islands to zero. This is a typical problem with the geometric techniques, the accuracy of heights and motions is sensitive to small navigation errors. In many cases with pairs of GOES satellites, adjustments need to me made to force alignment in the navigation. Finding reliable landmarks to adjust the navigation in polar regions is especially difficult. Certainly, where available the GOES results would be more useful than the Polder estimates. But the primary interest in using polar orbiter data is in areas with out two geosynchronous views.

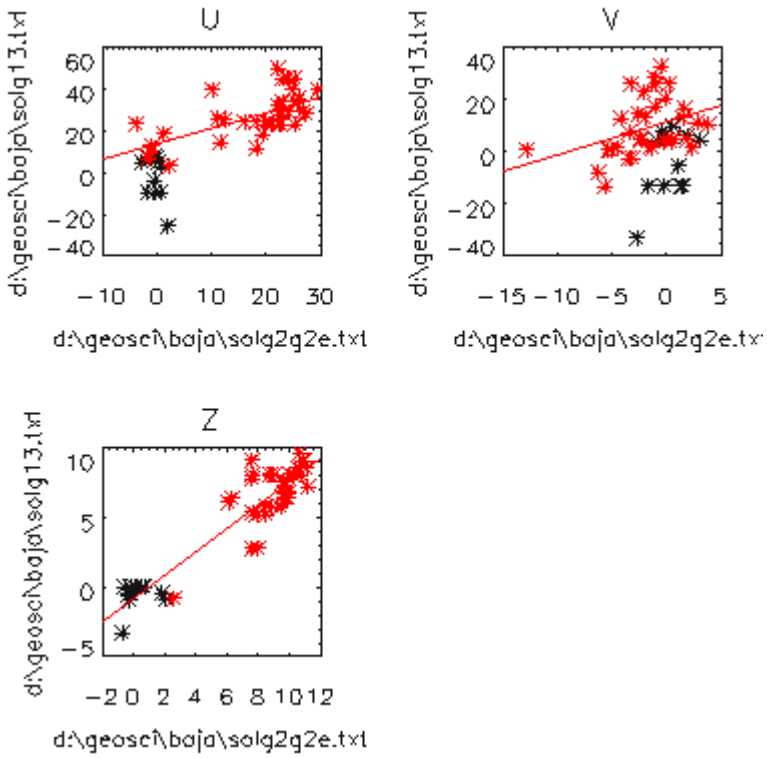

Figure 4. Scatter between GOES 8 and 9 results and Polder plus GOES 9 results. U and V are the components of the cloud motion and Z is the height (km).

4. Oxygen Heights

In addition to the bi-directional imaging capabilities of POLDER, there are two channels which measure the reflected radiance in the Oxygen A absorption band at 765 nm. The ratio of he two observed radiances provide a measure of the oxygen absorption between the satellite and the reflection surface, assumed to be a spectrally white reflector., Because the oxygen is well mixed in the atmosphere, this absorption is related to the height of the cloud (Parol et al. 1999). Figure 5 shows an image of the cloud top pressure estimate based on this differential absorption technique.

This shows some artifacts. The cirrus clouds over the Gulf of California are higher that those adjacent over the land. There is considerable variability from one view point to the next for the same cloud. It turns out that the cloud is not a simple reflecting surface. Some of the visible radiation is scattered within the cloud top and some of the radiation from ground penetrates the cloud (Parol et al. 1999). These contaminate the Oxygen absorption signals. Figure 5 is actually a composite of the minimum cloud height over the 14 views of the cloud masking some of the variability of the estimates.

Using the Tucson sounding, the pressures were converted to geometric height for comparison to the Asynchronous heights. Finally figure 6 shows a scatter plot of the geometric heights and the Oxygen heights. The Oxygen heights show considerable variability in space and from the many view points so these are the lowest heights in the region from the multiple view points.

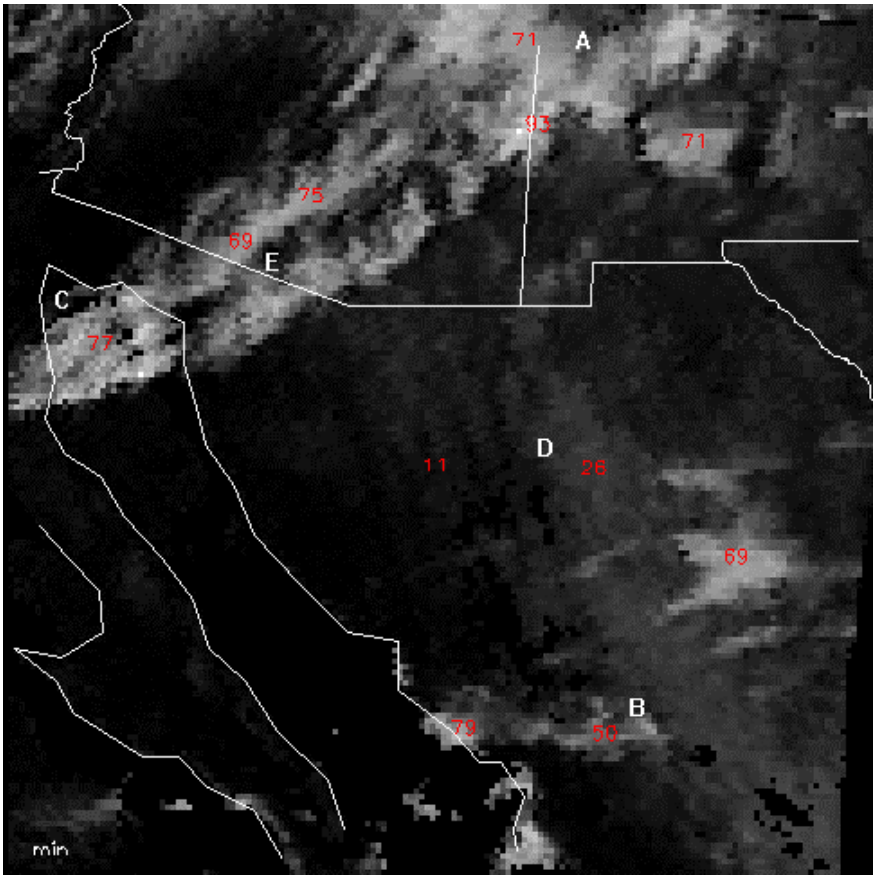

Figure 5. Image of Oxygen A band heights. The numbers are heights in hectometers derived from the Tuscon sounding. The minimum height from the 14 views of each location.

5. Discussion

The geometric cloud heights and motion have some quantitative information but high precision is not possible. Application to special case studies is possible to understand special meteorological events. There are several limits to their regular use: The pixel resolution is just barely able to detect cloud location changes. Organizing the data and verifying the navigation alignment between different satellites is not easily automated.

The standard way to estimate cloud top height is to use the cloud top temperature and a temperature profile estimate. For comparison the cloud heights in table 2 were estimated by interpolation from the Tucson sounding.

Table 2. Selected points from figure 5 analyzed several ways. Heights in km and temperature in Kelvin.

Table 2	Oxygen Z (km)	Geometric Z	GOES Temperature	Temperature > Z
A	5.6	4.7	234	9.3
B Cirrus ocean	8.6	8.6	242	8.2
C	8.0	6.8	243	8.1
D	8.5	6.9	228	10.
E	3.7	7.3	233	10.
F	7.4	5.1	242	8.2
G	7.0	6.8	243	8.1

The Oxygen A band heights show some skill but there are some artifacts with different backgrounds and cloud types. Using the geometric cloud height estimates could be used as a verification tool to better understand the variability of the Oxygen method and filter out the unphysical height estimates. These anomalous heights are an indication of other physical processes are occurring in the reflections from the cloud like multiple scattering in the cloud or transmission of light from the underlying surface.

Application of the technique to the MISR data from the TERRA satellite with its much better resolution should provide accurate geometric cloud heights.

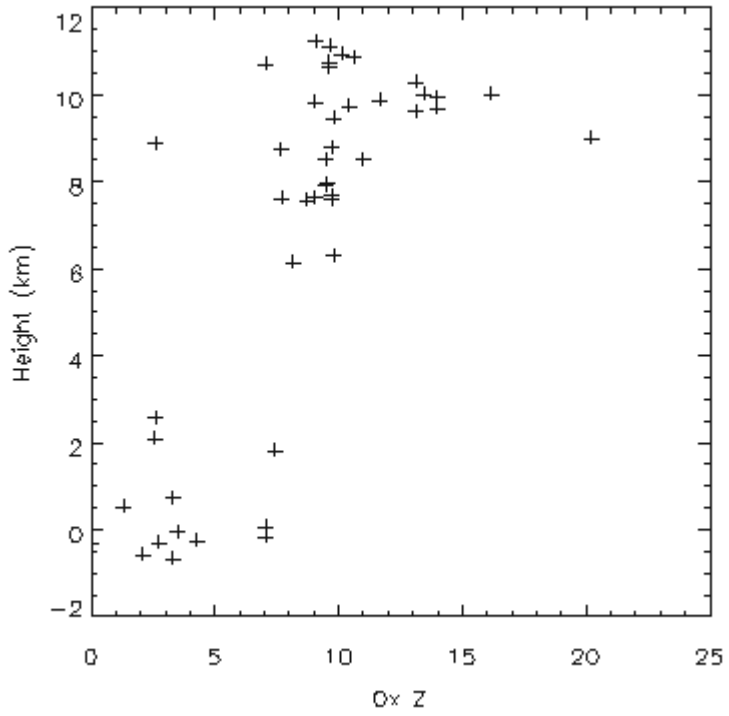

Figure 6. Comparison of geometric heights with Oxygen heights, Baja case. Asynchronous stereo height on the vertical axis and Oxygen A band cloud top pressures converted to height with a nearby sounding.

6. Conclusion

This study has shown that geometric techniques can be used with polar orbiter observations. The accuracy of the POLDER results is limited by the imager resolution and has limited information content. With smaller pixel resolution of MISR on the TERRA better results should be expected. The Oxygen results show considerable variability which demonstrates that the cloud transmission (surface contribution) and its spatial variability must be accounted for in a quantitative use of the oxygen cloud height product.

ACKNOWLEDGEMENTS

This work was supported by the Department of Defense Center for Geosciences/Atmospheric Research Agreement #DAAL01-98-2-0078. The results presented in this paper were obtained using data from CNES/POLDER onboard NASDA/ADEOS.

REFERENCES

Campbell, G.G., 1998, Asynchronous Stereo Height and Motion Analysis: Applications, *Proc. Fourth Winds Workshop*, EUMETSAT, EUM P24

Deschamps, O.Y., F.M. Breon, M. Leroy, A. Opodaire, A. Bricaud, J.C. Buriez, and G. Seze; 1994, The POLDER mission: Instrument characteristics and scientific objectives., *IEEE Trans. Geosci. Remote Sensing*, **32**, PP 598-614.

Parol, F., J-C Buriez, C. Vanbauce, P. Couvert, G. Seze, P. Goloub, and S. Cheinet, 1999, First results of POLDER "Earth radiation budget and clouds" operational algorithm, *Trans. On Geoscience and Remote Sensing*, **37**, No. 3, 1597-1612.

ON THE USE OF RAPID SCANS

Johannes Schmetz[1], Kenneth Holmlund[1],
Hans Peter Roesli[2] and Vincenzo Levizzani[3]

[1] EUMETSAT, D-64295 Darmstadt, Germany
[2] SMA, CH-6605 Locarno-Monti, Switzerland
[3] ISAO-CNR, I-40129 Bologna, Italy

ABSTRACT

Previous work on rapid scan images from geostationary satellites is summarised first. Then results from rapid scans with Meteosat-6 over the tropical region and the alpine area are reported. Wind fields from cloud and water vapour tracking in the water vapour channel (WV: 5.7 – 7.1 μm) with short interval scans are compared with the nominal 30-minute scans and generally more consistent wind fields are obtained with rapid scans. It is also shown that the upper level divergence of large scale tropical systems can be directly inferred from the wind field and that rapid scans provide higher divergence values. Finally perspectives for rapid scans from Meteosat Second Generation (MSG) are discussed.

1. Introduction

Previous work on rapid scan images from geostationary satellites has been mainly performed with GOES and GMS data. Recently rapid scans have been conducted with Meteosat-6 in support of the Mesoscale Alpine Program (MAP); preliminary results from this campaign and from test scans over the tropical belt are reported in this paper. A perspective in mind is to consider the use of the new generation of European geostationary satellites (MSG: Meteosat Second Generation) for taking images at intervals shorter than the routine scan interval of 15 minutes for the full disk. Currently image intervals of 30 minutes for full disk are considered as baseline and any shorter scan interval of the same area is considered as rapid scan. With the advent of MSG this definition becomes obsolete since 15 minute scans for the full disk become the standard. However previous work has shown that even shorter intervals are needed to properly observe convective events and short-lived clouds as tracers for the derivation of winds. Therefore this paper also discusses the use of MSG to support research on rapid scan applications in nowcasting and NWP; both may benefit from improved and more numerous atmospheric motion vectors and from a better understanding and parameterisation of deep convection.

2. Experience with Rapid Scans

Work on rapid scans from geostationary satellites has been mainly conducted by researchers in the US and by the Japan Meteorological Agency (JMA). Europe did perform rapid scans with Meteosat-1 in support of ALPEX (Alpine Experiment) in 1979, however it seems that the value of those efforts was never realised.

Hamada (1983) was among the first to suggest intervals of 15 minutes to better cope with the short lifetime and rapid deformation of cloud targets. Shenk (1991) substantiated this suggestion and provided a graphical presentation of the percent of useful tracers as a function of time interval between GOES (VAS) images. He argued that the optimum time interval for the tracking of cumulus type clouds over land is between 10 minutes and less than one minute, whereas displacement of high level cirrus clouds is fairly well depicted by the standard imaging interval of 30 minutes.

Other studies corroborate the suggestions by Shenk (1991). Uchida et al. (1991) studied low-level cloud motion winds around typhoons. They obtained winds of higher spatial density and closer to the typhoon centre when using 7.5 and 15 minutes as imaging intervals as opposed to 30-minute intervals. The 15-minute interval provides winds outside the 400 km radius from the typhoon centre whereas for the 30-minute interval the distance is 500 – 600 km. With 7.5-minute interval winds can be derived to a 200 km radius. The increase of low-level wind speed with proximity to the typhoon centre is also well depicted and increase from about 25 – 30 kts at 800 km distance to 55 kts at 200 km distance from the centre. It is important to mention that the Japan Meteorological Agency (JMA) makes a special effort to operationally derive low-level winds in the vicinity of typhoons (e.g. Takata, 1993). The cloud motion winds are used in the numerical analysis over the typhoon area and for the prediction of gale-force area winds by the forecasting division of JMA. In this context it interesting to note that the 3rd International Winds Workshop (Schmetz et al., 1997) recommended that imaging in research mode should be considered for quasi-operational application. The JMA practice to use 15-minute imagery to derive winds near typhoons was mentioned as a good example how research modes could soon become operational practice.

Work in the US on rapid scans started already in the 19-seventies. Rodgers et al. (1979) showed that high spatial resolution and short imaging intervals increase the number of low-level winds around a hurricane. The hypothesis of the work of Rodgers et al. (1979) was that low-level clouds around tropical storms are too short-lived to be tracked with standard 30- (or 15-) minute scan intervals. They derived cloud-tracked wind fields at high (200 hPa) and low altitudes (900 hPa) from rapid scans with SMS 2 at 7.5-minute intervals and with GOES-1 at 3 minute intervals, respectively, around tropical cyclones. The visible channel was used with spatial resolutions of 1, 2, 4 and 8 km. Those wind fields were compared with wind fields from 15- and 30-minute intervals: The result was that 10 (5) times as many clouds could be tracked with the rapid scans in comparison to the 30 (15) minute interval scans. They also demonstrated that the high temporal resolution necessitates a higher spatial resolution in order to get optimum results. A 2 km resolution was found adequate for low-level clouds over water. Generally, rapid scan full-resolution infrared and visible images minimised the 'incorrect winds' from tracking cloud elements which propagate by growing on one side and dissipating on the other side. Notable is also that the wind fields of Rodgers et al. (1979) had been validated with near simultaneous aircraft measurements. A similar study by Johnson and Suchman (1980) deriving winds from SMS in 1978 with 30, 15, 6 and 3 minute intervals concludes that nearly 10 times as many low-level cloud are extracted from 3 minute scans as compared to the 30 minute scans in cases of short lived clouds. They recommend scan interval of 6 – 10 minutes for the tracking of low-level clouds.

Purdom (1996) has also shown that very accurate mesoscale cloud track winds can be determined from rapid scans. Primarily he points out the much better target identification. A very interesting aspect is the use of a 'cloud or storm relative animation' which helps to identify secondary circulations around cloud systems. One minute or 30 second interval imagery provides the possibility to follow clouds even in complex weather situations.

Recently Velden et al. (2000) studied the optimal time lapse between images for different spectral channels on GOES- 10 for the derivation of winds. Generally speaking the number of winds, and quality too, increases with decreasing time intervals and increasing resolution; they found:

i) The optimum time interval for VIS images with 1 km resolution is 5 minutes
ii) For IR window images with 4 km resolution it is 10 minutes
iii) For water vapour images with 8 km resolution it is 30 minutes.

3. Rapid Scans with Meteosat-6

In preparation for and during the Mesoscale Alpine Programme (MAP, Levizzani et al. 1999) several rapid scans have been taken with Meteosat-6. Here we report on two cases of rapid scan images from the water vapour channel (WV: 5.7 – 7.1 μm) consisting each of three images: i) a rapid scan of the tropical belt from about 6.7° S to 9.5° N with 7.5-minute intervals and ii) a rapid scan over the Alpine

region from about 40.6° N to 53.5° N with 5-minute intervals. In both cases the rapid scan wind fields are compared with wind fields from standard intervals of 30 minutes. Vectors from clouds and water vapour moisture displacements were derived using the Meteosat Second Generation (MSG) prototype algorithm described in more detail by Holmlund (2000). The vectors were derived with an extraction grid of 16x16 pixels, a 24x24 pixel template and a search-area of 72x72 pixels using a standard cross-correlation technique. Overlap was confined to a maximum of 30% of the template area in order to avoid tracking of the same feature. The wind fields were quality controlled following Holmlund (1998) and vectors with are quality indicator (QI) higher than 0.2 were retained.

An attempt was also made to derive wind divergence from the vector fields. Earlier work (e.g. Schmetz et al., 1995) has shown that it is difficult to infer divergence fields directly from the wind vectors since the differentiation amplified the noisy character of the wind field. Therefore a QI-weighted Barnes filter was run over the wind vectors before computing the divergence with finite differences over areas of 3x3 grid-points as described in Holmlund (2000). The idea behind the derivation of divergence fields is to test whether this quantity can be derived in a sensible manner from rapid scans. If yes, the wind data could be used in the data assimilation of a numerical model in order to create upper level divergence fields and hence initiate model convection in the correct geographical location.

3.1 Tropical Rapid Scan

Figure 1 a and 1 b show the wind fields derived for the tropical Africa from three images with 7.5-minute intervals and 30-minute intervals, respectively. While both images indicate that the outflow of this large convective system of several hundred kilometres diameter can be derived with both scan intervals, it is clearly discerned that the rapid scan provides a more consistent wind field. The divergence derived from the rapid scan winds filtered with the Barnes scheme is shown in Figure 1c:

$$\nabla \cdot \vec{n} = -\frac{\partial w}{\partial p} \tag{1}$$

values of more 8. 10^{-5} m^{-1} are $\nabla \cdot \vec{n}$ observed. Using the relationship between horizontal wind divergence and the change of the vertical velocity ω with height pressure *p* we can estimate the mean vertical velocity in this tropical convective system from:

$$w(p) = w(p') - \int_{p'}^{p} \nabla \cdot \vec{n}\, dp \tag{2}$$

With the satellite derived divergence of: $\nabla \cdot \vec{n} = 8 \cdot 10^{-5} s^{-1}$

and the assumed boundary condition $w(p' = 100 hPa) = 0$

we obtain a vertical velocity of about 0.5 m/s at 300 hPa, which is quite a realistic value for a tropical convective system. Divergence fields have also been derived from the nominal 30-minute scans (results not shown). While the geographical pattern looks very similar to Figure 1c, the maximum value is smaller by about 15%.

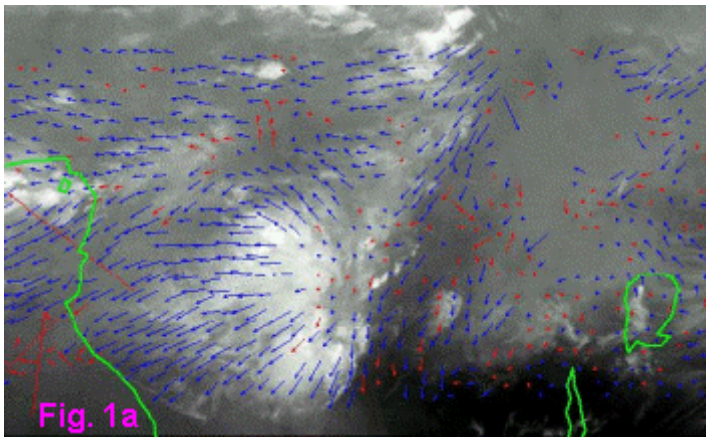

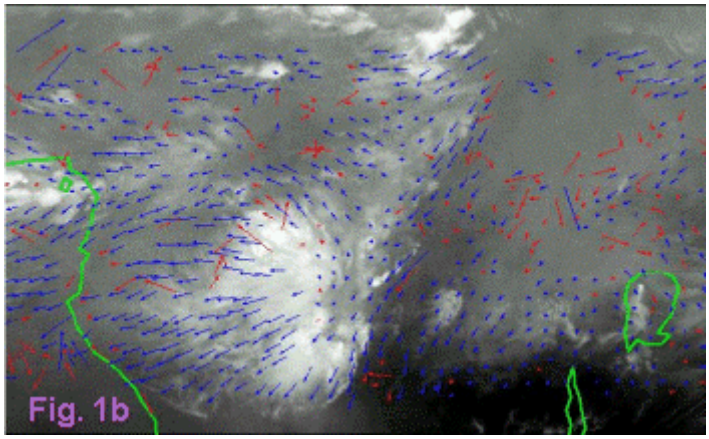

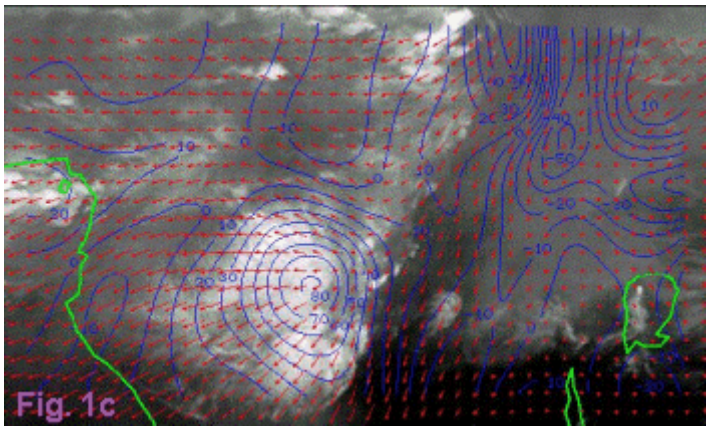

Figure 1. Wind fields derived from a triplet of WV images over tropical Africa (about 6.7° S to 9.5° N and 6.6° E to 36.1° E) from rapid scans with 7.5 minute intervals (Figure 1a) and nominal 30 minute scans (Figure 1b). Figure 1c shows the divergence field derived from Figure 1a; units are 10^{-6} s^{-1}, the maximum divergence value is higher than 8. 10^{-5} s^{-1}.

The success of the derivation of wind divergence from the wind vectors suggests that these data are useful indeed to trigger convection in the right geographical location in numerical weather prediction models. This would be clearly beneficial to the forecast models since they have deficiencies in predicting tropical deep convective systems correctly. However currently the potential benefit may be difficult to materialise because data assimilation systems do not handle the high density wind fields shown in Figures 1a and 1b. Instead they perform data thinning which may delete the information on the divergent flow.

We should also note that we tried to derive the divergence from the change of high level cloud cover A with time t:

$$\frac{1}{A}\frac{dA}{dt} = \nabla_h \cdot \bar{v} \qquad (3)$$

Unfortunately the tests did not succeed but provided unrealistic results presumably due to the high sensitivity to measurements of the cloud cover A. Further work with a finely tuned cloud classification scheme my lead to a better result. However it appears that the derivation of the divergence from the wind field is preferable anyway since it provides a continuous divergence field and not just a mean value for the whole convective system.

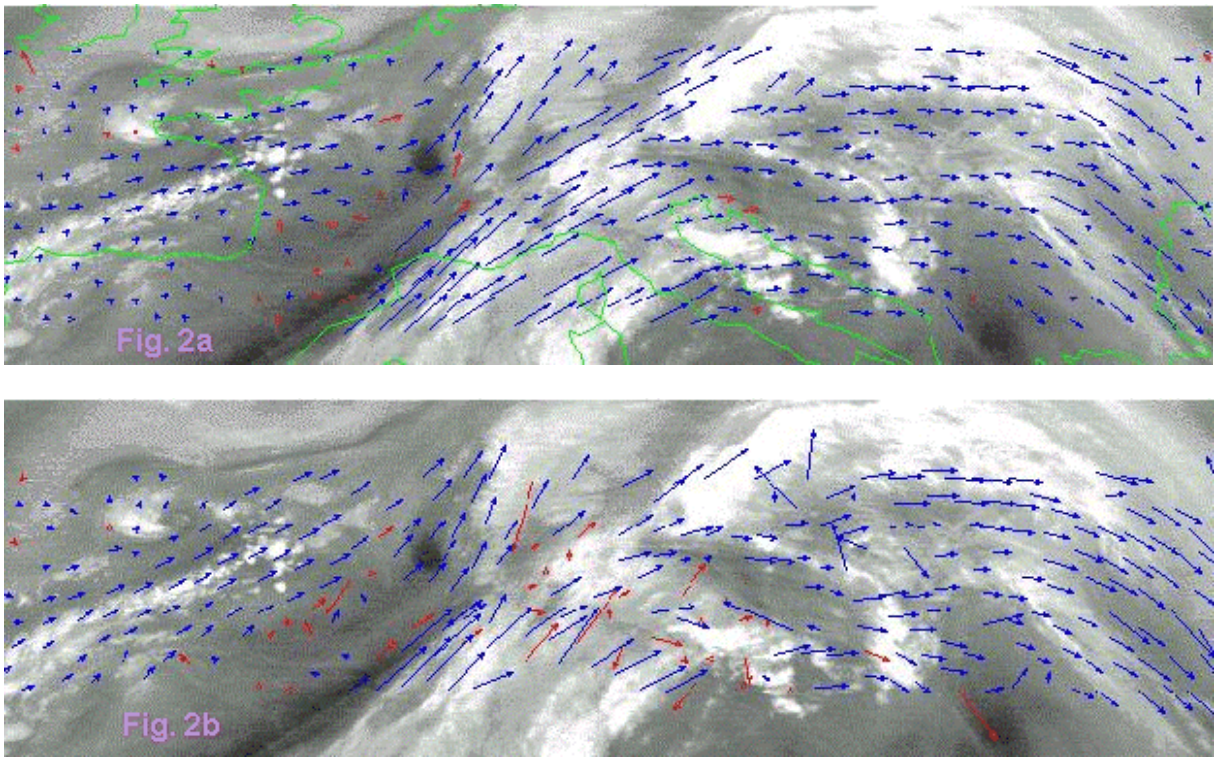

Figure 2. Wind fields derived from a triplet of WV images with rapid scans of 5 minute intervals (Figure 2a) and the nominal 30 minute scan (Figure 2b), respectively. The area covers the Alps and stretches from about 40.6° N to 53.5° N and 11.1° W to 28.5° E.

3.2 Rapid Scan for the Alpine Region

Figure 2 shows the comparison of wind fields derived from rapid scans with 5-minute intervals and 30-minute intervals, respectively. Clearly the tracking based on rapid scans (2a) provides a much better depiction of the flow. However, as the image contains cloudy and clear sky features in close proximity, which are all tracked, the flow does not correspond to one well defined altitude level. This makes the derivation of divergence fields rather difficult, which is in contrast to the tropical convective system in Figure 1 where mainly cirrus outflow has been tracked.

4. MSG Capabilities

The Meteosat Second Generation (MSG) satellite will provide 15-minute full disk imagery during nominal operations, i.e. the temporal image resolution is twice as good as for the present Meteosat satellite series. Even shorter scan periods than the nominal 15-minute repeat cycle are possible by

shortening the repeat cycle of image taking. A repeat cycle consists of a full cycle of image acquisition by the instrument, starting with the forward scan, followed by the repositioning of the scanning mirror and by the standby period where no scanning mirror motion takes place.

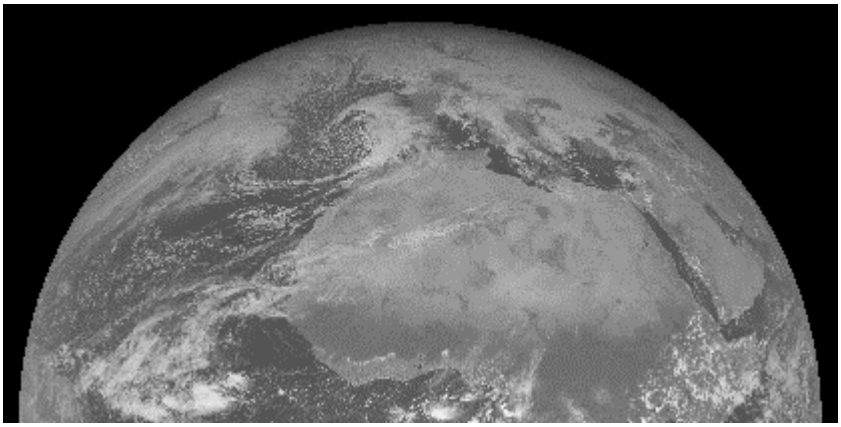

Figure 3a. Northern Hemisphere: 7’30’’ scan, i.e. 2 limited scans per 15 minutes, 1856 lines are scanned for 11 channels of MSG and 5568 lines for the HRVIS channel, which however has only half the E-W extension of the other channels.

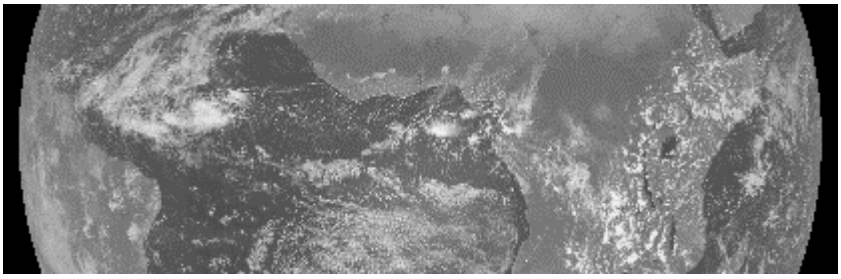

Figure 3b. Scan of tropical belt for a period of 5’, i.e. 3 limited scans per 15 minutes.

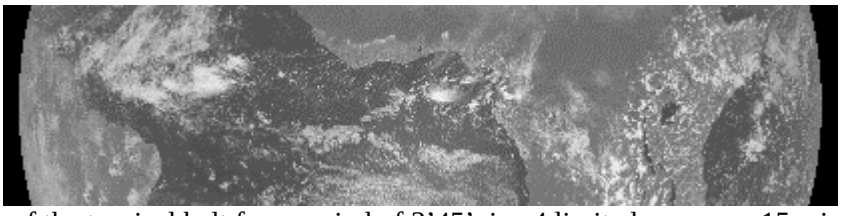

Figure 3c. Scan of the tropical belt for a period of 3’45’, i.e. 4 limited scans per 15 minutes.

For the MSG SEVIRI instrument the level 1.0 full disc images comprise 3834 by 3834 pixels for all channels except for the high-resolution visible channel, which comprises 5751 by 11235 pixels. The full disc is created within 12 minutes of forward scanning followed by a retrace and adjustment period of 3 minutes. For a limited scan a start and end line within the full disc view can be selected for the forward scan. It should be noted that a limited scan always covers the full width of a nominally scanned image line, i.e. the coverage is only limited in North-South direction. Figure 3 shows three examples of area coverage that can be obtained from MSG with different rapid scan intervals.

4.1 Science Issues to be Addressed with Rapid Scans

Geostationary satellites offer the unique possibility to observe atmospheric phenomena at time intervals that are compatible with their life cycle. As explicitly mentioned in the MSG Programme Proposal a ‘typical example for nowcasting is severe weather which has small features that undergo rapid development. This requires high spatial as well as high temporal resolution and rapid delivery of the data'. It is known that the rapid development of severe weather would require images taken at intervals of a few minutes in order to visualise the rapid changes in a comprehensible manner; generally speaking 15 minute or 30 minute intervals are not always sufficient.

In addition to the demonstrated utility of rapid scans for the derivation of winds (e.g. Velden et al., 2000), MSG could also provide data to address fundamental questions with regard to cloud development and convection or, generally speaking, the fast component of the hydrological cycle. Relevant questions are:

- It has been demonstrated that advanced cloud parameters (optical depth, cloud phase and effective particle size) can be inferred from MSG. This is very important for studies on cloud top structure that might help solving fundamental open questions (e.g. thermal structure, ice crystal injections above the storm, rotational features, waves). Will rapid scan be relevant for the study of very rapid phenomena at the cloud top?
- If the answer to the above question is yes, the question arises whether multispectral images, taken in rapid scan mode, will be relevant to operational nowcasting?
- Is the observation of rapid cloud development a good complement to observations of instability and what is the relative merit of both observations in nowcasting? Here the underlying thought is that forecasters may wish to see frequent updates of images over areas of rapid cloud development. This could complement a clear-sky instability product. Cloud development may also be a useful quantity for use in future short-range numerical forecast models.
- MSG has the potential to monitor tropical convection with rapid scans (e.g. with 7.5-minute intervals). Therefore it could be worth while to consider regular rapid scans (at least during certain periods) to conduct novel studies on tropical deep convection? Such image data and derived products could reveal important aspects of deep convection, e.g. one could observe the transition of water to ice, the outflow from convective systems and the corresponding water vapour transport. The data set could also serve as a stringent test of convective parameterisations in large scale models.
- Since rapid scans can provide better wind fields it may be useful to perform rapid scans operationally during certain times. For instance rapid scans during the Hurricane season over the tropical Atlantic could help the analysis of the early development of tropical easterly wave disturbances in numerical forecasting systems (Reed et al., 1986).

5. Conclusion

The utility rapid scans from geostationary satellites for the derivation of winds and for nowcasting application has been demonstrated by various researchers, mainly in the US and in Japan (see section 2). Europe has made little effort to utilise the potential of rapid scans until the most recent use of Meteosat-6 to support MAP in 1999 (Levizzani et al., 1998). This may be understood by the particular weather prevailing in Europe that often does not call for short interval observation of rapidly changing convective systems. However, it appears that the advantage of rapid scans for the derivation winds from short-lived clouds would already justify the scheduling of rapid scans (e.g. Velden et al., 2000).
With the advent of MSG multispectral images of rapidly developing convective systems might cast new light on our understanding of this part of the hydrological cycle. Specific questions are spelled out in section 4.1.

The paper has also shown that wind fields derived from rapid scans over the tropical belt and over the alpine region provide better and spatially more consistent wind fields, thus confirming results of earlier work. A novel result is the direct derivation of divergence fields of large scale tropical systems from the tracked wind field. Realistic divergence features with maxima above 8.10^{-5} s^{-1} have been obtained, whereby the rapid scan results provide 15 % higher divergence values than the nominal rapid scan intervals of 30 minutes. It is argued that the use of such high density winds (without data thinning) in numerical data assimilation systems for NWP would help the analysis and forecasting of large scale convective cloud systems.

REFERENCES

Hamada, T. (1983): On the optimal time-interval of satellite image acquisition for operational cloud motion wind derivation. Met. Center Technical Note, No. 7, 79 - 87.

Holmlund, K., 1998: The utilisation of statistical properties of satellite-derived atmospheric motion vectors to derive quality indicators. *Wea. Forecasting*, **13**, 1093 –1104.

Holmlund, K., 2000a: The Atmospheric Motion Vector Retrieval Scheme for Meteosat Second Generation. *Proceedings of the 5th International Winds Workshop*, Lorne, Australia

Holmlund, K., 2000b: The use of Observations error as an extension to Barnes interpolation scheme to derive smooth instantaneous vector fields from satellite-derived Atmospheric Motion Vectors. *Proceedings of the 5th International Winds Workshop*, Lorne, Australia.

Johnson, G. and D. Suchman, 1980: Intercomparison of SMS wind sets: A study using rapid-scan imagery. *Mon. Wea. Rev*., **108**, 1672 - 1688.

Levizzani, V., 1998: METEOSAT rapid scan during MAP-SOP. MAP Newsletter, 8

Purdom, J., 1996: Detailed cloud motions from satellite imagery taken at thirty second and three minute intervals. *Proceedings of the 3rd International Winds Workshop*, Ascona, Switzerland, 10 - 12 June 1996, EUM P-1. , pp. 137 - 145.

Reed, R. J., A. Hollingsworth, W. A. Heckley and F. Delsol, 1986: An evaluation of the performance of the ECMWF operational forecasting system in analysing and forecasting tropical easterly wave disturbances. Part 1: Synoptic investigation. Technical Report No. 58, ECMWF.

Rodgers, E., R. C. Gentry, W. Shenk and V. Oliver, 1979: The benefits of using short interval satellite images to derive winds for tropical cyclones, *Mon. Wea. Rev*., **107**, 575-584.

Shenk, W. E., 1991: Suggestions for improving the derivation of winds from geosynchronous satellites. Special Issue on Operational Satellites: Sentinels for the monitoring of climate and global change. *Global and Planetary Change*, **4**, 165-171.

Schmetz, J., C. Geijo, W. P. Menzel, K. Strabala, L. van de Berg, K. Holmlund and S. Tjemkes, 1995: Satellite observations of upper tropospheric relative humidity, clouds and wind field divergence. *Contrib. Atmosph. Physics*, **68**, 345 - 357.

Schmetz, J., H. P. Roesli and W. P. Menzel, 1997: Third International Winds Workshop (Meeting summary), *Bull. Amer. Meteor. Soc*., **78**, 893 – 896.

Takata, S., 1993: Current status of GMS wind and operational low-level wind derivation in a typhoon vicinity from short-time interval images. *Proceedings of the 2nd International Winds Workshop,* Ascona, Switzerland, 13 - 15 December 1993, EUM P-14, pp. 29 – 36.

Uchida, H., T. Oshima, T. Hamada, and S. Osano, 1991: Low-level cloud motion wind field estimated from GMS short interval images in typhoon vicinity. *Geophys. Mag*., **44**, 37-50.

Velden, C. S., D. Stettner and J. Daniels, 2000: Wind vector fields derived from GOES rapid-scan imagery. *Proceedings of the 10th Conference on Satellite Meteorology and Oceanography*. 9 – 14 January 2000, Long Beach California, American Meteorological Society, pp.20 - 23.

INVESTIGATIONS OF CROSS-CORRELATION AND EUCLIDEAN DISTANCE TARGET MATCHING TECHNIQUES IN THE MPEF ENVIRONMENT

Greg Dew[@] And Ken Holmlund[#]

[@]Logica
[#]EUMETSAT

ABSTRACT

Cross-Correlation and Euclidean Distance are two of the most common statistical techniques used for target matching. Calculation of the Cross-Correlation can be carried out in both the spatial and Fourier domain. Significant performance benefits are achieved by computing the Fourier domain Cross-Correlation using the Mixed Radix Fast Fourier Transform (FFT). This paper provides further results of a comparison of these techniques undertaken in the Meteorological Product Extraction Facility (MPEF) environment, by comparing the displacement vectors derived from pseudo-real imagery data, including analysis of behaviour in different contrast regions. The results show that the two techniques are well matched.

In assessing the relative benefits of alternative matching techniques, this paper additionally provides results for the Euclidean Distance method. It includes comparison with Cross-Correlation of the displacement vectors in different contrast regions and analyses where maximum discrepancy is observed between the two methods. The results indicate that differences between the two techniques are more apparent in lower contrast regions.

1. Introduction

The Meteorological Product Extraction Facility (MPEF) is being developed as part of the Meteosat Second Generation (MSG) Ground Segment. The Atmospheric Motion Vector (AMV) product, generated as part of the MSG MPEF, poses the highest CPU load. For calculating AMV there are three target matching techniques available; Cross-Correlation in the spatial domain, Cross-Correlation in the Fourier domain, and Euclidean Distance. Dew and Holmlund (1998) introduced the Mixed Radix Fast Fourier Transform (FFT) technique to be used for carrying out Cross-Correlation in the Fourier domain. This technique was shown to have significant performance benefits over the spatial domain method, and a preliminary comparison was undertaken of the wind vectors produced with the two techniques in the MPEF environment. This paper provides further comparisons, using simulated MSG MPEF data for 3 channels: WV6.2, VIS0.6 and IR10.8. It also carries out a similar comparison of the spatial domain Cross-Correlation and Euclidean Distance methods, with the view to isolating conditions under which the behaviour of the two techniques diverge.

Section 2 provides a theoretical overview of the target matching techniques, highlighting the performance benefits of the Mixed Radix FFT, and predicting potential differences in behaviour between the Euclidean Distance and Cross-Correlation methods. Section 3 analyses the two Cross-Correlation techniques, and compares the spatial domain and Mixed Radix FFT methods for a series of wind vectors generated from simulated MSG channel data, investigating potential areas of discrepancy across different contrast regions. Section 4 concentrates on comparing the spatial domain cross-correlation and Euclidean distance methods, using similar analysis criteria as for Section 3. Section 5 assesses the conclusions of the work carried out so far and provides recommendations for further investigations.

2. Overview of MSG MPEF target tracking techniques

2.1 Cross-Correlation

Cross-correlation is one of the standard statistical techniques used for target matching. Given a target area denoted by T and a search area by S, for a square target size, with side length N_T, the total number of pixels used to compute one correlation value is $N = N_T^2$. If the pixels within the target area are identified by (m,n) and the target location within the search area by (i,j), such that the target is always fully contained within the search area, then T_{mn} and $S_{i+m,j+n}$ uniquely identify pixel count values within the target and search areas. The cross-correlation between T and S can be normalised to prevent false correlation peaks arising from changes in the search area local means, and any local additive bias differences can also be removed. The expression for the cross-correlation is expanded to produce the cross-correlation coefficient defined by:

$$r_{ij} = \frac{\sum_{m=1}^{N_T}\sum_{n=1}^{N_T}\left(T_{mn}-m_T\right)\left(S_{i+m,j+n}-m_{Sij}\right)}{\left[\sum_{m=1}^{N_T}\sum_{n=1}^{N_T}\left(T_{mn}-m_T\right)^2\right]^{1/2}\left[\sum_{m=1}^{N_T}\sum_{n=1}^{N_T}\left(S_{i+m,j+n}-m_{Sij}\right)^2\right]^{1/2}} \qquad (1)$$

where

$$m_T = \frac{1}{N_T}^2 \sum_{m=1}^{N_T}\sum_{n=1}^{N_T} T_{mn} \quad \text{and} \quad m_{Sij} = \frac{1}{N_T}^2 \sum_{m=1}^{N_T}\sum_{n=1}^{N_T} S_{i+m,j+n}$$

The cross-correlation can also be implemented in the Fourier Domain by three Fourier transforms. Before normalisation and biases are removed, equation (1) can be expressed by :

$$R_{ij} = \left[F^{-1}\left\{F(S)F^*(T)\right\}\right]_{ij} \qquad (2)$$

Dew and Holmlund (1998) showed that a Mixed Radix FFT implementation is considerably more efficient than the traditional Radix-2 FFT, and the performance benefits compared to the spatial domain Cross-Correlation method are also significant (CPU load is approximately 60% for a 16/72 target/search area combination, and 20% for a 32/96 target/search area). In assessing the relative quality of the wind vectors produced for the two Cross-Correlation methods, results using real water wapour imagery (Dew and Holmlund, 1998) indicated a strong correlation between the Mixed Radix and the spatial domain correlation. Further results are provided in this paper in Section 3.

2.2 Euclidean Distance

The alternative template matching technique, Euclidean Distance or Sum of Squared Distance (SSD) can be expressed using the same terms and expressions as above to give an SSD coefficient:

$$ssd_{ij} = \frac{1}{N_T}^2 \sum_{m=1}^{N_T}\sum_{n=1}^{N_T}\left(S_{i+m,j+n}-T_{mn}\right)^2 \qquad (3)$$

While the the maximum of the correlation surface described in (1) provides the best match, it is the minimum of the SSD surface in (3) which gives the best target location. Equation (3) can be expanded, so that minimising the *ssd* surface is equivalent to maximising the expression:

$$pseudo\_ssd_{ij} = 2\sum_{m=1}^{N_T}\sum_{n=1}^{N_T} S_{i+m,j+n}T_{mn} - \sum_{n=1}^{N_T} S_{i+m,j+n}^{\ 2} \qquad (4)$$

By introducing the bias and normalisation terms to T and S, which are used to expand the Cross-Correlation term into (1), the ΣS^2 term in (4) becomes invariant and the *pseudo-ssd* surface simply equates to the

correlation surface of (1). Hence, the relative performance of the Euclidean Distance and Cross-Correlation matching techniques can be addressed by considering the affect of the normalisation and bias terms. The use of normalisation terms and removal of image biases have been shown to significantly improve the Cross-Correlation performance. The use of normalisation would be expected to be especially beneficial in high contrast search areas in which the search area local means are variable. In low contrast search areas, however, where the correlation surface has shallow slopes and a broad maxima, this may not be so important. In these cases, normalisation may degrade the accuracy of the surface peak location (in the limiting case of no contrast, the Cross-Correlation expression becomes undefined). It is possible that the Euclidean Distance technique will yield better quality results in these regions. This is investigated in this paper in Section 4.

3. Comparison of cross-correlation techniques

3.1 Criteria for Analysis

Dew and Holmlund (1998) provided preliminary results of investigations into validating the Mixed Radix FFT method against the spatial domain technique in the MPEF environment. Further results are presented for a series of wind vectors generated over the Earth's globe from simulated MSG MPEF WV6.2, IR10.8 and VIS0.6 channels. A statistical analysis has been undertaken for each channel which lists the number of vectors, speed bias, mean vector difference, RMS vector difference, mean speed , normalised RMS (RMS difference/mean speed) and mean search area contrast. The search area contrast associated with each target is defined in units of counts as the difference between the maximum and minimum local mean within the search area centred on the target. The statistics are also presented for three quality indices - all vectors, vectors with a quality index above 0.3, and vectors with a quality index above 0.6. A statistical analysis of the differences is carried out for the WV6.2 channel, highlighted in two histogram representations which respectively concentrate on separating the direction differences (degrees) and the speed differences (m/s) of the 24999 generated wind vectors into classes.

A further statistical analysis is undertaken to investigate the relative behaviour of the two techniques in different contrast regions, which concentrates on the WV6.2 channel. This is summarised into a histogram representation which separates into contrast regions the normalised RMS for the three quality indices. In addition, differences between the speed bias, mean vector difference, RMS difference and mean speed in a low and high contrast region are provided, and relative numbers of high quality winds for the two techniques in each region are also assessed.

3.2 Results and Discussion

3.2.1 General

Figure 1 provides an example to illustrate the observation that there is very good correspondence between the spatial domain and the Mixed Radix FFT technique. The FFT vectors are plotted in red and the spatial domain vectors are overlaid in yellow. Hence, where there is very good correspondence, the FFT vectors are obscured by those produced by the spatial domain technique. Each wind vector starts at the same point for the two techniques (i.e. target selection is independent of matching technique).

Figures 2 and 3 and Table 1 detail the statistics, which show that in over 80% of cases there is less than 0.1 m/s speed difference and in over 90% of cases there is less than 1.0 degree direction difference. As the quality index rises, the two methods further converge. Table 1 shows that the normalised RMS is reduced for the higher quality threshold. The table also shows that the normalised RMS is highest for the channel (WV6.2) in which the contrast is lowest. This has led to further analysis of the WV6.2 channel derived vectors in different contrast regions.

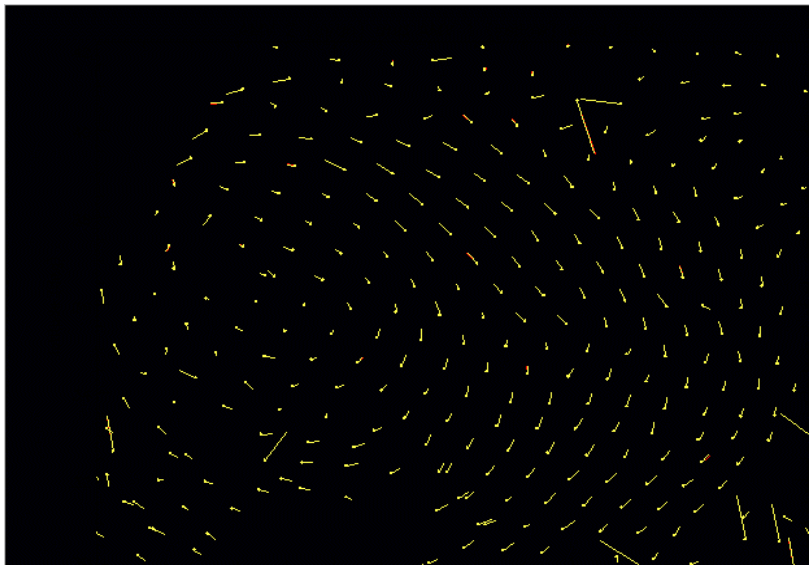

Figure 1. High Level View of a Wind Field (WV6.2) (Yellow: Spatial Domain Red: Mixed Radix FFT).

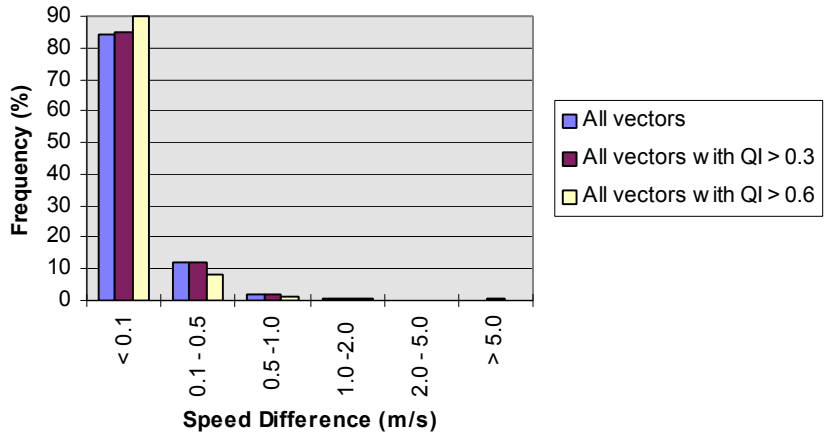

Figure 2. Frequency of Vectors in Speed Difference Classes (WV6.2) (Cross-Correlation Spatial Domain vs Mixed Radix Fourier Domain).

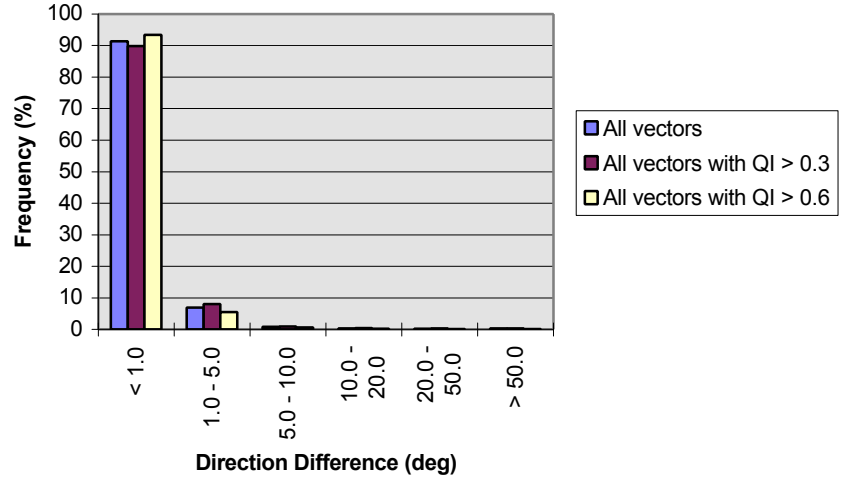

Figure 3. Frequency of Vectors in Direction Difference Classes (WV6.2) (Cross-Correlation Spatial Domain vs Mixed Radix Fourier Domain).

Table 1. Vector Difference Statistics (Cross-Correlation Spatial Domain vs Mixed-Radix Fourier Domain)

Channel	Quality	No of vectors	Speed bias	Mean vecdiff	RMS vecdiff	Mean speed	NRMS	Mean contrast
WV6.2	All	24999	0.00	0.22	2.22	23.95	0.093	76.62
	QI > 0.3	17609	0.02	0.21	1.87	18.62	0.101	79.03
	QI > 0.6	7225	0.01	0.12	1.19	16.79	0.071	88.21
IR10.8	All	17827	-0.00	0.04	0.39	14.04	0.028	260.01
	QI > 0.3	14105	-0.00	0.04	0.37	11.01	0.034	252.69
	QI > 0.6	8486	0.00	0.03	0.09	9.65	0.010	220.93
VIS0.6	All	19230	0.00	0.02	0.07	11.45	0.006	380.19
	QI > 0.3	15866	-0.00	0.02	0.04	9.06	0.005	381.79
	QI > 0.6	10247	0.00	0.01	0.03	7.76	0.004	370.67

3.2.2 Search Area Contrast

For all of the contrast regions, there is virtually no difference in the number of vectors above quality thresholds of 0.3 and 0.6 produced by the two techniques. Figure 4 shows how the normalised RMS varies across contrast regions. It indicates that for all vectors the normalised RMS decreases as the contrast increases, but this trend is reversed in the 150 -300 contrast region. The lowest contrast region (0- 25) produces the highest normalised RMS and the contrast region 100 -150 produces the lowest. Table 2 shows the vector difference statistics for these two regions.

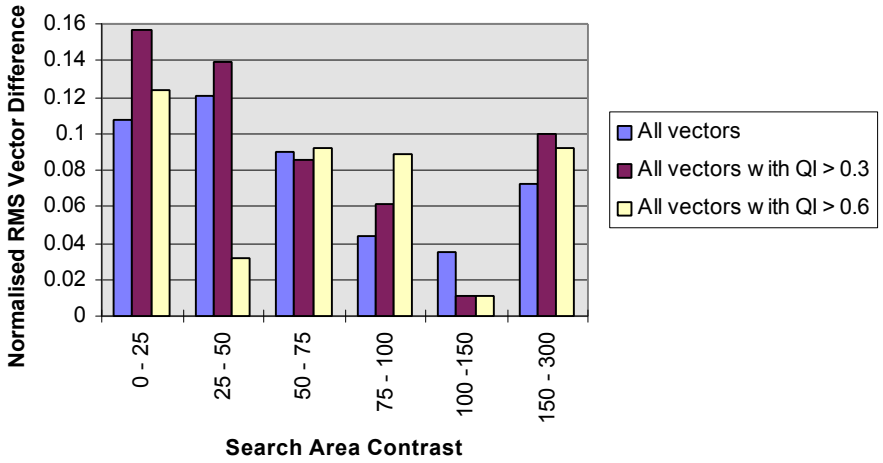

Figure 4. Normalised RMS Vector Difference in Search Area Contrast Classes (WV6.2)
(Cross-Correlation Spatial Domain vs Mixed-Radix Fourier Domain)

Table 2. Search Area Contrast Vector Difference Statistics (Cross-Correlation Spatial Domain vs Mixed-Radix Fourier Domain) (WV6.2)

Contrast	Quality	No of vectors	Speed bias	Mean vecdiff	RMS vecdiff	Mean speed	NRMS
0-25	All	1346	0.05	0.39	2.91	27.15	0.107
	QI > 0.3	865	0.05	0.44	3.21	20.50	0.156
	QI > 0.6	153	-0.04	0.31	2.01	16.22	0.124
100-150	All	4607	-0.00	0.08	0.71	19.90	0.036
	QI > 0.3	3517	0.00	0.06	0.19	16.64	0.011
	QI > 0.6	1932	0.00	0.05	0.17	15.73	0.011

4. Comparison of cross-correlation with Euclidian Distance technique

4.1 Criteria for Analysis

The criteria used for analysing differences between the Cross-Correlation (spatial domain) and Euclidean Distance techniques are identical to those used to compare the Mixed Radix FFT technique, hence are described in Section 3.1.

4.2 Results and Discussion

4.2.1 General

Figures 5 and 6 and Table 3 detail the statistics, which emphasise differences between the Cross-Correlation and Euclidean Distance techniques. In over 90% of cases there is greater than 0.1 m/s speed difference, and in over 35% of cases there is greater than 5 m/s speed difference. In over 80% of cases there is greater than 1.0 degree direction difference, and in over 25% of cases there is greater than 50 degree direction difference. The discrepancy reduces as the quality threshold increases. For a 0.6 quality threshold the distribution of speed and direction differences is more even, but 50% of vectors have a speed difference above 1.0 m/s and a direction difference above 5.0 degrees.

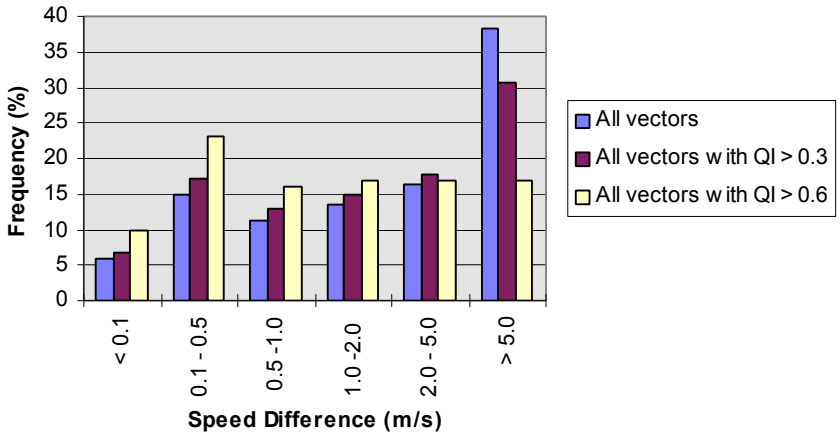

Figure 5. Frequency of Vectors in Speed Difference Classes (WV6.2) (Cross-Correlation vs Euclidean Distance).

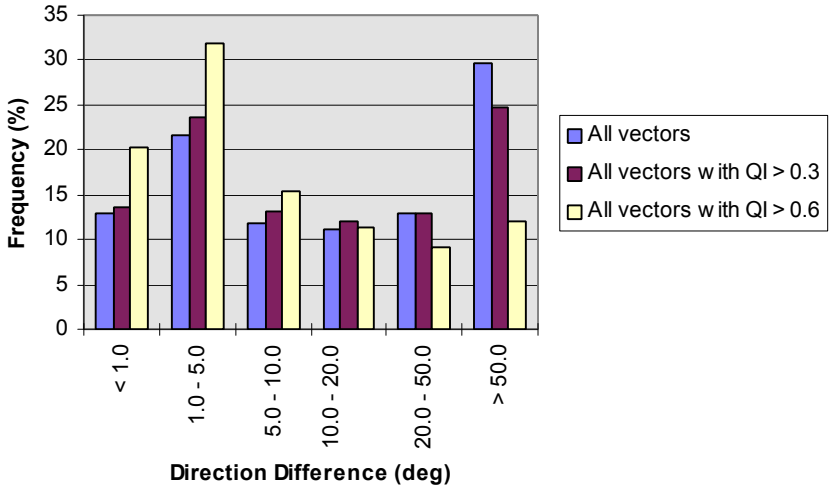

Figure 6. Frequency of Vectors in Direction Difference Classes (WV6.2) (Cross-Correlation vs Euclidean Distance).

Table 3. Vector Difference Statistics (Cross-Correlation Spatial Domain vs Euclidean Distance)

Channel	Quality	No of vectors	Speed bias	Mean vecdiff	RMS vecdiff	Mean speed	NRMS	Mean contrast
WV6.2	All	24999	-4.72	18.13	31.46	23.95	1.314	76.62
	QI > 0.3	17609	-1.29	12.78	24.26	18.62	1.303	79.03
	QI > 0.6	7225	-0.05	6.89	16.55	16.79	0.985	88.21
IR10.8	All	17827	0.14	8.23	21.08	14.04	1.501	260.01
	QI > 0.3	14105	1.37	5.80	16.49	11.01	1.497	252.69
	QI > 0.6	8486	1.43	3.19	10.94	9.65	1.134	220.93
VIS0.6	All	19230	1.86	9.30	24.63	11.45	2.151	380.19
	QI > 0.3	15866	2.70	6.64	20.01	9.06	2.208	381.79
	QI > 0.6	10247	2.26	3.69	14.89	7.76	1.919	370.67

For low quality vectors the results would not be expected to be significantly divergent for the Cross-Correlation spatial domain and Mixed Radix techniques because the respective correlation surfaces would be virtually identical. However, by definition, the Cross-Correlation and Euclidean Distance surfaces are different and, in cases where they are both ill-defined, are likely to produce significantly different maxima/minima locations. Hence, it would be expected that for low quality vectors the results would be significantly divergent, and hence affect the overall statistics.

The results are more convergent for higher quality vectors, but by focusing on a small region, Figure 7 illustrates the discrepancies between the two techniques, even in well defined wind fields. The Euclidean Distance vectors are plotted in red and the Cross-Correlation vectors are overlaid in yellow. Where there is very good correspondence, the Euclidean Distance vectors are obscured by the Cross-Correlation vectors. Figure 7 highlights the small direction and speed differences, where the speed bias is -0.22 and the Normalised RMS Vector Difference is 1.420. (Filtering out vectors below a quality of 0.6 leads to a speed bias of -0.59 and a Normalised RMS Vector Difference of 0.169). Hence, these results illustrate the differences between the two techniques even for well defined wind fields and high quality vectors.

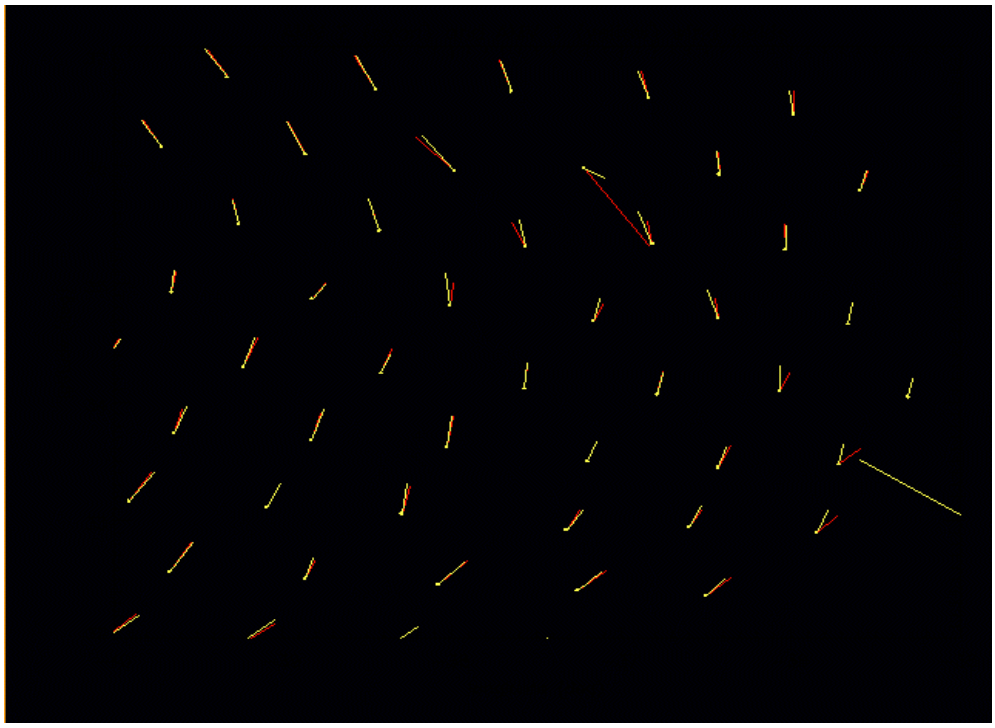

Figure 7. Low Level View of a Wind Field (WV6.2) (Yellow: Cross Correlation Red: Euclidean Distance) (All wind vectors).

4.2.2 Search Area Contrast

Figures 8 and 9 summarise the relative behaviour of the two techniques in different search area contrast regions. The Euclidean Distance technique generally produces more vectors with a quality index above 0.3 and 0.6 than the Cross Correlation technique (as opposed to the Mixed Radix FFT technique in which the numbers are virtually identical). This is illustrated in Figure 8 which shows the percentage difference in number of Euclidean Distance vectors, compared with Cross-Correlation, above the quality index thresholds of 0.3 and 0.6. It should be noted that when the quality index threshold is zero, the vector numbers will be identical. Figure 8 also shows that as the search area contrast decreases, the percentage difference increases, i.e. the relative quality of the Euclidean Distance vectors compared to Cross Correlation is greater for the lower contrast regions. Figure 9 further supports this view by showing that the Normalised RMS Vector Difference increases as the search area contrast decreases. Table 4 shows the vector difference statistics for the highest and lowest contrast regions to illustrate this point.

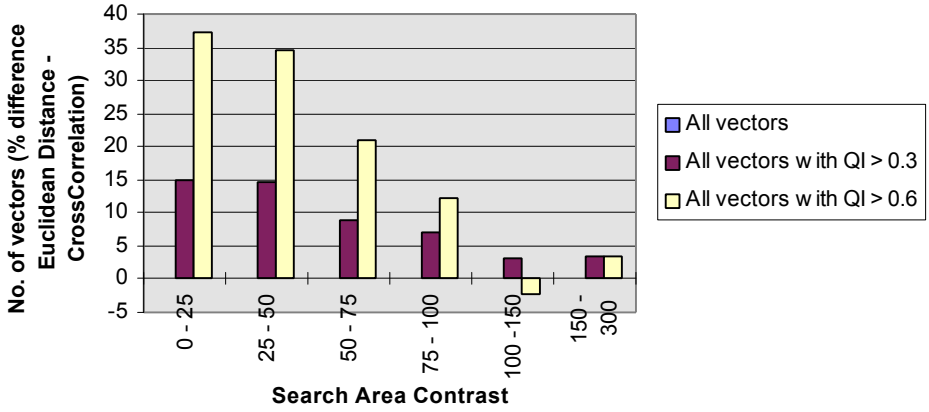

Figure 8. Percentage Difference in No. of Euclidean Distance to Cross Correlation Vectors.

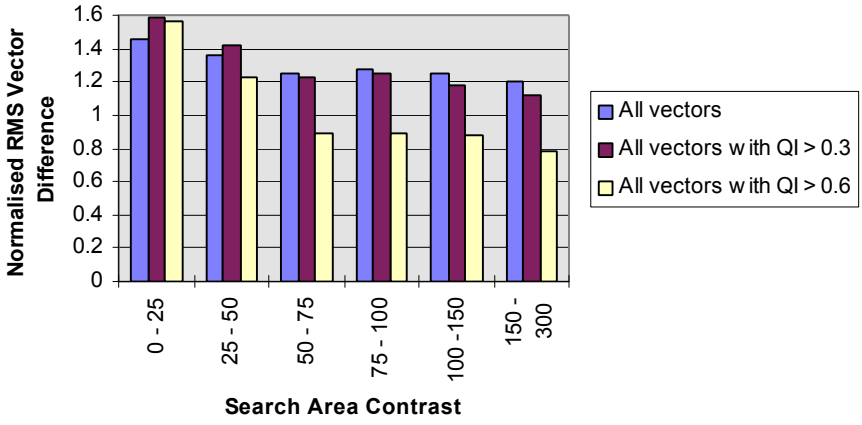

Figure 9. Normalised RMS Vector Difference in Search Area Contrast classes (WV6.2) (Cross-Correlation Spatial Domain vs Euclidean Distance).

Table 4. Search Area Contrast Vector Difference Statistics (Cross-Correlation Spatial Domain vs Euclidean Distance) (WV6.2)

Contrast	Quality	No of vectors	Speed bias	Mean vecdiff	RMS vecdiff	Mean speed	NRMS
0-25	All	1346	-5.60	29.06	39.53	27.15	1.456
	QI > 0.3	865	-0.10	22.39	32.49	20.50	1.585
	QI > 0.6	153	2.62	14.91	25.42	16.22	1.568
150-300	All	1860	-2.16	9.72	21.23	19.90	1.198
	QI > 0.3	1411	-0.57	7.23	16.46	14.68	1.121
	QI > 0.6	664	-0.05	3.95	10.26	13.05	0.787

5. Conclusions and recommendations

This paper has provided a comparison of three template matching techniques which are to be available for operational use in the MSG MPEF environment. The paper is essentially split into two areas. Firstly, validation of the Cross-Correlation Fourier domain Mixed Radix FFT technique has been carried out against the spatial domain method. Secondly, investigations have been undertaken into the performance of the Euclidean Distance technique compared to the Cross- Correlation spatial domain method.

The Mixed Radix FFT technique was introduced and validation commenced by Dew and Holmlund (1998). Further validation has since been undertaken for a large wind vector set using simulated MSG MPEF data, concentrating in particular on the WV6.2 channel. The results confirm a much stronger correlation between the Mixed Radix FFT and spatial domain methods. Preliminary investigations have been carried out into how the relative behaviour of the two techniques varies over different contrast regions. These suggest some small differences between the two techniques in lower contrast regions. However more investigations need to be undertaken before any constructive prognosis can be made.

Comparison of the Euclidean Distance technique to Cross-Correlation has been undertaken using the same simulated MSG MPEF data set, and also concentrating on WV6.2. The results show differences between the two techniques. This is best illustrated when analysing regions which produce good quality wind fields for both techniques, yet show minor discrepancies in wind speed and direction for a significant proportion of vectors. A strong correlation exists between search area contrast and the relative behaviour of the two techniques. As the contrast reduces, the Euclidean Distance technique produces a relatively larger number of high quality wind vectors compared to Cross Correlation. The divergence of wind speed and direction between the two techniques also increases as the contrast reduces.

It is important to emphasise that these investigations need to be taken forward by analysing real imagery data. Discrepancies between the two Cross-Correlation techniques may be exaggerated in the presence of noisy data, and this may provide a more decisive insight into possible variation with contrast. Similarly, in comparing the Euclidean Distance and Cross-Correlation techniques, the use of real imagery data would be a necessary validation procedure. It would also be prudent to investigate methods of statistically analysing future results with the aim of focusing on regions of interest and specific discrepancies in techniques.

This paper has assessed areas of discrepancy between the three matching techniques and the eventual aim is to achieve an understanding of which techniques are more beneficial in certain environments, hence enabling more intelligent selection in operational use.

REFERENCES

Dew, G. and Holmlund K., 1998: Improved Computing Efficiency in the Fourier Domain. Proc. Of the Fourth International Winds Workshop 20 - 23 October 1998, Saanenmoser, Switzerland. EUMETSAT EUM P 24, 289 - 298. [Available from EUMETSAT]

TRACKING LOW-LEVEL CLOUDS OVER LAND ON METEOSAT IMAGES

André Szantai, Françoise Désalmand, Michel Desbois, Pascal Lecomte

Laboratoire de Météorologie Dynamique, Ecole Polytechnique, 91128 Palaiseau, France

Patrick Perez, Stelios Zimeras, Patrick Bouthemy

IRISA, Campus de Beaulieu, 35042 RENNES, France

ABSTRACT

The tracking of reliable low-level cloud motion winds over land remains a difficult task. For this purpose, conventional computation techniques can be used and be associated to selection tests on vectors based on climatological characteristics of the expected winds. Such tests have been successfully used to extract monsoon winds over West-Africa during the rainy season from Meteosat VISible images. The number of vectors is increased by using rapid scan images. Other improvements include the use of the information from other channels (in particular the Water Vapour) to reject non low-level winds.

Methods based on the estimation of quasi-dense motion fields using optical flow techniques are introduced. Generic methods have been adapted to the highly deformable nature of cloud motion and to the photometric specificities of images at hand (low contrast and global variations of illuminations). Results of both types of methods are presented and compared.

1. Introduction

The tracking of low-level clouds over land has been considered as an almost impossible task at the nominal resolution of current Meteosat satellites (30 min between images), due to the short lifetime of these clouds and often to their small size (generally less than the size of a VISible pixel). Therefore low-level cloud motion winds (CMWs hereafter), when they are produced, are not used for assimilation or forecast in models over land (Ottenbacher et al., 1997). This study shows in section 2 that a limited number of CMWs associated to the monsoon flow over West-Africa can nevertheless be computed during the rainy season with images of Meteosat 7. In section 3, a test based on the correlation between the content of infrared (IR) and the water vapour (WV) channels is presented. This test can be used to eliminate vectors associated to high-level clouds. Section 4 shows the effect of using a reduced time interval between images on the number of low-level CMWs. In section 5, new techniques based on the computation of the optical flow enable the construction of dense cloud motion vector fields. Preliminary results obtained with these techniques are compared qualitatively with those obtained by the "classical" CMW computation method.

2. Statistics of cloud motion winds obtained with current Meteosat data

In this first step, we have tried to extract low-level CMWs associated to the monsoon flow over West-Africa during the summer months (rainy season) of 1998, with the standard temporal resolution of 30 min between images. A preliminary study (Désalmand et al., 1999) has shown that the visible (VIS) channel of Meteosat (with a solar angle correction) enabled a better tracking of low-level clouds than the IR channel. For this purpose, CMWs are computed on a regular grid with a standard method from a triplet of images:

- 2 raw wind fields are computed from image pairs (1, 2) and (2, 3). Displacements are obtained by minimising the Euclidean distance.
- Quality tests remove too small and too large vectors and collocated vectors in both fields with a large difference in direction and / or speed (temporal symmetry check).

Specific tests are then applied to extract low-level winds:

- Low level winds are selected with the help of the IR brightness temperature of the 10 % coldest pixels located inside the target window (BTIR). CMWs associated to a BTIR below a threshold value of 0°C are considered as medium- or high-level winds and therefore are excluded.
- Low level CMWs with a direction between 150 and 270° are then selected. These values correspond approximately to the climatological limits of the direction of the monsoon flow, which is observed over West Africa.

Each CMW which has successfully passed the previous tests is compared to its neighbour(s), if available (spatial symmetry check). If at least one neighbour vector with close characteristics is present, the tested CMW is considered eventually as a monsoon wind.

These quality tests do not take into account WV located above the clouds (which can reduce the observed BT_{IR} by a few degrees K), nor effects related to the partial coverage of a pixel by small clouds or to the semi-transparency of high-level clouds. A visual observation of IR images with the selected VIS CMWs shows that a minority of these winds are related to cirrus clouds associated to the outflow at the top of convective clusters. Such inconsistent vectors are tolerated at this stage because the main goal of this study is to show that the extraction of low-level winds over land is feasible.

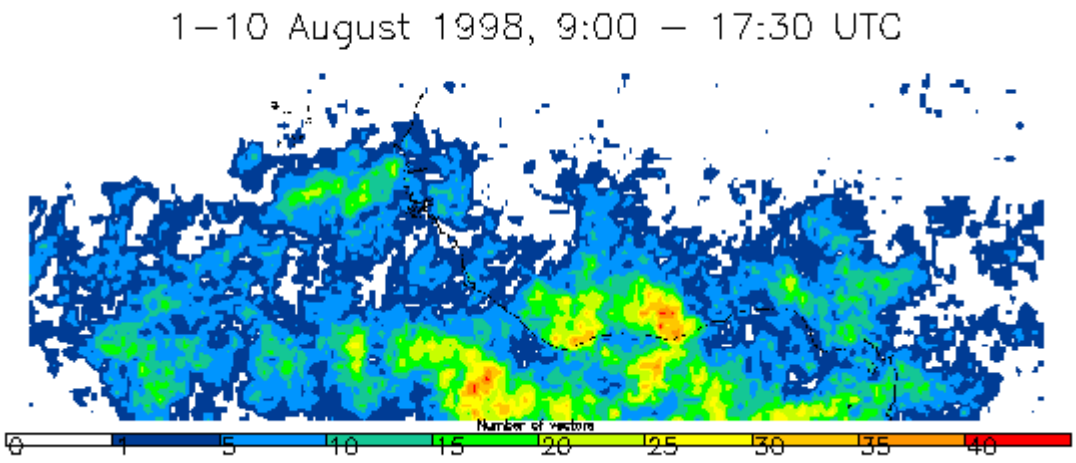

Figure 1. Isolines of the number of monsoon CMWs for the first ten-day period of August 1998.

Figure 1 represents the number of monsoon CMWs over West-Africa between 1 and 10 August 1998. Although the monsoon flow is a quasi-permanent feature of the atmospheric circulation in this area at this time of the year, it appears that the proportion of monsoon CMWs is small, compared to the number of theoretically possible observations (less than 26 %, for a possible maximum of 170 vectors at each grid point). This confirms the difficulty of tracking low-level clouds over land (furthermore high-level clouds which are part of mesoscale convective clusters mask the motion located at lower levels in some areas). Monsoon CMWs are frequently measured in specific, mainly lowland areas: over Ghana, the Ivory Coast and at a lesser extent over Nigeria. The same preferential locations have been observed during another ten-day period (1-10 July 1998), with fewer vectors.

3. Selection of low level CMWs with the IR/WV correlation

The correlation between the IR and WV pixel values over a limited area can be used to indicate the presence of high-level clouds (Xu et al., 1998). Therefore, we have computed the IR/WV correlation over the area covered by the target window used for the calculation of each (VIS) CMW. For the studied case (2 Aug. 1998, 12:00-12:30 UTC), the same methodology as in section 2 has been applied, but without any selection on the direction of the CMWs. It appears that a vast majority of low-level CMWs correspond to a low IR/WV correlation values (below 0.5). A few vectors with a high correlation value are associated to the motion of cirrus clouds. On the other hand, some vectors have a high correlation but have neighbours with low correlation values: in these cases, the motion of low-level clouds is measured below cirrus clouds. These cirrus are thin enough in the VIS channel to enable the calculation of a CMW but thick enough to be detected in the IR and WV channels (thus the high IR/WV correlation values).

The use of the IR/WV correlation as a selection criterion of low-level CMWs has been investigated on another case (5 July 1998, 12:00-12:30 UTC). The set of 1293 low-level CMWs selected with the test on the brightness temperature (BT_{IR} ³ 0°C) is compared to the 1377 CMWs selected with their low IR/WV correlation value (² 0.4) only (without applying the brightness temperature test, all other quality tests being the same). It appears that a vast majority of vectors is common to both sets (Figure 2). The vectors selected only by the correlation generally have a large speed and are related to high-level clouds.

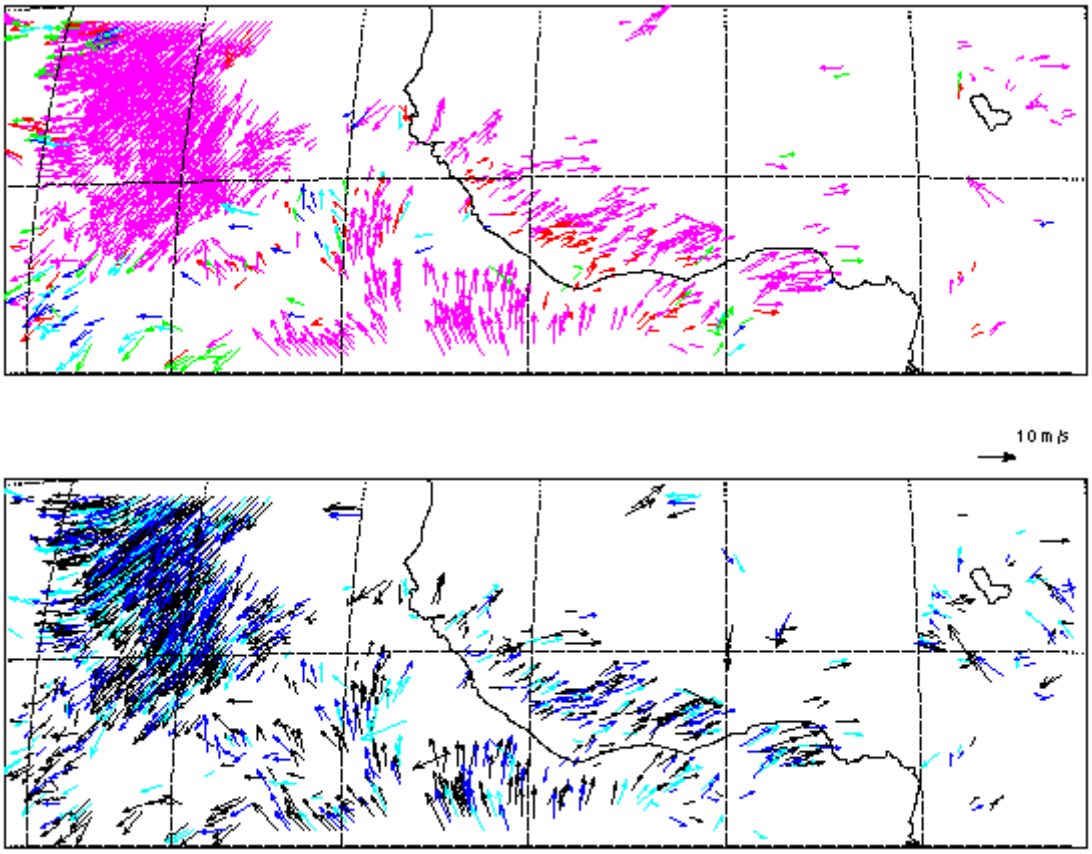

Figure 2. Top: vectors with high BT_{IR} (1293 vectors. Colour scale: blue - green - red - pink, with increasing brightness temperature above 0°C). Bottom: vectors with low IR/WV correlation (1377 vectors. Colour scale: black - dark blue - light blue, with increasing correlation, below 0.4).

From these two examples, we conclude that both tests extract almost similar sets of low-level CMWs.

But the BT_{IR} test is more efficient to remove high-level winds, and is also able to retain low-level winds measured under high-level (thin) cirrus clouds.

4. Cloud motion winds from rapid scan images

The effect of a reduced time interval between images on the number of low-level CMWs has been investigated with a series of Meteosat 6 images covering one day (28 July 1999) during daytime, with a 7.5 min time interval (rapid scan). These images centred on the equator cover the central Atlantic Ocean and West/Central-Africa. Three series of low-level CMWs have been computed with time intervals of 7.5, 15 and 30 minutes between images, with the same quality tests as in section 2 (with thresholds adapted to the reduced time interval and without selection on the wind direction).

Figure 3 shows the huge increase in the number of vectors when the time interval is reduced from 30 to 15 minutes (724 vs. 2592 vectors over land and over ocean). This number is further increased when a 7.5 min interval is used (3323 vectors). This increase in the vector number with the reduction of the time interval can be observed over land during the whole period of the study (figure 4). The fact that the lifetime of small low-level clouds, especially cumulus, is around 10-15 min and is closer to the reduced time intervals than the nominal 30 min between current Meteosat images can explain this increase in the number of vectors. The decrease observed after 11:00 UTC with 7.5 and 15 min time intervals can be explained by increased convection producing more convective cloud systems reaching high altitudes, and by the onset of dusk, which moves from east to west with time.

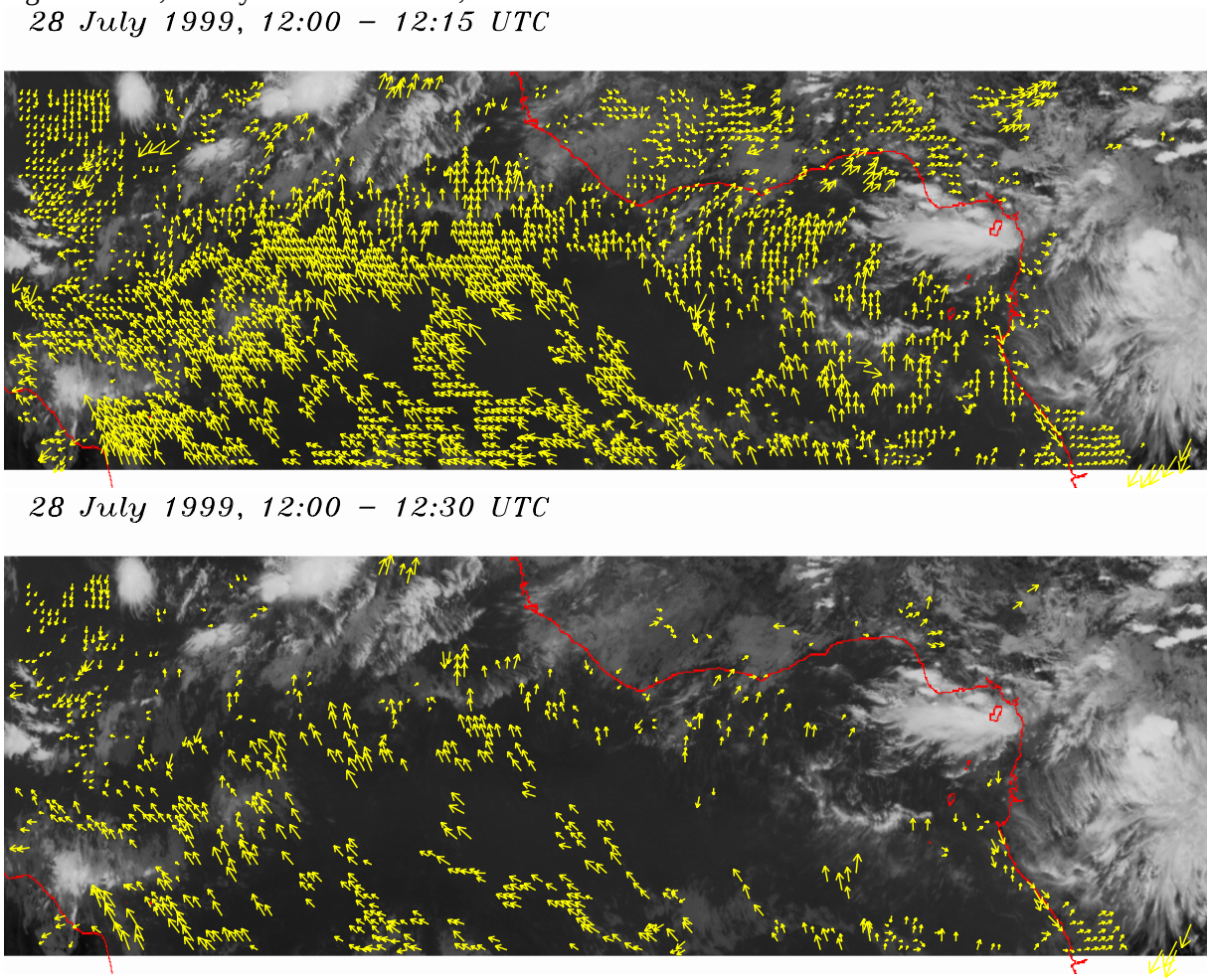

Figure 3. Low-level CMW fields with 30 min (bottom) and 15 min (top) time intervals, with the 12:00 UTC IR image.

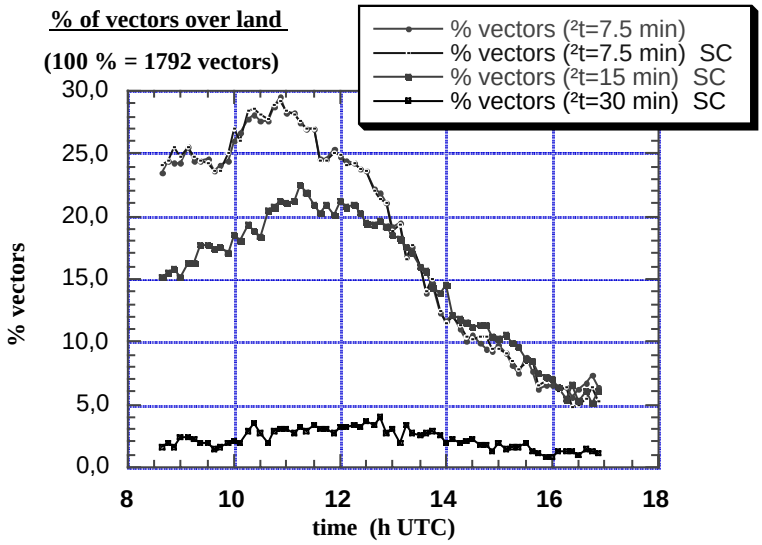

Figure 4. Percentage of vectors over land with different time resolutions (7.5 min : with (SC) and without correction of the solar angle, 15 and 30 min : with correction only (SC).

The effect of a solar correction of images (correction of the solar zenith angle) with a 7.5 min time interval has also been investigated. For such short time intervals, it appears that the number of selected CMWs is almost identical with and without a solar correction (top curves of figure 4). Very close solar illumination on a pair of images at any location explains that reliable CMWs can be computed with uncorrected images. (With a solar correction, CMWs cannot be computed reliably in the areas where the solar zenith angle reaches its maximal value, set to 75°. CMWs with higher values have nevertheless been computed, but without image correction.)

5. Dense vector fields

From an image processing point of view, the movement of the clouds leads to a spatial variation of the image or a sequence of images. The variation of the image introduces a motion at different instants. An effective way to extract information or to identify the shape of an object is to use the *optical flow*. An optical flow can be defined as *the transformation of the 3D motion of objects and cameras to a 2D motion on the image plane via a suitable projection system*. The presentation of the optical flow as a vector-values functions of continuous spatial co-ordinates can be defined as a motion field.

The main steps of the motion field modelling are introduced by:

1. Modelling the motion as a cost energy function including observation constraints and smoothness terms (Horn and Schunck, 1981),
2. Expressing the optical flow as a model, constant or affine (Stiller and Konrad, 1999),
3. Introducing robustness to reduce the differences between the data and the optic flow model,
4. Minimise the energy function using a general hierarchical optimisation framework, which is both multiresolution and multigrid with an adaptive way (Memin and Perez, 1998).

5.1 Modelling of the motion field

Let us define the unknown 2D motion field as ={s, s∈S} over a rectangular pixel lattice S and the intensity function at two consecutive instants t and t+1 as f(t)={f(s,t), s∈S}. Assuming a temporal constancy of the brightness, the optical flow constrained equation (OFCE) is given by:

$$\nabla \boldsymbol{f}(\boldsymbol{s},\boldsymbol{t})\omega_s + \boldsymbol{f}_t(\boldsymbol{s},\boldsymbol{t}) = \boldsymbol{0}$$

where, ∇f represents the spatial gradient of f with $\nabla \boldsymbol{f} = \left(\boldsymbol{f}_x, \boldsymbol{f}_y\right)^T$ and $f_t(s,t)$ is the temporal partial derivative of luminance f. The model assumes small displacements. The global estimation of the motion field can be achieved by optimising the following cost function (from Horn and Schunck (1981)):

$$\boldsymbol{U}(\omega, \boldsymbol{f}) = \sum_{s \in S} \left[\nabla \boldsymbol{f}(\boldsymbol{s},\boldsymbol{t})\omega_s + \boldsymbol{f}(\boldsymbol{s},\boldsymbol{t})\right]^2 + \boldsymbol{a} \sum_{<s,r> \in C} \left\|\omega_s - \omega_r\right\|^2$$

where, S is the set of pixel grid, C are the possible cliques for the neighbouring sites <s,r> (the 4-neighbourhood system in this case), and a>0 is the smoothing parameter controlling the balance between the two terms. The first term represents the interaction between the field (unknown variables) and the data (given variables), where the second term expresses the smoothness constraint. The disadvantages of this formulation are:

- The OFCE is not valid in case of large displacements, because of the linearisation,
- The real field is not globally smooth, containing probably discontinuities that might not be presented because of the quadratic cost function.

5.2 Robust estimators

To efficiently cope with the large deviations from the data model and the prior model, robust functions (Black and Anandan, 1996) are introduced and more precisely robust M-estimators. After this modification, the cost function takes the form:

$$\boldsymbol{U}(\boldsymbol{d}\omega, \boldsymbol{f}) = \sum_{s \in S} \rho_1\left[\nabla \boldsymbol{f}(\boldsymbol{s},\boldsymbol{t})\omega_s + \boldsymbol{f}(\boldsymbol{s},\boldsymbol{t})\right]^2 + \boldsymbol{a} \sum_{<s,r> \in C} \rho_2\left\|\boldsymbol{d}\omega_s - \boldsymbol{d}\omega_r\right\|^2$$

where, ρ_1 and ρ_2 are the two robust estimators (in this case the Leclerc estimator was used) and d_ω is the incremental displacement field. According to minimisation aspects, for the estimators (Black and Anandan, 1996; Geman and Reynolds, 1992), the cost function takes the form:

$$\boldsymbol{U}(\boldsymbol{d}\omega, \boldsymbol{f}) = \sum_{s \in S} \delta_s\left[\nabla \boldsymbol{f}(\boldsymbol{s},\boldsymbol{t})\boldsymbol{d}\omega_s + \boldsymbol{f}(\boldsymbol{s},\boldsymbol{t})\right]^2 + \phi_1(\delta_s) + \boldsymbol{a} \sum_{<s,r> \in C} \beta_{sr}\left|\boldsymbol{d}\omega_s - \boldsymbol{d}\omega_r\right|^2 + \phi_2(\beta_{sr})$$

where, δ_S are the weights of the data that controls the optical flow constrained equation and ρ_{Sr} are the weights that controls the velocity discontinuities.

5.3 Multiresolution-Multigrid approaches

For each instant t of the sequence, a pyramid of images $\{f^{(k)}\}$ is derived by successive Gaussian smoothing and regular resampling by a factor of 2. At coarsest level, displacements are reduced and cost function can be used. For the next resolution levels, only one incremental $d\omega^{(k)}$ is estimated to refine estimate $\hat{\omega}^{(k)}$, obtained from the previous level. The cost function depends on from three parameters: r_1, r_2 and r_3 that are approximately defined by the variances of the three robust models (interaction between the field and the data and smoothness constraints between different neighbouring structures).

For a faster convergence of the minimisation process, a multigrid approach is applied. The process partitions the image into lattice of size $2^{(k)}$ at the grid level k. The cost function can then be expressed according to the partition and a parametric model is estimated as an increment on each pixel. The displacement increment estimated on a pixel depends on the total displacement on the neighbourhood of this pixel; that implies the field could be continuous between the pixels and in this case no block effects are appeared.

When the grid level is changed, the partition of the grid is also changed (in an adaptive way). The number of blocks could be the criterion to measure the way the model fits the data or could be used as a prior knowledge for the structure of the particular application. Using this adaptive way of splitting the blocks, eventually there is a distinction between the regions of interests, where the estimation must be accurate, and the regions where information is useless.

5.4 Extension of the standard method

When the luminance is constant along its trajectories, the standard methods (see above) can be applied to estimate the optical flow field. This assumption is not valid in cases of spatial and temporal distortions as in fluid image sequences. As an extension, a new model is applied based on the continuity equation of fluid mechanics and a smoothness function considering the divergence and vorticity (curl) of the motion field. The basic idea is to have different penalisation for div(ω) and curl(ω) in the smoothness terms, to encourage one or the other quantity.
In this case the cost energy function takes the form:

$$U(d\omega, f) = \sum_{s \in S} \rho_1 \left[\nabla f(s,t) d\omega_s \exp\left[div(\omega_s) \right] + f(s,t) \right]^2 + \alpha \sum_{<s,r> \in C} \rho_2 \left\| d\omega_s - d\omega_r \right\|^2 +$$
$$\lambda \sum_{s \in S} \rho_2 \left[\left\{ div(\omega_s) - L_{div_s} \zeta_{div_s} \right\}^2 + \left\{ curl(\omega_s) - L_{curl_s} \zeta_{curl_s} \right\}^2 \right]$$

where $div(\omega_S)$ can be expressed as a product of two factors: L_{div} and ξ_{div}, $\lambda>0$ is a control parameter between the two factors of smoothness term.

5.5 Results

A dense vector field, which represents the motion of clouds at all levels, has been calculated with the improved method described above (28 July 1999, 12:00 - 12:07 UTC). On figure 5, the corresponding chart can be compared with the low-level CMW field obtained with the same images and the method described in sections 2 and 4. On both charts, the vectors show the same direction of motion. But more complete (quantitative) comparisons must be undertaken, especially in the areas where low- and high-level clouds are in contact.

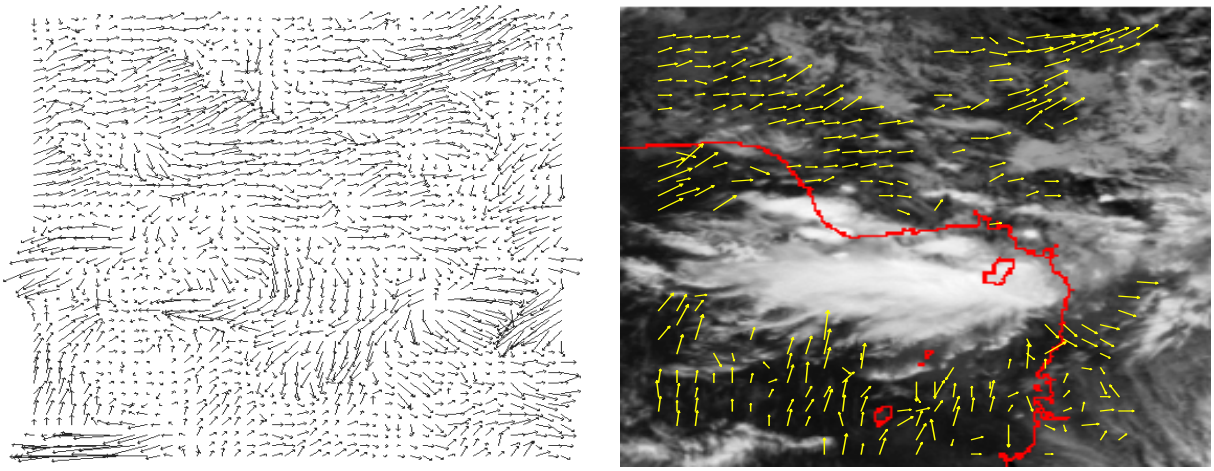

Figure 5: dense vector field calculated with the optical flow method (left) and low level CMWs obtained with the classical method (right, with IR image of 28 July 1999, 12:00 UTC)

6. Conclusion and prospects

This study confirms that a limited number of low-level CMWs can be computed over land in the tropics from VIS images with the time interval of 30 minutes between images, available on current Meteosat satellites. An important increase in the number of CMWs is observed when the time interval is reduced to 15 minutes and can be expected from future Meteosat Second Generation satellites which will have that time interval in operational mode. A further but smaller increase is observed during a part of daytime when the time interval is reduced to 7.5 minutes. In the latter situation, CMW fields are

almost identical whether a solar correction is applied or not; therefore we suggest suppressing this preliminary image processing.

The IR/WV correlation has been tested as an alternate parameter for the selection of low-level CMWs. It appears that the use of the IR brightness temperature (high values) enables a slightly better selection than the correlation (low values), but that a large majority of vectors are retained by both selection tests. Future improvements of the selection method are planned, they include a better height assignment and a semi-transparency correction.

A new method based on optical flow determination has been developed for the construction of dense cloud motion fields. A qualitative comparison shows that vectors in areas where low-level clouds are present have directions similar to the (limited number of) vectors available with conventional techniques. Quantitative comparisons in a near future will evaluate the quality of this method.

ACKNOWLEDGEMENT

This study was realised partly under EUMETSAT contract no. EUM/CO/99/699/KTH. The authors would also like to thank EUMETSAT for the financial help that enabled one of them to attend to this Winds Workshop.

REFERENCES

Black, M. and P. Anandan (1996). The robust estimation of multiple motions: parametric and piecewise smooth flow fields. *Computer Vision and Image Understanding*, **63**, 1, pp 75-104.

Désalmand, F., A. Szantai and M. Desbois (1999). An attempt to retrieve low cloud motion winds over land in the African monsoon flow on Meteosat pictures. *Geophys. Res. Lett*., **26**, pp 319-323.

Horn, B. K. P. and B. G. Schunck (1981). Determining optical flow. *Artificial Intelligence*, **17**, pp 185-203.

Memin, E. and P. Perez (1998). Optical flow estimation and object-based segmentation with robust techniques. *IEEE Trans. Pattern Anal. Machine Intell.*, **7, 5,** pp 703-719.

Ottenbacher, A., M. Tomassini, K. Holmlund, and J. Schmetz (1997). Low-level cloud motion winds from Meteosat high resolution visible imagery. *Wea. Forecasting* , **12**, pp 175-184.

Stiller, C. and J. Konrad (1999). Estimating motion in image sequences. *IEEE Signal Processing Magazine*, **16, 4**, pp 70-91.

Xu, J., Z. Qisong, F. Xiang and L. Jian (1998). Cloud motion winds from FY-2 and GMS-5 meteorological satellites. *Proc. Fourth International Winds Workshop*, Saanenmőser, Switzerland (20-23 Oct. 1998). Eds. JMA, EUMETSAT, WMO and NOAA. EUMETSAT : pp 41-48.

SESSION VI

NEW SPACE BORNE SYSTEMS

Chairperson: J. Schmetz

GIFTS-
A SYSTEM FOR WIND PROFILING FROM GEOSTATIONARY SATELLITES

William Smith, Wallace Harrison, Dwayne Hinton, Vickie Parsons and Allen Larar
NASA LaRC, Hampton Virginia (USA)

Henry Revercomb[1], Allen Huang[2], Christopher Velden[2], Paul Menzel[3], and Ralph Petersen[3]
[1]SSEC,[2] CIMSS, and [3]NOAA
University of Wisconsin, Madison WI (USA)

Gail Bingham and Ronald Huppi
Utah State University, Logan Utah (USA)

ABSTRACT

The Geostationary Imaging Fourier Transform Spectrometer (GIFTS) is a NASA New Millennium Program mission to validate a revolutionary new instrument capable of providing high density temperature and moisture profiles with very high vertical and temporal resolution from geostationary satellites. The GIFTS will fly on NASA's Earth Observing-3 geostationary satellite to be launched in 2004. The technology uses is a combination of large area format focal plane detector arrays, which enable frequent high spatial resolution coverage over large areas, with the Fourier Transform Spectrometer, which enables simultaneous high vertical resolution soundings for all detector elements of the array. It has been demonstrated, both theoretically through numerical model simulation and experimentally using an aircraft prototype instrument, that the vertical profile of wind velocity can be achieved by tracking the movement of small-scale moisture features observed as a function of altitude. The instrument concept, results from aircraft measurements and model simulations, and plans for the satellite implementation of the GIFTS are presented.

1. Introduction

The Geostationary Imaging Fourier Transform Spectrometer (GIFTS) combines new and immerging sensor and data processing technologies to acquire geophysical measurements that lead to revolutionary improvements in meteorological observations and forecasting. The GIFTS measurement concept uses a large area format focal plane detector array (128 x 128) in a Fourier Transform Spectrometer (FTS) (Smith et. al., 1979, Smith et. al., 1990) mounted on a geostationary satellite to enable the simultaneous gathering of high spectral resolution (as great as 0.3 cm –1) and high spatial resolution (4-km x 4-km pixel) Earth infrared radiance spectra over a large area (512-km x 512-km) of the Earth within a 10 second time interval. A low visible light level camera provides quasi-continuous imaging of clouds at 1-km spatial resolution. Extended Earth coverage is achieved by step scanning the instrument field of view in a contiguous fashion across any desired portion of the visible Earth. The radiance spectra observed at each time step are transformed to high vertical resolution (1-2 km) temperature and water vapor mixing ratio profiles using rapid profile retrieval algorithms. These profiles are obtained on a 4km grid and then converted to relative humidity profiles. Images of the horizontal distribution of relative humidity for atmospheric levels, vertically separated by approximately 2 km, are constructed for each spatial scan. The sampling period will range from minutes to an hour, depending upon the spectral resolution and the area coverage selected for the measurement. Successive images of clouds and the relative humidity for each atmospheric level are then animated to reveal the motion of small scale thermodynamic features of the atmosphere. Automated auto-correlation feature tracking programs are then used to compute the speed and direction of movement of these small scale features, providing a measure of the wind velocity distribution at each atmospheric level. The net result is a dense grid of temperature, moisture, and wind profiles which can also be used for atmospheric analyses and operational weather prediction. Feature tracking can be performed for mixing ratio profiles of O_3 and

CO, derived from their spectral radiance features observed by the instrument, providing a direct measure of the transport of these pollutant and greenhouse gases. It is the unique combination of the FTS and the large area format detector array (i.e., an imaging interferometer) and the geostationary satellite observation platform that enables the revolutionary tracer wind profile and trace gas transport remote sensing measurements. The optical layout of the GIFTS instrument is shown in Figure 1. The imaging FTS produces the interferometric patterns for spectral separation of scene radiation reaching the detector arrays. To limit the background signal, the FTS is thermally controlled at a low temperature. The high data rates generated by the focal plane arrays (FPAs) are reduced by loss-less compression techniques then passed to the telemetry system by low-power and -volume next-generation electronic components.

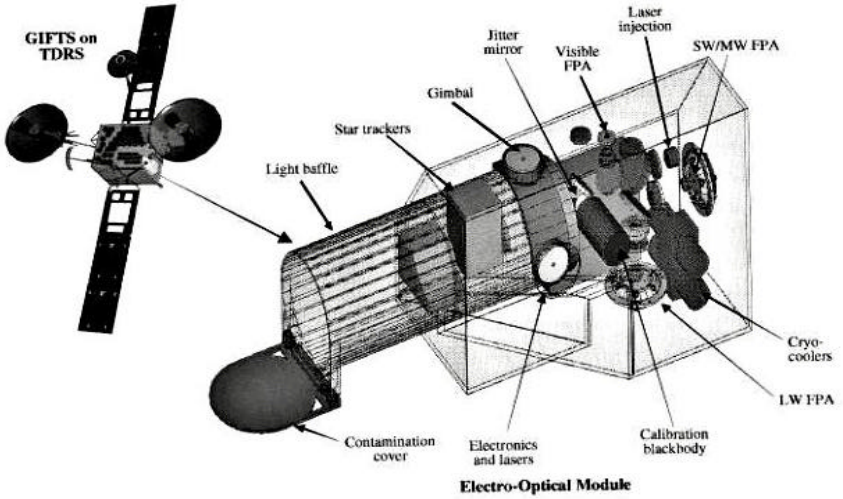

Figure 1. GIFTS Optical System.

2. GIFTS data products

2.1 Temperature, Moisture, and Wind Profiles

GIFTS measurements will be used to determine temperature and moisture profiles with unprecedented high spatial and temporal resolution. These measurements will produce wind profiles and record thermodynamic and dynamic features of the turbulent atmosphere and the evolution of severe storm systems, including tornadoes and hurricanes. Wind profile estimates can be diagnosed through the direct real-time assimilation of GIFTS retrieved temperature and water vapor profile data, in a mesoscale numerical model. Alternatively, vertical profiles of wind velocity can be estimated by tracking the horizontal displacement of features in the retrieved water vapor profiles. A similar feature-tracking approach is now used operationally and has been shown to provide improved weather forecasts on both regional and global scales. However, the current Geostationary Operational Environmental Satellite (GOES) application only provides upper tropospheric winds from images of radiance for a single water vapor channel (Stewart et. al., 1985, Velden et. al., 1997). More complete vertical profiles of wind velocity are needed to realize the full potential of satellite measurements to greatly improve both regional scale intense weather forecasts and global scale synoptic weather predictions. The capability of GIFTS to observe small scale atmospheric water vapor features for inferring the wind field has been investigated through (1) the analysis of National Polar-Orbiting Environmental Satellite System (NPOESS) Aircraft Sounder Test-bed Interferometer (NAST-I) data and (2) the simulation of GIFTS measurements for the hurricane Bonnie landfall in 1998. NAST-I has similar spectral and spatial measurement properties to the GIFTS, and the hurricane simulation used a very sophisticated Nonhydrostatic Mesoscale numerical Model (NMM) (Tripoli, 1992). The results of these supporting studies are shown in detail on the GIFTS web pages at http://its.ssec.wisc.edu/~bormin/GIFTS/.

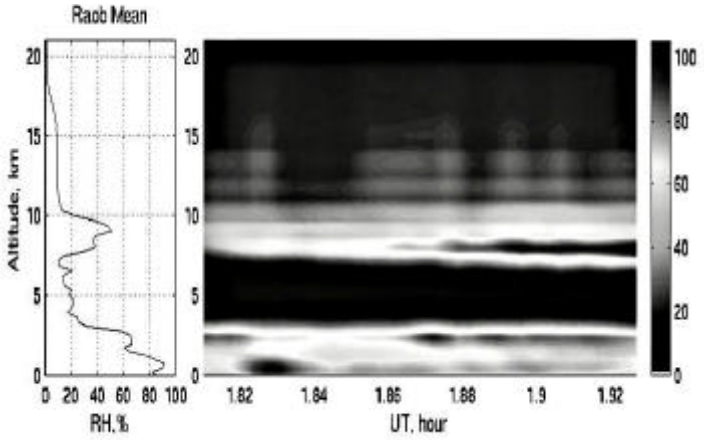

Figure 2. Horizontal cross-section (75 km) of relative humidity derived from NAST-I radiances observed from the NASA ER-2 flying over Andros Island Bahamas on September 14, 1998. The average of several radiosondes released during the aircraft overpass is shown.

Figure 2 displays the high vertical resolution sounding capability of a high spectral resolution passive remote sounder. Moist and dry layers of 1- to 2-km atmospheric depth are clearly resolved with the NAST-I system. This same vertical resolving power will be achieved with GIFTS. Using the NMM, fields of atmospheric temperature, water vapor, and wind velocity were output at 6-km spatial resolution and a 10-min time interval. The vertical distribution of cloud water content and microphysical properties were also output for each model grid point. These fields were used with a radiative transfer model to simulate GIFTS spectral radiance observations. Expected instrument noise was added to the simulated radiances. Temperature and moisture profiles were then produced for each model grid point and time step to simulate GIFTS. Figure 3 is the derived horizontal wind vectors derived from GIFTS NMM simulated radiance observations for hurricane Bonnie. The ability of GIFTS to observe the vertical structure of the hurricane circulation is clearly shown. The wind velocity errors to be derived from GIFTS will be much smaller than those associated with current geostationary satellite water vapor radiance tracer results as a result of the much higher vertical resolution of the GIFTS. The revolutionary aspect of GIFTS is that it provides access to the vertical dimension of the wind field, with accurate altitude assignment.

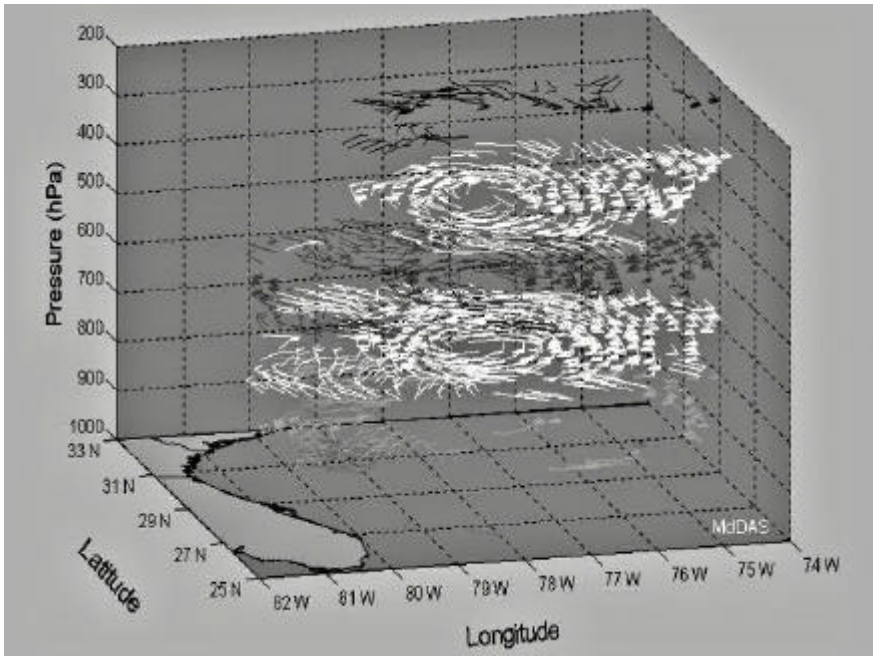

Figure 3. Wind vectors derived from NMM simulated GIFTS radiances for Hurricane Bonnie on Aug.26 1998.

2.2 Trace Gas Concentrations

GIFTS measurements will also be used to determine the time varying spatial distribution of CO and O_3 with a 3- to 11-km vertical resolution, decreasing with increasing altitude. The vertical resolving power is illustrated in Figure 4: Vertical resolution functions for GIFTS retrieved carbon monoxide and ozone profiles at 0.6- and 0.3 cm^{-1} spectral resolutions, dashed and solid curves, respectively (courtesy of Nikita Pougatchev, CNU).

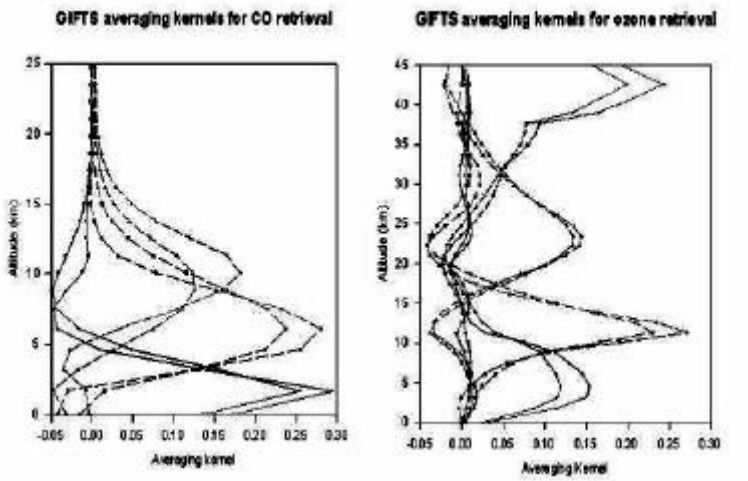

Figure 4. obtained using the EOS-CHEM platform Thermal Emission Spectrometer (TES) level-2 algorithm software.

The GIFTS capability to track vertically resolved trace gas concentrations together with the Water vapor winds is important for monitoring the global transport of pollutant gases resulting from biomass burning and industrial sources. Global Tropospheric Experiment (GTE) data have shown that this transport takes place at middle tropospheric levels (Pougatchev, 1999). Thus, GIFTS water vapor and trace gas motion sensing ability will provide a unique measure of chemical pollutant episode evolution and transport

3. Measurement characteristics

GIFTS will view areas of the Earth with a linear dimension of about 500-km, anywhere on the visible disk for a period between 0.125 and 25.0 sec, depending on the data application (i.e., imaging, sounding, or chemistry). GIFTS uses two detector arrays to cover the spectral bands 685 to 1130 cm^{-1} and 1650 to 2250 cm^{-1} (Figure 5) and a Michelson interferometer to achieve a wide range of spectral resolutions (Table I).

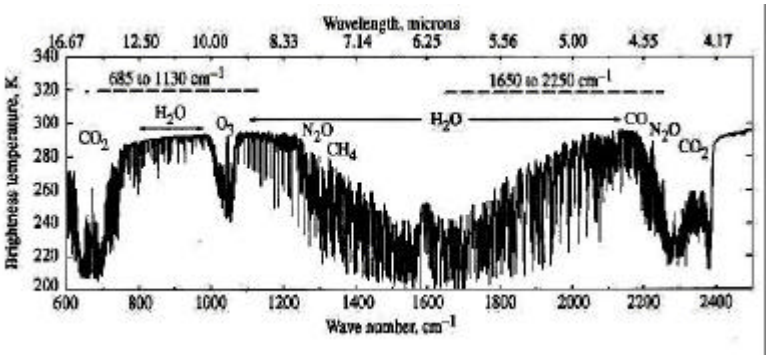

Figure 5. GIFTS spectral coverage with 2 detector arrays with spectral features of key radiatively active atmospheric trace gases.

These spectral characteristics achieve all scientific objectives of GIFTS, as well as the sounding accuracy desired for a future operational sounding system. The Michelson interferometer, or FTS, approach for geostationary satellite applications allows spectral resolution to be easily traded for greater area coverage or higher temporal resolution.

Table I: Five example GIFTS operating modes

Visible Resolution= 1 km; IR Resolution = 4 km

Mode	Resolution		Coverage	
	Spectral	OPD	Area	Time*
Stare Mode	0.3-36 cm-1	0.014-1.744 cm	512 km	<1-20 sec
Regional Imaging	36 cm-1	0.014 cm	6,000 km	3 min
Global Sounding	18 cm-1	0.027 cm	10,000 km	7 min
Regional Sounding and Chemistry	0.6 cm-1	0.872 cm	6000 km	25 min
Self Validation**	0.3 cm-1	1.744 cm	1000 km	60 min
Assumes a constant data rate associated with a Michelson mirror scan velocity of 0.17cm/sec and 1 sec telescope pointing step time. ** Provides radiometric precision better than 0.1 K over all wavelengths				

Table I shows the areal coverage, measurement frequency, spectral resolution, and geophysical measurement for example modes of operation for GIFTS. Quasi-continuous imagery of localized areas and minute-interval imagery of large scale areas can be achieved. Full disk sounding coverage can be obtained every 7 min at contemporary sounder spectral resolutions (e.g., 18 cm $^{-1}$). High vertical resolution soundings and atmospheric chemistry measurements of GIFTS require 0.6 cm $^{-1}$ spectral resolution and a longer stare time, thereby reducing the area coverage and/or frequency of observation relative to the imagery mode of operation. Nevertheless, GIFTS can cover a major portion of the visible disk with high vertical resolution soundings in less than 0.5 hour. This feature is important for obtaining wind profiles from geostationary temperature and moisture sounding data. A relatively long dwell time and a more limited area coverage "self validation mode" of operation will enable 0.3-cm^{-1} spectral resolution radiances to be achieved with very high radiometric precision. The self validation mode will be for radiance, sounding, and chemistry product validation of the routine larger area, higher frequency, spectra and geophysical products provided by the global and regional sounding and chemistry modes of operation. GIFTS can achieve good simultaneity with Earth orbiting satellite observations to enhance overall ESE science mission objectives.

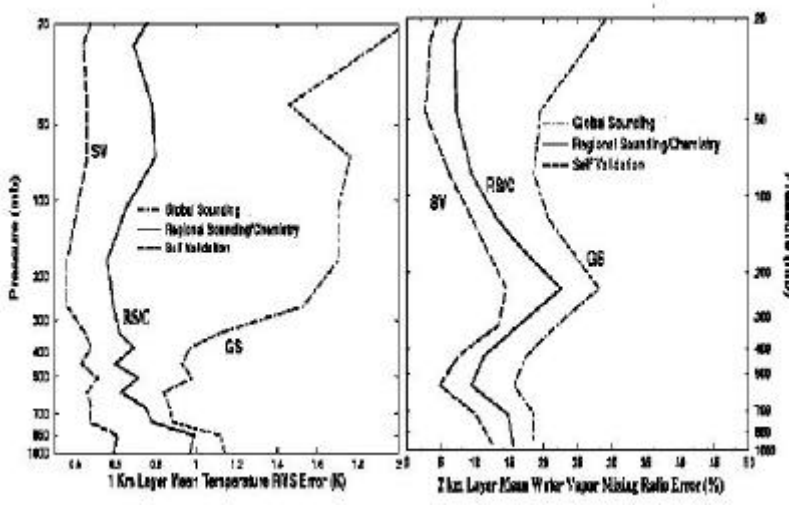

Figure 6. Profile RMS errors for 3 GIFTS sounding modes of operation shown in Table 1 using expected radiometric noise performance

The expected sounding performance of GIFTS has been determined by radiance simulation. The results for the three example sounding modes of operation (Table 1) are shown in Figure 6. The radiometric noise and accuracy requirements for this retrieval of temperature and water vapor in the Regional Sounding and Chemistry mode with 10 sec dwell time are: (1) Noise Equivalent Radiance (NEN) in the LW spectral band (685-1130 cm $^{-1}$) <0.2 mW/m 2 sr cm $^{-1}$, (2) NEN in the SW/MW spectral band (1650-2250 cm $^{-1}$) <0.06 mW/m 2 sr cm $^{-1}$, and (3) Absolute calibration accuracy better than 1 K brightness temperature for Earth scene brightness temperatures > 190 K for the LW and >240 K for the SW/MW band. Periodic views of onboard references and cold space will be used to realize this high calibration accuracy. Achieving these radiometric requirements for the primary high spectral resolution sounding mode is sufficient to insure the performance of other GIFTS imaging and sounding modes. The only other necessary constraints are that the time required to point the field-of-view to an adjacent region on Earth be less than 1 sec and that the pointing knowledge be better than 0.4 km for wind determination.

4. Summary

GIFTS will be put into geostationary orbit in 2004 to demonstrate the ability to obtain revolutionary improvements in weather and air quality forecasts using its high temporal and spatial resolution temperature and moisture products. GIFTS is the experimental forerunner of a global operational system of advanced sounders. A global system will enable these revolutionary improvements to be achieved on a world-wide basis as needed to realize the full potential of the GIFTS measurement approach.

REFERENCES

Smith, W. L., H. B. Howell, and H. M. Woolf, 1979: The use of interferometric radiance measurements for sounding the atmosphere. *J. Atmos. Sci.*, **36**, 566-575.

Smith, W. L., H. E. Revercomb, D. D. LaPorte, L. A. Sromovsky, S. Silverman, H. M. Woolf, H. B. Howell, R. O. Knuteson, and H.-L. Huang, 1990: GHIS - The GOES High resolution Interferometer Sounder. *J. Appl. Meteor*., **29**, 1189-1204.

Stewart, T. R., C. M. Hayden, and W. L. Smith, 1985: A note on water vapor wind tracking using VAS data on McIDAS. *Bull. Amer. Meteor. Soc*., **66**, 1111-1115. Sounder (HIS) observations. *J. Appl. Meteor.*, **29**, 658-662.

Tripoli,G.J., 1992: A Nonhydrostatic Mesoscale Model Designed to Simulate Scale Interaction. *Mon. Wea. Rev.*, **120**, 1342-1359.

Velden, C.S., C. M. Hayden, S.J. Nieman, W.P. Menzel, S. Wanzong and J. S. Goerss, 1997: Upper-tropospheric winds derived from geostationary satellite water vapor observations. *Bull. Amer. Meteor. Soc.*, **78**, 173-195.

Pougatchev,N.S., 1999: PEM Tropics Carbon Monoxide Measurements in Historical Context. *J. Geophysical Research* (in press).

WIND ENERGY MAPPING USING SYNTHETIC APERTURE RADAR

C. B. Hasager

Risoe National Laboratory, Wind Energy and Atmospheric Physics Dept.,
P.O.Box 49, 4000 Roskilde, Denmark
Charlotte.hasager@risoe.dk

ABSTRACT

Wind energy *off-shore* is gaining much interest due to the high wind power potentials. The need is to map wind climatology and regional wind patterns in coastal regions. In the WEMSAR (Wind Energy Mapping using Synthetic Aperture Radar) project three European sites will be covered near Norway, Denmark and Italy. Data to be used are from the ERS-2 C-band scatterometer with a 50 km resolution, from ERS-2 Ku-band and Topex Poseidon Ku-Band altimeter with a 7 km resolution and from SAR. The SAR data will be block averaged into 400 m resolution from ERS-2 C_VV, Radarsat C_HH and Envisat ASAR C_VV and C_HH beginning year 2000. For SAR data, the algorithm CMOD IFRE2 (Institute Francaise de Recherche pour L'Exploitation de la Mer) is used based on 3433 collocated pairs of buoys of NOAA and ECMWF (European Centre for Medium Range Weather Forecasts) with the accuracy of ∀2 m/s for a single retrieval. In the validation part of the WEMSAR project for wind energy retrieval, the ESA SAR (SAR.PRI (precision image format)) will be used because of the need for absolute calibration. Validation data are from long-term off-shore and coastal meteorological masts at the sites. Some masts are dedicated to wind power measurements including the roughness of sea and wave height. Optimal validation is crucial as wind energy varies with the third power of the wind speed. Also, the 10 or 19.5 m wind speeds will have to be calculated into 50-100 m height, i.e. the hub height of modern 600-1500 kW wind turbines. This calculation includes stability correction of the wind profiles. Wind analysis at mesoscale (1 km grid) with the non-hydrostatic KAMM (Karlsruhe Atmospheric Mesoscale Model) and WAsP (the Risoe Wind Atlas Analysis and Application Program) for micro-siting will be used. The aim is to link from meteorological mast data to spatial mapping of the wind energy potential based on satellite SAR data in coastal areas.

1. Introduction

There are global plans for reduction of the CO_2 emissions according to the Kyoto protocol (IGBP, 1998). At the same time, the demand for electrical power is increasing in most societies. Therefore renewable energy sources are of interest. Wind power is one of the renewable energy sources that may contribute significantly worldwide. Today roughly 7% of the Danish power consumption is supplied by wind power. Within the next 30 years it is planned by the Danish government, that renewable sources (mainly wind power) should supply 35% of the total Danish electricity consumption. To achieve this goal the utilities take great interest in siting of wind turbines.

In many parts of the world where wind turbines are being planned, environmental authorities and local interest groups hold the point of view that wind turbine should not be placed due to e.g. bird migration, dwellings, tourism and so on. Therefore the number of attractive sites is limited. This has caused an interest in *off-shore siting* as the wind potential is relatively high at sea. An example of the estimated wind power production on land and off-shore at the Vindeby site in Denmark is shown in Figure 1. It is clear that the wind power potential is very much larger off-shore than on land. At this site an off-shore wind turbine park (11 turbines) has produced energy since 1991 (Barthelmie et al., 1994).

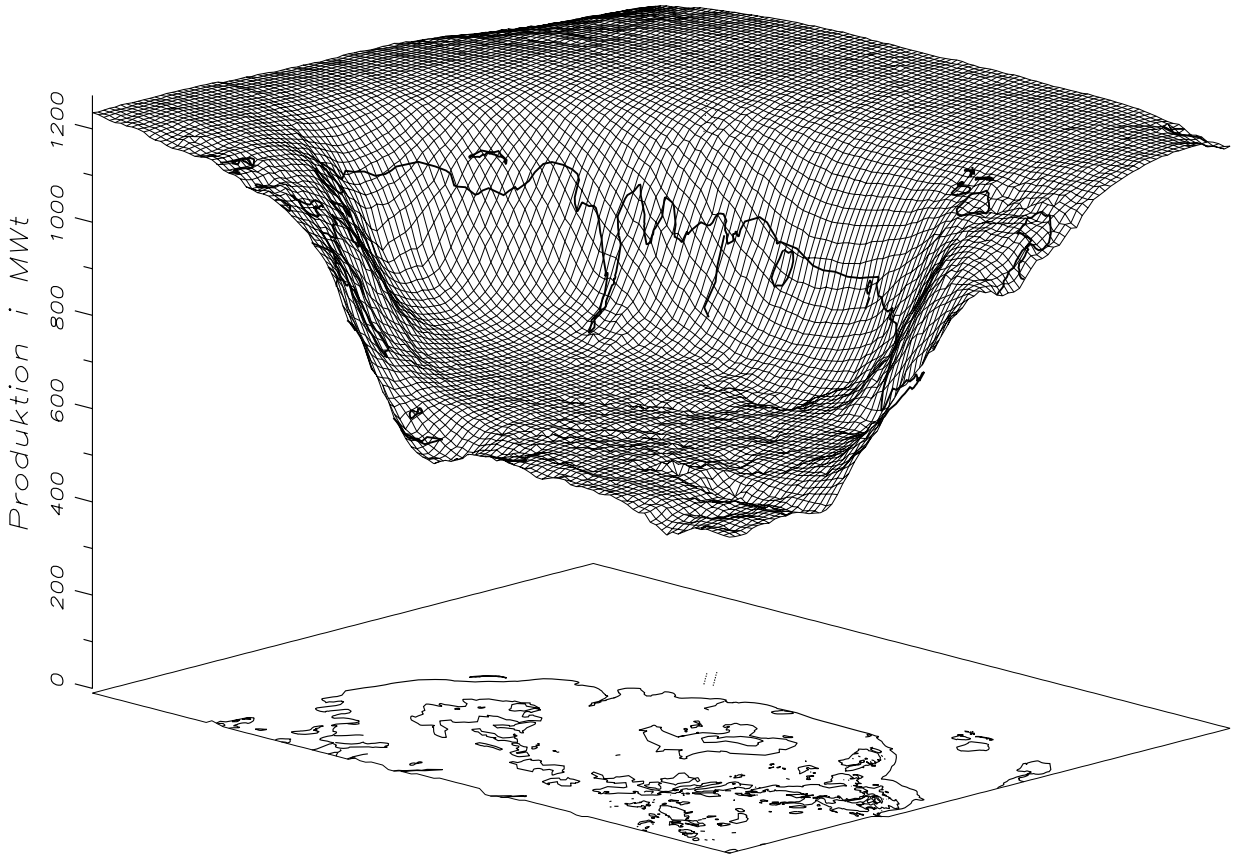

Figure 1. The estimated wind power production near Vindeby, Denmark. The Vindeby wind turbine farm is located 1 to 3 km off-shore (Courtesy of N.G. Mortensen).

Siting of wind turbines is usually performed by analysis of wind observations combined with information on orography, roughness and obstacles in the local terrain (Mortensen et al., 1993, Petersen et al., 1998). Wind statistics are obtained from long-term data series at one or few locations in the landscape and through modelling work calculated into maps for given areas, e.g. the European Wind Atlas (Troen and Petersen,1989). An investigation on the mapping of wind energy resources off-shore by use of SAR satellite data will be undertaken within a new project. Spatial data of wind observations will provide a novel information source to current micrositing models.

2. Satellite radars

Satellite radars include scatterometers, altimeters and synthetic aperture radar (SAR) systems. Currently in operation are the ERS-2 C-band (5.3 GHz, VV) scatterometer, the Topex-Poseidon Ku-band altimeter, the ERS-2 Ku-band altimeter (13.8 GHz), the ERS-2 SAR C-band (VV) and the RADARSAT-1 SAR C-band (HH). For wind energy mapping also data from sensors that previously have been in operation may be of interest, here mainly the ERS-1SAR scenes.

2.1 SAR

SAR data were collected first time from space with SEASAT in 1978. Since then other missions, among these the shuttle imaging radars (SIR), have delivered data (see Table 1) (from Hasager, 1997). However, only since ERS-1 was launched in 1991, has a continuous series of SAR data become available, currently provided by ERS-2 SAR and RADARSAT-1. In year 2000 the ASAR C-band (VV & HH) at ENVISAT will be launched and in year 2001 the RADARSAT-2 C-band (HH). Hence the future availability of SAR scenes is promising.

The radar antenna transmits microwaves with a controlled (known) strength, frequency and polarization. It is the backscattered signal of this electromagnetic radiation that is measured and projected onto a grid via a time- and space-dependent algorithm. For image processing it can be considered as a grid of pixels. The value in each pixel usually is the signal strength squared (with unit $Volt^2$ per pixel).

The mean reflection in a calibrated SAR image is called the backscatter coefficient, Φ_0. It is dimensionless. It is proportional to the effect. Φ_0 is defined as a measure of the expected return signal from randomly distributed scattering elements in an area of 1 m^2 in the horizontal plane. Φ_0 is a function of surface parameters such as roughness, geometry and dielectric properties. Furthermore it is a function of radar observation parameters such as frequency, polarisation and incidence angle. SAR data are polarimetric. This means that the received and transmitted signal matrix can be described from coordinates horizontal (H) and vertical (V) to the incidence angle, relative to nadir for a plane surface. Φ_0 has a very large dynamic range, roughly $1*10^5$, and therefore the values are recalculated with the logarithm (with base 10) into decibel (dB).

Table 1. SAR data available from satellites and shuttle missions. * means optically processed. All other scenes are digitally processed.

Name	Period	Band	Polarization	□ (□)
SEASAT	July-Sep. 1978	L	HH	22
SIR 1 (A)*	Nov. 1981	L	HH	50
SIR 2 (B)	Oct. 1984	L	HH	20-50
ALMAZ 1	1987-	S	HH	25-50
ALMAZ 2	May 91-Oct. 92	S	HH	25-50
ERS-1	July 1991-1996	C	VV	23
JERS-1	Feb. 1992-	L	HH	38.5
SIR 3(C)	Dec. 1993	L,C	HH VV HV VH	variable
		X	HH	variable
ERS-2	April 1995-	C	VV	23
RADARSAT	Nov. 1995-	C	HH	20-50

For technical reasons a chirp technique, i.e. a long pulse with modulations on the frequency, is emitted and after reception transformed into a short pulse value. The emitted pulses from the radar hit the objects in the resolution cell at the theoretically homogeneous scattering surface at different angles and times. Backscatter and surface penetration vary slightly according to the scattering media. The result is that the backscattered contribution from the various places within the resolution cell is changed to a different phase, power and polarization. Phase shift causes constructive or destructive interference to occur.

The SAR image constructed from a linear combination of all the individual scatters illuminated by the radar will vary around a mean value. When the amplitude is squared, the phase information is eliminated, but the brightness (intensity) differences are preserved. The standard deviation on brightness is dependent upon the number of looks. Number of looks refers to uncorrelated radar recordings of the same element under ideally the same conditions. To eliminate the unwanted scatter in Φ_0, the radar system is constructed so that it "sees" the object several times and the signals (effect

values) are averaged. Hence the variance of the intensity is reduced. It is a non-coherent averaging performed in raw signal data by dividing the antenna into more "seeing segments" and thereby obtaining a larger number of uncorrelated recordings of the same resolution cell. As the number of effective looks is not determined by the user of SAR data, other tools have to be used to get rid of unwanted variance around the mean, the so-called speckle noise (FAO, 1993).

Speckle is a statistic fluctuation or uncertainty associated with the brightness in each pixel. Speckle noise is multiplicative. This means that the higher the mean reflection, the larger the spread. So in an area mapped with dark grey tones (low Φ_0), the speckle will generally be less than in brighter areas. Users can reduce speckle either by filtering techniques or by block-averaging. Filtering is performed in image data by averaging a number of pixels in a moving window and assigning the centre pixels new (estimated) values based on the local statistics appearing within the window (e.g. Hasager, 1997). Block-averaging is done by averaging a number of cells. Hence the spatial resolution is decreased. For ERS SAR the resolution cells are 25 m * 25 m, and it is foreseen that a 400 m * 400 m resolution will be adequate for estimation of off-shore wind resources. The swath of ERS SAR is 100 km.

SAR recording is independent of sunlight and the atmospheric damping of microwaves is very small at wavelengths larger than 3 cm (< 10 GHz). It means that the C-band energy (5.6 cm wavelength) is transmitted practically undisturbed through the atmosphere. Clouds and precipitation do not effect the recording.

2.2 Retrieval of wind speed and direction from SAR

Physical principle of using SAR to estimate the wind speed is through the correlation between capillary waves at the sea surface and the backscattered signals. Although the CMOD4 (Stoffelen & Anderson, 1993, see Offiler, 1994) and CMOD IFRE2 algorithms were developed originally for scatterometer data, the models have been shown to be useful for SAR data too (e.g. Offiler, 1994, Mastenbroek, 1998, Korsbakken & Furevik, 1998).

The empirical methodology of retrieving wind speeds from C-band VV scatterometer is well-established. The method is based on derivation of fitting functions between ocean wind speeds and radar parameters. There are two well-know methods, the CMOD4 (Stoffelen and Anderson, 1993) (implemented at ESA in 1993 for operational fast-delivery wind product) and the CMOD IFR2 (Quilfen et al., 1998) (an off-line product from IFREMER, i.e. Institute Francaise de Recherche pour L'Exploitation de la Mer). CMOD IFRE2 is based upon wind speed data from 3433 collocated pairs of NOAA buoys and ECMWF model results. The estimated model tranfer function (MTF) is derived from the relationship between wind speed at 10 m, Φ_0, the incidence angle of the radar beam and the azimuth direction of the mean wind vector. The relationships are implemented in analytic form with the supplied coefficients used to generate look-up tables of as a function Φ_0, incidence angle of the radar beam and the wind direction (Offiler, 1994).

The models are very sensitive to Φ_0. Therefore SAR scenes in the precision image format, SAR.PRI, will be used because these can be further calibrated by the user (e.g. Scoon et al., 1996).

Wind direction can in some cases be estimated from wind streaks in the SAR scenes. If not, wind direction will have to be taken from NWP models or meteorological observations. Wind streaks were visible in approximately 65% of the scenes used in a study on winds in a coastal region in the Baltic Sea (Lehner et al., 1998, Horstmann et al. 1998). In this work the wind streak direction was determined by applying a two-dimensional Fourier transform (FFT) to a sub-set of the radar scene. It should be noted however, that the wind streaks will not be aligned with the mean wind vector but offset due to Ekman turning. For a Dutch waddensee study (Mastenbroek, 1998) this angular difference was found to be about 10°. In near-coastal regions (> 3 km from shore) the wind direction was shown to be measured from SAR wind streaks to an accuracy of 5°(Lehner et al., 1998). The angular deviation

between wind streaks and the mean wind vector will be dependent upon the height above surface, the static stability and internal boundary layer(s). This/these will be present for off-shore flow (i.e. flow from the land to the sea) as opposed to on-shore flow from the open sea (fetch-unlimited flow).

2.3 Roughness of the sea

It is well-known that the wind generates capillary waves at the sea surface and that Charnock's relation provides a formula to calculate the roughness (z_0 in m) from the friction velocity (u_* in m/s) and the acceleration of gravity (g in m s^{-2}). The equation reads $z_0=0.015u_*^2/g$ (Charnock, 1955 *in* Stull, 1991). Studies have shown that in fetch-limited seas the roughness is dependent upon fetch. In the Danish seas a constant of 0.018 seems more appropriate than the original value of 0.015. For open seas 0.011 is generally recommended (Johnson et al., 1998). It is important to include these roughness effects in microscale models (Astrup et al., 1999). A LINearized COMputational model (LINCOM) useful for flow over hilly terrain (Troen & de Baas, 1986), is combined with a microscale aggregation model useful for flow over terrain with variations in surface roughness (Hasager & Jensen, 1999) and a model for the sea surface roughness (Astup et al., 1999, Petersen et al. 1998). The parametrization yields relatively larger roughness near the shore and at larger distances approach the Charnock relationship. The roughness step change between the land and sea is a significant parameter.

Recently meteorological data sampled from sea-masts at the Vindeby site has been analysed in relation to fetch and stability, and it was demonstrated that the effect of stability is significant (Petersen et al. 1998, Lange and Højstrup, subm.). This supports the results of (Frank et al, subm) that demonstrates that a correct description of stratification is more important than applying a fetch dependent sea roughness.

Drawbacks of NWP and planetary boundary layer models (PBL) are that they are too coarse compared to SAR satellite data (Offiler, 1994). NWP/PBL results have been used extensively for comparison to e.g. scatterometer wind products. For SAR algorithms it becomes important to combine high-resolution mesoscale models e.g. KAMM with a 1 km resolution (Karlsruhe Atmospheric Mesoscale Model) and WasP micrositing model as well as long-term meteorological observations at sea-masts. Further, to ascertain the static stability, sea and land surface temperatures (SST/LST) should be derived from NOAA AVHRR and ATSR and combined with air temperature observations to the ocean wind speed observations. These methods will be used in a project in years 2000-2002. The project WEMSAR, Wind Energy Mapping Using Synthetic Aperture Radar, is a EU funded project with partners from the Nansen Environmental and Remote Sensing Center (Norway), NEG Micon and Risø (Denmark) and ENEA (Italy).

Studies on the state of the sea surface will be very important for improving the SAR wind derivations. The physical link between wind speed and generation of capillary waves is dependent upon a long list of factors e.g. tidal currents, slicks, bathymetry, wave age, temperature, viscosity, fetch, atmospheric stratification, coastal orography, land-sea breezes and low-level jets over cold seas (Petersen et al., 1998). Some of these parameters have been investigated in part in relation to methods for wind retrieval from SAR e.g. in the VIERS model (Janssen et al., 1998) and in so-called SWA (SAR Wind Algorithm) method originally developed by (Vachon et al. 1994, *see* Korsbakken et al., 1998).

2.4 Briefly on scatterometer and altimeter

Scatterometer data has a resolution of 50 km x 50 km and covers a swath of 500 km. The working principle is that a short pulse is emitted towards the surface and the returned signal is recorded. The incidence angles of the side-looking instrument are between 18° and 59°. The wind direction is not retrieved directly, but derived through a first guess approach on wind direction based on NWP. The backscatter from the three independent backscatter measures (fore, mid and aft beams) normally yields a 180° ambiguity on wind direction solved through triplets within a mathematical model (Ebuchi &

Graber, 1998, Kramer, 1996). The specification of 2 m s^{-1} or 10% in rms and ±20° in wind direction is met for the 2-24 m s^{-1} wind speed interval. In some cases (i.e. for a dataset where near-neutral stability is fulfilled) the accuracy is 1.5 m s^{-1} by the CMOD4 (Offiler, 1994).

The K-band altimeters on-board ERS and Topex-Poseidon have footprints varying from less than a km over calm seas to several km over rough sea. The resolution is 7 km. The altimeter transmits short pulses from nadir and receives the backscattered signals. From analysis of the form of the echo pulse and the timelag, it is feasible to estimate the height of the surface (ocean or land) and the significant wave height. Wind direction is not retrieved (Kramer, 1996).

ACKNOWLEDGEMENTS

Funding from EU in project ERK6-CT-1999-00017 is acknowledged.

REFERENCES

Astrup, P., Larsen, S.E., Rathmann, O. and Madsen, P.H., 1999: WAsP engineering –Wind flow modelling over land and sea. *In* Wind Engineering into the 21st Century, Larsen, Larose & Livesey (eds.). Balkema, Rotterdam, pp 179-184

Barthelmie, R.J, Courtney, M.S., Højstrup, J. & Sanderhoff, P., 1994: The Vindeby Project: A description. Risø Report R-741 (EN). Risø National Laboratory, Roskilde, Denmark

Ebuchi, N. & Graber, H. C., 1998: Directivity of wind vectors derived from the ERS-1/AMI scatterometer, *J. Geophys. Research,* **103**, pp 7787-7798

FAO, 1993: Remote Sensing Centre. Radar imagery. Theory and interpretation. Lecture Notes, ESA FAO Rome, p 103

Frank, H.P, Larsen, S.E., & Højstrup, J. (subm): Simulated wind power off-shore using different parameterizations for the sea surface roughness. *Wind Energy*.

Hasager, C.B., 1997: Surface fluxes in heterogeneous landscape. (Ph.D. thesis). Risø-R-922(EN). Risø National Laboratory, Roskilde, Denmark. p180

Hasager, C.B. and Jensen, N.O., 1999: Surface-flux aggregation in heterogeneous terrain. *Q. J. R. Meteor. Soc.,* **125**, pp 2075-2102

Horstmann, J., Koch, W., Lehner, S. and Rosenthal, W., 1998: Ocean wind fields and their variability derived from SAR, ESA-*Earth Observation Quarterly*, **59**, pp 8-12

Janssen, P.A.E.M., Wallbrink, H. Calkoen, C.J., von Halsema, D., Oost, W.A. and Snoeij, P. :VIERS-1 scatterometer model. *J. Geophys. Research,* **103**, pp 7807-7832

IGBP, 1998: The terrestrial carbon cycle: Implications for the Kyoto Protocol, *Science*, **280**, pp 1393-1394

Johnson, H. K., Højstrup, J., Vested, H.J. &Larsen, S.E., 1998: On the dependence of sea surface roughness on wind waves. *J. Phys. Oceanogr.,* **28**, pp 1702-1716

Korsbakken, E. & Furevik, B., 1998: Wind field retrieval from SAR compared with scatterometer wind field during ERS Tandam phase. ESA-*Earth Observation Quarterly*, **59**, pp 23-26

Korsbakken, E., Johannessen, J.A. and Johannessen, O.M., 1998: Coastal wind field retrievals from ERS synthetic aperture radar images. *J. Geophys. Research*, **103**, C4, pp 7857-7874

Kramer, H.J.., 1996: Observation of the Earth and Its Environment. Springer. 3rd enlarged ed., Berlin. p960

Lange, B. & Højstrup, J. (subm.): A validation study of WAsP for offshore applications. ICWE special issue of the J. of Wind Engineering and Industrial Aerodynamics (submitted)

Lehner, S., Horstmann, J., Koch, W. and Rosenthal, W., 1998: Mesoscale wind measurements using recalibrated ERS SAR images. *J. Geophys. Research*, **103**, pp 7847-7856

Mastenbroek, K., 1998: High-resolution wind fields from ERS SAR. ESA-*Earth Observation Quarterly*, **59**, pp 20-22

Mortensen, N.G., Landberg, L,, Troen, I. and Petersen, E.L.,, 1993: Wind Atlas analysis and application Program (WAsP). Risø National Laboratory, Roskilde, Denmark

Offiler, D., 1994: The calibration of ERS-1 satellite scatterometer winds*, J. Atmospheric and Oceanic Technology*, **11**, pp1002-1017

Petersen, E.L., Mortensen, N.G., Landberg, L., Højstrup, H. & Frank, H., 1998: Wind power meteorology. Part II: Siting and models. *Wind Energy* **1**, pp 55-72

Quilfen, Y., Chapron, B., Elfouhaily, T., Katsaros, K. and Tournadre, J., 1998: Observation of tropical cyclones by high-resolution scatterometry. *J. Geophys. Research,* **103**, pp 7767-7786

Scoon, A, Robinson, I.S. and Meadows, P.J., 1996: Demonstration of an improved calibration scheme for ERS-1 SAR imagery using a scatterometer wind model. *Int. J. Remote Sensing*, **17,** 2, pp 413-418

Stoffelen, A. and Anderson, D.L.T., 1993: Wind retrieval and ERS-1 scatterometer radar backscatter measurements. *Advance Space Research*, **13**, pp53-60

Stull, R.B., 1991: An introduction to boundary layer meteorology. Kluwer Academic Publishers. p666

Troen, I. & de Baas, A., 1986: A spectral diagnostic model for wind flow simulation in complex terrain. *Proceedings of the European Wind Energy Association Conference & Exhibition*, Rome, pp 37-41

Troen, I. and Petersen, E.L., 1989: European Wind Atlas. Risø National Laboratory, Roskilde, Denmark, p656.

THE ATMOSPHERIC DYNAMICS MISSION

P. Ingmann and J. Fuchs (*)

and the members of the ADMAG[1]

(*)ESA/ESTEC, P.O. Box 299, NL-2200 AG Noordwijk, The Netherlands

ABSTRACT

The primary aim of the Earth Explorer Atmospheric Dynamics Mission is to provide improved analyses of the global three-dimensional wind field by demonstrating the capability to correct the major deficiency in wind-profiling of the current GOS and GCOS. The ADM will provide the wind-profile measurements to establish advancements in atmospheric modelling and analysis. There is an intimate link between progress in climate modelling and progress in numerical weather prediction (NWP) as our understanding of the atmosphere is largely based on the experience of operational weather centres. Long-term data bases are being created by NWP data assimilation systems to serve the climate research community. It is widely recognised therefore that the impact of a new global atmospheric observing system on our understanding of atmospheric dynamics should be evaluated primarily in the context of operational weather forecasting.

New insights into the atmosphere through the provision of wind profiles are expected for NWP but also for climate research. The ADM is addressing one of the main areas discussed under Theme 2 of the 'ESA Living Planet Programme' (ESA, 1998). Although there are several ways of measuring wind from a satellite, only the active Doppler Wind Lidars (DWL) has the potential to provide the requisite data globally. It is the only candidate so far that can provide direct observations of wind profiles. In addition, a DWL will not only provide wind data but also has the potential to provide ancillary information on cloud top heights, vertical distribution of cloud, aerosol properties, and wind variability as by-products.

1. Introduction

The 'ESA Living Planet Programme' (ESA, 1998) describes the plans for the Agency's new strategy for Earth Observation in the post 2000 time frame. It marks a new era for European Earth Observation based on smaller more focused missions and a programme that is user driven, covering the whole spectrum of interests ranging from scientific research-driven Earth Explorer missions through to application-driven Earth Watch missions. The user community is therefore now able to look forward to a programme of more frequent but very specific missions directed at the fundamental problems of Earth system sciences.

Out of the nine Earth Explorer core missions identified in ESA SP-1196 (1-9), four core missions were selected for in-depth study, namely: the Land-Surface Processes and Interactions Mission (LSPIM); the Earth Radiation Mission (ERM); the Gravity Field and Steady-State Ocean Circulation Mission (GOCE); and the Atmospheric Dynamics Mission (ADM). In autumn 1999, GOCE and ADM were selected for implementation.

[1] The members of the Atmospheric Dynamics Mission Advisory Group (ADMAG) were:
P. Flamant/LMD, L. Isaksen/ECMWF, E. Källén/MISU, J. Pailleux/Météo France,
A. Stoffelen/KNMI, M. Vaughan/DERA, W. Wergen/DWD

The primary aim of the Earth Explorer Atmospheric Dynamics Mission is to provide improved analyses of the global three-dimensional wind field by demonstrating the capability to correct the major deficiency in wind-profiling of the current Global Observing System (GOS) and Global Climate Observing System (GCOS). The ADM will provide the wind-profile measurements to establish advancements in atmospheric modelling and analysis. There is an intimate link between progress in climate modelling and progress in numerical weather prediction (NWP) as our understanding of the atmosphere is largely based on the experience of operational weather centres. Long-term data bases are being created by NWP data assimilation systems to serve the climate research community. It is widely recognised therefore that the impact of a new global atmospheric observing system on our understanding of atmospheric dynamics should be evaluated primarily in the context of operational weather forecasting.

New insights into the atmosphere through the provision of wind profiles are expected for NWP, but also for climate research. The ADM is addressing one of the main areas discussed under Theme 2 of the 'ESA Living Planet Programme' (ESA, 1998). Although there are several ways of measuring wind from a satellite, the active Doppler Wind Lidar (DWL) is the only candidate so far that can provide direct observations of wind profiles, and thus has the potential to provide the requisite data globally. In addition, a DWL will not only provide wind data, but also has the potential to provide ancillary information on cloud top heights, vertical distribution of cloud, aerosol properties, and wind variability as by-products.

2. Global Wind Profile Measurements for Climate and NWP

Reliable instantaneous analyses and longer term climatologies of winds are needed to improve our understanding of atmospheric dynamics and the global atmospheric transport and the cycling of energy, water, aerosols, chemicals and other airborne materials. However, improvement in analysing global climate, its variability, predictability and change requires measurements of winds throughout the atmosphere. In order to do so, it is a pre-requisite to improve NWP, as progress in climate-related studies is intimately linked to progress in operational weather forecasting. The World Meteorological Organisation (WMO) states in their recent evaluation of user requirements and satellite capabilities that for global meteorological analyses measurement of wind profiles remains most challenging and most important (WMO, 1998).

After several decades of observations from space, direct measurements of the fully global, three-dimensional wind field are still lacking. Deficiencies, including coverage and frequency of observations, in the current observing system are impeding progress in both climate-related studies and operational weather forecasting while there is a clear requirement for a high-resolution observing system for atmospheric wind profiles.

At present, our information on the three-dimensional wind field over the oceans, the tropics and the southern hemisphere is indirect. It is severely limited by having to rely on mainly space-borne observation of the mass field and geostrophic adjustment theory. Improvements in the available wind data are needed urgently if we are to exploit fully the potential of recent advances in climate prediction and NWP and continue to make significant progress in the field, e.g. 4-DVAR assimilation.

The different types of observations currently available and constituting the Global Observing System (GOS) are documented in full detail in ESA (1996). They can be classified in the following way:

- *Surface data* – they are the synoptic reports from land stations and ships, the (moored and drifting) buoys, and also the scatterometer winds from satellites (such as ERS). They are all single level data, and cannot provide any information on atmospheric profiles.
- *Single-level upper-air data* – mainly aircraft reports and cloud motion winds derived from geostationary satellite imagery. More and more aircraft observations (wind and temperature) are

being made during ascent and descent phases, thus tending to become 'multi-level'. Their main deficiency is the poor data coverage.

- *Multi-level upper-air data* – mainly the radiosondes (Fig. 1) and the polar orbiting sounder data. Satellite sounders provide global coverage with radiance data, which can only be used indirectly for the definition of the mass field (temperature and humidity). Radiosondes are the only current observing system providing vertical profiles of the wind field, but they are available mainly from the continents in the northern hemisphere.

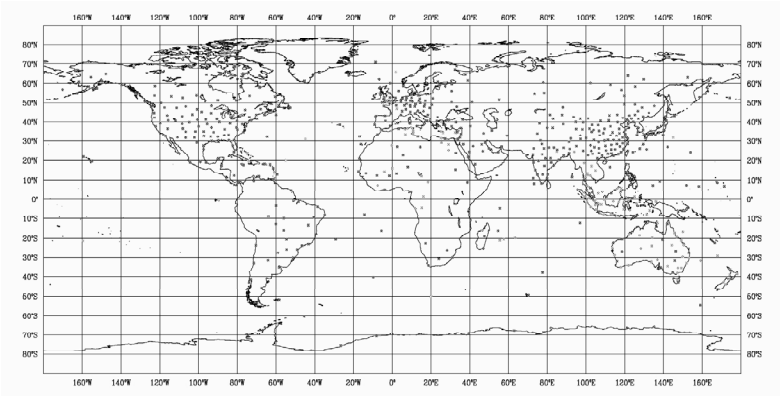

Figure 1. The radiosonde network – radiosonde/pilot ascents containing wind profile information that were available for the 6-hour time window centred around 12 UTC on 28 April 1999. Wind profile information is generally lacking over all ocean areas.

3. OSE and OSSE: Principles, Limitations and Some General Results

In order to assess the impact of wind profile data on NWP in a more quantitative way, Observing System Experiments (OSE) and Observing System Simulation Experiments (OSSE) have been run in NWP for at least twenty years. OSE are impact studies carried out with existing observations: two parallel data assimilations are carried out, with and without the observing system to be evaluated; resulting analyses and subsequent forecasts are then compared. OSSE are similar to OSE except the observations to be tested are simulated rather than real: simulated observations are produced from an NWP model integration assumed to be the 'known truth' and usually called the 'nature run'. For a quantitative assessment of a non-existing observing system like the global wind profiles, which may be produced by a space Doppler lidar in the next decade, OSSE are required.

In a recent OSSE performed in Germany it was shown that a system providing only a small number of wind profiles in place of the conventional wind observations over North America would recover more than half of this forecast degradation. Figure 2 (from the same study) illustrates that even at forecast range 0 (model initial state), systematically removing the North-American wind profiles produces wind uncertainties over almost the entire tropical area, indicating that the tropical flow is rather uncertain. This experiment provides a rough estimate of the potential impact of wind profile data available in a data sparse area of the size equivalent to North America. Forecasts started from the degraded analysis reduced the operational medium-range forecast skill by 20 hours.

Another interesting OSE was carried out by Isaksen (Ingmann et al., 1999) with the 1997 ECMWF global data assimilation and forecasting system. It evaluates the impact of all the radiosonde wind profiles above the planetary boundary layer (PBL) versus the impact of the radiosonde mass profiles (geopotential height), and also the impact of all available radiosonde information. The impact is found to be much larger than the impact of any single-level data observing system and equivalent to a big portion of the total radiosonde network impact which includes temperature and humidity information.

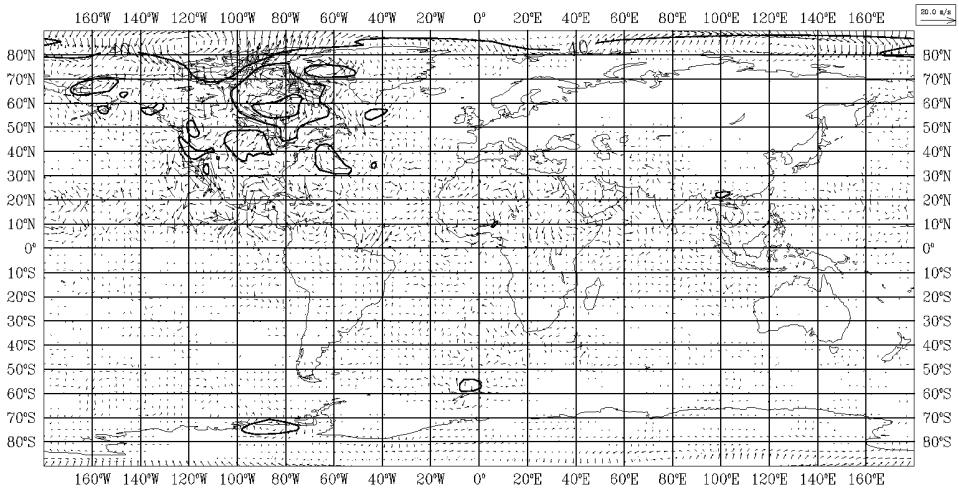

Figure 2. Degradation of the global wind field – analysis of differences in the geopotential height and wind field at 500 hPa between an 11 day long assimilation not using wind profile observation from radiosondes, pilots and aircraft over the United States and Canada and the control assimilation using all observations. The difference is valid for 30 January 1998, the contour interval for the height field is 20 m (from Cress, 1999).

4. The Need for Atmospheric Wind Fields for Climate Studies

Climate-change issues have received substantial attention in recent years due to the increasing awareness that human activities may substantially modify the future climate of the Earth. The globally averaged temperature has increased by about 0.6 degrees Celsius over the past hundred years and 1998 was the warmest year recorded on instrumental temperature record covering the last 150 years. These facts and other pieces of evidence suggest that an increased greenhouse effect due to human activities is starting to influence the global climate system. A very important question is thus to assess how a further future increase in greenhouse gases may affect this system. The most effective tools available to answer such questions are global and regional climate models, which to a very large extent resemble the corresponding NWP models. All the benefits of wind data discussed in the previous section relating to NWP models are also relevant to circulation models used for climate studies as both model types are based on the same physical and numerical principles. An illustration of the uncertainties involved in climate-change scenarios can be seen in Figure 3.

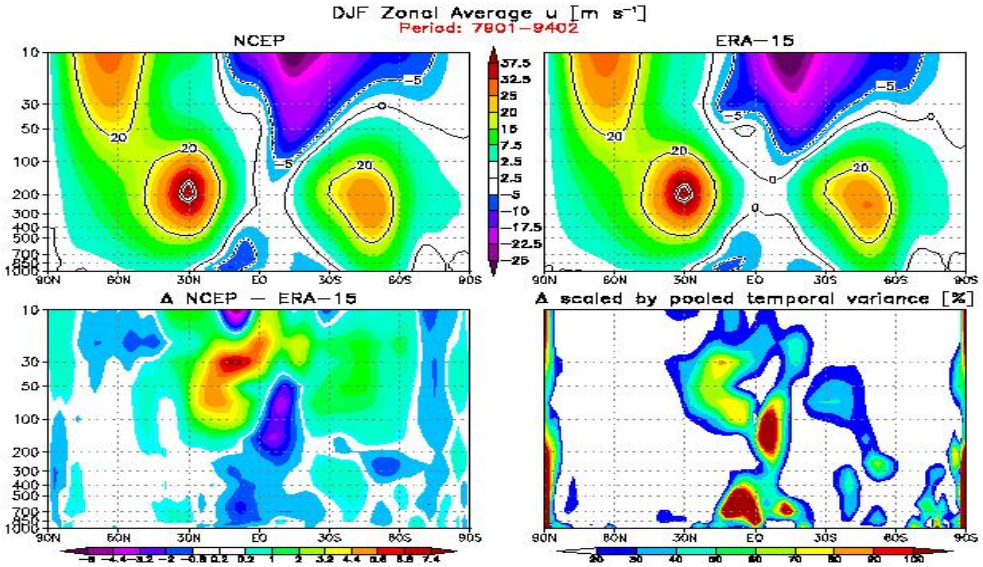

Figure 3. Comparison of NCEP (National Centre for Environmental prediction) and ERA (ECMWF Re-Analysis) derived zonal winds. Major differences are found mainly in the tropics and in the lower stratosphere.

5. Observational Requirements

Existing and planned systems will not meet the requirements for better wind profiles. In order to meet the numerical weather prediction, climate and atmospheric research objectives, an observing system is needed that provides three-dimensional winds over the globe. This means that it is essential to put significant effort into the development of a space-based system.

The WMO recognises the prime need for wind-profile data (WMO, 1998) and has defined a set of optimum wind-profile measurement requirements (WMO, 1996). User requirements for synoptic use are as or more stringent than those for climatological use. Quoting from WMO (1996): 'Various statements of requirements have been made, and both needs and capability change with time. The statements given here were the most authoritative at the time of writing, and may be taken as useful guides to development, but are not fully definite'. The WMO assigns great importance to wind-profile measurements. The realisation of their requirements would represent a major step forward in improving the quality of atmospheric flow analyses.

Current satellite capabilities for wind profiles consist of image-derived cloud motion winds (CMWs). However, it should be noted that in the absence of any appreciable wind-profiling capability, the current satellite winds mainly improve wind analysis in the tropics (e.g. Kelly, 1997, or Kållberg and Uppala, 1999), and thus do not at all meet the objectives. In order to give better guidance to developers of observation systems, the WMO has used the current satellite capability (i.e. CMW) to set a threshold below which no impact is expected from additional wind measurements.

Table 1. Observational requirements for an Atmospheric Dynamics Demonstrator Mission.

		Observational Requirements		
		PBL	Troposph.	Stratosph.
Vertical Domain	[km]	0-2	2-16	16-20
Vertical Resolution	[km]	0.5	1.0	2.0
Horizontal Domain		global		
Number of Profiles	[hour^{-1}]	100		
Profile Separation	[km]	> 200		
Temporal Sampling	[hour]	12		
Accuracy (Component)	[ms^{-1}]	2	2-3	3
Horizontal Integration	[km]	50		
Error Correlation		0.01		
Reliability	[%]	95		
Timeliness	[hour]	3		
Length of Observational Data Set	[yr]	3		

For a mission intended to demonstrate the feasibility of a full-scale spaceborne wind observing system to improve global atmospheric analyses, the requirements on data quality and vertical resolution are the most stringent and most important to achieve. Under this assumption, the horizontal density of observations is of the lowest priority amongst the requirements discussed in this chapter. The derivation of the coverage specification is supported by weather-forecast-impact experiments, which included the inputs of the conventional wind-profile network that is thin and irregular but of key importance. Moreover, the coverage specification reflects the WMO threshold requirements. Table 1 specifies the principal parameters for wind-profile observations that have been extracted from the above-mentioned WMO requirements and capabilities documents in view of demonstrating the capabilities.

6. The Technical Concept

The mission requires the measurement of horizontal wind velocity components from the lower part of the troposphere to the lower part of the stratosphere (up to 20 km altitude). The observation of a single component of the horizontal wind velocity is required to ease the instrument design since it has been shown to be adequate for the ADM. Furthermore, there is no particular requirement on the direction of the wind component to be measured.

The required instrumental accuracy for any horizontal line-of-sight (HLOS) wind component has been translated from the mission accuracy requirement of 2-3 ms^{-1}. The background representativeness error for a line-averaged wind component measurement has been quadratically subtracted from the mission accuracy requirement, yielding an instrumental accuracy requirement of 1-2 ms^{-1} for the HLOS wind component. It has to be noted that this representativeness error includes the contribution from the vertical wind component.

Stringent requirements on both wind accuracy and large vertical domain (up to 20 km) lead to consider an instrument concept relying on molecular backscatter at high altitude, where background aerosols become rare (Vaughan et al., 1999), and on aerosol backscatter at lower altitude. Figure 4 shows the baseline measurement profile.

The main characteristics of the proposed system feature a satellite flying in a Sun-synchronous dawn-dusk orbit of 400 km altitude, carrying a continuously operated lidar instrument

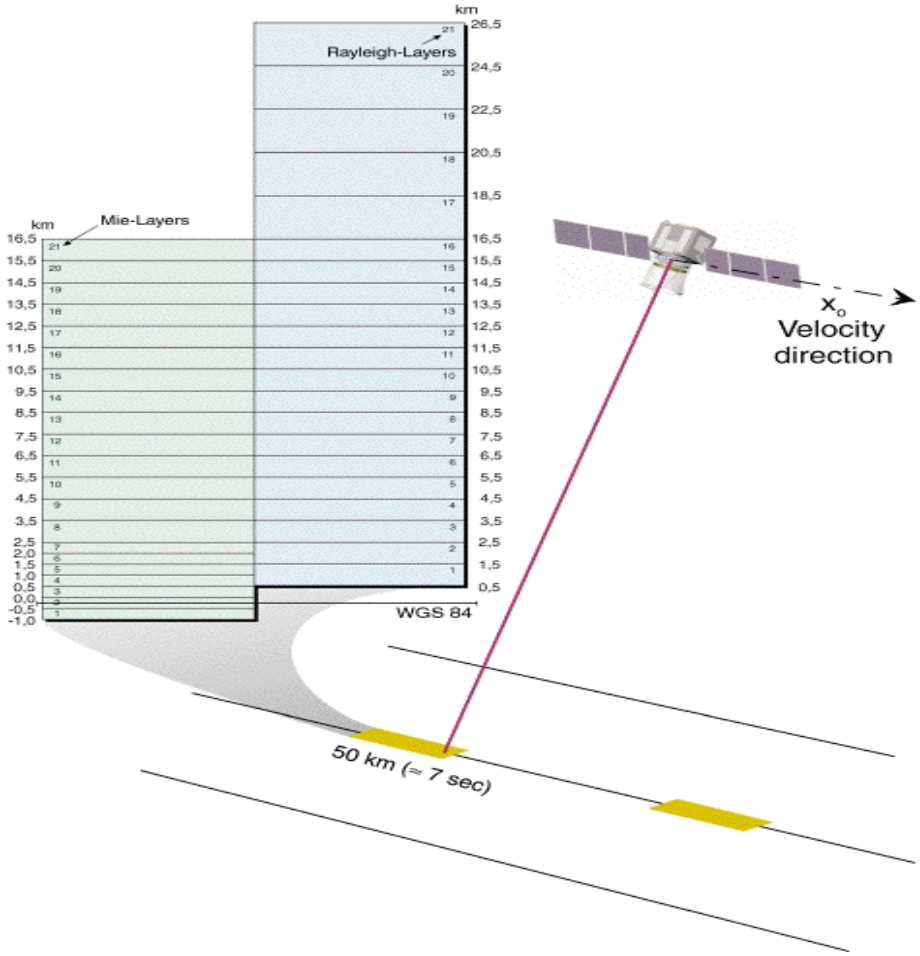

Figure 4. The baseline measurement profile depicting the mapping of atmospheric heights to layers measured by the detector. (ALADIN) whose main field of view is 35° off nadir and points to the anti-Sun side of the satellite track.

The performance requirements of the instrument require that an optical aperture of 1.1 m is needed, resulting in an outer diameter for the protecting baffle of about 1.2 m diameter, which dictates to some extent the dimensions of other satellite elements. A further consequence of the measurement performance requirements is the need to provide an excellent thermal stability, which affects the distribution of the units in the satellite. The baseline satellite configuration is shown in figure 5.

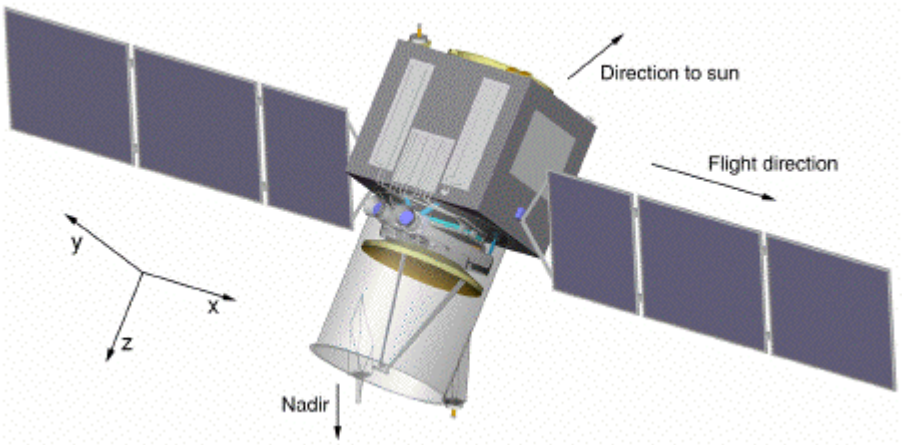

Figure 5. ADM baseline satellite configuration.

7. Programmatics

The US started with activities targeted at a DWL. The original concept was the LAWS (laser atmospheric wind sounder) concept. After refinement it was planned to embark a DWL on a shuttle for technology demonstration in 2001. However, this project was discontinued in 1999. In the context of the IPO (Integrated Program Office) NPOESS programme there are plans to embark an operational instrument in the 2007/8 time-frame. In Japan there are similar plans for a DWL called JLAWS (Japanese LAWS).

In the context of the European Space Agency's future Earth Observation *Living Planet Programme* (ESA, 1998) the Atmospheric Dynamics Mission is one of the two missions selected for implementation with a target launch date of 2006.

8. Conclusions

The Atmospheric Dynamics Earth Explorer Core Mission will for the first time provide direct observations on a global scale of atmospheric wind profiles over the depth of the atmosphere, a notable deficiency of current observing systems. These data will find wide application in advancing the performance of numerical models used in weather forecasting as these are suffering increasingly from the lack of such data. With these data it will also be possible to increase understanding of atmospheric processes occurring in tropical regions to the point where it will be possible to take proper account of them in climate models. The proposed concept meets the requirements of growth potential which is relevant in view of a future operational mission.

More detailed information on the scientific context and the mission implementation can be found in ESA (1999).

ACKNOWLEDGEMENT

The technical concept presented in this document is very much relying on the results of on-going work within European industry, namely by Dornier Satellitensysteme and Matra Marconi Space.

REFERENCES

Cress, A.,1999: Impact of wind profile observations on the German Weather Service's NWP system, Arbeitsergebnisse Nr. 56, Geschäftsbereich Forschung und Entwicklung, DWD, Offenbach. ISSN 1430-0281.

European Space Agency, 1996: Atmospheric Dynamics Mission, ESA SP-1196 (4).

European Space Agency, 1998: The Science and Research Elements of ESA's Living Planet Programme, ESA SP-1227, 105p.

European Space Agency, 1999: Atmospheric Dynamics Mission, Report for Mission Selection, ESA SP-1233 (4)

Ingmann, P., L. Isaksen, A. Stoffelen and G.-J. Marseille, 1999: On the Needs, Requirements and Feasibility of a Space-borne Wind Profiler, *Proc. of 'Fourth International Winds Workshop'*, Eumetsat, EUM P 24, 199-206.

Kållberg, P., and S. Uppala, 1999: Impact of Cloud Motion Winds in the ECMWF ERA15 Reanalysis, *Proc. of 'Fourth International Winds Workshop'*, Eumetsat, EUM P 24, 109-116.

Kelly, G.A., 1997: Influence of observations on the Operational ECMWF System, *WMO Bulletin*, 46, 336-342.

Vaughan, M., P. Flamant and C. Flesia, 1999: Scientific concept trade-off, ESA Contract No. 12510/97/NL/RE.

World Meteorological Organisation, 1996: Guide to Meteorological Instruments and Methods of Observation, 6th edition, *WMO-No.8*, Secretariat of the World Meteorological Organisation, Geneva, Switzerland.

World Meteorological Organisation, 1998: Preliminary Statement of Guidance Regarding How Well Satellite Capabilities Meet WMO User Requirements in Several Application Areas. WMO Satellite Reports SAT-21. *WMO/TD No 913*.

IMPACT ASSESSMENT OF A DOPPLER WIND LIDAR IN SPACE ON ATMOSPHERIC ANALYSES AND NUMERICAL WEATHER PREDICTION

G. J. Marseille, A. Stoffelen, F. Bouttier*, C. Cardinali*, S. de Haan, and D. Vasiljevic*

* Affiliated to the European Centre for Medium-range Weather Forecasts

Contract No. 13018/98/NL/GD
Phase A study of the Atmospheric Dynamics Explorer mission

ABSTRACT

Wind profiles from space would help to fill in data sparse areas over the oceans, the tropics, and the southern hemisphere. ESA has conducted a phase A study for the Earth Explorer Atmospheric Dynamics Mission (ADM). A polar satellite with a Doppler Wind Lidar (DWL) on board is proposed for this mission and which is described in this session by Ingmann. The DWL measures wind profiles in the troposphere and stratosphere up to 26.5 km height. Performance assessment studies have been performed for this system by simulation. In a statistical assessment it is investigated whether the DWL provides sufficient data quality in clear air, but also in cloudy regions. Obviously clouds are good scatterers, but could obstruct lower-lying air masses. We find that even in cloudy regions cloud penetration is sufficient to detect extreme tropospheric wind shear or the areas with large humidity flux in most cases. After the statistical assessment of performance an Observation System Simulation Experiment (OSSE) was performed. This experiment over a two-week period confirms earlier assessments that the ESA ADM will demonstrate the impact of space-borne DWL on atmospheric analyses, used for numerical weather prediction and climate analyses.

1. Introduction

ESA has recently approved a Doppler Wind Lidar (DWL) to fly on a free-flyer platform orbiting dawn-dusk at 400 km altitude. Rigorous trade-off studies during the Atmospheric Dynamics Mission (ADM) phase-A have resulted in the definition of a lidar concept, hereafter named ADM_UV, operating in the ultraviolet part of the spectrum at 355 nm laser wavelength. In order to guarantee the demonstration value of this mission for Numerical Weather Prediction (NWP) and in climate studies, extended atmospheric analyses and forecast runs are needed to better quantify this potential DWL impact and to address specific issues of concern during the ADM phase A study, such as profile quality and coverage.

The objective of this activity is demonstration of the impact on atmospheric circulation and on NWP of wind profiles from ADM_UV and comparison to the impact of conventional wind profiles (TEMP/PILOT) with respect to the existing Global Observing System (GOS). This demonstration is made by means of OSSEs (Observing System Simulation Experiments). It serves to consolidate the requirements for an operational mission by assessing the sensitivity of the impact of ADM_UV to key mission parameters to aid in the design of future operational missions, as well as to demonstrate the impact of the minimum useful requirements and performance of the Atmospheric Dynamics Earth Explorer Mission.

1.1 Background

The quality of state-of-the-art NWP is among other things determined by the availability and quality of meteorological observations. NWP models have improved much over the last decades, and advanced 4D-var techniques are now being used for the analysis. The spatial resolution of global circulation models has as well improved, which leads to a need for more observations on the sub-synoptic scales. On these scales the wind field, rather than the atmospheric temperature or humidity fields determines the atmospheric dynamics. Furthermore, the prime factor determining meteorological instability is vertical wind shear. In the tropics, for an accurate definition of the Hadley circulation, 3D wind information has been lacking. Conventional wind profile data lack coverage and a uniform distribution over the globe.

For the study of climate processes extensive reanalyses experiments are being conducted. These experiments use the technique of data assimilation, as used for NWP, to establish long time series of the weather in support of climate studies. In the OSSE evaluation we investigated extensively the analysis impact of wind profile data, thus supporting the climate application.

Recent OSEs (Observation System Experiments) by the European Centre for Medium-range Weather Forecasts (ECMWF) (Isaksen, 1998, and Kelly, 1997) have confirmed the relevance of tropospheric wind profile data for NWP. ECMWF tested this in a series of experiments where they excluded conventional wind profile observations (TEMP/PILOT), or parts thereof in the free troposphere, and compare to experiments where conventional (TEMP), or satellite (TOVS) temperature or humidity profile data, or single level observations, were excluded.

Complementary experimentation has been performed at the Deutcher Wetter Dienst (DWD) to test the impact of continental North American wind profile observations (Wergen, 1998). From these experiments, a few points are noteworthy. These experiments confirm largely the importance of wind profile data, compared to the importance of temperature/humidity data. Near-surface winds (PBL winds) seem less important than winds in the middle and upper troposphere. In the OSE experiments, a small number of (good quality) wind profiles already shows a positive impact on the quality of the NWP. TEMP/PILOT OSE work with the US National Center for Environmental Prediction, NCEP, NWP model confirms some of these conclusions. For these reasons, the ADM requirements have been focussing on quality rather than quantity over the last few years, in accordance with the WMO requirements. Moreover, past experience in data assimilation shows that quality can usually not be traded off against quantity without a degrading effect.

The results and conclusions of OSEs give an insight into the effect of a particular type of *existing* observation has in the *existing* data assimilation system. However, it is difficult to draw from this easily conclusions on the added value of supplementary measurements on the meteorological analyses and forecasts. This added value may be investigated through OSSEs. Météo France has made a first step. The work encompassed to run OSSE experiments with the French Arpege NWP model, in order to test the impact of the OSSE data base DWL wind profiles from a 10 micron laser attached to a free flyer satellite in a polar orbit (Cardinali et al, 1998). This scenario provided a wind profile density over the oceans comparable to the current density over land in the Northern Hemisphere. The assimilation experiments were performed with a low-resolution version of the NWP model (T42), and as expected the DWL impact could be well demonstrated.

DWL OSSEs performed in the United States indicate an impact even for low measurement accuracy. However, the forecast quality was almost exclusively based on DWL information from the Southern Hemisphere and therefore show obviously an improvement against the control analysis which did not contain relevant observations in this area.

For an operational system, the impact on NWP often depends on the skill of the data assimilation system used. Therefore it is worthwhile to perform an OSSE with the state-of-the-art ECMWF 4D-var system in order to consolidate the requirements for an operational mission. Based on past work (especially of ECMWF and Météo France, as well as preparatory work by KNMI), those additional questions have to be addressed. The main critical points to be considered are up-to-date model dynamics and resolution (desirable to have T319 L31), as well as the identification and consolidation of the driving key mission parameters.

1.2 Report outline

Chapter 2 discusses the general OSSE setup and required attributes. Most of necessary preparatory work to perform the OSSEs has been the result of many studies, started in the early 1990's (Stoffelen, 1994), (Becker, 1995), (Stoffelen and Marseille, 1998). The result of these studies is a database with simulated observations of conventional meteorological observation systems and three infrared lidar concepts that were proposed in the mid 1990's. The simulation of the ADM_UV concept is using the LIPAS simulation tool (Veldman, 1999). It includes simulation of data coverage according to the ADM user requirements and profile quality simulation according to expected instrument characteristics. Results of a pre-OSSE analysis to assess profile quality in clear air, *i.e.* without clouds, and the impact of clouds on atmospheric penetration are presented. Moreover shear and flux visibility are assessed in relation to clouds. After validation, the new concept is added to the OSSE database at ECMWF. Chapter 3 discusses results of the OSSEs performed to demonstrate the impact of the ADM_UV concept on NWP and atmospheric circulation analyses.

Table 1. MSE of analysis wind fields for the NoDWL and DWL experiments verified against the nature run. The mean is taken over 15 cases, i.e. analyses at 12 UTC from 19930206 until 19930220. The effective lidar impact (effect.) is defined as the difference of the MSE of the NoDWL and DWL experiment. The total lidar data impact equals the MSE of the differences of the analysed fields from the NoDWL and DWL experiments.

	500 hPa				200 hPa			
	NoDWL	DWL	effect.	total	NoDWL	DWL	effect.	total
Globe	20.98	12.52	8.46	14.11	27.88	15.78	12.10	18.86
N.Hemis	11.10	9.34	1.76	4.85	7.63	6.45	1.18	2.81
S.Hemis	31.73	14.75	16.98	25.58	40.61	16.63	23.98	32.20
Tropics	20.17	13.42	6.75	12.01	34.98	23.78	11.20	21.41
Europe	3.14	3.01	0.13	0.78	2.92	2.83	0.09	0.60
N.Atlantic	11.98	9.94	2.04	4.71	9.84	8.27	1.57	3.57
N.America	9.26	7.25	2.01	5.27	8.53	5.99	2.54	4.12

To compare the observational network as generated in Stoffelen et al. (1994) with the current operational network we compared the observation statistics of the OSSE with the operational observation statistics in the February period of 1999. The results are condensed in Table 2 and show that the OSSE uses more radiosondes (TEMPs), less AIREPs, less SATOBs and less DRIBUs.

Table 2. Global observation coverage and statistics of OSSE related to the operational system in 1999 for the same period, i.e. 5 February 18UTC to 16 February 12UTC. (o-b) Denotes the background departure and (o-a) the analysis departure.

	OSSE experiment			Operations 1999		
	NUMBER OF data	data RMS		number of data	data RMS	
		o - b	o - a		o - b	o - a
TEMP-wind[1] [m/s]	830,118	3.2	2.8	307,301	3.7	3.0
TEMP-T[1] [K]	400,290	3.8	3.7	402,404	3.0	2.8
TEMP-q[1] [kg/kg]	264,425	0.16E-2	0.15e-2	215,811	0.24e-2	0.23e-2
PILOT[1] [m/s]	328,870	3.2	2.8	241,334	3.7	3.0
AIREP-wind[1] [m/s]	100,060	5.8	5.3	920,698	4.3	4.0
AIREP-T[1] [K]	66,774	2.6	2.5	407,484	2.2	2.2
TOVS[1] [K]	0	-	-	2,347,298	6.5	5.0
LIDAR[1] [m/s]	532,992	4.2	3.4	0	-	-
SYNOPship-10U [m/s]	49,794	3.0	2.8	67,754	3.9	3.8
DRIBU-10U [m/s]	2,618	5.1	4.9	11,712	3.3	3.0
SCAT-10U[1] [m/s]	99,685	2.7	2.1	114,756	1.7	1.2
SYNOPland-2RH [%]	24,727	14.0	14.0	282,571	14.0	14.0
SYNOPship-2RH [%]	16,960	15.0	13.0	33,948	16.0	15.0
SATOB-wind [m/s]	37,576	4.3	4.1	981,886	5.3	5.2
PAOB (Pa)	3,255	229	207	3,353	307	273
RAOB-WIND [M/S]	1,183,830	3.9	3.5	855,975	5.2	4.6

[1] For instruments measuring profiles, the number of data equals the sum of data at all levels. The data RMS is an average over all levels.

[2] Only the closest 10m u-wind vector of the two available ambiguities is considered.

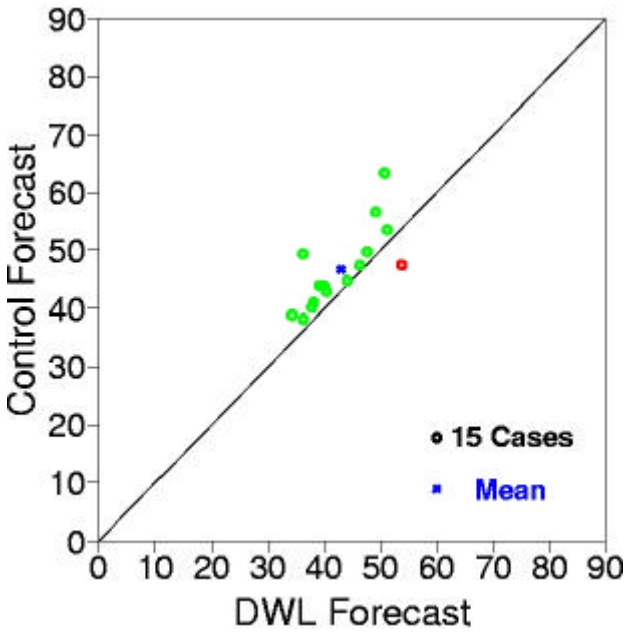

Figure 1. Comparison of control forecast and DWL forecast for 15 cases.

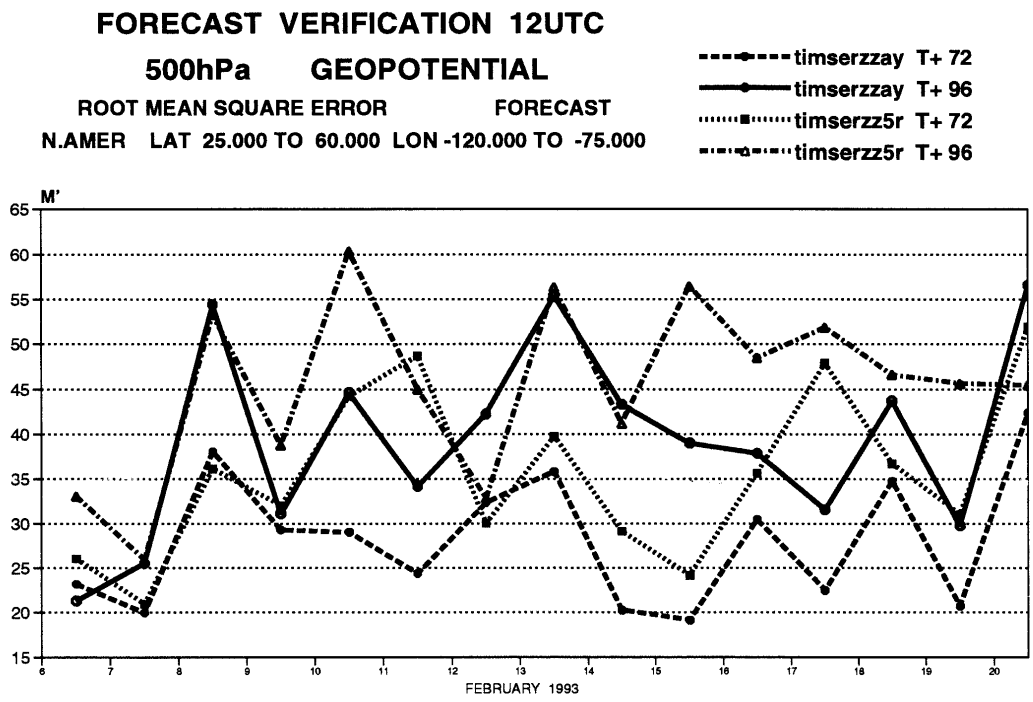

Figure 2. Comparison of reference run (NoDWL) with experiment run including lidar wind data. Analyzed period: 1993020512 – 1993022012, 6 hour assimilation window. Model: T319L31, no waves, no TOVS, no SSM/I, IFS cycle 21r1 + modification to allow the use of simulated HLOS winds form Doppler wind lidar data. 10-day forecasts were run once a day initiated with the analysis at 12 UTC.
az5r: Reference or control or NoDWL assimilation, no lidar winds.
zz5r: 10-day forecasts from az5r
azay: Same as az5r, including lidar wind data starting at 1993020518.
zzay: 10-day forecasts from azay

2. Observing System Simulation Experiments

This report addresses the use of OSSEs to assess the potential impact of the proposed ADM_UV DWL on atmospheric analyses and on NWP. More generally, OSSEs can be used to assess the potential impact of any new observing system. The basic elements of an OSSE are a state-of-the-art data assimilation system, a nature run "truth" and a database of simulated observations. The latter includes both simulated observations of conventional meteorological systems, covering a network similar to the operational network, and simulated observations of the new instrument to be assessed. Generation of the nature run and data base for conventional observation systems has been reported extensively in the past (Stoffelen et al, 1994), (Becker et al, 1995).

To build up a database of simulated observations one needs a description of the atmosphere over a certain time period. For this purpose, a "true" atmosphere is generated through a long integration period of a forecast model, initiated with an atmospheric analysis. This is called the "nature run". The nature run we use in this study was the result of a 30-day integration, initiated on 5 february 1993 00 UTC and ended on 7 march 1993 00 UTC. Integration was performed with the operational forecast model at ECMWF in 1993, *i.e.* T213 horizontal and 31 levels vertical resolution (Stoffelen, 1994). Mean atmospheric characteristics during the OSSE assimilation period, *i.e.* 6 February 1993 12UTC until 20 February 1993 12UTC are displayed in figures 1 and 2.

3. Conclusions

In this study we realistically simulated the UV Doppler Wind Lidar as proposed for the ESA Core Explorer Atmospheric Dynamics Mission, ADM_UV. ADM_UV was simulated, validated, and added to ECMWF OSSE database. In particular, a closer look was given to the nature run clouds, but no serious deficiencies were found. The relative lack of PBL clouds over the oceans as compared to satellite observations may be improved. However, we found that in the PBL over the ocean, the DWL impact is very limited due to the presence of the ASCAT scatterometer.

ADM_UV has a clear and demonstrable positive impact on the analyses and forecasts in the northern hemisphere. In the tropics and southern hemisphere the impact is overwhelmingly positive, but here the OSSE observing system is not representative of the real world observing system. In particular in the southern hemisphere, the incapability to realistically use satellite temperature sounding measurements is regretful. However, based on current operational experience at ECMWF, this is of little limitation in the northern hemisphere.

The average benefit of lidar data on medium-range forecast in the OSSE was about 0.25 days in the northern hemisphere (above 20N). Local impacts varied and were up to 0.5 days, for example for Europe. To test the significance of our results we verified that time series of forecast impact showed sufficient variability. On the other hand, in a clear majority of cases was the DWL forecast better than the control.

Good quality ADM_UV wind observations have a clear and beneficial impact on the analyses. Some large and beneficial forecast impacts of ADM_UV can traced back to areas with large analysis impact.
However, inaccurate ADM_UV data causes locally negative impacts. This occurs probably because those observations are not properly weighted against the background model fields in the analysis. In the local absence of good quality observations the background error estimate becomes poor, probably frequently resulting in detrimental observation impacts in the analysis. In areas with extensive high-level cloud cover negative impacts were most frequent. We may conclude from this that:
The tuning of data assimilation systems is very important for achieving beneficial observation impact and OSSE could be used for this; Quality control on real observations is very important in cloudy regions.

Wind profile observations are of key importance to the GOS, as demonstrated here again. However, the operational profile network is expected to further decrease in the future. As an illustration of this fact we note that the conventional wind profile network in operations is much smaller than that used in the OSSE. This will result in a larger impact of satellite data in the future in the northern hemisphere, both for mass and wind observations. Moreover, the simulated quality in the OSSE data base was too optimistic for the conventional wind profiles. This somewhat reduces the improvements brought by ADM_UV in the OSSE. On the other hand, more AIREP are available nowadays, mainly resulting in tropopause flight level observations, but also some profiles near airports. We rigorously tested the presence of a so-called fraternal twin problem, but found no substantial evidence of such a problem.

4. Recommendations

Although we have verified in this study that ADM_UV is indeed capable of demonstrating the potential value of space-borne wind profile observations for improving atmospheric analyses and NWP, this study was of a limited nature and more experimentation is recommendable.
OSSEs for other and more periods would reveal more about the significance of the results that we have found here. A two-week assimilation period is generally though of as the minimum to be able to demonstrate impact with an OSE or OSSE.

Moreover, it will be useful to study several scenarios of ADM_UV, such as for example a best and worst case scenario based on different instrumental and sampling options, or for different ways of data processing, in particular to test quality control.

OSSE can be used to tune data assimilation systems.

Quality control is very important. In the OSSE low–quality ADM_UV observations showed often detrimental impact. LITE observations may be useful to investigate the interaction of a lidar with a cloudy atmosphere and to study quality control issues. Also air and ground measurements may help to verify processing schemes.

Where ADM_UV is designed to demonstrate the capability of a space-borne DWL, OSSE could be used to study scenarios for an operational meteorological mission to be implemented when ADM_UV has successfully flown. Options for targeting LOS profiles, multiple LOS or even multiple satellites could be tested.

To avoid the fraternal twin problem we recommend the use of a foreign model for the production of the nature run. These fields can then be interpolated and processed in any location to provide an OSSE data base in standard meteorological format. The ECMWF has a great capability to run OSSEs on such input.

OSSEs including TOVS data would be better capable of assessing the relative benefit of temperature and wind sounding in the southern hemisphere and tropics. Simulation of AIRS or IASI or other new observation systems is also worthwhile. However, we note that for these observations, cloud clearing is a major issue and consequently error properties are complex and more difficult to simulate realistically.

ACKNOWLEDGEMENT

We acknowledge staff at ECMWF and Météo France for supporting this study. Special acknowledgement goes to ECMWF for maintaining the OSSE data base and nature run in their archives.

REFERENCE:

Becker, B. and H. Roquet, 1995, Extension of the OSSE data base to Scatterometer and ATOVS Data, Final Report Part II, ECMWF.

Cardinali, Carla, Jean Pailleux, Jean-Noël Thépaut, 1998, Use of simulated Doppler Wind Lidar data in NWP: an impact study, CNRS, Météo France.

Courtier, P., et al, 1998, The ECMWF implementation of three dimensional variational assimilation (3D-Var). Part I: Formulation, *Quart. J. Royal Meteor. Soc.* 124, 1783-1808.

Courtier, P., et al, 4D-Var, ECMWF documents, 1999.

Fabre, F., D. Morançais, 1998, ALADIN Incoherent DWL, Performance model description & Preliminary Analysis and concept design, Matra Marconi Space, 26/11/1998

Holton, J.R. An introduction to dynamic meteorology, 3rd edition, 1992.

M. Musatani, K.A. Campana, 1999, Note on Cloud Cover of the ECMWF Nature run used for OSSE/NPOESS project
(http://sgi62.wwb.noaa.gov:8080/research/osse/index.www,html)

Isaksen, Lars, 1998, Presentation at the EOPP Seminar on Atmospheric Dynamics, ECMWF, October 1998.

Rohn, M., G. Kelly, and R. Saunders, Experiments with Atmospheric Motion Vectors at ECMWF, Proc. *Fourth International Winds Workshop* from 20-23 October 1998, Saanenmöser, Switzerland, EUM P 24, printed at EUMETSAT, Darmstadt, Germany.

Stoffelen et al, 1994, Theoretical Studies of the Impact of Doppler Wind Lidar Data - Preparation of a data base, ESA-CR(P)-3943.

Stoffelen, A. and G.J. Marseille, 1998, Study on the Utility of A Doppler Wind Lidar for Numerical Weather Prediction and Climate, ESA-CR11982, 1998

Vaughan, N.J. Geddes, P.H. Flamant, C Flesia, 1998, Establishment of a backscatter coefficient and atmospheric database, ESA-CR12510.

Veldman, S.M, H.A. Knobbout, A. Stoffelen, G.J. Marseille and E.A. Kuijpers, 1999, LIPAS, executive summary, ESA, 3-9132/97, in progress.

Wauben, W.M.F., 1996, A new Algorithm for total ozone retrieval from direct sun measurements with a filter instrument, KNMI technical report.

Wergen, Werner, 1998, Presentation at the EOPP Seminar on Atmospheric Dynamics, DWD, October 1998

Wilks, D.S., Statistical Methods in the Atmospheric Sciences, 1995

World Meteorological Organisation, 1998: Preliminary Statement of Guidance Regarding How Well Satellite Capabilities Meet WMO User Requirements in Several Application Areas. WMO satellite reports SAT-21. *WMO/TD No 913*.

COMBINED CAPABILITIES OF DATA FROM ACTIVE AND PASSIVE SATELLITE INSTRUMENTS TO DEFINE ATMOSPHERIC MOTION

James F. W. Purdom
Director, Office of Research and Applications
NOAA/NESDIS

Integrity is the watch word of science. It is important that as we move to the future that we insure the integrity of our work. Too often, a scientist can become so involved in a particular product or area that the product becomes an area unto itself. This can lead to a sense of loyalty to the product, along with a lack of objectivity. This can be dangerous, because once it is perceived by the community at large that a scientist has lost objectivity, then all past work might be brought unrightly into question. Thus, this talk will focus into looking at lessons from the past that can help us not to fall into the trap of introspection without scientific dissection of that process. This talk will cover several areas:

a) Some Lessons from The Past
b) Cloud Location, Type and Movement
c) Cloud Motions and Winds
d) The Atmosphere in Motion
e) Thoughts on Assimilation and NWP

Most of the focus will be on topic (a) - how did we get where we are, and what lessons should we carry forward as we continue to develop our science. The presentation related to this paper can be down-loaded from ftp://orbit35i.nesdis.noaa.gov/pub/ora/purdom/5thWW/[1].

Perhaps the brightest, most scientifically talented person that I have ever been involved with is Ted Fujita. Ted was one of the original leaders in determining how to best utilize satellite data for a variety of scientific applications. We often think of Ted as a superstar in the area of mesoscale meteorology and tornadoes. That is certainly true, but Ted was also a superstar in the area of satellite meteorology. Why? There were a number of reasons: a) Ted was an expert in atmospheric science; b) Ted's curiosity was boundless; c) Ted was meticulous, you could see that from his early writings in Tellus on mesoscale meteorology - a field which he practically invented; d) Ted's analyses were works of art, but more than that they were precise and always dynamically correct. He knew what he was doing, and with his knowledge of the atmosphere, he knew why? Ted received many awards throughout his career, significant to our science: In 1985 at the 25th anniversary of weather satellites, Ted received a special award for his contributions that led to the success of the U.S. weather satellite program. Ted was cited for 'creative scientific leadership as an enthusiastic pioneer in the use of satellite imagery to analyze and predict mesoscale weather phenomena and to understand severe thunderstorms.'

Ted's pioneering work in the early days of satellite meteorology (for which he was recognized in 1967 with the American Meteorological Society's Clarence Leroy Meisinger Award for pioneering research on mesometeorological analysis and broad contributions to the use of meteorological satellites) made possible much of what we do today. Ted developed the necessary rectification and analysis techniques to make those TIROS satellite photographs useful for estimating the velocity of both low and high level winds. For example, shortly after the launch of TIROS 1, in the study of a 1960 south Pacific tropical storm, Fujita analyzed clouds to provide information about the direction of low level winds and the vertical wind shear between 700 and 200 hPa. He also showed how cloud shadows in these early satellite pictures could be used to quantitatively determine cloud top height (a problem we are still coming to grips with today).

Ted began his career by defining mesoscale meteorology, and under his guidance the Mesometeorology Research Project (MRP) came into being at the University of Chicago. It wasn't long after the launch of TIROS-1 that, recognizing the importance of satellites to meteorology, the MRP changed to SMRP the

[1] If you want to access the ftp site, please note that you should place the power point presentation and AVI loops into the same folder, then open the power point presentation. That way, the loops will link directly.

Satellite and Mesometeorology Project. The SMRP Research Papers soon became classics in atmospheric research, and are still referred to today.

The Applications Technology Satellite (ATS) era marked the beginning of measurements of cloud motion vectors (cmv's) from space based data. Fujita was there from the beginning, along with Vern Suomi, paving the path for us to follow. Originally, creating cmv's was a manually intensive process. While intensive, such activity had the distinct advantage of engaging the analysts mind into the process. Which cloud, what part of a cloud should be tracked. Which cmv's were representative of the motion of the atmosphere and which were not. Fujita, through his training and research in mesometeorology understood the atmosphere; he knew why the wind was blowing a certain direction and WHY. What he tracked was not a mystery but a revelation for us all. In performing such exquisite scientific work, Fujita lay a challenge for all to follow, as both a scientist and teacher. His QC (Quality Control) indicator was his knowledge and atmospheric dynamics.

An early ATS-1 series of images, from March 6, 1967 were used by Fujita to provide a detailed analysis of cloud motions over the Pacific Ocean area. Using conventional atmospheric analyses, Fujita determined how winds on the synoptic scale should behave, and how the cloud patterns and motions should relate to that. Then, using a series of images over the region, mesoscale cloud tracking was performed. Cloud patterns were selected for computation of cloud velocities, and low, middle, high and unknown initial positions were subjectively assigned. But those subjective assignments were not a mere guesses; they were based on atmospheric physics and understanding. Velocities were computed from cloud displacements between 1223 and 1354 Hawaii Standard Time. Heights were assigned according to cloud movement. From the March 6, 1967 detailed analysis of cloud motions over the Pacific Ocean area, Fujita showed that analysis of ATS cmv's plus conventional data revealed convergence at the 850 hPa level, with large convective clouds forming on the convergence line. This measurement of cloud motions and relating them to dynamic processes in the atmosphere was what was important. This revealing of dynamic processes was utmost in the mind of Fujita and other scientists working in the area of cmv determination in the early days. What, how, why - these were the watch words.

It was recognized early on that humans played an important role in the measurement and determination of cmv's, for the identification of gravity waves, mountain waves, cloud edge erosion and movements that were not direct measurements of the wind. Those phenomena were important, in that they were reflective of various atmospheric processes, but not cmv's in the way we today relate a cmv to a wind

It was recognized early on by Fujita and other pioneers that there was a relationship between image frequency, spatial resolution and the ability to resolve the motion of atmospheric features. For example, early experiments by Shenk and others at NASA, NOAA and in the University community were made to determine life cycles of cumulus over land and water; as well as to study cirrus lifetimes. These aircraft experiments were important components of what evolved into trials of taking images at more frequent that normal intervals (now known as rapid scan) to determine our ability to use cloud motions to determine winds at the mesoscale.

In his cmv research, Fujita showed that it was important to track the appropriate part of a cloud to determine the "wind." For example, Fujita showed that cmv's in various parts of a Florida thunderstorm anvil reveal that the leading edge of a drifting anvil cloud moves faster than the central region of the cloud. Fujita showed, what many of us realized, that the motions of a thunderstorm anvil were not representative of the wind field, but rather were representative of the thunderstorm's divergence at anvil level, plus the wind field into which it evolved. Furthermore, Fujita was the first to make Lear Jet flights (early 1970s) during which thunderstorm overshooting tops were photographed at 30 second intervals to study the dynamics of overshooting tops. In studying those tops, Fujita noted the existence of cirrus in the stratosphere, "jumping cirrus," which streamed downwind from the thunderstorm updraft area (the overshooting top region). In those studies of overshooting tops, many of the things revealed in 30 second and one minute interval GOES visible imagery were recognized. They included strong overshooting with downstream cirrus above the broad anvil top. We now realize that such cirrus often spreads hundreds of miles downwind, and may be

related to winds in the stratosphere. Current research of one minute and 30 second interval imagery (super rapid scan) has revealed that clouds all levels are easily followed, and that any number of cmv's might be derived. The question is: "what is the purpose of these winds?" Some of those super mesoscale cmv's are measurements that are representative on the synoptic scale, others are representative of the mesoscale, while some of the measurements reveal the effect of dynamic pressure as winds slow as they approach a mature thunderstorm. When we develop our cmv's today, are we selective and filter out winds that are inappropriate for a given application? In the image, the circle represents a 100 km radius: notice the variability of cirrus motions within that region. Which would you pick, what density, what application?

More than any of us, I believe, Fujita understood the importance of understanding cloud motions from satellites and the importance of their correct utilization in atmospheric science. Fujita was among the first to use stereo from the ground to track clouds and assign their correct heights and motions. We should all understand how important it is to place a cmv at the proper level, especially when wind speeds are strong - recall that while acceleration is directly proportional to horizontal gradients in the mass field, it is proportional to the square of the wind speed (V squared over 2). Thus errors at high wind speeds can be much more damaging for certain applications than similar errors at low wind speeds. But, imagine further the havoc that can result when these winds are placed at the wrong height in a highly energetic region such as the jet stream (a compounding error).

At the second wind workshop in Tokyo, Fujita and I showed results from experiments where ground based stereo cmv's were compared with cmv's derived from GOES data. The GOES cmv's height was determined using cloud shadows, while Fujita tracked the clouds over the same region using his ground based stereo camera system. Fujita stereoscopic whole sky cameras produced many more vectors than were produced with the GOES imagery (as might be expected). Most important, his measurements validated GOES cmv's to be within 1 m/s and 10 deg and 0.5 km. GOES cmv's ranged from 15.7 to 17.1 m/s from 314 to 315 degrees; CO2 slicing and cloud shadows agree on 10.5 km heights for pelican shaped cloud. The winds done for this example were produced in a research environment. Their verification statistics is what we should strive for operationally.

As satellite meteorologists, one of the tenets of which we should be acutely aware is that when we are observing the earth/atmosphere, "each spatial element has a continuous spectrum that may be used to analyze the surface and the atmosphere." In satellite meteorology, we have tended to use "chunks" of the spectrum (channels over selected wavelengths) for our analysis. As we move to the future, this is most definitely the way we DO NOT want to go for a number of applications. After hearing Bill Smith's talk on GIFTS, that seems rather obvious.

NASA has an instrument called AVIRIS, which currently flies on an aircraft. That instrument takes about 240 samples of the spectrum between around 400 and 2400 nanometers (0.4 to 2.4 microns). That very high resolution data may be used to analyze the spectrum in more detail (at each pixel). For example, fire, smoke, land surface and cloud appear very different depending on the wavelength used to observe a scene. While smoke shows up very well at short wavelengths, at long wavelengths we can virtually see right through it! At those longer wavelengths, the heat from the fire can be detected. However, as interesting as the finding and tracking of smoke may be, that is nothing (relatively speaking) when compared to water vapor. If we look at the same scene, using different portions of the AVIRIS spectrum, at 15 minute intervals, we can actually follow plumes of water vapor as they evolve and move. It is this type capability to which we need to evolve!

With our (USA) current GOES we can track motion in five channels. The current GOES is an adaptive observing platform, which allows for different temporal frequencies of observation depending on the feature of meteorological interest. What is interesting with respect to multispectral imaging, is that depending on channel, we can detect cloud phase, temperature, motion, and using stereo or shadows we can assign a fairly precise height. With the infrared channel centered at 6.7 microns, we detect water vapor, but over a fairly deep region in the atmosphere. I believe that great strides forward will be made in the area of motion

tracking from satellites when we move out of the channel era and into the era of spectrometers and interferometers.

Tracking of clouds and features in “water vapor” imagery has added a great deal to our knowledge of motions in the broad scale atmosphere. The ability to determine water vapor winds is certainly one of the major accomplishments over the past decade. But while this accomplishment is in its own way monumental, we must not rest on out laurels, but must go back and do as Fujita would have done. We have a motion, it’s now time to take apart its components, give it a good hard scientific look and define where it fits into the big picture. In this area, we need to be careful to work closely with the modeling community to provide the best data possible - while reminding that community of what the measurement they are using represents. I never cease to be amazed when someone makes the observation that while certain types of observations improved an initial analysis, they did not improve, or show a positive impact on the forecast. Think about it.

The ability to provide high density winds, at several levels, remains an important contribution of the satellite community. These winds serve a variety of users. A bench forecaster may use cmv’s and be satisfied to know that the jet stream or low’s position relative to a forecast, and that the winds are strong. However, for a numerical model application that same success might be a disaster if the winds are placed at the incorrect height, or are in a thunderstorm region where they do not represent the atmosphere’s free stream flow. In the former case the cmv can ruin the forecast because it produces unrealistic shears and accelerations into the data field, in the other case the cmv can ruin the forecast because the model lacks the sophistication to use the information. I’m sure one day models will evolve to the level of sophistication needed where they will know convection is present and can use such information as cmv’s in deep convective regions - but they are not there today.

But, in any case, it is important to note that cmv’s play an important role as part of a global observing system where rawinsondes only provide limited global coverage (mostly in the northern hemisphere). It is also important to realize that it is both the mass and the wind fields play an important role in numerical weather prediction. For example, HIRS provides near global coverage every 12 hours. But, those HIRS data are not currently used where there are clouds NOR are the surface sensing channels used over land. I often wonder how much of the lack of impact of satellite sounding (and wind) data in the northern hemisphere is due to its under utilization over land - just look at the percentage of the northern hemisphere, versus the southern, which is covered by land. With microwave data, we can see through most clouds. However, in current NWP that data is under sampled (in some models it’s as poorly as one AMSU sample every 7 AMSU data points), and as with HIRS, AMSU data is not used over land. I personally believe that statements about the “non-impact” or poor or negative impact of satellite data in the northern hemisphere are due to poor models, their inadequate parameterizations and data assimilation systems, and not the quality of satellite observations - but that is another story for another day - or is it? For example we can measure, or infer winds from a variety of satellite based sensors. From QuikSCAT we can measure ocean surface wind speed, representative over 35 to 50 km square areas. ERS-2 provides us with similar capabilities over the ocean. With these systems, aside from the winds themselves, we get accurate locations of low pressure centers, hurricanes, fronts and trough lines. Are these data able to be used effectively in models? In some instances yes. But what happens when the observations stray too far from the model first guess? Most often the observations “loose their influence” due to the lack of match with the model first guess field. Then one might ask, “How can we justify verifying our satellite derived cmv’s against models, especially in data sparse areas?” I believe that is a valid question and concern.

Synthetic Aperture Radar also provides very accurate wind speed information, and on very small scales. Alaska Mariners call them williways - sudden, cold winds that blow from the coast without warning, churning the calmest seas. Using satellite imaging technology designed for other uses, like making topographical maps and gauging the thickness of sea ice, scientists with the National Oceanic and Atmospheric Administration are taking pictures of sea-level winds, including williways. The images they're producing are already making a difference. "The impression we're getting from the mariners out there is

a big 'wow' " said Gary Hufford, regional scientist for the National Weather Service in Alaska. "The device that can spot williways is synthetic aperture radar, or SAR. SAR is unique in that it can provide a picture of the winds through narrow mountain passes. Another satellite-mounted tool, a scatterometer, was designed specifically to gather wind information

over wide regions." While a scatterometer cannot spot williways, it does give wind direction which SAR cannot.

Let's focus on a real problem and see some of the things that can be done with satellite observations, aside from the ones that have been discussed thus far. Hurricane Mitch was one of the deadliest hurricanes ever. It was a category five hurricane that stalled and then drifted slowly southward into Central America, producing devastating flooding in Honduras, Nicaragua, and El Salvador. Its motion was continuously monitored (30 minute intervals) using GOES satellite data; yet model predictions for its movement were poor. How could that be? CMV's were derived on a routine basis. Aircraft flights were made into the storm. Its center location was well known. I cannot provide the answer, but believe its solution lies in improving the utilization of satellite data of all types in NWP : 1) full resolution AMSU and HIRS data; 2) full utilization over land; 3) use of precipitation information from satellites; 4) better models and assimilation systems; 5) use of full resolution, satellite derived ocean surface wind data ; 6) use of winds derived from AMSU (to follow); 7) better use of satellite derived sea surface temperature and altimetry; and, 8) other areas which run the gamut from improved satellite measurements to better model physics and improved parameterization schemes. But let's look at a few areas.

With geostationary satellites, observing frequency is important when analyzing a phenomena. A movie loop made from 30 minute interval imagery centered on the eye of Hurricane Mitch provides the illusion of strong anticyclonic rotation about the eye wall. Nothing could be further from the truth. Mitch was an extremely strong storm: what is observed at 30 minute intervals is simply a stroboscope effect. The features being observed made 300 degrees of clockwise rotation between successive images. When viewed at 30 minute intervals, they appear to move 60 degrees counterclockwise! This is consistent with the strong winds with Mitch. Thus, to correctly observe and analyze cloud feature motions in the eye wall in strong storms, an imaging frequency more rapid than 30 minutes is required. How much more frequently? With GOES, images as frequently as once every minute have been made of hurricanes. Those images, when animated (as is the case with hurricane Luis), clearly show strong cyclonic rotation along the eye wall, as well as the development of small vortices along the eye wall. CMV's made from those data have been used to show the deep cyclonic rotation extends to the hurricane's cirrus canopy, with a sharp ridge separating the inner region of cyclonic low from the broader anticyclonic outflow at hurricane canopy level. Does the extent of the cyclonic flow at canopy level relate to storm intensity - it should, and this phenomena deserves further investigation. It can only be observed with "super rapid scan" satellite imagery at resolutions comparable to today's visible image data (1 km).

With current AVHRR imagery we are able to make very nice color images using three channels composites that separate out high clouds from low clouds and ground. No doubt we will learn to improve on that by using multichannel data from MODIS, or MSG, which should also be able to provide further information on cloud particle size and phase. However, as has been demonstrated in this conference, very accurate height assignments can be made using polar orbiting (AVHRR) and geostationary (GOES and METEOSAT) satellite imagery. But what did we learn from that exercise? One point that resurfaced was the importance of the original work of Fujita on rectification, registration and navigation. Others more subtle were the importance of taking into account the curvature of the earth along the cloud trajectory path. There was also the realization that with the computer power available today, that there are opportunities to improve cloud height assignment by using multiple satellite views - beyond that is the exciting opportunity to investigate cloud properties by removing that ambiguity (height) and the applying multispectral analysis!

It is important to realize that the new polar orbiting satellite instrument AMSU (Advanced Microwave Sounding Unit) is providing valuable observations of the atmosphere, especially ia and around hurricanes. When one performs a simple retrieval of temperature (using climatology as a base) and then subtracts out

the mean sounding for the area, you are left with a temperature anomaly field which is solely due to the AMSU temperature observation. Such AMSU derived anomaly fields depict the warm core of hurricanes very well. This is exceptionally important, as will be shown momentarily, because it allows us to develop realistic renderings of a hurricane's wind field from full resolution AMSU data. BUT, realize that these fields were derived using full resolution AMSU data, while models use only a smattering of the available AMSU data. When we realize that we can observe the hurricane's warm core, and that model assimilation system greatly
under sampling AMSU and may not even see the warm region, then go back to the tenant that satellite data is having minimal impact on models is - incredible, simply incredible.

It is instructive to take a look at the information derived from a particular case; hurricane Floyd on September 14, 1999. This was a case where heavy rains and cloud liquid water were located in the northern part of the storm near the eye wall. Because AMSU-A is contaminated at lower levels by heavy rain, when a temperature anomaly is computed, the heavy rain area will show a negative anomaly. When one derives the wind field using rain contaminated anomaly data, the result is an unrealistic anticyclonic circulation away at low levels. Research is underway to best determine how to remove the low level rain contaminated region and replace it with a realistic temperature field. When that is done, the circulation pattern is realistic, although the very strong winds at the eye wall are not reproduced. That is partly because of the footprint size of the AMSU observation. What is very promising, however, is the ability to derive the three dimensional wind field for the hurricane and its environment using AMSU data and a non-linear balance equation. In two dimensional depictions the strong winds around the eye wall are not reproduced, as expected, however, the asymmetric nature of the broad scale flow is captured. For the case of hurricane Floyd, the asymmetric flow compared very favorably with aircraft reconnaissance data. Indeed, while the high wind region around the eye was not well depicted, the outer winds and those of the environment verified very well, as one might expect because of the larger scale coupling between winds and mass field away from the eye region.

AMSU is a global observing tool. It's ability to detect the driving force of the hurricane (warm core), should be expected to, and does, detect baroclinic features at more northern and southern latitudes. Just as the hurricane's warm core can be detected, so can the baroclinic nature of the jet stream. When AMSU is applied in a similar manner as with hurricanes in the westerlies, very good depictions of the flow are yielded. In an experiment underway at CIRA, AMSU derived winds are being compared with winds over Bermuda, where rawinsonde releases roughly coincide with AMSU overpasses. The flow fields that are being derived using AMSU data look very realistic. The accuracy of the AMSU wind derived at the rawinsonde site compares very well with "rawinsonde truth." This brings us to what I believe is an important juncture with our research using satellite data to derive atmospheric winds. We have a variety of tools that can be used for winds: AMSU, radar scatterometry (ERS-2, QuikSCAT), passive microwave (SSM/I), and geostationary satellite cloud tracking and water vapor motion. How can they best be put together? We know that with AMSU there is the opportunity for winds using a nonlinear balance equation, and that some of those winds are in regions where clouds are being tracked at precisely the same time with geostationary satellites, and in such a situation stereo might be able to be employed for determining cloud height. Can these sets of data be combined to develop an improved product? What about in regions of strong dynamics where the AMSU might miss the highest wind speeds, but where the geostationary satellite's cmv's will find them. How does scatterometry fit into this? With that tool we have a good measure of winds at the surface. There's a lot of good research to do, and I believe our end product can be greatly improved by combining these "non-conventional" winds with cmv's from rapid scan imagery. Maybe we can get close to the magic 1 m/sec.

Where do we go from here. We certainly must move forward with a strong research component; a component grounded in science. Let's take a lesson from the giant's who helped give us the opportunity to be involved in the exciting field of satellite meteorology. We owe them scientific integrity, we owe it to ourselves, and we owe it to those who follow in our footsteps. We are not merely generating winds to compare with rawinsondes and improve our verification statistics. Winds that are "errors" for one scale of motion may be important information for another. We must look to the opportunity provided by hyperspectral data which will be available from systems such as GIFTS. GIFTS promises to be a major part

of the future for geostationary observing platforms, and ALL countries involved in developing and providing geostationary satellite data must become be involved in GIFTS validation and assessment activities. We must prepare for the veritable onslaught of data that will be available in the future, with higher spatial resolution, more frequent interval sampling, multiple satellites, and interferometry. Satellites have limited life times, we must optimize their utilization both for monetary reasons and for our personal satisfaction as a science community. It is imperative that we work with the NWP community to improve the utilization of satellite data in that important tool. It is unrealistic to think that we will improve forecasting without improvements in NWP and coincident improvements in the assimilation of satellite data and products. Those products include winds, precipitation, cloud type and a variety of other pieces of information. The future is exceptionally challenging, and we must work with our users to insure that future is brought to a clear and exciting reality.

LIST OF PARTICIPANTS
FIFTH INTERNATIONAL WINDS WORKSHOP
28 February – 3 March 2000

R. C. Bhatia
Satellite Meteorology Division
India Meteorological Department
Mausam Bhavan, Lodi Road
New Delhi - 110 003
INDIA
Telephone: +91-11-4626021
Telefax: +91-11-4699216 or 4623220
e-mail: rcbhatia@imd.ernet.in

W. Bourke
BMRC - Bureau of Meteorology Research Centre
13th Floor, Celsius House
150 Lonsdale Street
P.O. Box 1289K GPO
Melbourne Vic 3001
AUSTRALIA
Telephone: +61-3-9669-4425
Telefax: +61-3-9669-4660
e-mail: w.bourke@bom.gov.au

G. G. Campbell
Cooperative Institute for Research in the Atmosphere
Colorado State University
Ft. Collins, CO 80523
USA
Telephone: +1-970-491-8497
Telefax: +1-970-491-8241
e-mail: campbell@cira.colostate.edu

J. Daniels
NOAA/NESDIS
WWBG, E/RA2, Room 601
5200 Auth Road
Camp Springs, Maryland 20746
USA
Telephone: +1-301-763-8204
Telefax: +1-301-763-8580
e-mail: jdaniels@nesdis.noaa.gov

S. S. Elliott
EUMETSAT
Am Kavalleriesand 31
64295 Darmstadt
GERMANY
Telephone: +49-6151-807-385 or 365
Telefax: +49-6151-807-304
e-mail: elliott@eumetsat.de

J. L. Evans*
Pennsylvania State University
University Park, PA 16803
USA
*Presently on leave at:
Bureau of Meteorology Research Center
P.O. Box 1289K
Melbourne VIC 3001
AUSTRALIA
Telephone: +61-3-9669-4421
Telefax: +61-3-9669-4660
e-mail: evans@essc.psu.edu (works in Australia and USA)

J. M. Fernández
Instituto Nacional de Meteorologia
Ap. 285
28071 Madrid
SPAIN
Telephone: +34-91-581-9664
Telefax: +34-91-581-9846
e-mail: serdan@inm.es

D. Griersmith
Bureau of Meteorology - Satellite Section
13th Floor, Celsius House
150 Lonsdale Street
P.O. Box 1289K GPO
Melbourne Vic 3001
AUSTRALIA
Telephone: +61-3-9669-4594
Telefax: +61-3-9669-4736
e-mail: d.griersmith@bom.gov.au

C. B. Hasager
Risoe National Laboratory
Wind Energy and Atmospheric Physics Department
P.O. Box 49
Frederiksborgvej 399
4000 Roskilde
DENMARK
Telephone: +45-4677-5014
Telefax: +45-4677-5970
e-mail: charlotte.hasager@risoe.dk

D. E. Hinsman
World Meteorological Organization
Case Postale 2300
1211 Geneva 2
SWITZERLAND
Telephone: +41-22-730-8285
Telefax: +41-22-730-8181
e-mail: hinsman@www.wmo.ch

K. Holmlund

EUMETSAT
Am Kavalleriesand 31
64295 Darmstadt
GERMANY
Telephone: +49-6151-807-599
Telefax: +49-6151-807-838
e-mail: holmlund@eumetsat.de

N. B. Ingleby
Meteorological Office
NWP Division
London Road
Bracknell, RG 12 2SZ
UNITED KINGDOM
Telephone: +44-1344-856447
Telefax: +44-1344-854026
e-mail: pbutterworth@meto.govt.uk

P. Ingmann
ESA/ESTEC
Earth Sciences Division
Postbus 299
2200 AG Noordwijk
THE NETHERLANDS
Telephone: +31-71-565-4459
Telefax: +31-71-565-5675
e-mail: pingmann@estec.esa.nl

A. R. Irving
NOAA/NESDIS/SSD/IPB
5200 Auth Road
Camp Springs, Maryland 20746
USA
Telephone: +1-301-763-8142 ext. 136
Telefax: +1-301-899-9196
e-mail: rirving@nesdis.noaa.gov

D. Jasper
BMRC - Bureau of Meteorology Research Centre
13th Floor, Celsius House
150 Lonsdale Street
P.O. Box 1289K GPO
Melbourne Vic 3001
AUSTRALIA
Telephone: +61-3-9669-4046
Telefax: +61-3-9669-4660
e-mail: d.jasper@bom.gov.au

G. Kelly
ECMWF
Shinfield Park
Reading, Berkshire RG2 9AX
UNITED KINGDOM
Telephone: +44-118-949-9651
Telefax: +44-118-986-9450
e-mail: graeme.kelly@ecmwf.int

P.N. Khanna
India Meteorological Department
Satellite Meteorology Division
Mausam Bhavan, Lodi Road
New Delhi – 110 003
INDIA
Telephone: +91-11-4642249 or 4626019
Telefax: +91-11-4642249 or 4623220
e-mail: pnk@imd.ernet.in

F. Lalaurette
ECMWF
Shinfield Park
Reading, Berkshire RG2 9AX
UNITED KINGDOM
Telephone: +44-118-949-9420
Telefax: +44-118-986-9450
e-mail: f.lalaurette@ecmwf.int

M. Manton
BMRC - Bureau of Meteorology Research Centre
13th Floor, Celsius House
150 Lonsdale Street
P.O. Box 1289K GPO
Melbourne Vic 3001
AUSTRALIA
Telephone: +61-3-9669-4444
Telefax: +61-3-9669-4660
e-mail: m.manton@bom.gov.au

J. Le Marshall
BMRC - Bureau of Meteorology Research Centre
13th Floor, Celsius House
150 Lonsdale Street
P.O. Box 1289K GPO
Melbourne Vic 3001
AUSTRALIA
Telephone: +61-3-9669-4420
Telefax: +61-3-9669-4660
e-mail: j.lemarshall@bom.gov.au

W. P. Menzel
NOAA/NESDIS
1225 West Dayton St.
Madison, WI 53706
USA
Telephone: +1-608-263-4930
Telefax: +1-608-262-5974
e-mail: paul.menzel@ssec.wisc.edu

T. Olander
University of Wisconsin - CIMSS
1225 West Dayton Street
Madison, WI 53706
USA
Telephone: +1-608-265-8005
Telefax: +1-608-262-5974
e-mail: timo@ssec.wisc.edu

N. Pescod
BMRC - Bureau of Meteorology Research Centre
13th Floor, Celsius House
150 Lonsdale Street
P.O. Box 1289K GPO
Melbourne Vic 3001
AUSTRALIA
Telephone: +61-3-9669-4749
Telefax: +61-3-9669-4660
e-mail: n.pescod@bom.gov.au

J. F. W. Purdom
NOAA/NESDIS
Office for Research and Applications
E/RA, World Weather Building/Room 701
5200 Auth Road
Camp Springs, Maryland, 20746
USA
Telephone: +1-301-763-8127
Telefax: +1-301-763-8108
e-mail: jpurdom@nesdis.noaa.gov

K. Puri
BMRC - Bureau of Meteorology Research Centre
13th Floor, Celsius House
150 Lonsdale Street
P.O. Box 1289K GPO
Melbourne Vic 3001
AUSTRALIA
Telephone: +61-3-9669-4433
Telefax: +61-3-9669-4660
e-mail: k.puri@bom.gov.au

S. R. H. Rizvi
National Centre for Medium Range Weather Forecasting
Department of Science & Technology
Mausam Bhavan Complex
Lodi Road
P.O. Box 3103
New Delhi 110003
INDIA
Telephone: +91-11-4694639
Telefax: +91-11-4690108
e-mail: rizvi@ncmrwf.ernet.in

R. Sarrazin
Canadian Meteorological Centre
Atmospheric Environment Service
2121 Trans-Canada Highway
North Service Road
Dorval, Quebec H9P 1J3
CANADA
Telephone: +1-514-421-4655
Telefax. +1-514-421-4657
e-mail: real.sarrazin@ec.gc.ca

J. Schmetz
EUMETSAT
Am Kavalleriesand 31
64295 Darmstadt
GERMANY
Telephone: +49-6151-807-590
Telefax: +49-6151-807-838
e-mail: schmetz@eumetsat.de

W. L. Smith
NASA Langley Research Center
Atmospheric Sciences
21 Langley Boulevard
Hampton, VA 23681-2199
Mail Stop 401
USA
Telephone: +1-757-864-5914
Telefax: +1-757-864-8197
e-mail: bill.l.smith@larc.nasa.gov

B. Soden
NOAA/GFDL (Geophysical Fluid Dynamics Laboratory)
P.O. Box 308
Princeton, N. J. 08542
USA
Telephone: +1-609-452-6575
Telefax: +1-609-987-5063
e-mail: bjs@gfdl.gov

C. Spinoso
BMRC - Bureau of Meteorology Research Centre
13th Floor, Celsius House
150 Lonsdale Street
P.O. Box 1289K GPO
Melbourne Vic 3001
AUSTRALIA
Telephone: +61-3-9669-4000
Telefax: +61-3-9669-4660
e-mail: c.spinoso@bom.gov.au

A. Stoffelen
KNMI
Postbus 201
3730 AE de Bilt
THE NETHERLANDS
Telephone: +31-30-22-06-585
Telefax: +31-30-22-10-407
e-mail: ad.stoffelen@knmi.nl

X. Su
NOAA
Environmental Modelling Center
National Center for Environmental Prediction
5200 Auth Road
Camp Springs, MD 20742
USA
Telephone: +1-301-763-8000 ext. 7271
Telefax: +1-301-763-8545
e-mail: xsu@ncep.noaa.gov

A. Szantai
Laboratoire de Météorologie Dynamique
Ecole Polytechnique
91128 Palaiseau
FRANCE
Telephone: +33-1-69-33-31-95
Telefax: +33-1-69-33-30-05
e-mail: szantai@lmd.polytechnique.fr

Y. Tahara
Japan Meteorological Agency
Numerical Prediction Division
1-3-4 Otemachi, Chiyodaku
Tokyo 100-8122
JAPAN
Telephone: +81-3-3211-8408
Telefax: +81-3-3211-8407
e-mail: y-tahara@naps.kishou.go.jp

C. Tingwell
BMRC - Bureau of Meteorology Research Centre
13th Floor, Celsius House
150 Lonsdale Street
P.O. Box 1289K GPO
Melbourne Vic 3001
AUSTRALIA
Telephone: +61-3-9669-4239
Telefax: +61-3-9669-4660
e-mail: c.tingwell@bom.gov.au

M. Tokuno
Meteorological Satellite Center/Japan Meteorological Agency
3-235, Nakakiyoto, Kiyose-shi
Tokyo 204-0012
JAPAN
Telephone: +81-424-93-4981
Telefax: +81-424-92-2433
e-mail: tokuno@msc.kishou.go.jp

C. Velden
University of Wisconsin - CIMSS
1225 West Dayton St.
Madison, Wisconsin 53706
USA
Telephone: +1-608-262-9168
Telefax: +1-608-262-5974
e-mail: chrisv@ssec.wisc.edu

J. Xu
National Satellite Meteorological Center
China Meteorological Administration
Bashiqiao Road 46, Western Suburb
Beijing 100081
CHINA
Telephone: +86-10-6840-6367
Telefax: +86-10-6217-2724
e-mail: wsk@rays.cma.gov.cn

Q. Zhang
National Satellite Meteorological Center
China Meteorological Administration
Bashiqiao Road 46, Western Suburb
Beijing 100081
CHINA
Telephone: +86-10-6840-8540
Telefax: +86-10-6217-2724
e-mail: wsk@rays.cma.gov.cn or qsz@nsmc.cma.gov.cn